Quantum kinetic description of the spin dynamics in diluted magnetic semiconductors

Von der Universität Bayreuth
zur Erlangung des Grades eines
Doktors der Naturwissenschaften (Dr. rer. nat.)
genehmigte Abhandlung

von

Moritz Cygorek

geboren in Neustadt a. d. Waldnaab

1. Gutachter: Prof. Dr. Vollrath Martin Axt
2. Gutachter: Prof. Dr. Stephan Kümmel

Tag der Einreichung: 21.09.2016
Tag des Kolloquiums: 22.02.2017

Quantum kinetic description
of the spin dynamics in
diluted magnetic semiconductors

Von der Universität Bayreuth
zur Erlangung des Grades eines
Doktors der Naturwissenschaften (Dr. rer. nat.)
genehmigte Abhandlung

von

Moritz Cygorek

geboren in Neustadt a. d. Waldnaab

1. Gutachter: Prof. Dr. Vollrath Martin Axt
2. Gutachter: Prof. Dr. Stephan Kümmel

Tag der Einreichung: 21.09.2016
Tag des Kolloquiums: 22.02.2017

Abstract

The spin dynamics in optically excited paramagnetic diluted magnetic semiconductors is investigated. To this end, a quantum kinetic density matrix theory which was developed by Christoph Thurn is applied, analyzed and extended.

Earlier studies which mainly concentrated on the case of a vanishing magnetization of the magnetic impurities revealed that the spin dynamics of optically excited electrons in three-dimensional systems is well reproduced by rate equations, where the rates can be derived from the Markovian limit of the quantum kinetic equations and coincide with the result of Fermi's golden rule. In two-dimensional systems, however, deviations between quantum kinetic simulations and results of Markovian rate equations in the form of non-monotonic overshoots of the carrier spin polarization below its asymptotic value for long times have been discovered.

In the present thesis, first, Thurn's quantum kinetic theory is applied to the case of finite impurity magnetization and equations in the Markovian limit are derived which reproduce well the quantum kinetic results and whose form has notable similarities to Landau-Lifshitz-Gilbert equations. The derived effective equations are then applied to study the competition between the spin-orbit coupling and the carrier-impurity exchange interaction. For this purpose, the quantum kinetic equations are extended and in addition to the exchange interaction, also $\mathbf{k}$-dependent effective fields together with carrier and impurity Zeeman energies are accounted for. This further enables the derivation of explicit expressions for the magnetic-field dependence of the spin transfer rates from the quantum kinetic equations. In contrast to the prevalent theories in the literature, the rate equations obtained here conserve the single-particle energies.

The causes and conditions for the appearance of non-Markovian effects are investigated more thoroughly. It is found that the non-Markovian behavior of the spin dynamics is particularly pronounced if carriers are excited in close proximity to the band edge. Accounting explicitly for the correlations between carriers and impurities in the quantum kinetic theory enables a discussion of genuine many-body effects like a renormalization of the precession frequency of the carrier spins for a finite impurity magnetization and a build-up of correlation energy.

Subsequently, the optical excitation of diluted magnetic semiconductors is taken into account on a quantum kinetic level in order to identify optimal excitation conditions for the detection of non-Markovian effects. Furthermore, it is investigated whether an efficient control of the spin dynamics in semiconductors with spin-orbit interaction by excitation with light with orbital angular momentum (twisted light) is possible. However, it is found that in extended systems, the spin dynamics after the optical excitation is nearly independent of the orbital angular momentum of the light.

Finally, the quantum kinetic theory is extended to account also for the scattering of carriers at a non-magnetic impurity potential which, in addition to the magnetic carrier-impurity interaction, originates from the doping with magnetic ions. It is found that the non-magnetic scattering leads to a redistribution of carriers in $\mathbf{k}$-space, which can strongly

suppress some of the non-Markovian effects. Simultaneously, the build-up of strong non-magnetic correlations also results in a considerable enhancement of genuine many-body effects and increases the regime of parameters in which a significant renormalization of the carrier spin precession frequency can be expected.

Kurzzusammenfassung

Die Spindynamik in optisch angeregten paramagnetischen verdünnt magnetischen Halbleitern wird untersucht. Zu diesem Zweck wird eine quantenkinetische Dichtematrixtheorie, die von Christoph Thurn entwickelt wurde, verwendet, analysiert und erweitert.

Frühere Studien, die sich hauptsächlich auf den Fall verschwindender Magnetisierung der magnetischen Dotieratome konzentrierten, ergaben, dass die Spindynamik optisch angeregter Elektronen in dreidimensionalen Systemen gut mit Ratengleichungen reproduziert werden kann, wobei die Raten aus dem Markovschen Grenzfall der quantenkinetischen Gleichungen hergeleitet werden können und mit dem Ergebnis von Fermis Goldener Regel übereinstimmen. In zweidimensionalen Systemen konnten jedoch Abweichungen zwischen quantenkinetischen Simulationen und den Ergebnissen der Markovschen Ratengleichungen in der Form eines nicht-monotonen Überschwingens der Ladungsträgerspinpolarisation über ihren asymptotischen Wert für lange Zeiten aufgezeigt werden.

In dieser Arbeit wird zunächst Thurns quantenkinetische Theorie auf den Fall endlicher Magnetisierung der magnetischen Ionen angewandt und Gleichungen im Markovschen Grenzfall hergeleitet, die die quantenkinetischen Ergebnisse gut reproduzieren und deren Form deutliche Ähnlichkeiten mit Landau-Lifshitz-Gilbert-Gleichungen aufweist. Die hergeleiteten effektiven Gleichungen werden anschließend benutzt, um die Konkurrenz zwischen Spin-Bahn-Wechselwirkung und Austauschwechelwirkung zwischen Ladungsträgern und magnetischen Dotieratomen zu untersuchen. Dazu werden die quantenkinetischen Gleichungen erweitert und zusätzlich zur Austauschwechselwirkung auch $\mathbf{k}$-abhängige effektive Felder zusammen mit Zeeman-Energien für Ladungsträger und magnetische Ionen berücksichtigt. Dies ermöglicht auch die Herleitung von expliziten Ausdrücken für die Magnetfeldabhängigkeit der Spin-Transfer-Raten aus den quantenkinetischen Gleichungen. Im Gegensatz zu den gängigen Theorien in der Literatur erhalten die hier gewonnenen Ratengleichungen die Ein-Teilchen-Energie.

Zudem werden die Ursachen und Bedingungen für das Auftreten nicht-Markovscher Effekte näher untersucht. Dabei ergibt sich, dass sich nicht-Markovsches Verhalten der Spindynamik besonders deutlich zeigt, wenn Ladungsträger in unmittelbarer Nähe zur Bandkante angeregt werden. Die explizite Berücksichtigung der Korrelationen zwischen Ladungsträgern und Dotieratomen in der quantenkinetischen Theorie ermöglicht die Diskussion reiner Vielteilcheneffekte, wie z.B. einer Renormierung der Präzessionsfrequenz der Ladungsträgerspins für endliche Magnetisierungen der Dotieratome und den Aufbau von Korrelationsenergie.

Danach wird die optische Anregung von verdünnt magnetischen Halbleitern auf der Ebene der Quantenkinetik berücksichtigt, um optimale Anregungsbedingungen für den Nachweis nicht-Markovscher Effekte zu identifizieren. Außerdem wird untersucht, ob eine effiziente Kontrolle der Spindynamik in Halbleitern mit Spin-Bahn-Wechselwirkung durch Anregung mit Licht mit Bahndrehimpuls (Twisted Light) möglich ist. Jedoch zeigt sich, dass in ausgedehnten Systemen die Spindynamik nach der optischen Anregung nahezu unabhängig vom Bahndrehimpuls des Lichts ist.

Schließlich wird die quantenkinetische Theorie noch erweitert, um der Streuung von Ladungsträgern an nichtmagnetischen Störpotentialen Rechnung zu tragen, die zusätzlich zur magnetischen Ladungsträger-Dotieratom-Wechselwirkung durch die Doterung mit magnetischen Ionen zustande kommt. Dabei ergibt sich, dass die nichtmagnetische Streuung zu einer Umverteilung von Ladungsträgern im $\mathbf{k}$-Raum führt, die einige der nicht-Markovschen Effekte in der Spindynamik deutlich unterdrücken kann. Gleichzeitig führt der Aufbau starker nichtmagnetischer Korrelationen auch zu einer deutlichen Verstärkung echter Vielteilcheneffekte und vergrößert den Parameterbereich, in dem eine signifikante Renormierung der Ladungsträgerspinpräzessionsfrequenz zu erwarten ist.

Contents

Part I.

Introduction & Background

1. Introduction

1.1. Motivation

The idea behind the spintronics paradigm [1, 2] is to utilize the spin degree of freedom of carriers instead of or in addition to the charge degree of freedom used in conventional electronic devices in order to enhance their properties with respect to, e.g., processing speed or power consumption [2]. So far, technological applications of spintronics are mostly confined to metallic magnetic devices [3], such as hard disk read heads based on the giant magnetoresistance effect in ferromagnetic–non-magnetic–ferromagnetic sandwich structures [4, 5]. This effect exploits the fact that the transmission of carriers through a non-magnetic–ferromagnetic interface strongly depends on the direction of the carrier spin with respect to the magnetization of the ferromagnet. Similar effects constitute the basis for a number of proposals for more advanced spintronics devices, such as spin valves and spin transistors [1, 3, 6] or magnetoresistive random access memories (MRAMs) [7]. However, some of these devices, in particular the spin transistors, require not only the control of the number of spin-up and spin-down electrons, but also of the coherences between spin-up and spin-down states of the individual carriers. Due to the large number of carriers in a metal, the carrier-carrier scattering leads to a fast dephasing of electron spins, making spin transistors based on metallic devices unlikely [3]. This difficulty can be overcome if the non-magnetic parts of the heterostructures are composed of semiconductor materials, whose spin dephasing times can be up to 3 orders of magnitude longer than in metallic systems [3].

However, the semiconductor spintronics approach faces a new problem: The electrical spin injection from a metallic ferromagnetic to a semiconductor is very inefficient due to the conductivity mismatch between the metal and the semiconductor [8]. One strategy to circumvent the conductivity mismatch problem is to use magnetic semiconductors instead of the ferromagnetic metal as a spin injector [9]. To make a semiconductor magnetic, it can be doped with transition metal elements, which have a partially filled d shell resulting in a strong magnetic moment. The systems obtained this way form the material class of diluted magnetic semiconductors (DMS) [10]. While most DMS are paramagnetic, ferromagnetism can be achieved in certain materials, e.g., $Ga_{1-x}Mn_xAs$, if the doping concentration x exceeds a few percent [11]. The reason for this is that the substitutional incorporation of group-II Mn ions on lattice positions of group-III Ga ions leads also to a strong p-doping of the DMS. These holes mediate an effective magnetic impurity-impurity interaction responsible for the ferromagnetism [12]. The main obstacle for commercial applications based on ferromagnetic DMSs is that the Curie temperatures are usually well below room temperature [13]. To this day, the details of the microscopic mechanism responsible for ferromagnetism in $Ga_{1-x}Mn_xAs$ are still debated [14] and investigations in this direction continue [15].

While most proposals for applications rely on spin-dependent transport properties, a

more fundamental understanding of the spin physics of DMS is often obtained by optical means: Information about the formation of exciton, trion and donor acceptor states as well as the impurity magnetization via the carrier spin splitting can be obtained by photoluminescense measurements [16] and the magnetization dynamics in DMS can be extracted, e.g., from time-resolved magneto-optical Kerr rotation [17, 18], Faraday rotation [19] or circular dichroism [20] experiments. Although the time evolution of the carrier spin has been probed since the 90s, there is so far no microscopic theory that can accurately predict such basic quantities as the carrier spin decay rate and its magnetic field dependence, even in the simplest cases like in n-doped very dilute magnetic $Cd_{1-x}Mn_xTe$ quantum wells [21].

In order to advance the theoretical understanding of the spin dynamics in DMS, Christoph Thurn laid the grounds for a comprehensive quantum kinetic description based on a density matrix theory taking into account the many-body correlations between carriers and impurities in DMS [22–24]. This theory enables the study of coherent optical excitation of electrons from the valence to the conduction band and the onset of a precession of the carrier and impurity spins as well as spin-flip scattering mediated by the carrier-impurity correlations. It was found that in certain situations, the carrier-impurity spin transfer dynamics can deviate strongly from a simple exponential behavior [23, 24], which is predicted by theories that do not take into account the finite memory due to the build-up of carrier-impurity correlations, such as models based on rate equations [21, 25–27] or on a projection operator method [28].

However, the accuracy of the microscopic approach entails the drawback that the derived equations of motion are lengthy and numerically challenging. The complexity of the equations makes it difficult to develop an intuition about the physical meaning of the individual terms in the equations. The numerical demands impede a brute-force approach to an exhaustive investigation of the dependence of the spin dynamics on the material parameters and excitation conditions. Furthermore, so far, only the s/p-d exchange interaction between carriers and impurities as well as the light-matter interaction for the description of the optical excitation has been considered, whereas in realistic samples a number of other interactions might influence the spin dynamics. These include non-parabolicities and spin-orbit coupling terms in the crystal Hamiltonian [29, 30], confinement and strain effects in quantum wells and heterostructures [31], non-magnetic impurity scattering [25], acceptor bound states, e.g., in GaMnAs [13, 15], Coulomb correlations causing exciton and trion formation [32–34] and carrier-carrier exchange interactions [35], effects due to the disorder in the distribution of impurity positions as well as an inhomogeneous impurity magnetization [36] and, finally, the interaction with external electric and magnetic fields used in experiments, e.g., in time-resolved magneto-optical Kerr measurements [19].

Thus, Thurn's work marks only the beginning of a comprehensive and systematic investigation of a number of different aspects of the spin dynamics in DMS based on a quantum kinetic description. In the present thesis, Thurn's quantum kinetic theory is analyzed in great detail and numerical simulations as well as analytical limiting cases are presented that enable a more thorough understanding of the phyiscs captured in the quantum kinetic theory. Besides investigating Thurn's quantum kinetic equations in cases which have been largely unexplored so far, the theory is extended to incorporate other interactions, such as external magnetic fields, spin-orbit coupling effects and non-magnetic impurity scattering on a quantum kinetic level.

In particular, we discuss under which circumstances a Markovian description in terms of rate equations is appropriate and when genuine quantum kinetic effects beyond the Markovian approximation become important. In cases, where the Markovian picture is justified, carrier-impurity spin transfer rates are derived, which is not straightforward in the presence of an external magnetic field and non-zero impurity magnetization. Also, non-perturbative many-body correlation effects are investigated which have a number of different consequences, such as a renormalization of the precession frequencies in the presence of an external magnetic field or the release of energy due to the build-up of strong carrier-impurity correlations, which results in characteristic signatures in the spin dynamics of optically excited DMS.

1.2. Outline

This thesis is based on 10 publications which can be found at the end of this document in part IV. In order to make the subject of these publications more accessible, we first provide the reader with a basic summary of the usual description of the spin dynamics in non-magnetic semiconductors and DMS in the literature in chapter 2. Since the publications presented in this thesis rely heavily on the previous work by Christoph Thurn, we recapitulate Thurn's quantum kinetic theory to the necessary extent in chapter 3.

The publications are introduced in part II where, first, in chapter 4, the open questions after Thurn's work are summarized and, after the necessary concepts are introduced, a more detailed overview of the publications is given. In chapter 5, Thurn's quantum kinetic theory is applied to the case of non-zero impurity magnetization and it is discussed how effective equations can be derived in the Markov limit that reproduce well the full quantum kinetic spin dynamics in bulk DMS. The Markovian equations are then used in chapter 6 to study the interplay between the carrier-impurity interaction and spin-orbit coupling in the form of Dresselhaus and Rashba fields. Subsequently, it is discussed in chapter 7 under which circumstances the results of the quantum kinetic equations deviate from the predictions of a Markovian effective single-particle description. In chapter 8, it is studied how the spin dynamics can be controlled by the optical excitation conditions such as the duration of a pump pulse or the orbital angular momentum of the light. After that, the influence of the scattering of carriers at a spin-independent disorder potential originating from the magnetic doping of the semiconductor is investigated in chapter 9.

Finally, the central findings of the publications are summarized and some suggestions and preliminary results for further studies are presented in part III.

2. Spin dynamics in DMS: state of the art

2.1. Spin dynamics in non-magnetic semiconductors

Before discussing the spin dynamics in DMS, it is necessary to acquire a rough understanding about the basic notions and practices in the more general field of spin physics in, in general, non-magnetic semiconductors. This topic has a long history and it is beyond the scope of this thesis to cover it in detail. For a more comprehensive review, the reader is referred to the review article of *Wu et al.* [37] which is the basis for the following summary.

2.1.1. Basic band structure and optical excitation

The most frequently studied DMS are based on II-VI and III-V compound semiconductors [13], which typically crystallize in zinc-blende structure and have a direct band gap at the Γ-point ($\mathbf{k}$=0). There, the lowest conduction band states have s-type symmetry and are two-fold degenerate, while the highest valence band is of p-type and contains 6 valence subbands in total [38]. At $\mathbf{k} = 0$, the energy eigenstates of the crystal Hamiltonian can be written as Bloch states composed of plane waves and periodic Bloch functions that are eigenstates of the total angular momentum operator $\mathbf{j} = \mathbf{l} + \mathbf{s}$, where $\mathbf{l}$ is the orbital angular momentum of the periodic Bloch function and $\mathbf{s}$ is the spin [39]. Furthermore, it can be shown that, in the absence of external fields, confinement and strain, the valence band forms a set of 4 degenerate heavy- and light-hole subbands corresponding to $j = \frac{3}{2}$ and 2 split-off subbands with $j = \frac{1}{2}$, which are typically energetically far below the heavy- and light hole states. For $\mathbf{k} \neq 0$ or in the presence of a confinement potential or strain, the symmetry is reduced and heavy- ($j_z = \pm\frac{3}{2}$) and light holes ($j_z = \pm\frac{1}{2}$) are split from each other. This situation is depicted in Fig. 2.1.

In addition to the band structure, Fig. 2.1 also shows the allowed transitions between the conduction band and the heavy- and light-hole subbands for optical excitation with circularly polarized light. From these selection rules it is immediately clear how one can, in principle, study the spin dynamics in semiconductors experimentally. If the heavy- and light-hole bands are significantly split and the semiconductor is excited by a laser beam with circular polarization, say σ^-, which is tuned in resonance with the heavy-hole–conduction-band transition energy, only conduction band electrons with spin $s_z = +\frac{1}{2}$ are excited and valence band electrons with $j_z = +\frac{3}{2}$ are removed, i.e., holes with total angular momentum $j_z = -\frac{3}{2}$ are generated. This procedure is called optical orientation [40] and also works to some degree in the case where heavy- and light-hole bands are degenerate, since the heavy-hole–conduction-band and light-hole–conduction-band transitions have different strengths.
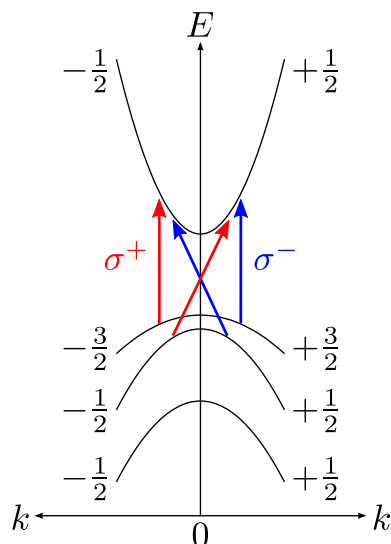
Figure 2.1.: Schematic of a band structure of a direct band gap semiconductor in the presence of confinement or stain. The states at $\mathbf{k} = 0$ are eigenstates to the j_z operator with eigenvalues $\pm\frac{3}{2}$ and $\pm\frac{1}{2}$, respectively. The total-angular-momentum selection rule between the conduction band (highest parabola) and the heavy- (second parabola) and light-hole band (third parabola) for optical excitation with light with helicity $\sigma^\pm$ are depicted. Transitions from the split-off band (lowest parabola) are not shown.

In the simplest case, information about the spin dynamics can be extracted by looking at the polarization of the photoluminescence after a short circularly polarized pump pulse. Alternatively, one can consider the change of certain response functions in the presence of spin-polarized carriers, which can be tested experimentally, e.g. by probing the system with a second light pulse that is delayed with respect to the pump pulse. Such pump-probe experiments are the basis for most modern setups and enable a tracking of the carrier spin polarization with time-resolutions of about 200 fs [18, 19].

2.1.2. k-dependent effective magnetic fields

The spin dynamics in semiconductors immediately after the optical orientation is determined by contributions to the Hamiltonian which do not commute with the spin operator. For the conduction band electrons, these terms can be written in the form of a $\mathbf{k}$-dependent effective magnetic field. To understand the origin of these effective fields, one has to study the band structure beyond the parabolic approximation depicted in Fig. 2.1. The effective field can be obtained directly from $\mathbf{k}.\mathbf{p}$-theory, which is extensively covered in the books by *Bastard* [31] or *Winkler* [39]. Here, we only sketch the essential steps that are necessary to understand the origin of the effective field.

In general, the electrons in a semiconductor are subject to the Coulomb interaction with nuclei and other electrons. This leads to a complicated many-body problem that requires some approximations in order to be solvable. Often, one tries to find a suitable effective single-particle theory for semiconductor electrons, where the Coulomb interactions are modeled by an effective single-particle crystal potential V_0. The exact form of the crystal potential is unknown, but it is assumed that the crystal potential has the same symmetry as the crystal itself. The discrete translational invariance of the crystal lattice has the consequence that, according to the Bloch theorem, the electronic energy

eigenstates of the crystal Hamiltonian can be written as products of plane waves and periodic Bloch functions $u_{n\mathbf{k}}(\mathbf{r})$, i. e.,

$$\psi_{n\mathbf{k}}(\mathbf{r}) = \frac{1}{\sqrt{V}}e^{i\mathbf{k}\cdot\mathbf{r}}u_{n\mathbf{k}}(\mathbf{r}), \tag{2.1}$$

where $u_{n\mathbf{k}}(\mathbf{r})$ has the same periodicity as the crystal lattice. Here, n labels the different subbands.

In typical direct gap II-VI and III-V semiconductors, the Γ-point ($\mathbf{k} = 0$) is a high symmetry point, where the periodic Bloch functions $u_{n\mathbf{k}=0}(\mathbf{r})$ of bulk systems[1] coincide with the eigenstates of the j_z operator (cf. situation depicted in Fig. 2.1). Together with the degeneracies of the subbands known from symmetry considerations this enables a description of the crystal Hamiltonian at $\mathbf{k} = 0$ with only a few independent parameters, which can be obtained in optical experiments. At $\mathbf{k} \neq 0$, the periodic Bloch functions $u_{n\mathbf{k}\neq0}$ are not known, but since the periodic Bloch functions u_{n0} at $\mathbf{k} = 0$ form a complete basis in the set of lattice-periodic functions, the states $u_{n\mathbf{k}}$ at $\mathbf{k} \neq 0$ can be decomposed into linear combinations of the periodic functions at $\mathbf{k} = 0$.

With this in mind, we can formulate the idea of $\mathbf{k}.\mathbf{p}$-theory: The crystal Hamiltonian is written in the form of a matrix in the basis of states similar to the Bloch states in Eq. (2.1), except that the known periodic Bloch functions u_{n0} at $\mathbf{k} = 0$ are used instead of $u_{n\mathbf{k}}$. This yields an eigenvalue problem for every $\mathbf{k}$-state in the form of a matrix diagonalization. The matrix elements of the crystal Hamiltonian are, in general, unknown, but they can be formally expanded in terms of polynomials in $\mathbf{k}$. Group theory is used to classify these polynomials according to their transformation properties. Only a small subset of polynomials of a given order in $\mathbf{k}$ are compatible with the crystal symmetry, which drastically reduces the number of free parameters in the off-diagonal elements.

Usually [31, 39], only terms up to $\mathcal{O}(\mathbf{k}^2)$ are taken into account and one focuses on the 8 subbands depicted in Fig. 2.1. In the basis described above, the crystal Hamiltonian has off-diagonal elements between conduction and valence band states. However, in many situations it is sufficient to concentrate either on the conduction band or on the valence band. To this end, it is useful to block-diagonalize the crystal Hamiltonian by a suitable unitary transformation described by a matrix $U_{\mathbf{k}}$ which is chosen such that the interband mixing terms vanish and the transformed effective conduction band and valence band states are decoupled:

---

[1]Note that this is only the case for the three-dimensional $\mathbf{k}$-vector in bulk systems. In confined systems, the decomposition of low-energy eigenstates of the confinement problem in plane waves has contributions of states with significant wave vector components along the confinement directions, which can lead to a significant mixing of bands [41].

$$
\begin{pmatrix}
* & * & * & * & * & * & * & * \\
* & * & * & * & * & * & * & * \\
* & * & * & * & * & * & * & * \\
* & * & * & * & * & * & * & * \\
* & * & * & * & * & * & * & * \\
* & * & * & * & * & * & * & * \\
* & * & * & * & * & * & * & * \\
* & * & * & * & * & * & * & *
\end{pmatrix}
\longrightarrow
\begin{pmatrix}
* & * & 0 & 0 & 0 & 0 & 0 & 0 \\
* & * & 0 & 0 & 0 & 0 & 0 & 0 \\
0 & 0 & * & * & * & * & * & * \\
0 & 0 & * & * & * & * & * & * \\
0 & 0 & * & * & * & * & * & * \\
0 & 0 & * & * & * & * & * & * \\
0 & 0 & * & * & * & * & * & * \\
0 & 0 & * & * & * & * & * & *
\end{pmatrix}
$$

$$H_0(\mathbf{k}) \qquad\qquad\qquad U_\mathbf{k}^+ H_0(\mathbf{k}) U_\mathbf{k}$$

Since the crystal Hamiltonian is diagonal at $\mathbf{k} = 0$, these band mixing terms are of the order $\mathcal{O}(\mathbf{k}^1)$. Thus, the block-diagonalization can be done perturbatively in terms of $\mathbf{k}$. This procedure is known as Löwdin partitioning [42] and is mathematically equivalent to a Schrieffer-Wolff transformation [43] or a Foldy-Wouthuysen transformation [44].

This has two major consequences: First of all, the unitary transformation changes the basis states so that the new effective conduction band states have some contributions from the original valence bands. In particular, the new basis states are not exact eigenstates of the total angular momentum operator j_z. Second, the Löwdin partitioning introduces new contributions to the Hamiltonian in the basis of the new conduction band states. Because the conduction band consists of only two subbands, one can rewrite the conduction band part $H^c(\mathbf{k})$ of the crystal Hamiltonian $U_\mathbf{k}^+ H_0(\mathbf{k}) U_\mathbf{k}$ in terms of a spin independent part $E_\mathbf{k}$ and a Zeeman-like term with an $\mathbf{k}$-dependent effective magnetic field $\mathbf{\Omega_k}$:

$$H^c(\mathbf{k}) = E_\mathbf{k}\mathbf{1} + \hbar\mathbf{\Omega_k} \cdot \mathbf{s}, \tag{2.2}$$

where $\mathbf{1}$ is the 2×2 identity matrix and $\mathbf{s} = \frac{1}{2}\boldsymbol{\sigma}$ with the vector of Pauli matrices $\boldsymbol{\sigma}$.

The general properties of the effective magnetic field $\mathbf{\Omega_k}$ follow from symmetry considerations. For example, without external magnetic fields the total Hamiltonian is invariant under time reversal. This leads to Kramers degeneracy, which means that the effective field is antisymmetric with respect to the wave vector $\mathbf{\Omega_{-k}} = -\mathbf{\Omega_k}$. If the system is also invariant under inversion, so that $\mathbf{\Omega_{-k}} = \mathbf{\Omega_k}$, the effective magnetic field vanishes. Thus, the presence of $\mathbf{\Omega_k}$ requires some mechanism of breaking of the inversion symmetry. In zinc-blende structures, this symmetry breaking is provided by the crystal structure. This results in the Dresselhaus field [29]

$$\mathbf{\Omega_k}^D = \frac{2}{\hbar}\gamma_D \begin{pmatrix} k_x(k_y^2 - k_z^2) \\ k_y(k_z^2 - k_x^2) \\ k_z(k_x^2 - k_y^2) \end{pmatrix}, \tag{2.3}$$

where γ_D is a material parameter that describes the strength of the Dresselhaus field. Other sources of inversion symmetry breaking are asymmetric confinement potentials in semiconductor heterostructures or an external electric field. This leads to the Rashba field [30], which in two dimensions reads

$$\mathbf{\Omega_k}^R = \frac{2}{\hbar}\alpha_R \begin{pmatrix} k_y \\ -k_x \end{pmatrix}, \tag{2.4}$$

where α_R is the Rashba parameter. In a more microscopic picture, the effective magnetic fields can be related to spin-orbit coupling.

The consequences of **k**-dependent effective magnetic fields for the spin dynamics in DMS are discussed in [Pub3], [Pub4] and [Pub5]. Their influence on the spin dynamics in non-magnetic semiconductors is described next.

2.1.3. Spin relaxation mechanisms in non-magnetic semiconductors

A comprehensive review of the spin dynamics in non-magnetic semiconductors is given in Ref. [37]. Here, we present a rough overview of the most important spin dephasing and relaxation mechanisms in non-magnetic semiconductors that compete with the magnetic-impurity-induced spin dynamics in DMS.

As shown in the previous section, several sources contribute to an effective **k**-dependent magnetic field for the electron spins. When a non-equilibrium electron spin polarization is induced by optical orientation, these spins start to precess about the effective field. Since the effective magnetic field depends on the wave vector, spins of electrons with different wave vectors precess, in general, about different axes with different frequencies. This leads to a dephasing of the ensemble of electron spins [45].

During the precession and dephasing, the carriers in semiconductors are subject to scattering at different sources, such as other carriers, impurities or phonons. In the literature [37, 46–48], the spin dephasing is usually described in terms of a stochastic process in which the wave vector of an electron is changed abruptly after a characteristic momentum relaxation time τ_p. This, in turn, changes the effective magnetic field $\boldsymbol{\Omega_k}$ for the electron spin. If the momentum relaxation rate τ_p^{-1} is large compared with the typical precession frequency, the electron spins do not have the time to precess significantly before they get scattered again, which effectively freezes the spin. This motional-narrowing-type of behavior leads to a spin dephasing time inversely proportional to the momentum relaxation time. This process is referred to as the D'yakonov-Perel' (DP) mechanism [46].

Another process in which the spin is influenced by momentum scattering is the Elliot-Yafet (EY) mechanism [47, 48]. This mechanism relies on the fact that, because of the mixing between conduction and valence band states for $\mathbf{k} \neq 0$, the states in the effective conduction subbands after Löwdin partitioning are no longer spin eigenstates. Thus, the scattering between energy eigenstates with different wave vectors has a finite chance of inducing a flipping of the carrier spin, even if the interaction responsible for the scattering is itself spin-independent, i.e., it commutes with the spin operator. In contrast to the DP mechanism, EY predicts the spin relaxation rate to be proportional to the rate of momentum scattering.

If there is a large number of holes in the semiconductor, electrons can also exchange their spins with the holes, which is another relaxation channel for electron spins. This is the essence of the Bir-Aronov-Pikus (BAP) mechanism [35].

Typically, the spin dynamics in non-magnetic semiconductors is dominated by DP and is only challenged by BAP in strongly p-doped bulk systems [49].

For holes, the situation is much less clear, since in many cases the strong intraband mixing leads to a very fast dephasing of hole spins, which is hard to resolve experimentally. Also, the simple picture of a precessing spin vector is not applicable for the holes, because the heavy and light holes form a spin-$\frac{3}{2}$ system, which cannot be represented by a dipole alone. Instead, for the heavy and light holes the quadrupole and octopole

parts have to be considered in the calculations [50]. On the other hand, in very narrow quantum wells, where the heavy- and light-hole bands are substantially split, transitions between them are energetically forbidden. Therefore, this splitting effectively pins the spins of the heavy holes. Already this short discussion shows that the situation of the valence band is complicated. Thus, for most of the thesis, we focus on the conduction band.

2.2. Spin dynamics in DMS in the literature

Now, we introduce the DMS materials under investigation as well as the carrier-impurity interaction, before we review the spin dynamics in DMS as it is usually covered in the literature.

2.2.1. DMS materials

Diluted magnetic semiconductors are obtained when transition metal ions, which possess a partially filled d shell, are incorporated into a conventional semiconductor.

The most frequently studied DMS are Mn-doped II-VI semiconductors, e.g., CdTe or ZnSe, and III-V semiconductors, such as GaAs [13]. The main difference between these two classes of DMS is that Mn can isoelectrically substitute the group-II elements in II-VI semiconductors, while the incorporation of Mn at positions of the group-III elements concurrently results in p-doping of the DMS. The excess holes in III-V materials can mediate a ferromagnetic interaction between different magnetic impurities. The ferromagnetic order in $Ga_{1-x}Mn_xAs$ has been verified experimentally in the 1990s [11]. However, the Curie temperature is way below room temperature, which is a major impediment for technological applications of ferromagnetic $Ga_{1-x}Mn_xAs$.

Although the ferromagnetism in $Ga_{1-x}Mn_xAs$ is an interesting property, we study exclusively II-VI DMS in this thesis because III-V DMS are much harder to model theoretically. The reason for this is that the large number of donors in III-V DMS and the holes introduce many additional complications compared with II-VI based systems. For example, the holes can be bound to the acceptors. If the wave functions of the carriers bound to the acceptors overlap, an impurity band can form in the band gap [15]. Also, a large number of holes enhances electron spin relaxation via the BAP mechanism [49] and, in general, leads to screening effects as well as to scattering [51]. Nevertheless, one can expect that the theory developed for II-VI DMS in this thesis can also be applied to the case of $Ga_{1-x}Mn_xAs$, if it is extended correspondingly.

The II-VI DMS considered here are usually paramagnetic with small antiferromagnetic corrections due to the superexchange between Mn impurities at nearest-neighbor cation sites [13, 52]. The Mn impurities in II-VI DMS effectively provide nearly independent local magnetic moments which interact with the quasi-free carriers in the semiconductor. In order to be able to treat the half-filled d-shell of a Mn impurity as a localized spin-$\frac{5}{2}$ system, two conditions have to be fulfilled. First, the lifting of the degeneracy of the d-states caused, e.g., by a crystal field splitting must be much smaller than the Hund's rule coupling. For example, in the case of $LaCoO_3$, the d-orbitals of Co are split into sixfold degenerate t_{2g} and fourfold degenerate e_g states due to the tetragonal crystal field splitting, so that for low temperatures, all of the six d-electrons of Co occupy the

lower-energetic t_{2g} states and form a state with a total magnetic moment of zero [53]. However, for the II-VI DMS considered here, the Hund's rule coupling dominates and the five d-electrons of Mn indeed form a spin-$\frac{5}{2}$ system [10]. Furthermore, the d-states have to be energetically separated from the band edges. Otherwise, quasi-free carrier can hop on and off the d-states, which again invalidates the picture of the d-states forming a well-defined localized spin-$\frac{5}{2}$ system. This condition is also well met in II-VI DMS [10].

These findings allow us to describe the II-VI DMS in the present thesis by the band structure of the non-magnetic II-VI material together with an effective interaction between the semiconductor carriers and localized spin-$\frac{5}{2}$ systems comprised of the d-shell electrons of the Mn impurities.

2.2.2. Carrier-impurity interaction

The interaction between conduction band carriers and magnetic impurities in DMS is modeled by [25, 54]

$$H_{sd} = J_{sd} \sum_{iI} \hat{\mathbf{S}}_I \cdot \hat{\mathbf{s}}_i \, \delta(\mathbf{R}_I - \mathbf{r}_i), \tag{2.5a}$$

$$H_{\mathrm{imp}} = J_0 \sum_{iI} \delta(\mathbf{R}_I - \mathbf{r}_i), \tag{2.5b}$$

where H_{sd} is the spin-dependent part and H_{imp} is the spin-independent part of the interaction between the s-type conduction band electrons and the d-electrons of the Mn impurities. Here, J_{sd} and J_0 are the coupling constants, $\hat{\mathbf{S}}_I$ and $\hat{\mathbf{s}}_i$ are the impurity and electron spin operators and $\mathbf{R}_I$ as well as $\mathbf{r}_i$ are the positions of the I-th impurity and the i-th electron, respectively.

Similarly, for holes, the spin-dependent part of the effective Hamiltonian is:

$$H_{pd} = J_{pd} \sum_{jI} \hat{\mathbf{S}}_I \cdot \hat{\mathbf{s}}_j^h \delta(\mathbf{R}_I - \mathbf{r}_j^h), \tag{2.6}$$

with valence band coupling constant J_{pd} and operators of the j-th hole spin and position $\hat{\mathbf{s}}_j^h$ and $\mathbf{r}_j^h$.

The effective Hamiltonians describe a localized interaction between carriers and magnetic impurities. Since a Hamiltonian of the same form as the s-d interaction is also important in the discussion of the Kondo effect in magnetically doped metallic alloys [55], H_{sd} is often referred to as the Kondo Hamiltonian.

A discussion of how the effective Hamiltonians can be derived from microscopic band structure calculations is given in Ref. [56]. The coupling constants J_{sd} and J_{pd} have two different contributions [56, 57]: First, the direct or potential exchange stems from the exchange part of the Coulomb interaction between the quasi-free semiconductor carriers and the d-electrons of the Mn impurities in the Hartree-Fock picture. Second, a hybridization of the semiconductor band states and the Mn d-electrons enables a virtual hopping between these states. The hopping is suppressed by the strong energetic penalty involved in adding or removing an electron to and from the Mn d-tates. This allows for a perturbative treatment of the hopping by a Schrieffer-Wolff transformation [43] yielding

a contribution to the effective conduction and valence band Hamiltonians of the form of H_{sd} and H_{pd}. This contribution is referred to as the kinetic exchange [58].

Note that the hybridization between s-type conduction band states and the d-states of the impurities is forbidden by symmetry [56, 58]. This is the reason why the valence band coupling constant J_{pd} is typically much stronger than the conduction band coupling constant J_{sd} and has the opposite sign for most II-VI DMS [54].

The magnetic carrier-impurity interaction is always accompanied by the non-magnetic impurity interaction H_{imp} with similar microscopic origins [59]. Because H_{imp} commutes with the spin operators and therefore acts only indirectly on the carrier spin via scattering in $\mathbf{k}$-space, it is often not taken into account in theoretical studies of the spin dynamics in DMS. For most of the publications in this thesis, we also neglect the spin-independent part of the carrier-impurity interaction and adjourn the discussion of its effects on the spin dynamics in DMS to [Pub10].

2.2.3. Mean-field and virtual-crystal approximation

Some effects of the s-d exchange interaction on the carrier spins can already be obtained in the simple picture provided by the mean-field and virtual-crystal approximations. In the mean-field approximation, it is assumed that, in the description of the quasi-free carriers, the impurity spins are regarded as classical vectors, so that the electrons are subject to an effective mean-field Hamiltonian

$$H_{sd}^{\text{MF}} = J_{sd} \sum_{iI} \langle \hat{\mathbf{S}}_I \rangle \cdot \hat{\mathbf{s}}_i \, \delta(\mathbf{R}_I - \mathbf{r}_i). \tag{2.7}$$

In the virtual-crystal approximation, the impurities are assumed to be positioned regularly in the crystal lattice instead of randomly. This is achieved by smearing out the δ-function and replacing $\delta(\mathbf{R}_I - \mathbf{r}_i) \to \frac{1}{V}$. Thus, the s-d Hamiltonian in mean-field and virtual-crystal approximation reads

$$H_{sd}^{\text{MF/VC}} = \frac{J_{sd} N_{\text{Mn}}}{V} \sum_i \langle \hat{\mathbf{S}} \rangle \cdot \hat{\mathbf{s}}_i, \tag{2.8}$$

where N_{Mn} is the number of magnetic impurities and $\langle \hat{\mathbf{S}} \rangle$ is the average spin per impurity.

Recalling that the Zeeman energy of an electron in an external magnetic field $\mathbf{B}$ is

$$H_Z^e = \sum_i g_e \mu_B \mathbf{B} \cdot \hat{\mathbf{s}}_i, \tag{2.9}$$

with an effective g-factor g_e, one can immediately see that, on this level of theory, the impurity magnetization acts exactly like an external magnetic field. Thus, both contributions, the mean-field/virtual-crystal s-d interaction and the Zeeman energy, can be combined into a single term. The enhancement of the effective magnetic field for the electrons due to the magnetic impurities is then referred to as the giant Zeeman effect and can be measured experimentally by investigating the corresponding energetic shifts between the spin-up and spin-down subbands [54].

The giant Zeeman effect has the immediate consequence for the spin dynamics that the precession of carrier spins in the presence of an external magnetic field is enhanced

the same way as the spin splitting, which is verified experimentally, e.g., in Ref. [19]. However, the simple picture of the giant Zeeman effect as an enhancement of the g-factor is not always applicable. For example, after optical orientation of carrier spins in DMS perpendicular to an external magnetic field, the impurity spins precess about the field caused by the carrier spins. Thus, the impurity magnetization is tilted out of its equilibrium direction. Then, the resulting finite component of the impurity magnetization perpendicular to the external field starts to precess about the external field, which produces characteristic oscillatory signatures in the signals of optical pump-probe experiments [60]. Similarly, the precession of carrier and impurity spins about each other can give rise to collective carrier-impurity precession modes [61], which are not captured by a simple enhancement of the electron g-factor due to the giant Zeeman effect, but they can be described in the mean-field and virtual-crystal approximation.

However, it is noteworthy that, on the level of the mean-field and virtual-crystal approximation, no changes in the spins are predicted if the impurity and carrier spins are aligned parallel to each other. Therefore, this approximation is not capable of describing a genuine transfer of a non-equilibrium spin polarization from the carriers to the impurities and vice-versa.

2.2.4. Rate equations for spin-flip scattering

Beyond the mean-field and virtual-crystal approximation, the Hamiltonian H_{sd} also describes a spin-flip scattering of electrons at the impurities, which is usually described in the literature in terms of rate equations derived by Fermi's golden rule [16, 25, 26, 62, 63]. There are also some other approaches which enable an extraction of the spin-flip scattering rates, such as the kinetic spin Bloch equations [27] or a theory based on a projection operator method [28]. The results of the different approaches coincide with Fermi's golden rule for vanishing external magnetic field, but they differ for non-zero **B**. In the case of **B** = 0, the carrier-impurity spin transfer rate τ_{sd}^{-1} for a quantum well with width d is [23]

$$\frac{1}{\tau_{sd}} = I \frac{J_{sd}^2 N_{\mathrm{Mn}} m^*}{\hbar^3 V d} \langle S^2 \rangle, \tag{2.10}$$

where m^* is the effective electron mass and $I = d \int_{-\frac{d}{2}}^{\frac{d}{2}} dz \, |\psi(z)|^4$ is a factor depending on the form of the z-envelope of the carrier wave function in the quantum well.

It is expected that the spin-flip scattering is the dominant process for the decay of the carrier spin in DMS quantum wells [27, 37]. This is supported by the fact that the carrier spin decay measured in experiments is proportional to the impurity concentration [21]. However, the predicted rates are a factor of ≈ 5 too small to explain the experiments quantitatively [21]. It was argued [18, 64] that if excitons are excited instead of uncorrelated electrons and holes, the effective mass m^* that enters in the rate has to be replaced by the exciton mass. Although this gives the right tendencies, a number of questions remain. For example, for the experiments in Ref. [21], the DMS were actually n-doped in order to suppress excitonic effects by screening.

Furthermore, for low temperatures of the order of 2 K, a minimum of the carrier spin

decay time has been found experimentally [21]. This was attributed to inhomogeneity effects resulting, e.g., from different local temperatures within the laser spot [21]. For bulk DMS, where the spin-flip scattering time is rather large, it was argued [65] that such spacial inhomogeneity effects lead to a dephasing of spins more than one order of magnitude faster than the *s-d* spin transfer time predicted by Fermi's golden rule. Other effects related to spacial inhomogeneities in DMS are the formation of complexes comprised of quasi-free carriers with wave functions within a finite volume that includes a number of spin polarized magnetic impurities, the so-called magnetic polarons [36, 66–72]. However, these inhomogeneity effects strongly depend on the preparation and excitation of the sample. In the present thesis, we focus on the spin dynamics of an on average homogeneous DMS system and we do not account for the effects related to a spatially varying local temperature or the formation of magnetic polarons.

2.2.5. Prospects of a quantum kinetic theory for the spin dynamics in DMS

In the present thesis, a quantum kinetic theory for the description of the spin dynamics in DMS is presented. The main reason for developing such a theory, which is much more complicated than the Fermi's-golden-rule-type rate equations described earlier, is that it is also more accurate and requires less assumptions. In particular, the derivation of the quantum kinetic theory does not rely on perturbative arguments in terms of the carrier-impurity interaction and is applicable even if H_{sd} is strong.

In the absence of an external magnetic field and for vanishing impurity magnetization, rate equations can be obtained in the Markov limit of the quantum kinetic theory. The rates derived in this way also coincide with the golden rule value in Eq. (2.10). However, in certain situations, such as in low-dimensional systems, the full quantum kinetic theory yields results that can deviate from a simple rate-type exponential decay [23].

Furthermore, the Markov limit of the quantum kinetic theory can also be constructed in the case of a non-vanishing impurity magnetization and a finite external magnetic field. This makes it possible to extract the magnetic-field dependence of the rates from the quantum kinetic theory. While Fermi's golden rule only gives transition rates between energy eigenstates, the Markov limit of the quantum kinetic theory also provides an expression for the perpendicular spin transfer rate, i.e., the rate by which the carrier spins perpendicular to the impurity magnetization are transferred to the impurity system. For non-zero magnetic field we find an effective rate-like description that automatically conserves the total single-particle energies in spin-flip scattering events, while the kinetic spin Bloch equations approach in Ref. [27] and the projection operator method of Ref. [28] end up with different rate equations that are not compatible with the conservation of the total single-particle energy.

Also, the density matrix theory enables a fully coherent treatment of the optical excitation. This allows us, e.g., to investigate the carrier-impurity spin transfer even within the time frame of the pump pulse duration, which is relevant for developing protocols for the optical control of the spins in DMS.

Furthermore, the quantum kinetic theory described in this thesis explicitly accounts for correlations between carriers and magnetic impurities. Some hints towards why the carrier-impurity correlations are indeed important in DMS can be found in the litera-

ture: First of all, the *s-d* Hamiltonian also appears in the theory of the Kondo-effect [55]. There, the quantity of interest is the resistivity of metals with magnetic impurities for low temperatures T. While a theoretical description based on perturbation theory predicts a logarithmic divergence of the resistivity at $T \to 0$ [55], measurements show that the resistivity actually converges towards a finite value in this limit. This was later explained by the formation of a many-particle state, where each impurity forms a spin-singlet with a few carriers and is therefore screened from the other carriers in the metal. The fact that this state is a real many-particle state that is not separable into single-particle contributions reflects strong quantum mechanical correlations between the carriers and impurities. Although the conditions in DMS are very different from those in metals with magnetic impurities, the relation to the Kondo-effect is a strong motivation for studying the carrier-impurity correlations in DMS. Moreover, *Perakis et al.* [73] studied the effects of carrier-impurity correlations in ferromagnetic $Ga_{1-x}Mn_xAs$ within a theory based on Green's functions and found that the correlations indeed influence the spin stiffness and Gilbert damping in this system. Note also that *Morandi et al.* [74] derived a third-order perturbation theory based on Green's functions in an Abrikosov pseudofermion formulation for the investigation of the magnetization dynamics in ferromagnetic $Ga_{1-x}Mn_xAs$. The study came across uncontrolled Kondo-like divergences. This makes an application of the theory questionable, but it also highlights the importance of carrier-impurity correlations in DMS. In the quantum kinetic theory described in this thesis, we also find Kondo-like divergences. These appear in the correlation energy and in a renormalization of the carrier spin precession frequency when treated in the Markov limit. However, these divergences are integrable and finite values are obtained when the carrier distribution has a non-zero spectral width.

Another advantage of our quantum kinetic approach is that it can easily be extended to incorporate other interactions. This allows us to study the interplay between the *s-d* interaction and the spin-orbit coupling as well as the non-magnetic scattering of carriers due to the interaction H_{imp} on a quantum kinetic level.

3. Thurn's quantum kinetic equations

The present thesis is based on previous works conducted as part of Christoph Thurn's PhD thesis [75]. Therefore, it is necessary to summarize the central aspects of Thurn's quantum kinetic theory [22] and some first numerical results in the case of vanishing impurity magnetization and zero magnetic field [23, 24], which is the subject of this chapter.

3.1. General remarks

The goal of Ref. [22] was the development of a microscopic theory of the spin physics in DMS in terms of a quantum kinetic theory. This approach starts with a given Hamiltonian and yields equations of motion for the relevant density matrices. It is motivated by pump-probe measurements where the time evolution of quantities related to the density matrices, e.g., the total carrier spin parallel or perpendicular to a quantum well plane, can be monitored experimentally [19].

As is always the case in condensed matter physics, where a macroscopic number of carriers can contribute to the observed signals, some approximations have to be applied in order to establish a numerically feasible solution to the complicated many-body problem, while still maintaining the relevant physical features. In the case of Thurn's quantum kinetic theory, the many-body problem was tackled using a correlation expansion scheme [76].

In a semiclassical mean-field treatment, where the impurity spins and the quasi-free carriers in the DMS are treated as independent (uncorrelated) variables, the main effect of the magnetic impurities is to provide an additional effective magnetic field for the carriers. In contrast, the quantum kinetic treatment of Ref. [22] also accounts for the correlations between the quasi-free carriers and the magnetic impurities beyond the mean-field approximation. The central assumption for finding a closed set of equations of motion in the quantum kinetic theory is that higher correlations, such as the carrier-carrier as well as the impurity-impurity correlations, are negligible. Accounting for these correlations is, in principle, straightforward, but blows up the complexity of the equations of motion and the numerical demands even further.

One of the most important effects of the carrier-impurity correlations on the spin dynamics, which is not captured by the mean-field approximation, is that the correlations mediate spin-flip scattering processes between the carrier and impurity subsystems. In contrast to rate equations, where the spin-flip scattering processes are assumed to be instantaneous, accounting explicitly for the carrier-impurity correlations in the quantum kinetic theory introduces a finite memory, i.e., a non-zero duration of spin-flip scattering processes.

3.2. Quantum kinetic theory

3.2.1. Hamiltonian and basis states

The first step in setting up quantum kinetic equations of motion is the choice of the model Hamiltonian and the basis states in which the Hamiltonian is expressed. As usual in solid state theory, a formulation in terms of creation and annihilation operators for Bloch states in second quantization is employed for the description of a macroscopic number of delocalized carriers in the DMS. As discussed earlier, the elementary interaction between quasi-free carriers and magnetic impurities can be described by a Kondo-Hamiltonian [cf. Eq. (2.5a)]. In second quantization for the carriers, the *s-d* interaction has the form:

$$H_{sd} = \frac{J_{sd}}{V} \sum_{I} \sum_{\mathbf{k}l\mathbf{k}'l'} \hat{\mathbf{S}}_I \cdot \mathbf{s}_{ll'} c_{l\mathbf{k}}^\dagger c_{l'\mathbf{k}'} e^{i(\mathbf{k}'-\mathbf{k})\mathbf{R}_I}, \tag{3.1}$$

where $c_{l\mathbf{k}}^\dagger$ and $c_{l\mathbf{k}}$ are the creation and annihilation operator of Bloch electrons with wave vector $\mathbf{k}$ in the conduction subband l and $\mathbf{s}_{ll'} = \frac{1}{2}\boldsymbol{\sigma}_{ll'}$ are the conduction band spin matrices proportional to the vector of Pauli matrices $\boldsymbol{\sigma}$.

Now, it is crucial to find a suitable representation of the magnetic impurity spins $\hat{\mathbf{S}}_I$ at positions $\mathbf{R}_I$. In the spirit of the correlation expansion, the most obvious representation is the average spin $\langle \hat{\mathbf{S}}_I \rangle$ of the I-th impurity. However, one finds that terms of the form $\langle \hat{S}_I^i \hat{S}_J^j \rangle$ enter in the equations of motion, so that this approach has the disadvantage that second moments of the impurity spins cannot be expressed in terms of average values (first moments) if the impurity spin is larger than $\frac{1}{2}$. Therefore, one would have to derive equations of motion for the second moments, which, in turn, depend on the third moments. Formally, there are only 36 degrees of freedom for a spin-$\frac{5}{2}$ system such as Mn, but the factorization of higher moments is cumbersome.

Instead, Thurn used a representation for impurity spins comprised of the single-particle impurity density operators $\hat{P}_{n_1 n_2}^I = |I, n_1\rangle\langle I, n_2|$ in the basis $|I, n\rangle$ of the spin states for the I-th impurity, which are eigenstates to the $\hat{S}_I^z$ operator with eigenvalues $n \in \{-\frac{5}{2}, -\frac{3}{2}, \ldots, \frac{5}{2}\}$. Neglecting the impurity-impurity correlations at different positions $\mathbf{R}_I$ and $\mathbf{R}_J$ enables a factorization according to [22]

$$\langle \hat{P}_{n_1 n_2}^I \hat{P}_{n_3 n_4}^{J \neq I} \rangle = \langle \hat{P}_{n_1 n_2}^I \rangle \langle \hat{P}_{n_3 n_4}^{J \neq I} \rangle, \tag{3.2a}$$

$$\langle \hat{P}_{n_1 n_2}^I \hat{P}_{n_3 n_4}^I \rangle = \langle I, n_1 | I, n_2 \rangle \langle I, n_3 | I, n_4 \rangle = \delta_{n_2 n_3} \langle \hat{P}_{n_1 n_4}^I \rangle, \tag{3.2b}$$

which allows for a more compact notation of the equation of motion for the impurity degrees of freedom. In other works [74], a pseudo-fermion approach was used to describe the impurity spins in DMS. However the perturbative Green's functions study of Ref. [74] suffers from uncontrolled divergences, which inhibit a clear physical picture as well as a direct comparison with Thurn's quantum kinetic theory.

With the impurity spins expressed in terms of the operator $\hat{P}_{nn'}^I$ and the carriers described in second quantization, the *s-d* interaction takes the form [22]:

$$H_{sd} = \frac{J_{sd}}{V} \sum_{Inn'} \sum_{\mathbf{k}l\mathbf{k}'l'} \mathbf{S}_{nn'} \cdot \mathbf{s}_{ll'} c_{l\mathbf{k}}^\dagger c_{l'\mathbf{k}'} \hat{P}_{nn'}^I e^{i(\mathbf{k}'-\mathbf{k})\mathbf{R}_I}, \tag{3.3}$$

where $\mathbf{S}_{nn'}$ are the spin matrices of a spin $\frac{5}{2}$ system, which can be found, e. g., in appendix A of Ref. [22]. H_{sd} together with the corresponding term for the p-d interaction between holes in the valence band, the parabolic free-carrier band structures and the light-matter interactions form the starting point of the correlation expansion of Ref. [22]. For the summary of Thurn's quantum kinetic theory, we focus on the conduction band and take the laser excitation into account by choosing corresponding non-equilibrium initial values for carrier spins and occupations at $t = 0$, so that the total Hamiltonian in this description is comprised of only H_{sd} and an effective mass Hamiltonian H_0 for the two-fold degenerate conduction band.

3.2.2. Correlation expansion

The carrier and impurity spin polarization can be extracted from the single-particle density matrices $\langle c^\dagger_{l_1 \mathbf{k}_1} c_{l_2 \mathbf{k}_1} \rangle$ and $\langle \hat{P}^I_{n_1 n_2} \rangle$. From the Heisenberg equations of motion, one finds for the carrier density matrix:

$$-i\hbar \frac{\partial}{\partial t} \langle c^\dagger_{l_1 \mathbf{k}_1} c_{l_2 \mathbf{k}_1} \rangle = \langle [H_0, c^\dagger_{l_1 \mathbf{k}_1} c_{l_2 \mathbf{k}_1}] \rangle + \langle [H_{sd}, c^\dagger_{l_1 \mathbf{k}_1} c_{l_2 \mathbf{k}_1}] \rangle, \qquad (3.4)$$

where the first commutator vanishes in the case of an effective mass Hamiltonian H_0. After inserting the expression for H_{sd} from Eq. (3.3), the second term of Eq. (3.4) yields

$$\frac{J_{sd}}{V} \sum_{Inn'} \sum_{kl} \mathbf{S}_{nn'} \cdot \left(\mathbf{s}_{ll_1} \langle c^\dagger_{l\mathbf{k}} c_{l_2 \mathbf{k}_1} \hat{P}^I_{nn'} \rangle e^{i(\mathbf{k}_1 - \mathbf{k})\mathbf{R}_I} - \mathbf{s}_{l_2 l} \langle c^\dagger_{l_1 \mathbf{k}_1} c_{l\mathbf{k}} \hat{P}^I_{nn'} \rangle e^{i(\mathbf{k} - \mathbf{k}_1)\mathbf{R}_I} \right). \qquad (3.5)$$

It is now clear that the carrier-impurity correlations $\langle c^\dagger_{l_1 \mathbf{k}_1} c_{l_2 \mathbf{k}_2} \hat{P}^I_{n_1 n_2} \rangle$ influence the carrier spin dynamics. To distinguish the mean-field contributions from the true correlation effects, it is instructive to factorize [76] according to

$$\langle c^\dagger_{l_1 \mathbf{k}_1} c_{l_2 \mathbf{k}_2} \hat{P}^I_{n_1 n_2} \rangle = \langle c^\dagger_{l_1 \mathbf{k}_1} c_{l_2 \mathbf{k}_2} \rangle \langle \hat{P}^I_{n_1 n_2} \rangle + \delta \langle c^\dagger_{l_1 \mathbf{k}_1} c_{l_2 \mathbf{k}_2} \hat{P}^I_{n_1 n_2} \rangle, \qquad (3.6)$$

where the first term on the r.h.s. is the mean-field part and $\delta \langle c^\dagger_{l_1 \mathbf{k}_1} c_{l_2 \mathbf{k}_2} \hat{P}^I_{n_1 n_2} \rangle$ are the true correlations or cumulants. Henceforth, when the term correlations is used, we refer to the true correlations as opposed to the expressions of the form of the l.h.s. of Eq. (3.6).

Another problem that is evident from Eq. (3.5) is that the positions of the impurity ions $\mathbf{R}_I$ appear explicitly in the time evolution of the carrier density matrix. However, the number of impurity ions is a macroscopic quantity, so that the impurities cannot be taken into account individually. Rather, some distribution of impurity ions has to be assumed and an averaging over this distribution has to be performed in order to enable the calculation of the time evolution of the carrier spins. Thus, the impurity positions become (classical) random variables that also have to be accounted for in a rigorous correlation expansion scheme. Then, Eq. (3.5) becomes

$$\frac{J_{sd}}{V} \sum_{Inn'} \sum_{kl} \mathbf{S}_{nn'} \cdot \left(\mathbf{s}_{ll_1} \langle c^\dagger_{l\mathbf{k}} c_{l_2 \mathbf{k}_1} \hat{P}^I_{nn'} e^{i(\mathbf{k}_1 - \mathbf{k})\mathbf{R}_I} \rangle - \mathbf{s}_{l_2 l} \langle c^\dagger_{l_1 \mathbf{k}_1} c_{l\mathbf{k}} \hat{P}^I_{nn'} e^{i(\mathbf{k} - \mathbf{k}_1)\mathbf{R}_I} \rangle \right), \qquad (3.7)$$

where the brackets now also include an averaging over the random impurity positions $\mathbf{R}_I$. Note that the dependence on $\mathbf{R}_I$ disappears for $\mathbf{k} = \mathbf{k}_1$, so that in this case the

factorization has to be performed as in Eq. (3.6). For $\mathbf{k}_1 \neq \mathbf{k}_2$, the factorization of the terms in Eq. (3.7) is [22]:

$$\langle c_{l_1\mathbf{k}_1}^\dagger c_{l_2\mathbf{k}_2} \hat{P}_{nn'}^I e^{i(\mathbf{k}_2-\mathbf{k}_1)\mathbf{R}_I}\rangle = \langle c_{l_1\mathbf{k}_1}^\dagger c_{l_2\mathbf{k}_2}\rangle\langle\hat{P}_{nn'}^I\rangle\langle e^{i(\mathbf{k}_2-\mathbf{k}_1)\mathbf{R}_I}\rangle + \delta\langle c_{l_1\mathbf{k}_1}^\dagger c_{l_2\mathbf{k}_2}\hat{P}_{nn'}^I\rangle\langle e^{i(\mathbf{k}_2-\mathbf{k}_1)\mathbf{R}_I}\rangle$$

$$+ \delta\langle\hat{P}_{nn'}^I e^{i(\mathbf{k}_2-\mathbf{k}_1)\mathbf{R}_I}\rangle\langle c_{l_1\mathbf{k}_1}^\dagger c_{l_2\mathbf{k}_2}\rangle + \delta\langle c_{l_1\mathbf{k}_1}^\dagger c_{l_2\mathbf{k}_2} e^{i(\mathbf{k}_2-\mathbf{k}_1)\mathbf{R}_I}\rangle\langle\hat{P}_{nn'}^I\rangle$$

$$+ \delta\langle c_{l_1\mathbf{k}_1}^\dagger c_{l_2\mathbf{k}_2}\hat{P}_{nn'}^I e^{i(\mathbf{k}_2-\mathbf{k}_1)\mathbf{R}_I}\rangle. \tag{3.8}$$

The first two terms on the r.h.s. of Eq. (3.8) vanish if an on average homogeneous distribution of impurities with $\langle e^{i(\mathbf{k}_2-\mathbf{k}_1)\mathbf{R}_I}\rangle = \delta_{\mathbf{k}_2\mathbf{k}_1}$ is assumed and $\mathbf{k}_1 \neq \mathbf{k}_2$. A non-vanishing value of $\delta\langle\hat{P}_{nn'}^I e^{i(\mathbf{k}_2-\mathbf{k}_1)\mathbf{R}_I}\rangle$ implies a correlation between the spin and the position of impurities. These correlations correspond to spin waves with wave vector $(\mathbf{k}_2 - \mathbf{k}_1)$. However, the third term on the r.h.s. of Eq. (3.8) also vanishes for $\mathbf{k}_1 \neq \mathbf{k}_2$ in an on average spatially homogeneous system, where $\langle c_{l_1\mathbf{k}_1}^\dagger c_{l_2\mathbf{k}_2}\rangle \propto \delta_{\mathbf{k}_1,\mathbf{k}_2}$ is diagonal with respect to the wave vector. Thus, only the last two terms of Eq. (3.8) remain. Note that correlations of the type $\delta\langle c_{l_1\mathbf{k}_1}^\dagger c_{l_2\mathbf{k}_2} e^{i(\mathbf{k}_2-\mathbf{k}_1)\mathbf{R}_I}\rangle$ also build up when scattering at non-magnetic impurities due to the Hamiltonian H_{imp} defined in Eq. (2.5b) is considered. In the equations of motion for the correlations in Ref. [22], all correlations higher than $\delta\langle c_{l_1\mathbf{k}_1}^\dagger c_{l_2\mathbf{k}_2} e^{i(\mathbf{k}_2-\mathbf{k}_1)\mathbf{R}_I}\rangle$ and $\delta\langle c_{l_1\mathbf{k}_1}^\dagger c_{l_2\mathbf{k}_2}\hat{P}_{nn'}^I e^{i(\mathbf{k}_2-\mathbf{k}_1)\mathbf{R}_I}\rangle$ have been dropped after the factorization. Special care has to be taken that the fermionic antisymmetry in factorizations of electronic four-point averages is fulfilled, so that, e.g.,

$$\langle c_{l_1\mathbf{k}_1}^\dagger c_{l_2\mathbf{k}_2}^\dagger c_{l_3\mathbf{k}_3} c_{l_4\mathbf{k}_4}\rangle \to \langle c_{l_1\mathbf{k}_1}^\dagger c_{l_4\mathbf{k}_4}\rangle\langle c_{l_2\mathbf{k}_2}^\dagger c_{l_3\mathbf{k}_3}\rangle - \langle c_{l_1\mathbf{k}_1}^\dagger c_{l_3\mathbf{k}_3}\rangle\langle c_{l_2\mathbf{k}_2}^\dagger c_{l_4\mathbf{k}_4}\rangle, \tag{3.9}$$

where the true carrier-carrier correlations are neglected in the truncation scheme. Note that, in order to obtain physical results in the limit $V \to \infty$, the relation (3.2b) for products of impurity operators at the same position ($I = J$) has to be applied before the factorization.

In Ref. [22], the dynamical variables of the quantum kinetic equations for conduction band electrons were defined as:

$$C_{l_1\mathbf{k}_1}^{l_2} = \langle c_{l_1\mathbf{k}_1}^\dagger c_{l_2\mathbf{k}_1}\rangle, \tag{3.10a}$$

$$M_{n_1}^{n_2} = \langle\hat{P}_{n_1n_2}^I\rangle, \tag{3.10b}$$

$$\bar{C}_{l_1\mathbf{k}_1}^{l_2\mathbf{k}_2} = V\delta\langle c_{l_1\mathbf{k}_1}^\dagger c_{l_2\mathbf{k}_2} e^{i(\mathbf{k}_2-\mathbf{k}_1)\mathbf{R}_I}\rangle, \tag{3.10c}$$

$$\bar{K}_{l_1n_1\mathbf{k}_1}^{l_2n_2\mathbf{k}_2} = V\delta\langle c_{l_1\mathbf{k}_1}^\dagger c_{l_2\mathbf{k}_2}\hat{P}_{n_1n_2}^I e^{i(\mathbf{k}_2-\mathbf{k}_1)\mathbf{R}_I}\rangle. \tag{3.10d}$$

The factors V are introduced to keep the correlations finite in the limit $V \to \infty$. Note also that the dynamical variables are independent of the impurity index I due to the averaging over the impurity distribution. While the equations of motion in Ref. [22] were explicitly written down for the correlations $\bar{C}_{l_1\mathbf{k}_1}^{l_2\mathbf{k}_2}$ and $\bar{K}_{l_1n_1\mathbf{k}_1}^{l_2n_2\mathbf{k}_2}$, it turns out in [Pub1] that the equations of motion can be simplified by summarizing the correlations to

$$Q_{l_1n_1\mathbf{k}_1}^{l_2n_2\mathbf{k}_2} = M_{n_1}^{n_2}\bar{C}_{l_1\mathbf{k}_1}^{l_2\mathbf{k}_2} + \bar{K}_{l_1n_1\mathbf{k}_1}^{l_2n_2\mathbf{k}_2} = V\langle c_{l_1\mathbf{k}_1}^\dagger c_{l_2\mathbf{k}_2}\hat{P}_{n_1n_2}^I e^{i(\mathbf{k}_2-\mathbf{k}_1)\mathbf{R}_I}\rangle, \qquad \mathbf{k}_1 \neq \mathbf{k}_2, \tag{3.11}$$

since the mean-field contribution is exactly the term that is obtained from the average $\langle c_{l_1\mathbf{k}_1}^\dagger c_{l_2\mathbf{k}_2}\hat{P}_{n_1n_2}^I e^{i(\mathbf{k}_2-\mathbf{k}_1)\mathbf{R}_I}\rangle$ for $\mathbf{k}_1 = \mathbf{k}_2$. Note that the factorization into the true correlations in Ref. [22] was necessary for the correct identification of higher order correlations

that are neglected.

The corresponding equations of motion for the density matrices and the correlations in the conduction band are given in [Pub1].

3.3. Theoretical findings

The quantum kinetic equations of motion are the main result of Ref. [22]. However, already at this point, it is possible to discuss some features of the theory.

First of all, it is found that the mean-field theory, which describes the giant Zeeman effect and a precession of carrier and impurity spins about each other, is obtained from the quantum kinetic theory if the correlations are set to zero. Furthermore, if the averaging over the impurity distribution is performed on the level of the Hamiltonian, which corresponds to the virtual-crystal approximation, the same result is obtained as in the mean-field case. In particular, in the situation of a vanishing impurity magnetization, the mean-field and virtual-crystal approximations predict no change of the initial carrier spin at all.

A successful test of the soundness of the theory is that the equations of motion can be shown to conserve the total number of electrons as well as the total energy including the correlation energies. Also, the total spin comprised of carrier and impurity spins is conserved.

A Taylor-expansion in terms of short times, i.e., a few time steps in the equations of motion corresponding to a few fs, shows that, in the first step, the correlations are built up, which, in turn, change the single-particle density matrices in the second step. Thus, the change of the single-particle observables is quadratic in time as can be expected from a time-reversible quantum kinetic theory. Also, a redistribution of carriers in **k**-space is already indicated by such an analysis.

3.4. Markov limit

After the derivation of the quantum kinetic theory, it is instructive to compare it to rate equations obtained from Fermi's golden rule. This was done in Ref. [23] for the case of vanishing impurity magnetization.

It turns out that the same rate equations can also be derived directly from the quantum kinetic theory in the Markovian limit, i.e., if it is assumed that the memory provided by the correlations is short. The procedure of deriving the Markov limit of the quantum kinetic theory according to Ref. [23] is sketched schematically as follows:

First, assume that the equations of motion for the correlations have the form

$$-i\hbar\frac{\partial}{\partial t}Q = -\hbar\Delta\omega Q + b, \tag{3.12}$$

where $(-\hbar\Delta\omega Q)$ is the homogeneous part and b is the source term, which only depends on the single-particle density matrices C and M. If b is regarded as a function of time,

Eq. (3.12) can be formally integrated. The Markov limit is established by

$$Q(t) = \frac{i}{\hbar} \int\limits_{-\infty}^{t} dt' \, e^{i\Delta\omega(t'-t)} b(t') \approx \frac{i}{\hbar} b(t) \int\limits_{-\infty}^{t} dt' \, e^{i\Delta\omega(t'-t)} = \frac{i}{\hbar} b(t) \Big(\pi\delta(\Delta\omega) - \frac{i}{\Delta\omega} \Big). \quad (3.13)$$

The l.h.s. of Eq. (3.13) has the form of a memory integral over the values of the single-particle quantities contained in b at past times $t' \leq t$. The assumption of a short memory means that only the value of the source term at $t' = t$ is relevant. Evaluating $b(t') \approx b(t)$ at t leads to the r.h.s. of Eq. (3.13), where the memory integral can be calculated analytically. The correlations appearing in the equations of motion for the single-particle density matrices can then be replaced by the Markovian expressions according to Eq. (3.13). The real part of the memory integral yields a δ-function which, when inserted into the equation for the carrier density matrix, leads to an expression equivalent to Fermi's golden rule. For zero impurity magnetization, the imaginary part does not enter in the equations of motion for the single-particle density matrices.

A more formal and comprehensive derivation of the Markov limit for more general situations is presented in [Pub5].
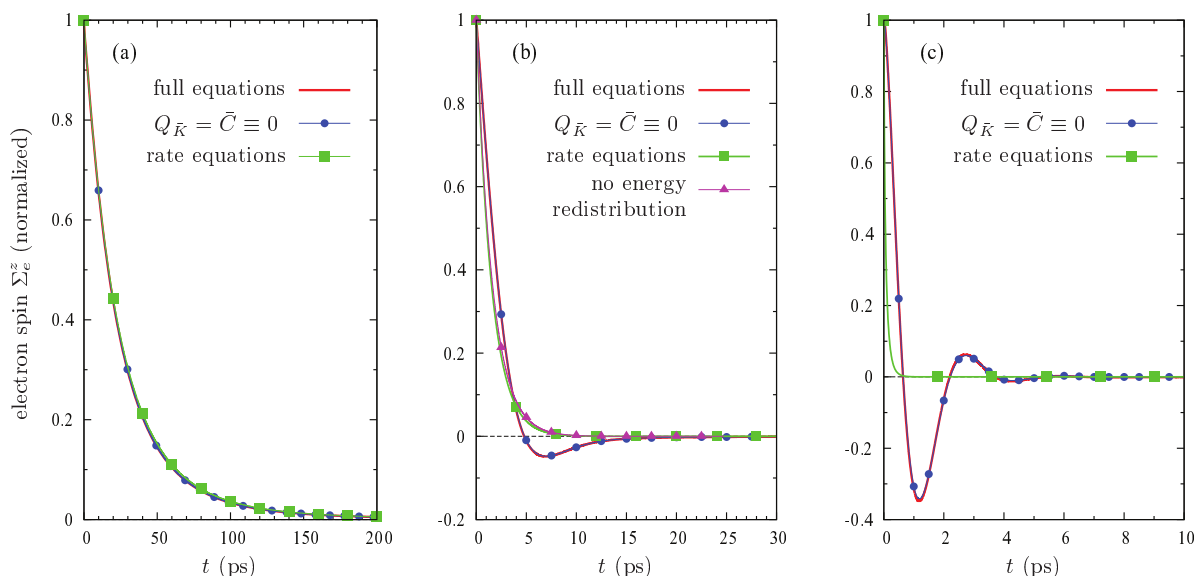
3.5. Results for zero impurity magnetization

In Ref. [23], the spin dynamics in a DMS at zero magnetic field and vanishing impurity magnetization has been investigated in simulations in which the optical excitation has been modeled by choosing the corresponding values for initial non-equilibrium carrier spins and occupations.

Figure 3.1 shows the time evolution of the carrier spin polarization for an initially spin polarized Gaussian spectral carrier distribution centered at the conduction band edge in a Mn-doped ZnSe DMS in three, two and one dimensions. Note that the number of magnetic impurities N_{Mn} is much larger than the number of optically induced carriers N_e, so that the impurities act effectively as a spin bath for the carriers. Thus, the initial carrier spin can be completely transferred to the impurity system so that the average carrier spin polarization approaches zero at long times $t \to \infty$. The full quantum kinetic theory predicts this decay to be exponential in a bulk system, whereas in lower dimensions deviations from the exponential behavior can be found. These deviations show up as overshoots or oscillations.

Some of the source terms in the quantum kinetic equations can be neglected in the calculations while still virtually the same spin dynamics is obtained, as depicted by the blue circles in Fig. 3.1. The remaining numerically relevant terms in the equations of motion for the correlations yield equations of the form of Eq. (3.12) and make it possible to formulate the Markov limit of the theory and to derive expressions for the carrier-impurity spin transfer rates. The green squares in Fig. 3.1 depict an exponential decay with these rates and serve as a point of reference for the discussion of the differences between the quantum kinetic and the Markovian results.

In Ref. [23], the discussion of the origin of the non-Markovian behavior in lower-dimensional samples focuses on the finding that a significant redistribution of carrier occupations in $\mathbf{k}$-space in the situation with pronounced non-Markovian features is found.

Figure 3.1.: From Ref. [23]: Time evolution of an initial carrier spin in a $Zn_{0.93}Mn_{0.07}Se$ DMS in a bulk system (a), a quantum well (b) and a quantum wire (c) for vanishing impurity magnetization. The red solid line shows the results of the full quantum kinetic theory, the green squares are the results of rate equations according to Fermi's golden rule and the blue circles correspond to calculations where only a numerical relevant subset of terms in the quantum kinetic theory is accounted for. In particular, the correlations $\bar{C}$ as well as source terms $Q_{\bar{K}}$ in the equations of motion for the correlations $\bar{K}$ are neglected, where $Q_{\bar{K}}$ comprises all terms containing correlations or terms of higher than linear order in the electron density [23]. Calculations where the shape of the carrier occupations in **k**-space are fixed are shown as pink triangles in the case of the quantum well (b).

For example, manually enforcing the shape of the carrier distribution to remain the same as at $t = 0$ [pink triangles in Fig. 3.1(b)] leads to the same spin dynamics as the rate equations. The relation between the non-Markovian behavior and the carrier redistribution can be understood as follows: While in the Markov limit, as in Fermi's golden rule, the redistribution of carriers is confined to final states within the same kinetic energy shell as the initial state, deviations from the Markov limit are associated with a finite broadening of the energy selection rule according to the energy-time uncertainty relation.

Furthermore, in Ref. [23], an explanation for the fact that the deviations from the Markovian rate equations are more pronounced in lower-dimensional systems is suggested by a comparison with a quantum dot (zero dimensions): A quantum dot can be described as a few-level system, where an interaction between the discrete states leads to a coherent Rabi-flop behavior in the form of oscillations. Thus, the one- and two-dimensional cases are regarded as intermediate situations between the zero-dimensional coherent case and the incoherent bulk result.

It is shown analytically in Ref. [23] that the overall shape of the time evolution of the carrier spin depends on the material parameters via a parameter F, which in two dimensions takes the form $F = m^* J_{sd}^2 N_{Mn}/V d$, where m^* is the effective mass in the conduction band, J_{sd} is the s-d coupling constant, N_{Mn} is the number of magnetic impurities and V and d are the volume and the width of the quantum well, respectively. The deviations from the rate-like behavior of the spin dynamics are found to be stronger for larger values of the parameter F.

In contrast, the investigation of the dependence of the spin dynamics on the initial spectral electron distributions, i.e., on the properties of the exciting laser pulse, relies on the numerical integration of the quantum kinetic equations. It is found that, even if the material parameters are chosen to maximize F while still being in a reasonable range for realistic DMS, the non-Markovian features disappear if the initial carrier distribution is either too broad (of the order of a few meV) or the center of the Gaussian peak is shifted towards higher energies.

The fact that the non-Markovian effects depend on the properties of the exciting laser beam is exploited in Ref. [24], where a two-color experiment with laser beams of different central frequencies and opposite circular polarizations is proposed, where the total spin optically induced into the sample is zero, but still pronounced oscillations in the time evolution of the carrier spin polarization in a DMS quantum well are predicted. These oscillations in the carrier spin polarization have a magnitude of the order of 1% and they are visible even a few ps after the fs-pulses are gone. From a technical point of view, a novelty of Ref. [24] compared with Ref. [23] is that the laser pulse and the valence band were taken into account numerically. The results are very similar to those obtained by calculations where the optical exciation is taken into account by the choice of suitable initial values for the carrier spins and occupations. This justifies the procedure of using the corresponding initial values in Ref. [23] and in the studies described in the present thesis.

Part II.

Quantum kinetic description of the spin dynamics in DMS

4. Open questions after Thurn's work

The full set of Thurn's quantum kinetic equations derived in Ref. [22] spans four pages. Because of the sheer size and complexity of the quantum kinetic equations, many physical features that are already present in Thurn's quantum kinetic theory are concealed in some of the source terms. The large parameter space and the numerical demands make it difficult to infer the physical content from brute-force calculations of the quantum kinetic equations for a vast number of different situations, material parameters and initial conditions. This is also the reason why the numerical investigations in Refs. [23] and [24] are confined to the relatively transparent case of zero impurity magnetization. Situations with non-vanishing Mn spins are not addressed in these publications, although the quantum kinetic theory of Ref. [22] is capable of describing these cases, too. Furthermore, the explanation of the non-Markovian behavior in Ref. [23] is somewhat unsatisfactory, because no clear criterion is provided for when to expect that golden-rule-like rate equations are a good approximation and under which circumstances they fail to accurately reproduce the spin dynamics predicted by the quantum kinetic theory.

Moreover, the description of realistic DMS requires to take into account additional interactions and Hamiltonians, such as the scattering at non-magnetic impurities, the Zeeman energies in the presence of an external magnetic field or spin-orbit coupling effects. The latter can be described by effective magnetic fields that lead to a non-vanishing commutator between the crystal Hamiltonian and the carrier spin operators, which complicates the analysis of the quantum kinetic equations even further.

These open questions are the starting point for the studies carried out within the present thesis: First, the quantum kinetic theory of Ref. [22] is applied to the case of non-zero impurity magnetization in [Pub1] and [Pub2] in a bulk system, where the complications due to non-Markovian effects are negligible [23]. In this context, the different source terms in the equations for the correlations are interpreted, which facilitates a physical intuition about the processes described in the quantum kinetic theory. A more thorough take on the origin of the non-Markovian effects in two-dimensional systems is presented in [Pub6] and the correlation-induced renormalization of the carrier spin precession frequency is discussed in [Pub7]. Furthermore, the theory is extended to incorporate spin-orbit coupling effects and an external magnetic field. The interplay between s-d and spin-orbit interactions is investigated in [Pub3] and [Pub4] in the Markov limit and a full quantum kinetic treatment of the s-d, the spin-orbit and the Zeeman interactions is presented in [Pub5]. There, also expressions for the magnetic-field dependence of the carrier-impurity spin transfer rates are derived and compared with the results of other theories in the literature.

In these studies, the optical excitation is modeled by choosing corresponding initial carrier occupations. In [Pub8], the optical excitation is taken into account on a quantum kinetic level. On this level of theory, we work out for which excitation conditions, i.e., pulse durations and magnetic field strengths, the non-Markovian effects are particularly pronounced.

In [Pub9], we investigate the effects of the excitation of semiconductors with twisted light, i.e., light with orbital angular momentum, on the subsequent spin dynamics induced by the Rashba interaction. In particular, we discuss the possibility of spin control via the orbital angular momentum of the impinging light beam.

Finally, in [Pub10], we study how the spin dynamics in DMS is modified if the non-magnetic interaction between carriers and impurities is accounted for.

5. Spin transfer dynamics for non-zero impurity magnetization

In this chapter, we discuss the quantum kinetic theory in the case of a non-zero impurity magnetization. We focus on a bulk system, where according to Ref. [23] no significant non-Markovian effects are expected and rate equations derived using Fermi's golden rule provide a very good description of the spin dynamics for vanishing impurity magnetization.

For a non-zero impurity magnetization, a distinction between the carrier spin components parallel and perpendicular to the impurity magnetization arises naturally. It is clear that in order to obtain the corresponding parallel and perpendicular spin transfer rates, Fermi's golden rule reaches its limits, in particular, because it only describes transitions between energy eigenstates and, thus, makes no statement about the dynamics of the perpendicular carrier spin component, i.e., the loss of coherence between spin-up and spin-down states.

This is, however, not a problem for the quantum kinetic theory, which describes the dynamics not only of the spin-up and spin-down occupations, but also of their coherences by accounting for the off-diagonal elements of the density matrices with respect to the spin indices. The Markov limit of the quantum kinetic equations is established and discussed in detail in [Pub1] and [Pub2]. The result is a set of effective rate equations for both, the parallel and perpendicular carrier spins with respect to the impurity magnetization and the corresponding rates are expressed in terms of the microscopic parameters of the Hamiltonian.

Although the steps involved in the derivation of these equations are, in principle, very similar to that in the case of vanishing impurity magnetization, which was sketched in Eq. (3.13), a number of complications arise when the impurity spin is non-zero: First, switching from the carrier density matrix to the carrier spin parallel and perpendicular to the impurity magnetization as dynamical variables leads to effective equations where higher moments of the impurity spin appear. For example, for the spin-$\frac{5}{2}$ Mn impurities, the second moments

$$\langle S^i S^j \rangle = \sum_{n_1 n_2 n_3} S^i_{n_1 n_2} S^j_{n_2 n_3} M_{n_1 n_3} \tag{5.1}$$

cannot be expressed in terms of the averages $\langle S^i \rangle$ alone.

In [Pub1], a number of algebraic manipulations are required to end up with relatively simple equations that can be interpreted more intuitively and solved analytically. These equations bear a striking resemblance to Landau-Lifshitz-Gilbert equations, which are usually derived phenomenologically. However, the fact that the impurity and carrier spins are quantum mechanical objects and not classical vectors has very important consequences. For example, the classical version of the Landau-Lifshitz-Gilbert equations

predicts that the spins remain unchanged if impurity and carrier spins are aligned parallel to each other. In contrast, the quantum corrections obtained in [Pub1] lead to a spin transfer between the carrier and impurity systems even in this case.

Further complications that arise when a finite impurity magnetization is taken into account are related to the importance of certain source terms in the equations for the correlations. Concentrating on the conduction band and simplifying Thurn's original equations [22] by rewriting them in terms of the correlations Q defined in Eq. (3.11) yields the following equations of motion, which are the starting point of [Pub1]:

$$-i\hbar\frac{\partial}{\partial t}M_{n_1}^{n_2} = J_{sd}\frac{1}{V}\sum_{\mathbf{k}nll'}\mathbf{s}_{ll'}\Bigg[C_{l\mathbf{k}}^{l'}\big(\mathbf{S}_{nn_1}M_n^{n_2} - \mathbf{S}_{n_2n}M_{n_1}^n\big)$$
$$+ \frac{1}{V}\sum_{\mathbf{k}'}\big(\mathbf{S}_{nn_1}Q_{ln\mathbf{k}}^{l'n_2\mathbf{k}'} - \mathbf{S}_{n_2n}Q_{ln_1\mathbf{k}}^{l'n\mathbf{k}'}\big)\Bigg], \tag{5.2a}$$

$$-i\hbar\frac{\partial}{\partial t}C_{l_1\mathbf{k}_1}^{l_2} = J_{sd}\frac{N_{\mathrm{Mn}}}{V}\sum_{nn'l}\mathbf{S}_{nn'}\Bigg[M_n^{n'}\big(\mathbf{s}_{ll_1}C_{l\mathbf{k}_1}^{l_2} - \mathbf{s}_{l_2l}C_{l_1\mathbf{k}_1}^l\big)$$
$$+ \frac{1}{V}\sum_{\mathbf{k}}\big(\mathbf{s}_{ll_1}Q_{ln\mathbf{k}}^{l_2n'\mathbf{k}_1} - \mathbf{s}_{l_2l}Q_{l_1n\mathbf{k}_1}^{ln'\mathbf{k}}\big)\Bigg], \tag{5.2b}$$

$$\Big(-i\hbar\frac{\partial}{\partial t} + E_{\mathbf{k}_2} - E_{\mathbf{k}_1}\Big)Q_{l_1n_1\mathbf{k}_1}^{l_2n_2\mathbf{k}_2} = \underbrace{b_{l_1n_1\mathbf{k}_1}^{l_2n_2\mathbf{k}_2\,I.1} + b_{l_1n_1\mathbf{k}_1}^{l_2n_2\mathbf{k}_2\,I.2}}_{=:b_{l_1n_1\mathbf{k}_1}^{l_2n_2\mathbf{k}_2\,I}} + \underbrace{b_{l_1n_1\mathbf{k}_1}^{l_2n_2\mathbf{k}_2\,II.1} + b_{l_1n_1\mathbf{k}_1}^{l_2n_2\mathbf{k}_2\,II.2}}_{=:b_{l_1n_1\mathbf{k}_1}^{l_2n_2\mathbf{k}_2\,II}}$$
$$+ \underbrace{b_{l_1n_1\mathbf{k}_1}^{l_2n_2\mathbf{k}_2\,III.1} + b_{l_1n_1\mathbf{k}_1}^{l_2n_2\mathbf{k}_2\,III.2}}_{=:b_{l_1n_1\mathbf{k}_1}^{l_2n_2\mathbf{k}_2\,III}}, \tag{5.2c}$$

with source terms

$$b_{l_1n_1\mathbf{k}_1}^{l_2n_2\mathbf{k}_2\,I.1} = J_{sd}\sum_{nl}\big(\mathbf{S}_{nn_1}\mathbf{s}_{ll_1}C_{l\mathbf{k}_2}^{l_2}M_n^{n_2} - \mathbf{S}_{n_2n}\mathbf{s}_{l_2l}C_{l_1\mathbf{k}_1}^lM_{n_1}^n\big), \tag{5.2d}$$

$$b_{l_1n_1\mathbf{k}_1}^{l_2n_2\mathbf{k}_2\,I.2} = -J_{sd}\sum_{nll'}\mathbf{s}_{ll'}C_{l\mathbf{k}_2}^{l_2}C_{l_1\mathbf{k}_1}^{l'}\big(\mathbf{S}_{nn_1}M_n^{n_2} - \mathbf{S}_{n_2n}M_{n_1}^n\big), \tag{5.2e}$$

$$b_{l_1n_1\mathbf{k}_1}^{l_2n_2\mathbf{k}_2\,II.1} = J_{sd}\sum_{nn'l}\mathbf{S}_{nn'}M_n^{n'}\frac{N_{\mathrm{Mn}}}{V}\big(\mathbf{s}_{ll_1}Q_{ln\mathbf{k}_1}^{l_2n_2\mathbf{k}_2} - \mathbf{s}_{l_2l}Q_{l_1n\mathbf{k}_1}^{ln_2\mathbf{k}_2}\big), \tag{5.2f}$$

$$b_{l_1n_1\mathbf{k}_1}^{l_2n_2\mathbf{k}_2\,II.2} = J_{sd}\sum_{nll'}\mathbf{s}_{ll'}\frac{1}{V}\sum_{\mathbf{k}}C_{l\mathbf{k}}^{l'}\big(\mathbf{S}_{nn_1}Q_{l_1n\mathbf{k}_1}^{l_2n_2\mathbf{k}_2} - \mathbf{S}_{n_2n}Q_{l_1n_1\mathbf{k}_1}^{l_2n\mathbf{k}_2}\big), \tag{5.2g}$$

$$b_{l_1n_1\mathbf{k}_1}^{l_2n_2\mathbf{k}_2\,III.1} = J_{sd}\sum_{nl}\Bigg\{\frac{1}{V}\sum_{\mathbf{k}}\Big[\mathbf{S}_{nn_1}\mathbf{s}_{ll_1}Q_{ln\mathbf{k}}^{l_2n_2\mathbf{k}_2} - \mathbf{S}_{n_2n}\mathbf{s}_{l_2l}Q_{l_1n_1\mathbf{k}_1}^{ln\mathbf{k}}\Big]\Bigg\}, \tag{5.2h}$$

$$b_{l_1n_1\mathbf{k}_1}^{l_2n_2\mathbf{k}_2\,III.2} = -J_{sd}\sum_{nll'}\mathbf{s}_{ll'}\Bigg\{\frac{1}{V}\sum_{\mathbf{k}}C_{l_1\mathbf{k}_1}^{l'}\Big[\mathbf{S}_{nn_1}Q_{ln\mathbf{k}}^{l_2n_2\mathbf{k}_2} - \mathbf{S}_{n_2n}Q_{l_1n\mathbf{k}}^{l_2n\mathbf{k}_2}\Big]$$
$$+ \frac{1}{V}\sum_{\mathbf{k}}C_{l\mathbf{k}_2}^{l_2}\Big[\mathbf{S}_{nn_1}Q_{l_1n\mathbf{k}_1}^{l'n_2\mathbf{k}} - \mathbf{S}_{n_2n}Q_{l_1n_1\mathbf{k}_1}^{l'n\mathbf{k}}\Big]\Bigg\}. \tag{5.2i}$$

The above subdivision of the source terms into the different $b_{l_1n_1\mathbf{k}_1}^{l_2n_2\mathbf{k}_2\,X}$ introduced in [Pub1]

helps to bring order into this set of equations and makes an interpretation and an estimation of the relative importance of the different terms easier.

The terms on the r.h.s. of Eqs. (5.2) are interpreted as follows: The first lines of Eqs. (5.2a) and (5.2b) represent the mean-field contributions to the dynamics of the single-particle density matrices. They describe the mutual precession of the carrier and impurity spins about each other. The second lines of Eqs. (5.2a) and (5.2b) contain the correlation-induced changes of the single-particle density matrices. Equation (5.2c) suggests that, for small coupling constants J_{sd}, where the source terms $b_{l_1 n_1 \mathbf{k}_1}^{l_2 n_2 \mathbf{k}_2 X}$ tend to zero, the correlations oscillate with a frequency corresponding to the difference of kinetic energies $(E_{\mathbf{k}_2} - E_{\mathbf{k}_1})$ of electronic states with wave vectors $\mathbf{k}_1$ and $\mathbf{k}_2$. The source terms $b_{l_1 n_1 \mathbf{k}_1}^{l_2 n_2 \mathbf{k}_2 I}$ are responsible for starting the dynamics of the correlations, since all other terms are initially zero if the correlations are zero. The terms $b_{l_1 n_1 \mathbf{k}_1}^{l_2 n_2 \mathbf{k}_2 I}$ are comprised of $b_{l_1 n_1 \mathbf{k}_1}^{l_2 n_2 \mathbf{k}_2 I.1}$ which is linear and $b_{l_1 n_1 \mathbf{k}_1}^{l_2 n_2 \mathbf{k}_2 I.2}$ that is quadratic in the electron density matrix $C_{l_1 \mathbf{k}_1}^{l_2}$. As more thoroughly discussed in [Pub2], one important effect of $b_{l_1 n_1 \mathbf{k}_1}^{l_2 n_2 \mathbf{k}_2 I.2}$ is to ensure the correct Pauli blocking behavior. By comparison with the mean-field terms of Eqs. (5.2a) and (5.2b), the source terms $b_{l_1 n_1 \mathbf{k}_1}^{l_2 n_2 \mathbf{k}_2 II}$ are identified as terms which describe a precession-type motion of the correlations about the total impurity $(b_{l_1 n_1 \mathbf{k}_1}^{l_2 n_2 \mathbf{k}_2 II.1})$ and carrier $(b_{l_1 n_1 \mathbf{k}_1}^{l_2 n_2 \mathbf{k}_2 II.2})$ spins. $b_{l_1 n_1 \mathbf{k}_1}^{l_2 n_2 \mathbf{k}_2 III}$ are terms that connect correlations with different wave vectors.

In order to be able to apply the Markov approximation, it is necessary to write the equations for the correlations in the form of Eq. (3.12), where the source terms b only depend on the single-particle variables and not on the correlations themselves. Note that only the source terms $b_{l_1 n_1 \mathbf{k}_1}^{l_2 n_2 \mathbf{k}_2 I}$ have the desired form, while $b_{l_1 n_1 \mathbf{k}_1}^{l_2 n_2 \mathbf{k}_2 II}$ and $b_{l_1 n_1 \mathbf{k}_1}^{l_2 n_2 \mathbf{k}_2 III}$ contain correlations. Nevertheless, the Markov limit of the quantum kinetic theory can be established by assuming that $b_{l_1 n_1 \mathbf{k}_1}^{l_2 n_2 \mathbf{k}_2 II}$ and $b_{l_1 n_1 \mathbf{k}_1}^{l_2 n_2 \mathbf{k}_2 III}$ are less important than $b_{l_1 n_1 \mathbf{k}_1}^{l_2 n_2 \mathbf{k}_2 I}$. An argument in favor of this assumption is that the former are of higher order in the coupling constant J_{sd} than the latter, since the correlations, which are zero before the laser pulse, are built up over time and are linear in J_{sd}. Thus, the effects of the source terms $b_{l_1 n_1 \mathbf{k}_1}^{l_2 n_2 \mathbf{k}_2 II}$ and $b_{l_1 n_1 \mathbf{k}_1}^{l_2 n_2 \mathbf{k}_2 III}$ on the carrier and impurity density matrices are of the order $\mathcal{O}(J_{sd}^3)$, whereas $b_{l_1 n_1 \mathbf{k}_1}^{l_2 n_2 \mathbf{k}_2 I}$ causes changes in second order.

In the Markov limit of the quantum kinetic equations where $b_{l_1 n_1 \mathbf{k}_1}^{l_2 n_2 \mathbf{k}_2 II}$ and $b_{l_1 n_1 \mathbf{k}_1}^{l_2 n_2 \mathbf{k}_2 III}$ are neglected, the equation of motion for the carrier spin $\mathbf{s}_{\mathbf{k}_1} = \sum_{l_1 l_2} \mathbf{s}_{l_1 l_2} C_{l_1 \mathbf{k}_1}^{l_2}$ in the states with wave vector $\mathbf{k}_1$ is:

$$
\begin{aligned}
\frac{\partial}{\partial t} \mathbf{s}_{\mathbf{k}_1} = & \left[\frac{J_{sd} N_{\mathrm{Mn}}}{\hbar V} + \frac{J_{sd}^2 N_{\mathrm{Mn}}}{\hbar^2 V^2} \sum_{\mathbf{k}} \mathcal{P} \frac{1}{2} \frac{n_{\mathbf{k}} - 1}{\omega_{\mathbf{k}_1} - \omega_{\mathbf{k}}} \right] (\langle \mathbf{S} \rangle \times \mathbf{s}_{\mathbf{k}_1}) \\
& + \pi \frac{J_{sd}^2 N_{\mathrm{Mn}}}{\hbar^2 V^2} \sum_{\mathbf{k}} \delta(\omega_{\mathbf{k}_1} - \omega_{\mathbf{k}}) \left[\langle \mathbf{S} \rangle \frac{4 \mathbf{s}_{\mathbf{k}_1}^2 - n_{\mathbf{k}_1}^2 + 2 n_{\mathbf{k}_1}}{4} \right. \\
& + (\mathbf{s}_{\mathbf{k}} \times (\mathbf{s}_{\mathbf{k}_1} \times \langle \mathbf{S} \rangle)) + \left. \frac{\langle \mathbf{S} \times (\mathbf{S} \times \mathbf{s}_{\mathbf{k}}) \rangle + \langle (\mathbf{s}_{\mathbf{k}} \times \mathbf{S}) \times \mathbf{S} \rangle}{2} \right],
\end{aligned} \tag{5.3}
$$

where $n_{\mathbf{k}_1} = \sum_l C_{l \mathbf{k}_1}^l$ are the carrier occupations at wave vectors $\mathbf{k}_1$ and $\omega_{\mathbf{k}} = \frac{E_{\mathbf{k}}}{\hbar}$ is the

frequency corresponding to the kinetic energy $E_{\mathbf{k}}$ of an electron with wave vector $\mathbf{k}$.

The first line in Eq. (5.3) describes a precession of the carrier spin around the effective field provided by the impurity magnetization. The precession frequency is renormalized by contributions stemming from the carrier-impurity correlations. This renormalization is discussed in more detail in [Pub7]. The second line is responsible for the transfer of an excess impurity magnetization to the carrier subsystem, while the last line contains damping terms, which are similar to the corresponding terms in the phenomenological Landau-Lifshitz-Gilbert equation for the dynamics of a magnetization density $\mathbf{M}(\mathbf{r})$ in an external field $\mathbf{H}$ [77]
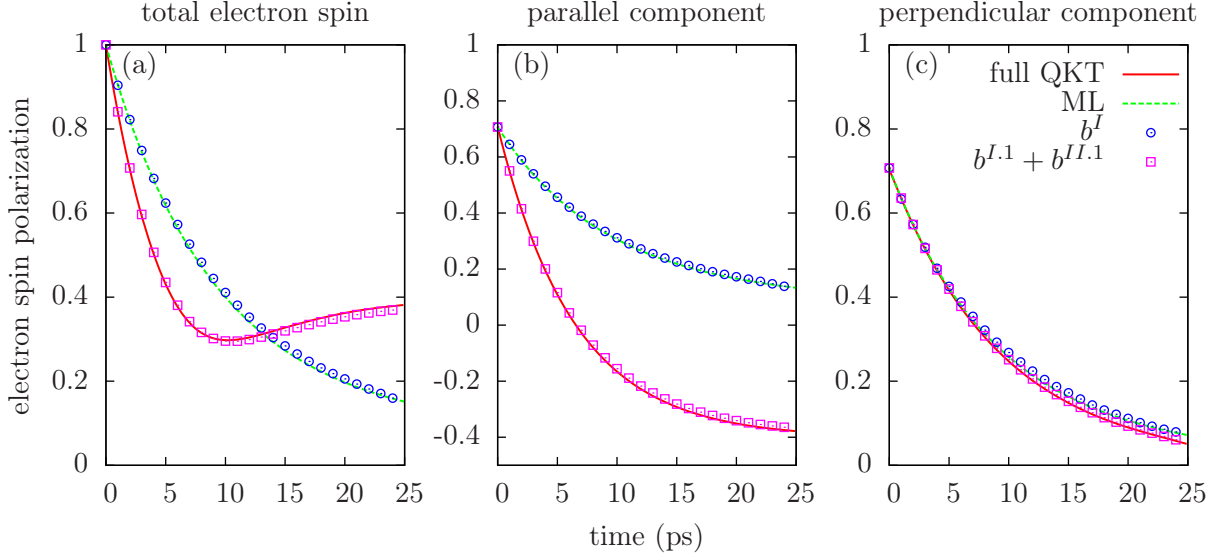
$$\frac{\partial}{\partial t}\mathbf{M} = \gamma\mathbf{M} \times \mathbf{H} - \frac{\lambda}{M^2}\mathbf{M} \times \left(\mathbf{M} \times \mathbf{H}\right). \tag{5.4}$$

In contrast to the original Landau-Lifshitz-Gilbert equation (5.4), where the magnetization $\mathbf{M}$ is already a quantum-mechanically averaged quantity, the average in the term $\langle \mathbf{S} \times \left(\mathbf{S} \times \mathbf{s_k}\right)\rangle + \langle\left(\mathbf{s_k} \times \mathbf{S}\right) \times \mathbf{S}\rangle$ in the Markovian effective equation (5.3) has to be taken *after* the evaluation of the cross product. This has the consequence that this term is non-zero in the case where $\langle\mathbf{S}\rangle$ and $\langle\mathbf{s_k}\rangle$ are parallel to each other, whereas the original Landau-Lifshitz-Gilbert equations (5.4) predict no change of the spins in this case.

However, the numerical calculations performed in [Pub1] show that the Markovian rate equations obtained by neglecting $b_{l_1 n_1 \mathbf{k}_1}^{l_2 n_2 \mathbf{k}_2 \, II}$ and $b_{l_1 n_1 \mathbf{k}_1}^{l_2 n_2 \mathbf{k}_2 \, III}$ are not generally applicable, because they produce significantly different results compared with the full quantum kinetic calculations, although they were performed for a bulk system, where it was shown in Ref. [23] that finite-memory effects are of minor importance and both calculations agree in the case of zero impurity magnetization. The results of the corresponding calculations are shown in Fig. 5.1. In order to pinpoint the origin of these discrepancies, a systematic study of the importance of the difference source terms is performed. It is found that the source term $b_{l_1 n_1 \mathbf{k}_1}^{l_2 n_2 \mathbf{k}_2 \, II.1}$, which describes the precession-type motion of the correlations about the impurity magnetization, is extremely important despite leading to changes in the single-particle variables in the order $\mathcal{O}(J_{sd}^3)$. If the term $b_{l_1 n_1 \mathbf{k}_1}^{l_2 n_2 \mathbf{k}_2 \, II.1}$ is not accounted for, in particular the asymptotic value of the carrier spin component parallel to the impurity magnetization for large times is not correctly reproduced.

The central point of [Pub2] is that, after some further manipulations and introducing suitable new dynamical variables for the correlations, it is possible to include $b_{l_1 n_1 \mathbf{k}_1}^{l_2 n_2 \mathbf{k}_2 \, II.1}$ as a contribution to the homogeneous part of the differential equation (3.12). This way, one obtains effective equations which produce almost the same results for the spin dynamics as the quantum kinetic theory in bulk systems, even for non-vanishing impurity magnetization. These effective equations are:

$$\frac{\partial}{\partial t}n_{\mathbf{k}_1}^{\uparrow/\downarrow} = \sum_{\mathbf{k}} \left\{ \mathrm{Re}(G_{\omega\mathbf{k}}^{\omega\mathbf{k}_1})\frac{b^{\|}}{2}\left[n_{\mathbf{k}}^{\uparrow/\downarrow} - n_{\mathbf{k}_1}^{\uparrow/\downarrow}\right] \right.$$
$$\left. + \mathrm{Re}(G_{\omega\mathbf{k}}^{\omega\mathbf{k}_1 \pm \omega_M})\left[b^{\pm}n_{\mathbf{k}}^{\downarrow/\uparrow} - b^{\mp}n_{\mathbf{k}_1}^{\uparrow/\downarrow} \mp 2b^0 n_{\mathbf{k}_1}^{\uparrow/\downarrow}n_{\mathbf{k}}^{\downarrow/\uparrow}\right] \right\} \tag{5.5a}$$

Figure 5.1.: From [Pub1]: Time evolution of the modulus (a), the parallel component (b) and the perpendicular (c) component of the total carrier spin with respect to the impurity magnetization in a $Zn_{0.93}Mn_{0.07}Se$ bulk DMS with initial carrier spin polarization tilted 45° away from the direction of the impurity magnetization and initial spectral carrier distribution modeled by a Gaussian with a standard deviation of $E_s = 3$ meV centered at the band edge. The red solid line (full QKT) depicts the full quantum kinetic results, while the blue circles and pink triangles show the results of calculations where only the source terms b^I or $b^{I.1}$ and $b^{II.1}$, respectively, have been accounted for in the equation of motion for the correlations. The green dashed line (ML) represents the results according to the Markovian equation of motion obtained by considering only the source terms b^I.

$$
\frac{\partial}{\partial t}\mathbf{s}_{\mathbf{k}_1}^\perp = -\sum_{\mathbf{k}} \left[\operatorname{Re}(G_{\omega_{\mathbf{k}}}^{\omega_{\mathbf{k}_1}-\omega_M})\left(\frac{b^+}{2}-b^0 n_{\mathbf{k}}^\uparrow\right)\mathbf{s}_{\mathbf{k}_1}^\perp \right.
$$
$$
\left. + \operatorname{Re}(G_{\omega_{\mathbf{k}}}^{\omega_{\mathbf{k}_1}+\omega_M})\left(\frac{b^-}{2}+b^0 n_{\mathbf{k}}^\downarrow\right)\mathbf{s}_{\mathbf{k}_1}^\perp + \operatorname{Re}(G_{\omega_{\mathbf{k}}}^{\omega_{\mathbf{k}_1}})\frac{b^\parallel}{2}\left(\mathbf{s}_{\mathbf{k}}^\perp + \mathbf{s}_{\mathbf{k}_1}^\perp\right)\right]
$$
$$
+ \frac{\langle\mathbf{S}\rangle}{|\langle\mathbf{S}\rangle|} \times \left[\omega_M - \sum_{\mathbf{k}}\left\{\operatorname{Im}(G_{\omega_{\mathbf{k}}}^{\omega_{\mathbf{k}_1}-\omega_M})\left(\frac{b^+}{2}-b^0 n_{\mathbf{k}}^\uparrow\right)\right.\right.
$$
$$
\left.\left. - \operatorname{Im}(G_{\omega_{\mathbf{k}}}^{\omega_{\mathbf{k}_1}+\omega_M})\left(\frac{b^-}{2}+b^0 n_{\mathbf{k}}^\downarrow\right)\right\}\right]\mathbf{s}_{\mathbf{k}_1}^\perp, \tag{5.5b}
$$

where $n_{\mathbf{k}}^\uparrow$ and $n_{\mathbf{k}}^\downarrow$ are the spin-up and spin-down occupations of the states with wave vector $\mathbf{k}$ and $\mathbf{s}_{\mathbf{k}}^\perp$ is the corresponding perpendicular spin component with respect to the impurity magnetization. The precession frequency of the carrier spins in the mean field due to the impurity magnetization is $\omega_M = \frac{J_{sd}N_{\mathrm{Mn}}}{\hbar V}|\langle\mathbf{S}\rangle|$. The factors $b^\parallel = \langle S^{\parallel 2}\rangle$, $b^0 = \frac{1}{2}\langle S^\parallel\rangle$ and $b^\pm = \langle S^{\perp 2}\rangle \pm \frac{1}{2}\langle S^\parallel\rangle$ depend only on the impurity spin state. $S^\parallel = \hat{\mathbf{S}}\cdot\frac{\langle\hat{\mathbf{S}}\rangle}{|\langle\hat{\mathbf{S}}\rangle|}$ is the component of the impurity spin operator parallel to the direction of its average value and $\langle S^{\perp 2}\rangle = \frac{1}{2}\left(\langle S^2\rangle - \langle S^{\parallel 2}\rangle\right)$. The memory function $G_{\omega_{\mathbf{k}}}^{\omega_{\mathbf{k}_1}}$ is defined by

$$
G_{\omega_{\mathbf{k}}}^{\omega_{\mathbf{k}_1}} = \frac{J_{sd}^2 N_{\mathrm{Mn}}}{\hbar^2 V^2}\int_{-t}^{0} dt'\, e^{i(\omega_{\mathbf{k}}-\omega_{\mathbf{k}_1})t'} \tag{5.6}
$$

and has to be regarded as an integral operator where the terms on the right of $G_{\omega_{\mathbf{k}}}^{\omega_{\mathbf{k}_1}}$ in Eqs. (5.5) have to be evaluated at times t'. When this finite memory is kept, Eqs. (5.5) are equivalent to Eqs. (5.2) without the terms $b_{l_1 n_1 \mathbf{k}_1}^{l_2 n_2 \mathbf{k}_2 III}$. As described earlier, the Markov limit is easily established by neglecting the memory, i.e., evaluating the terms appearing after $G_{\omega_{\mathbf{k}}}^{\omega_{\mathbf{k}_1}}$ at t and taking the limit $t \to \infty$ in the lower limit of the memory integral. Then, one obtains:

$$G_{\omega_{\mathbf{k}}}^{\omega_{\mathbf{k}_1}} \approx \frac{J_{sd}^2 N_{\mathrm{Mn}}}{\hbar^2 V^2} \left\{ \pi \delta(\omega_{\mathbf{k}} - \omega_{\mathbf{k}_1}) - \mathcal{P} \frac{i}{\omega_{\mathbf{k}} - \omega_{\mathbf{k}_1}} \right\}, \tag{5.7}$$

where $\mathcal{P}$ denotes the principal value. In the Markov limit, Eqs. (5.5) become effective rate equations. In addition, the imaginary part of the memory function acts like an effective magnetic field about which the carrier spins precess. This correlation-induced frequency renormalization is discussed in more detail later in the context of [Pub7].

It is instructive to compare the effective equations (5.5) in the Markov limit with rate equations based on Fermi's golden rule. The latter is concerned with transitions between energy eigenstates and, thus, is only applicable for the transitions between spin-up and spin-down states. Fermi's golden rule does not make any prediction for the perpendicular spin component similar to Eq. (5.5b). However, one can easily check that in the case of zero impurity magnetization, Eqs. (5.5a) and (5.5b) coincide.

Indeed, Eq. (5.5a) for the spin-up and spin-down occupations predicts the same carrier-impurity spin transfer rate as Fermi's golden rule, if the splitting of the bands due to the mean-field contribution of H_{sd} is taken into account for the basis states between which the golden-rule transitions are formulated. This splitting enters in the effective equations via the precession-type motion of the correlations described by the source terms $b_{l_1 n_1 \mathbf{k}_1}^{l_2 n_2 \mathbf{k}_2 II.1}$. Thus, there is a correspondence between the precession of the correlations and energetic shifts of the energy eigenstates. This finding leads us to the important conclusion that the classification of the source terms $b_{l_1 n_1 \mathbf{k}_1}^{l_2 n_2 \mathbf{k}_2 X}$ in terms of orders of J_{sd} in [Pub1] does not reliably predict the relative importance of the source terms for the spin dynamics, since this perturbative treatment does not capture the energetic shifts due to the mean-field contribution of H_{sd} correctly.

With this insight, the argument that the $b_{l_1 n_1 \mathbf{k}_1}^{l_2 n_2 \mathbf{k}_2 III}$ can be neglected because they are of higher order in the coupling constant seems no longer valid. However, there is also another argument for the insignificance of $b_{l_1 n_1 \mathbf{k}_1}^{l_2 n_2 \mathbf{k}_2 III}$: These terms describe the effects of correlations on other correlations with different wave vectors. Since the correlations oscillate fast with the frequency depending on the wave vector, the different contributions from the different correlations in general interfere destructively, so that $b_{l_1 n_1 \mathbf{k}_1}^{l_2 n_2 \mathbf{k}_2 III}$ will usually be very small. Nevertheless, these arguments are only qualitative and the fact that $b_{l_1 n_1 \mathbf{k}_1}^{l_2 n_2 \mathbf{k}_2 III}$ are indeed of minor importance is best proven by comparing numerical simulations of the quantum kinetic equations with and without accounting for $b_{l_1 n_1 \mathbf{k}_1}^{l_2 n_2 \mathbf{k}_2 III}$ as was done in [Pub1].

Note that the source term $b_{l_1 n_1 \mathbf{k}_1}^{l_2 n_2 \mathbf{k}_2 II.2}$, which describes a precession of the correlations about the total carrier spin, is not as important as $b_{l_1 n_1 \mathbf{k}_1}^{l_2 n_2 \mathbf{k}_2 II.1}$, since the number of carriers is much smaller than the number of impurities. Furthermore, the quadratic term in the electron variables $n_{\mathbf{k}_1}^{\uparrow/\downarrow} n_{\mathbf{k}}^{\downarrow/\uparrow}$, which originates from the source terms $b_{l_1 n_1 \mathbf{k}_1}^{l_2 n_2 \mathbf{k}_2 I.2}$ in Eqs. (5.2),

automatically gives the correct Pauli-blocking behavior, which otherwise has to be put in by hand in golden-rule-type rate equations [28].

Furthermore, it is noteworthy that the energetic shift between spin-up and spin-down states enforces a separate treatment of the spin-up/spin-down occupations and the perpendicular spin components. Thus, the effective equations (5.5) cannot be written in the form of a single Landau-Lifshitz-Gilbert-like equation similar to Eq. (5.3). Nevertheless, the Landau-Lifshitz-Gilbert-like equations can still be useful as an intuitive approximate picture for complicated cases where, e.g., the carrier and impurity spins are canted with respect to each other, because Eq. (5.3) directly follows from Eqs. (5.5) if the spin splitting ω_M in the memory function are neglected.

To summarize, deriving effective equations of motion (5.5) not only allows a drastic speed-up of the numerics and provides rates for the transfer of parallel as well as perpendicular carrier spins to the magnetic impurities, but also sheds light on the meaning of the different source terms in the quantum kinetic description. In particular, we find that the precession-type motion of the correlations corresponds to the energetic shifts of the single-particle states due to the mean-field contribution of the s-d interaction. Furthermore, we see that perturbative arguments with respect to the coupling constant J_{sd} can give a wrong impression and have to be handled with care. While there are some similarities between the effective equations and the Landau-Lifshitz-Gilbert equation, we find also significant differences originating from the quantum mechanical nature of the spins and the energetic shifts between spin-up and spin-down states.

6. Spin dynamics in DMS with spin-orbit coupling and external fields

6.1. Interplay between s-d and spin orbit interactions

As described in chapter 2, the spin dynamics in non-magnetic semiconductors is often dominated by the D'yakonov-Perel' mechanism. This process requires a $\mathbf{k}$-dependent effective magnetic field $\boldsymbol{\Omega}_{\mathbf{k}}$ for the carrier spins which originates from spin-orbit coupling. Here, we discuss the interplay between such spin-orbit coupling effects and the s-d exchange interaction for the spin dynamics in DMS, which is presented in [Pub3], [Pub4] and [Pub5].

For typical DMS studied in the literature [21] with a Mn concentration of $\sim 0.1 - 10\%$, the s-d interaction leads in general to a much faster spin dynamics than the dephasing in the effective field. However, in [Pub3] we show how a regime can be reached where both contributions are of comparable strength. In bulk systems with the Dresselhaus fields, the effective field is proportional to k^3. Thus, the effects of the spin-orbit interaction are more pronounced when excitation schemes with laser frequencies larger than the band gap are used. This leads to the excitation of carriers with large kinetic energies and wave vectors. Another approach for enhancing the effects of the spin-orbit interaction is using DMS materials with small band gaps. This is because the effective fields result from mixing between conduction and valence band states, which is inversely proportional to the band gap. In CdTe, the band gap can be very efficiently controlled by doping with Hg [78].

The level of theory used for the calculations in [Pub3] and [Pub4] is that of the effective rate equations (5.5) in the Markov limit derived in [Pub2], where a $\mathbf{k}$-dependent precession of the carrier spins about the field $\boldsymbol{\Omega}_{\mathbf{k}}$ is added to the equations:

$$\frac{\partial}{\partial t}\big|_{SO}\mathbf{s}_{\mathbf{k}} = \boldsymbol{\Omega}_{\mathbf{k}} \times \mathbf{s}_{\mathbf{k}}, \tag{6.1}$$

where $\frac{\partial}{\partial t}\big|_{SO}$ denotes to contribution to the time evolution of the spins due to the spin-orbit coupling effects.

Figure 6.1 shows the main results of [Pub3] for the situation of a bulk $Zn_{0.997}Mn_{0.003}Se$ DMS with a Dresselhaus field and a $Hg_{0.997-y}Cd_yMn_{0.003}Te$ quantum well with a Rashba field, where y is tuned so that the Rashba coefficient has a value of $\alpha_R = 4.87$ meVnm. The initial average impurity spin is set to $0.1\hbar$ and the initial carrier distribution is a Gaussian peak centered at 10 meV above the band gap with a standard deviation of 3 meV. The initial carrier spins are polarized $45°$ with respect to the impurity magnetization. For the quantum well, the growth direction coincides with the direction of the
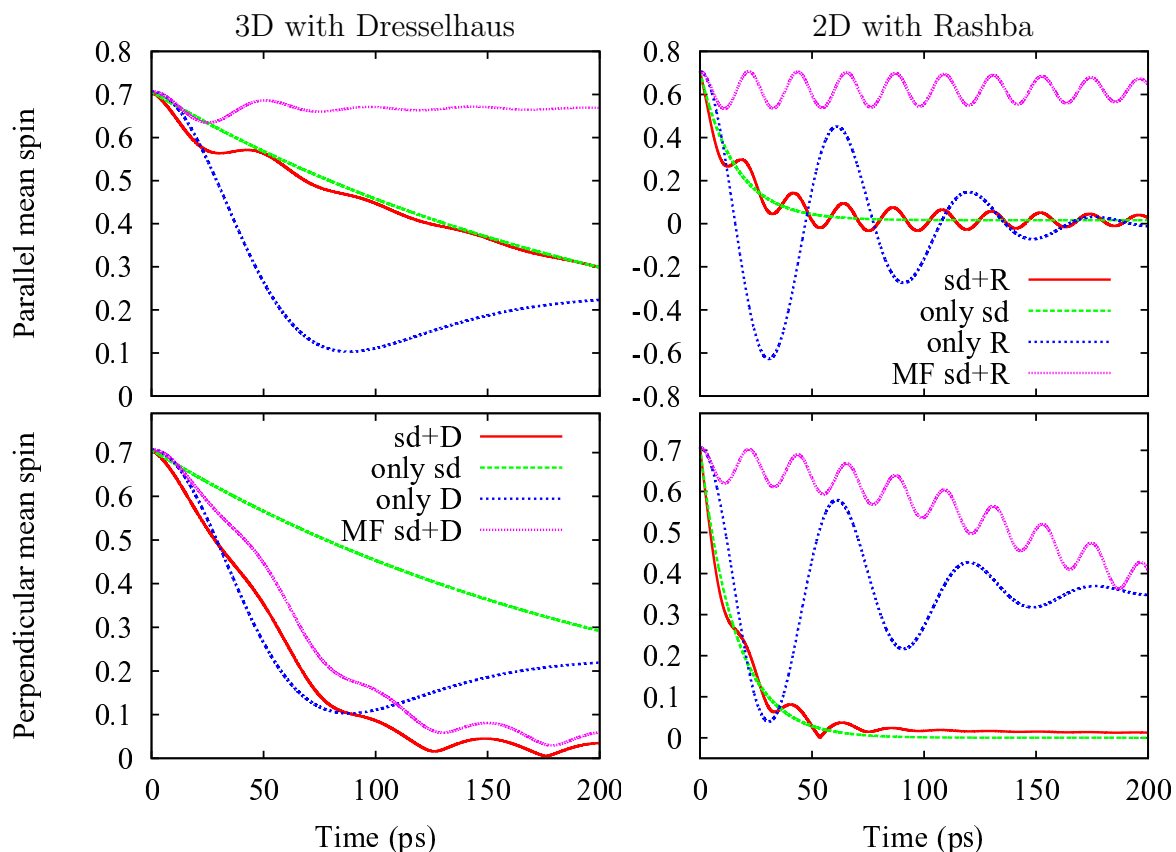
Figure 6.1.: After [Pub3]: Interplay of *s-d* and spin-orbit interactions in the dynamics of the modulus of the parallel and perpendicular carrier spin components in a bulk (3D) DMS with a Dresselhaus field and a quantum well (2D) with a Rashba field. Key: sd: including the *s-d* interaction, D: including the Dresselhaus field, R: including the Rashba field, MF: mean-field approximation of the *s-d* interaction.

impurity magnetization.

It can be seen in Fig. 6.1 that the dynamics including the *s-d* interaction and spin-orbit effects (red solid lines) is very different from the dephasing in the effective fields alone (blue dotted lines). The *s-d* interaction alone (green dashed lines), on the other hand, reproduces well the tendencies in the decay in most of the calculations where both interactions are present. Only the perpendicular spin component in the three-dimensional case decays on a time scale defined by the dephasing in the **k**-dependent field rather than the *s-d* spin transfer rate.

In all situations presented in Fig. 6.1, one can find pronounced oscillations with approximately the mean-field precession frequency of the carrier spins superimposed on the decay in the simulations accounting for both interactions, which is not reproduced when only the *s-d* interaction is considered. These oscillations can be explained by considering the total effective magnetic field $\tilde{\boldsymbol{\Omega}}_{\mathbf{k}} = \boldsymbol{\Omega}_{\mathbf{k}} + \boldsymbol{\omega}_M$ composed of the **k**-dependent field $\boldsymbol{\Omega}_{\mathbf{k}}$ and the mean-field carrier spin precession frequency $\boldsymbol{\omega}_M = \frac{J_{sd}N_{\mathrm{Mn}}}{\hbar}\langle\mathbf{S}\rangle$. Thus, in the mean-field description, an electron spin precesses about the total effective field $\tilde{\boldsymbol{\Omega}}_{\mathbf{k}}$. This mixes the contributions to the carrier spin parallel and perpendicular to the impurity magnetization and thereby introduces the oscillations also in the parallel component. For the perpendicular electron spin component, the mean field due to the impurity spins $\boldsymbol{\omega}_M$ notably reduces the dephasing caused by the **k**-dependent fields, which can be seen by

comparing the mean-field calculations (pink dotted lines) with the simulation considering only the spin-orbit interaction (blue dotted lines).

In [Pub4], we investigate in more detail the spin dynamics caused by the *s-d* and the Rashba interaction and study in particular the dependence of the time evolution of the spin on the excess kinetic energy E_c, i.e., the center of the peak in the initial spectral carrier distribution measured from the band edge. In this investigation we find that, while the *s-d* interaction predicts an exponential decay of the carrier spin in the Markov limit, the dephasing of carrier spins in the Rashba field leads to a time evolution of the spins that can be fitted well by an oscillation with a Gaussian envelope. Thus, whether the spin dynamics has a Gaussian or an exponential shape can help to distinguish the regime of dephasing from the regime of spin transfer in the combined dynamics.

6.2. Precession of correlations in a k-dependent effective field

The effective magnetic field $\mathbf{\Omega_k}$ depends explicitly not only on the modulus $k = |\mathbf{k}|$ of the wave vector, but also on its angle $\varphi_\mathbf{k}$. In particular, it follows from Kramers degeneracy that $\mathbf{\Omega_{-k}} = -\mathbf{\Omega_k}$ so that averaging over the angle $\varphi_\mathbf{k}$ would predict no effect on the spin dynamics at all. Thus, the averaging over the angle in $\mathbf{k}$-space, which was employed before to enable a reduction of the space to be discretized from 4 to 2 dimensions for quantum wells and from 6 to 2 in bulk systems, is no longer acceptable. This makes it hard to use the full quantum kinetic theory for extensive studies of the interplay between spin-orbit effects and the *s-d* interaction with a large number of parameters.

In the studies of the interplay between the *s-d* and the spin-orbit interaction in [Pub3] and [Pub4], the precession of the carrier spins in the $\mathbf{k}$-dependent effective field was added by hand to the dynamics described by the effective equations (5.5), which were derived in [Pub2] for the case without a $\mathbf{k}$-dependent field. Thus, effects like the precession of the correlations in the $\mathbf{k}$-dependent effective field were not taken into account.

In [Pub5], the derivation of effective equations in the spirit of Eqs. (5.5) is generalized in several aspects. Not only do we take into account the effects of a possibly $\mathbf{k}$-dependent field on the precession dynamics of the carrier-impurity correlations, but we also consider an external magnetic field via the Zeeman terms for the carrier and impurity spins. If the impurity Zeeman energy is accounted for, the source term $b_{l_1 n_1 \mathbf{k}_1}^{l_2 n_2 \mathbf{k}_2 \, II.2}$ is no longer negligible. Thus, the generalization complicates the theoretical description significantly. Most importantly, since the correlations possess two $\mathbf{k}$-indices, two different carrier spin precession frequencies enter in the dynamics for the correlations $Q_{l\mathbf{k}_1}^{\alpha \mathbf{k}_2} = \sum_{l_1,l_2,n_1,n_2} s_{l_1 l_2}^\alpha S_{n_1 n_2}^l Q_{l_1 n_1 \mathbf{k}_1}^{l_2 n_2 \mathbf{k}_2}$. In [Pub5], we obtain the equation of motion for the correlations

$$\frac{\partial}{\partial t} Q_{l\mathbf{k}_1}^{\alpha \mathbf{k}_2} = -i(\omega_{\mathbf{k}_2} - \omega_{\mathbf{k}_1}) Q_{l\mathbf{k}_1}^{\alpha \mathbf{k}_2} + \sum_\gamma (A_{\mathbf{k}_1} + A_{\mathbf{k}_2}^*)_{\alpha\gamma} Q_{l\mathbf{k}_1}^{\gamma \mathbf{k}_2} + \sum_{i,j} \epsilon_{ijl} \omega_{Mn}^i Q_{j\mathbf{k}_1}^{\alpha \mathbf{k}_2} + b_{l\mathbf{k}_1}^{\alpha \mathbf{k}_2 \, I},$$

(6.2)

where $b_{l\mathbf{k}_1}^{\alpha \mathbf{k}_2 \, I} = \sum_{l_1,l_2,n_1,n_2} s_{l_1 l_2}^\alpha S_{n_1 n_2}^l b_{l_1 n_1 \mathbf{k}_1}^{l_2 n_2 \mathbf{k}_2 \, I}$. Note that in the above definition of the cor-

relations the Latin indices run from 1 to 3 while the Greek indices include also the 0. Furthermore we define $s_{l_1 l_2}^0 = \delta_{l_1 l_2}$. The 4×4 matrices $A_{\mathbf{k}_1}$ are defined by

$$A_{\mathbf{k}_1} = \begin{pmatrix} 0 & \left(i\boldsymbol{\Omega}'_{\mathbf{k}_1}\right)^T \\ \left(\frac{i}{4}\boldsymbol{\Omega}'_{\mathbf{k}_1}\right) & \frac{1}{2}\left[\boldsymbol{\Omega}'_{\mathbf{k}_1}\right]_\times \end{pmatrix}. \tag{6.3}$$

$\left(\left[\boldsymbol{\Omega}'_{\mathbf{k}_1}\right]_\times\right)_{ij} = \sum_l \epsilon_{ijl}\left(\Omega'_{\mathbf{k}_1}\right)^l$ is the 3×3 cross product matrix. The total mean-field precession axes and frequencies are

$$\boldsymbol{\omega}_e = \frac{g_e \mu_B}{\hbar}\mathbf{B} + \frac{J_{sd}N_{\mathrm{Mn}}}{\hbar V}\langle\mathbf{S}\rangle \tag{6.4a}$$

$$\boldsymbol{\Omega}'_{\mathbf{k}} = \boldsymbol{\Omega}_{\mathbf{k}} + \boldsymbol{\omega}_e \tag{6.4b}$$

$$\boldsymbol{\omega}_{\mathrm{Mn}} = \frac{g_{\mathrm{Mn}} \mu_B}{\hbar}\mathbf{B} + \frac{J_{sd}}{\hbar V}\sum_{\mathbf{k}} \mathbf{s}_{\mathbf{k}}. \tag{6.4c}$$

In order to apply the same steps as in [Pub2] to derive an integral expression for the correlations, the homogeneous part of Eq. (6.2) has to be solved. Determining the solution including the inhomogeneities $b_{l\mathbf{k}_1}^{\alpha\mathbf{k}_2 I}$ requires the inversion of the homogeneous solution. This step can be done straightforwardly only if one has to deal with simple precessions where the time evolution can be described by rotation matrices. The procedure is more complicated in the present case where the precession-type motion of the correlations in the $\mathbf{k}$-dependent field $\boldsymbol{\Omega}'_{\mathbf{k}}$ is described by the matrices $A_{\mathbf{k}_1}$.

Nevertheless, we show in [Pub5] that it is possible to analytically calculate the matrix exponential $\exp(A_{\mathbf{k}_1}t)$ and thereby its inverse $\exp(-A_{\mathbf{k}_1}t)$. This enables us to analytically solve the homogeneous part of Eq. (6.2) and to obtain integral expressions for the correlations that can be integrated analytically in the Markov limit.

The results of the numerical simulations of the spin dynamics on this level of theory are shown in [Pub5] to coincide with the predictions of the theory used in [Pub3] without taking into account the precession of the correlations about the $\mathbf{k}$-dependent effective field $\boldsymbol{\Omega}_{\mathbf{k}}$. In fact, we were not able to find any set of realistic parameters and excitation conditions for which a visible difference in the spin dynamics between the two levels of theory is observable. This finding justifies retrospectively the application of the theory in [Pub3] and [Pub4] for the discussion of the interplay between the *s-d* exchange interaction and the spin-orbit coupling.

6.3. Magnetic-field dependence of the spin transfer rates

The generalization of the derivation of Markovian equations from the quantum kinetic theory in [Pub5] allows us to fully include the Zeeman energies of carriers and impurities in the derivation of Markovian expressions for the parallel and perpendicular spin transfer rates in the presence of an external magnetic field $\mathbf{B}$ if spin-orbit fields are negligible.

In this case, the central difference between the theory of [Pub2] and [Pub5] is that the Zeeman terms are accounted for in the latter which leads to a non-negligible precession of the correlations around the impurity spin precession axis $\boldsymbol{\omega}_{\mathrm{Mn}}$ originating from the term corresponding to $b_{l_1 n_1 \mathbf{k}_1}^{l_2 n_2 \mathbf{k}_2 II.2}$ in the quantum kinetic equations (5.2). As a result, we obtain
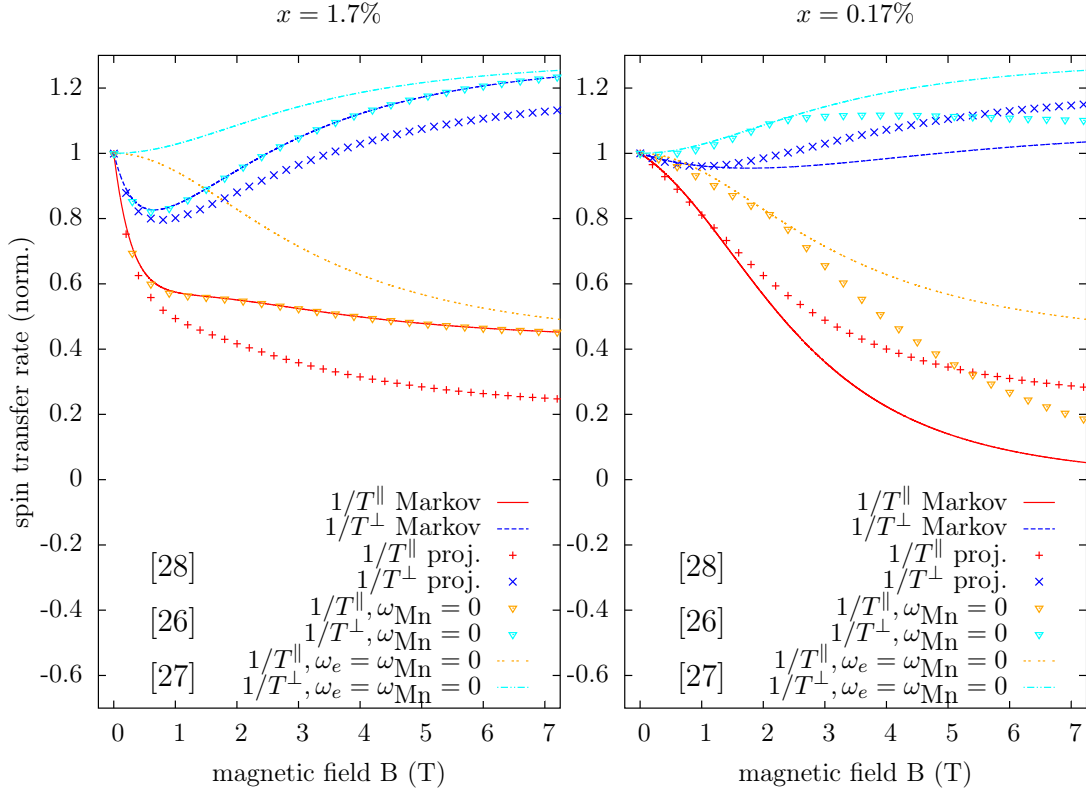
Figure 6.2.: Adapted from [Pub5]: Magnetic-field dependence of the parallel $(1/T^{\parallel})$ and perpendicular $(1/T^{\perp})$ spin transfer rates normalized to the Fermi's golden rule value at $\mathbf{B} = 0$. The Markovian results derived from the full quantum kinetic theory in [Pub5] are represented by the red and blue lines. The results of the projection operator formalism of Ref. [28] are depicted as pluses and crosses. Calculations neglecting the impurity spin splitting $\hbar\omega_{\mathrm{Mn}}$, as is done, e.g., in Ref. [26], are show as orange and cyan triangles. The level of theory in Ref. [27] corresponds to disregarding the impurity spin splitting as well as the carrier spin splitting. The corresponding results are depicted as the orange and cyan lines. The calculations were made for an 8 nm wide CdTe-based DMS quantum well with doping concentration x and a thermal carrier distribution with temperature $T = 4$ K.

in the Markovian limit the same equations as Eqs. (5.5), except that the band splitting $\hbar\omega_M$ in the memory functions has to be replaced by $\hbar\omega_e - \hbar\omega_{\mathrm{Mn}}^{\parallel}$, where $\omega_{\mathrm{Mn}}^{\parallel} = \boldsymbol{\omega}_{\mathrm{Mn}} \cdot \frac{\boldsymbol{\omega}_e}{\omega_e}$. The reason for this is that H_{sd} conserves the spin and therefore a spin-flip of a carrier is necessarily accompanied with a flop of an impurity spin in the opposite direction. In the presence of an external magnetic field $\mathbf{B}$, this flop of the impurity spin results in an energy penalty due to the impurity Zeeman term. Thus, in order to conserve the spin as well as the total single-particle energies, the difference in kinetic energies of the states involved in a spin-flip scattering process has to compensate the change of the total magnetic energies of carriers and impurities $\hbar\omega_e - \hbar\omega_{\mathrm{Mn}}^{\parallel}$.

Interestingly, this correction of the kinetic energy difference due to the impurity Zeeman energy is often disregarded in the literature [26], even if it is, in principle, accessible by a golden-rule approach, at least for the parallel spin transfer. In Ref. [27], also the conduction band spin splitting $\hbar\omega_e$ has been neglected. In Ref. [28], a projection operator method was used to investigate the magnetic-field dependence of the spin transfer rates in DMS. The equations obtained there also contain kinetic energy differences of $\hbar\omega_e + \hbar\omega_{\mathrm{Mn}}^{\parallel}$, which are not compatible with the conservation of the single-particle en-

ergies. We attribute this to an error in Ref. [28], where only the positive frequency component of the carrier spin precession is accounted for and the negative frequency component is disregarded.

The results for the magnetic-field dependence of the spin transfer rates are shown in Fig. 6.2 for a $Cd_{1_x}Mn_xTe$ quantum well with doping concentration $x = 1.7\%$ and $x = 0.17\%$, respectively. Beside the spin transfer rates obtained in the Markovian limit from the full quantum kinetic theory, also the rates obtained by the projection operator formalism of Ref. [28] are presented in Fig. 6.2 as well as the rates calculated neglecting either only the impurity spin splitting $\hbar\omega_{Mn}$ or the impurity and the carrier spin splittings $\hbar\omega_{Mn}$ and $\hbar\omega_e$, which corresponds to the levels of theory in Refs. [26] and [27], respectively.

It can be seen that neglecting the spin splittings can lead to quantitatively and qualitatively different behavior of the rates with increasing magnetic fields. The most striking differences become obvious in the parallel spin transfer rate for large magnetic fields and low doping concentrations.

Another aspect in which our theory is generalized in [Pub5] is that we do not regard the DMS quantum well as an ideal 2D system, but as a quasi-two-dimensional system with a non-constant envelope of the carrier wave function along the growth direction $\psi(z)$, which enhances the spin transfer rate by a factor of $I = d \int_{-\frac{d}{2}}^{\frac{d}{2}} dz |\psi(z)|^4$. This was also found in studies using other approaches to obtain the spin transfer rates, such as in Refs. [28, 79] and [21]. Beside the enhancement of the rates, taking into account the z-dependence of the correlations also allows for a connection of our theory to the description of collective carrier-impurity precession modes discussed in the literature [80–84]. There, the carrier-impurity correlations are neglected and the spin transfer is modeled by a phenomenological rate. With the theory described in [Pub5], we are able to extract an explicit expression for the spin transfer rate in the situation where the collective precession modes are relevant.

To summarize, in [Pub3], [Pub4] and [Pub5], we derive effective equations for the investigation of the interplay between the spin-orbit coupling and the s-d interaction in the spin dynamics in DMS and we study numerically situations where both interactions compete with equal strength. Our theory contains many features such as an enhancement of the rate due to the form of the carrier wave function envelope and it can be used to find expressions for the carrier-impurity spin transfer rates in the presence of an external magnetic field. In contrast to most approaches found in the literature, our description based on the Markov limit of a full quantum kinetic theory conserves the total single-particle energy and allows not only a derivation of the transfer rate for the parallel carrier spin component, but also for the perpendicular component of the carrier spin with respect to the external magnetic field, which is not accessible by Fermi's golden rule but is relevant for the description of experiments in Voigt geometry.

7. Quantum kinetic features and correlation effects

7.1. Proximity to the band edge as origin of non-Markovian effects

Already in the first numerical simulations of Thurn's quantum kinetic equations [23] genuine quantum kinetic features were found in the spin dynamics in DMS quantum wells, which deviates visibly from an exponential decay. In particular, a non-monotonic time evolution of the total carrier spin has been identified as a characteristic signature for quantum kinetic effects. However, Ref. [23] does not provide a comprehensive explanation of why these overshoots happen and what exactly the criteria for the appearance of these effects are. The idea behind [Pub6] is to shed light on the origin of the quantum kinetic effects by focusing on the smallest set of equations which is able to reproduce the overshoots. This way, we can extract the mathematical essence of the quantum kinetic effects.

The starting point are the effective equations (5.5) in the case of zero magnetic field and impurity magnetization and low carrier concentration, so that Pauli-blocking effects can be neglected. Taking the finite memory into account, i.e., interpreting the memory function $G_{\omega_{\mathbf{k}}}^{\omega_{\mathbf{k}_1}}$ as an integral operator, we find:

$$\frac{\partial}{\partial t} s_{\omega_1}(t) = -\frac{\eta}{\pi} \int\limits_0^t dt' \int\limits_0^{\omega_{BZ}} d\omega \; \cos[(\omega_1 - \omega)(t - t')] \Big[s_{\omega_1}(t') + \frac{1}{4} \big(s_\omega(t') - s_{\omega_1}(t') \big) \Big], \quad (7.1)$$

where $\eta = \frac{35}{12} \frac{J_{sd}^2 m^* N_{\mathrm{Mn}}}{\hbar^3 V d}$ is the spin transfer rate obtained in the Markov limit. Here, we have performed the quasi-continuous limit and replaced the sum over the $\mathbf{k}$-states in the first Brillouin zone by an integral over the kinetic energy $\hbar\omega = \frac{\hbar^2 \mathbf{k}^2}{2m^*}$, where the finite volume of the Brillouin zone translates into a cut-off frequency ω_{BZ}. Furthermore, we focus on the isotropic case in which the angle $\varphi_{\mathbf{k}}$ of the wave vector $\mathbf{k}$ is not important and the carrier spins s_ω can be labeled by the frequency ω instead of the wave vector $\mathbf{k}$.

We further assume that the spectral spin density s_ω is a smooth function of ω and, as the Markov limit suggests, scattering only occurs between nearby states with similar energies $\hbar\omega$. This motivates us to simplify Eq. (7.1) even further by neglecting the term $\frac{1}{4}\big(s_\omega(t') - s_{\omega_1}(t') \big)$. Although there is no quantitative *a priori* justification for this approximation, we find that the numerical solution of the integro-differential equation (7.1) and the full quantum kinetic equation produce very similar results for the time evolution of the total spin.

When the scattering to states with different values of ω is neglected, Eq. (7.1) becomes an integro-differential equation with respect to the time, where ω_1 only plays the role

of a parameter instead of introducing a second dimension. In this approximation, the ω-integral can be evaluated analytically. We obtain

$$\frac{\partial}{\partial t} s_{\omega_1}(t) = -\frac{\eta}{\pi} \int_0^t dt' \left[\frac{\sin[(\omega_{BZ} - \omega_1)(t' - t)]}{t' - t} + \frac{\sin[\omega_1(t' - t)]}{t' - t} \right] s_{\omega_1}(t'). \qquad (7.2)$$

The energy scale defined by the cut-off ω_{BZ} is much larger than any other energy considered here. Therefore, the cut-off can be considered as infinite, which enables the simplification

$$\frac{\sin[(\omega_{BZ} - \omega_1)(t' - t)]}{t' - t} \rightarrow \pi \delta(t - t') \text{ for } \omega_{BZ} \rightarrow \infty. \qquad (7.3)$$

Note that the upper limit of the time integral in Eq. (7.2) coincides with the zero in the argument of the δ-function, so that only half of the δ-function contributes to the time integral.

In the limit $\omega_{BZ} \rightarrow \infty$, the only two time scales of the problem are the Markovian rate η and the inverse frequency ω_1^{-1}. Thus, we can rewrite the problem in the form of an integro-differential equation with a single dimensionless parameter $\xi := \frac{\omega_1}{\eta}$, if the time is also rescaled by $\tau := \eta t$:

$$\frac{\partial}{\partial \tau} \Phi_\xi(\tau) = -\frac{1}{2} \Phi_\xi(\tau) - \frac{1}{\pi} \int_0^\tau d\tau' \frac{\sin[\xi(\tau' - \tau)]}{\tau' - \tau} \Phi_\xi(\tau'). \qquad (7.4)$$

Since the dimensionless equation (7.4) is linear in Φ_ξ, we can, without loss of generality, set $\Phi_\xi(0) = 1$. This initial condition together with Eq. (7.4) defines the set of functions $\Phi_\xi(\tau)$ which are at the core of the mathematical description of the quantum kinetic effects.

A first step towards the evaluation of these functions is a Taylor-expansion of $\Phi_\xi(\tau)$ at $\tau = 0$. The i-th derivatives $\Phi_\xi^{(i)}$ at $\tau = 0$ can be related to each other using the integro-differential equation (7.4), which yields the recursion relation

$$\Phi_\xi^{(i)} = -\frac{1}{2} \Phi_\xi^{(i-1)} - \frac{1}{\pi} \sum_{0 \leq 2m \leq i-2} \frac{(-1)^m}{2m + 1} \xi^{(2m+1)} \Phi_\xi^{(i-2-2m)}. \qquad (7.5)$$

In order to see that the functions Φ_ξ are indeed able to reproduce the physical effect of the quantum kinetic overshoots and to confirm the validity of the recursion relation (7.5), we compare the quantum kinetic calculations for the situation studied in Ref. [23] with the results obtained by calculating the derivatives $\Phi_\xi^{(i)}$ to high orders (up to 300) using the recursion relation (7.5) and evaluating $\Phi_\xi(\tau)$ by its Taylor expansion. The latter method is similar to the so-called *differential transform method* (DTM) [85].

Figure 7.1(a) shows the direct comparison of the results of the spin dynamics according to the quantum kinetic theory and the differential transform method. One can see that the DTM method perfectly reproduces the results of the quantum kinetic theory as far as the time evolution of the total spin is concerned. The spectral distribution of the spins, however, is slightly different in the quantum kinetic theory [Fig. 7.1(d)] and the DTM
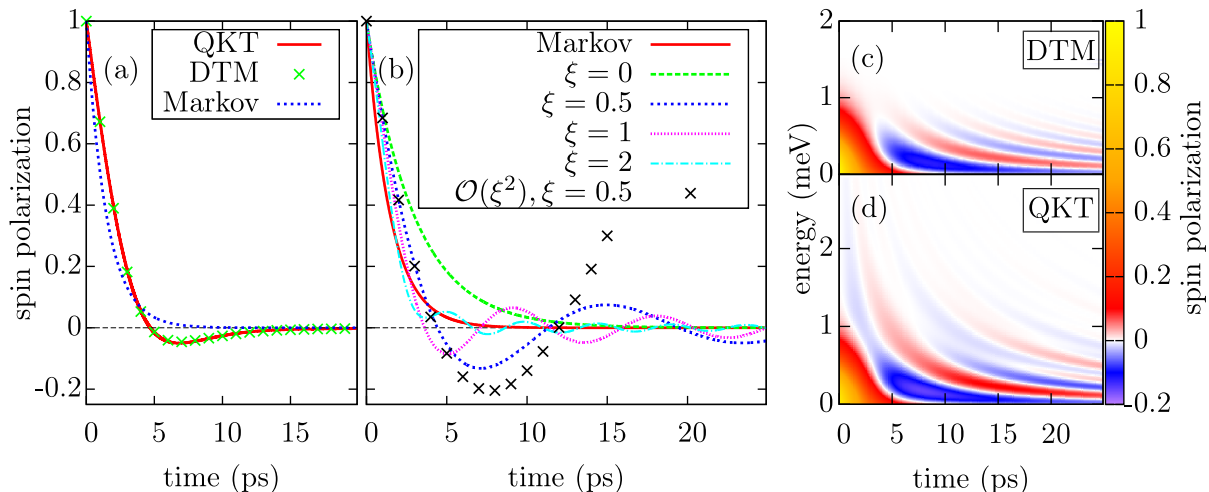
Figure 7.1.: From [Pub6]: (a): Comparison of the spin dynamics simulated by the full quantum kinetic theory (QKT) and the DTM method of [Pub6] for the case of the $Zn_{0.93}Mn_{0.07}Se$ quantum well studied in Ref. [23]. (b): Spin dynamics of electrons with a defined value of the kinetic energy $\hbar\omega$, which is expressed in terms of the parameter $\xi = \frac{\omega}{\eta}$ with Markovian rate η. (c)+(d): Time-resolved spectral distribution of spins according to the quantum kinetic theory (d) and the differential transform method (c).

[Fig. 7.1(c)] due to the scattering to different states in the full quantum kinetic theory that is not included in the DTM calculation, because, there, the term proportional to $\frac{1}{4}(s_\omega(t') - s_{\omega_1}(t'))$ in Eq. (7.1) is neglected.

Fig. 7.1(b) shows the results of the DTM calculations for electrons with defined kinetic energies and therefore fixed values of ξ, which corresponds to the functions $\Phi_\xi\left(\frac{t}{\eta}\right)$. One can clearly observe that for large values of ξ the function $\Phi_\xi(\tau)$ approximates the Markovian result, which is an exponential decay with the rate η. The reason for this is that, for large values of the kinetic energy $\omega_1 \gg \eta$, the limit of $\omega_1 \to \infty$ leads to a second δ-function in Eq. (7.2), similar to that obtained in the limit $\omega_{BZ} \to \infty$ for the cut-off frequency. In the opposite limit $\omega_1 \to 0$, the second term in Eq. (7.4) vanishes and the solution of Eq. (7.4) is simply an exponential decay with half of the rate η. In the intermediate regime, oscillations are superimposed on the decay. For a carrier distribution with a finite width, these oscillations partially interfere destructively, producing the overshoot in the time evolution of the total spin in Fig. 7.1(a).

Now, criteria for the appearance of quantum kinetic overshoots can be formulated: Deviations from the Markovian behavior require an excitation of carriers very close to the band edge, where the energy scale $\hbar\eta$ is defined by the Markovian rate. We can now also understand why the overshoots are only present in two and one dimensions, since in three dimensions the density of states goes to zero for $\omega \to 0$ so that there are only very few carrier states in the region of interest.

7.2. Mathematical considerations regarding finite memory effects

In this section, we point out some interesting aspects from the mathematical physics point of view, which are captured by the integro-differential equation (7.2) but are neither

discussed in [Pub6] due to length restrictions of the proceedings format, nor published elsewhere, since these aspects are rather formal and only qualitative conclusions are reached. Nevertheless we believe that some general insights can be gained from these considerations.

First, recall that applying Eq. (7.3) also for $\omega_1 \to \infty$ yields the Markovian result, which is equivalent to Fermi's golden rule. In this sense, Eq. (7.2) can be used as a model for studying deviations from the Markovian behavior in more general settings, not only for the spin transfer in DMS. In particular, one can ask whether it is possible to derive a general systematic approximation scheme for solutions of equations similar to Eq. (7.2), which to first order gives the Markovian behavior predicted by Fermi's golden rule but provides corrections, if higher orders are taken into account. Such a systematic approximation would be able to describe situations with short but finite memories.

The question of whether the memory in the situation considered in [Pub6] is short or long is, in fact, quite tricky. Usually, a memory is called short when it decays exponentially. An algebraic decay of the form $\frac{1}{\Delta t^n}$ is typically considered to be long. Thus, the memory kernel in Eq. (7.2) formally belongs to the latter case. However, because oscillations with frequency ω_1 are superimposed on the decay of the memory, quantities averaged over an interval of values for ω_1 with a finite width are subject to dephasing. This is also the reason why $\frac{\sin(\omega t)}{t} \to \pi\delta(t)$ for $\omega \to \infty$, which is the shortest possible kind of memory despite $\frac{1}{t}$ being long-range. Thus, in this situation the decay is formally algebraic suggesting a long memory, but average quantities effectively experience a dephasing and therefore a short memory. Such a dephasing can also affect the microscopic, non-averaged quantities, if there is some kind of cross-talk between the s_ω for different values of ω. In the situation considered here, the terms $\frac{1}{4}(s_\omega - s_{\omega_1})$ in Eq. (7.1) mediate such a cross-talk. Also phonons and non-magnetic impurity scattering provide sources for an effective averaging of the microscopic quantities. However, the shortening of the memory for the microscopic quantities is hard to capture quantitatively.

Despite the effective shortening of the memory due to dephasing, the fact that the memory is formally long leads to complications regarding approximate solutions of Eq. (7.2). For example, one could expect due to the effectively short memory that only the values of $s_\omega(t')$ around $t' \approx t$ matter in the memory integral in Eq. (7.2) and a Taylor-expansion of $s_\omega(t')$ about $t' \approx t$ is helpful. However, note that in

$$\int\limits_0^t dt' \, \frac{\sin[\omega_1(t'-t)]}{t'-t} \left(s_{\omega_1}(t) + s_{\omega_1}^{(1)}\big|_t (t'-t) + \frac{1}{2} s_{\omega_1}^{(2)}\big|_t (t'-t)^2 + \dots \right), \qquad (7.6)$$

only the first term, which gives the Markovian result, has a converging asymptotic behavior at $t \to \infty$, while the second term results in an undamped oscillation and the higher order terms diverge. Thus, one idea to solve this problem is to search for an infinite subset of terms in this expansion that can be summed up analytically. This was the original motivation for employing the differential transform method in [Pub6]. With the recursion relation (7.5), it is possible to identify contributions to the solutions $s_{\omega_1}(t)$ of the form of sine and cosine integrals and higher integrals thereof. The recursion relation also allows us to provide analytic results for the solutions $\Phi_\xi(\tau)$ of Eq. (7.4) up to an arbitrary order in ξ. The results up to second order are shown as the black crosses in Fig. 7.1(b) for a value of $\xi = 0.5$. However, we were not able to extract a subset of terms
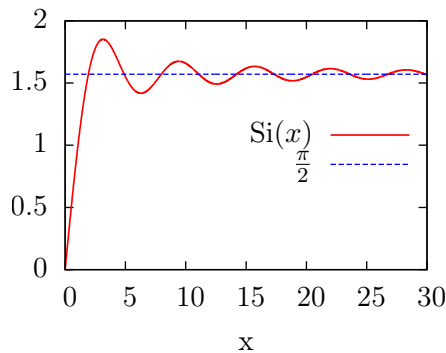
Figure 7.2.: Sine integral

which reproduce significant parts of the dynamics found in the full numerical calculations and also show the correct asymptotics at $t \to \infty$.

Another approach for the solution of Eq. (7.4) is a Laplace transformation, in particular, because Eq. (7.4) is linear in $\Phi_\xi(\tau)$. However, the Laplace transform of $\Phi_\xi(\tau)$ has a complicated form with a complex logarithm in the denominator. We did not find any reasonable approximation that enables an analytic inversion of the Laplace transformation.

Note also that studying Eq. (7.2) enables us to get some fundamental insights into how the exponential solutions to rate equations, e.g., from Fermi's golden rule, can be reconciled with the microscopic time-reversibility of the Schrödinger equation. The full quantum kinetic theory is time-reversible, which can be seen from the fact that the dynamics starts quadratically in time [22]. However, the Markov limit predicts an exponential decay, which starts linearly in time and thereby destroys the time-reversibility. Here, we can pinpoint this loss of time-reversibility to the assumption of $\omega_{BZ} \to \infty$, since before this step, the solution to the integro-differential equation starts quadratically in time and after it, a non-zero value of the first derivative $\Phi_\xi^{(1)}$ is obtained. To further understand this transition, we focus on the simplest case $\omega_1 = 0$. Then Eq. (7.2) becomes

$$\frac{\partial}{\partial t} s_0(t) = -\frac{\eta}{\pi} \int_0^t dt' \frac{\sin[(\omega_{BZ})(t' - t)]}{t' - t} s_0(t'). \tag{7.7}$$

Assuming that ω_{BZ} is very large, but finite, and that the memory is short enough so that $s_0(t') \approx s_0(t)$ is a good approximation, we find

$$\frac{\partial}{\partial t} s_0(t) \approx -\frac{\eta}{2} \left[\frac{2}{\pi} \mathrm{Si}(\omega_{BZ} t) \right] s_0(t), \tag{7.8a}$$

$$\mathrm{Si}(x) = \int_0^x dx' \frac{\sin(x')}{x'}, \tag{7.8b}$$

with the sine integral $\mathrm{Si}(x)$, which is depicted in Fig. 7.2. There, one can see that the sine integral starts linearly in x, reaches a maximum at $x = \pi$ and starts to oscillate with a decaying amplitude about an asymptotic value of $\frac{\pi}{2}$. For the solution of Eq. (7.8a) this means that, on a coarse-grained time scale $\bar{t} \gg \frac{1}{\omega_{BZ}}$ where the sine integral is essentially

constant with $\mathrm{Si}(x) \approx \frac{\pi}{2}$, one finds for the coarse-grained time evolution of the spin:

$$\frac{\partial}{\partial t}\bar{s}_0(\bar{t}) \approx -\frac{\eta}{2}\bar{s}_0(\bar{t}) \Longrightarrow \bar{s}_0(\bar{t}) = \bar{s}_0(0)e^{-\frac{\eta}{2}\bar{t}} = \bar{s}_0(0)\left(1 - \frac{\eta}{2}\bar{t}\right) + \mathcal{O}(\bar{t}^2), \qquad (7.9\text{a})$$

which starts linearly in time, whereas a formal Taylor expansion of Eq. (7.7) gives

$$\frac{\partial}{\partial t}s_0(t) \approx -\frac{\eta}{2}\big(t + \mathcal{O}(t^2)\big)s_0(t) \Longrightarrow s_0(t) = s_0(0) + \mathcal{O}(t^2), \qquad (7.9\text{b})$$

which remains quadratic in time. Thus, the contradiction between the time-reversibility in the microscopic picture and the exponential behavior predicted by rate equations is resolved by the fact that the latter describe an approximate behavior on a coarse-grained time scale, whereas, actually, oscillations with frequencies corresponding to the cut-off ω_{BZ} are superimposed on the decay in the microscopic picture.

7.3. Carrier-impurity correlation effects beyond spin-flip scattering

Historically, one of the first investigations of solid state systems where magnetic impurities play a key role were unintentionally magnetically doped metals. Already in the 1930s, measurements of the low-temperature conductivity in gold wires showed that the resistivity first decreases with decreasing temperature, but then it reaches a minimum and starts to increase logarithmically at even lower temperatures [86]. It was *Kondo* who explained this logarithmic divergence in the resistivity with the presence of magnetic iron impurities in the gold wire [55], which is therefore called the *Kondo effect*. This work, which uses a third-order perturbative treatment of the Kondo Hamiltonian H_{sd} for the calculation of transition probabilities, appeared in the 1960s. Experiments at even lower temperatures T show that the resistivity in these Kondo systems actually reaches a constant value at $T \to 0$ [87]. A satisfactory theoretical explanation of this very-low-temperature regime was missing for quite some time. This was known as the *Kondo problem*. Today, the Kondo problem is generally considered to be solved by a non-perturbative description of strongly correlated many-particle states [59]: At very low temperatures, a few of the quasi-free carriers in the metal form singlet spin states with the magnetic impurities. This way, the magnetic interaction is effectively screened for all the other quasi-free carriers. The singlet formation implies that the ground state of this system is a state with strong correlations between the quasi-free carriers and the magnetic impurities.

In the context of DMS, the Kondo-type correlations are rarely discussed. The reason for this is that the number of free carriers in metals is much higher than in semiconductors. While for the magnetically doped metals the number of carriers is much larger than the number of magnetic impurities $N_e \gg N_{\mathrm{Mn}}$, the DMS are typically in the opposite limit $N_e \ll N_{\mathrm{Mn}}$. For this reason, it has been argued [88] that the Kondo physics is of minor importance for the spin phyics in DMS. On the other hand, a perturbative many-body description of the spin dynamics in DMS based on Green's functions [74] found Kondo-like logarithmic divergences, which makes this treatment ill-defined but implies that carrier-impurity correlations can indeed be significant in DMS. Moreover, it

was found that the carrier-impurity correlations can have a strong impact on, e.g., spin stiffness and Gilbert damping in ferromagnetic $Ga_{1-x}Mn_xAs$ [73].

In this section, we discuss the importance of carrier-impurity correlations for the spin physics in DMS as presented in [Pub7]. Beside the spin transfer between carriers and impurities in spin-flip scattering processes mediated by the correlations, the correlations renormalize the carrier spin precession frequency with respect to its mean-field value. Furthermore, the formation of carrier-impurity correlations leads to a build-up of carrier-impurity correlation energy, for which we derive analytic expressions in the Markovian approximation in [Pub7]. For both quantities, we find Kondo-like logarithmic divergences which are, however, integrable and do not lead to problems in the theory like in other approaches [74].

The starting point of this discussion is the effective equation for the carrier spin component perpendicular to the impurity magnetization derived in Ref. [Pub2]. For the sake of clarity, we consider the case of low carrier densities, where only terms linear in the electron variables $s_{\mathbf{k}_1}^\perp$ and $n_{\mathbf{k}_1}^{\uparrow/\downarrow}$ are important. Then, Eq. (5.5b) becomes

$$\frac{\partial}{\partial t}s_{\mathbf{k}_1}^\perp = -\sum_{\mathbf{k}}\left[\operatorname{Re}(G_{\omega_{\mathbf{k}}}^{\omega_{\mathbf{k}_1}-\omega_M})\frac{b^+}{2}s_{\mathbf{k}_1}^\perp + \operatorname{Re}(G_{\omega_{\mathbf{k}}}^{\omega_{\mathbf{k}_1}+\omega_M})\frac{b^-}{2}s_{\mathbf{k}_1}^\perp + \operatorname{Re}(G_{\omega_{\mathbf{k}}}^{\omega_{\mathbf{k}_1}})\frac{b^\parallel}{2}\left(s_{\mathbf{k}}^\perp + s_{\mathbf{k}_1}^\perp\right)\right]$$
$$+ \left[\omega_M - \sum_{\mathbf{k}}\left\{\operatorname{Im}(G_{\omega_{\mathbf{k}}}^{\omega_{\mathbf{k}_1}-\omega_M})\frac{b^+}{2} - \operatorname{Im}(G_{\omega_{\mathbf{k}}}^{\omega_{\mathbf{k}_1}+\omega_M})\frac{b^-}{2}\right\}\right]\left(\frac{\boldsymbol{\omega}_M}{|\boldsymbol{\omega}_M|}\times s_{\mathbf{k}_1}^\perp\right), \quad (7.10)$$

where $\boldsymbol{\omega}_M = \frac{J_{sd}N_{Mn}}{\hbar V}\langle\mathbf{S}\rangle$. While the real part of the memory function describes the decay of the perpendicular carrier spin caused by spin transfer processes between carriers and impurities, the imaginary part renormalizes the carrier spin precession frequency. In the Markov limit, one finds

$$\operatorname{Im}\left(G_{\omega_{\mathbf{k}}}^{\omega_{\mathbf{k}_1}}\right) = \frac{J_{sd}^2 N_{Mn}}{\hbar^2 V^2}\int\limits_{-t}^{0} dt'\ \sin[(\omega_{\mathbf{k}}-\omega_{\mathbf{k}_1})t'] \approx -\frac{J_{sd}^2 N_{Mn}}{\hbar^2 V^2}\mathcal{P}\frac{1}{\omega_{\mathbf{k}}-\omega_{\mathbf{k}_1}}. \quad (7.11)$$

In the quasi-continuous limit, the $\mathbf{k}$-sum in Eq. (7.10) can be replaced by an integral over the density of states $D(\omega)$

$$\sum_{\mathbf{k}}\ldots \longrightarrow \int\limits_{0}^{\omega_{BZ}} d\omega\ D(\omega)\ldots, \quad (7.12)$$

with a cut-off frequency ω_{BZ} chosen so that $\hbar\omega_{BZ}$ corresponds to the width of the conduction band.

In two dimensions, the spectral density of states $D(\omega) = \frac{Am^*}{2\pi\hbar}\Theta(\omega)$ is step-like, yielding a renormalization $\Delta\omega^{2D}(\mathbf{k}_1)$ of the spin precession frequency for an electron with wave

vector $\mathbf{k}_1$

$$\Delta\omega^{2D}(\mathbf{k}_1) = \frac{J_{sd}^2 N_{\mathrm{Mn}}}{\hbar^2 V^2} \frac{Am^*}{2\pi\hbar} \left[\ln\left|\frac{\omega_{BZ} - (\omega_{\mathbf{k}_1} - \omega_M)}{\omega_{\mathbf{k}_1} - \omega_M}\right| \left(\frac{1}{2}\langle S^{\perp 2}\rangle + \frac{1}{4}\langle\mathbf{S}\rangle \cdot \frac{\boldsymbol{\omega}_M}{|\boldsymbol{\omega}_M|}\right) \right.$$
$$\left. - \ln\left|\frac{\omega_{BZ} - (\omega_{\mathbf{k}_1} + \omega_M)}{\omega_{\mathbf{k}_1} + \omega_M}\right| \left(\frac{1}{2}\langle S^{\perp 2}\rangle - \frac{1}{4}\langle\mathbf{S}\rangle \cdot \frac{\boldsymbol{\omega}_M}{|\boldsymbol{\omega}_M|}\right) \right]. \tag{7.13}$$

Thus, the Markovian expression for the renormalization of the spin precession frequency of an electron with wave vector $\mathbf{k}_1$ diverges logarithmically for $\omega_{\mathbf{k}_1} \to \omega_M$ and $\omega_{BZ} \to \infty$. If, however, a non-singular carrier distribution of carriers is considered, the precession frequency of the total spin is always finite, since the logarithmic divergence is integrable. Furthermore, the divergence is only present in the Markov limit, i.e., at $t \to \infty$. However, the perpendicular carrier spin component eventually decays to zero, so that a diverging frequency renormalization can never be observed.

From Eq. (7.13) it can be seen that the frequency renormalization depends on the value of the cut-off energy $\hbar\omega_{BZ}$. In typical semiconductors, the bandwidth of the conduction band is on the order of a few eV. Accounting for the whole conduction band in the integration of the full quantum kinetic equation is, however, not feasable. This can be easily seen by the following estimation: The correlations oscillate approximately with $\cos[(\omega_{\mathbf{k}_1} - \omega_{\mathbf{k}_2})t]$. For $\omega_{\mathbf{k}_1} - \omega_{\mathbf{k}_2} \approx \omega_{BZ}$, the oscillation period corresponds to hundreds of attoseconds. On the other hand, the spin dynamics takes place on a scale of ~ 10 ps, which is 5 orders of magnitude larger. Conversely, the time scale of 10 ps for the spin dynamics implies the necessity to resolve $\omega_{\mathbf{k}_1} - \omega_{\mathbf{k}_2}$ on a scale of 10-100 µeV, which is 4 to 5 orders of magnitude smaller than the typical cut-off energy $\hbar\omega_{BZ}$. Moreover, the solution of the full quantum kinetic equation is quadratic in the number of discretization points N_k of the $\mathbf{k}$-space.

Here, we solve this problem using a similar approach as the no-scattering-approximation in [Pub6]: We assume that the perpendicular carrier spin is a smooth function of $\mathbf{k}$ and we replace $\mathbf{s}_{\mathbf{k}}^{\perp}$ by $\mathbf{s}_{\mathbf{k}_1}^{\perp}$ in Eq. (7.10). This approximation is justified for the investigation of the renormalization of the precession frequency because $\mathbf{s}_{\mathbf{k}}^{\perp}$ only appears in a term that is also proportional to the real part of the memory function and it does not influence the spin precession frequency. As a result, the equations of motion for $\mathbf{s}_{\mathbf{k}_1}^{\perp}$ with different values of $\mathbf{k}_1$ decouple and become of the order $\mathcal{O}(N_k^1)$ for each value of $\mathbf{k}_1$. Integrating over the results for different values of $\mathbf{k}_1$ can be done on a much coarser energy scale, since the resulting functions $\mathbf{s}_{\mathbf{k}_1}^{\perp}(t)$ are smooth in $\mathbf{k}_1$. Also a restriction to a spectral region close to the conduction band edge is possible for the integration over $\mathbf{k}_1$.

In order to keep the memory effects, the memory function $G_{\omega_{\mathbf{k}}}^{\omega_{\mathbf{k}_1}}$ has to be regarded as a time integral operator and the effective equations become integro-differential equations. After applying the approximation $\mathbf{s}_{\mathbf{k}}^{\perp} \approx \mathbf{s}_{\mathbf{k}_1}^{\perp}$, these integro-differential equations can be transformed into ordinary differential equations by introducing auxiliary functions, which mathematically play a similar role as the carrier-impurity correlations in the full quantum kinetic theory. This procedure allows us to account for memory effects while still spectrally resolving the full conduction band.

From the numerical calculations for δ-like initial carrier distributions shown in Fig. 7.3(a), it is found that the Markovian expression in Eq. (7.13) for the frequency renormalization yields virtually the same result as a fit to the simulations including the memory, even for carriers close to the divergences. The calculations shown in Fig. 7.3(b) using
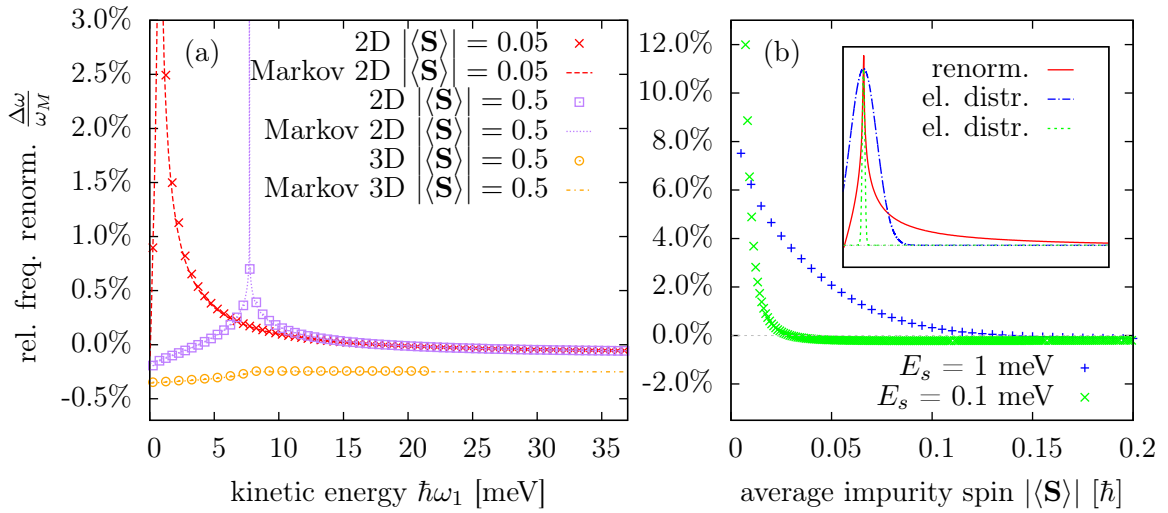
Figure 7.3.: Adapted from [Pub7] (sign according to the erratum): (a): Relative frequency renormalization $\Delta\omega/\omega_M$ as a function of the kinetic energy of a single electron for an average impurity spin of $0.5\hbar$ and $0.05\hbar$, respectively, in two- and three-dimensional systems. The lines represent the results of the Markovian expressions, whereas the points show the results of fits to simulations including a finite memory using Eqs. (15) of [Pub7]. (b): Relative frequency renormalization as a function of the average impurity spin for a Gaussian electron occupation with standard deviation E_s centered at the singularity of the renormalization (cf. inset).

more realistic initial carrier distributions with finite widths predict a renormalization of a few percent for small impurity magnetizations. Note that it is necessary for the detection of the precession frequency that the impurity magnetization is finite and the oscillations are not overdamped. Thus, there is a limited range of parameters for which a significant detectable renormalization of the precession frequency is predicted in [Pub7].

Beside the frequency renormalization, also the carrier-impurity correlation energy is extracted in [Pub7] from the quantum kinetic theory as a functional of the occupations $n_{\mathbf{k}_1}^{\uparrow}$ and $n_{\mathbf{k}_1}^{\downarrow}$. To this end, the Markovian expression for the correlations is inserted into the definition of the correlation-energy:

$$\langle H_{sd}^{\mathrm{cor}}\rangle = \langle H_{sd}\rangle - \underbrace{\langle H_{sd}^{\mathrm{MF}}\rangle}_{:=\sum_{\mathbf{k}} \hbar\boldsymbol{\omega}_M\cdot\mathbf{s}_{\mathbf{k}}} = \frac{J_{sd}N_{\mathrm{Mn}}}{V^2}\sum_{\mathbf{k}_1\mathbf{k}_2}\sum_{i} Q_{i\mathbf{k}_1}^{i\mathbf{k}_2}. \tag{7.14}$$

The explicit expression for the correlation energy depends on the memory function $G_{\omega_{\mathbf{k}_1}}^{\omega_{\mathbf{k}_2}}$ only via its imaginary part. Thus, in two dimensions, one obtains the same kind of logarithmic divergences in the correlation energy as in the frequency renormalization. Numerical estimates yield values of the correlation energy per electron of several hundred μeV, which is of the same order of magnitude as thermal energies in Helium-cooled systems. Thus, the correlation energy might also be relevant for thermodynamic considerations, such as for the formation of free or bound magnetic polarons that are mostly discussed in the literature in a semiclassical picture without accounting for carrier-impurity correlations [36, 66, 72, 89, 90].

So far, we have summarized the logarithmic divergences found in the renormalization of the carrier spin precession frequency and the correlation energy in two dimensions. The three-dimensional case is also discussed in [Pub7]. Due to the difference in the density of

states, also the expressions for the frequency renormalization and the correlation energy are different in two and three dimensions. As can be seen in Fig. 7.3(a), there are no divergences in three dimensions and, there, the correlation effects are, in general, weaker than in lower-dimensional systems.

8. Optical excitation

## 8.1. Quantum kinetic treatment of the light-matter interaction

The predictions of genuine quantum kinetic effects, such as the non-monotonic dynamics of the carrier-impurity spin transfer, are yet to be tested experimentally. In order to pave the way to a future experimental confirmation of our predictions, it is useful to figure out what excitation conditions lead to particularly pronounced quantum kinetic effects.

In [Pub8], we address the question of how the strength of the deviations from the Markovian behavior depends on the duration of a pump pulse. Furthermore, we compare two different materials, $Cd_{1-x}Mn_xTe$ and $Zn_{1-x}Mn_xSe$, for the suitability for experiments highlighting the non-Markovian features. Finally, the dependence of the strength of the quantum kinetic effects on an external magnetic field is investigated.

An important difference between the theory in [Pub8] and the approaches studied before in this thesis is that the optical excitation is taken into account on a quantum kinetic level instead of resorting to initial-value calculations. Thurn's original quantum kinetic theory [22] already contains the light-matter interaction as well as the valence band and the interband coherences. Also, the optical excitation has been taken into account explicitly in a first quantum kinetic calculation in Ref. [24] for the case of the same $Zn_{0.93}Mn_{0.07}Se$ quantum well that was also studied in Ref. [23] using initial-value calculations. These studies showed that the non-Markovian features in the results of the initial-value calculation are indeed also predicted in calculations where the optical excitation is treated on a quantum kinetic level.

However, only a single set of material parameters and excitation conditions was considered in Ref. [24]. In [Pub8], calculations for a number of different situations are presented. First of all, a comparison is made between the spin dynamics in $Cd_{1-x}Mn_xTe$ and $Zn_{1-x}Mn_xSe$ after an excitation with a circularly polarized pump pulse with pulse duration $\tau_L = 1.7$ ps. It is found that the non-Markovian features are more pronounced in the case of $Zn_{1-x}Mn_xSe$. This can be explained by the fact that the effective conduction band mass in ZnSe is about twice as large as the effective mass in CdTe and the spin transfer rate η is proportional to the effective mass. As found in [Pub6], the deviations from the Markovian behavior are particularly strong for an excitation close to the band edge, where the spectral distance of the carriers to the band edge has to be compared with the energy scale $\hbar\eta$ corresponding to the spin transfer rate η. The optical excitation of a similar electron distribution in $Zn_{1-x}Mn_xSe$ and $Cd_{1-x}Mn_xTe$ results in an occupation of states which, in $Zn_{1-x}Mn_xSe$, is closer to the band edge when measured on the scale $\hbar\eta$. Since this closer proximity of the optically excited states to the band edge in $Zn_{1-x}Mn_xSe$ leads to a deeper memory, the non-Markovian features, such as the non-monotonicity in the spin dynamics, are more pronounced.

Second, we investigate the changes in the shape of the time evolution of the carrier
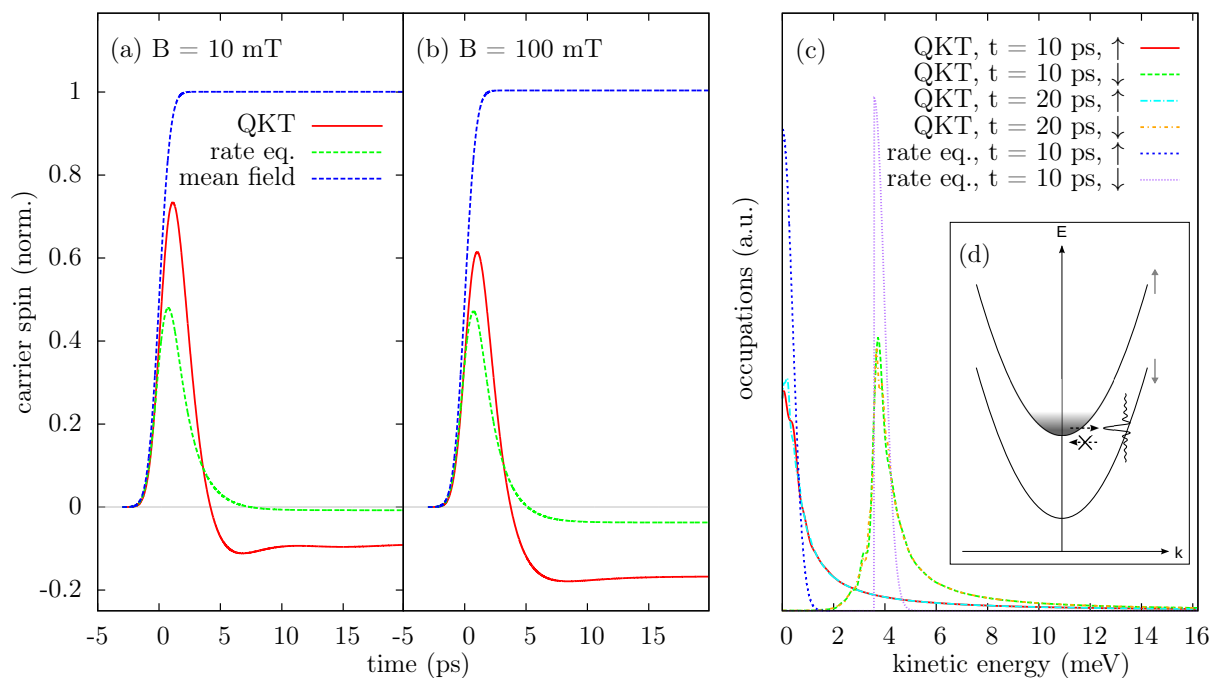
Figure 8.1.: From [Pub8]: Time evolution of the total carrier spin in a 4 nm wide $Zn_{0.93}Mn_{0.07}Se$ quantum well after optical excitation with a pulse duration of $\tau_L = 1.7$ ps in the presence of a magnetic field of $B = 10$ mT (a) and $B = 100$ mT (b), respectively. (c): Occupations of spin-up and spin-down electron states at different times t with respect to the center of the laser pulse. (d): Diagram depicting the spin-flip scattering between spin-up and spin-down subbands.

spin polarization when lasers with different pulse durations τ_L are used for the optical excitation. As expected from the results of the initial-value calculations, we find that, for short pulse durations τ_L compared with the spin transfer time η^{-1}, the optical excitation leads to a spectrally broad carrier distribution with most of the electrons occupying states with kinetic energies above $\hbar\eta$. Thus, the non-Markovian features are diminished. For long pulse durations, the spin transfer is already active during the optical excitation and one might expect that the non-Markovian effects are smeared out. However, the characteristic non-monotonic time evolution of the non-Markovian dynamics can still be found in calculations where the pulse duration τ_L is about three times longer than the spin transfer time η^{-1}. Our findings indicate that the optimal pulse duration for experiments aimed at detecting the genuine quantum kinetic features in the spin dynamics in DMS is slightly longer than the spin transfer time of the system under investigation.

Finally, in [Pub8], it is studied how an external magnetic field influences the quantum kinetic features in the spin dynamics in DMS. To this end, the quantum kinetic theory of Ref. [22] is extended to include not only the optical excitation on a quantum kinetic level, but also the Zeeman energies for carriers and impurities. The effects of an external magnetic field along the growth direction on the spin dynamics in a $Zn_{0.93}Mn_{0.07}Se$ quantum well are shown in Fig. 8.1.

Two effects of the external field on the quantum kinetic features are clearly seen in Fig. 8.1: First of all, the non-monotonicity of the time evolution of the spin polarization is suppressed when an external magnetic field is present. This is due to the fact that the spin-flip scattering leads to an occupation of electronic states with kinetic energies

increased by $\hbar\omega_e - \hbar\omega_{\text{Mn}}$ with respect to the original states. This drives the carrier distribution away from the band edge, which according to [Pub6] reduces the non-Markovian effects.

Second, the stationary value of the carrier spin obtained at long times t is drastically different in the quantum kinetic simulation compared with the Markovian result. To understand this, it is useful to look at the spectral redistribution of carriers [cf. Fig. 8.1(c)] after the optical excitation close to the band edge. While the distribution of the scattered electrons is a replica of the original distribution at the band edge shifted by $\hbar\omega_e - \hbar\omega_{\text{Mn}}$ according to the Markovian calculation, the quantum kinetic calculation predicts a broadening of the distribution of the scattered electrons. A broadening of carrier distributions in quantum kinetic calculations is usually attributed to the energy-time uncertainty [91, 92]. Interestingly, in the case studied here, the width of this distribution does not contract with time, so that, here, the energy-time uncertainty is ruled out as the main cause of the broadening. Instead, the reason for the broadening of the distribution of scattered electrons in the present case is that the *s-d* interaction builds up strong correlations between carriers and impurities so that the single-particle picture becomes invalid. The quantum kinetic calculation conserves the total energy including, beside the single-particle energies, also the many-body carrier-impurity correlation energy. The latter is responsible for the apparent non-conservation of the single-particle energy in spin-flip scattering processes.

The width of the distribution of scattered electrons has an influence on the dynamics of the total spin mainly by the occupation of spin-down states with kinetic energies below $\hbar\omega_e - \hbar\omega_{\text{Mn}}$. For these states, the backscattering to the spin-up subband is strongly suppressed, since there are no states in the spin-up band with matching single-particle energies to which they can scatter back. Thus, the scattering from the spin-up to the spin-down band is preferred to the scattering in the opposite direction. In this sense, the spin-flip scattering in the presence of an external field has some similarities to a quantum ratchet [93].

To summarize, [Pub8] predicts that the non-Markovian effects are most likely observable in ZnSe based DMS excited with pump pulses with pulse durations on the order of or slightly longer than the spin transfer rate. For a non-zero external magnetic field and in the absence of other relaxation and thermalization mechanisms, the quasi-stationary value of the spin polarization at long times can serve as an indicator for genuine quantum kinetic effects.

8.2. Optical excitation using twisted light

A relatively new area of research is the study of light with orbital angular momentum or twisted light [94]. Earlier work by *Quinteiro* and *Tamborenea* [95] suggests that the orbital angular momentum of twisted light can, in principle, be transferred to optically induced carriers in semiconductors. In the context of DMS, it is an interesting question whether this mechanism can be used to control the carrier spins and, via the *s-d* interaction, the spins of magnetic impurities in DMS.

To understand the concept of twisted light, it is necessary to go beyond the picture of a spatially homogeneous electromagnetic field of the laser beam. The propagation of a monochromatic light beam is described by the Helmholtz equation [96] which can

directly be derived from the homogeneous Maxwell's equations. Considering a light beam traveling along the z axis, one can apply the paraxial approximation to the Helmholtz equation. Then, the transverse spatial part $v(x, y)$ of an amplitude of the electromagnetic field (E or B) has to obey

$$\left(\frac{\partial^2}{\partial x^2} + \frac{\partial^2}{\partial y^2} + k_\perp^2\right)v(x, y) = 0, \tag{8.1}$$

A set of solutions to the paraxial Helmholtz equation (8.1) in polar coordinates is [96]

$$v(\rho, \phi) = v_0 J_m(k_\perp \rho)e^{im\phi}, \tag{8.2}$$

where $J_m(x)$ are Bessel functions and m is an integer. These solutions to the Helmholtz equations are dispersionless, i.e., they do not change their form while propagating along the z direction. The vector potential in Coulomb gauge corresponding to such a Bessel beam in the paraxial approximation is [95]

$$\mathbf{A}(\mathbf{r}, t) = \text{Re}\left\{A_0 e^{i(q_z z - \omega t)}\boldsymbol{\epsilon}_\pm J_l(q_r r)e^{il\phi}\right\}, \tag{8.3}$$

where l is the orbital angular momentum of the light, q_z and q_r are the linear momenta in the z direction and the radial direction, respectively, and $\boldsymbol{\epsilon}_\pm = \mathbf{e}_x \pm i\mathbf{e}_y$ is the polarization direction of the light, where $\mathbf{e}_{x/y}$ are the unit vectors in the x and y directions.

Most experiments involving optical excitation of semiconductors by laser beams use classical light, which has an average orbital angular momentum of zero. In Ref. [95], the matrix elements for the excitation of semiconductor quantum wells with twisted light for arbitrary values of m were derived using the minimal coupling Hamiltonian together with the expression for the vector potential in Eq. (8.3). It was also shown analytically that light with orbital angular momentum l induces only transitions between valence and conduction band states with envelope orbital angular momenta differing by l. This orbital angular momentum selection rule follows directly from the conservation of the linear momentum in the absorption process.

The goal of [Pub9] is to follow up on the advances made in Ref. [95] and present numerical simulations of the optical excitation based on the transition matrix elements derived in Ref. [95]. Besides simulating the optical excitation, also the subsequent spin dynamics in the presence of a Rashba field is calculated in [Pub9], which enables an investigation of the transfer of the envelope orbital angular momentum from the optically excited carriers to the carrier spin degree of freedom.

Some technical difficulties arise when studying the optical excitation of quantum wells with twisted light. First of all, the cylindrical symmetry of Bessel modes as well as their spatial localization make it difficult to investigate the excitation in the commonly used picture of an ideal quantum well with an infinite area and rectangular boundaries. Instead, we consider cylindrical quantum disks with finite radii R and we are especially interested in the limit $R \to \infty$, which corresponds to an extended quantum well. The electronic eigenstates of a finite-size quantum disk in zylindrical coordinates (r, ϕ, z) are

$$\psi_{bm\nu}(r, \phi, z) = \mathcal{N}_{m\nu} J_m(k_{m\nu}r)e^{im\phi}\Phi_b(z), \tag{8.4}$$

where $\mathcal{N}_{m\nu}$ is a normalization constant, $k_{m\nu} = u_{m,\nu}/R$ with $u_{m,\nu}$ being the ν-th root
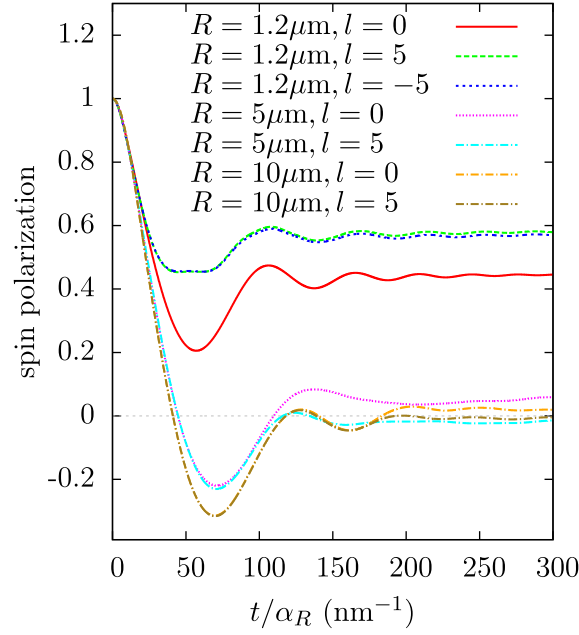
Figure 8.2.: From [Pub9]: Time evolution of the electron spin polarization after optical excitation with light with orbital angular momentum l for quantum disks with radii R.

of the m-th Bessel function J_m and b comprises the spin and band indices. The term $\mathcal{N}_{m\nu} J_m(k_{m\nu}r)e^{im\phi}$ plays the role of the envelope of the carrier wave function, which corresponds to the plane wave $\frac{1}{\sqrt{A}}e^{\mathbf{k}\cdot\mathbf{r}}$ in an infinite quadratic quantum well. Similarly, Φ_b replaces the periodic Bloch function in the infinite well. It is noteworthy that the states $\psi_{bm\nu}$ comprise three different angular momenta, viz., the spin and the orbital angular momentum within one unit cell contained in Φ_b as well as the envelope orbital angular momentum m.

For the simulations in [Pub9], the matrix elements of the light-matter interaction as well as the Rashba interaction in the basis of the orbital momentum eigenstates $\psi_{bm\nu}$ have to be calculated. This calculation reveals that the twisted light excites states with defined envelope orbital angular momenta, i.e., only diagonal elements of the carrier density matrix with respect to m. Furthermore, for each excited conduction band electron with envelope orbital angular momentum m, also a hole is excited in the valence band with envelope orbital angular momentum $l - m$. Thus, the orbital angular momentum of the light l is completely transferred to the envelope orbital angular momenta of the carriers.

Focusing on the conduction band ($b = c$), the matrix elements of the Rashba interaction H_R in the orbital momentum eigenstate basis are

$$\langle\psi_{c'm'\nu'}|H_R|\psi_{c,m,\nu}\rangle = \frac{\hbar\alpha_R k_{m\nu}k_{m'\nu'}}{R(k_{m\nu}^2 - k_{m'\nu'}^2)}\left(s_{c'c}^+\delta_{m',m-1} - s_{c'c}^-\delta_{m',m+1}\right), \qquad (8.5a)$$

which for large values of R becomes

$$\langle\psi_{c'm'\nu'}|H_R|\psi_{c,m,\nu}\rangle \to \hbar\alpha_R k\delta(k - k')\left(s_{c'c}^+\delta_{m',m-1} - s_{c'c}^-\delta_{m',m+1}\right). \qquad (8.5b)$$

Thus, the Rashba interaction increases the spin, while the envelope orbital angular momentum is decreased and vice versa. For $R \to \infty$, k corresponds to the modulus of the

carrier wave vector and remains unchanged under the action of Rashba interaction.

Figure 8.2 shows the time evolution of the carrier spin polarization after the optical excitation with a circularly polarized twisted light beam. Note that the spin dynamics does not depend on the sign of the orbital angular momentum l of the exciting light pulse and for large radii R also the dependence on the modulus of l becomes negligible. We explain this behavior as follows: When the Rashba interaction acts on a spin-up electron with envelope orbital angular momentum m, it flips its spin and increases m by 1. When the Rashba interaction acts a second time on the electron, it can only flip its spin back to the spin-up state and the envelope orbital angular momentum decreases again to m, so that the initial state is restored. This behavior is almost independent of the value of m of the initial state. The slight differences in the spin dynamics after optical excitation with light with different orbital angular momenta originate from the irregularities of the roots of the Bessel functions which determine the prefactor of the Rashba matrix element in Eq. (8.5a) and are therefore only important if the radius of the quantum disk is so small that the optical excitation spectrally resolves the individual states. This is consistent with the findings of Ref. [97] that twisted light can, in principle, be used to control the spin states in quantum dots.

However, in extended systems $(R \to \infty)$, the spin dynamics cannot be efficiently controlled by tuning the orbital angular momentum of the exciting light. Therefore, it is not very promising to try to control spins of magnetic impurities in extended DMS by the twisted light via the cascade of the optical excitation of quasi-free carriers, the subsequent transfer of angular momentum to the spin by the spin-orbit interaction and the ensuing carrier-impurity spin transfer caused by the s-d interaction.

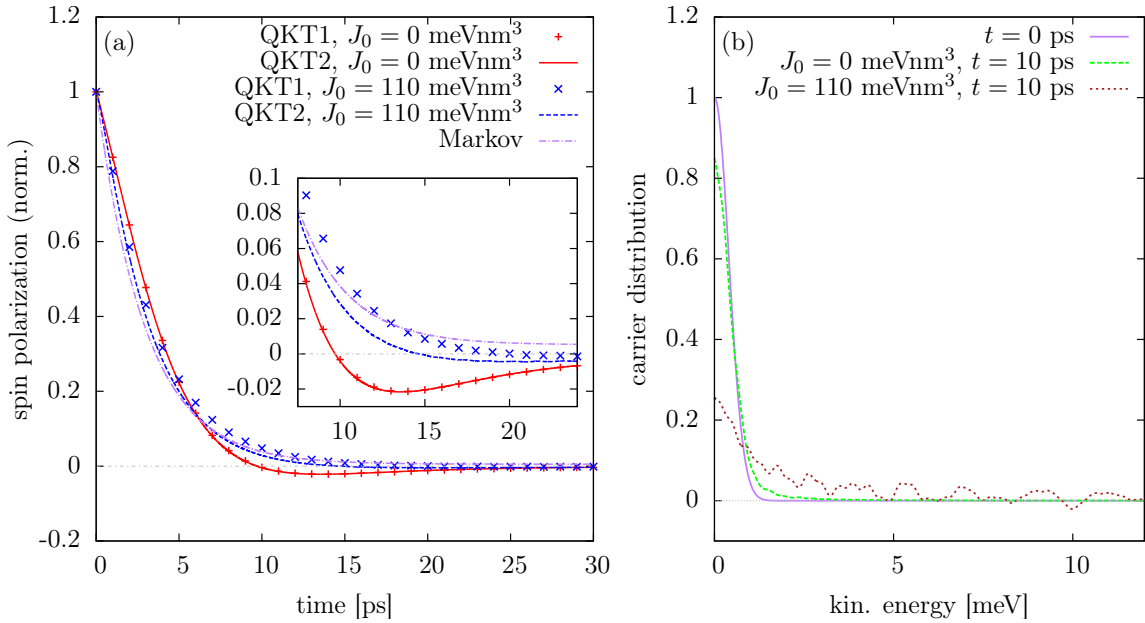# 9. Influence of non-magnetic impurity scattering

If semiconductors are doped isoelectrically with non-magnetic impurities, the main effect on the quasi-free carriers in the semiconductor is that they experience a change in the local crystal potential. This local potential breaks the translational crystal symmetry and leads to a coupling between states with different wave vectors. If the local potential is small, it is instructive to consider the picture in which carriers in plane wave states are scattered at the impurities and change their wave vectors. The goal of [Pub10] is to understand how such a non-magnetic local potential affects the spin dynamics in DMS, where both, the magnetic and non-magnetic potentials [cf. Eqs. 2.5 in section 2.2.2] are present.

In the case of CdTe, the incorporation of Mn impurities leads concurrently to a non-magnetic local potential with a coupling constant J_0 which is about a factor of 7 larger than the magnetic coupling constant J_{sd} [98]. Despite its strength, the non-magnetic carrier-impurity interaction is usually neglected in the description of the spin dynamics in DMS because it commutes with the spin-operators and therefore influences the spin dynamics only indirectly. However, as discussed above, our quantum kinetic theory shows that the spin dynamics in DMS can depend on the dynamical redistribution of carriers in $\mathbf{k}$-space. Since such a carrier redistribution is also facilitated by scattering at a non-magnetic local potential, the latter might have an influence, e.g., on the non-Markovian effects in the spin dynamics in DMS.

In [Pub10], the quantum kinetic theory is extended to incorporate beside the magnetic s-d interaction and the Zeeman energies of carriers and impurities in an external field also the non-magnetic carrier-impurity interaction. Following the line of [Pub5], the Markovian limit of the quantum kinetic theory is derived. Furthermore, the Markovian expressions for the correlation energies and the renormalization of the carrier spin precession frequencies are presented, where, in contrast to [Pub7], also the non-magnetic carrier-impurity correlations are taken into account.

Using this theory, numerical simulations are presented in [Pub10] for the case of a $Cd_{0.93}Mn_{0.07}Te$ quantum well where the optical excitation is modeled by choosing a spin polarized Gaussian initial carrier distribution with a standard deviation of $E_s = 0.4$ meV. The results of the calculations for the case of vanishing magnetic field are shown in Fig. 9.1(a). While the quantum kinetic theory without the non-magnetic impurity scattering predicts an overshoot of the spin polarization below its asymptotic value at long times, accounting for non-magnetic impurity scattering in the quantum kinetic theory leads to a monotonic time evolution of the spin polarization close to the Markovian result.

In Fig. 9.1(b), the distribution of carriers in $\mathbf{k}$-space at $t = 10$ ps is shown for calculations with and without impurity scattering. In the calculation without non-magnetic impurity scattering, the initial carrier distribution is slightly broadened. If the non-

Figure 9.1.: Form [Pub10]: (a): Spin dynamics in a 4 nm wide $Cd_{0.93}Mn_{0.07}Te$ quantum well with ($J_0 = 110$ meVnm^3) and without ($J_0 = 0$) non-magnetic impurity scattering calculated using the full quantum kinetic equations of [Pub10] (QKT1), using quantum kinetic equations neglecting source terms for correlations similar to $b_{l_1 n_1 \mathbf{k}_1}^{l_2 n_2 \mathbf{k}_2 III}$ (QKT2) and using the Markovian limit of QKT2. The inset shows a magnification of the region where the simulation without non-magnetic scattering predicts a non-monotonic behavior. (b): Spectral distribution of carriers at $t = 0$ and $t = 10$ ps.

magnetic impurity scattering is accounted for, the redistribution of carriers is very much enhanced, so that states with kinetic energies of a few meV above the initial peak are occupied. Since, as explained in [Pub6], the non-Markovian features in the spin dynamics are only strong for carriers very close to the band edge, the redistribution of carriers to states with much higher kinetic energy suppresses the non-Markovian behavior drastically.

The substantial redistribution of carriers in **k**-space for $B = 0$ is at odds with the conservation of the single-particle energies. Note, however, that the strong non-magnetic carrier-impurity interaction leads to the formation of correlations with a significant amount of (negative) correlation energy, as depicted in Fig. 9.2. This correlation energy compensates the increase of the kinetic energy of the carriers. Furthermore, Fig. 9.2 shows that the analytic expressions for the correlation energies derived in [Pub10] in the Markov limit reproduce the correlation energies obtained from the quantum kinetic simulations very well after a quasi-stationary value of the correlation energy is reached.

The fact that the non-magnetic impurity scattering, which is always present in DMS, suppresses the characteristic features of non-Markovian behavior in the case of the conduction band of Mn-doped CdTe raises the question whether there are actually situations in which non-Markovian behavior can be expected to appear in real DMS samples. To this end, we study in [Pub10] the spin dynamics in a degenerate valence band in a $Cd_{0.93}Mn_{0.07}Te$ quantum well and we simulate the spin dynamics using the material parameters for heavy holes. Since the magnetic coupling constant in the valence band of Mn-doped CdTe is about 4 times larger than in the conduction band [54] and the non-magnetic coupling constant is very small in the valence band [99], the non-Markovian
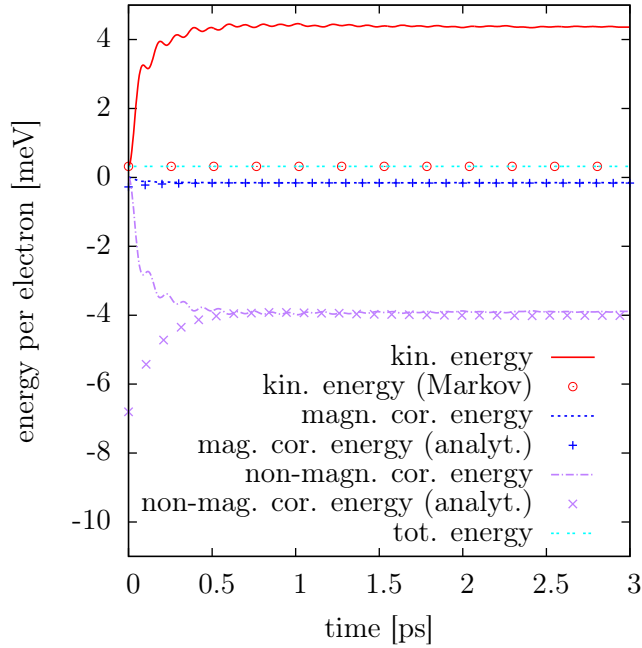
Figure 9.2.: From [Pub10]: Kinetic and correlation energies per electron according to the quantum kinetic calculation including non-magnetic impurity scattering (lines). The results of the analytic expressions for the correlation energies for the occupations obtained from the quantum kinetic simulation are shown as pluses and crosses. The kinetic energy according to the Markovian calculation is depicted by the circles.

effects are found to be more pronounced and no suppression due to the non-magnetic impurity scattering is observable in the valence band. Of course, a more realistic valence band structure requires to take into account the confinement potential, strain and the spin-orbit coupling. These effects lead, e.g., to a splitting between the heavy-hole and light-hole bands. Thus, the results of these calculations are not expected to describe comprehensively the hole spin dynamics in a real DMS quantum well, but they show that, in the valence band, the non-magnetic impurity scattering does not suppress the non-Markovian effects in the spin dynamics in DMS.

Furthermore, the influence of the non-magnetic impurity scattering on the spin dynamics in DMS in the presence of an external magnetic field parallel and perpendicular to the initial carrier spin polarization is discussed in [Pub10]. If the initial carrier spin polarization is parallel to the external field, it was already shown in [Pub8] that the quantum kinetic theory and its Markov limit predict very different stationary values of the carrier spin polarization. This is related to a broadening of the distribution of scattered carriers, which is enabled by the release of magnetic carrier-impurity correlation energy. In [Pub10] it is found that the non-magnetic carrier-impurity interaction leads to additional contributions to the carrier-impurity correlation energies, which enhances the broadening of the scattered carrier distribution and thereby increases the difference between the stationary values of the carrier spin polarizations according to the quantum kinetic and the Markovian calculations.

If an external magnetic field is applied perpendicular to the initial carrier spin polarization, the carrier spins precess about the effective magnetic field due to the external field and the impurity magnetization. It was shown in [Pub7] that the carrier spin precession frequency is renormalized due to the magnetic carrier-impurity interaction. In

[Pub10], we find that, when the non-magnetic interaction between carriers and impurities is considered, a new contribution to the frequency renormalization appears, which is absent if either the magnetic or the non-magnetic interaction is disregarded. In the case of the conduction band of $Cd_{1-x}Mn_xTe$, the magnetic and non-magnetic coupling constants have different signs, which results in a partial cancellation of the purely magnetic contribution to the renormalization and the new contribution due to the non-magnetic impurity scattering. In contrast to the purely magnetic contribution, which is only significantly strong in a narrow regime of excitation conditions, the new contribution is important in many more situations. Because the magnitude of the frequency renormalization is of the order of a few percent of the mean-field value of the precession frequency, it can be expected that the renormalization of the precession frequency is strong enough to be observable in experiments.

In summary, non-magnetic scattering of electrons at the impurities in DMS leads to a suppression of some non-Markovian effects in the spin dynamics in certain situations, such as in the conduction band of Mn-doped CdTe. The non-magnetic interaction leads also to the build-up of non-magnetic carrier-impurity correlations with significant correlation energies facilitating a strong redistribution of carriers in $\mathbf{k}$-space. In the presence of an external magnetic field, the correlations are responsible for significantly modifying the asymptotic value of the carrier spin polarization parallel to the external field at long times. Furthermore, the magnetic and non-magnetic carrier-impurity correlations renormalize the carrier spin precession frequencies about a few percent.

Part III.

Conclusion

10. Summary & Outlook

10.1. Summary

In this thesis, a quantum kinetic description of the spin dynamic in diluted magnetic semiconductors was presented including a number of interactions: the magnetic s-d exchange interaction between carriers and magnetic impurities, the Zeeman energies of carriers and impurities, spin-orbit interactions in the form of $\mathbf{k}$-dependent effective fields, the light-matter interaction as well as the non-magnetic interaction between carriers and impurities.

Earlier studies [23, 24] focused on the s-d interaction and the case of zero magnetic field and impurity magnetization and demonstrated that in some cases, such as in two-dimensional diluted magnetic semiconductors, the quantum kinetic theory yields a spin dynamics that cannot be captured by Markovian rate equations. In other cases, in particular in bulk DMS, the quantum kinetic theory predicts an exponential decay of the optically induced carrier spins, which, for the case of vanishing magnetic field and impurity spin, agrees well with rate equations where the spin-transfer rate is obtained by Fermi's golden rule.

In [Pub1] and [Pub2], we showed how Markovian effective equations can be derived from the quantum kinetic theory that reproduce well the dynamics predicted by the quantum kinetic calculations for three-dimensional systems, even in the case with non-zero impurity magnetization. In comparison with Fermi's golden rule, the approach presented here has the advantage that one obtains equations not only for the carrier spin component parallel to the impurity magnetization, but also for the perpendicular component, which is relevant for the description of experiments in Voigt geometry. The effective equations show some similarities to the phenomenological Landau-Lifshitz-Gilbert equations. However, the effective equations contain corrections due to the quantum mechanical nature of the impurity spins as well as energetic splittings and Pauli-blocking effects. The energetic splittings in the Markov limit are found to be related to a precession-type motion of the carrier-impurity correlations, which is important for a suitable description of the spin dynamics, although the source terms responsible for the precession of the correlations are higher than leading order in the coupling constant J_{sd}.

The effective equations derived in [Pub2] were applied to study the interplay between the spin-orbit coupling and the s-d interaction in diluted magnetic semiconductors with strong Rashba and Dresselhaus fields in [Pub3], [Pub4] and [Pub5]. It was found that in narrow band gap materials and for optical excitations well above the band gap, the spin-orbit coupling can compete with the exchange interaction. In this situation, the spin dynamics can become quite complex. For example, in the presence of strong spin-orbit fields, not only the spin component perpendicular to the impurity magnetization shows oscillations with approximately the frequency corresponding to the precession in the mean field of the impurity magnetization, but similar oscillations are also superimposed

on the decay of the parallel carrier spin component. In many cases, the dephasing of carrier spins in the **k**-dependent spin-orbit field is strongly suppressed by the effective field originating from the impurity magnetization. Moreover, while the *s-d* interaction leads to an exponential decay of the carrier spins in the Markov limit, we find that the dephasing in an **k**-dependent effective field is better described by a Gaussian time evolution than by an exponential decay.

Taking the Zeeman energies of carriers and impurities into account in [Pub5] allows us to derive expressions for the magnetic-field dependence of the parallel and perpendicular carrier-impurity spin transfer rates. In contrast to earlier works in the literature, our approach yields results that conserve the total single-particle energies in individual spin-flip scattering processes.

The origin of non-Markovian features in the spin dynamics in diluted magnetic semi-conductors was investigated in [Pub6]. It turns out that for a vanishing magnetic field, the shape of the time evolution of the spin of a single electron with a defined kinetic energy depends approximately only on the spectral distance to the band edge, i.e., on the ratio between the kinetic energy and the Markovian spin transfer rate. The non-Markovian effects are important if the excited carriers are spectrally very close to the band edge and the non-Markovian behavior disappears if the spectral distance to the band edge is large.

Taking explicitly the carrier-impurity correlations into account in the quantum kinetic theory enabled us to study many-body effects in diluted magnetic semiconductors in [Pub7], such as a renormalization of the carrier spin precession frequency and the build-up of correlation energy. In two-dimensional systems, logarithmic divergences similar to those appearing in the Kondo effect were found. However, these divergences do not lead to unphysical results in the spin dynamics, since, on the one hand, they are integrable and yield finite values when weighted with a non-singular carrier distribution. On the other hand, the divergences are predicted only in the Markovian limit assuming $t \to \infty$ while for finite times t finite values are obtained.

The theory was extended in [Pub8] to incorporate simultaneously the optical excitation as well as the Zeeman energies on a quantum kinetic level. This study predicts non-Markovian features in the spin dynamics as expected from the initial-value calculations presented in previous works. A non-monotonic time evolution of the carrier spin polarization is found not only in situations where the laser pulse duration is comparable to the Markovian spin transfer time, but signatures of non-Markovian behavior are also obtained if the pulse duration is longer. Furthermore, in [Pub8], the optical excitation in the presence of an external magnetic field was discussed. While the non-monotonic behavior of the spin dynamics is suppressed in an external field, the external field opens up another possibility to detect quantum kinetic features, because significantly different stationary values of the carrier spin polarization at long times are obtained in simulations using the quantum kinetic equations and in the Markovian calculations. This is a consequence of a correlation-induced broadening of the distribution of spin-flip-scattered carriers, which is not related to the energy-time uncertainty, but rather a genuine many-body effect.

The investigation of the possibility to efficiently control the spins in semiconductors via the spin-orbit interaction and optical excitation using twisted light in [Pub9] leads to the conclusion that this is only possible in systems which are small enough so that the individual energy levels of the carriers can be resolved. In contrast, towards the

quasi-continuous limit, the spin dynamics becomes more and more independent of the orbital angular momentum of the light.

Finally, the influence of non-magnetic scattering at impurities on the spin dynamics in diluted magnetic semiconductors was discussed in [Pub10]. In the conduction band of Mn-doped CdTe, the scattering at the spin-independent local potential caused by the incorporation of the Mn impurities results in a strong suppression of the non-Markovian effects in the spin dynamics. Model calculations show that this is not expected to be the case in the valence band of $Cd_{1-x}Mn_xTe$. The non-magnetic carrier-impurity interaction leads to the build-up of non-magnetic carrier-impurity many-body correlations that are, in the case of the conduction band of $Cd_{1-x}Mn_xTe$, much stronger than the magnetic correlations. As a consequence, the redistribution of carriers in **k**-space, the correlation energies, the renormalization of the carrier spin precession frequency as well as the changes of the asymptotic values of the carrier spin polarization for long times compared with the Markovian results in the presence of an external magnetic field are significantly enhanced.

10.2. Outlook

Although a number of interactions are already included in the present quantum kinetic description of the spin dynamics in diluted magnetic semiconductors, some important effects that are present in real samples have not been discussed so far. Most of these effects can, in principle, be incorporated into the quantum kinetic framework. For a few of them, there is already work in progress at the time of the writing of this thesis.

10.2.1. Exciton spin dynamics

It is known [100] that the optical excitation of intrinsic semiconductors leads directly to the creation of excitons rather than free electrons and holes. It is therefore interesting to investigate the role of the Coulomb correlations between electrons and holes for the decay of the spin polarization detected in experiments. For example, as a consequence of the conservation of momentum, usually only excitons with center of mass momentum $\mathbf{K} \approx 0$ are optically excited, where strong non-Markovian effects are expected. Moreover, the question arises whether the carrier-impurity interactions can induce transitions between 1s and 2s exciton states. Reformulating the quantum kinetic theory and simulating the exciton spin dynamics in diluted magnetic semiconductors is a project that is currently carried out by Florian Ungar. Some preliminary results show that a large part of the quantum kinetic theory presented in the present thesis is relevant in the discussion of the exciton spin dynamics, but there are also a number of new challenges, since, e.g., the shape of the excitonic wave functions enters in the equations of motion. Understanding the spin dynamics of excitons is crucial for connecting the quantum kinetic theory with experiments. For example, in order to suppress exciton formation and to detect only free conduction band electrons, some experiments used n-doped CdMnTe samples [21]. Other studies [33], however, indicate that upon optical excitation n-doped CdTe tends to facilitate the formation of trions due to the relatively strong binding energies in CdTe. Thus, experiments on the spin dynamics in diluted magnetic semiconductors are easier to perform on excitons than on quasi-free conduction band electrons. Therefore, a quantum

kinetic theory for the exciton spin dynamics could bridge the gap between the theory presented in this thesis and experiments.

10.2.2. Spin dynamics in the valence band

The theoretical description of the valence band in diluted magnetic semiconductors is both interesting and challenging. It is interesting, since ferromagnetism in DMS has only been demonstrated in systems with a large number of holes, such as in GaMnAs or strongly p-doped CdMnTe, whereas ferromagnetism mediated by conduction band electrons could not be verified experimentally [13, 79]. This is due to the fact, that the carrier-impurity interaction in the valence band is typically about a factor of 4 stronger in the valence band than in the conduction band [54]. Furthermore, it was found in [Pub10] that non-magnetic impurity scattering, which suppresses characteristic features of non-Markovian behavior in the spin dynamics of conduction band electrons in Mn-doped CdTe, is very inefficient in the valence band. Thus, non-Markovian signatures in the spin dynamics are expected to be more clearly observable in the valence band than in the conduction band. Furthermore, a comprehensive description of the spin dynamics of excitons requires taking into account the hole spin dynamics.

However, the theoretical description of the hole spin is challenging, because, for a realistic description, one has to account at least for the 4 subbands comprised of the heavy-hole and light-hole bands, which can be significantly coupled for $\mathbf{k} \neq 0$. In principle, it is straightforward to formulate a quantum kinetic theory for the spin dynamics in the valence band by replacing the kinetic energy H_0 and the $\mathbf{k}$-dependent effective field by a Luttinger Hamiltonian [37, 39, 101], but, as in the discussion of the $\mathbf{k}$-dependent effective spin-orbit fields, it is necessary to resolve the angles of the wave vector, which increases the numerical demands enormously. A similar problem is faced in the microscopic quantum kinetic description of the D'yakonov-Perel' mechanism, which is the topic of Michael Cosacchi's Bachelor thesis. There, he shows that the computation time of quantum kinetic calculations can be strongly reduced when the corresponding density matrices and correlations are Fourier decomposed with respect to the polar angles of the wave vectors $\mathbf{k}$. The calculations converge fast and only a few Fourier coefficients have to be accounted for. We expect that a similar approach makes full quantum kinetic calculations of the hole spin dynamics in DMS feasible.

In the conduction band, it is possible to derive Markovian equations, which enable a more intuitive understanding of the processes involved in the spin dynamics in diluted magnetic semiconductors. In order to derive the Markov limit, it is, however, necessary to invert the mean-field dynamics. This is relatively easy for the conduction band, which, in a mean-field description, can be decomposed into a set of decoupled effective two-level systems, or, equivalently, one dipolar spin vector for each wave vector $\mathbf{k}$. For the valence band where the heavy and light holes have to be considered, obtaining the mean-field dynamics of the hole spins involves calculating the exponential of a 4×4 matrix, which is, in general, hard to do analytically.

One idea to retain an intuitive rate-type description also for the hole spin dynamics is to use the fact that in narrow quantum wells the heavy- and light-hole bands are often split considerably. Thus, by tuning the laser frequency correspondingly, one can selectively excite, e.g., lower-energetic heavy holes. This led *Merkulov et al.* [102] to consider the heavy and light holes separately as effective pseudospin-$\frac{1}{2}$ systems with anisotropic g-

factors. However, this treatment neglects the **k**-dependent coupling between heavy and light holes contained in the Luttinger Hamiltonian, which can cause a fast dephasing of the hole spins. Thus, we propose a more rigorous derivation of the effective heavy- and light-hole subsystems: If the heavy-hole–light-hole splitting is large, the effects of the coupling to the light holes can be treated perturbatively by a Schrieffer-Wolff transformation. Preliminary calculations show that this procedure yields corrections to the effective heavy-hole Hamiltonian of the order $\mathcal{O}\left(\omega_h^3 k^0\right) + \mathcal{O}\left(\omega_h^1 k^2\right)$ in third order in the inverse band splitting, where ω_h is the magnitude of the effective magnetic field for the valence band holes comprised of an external field and the field due to the impurity magnetization in mean-field approximation. This way, the dynamics of the hole spins is described by an effective two-level system for each value of the wave vector and one can derive Markovian equations from the quantum kinetic theory, from which effective heavy- and light-hole spin transfer rates can be extracted.

10.2.3. Modified inhomogeneous g-factor mechanism in DMS

In three-dimensional diluted magnetic semiconductors, the decay of the carrier spin after optical excitation is experimentally found to be much faster than predicted by the spin transfer rates according to Fermi's golden rule [65]. To explain these findings, it was assumed that the impurity spin polarization in the sample is inhomogeneous. When the carriers move through the semiconductor, the carrier spins therefore experience a dephasing. Since the carrier-impurity spin transfer times in three-dimensional systems are rather large, the dephasing can be more efficient and can dominate the decay of the total carrier spin polarization. This picture was also used to explain qualitatively the non-monotonic magnetic-field dependence of the spin relaxation times measured in some experiments [21] in DMS quantum wells.

It is noteworthy that a non-monotonic spin relaxation time is also found in non-magnetic GaAs [103]. There, the effect was explained by invoking the inhomogeneous-g-factor mechanism: The Schrieffer-Wolff transformation which has been used to derive the **k**-dependent effective fields for the description of spin-orbit coupling effects mixes conduction and valence band states. Due to the conduction-band–valence-band mixing, the effective electron g-factor becomes **k**-dependent. This leads to a dephasing of the carrier spins that has its origins in **k**-space and not in real space.

In the case of diluted magnetic semiconductors, the mixing between the conduction and valence bands results in a contribution to the carrier-impurity interaction in the effective conduction band originating from the *p-d* interaction in the valence band. Thus, the carrier-impurity interaction for the effective conduction band electrons becomes **k**-dependent. Because the carrier-impurity interaction in DMS is usually much stronger than the Zeeman term, the dephasing in the **k**-dependent field for electrons caused by the impurity magnetization is expected to be much more efficient than the original inhomogeneous-g-factor mechanism for a **k**-dependent g-factor alone. It is an interesting question what contribution to the fast dephasing of carrier spins in three-dimensional diluted magnetic semiconductors reported in Ref. [65] comes from such an inhomogeneous-g-factor-type mechanism in DMS.

In narrow quantum wells where the lowest confinement state has a significant value of $\langle k_z^2 \rangle \approx \left(\frac{\pi}{d}\right)^2$, the strongly **k**-dependent band mixing has been shown to lead to a significant change of the effective coupling constant measured by spin-flip Raman scattering

and by the giant Zeeman splitting of excitons [57]. However, this study only considered static quantities at the band edge ($k_x = k_y = 0$) and made no predictions regarding the influence on the spin dynamics.

We now present preliminary results for the effects of the inhomogeneous-g-factor-type mechanism mentioned above on the spin dynamics in DMS, where we employ a second order Schrieffer-Wolff transformation as in Ref. [57], but we allow for non-zero values of k_x and k_y: We apply the transformation matrix that block-diagonalizes an 8×8 Kane Hamiltonian up to second order in $\mathbf{k}$ to the spin matrices $\mathbf{s}^e$ and $\mathbf{s}^h$ in the s-d and p-d carrier-impurity exchange interactions for conduction and valence band electrons and restrict ourselves to the effective conduction band block obtained after block-diagonalization of the crystal Hamiltonian H_0. In the mean-field approximation, the effective carrier-impurity interaction H_{sd}^{eff} comprised of contributions from the original Hamiltonians H_{sd} and H_{pd} reads:

$$H_{s/p-d}^{\text{eff}} \overset{\text{MF}}{\approx} \frac{N_{\text{Mn}}}{V} \sum_{\sigma\sigma'\mathbf{k}} \sum_{ij} \langle S^i \rangle \mathcal{J}_{ij}(\mathbf{k}) s_{\sigma\sigma'}^j \tilde{c}_{\sigma\mathbf{k}}^\dagger \tilde{c}_{\sigma'\mathbf{k}}, \tag{10.1}$$

where $\tilde{c}_{\sigma\mathbf{k}}^\dagger$ now creates effective conduction band electrons with pseudospin-index σ. Thus, the effective coupling constant $\mathcal{J}_{ij}(\mathbf{k})$ is now a matrix

$$\mathcal{J}_{ij} = \left[J_{sd} + (-J_{sd}\lambda_1 + \gamma J_{pd}\lambda_2)k^2 \right]\delta_{ij} - \gamma J_{pd}\lambda_3 2k_i k_j, \tag{10.2a}$$

$$\lambda_1 = \frac{2P^2}{3E_g^2} + \frac{P^2}{3(E_g + \Delta_0)^2} \approx 0.279 \text{ nm}^2, \tag{10.2b}$$

$$\lambda_2 = \frac{4P^2}{9E_g^2} + \frac{P^2}{9(E_g + \Delta_0)^2} + \frac{4P^2}{9E_g(E_g + \Delta_0)} \approx 0.268 \text{ nm}^2, \tag{10.2c}$$

$$\lambda_3 = \frac{P^2}{9E_g^2} + \frac{P^2}{9(E_g + \Delta_0)^2} - \frac{2P^2}{9E_g(E_g + \Delta_0)} \approx 0.005 \text{ nm}^2, \tag{10.2d}$$

where the standard parameters for CdTe [39] have been used. A large part of the valence band coupling constant J_{pd} stems from virtual hopping and depends on the energy difference between the valence band electrons and the energy levels corresponding to a Mn impurity occupied with 4 and 6 electrons, respectively. For effective conduction band electrons, one has to replace the valence band energy by the conduction band energy, i.e., the energy difference is changed by a value corresponding to the band gap E_g. This leads to a modification of the value of J_{pd} by the factor $\gamma \approx 1.36$ for effective conduction band electrons [57]. It is noteworthy that the factor λ_3, which determines the anisotropic part of the coupling constant $\mathcal{J}_{ij}$, is about two orders of magnitude smaller than the factors λ_1 and λ_2, so that the anisotropy can be neglected.

To estimate the effects of the band mixing on the spin dynamics, we calculate the spin dynamics after optical excitation of a Gaussian electron distribution centered at $\mathbf{k} = 0$ with a standard deviation of $E_s = 3$ meV with initial spin polarization perpendicular to an external magnetic field with $B = 100$ mT in the quantum well plane. For the calculations, the Markovian rate equations according to [Pub5] are used where J_{sd} is substituted by the isotropic part of $\mathcal{J}_{ij}$ at $k_x = k_y = 0$ in the expression for the rates. For the precession of the carrier spins, the dependence of the isotropic part of $\mathcal{J}_{ij}$ on k_x and k_y is accounted for.
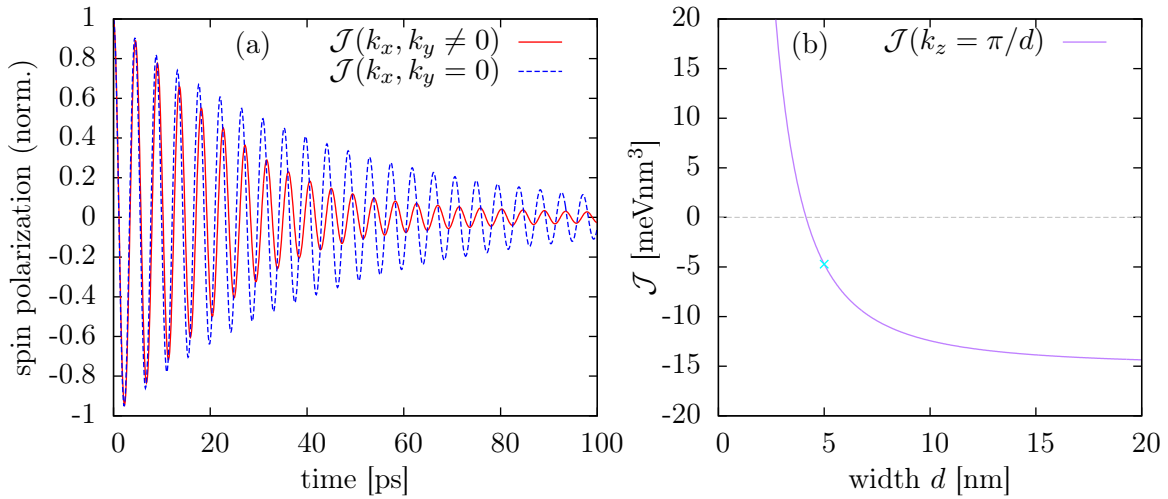
Figure 10.1.: (a): Time evolution of the spin polarization perpendicular to an external magnetic field $B = 100$ mT with (red solid line) and without (blue dashed line) accounting for dephasing due to the dependence of the isotropic part of $\mathcal{J}_{ij}$ on k_x and k_y in a quantum well with width $d = 5$ nm. The initial carrier occupation is a Gaussian with a standard deviation $E_s = 3$ meV centered at the band edge. (b): Dependence of the isotropic part of $\mathcal{J}_{ij}$ on the quantum well width (purple solid line). The value for $d = 5$ nm used in the calculation in (a) is highlighted by the cyan cross in (b).

The results for the spin dynamics are shown in Fig. 10.1(a). It is found that the spin decays about 40% faster if the dephasing due to the **k**-dependence of the effective coupling constant is accounted for. In Fig. 10.1(b), the dependence of the effective coupling constant at $k_x = k_y = 0$ on the width of the quantum well is presented, where it is assumed that the width defines the wave vector in the growth direction via $\sqrt{\langle k_z^2 \rangle} \approx \frac{\pi}{d}$. While the bulk value of the effective coupling constant for the conduction band in CdTe is negative, the coupling constant crosses the zero and eventually becomes positive for very narrow quantum wells.

Even on this level of theory, we find that an inhomogeneous-g-factor-type mechanism in DMS can indeed significantly influence the spin dynamics in DMS. However, more work is needed to describe this mechanism on a quantum kinetic level. One major challenge is that, in H_{sd} and H_{pd}, creation and annihilation operators with two different wave vectors **k** and **k**′ appear, so that a unitary transformation of these Hamiltonians actually leads to a dependence of the effective coupling constant on two wave vectors, which makes the bookkeeping and interpretation more difficult. For this reason, the problem of rigorously deriving a quantum kinetic description of this mechanism is beyond the scope of this thesis and will be addressed in the future.

An interesting aspect in this context is that the mechanism proposed above predicts a particularly strong dephasing if the carrier distribution in **k**-space is rather broad. In [Pub10], it was found that the non-magnetic carrier-impurity interaction leads to a significant redistribution of carriers in **k**-space that results in very broad distributions and therefore promotes such a spin dephasing. Thus, it can be expected that quantum kinetic effects such as the build-up of correlation energy, which facilitates the scattering to states with higher kinetic energy, are indeed necessary for an accurate description of the dephasing of carrier spins due to the **k**-dependent mixing of conduction and valence band states.

10.2.4. Further investigations

A number of other extensions to the quantum kinetic theory can be thought of. For example, the correlation expansion can be truncated at a higher level. This enables an investigation of the formation of impurity-impurity correlations, or the description of carrier-carrier scattering in diluted magnetic semiconductors. Furthermore, it is interesting to consider disorder effects like the clustering of magnetic impurities and the direct interaction between impurities at neighboring cation sites. For large magnetic fields, it is desirable to consider the effects of Landau quantization.

Another promising line of research is to reformulate the quantum kinetic theory so that it can be used to describe also spin transport phenomena, which is a topic that is particularly interesting for applications of diluted magnetic semiconductors in spintronics devices.

Furthermore, as can be seen by the analogies of the spin physics in diluted magnetic semiconductors to the Kondo effect in metals with magnetic impurities, there is no fundamental limitation of the quantum kinetic theory to the usual II-VI diluted magnetic semiconductors. Thus, the theory can, in principle, also be applied to other materials like graphene or transition metal dichalcogenides provided that technological advances enable a magnetic doping of these materials. In particular, it is interesting to study the effects of magnetic doping on the spin dynamics in HgTe/CdTe quantum wells, since they are, on the one hand, compatible with magnetic doping, on the other hand, they can form topological insulators [104, 105].

Thus, the quantum kinetic description of the spin dynamics in diluted magnetic semiconductors presented in this thesis not only yields results for the cases studied in this work but also enables further studies for other systems and situations.

Acknowledgement

I like to express my gratitude towards a number of people who have supported me in my professional and private life during my studies and research at the Universität Bayreuth.

Especially, I am grateful to my supervisor Martin Axt for sharing his expertise and time and giving me the freedom to choose the directions of my research. He also provided me and the other group members with the opportunity to attend a number of international conferences, which allowed me to broaden my horizon and to get in contact with other scientists.

Furthermore, I want to emphasize that the present work would literally not have been possible without the diligent work of Christoph Thurn, who developed the truncation scheme used in the present thesis. He put considerable effort in checking the consistency of the huge set of equations that he derived. Moreover, he supervised me during the time of my Diploma thesis and he taught me many things about working in science and research.

I also like to thank the other present and former members of our group, Alexei Vagov, Andreas Barth, Martin Glässl, Jan Steffan, Tim Seidelmann and Kevin Keil for the vivid discussions and especially those with whom I have directly worked together, Florian Ungar, Michael Cosacchi and Pablo I. Tamborenea, for the pleasant and constructive atmosphere and their patience during our discussions. Furthermore, André Brand was always available to share his knowledge about mathematical and numerical questions and Markus Hilt kept the computers running.

Most importantly, I am greatly indebted to my family for their unconditional support and my girlfriend Kerstin Pramberger for the love and joy she brings into my life. Finally, I want to thank my friends, in particular Christiane Jungnickel and the members of the Taekwondo sports group at the Universität Bayreuth for keeping me company during my years in Bayreuth.

Bibliography

[1] I. Žutić, J. Fabian, and S. Das Sarma, Rev. Mod. Phys. **76**, 323 (2004).

[2] S. A. Wolf, D. D. Awschalom, R. A. Buhrman, J. M. Daughton, S. von Molnár, M. L. Roukes, A. Y. Chtchelkanova, and D. M. Treger, Science **294**, 1488 (2001).

[3] D. Awschalom and M. Flatté, Nat. Phys. **3**, 153 (2007).

[4] M. N. Baibich, J. M. Broto, A. Fert, F. Nguyen Van Dau, F. Petroff, P. Etienne, G. Creuzet, A. Friederich, and J. Chazelas, Phys. Rev. Lett. **61**, 2472 (1988).

[5] G. Binasch, P. Grünberg, F. Saurenbach, and W. Zinn, Phys. Rev. B **39**, 4828 (1989).

[6] S. Datta and B. Das, Appl. Phys. Lett. **56**, 665 (1990).

[7] J. Åkerman, Science **308**, 508 (2005).

[8] G. Schmidt, D. Ferrand, L. W. Molenkamp, A. T. Filip, and B. J. van Wees, Phys. Rev. B **62**, R4790 (2000).

[9] R. Fiederling, M. Keim, G. Reuscher, W. Ossau, G. Schmidt, A. Waag, and L. W. Molenkamp, Nature **402**, 787 (1999).

[10] J. K. Furdyna, J. Appl. Phys. **64**, R29 (1988).

[11] H. Ohno, A. Shen, F. Matsukura, A. Oiwa, A. Endo, S. Katsumoto, and Y. Iye, Appl. Phys. Lett. **69**, 363 (1996).

[12] T. Dietl, H. Ohno, F. Matsukura, J. Cibert, and D. Ferrand, Science **287**, 1019 (2000).

[13] T. Dietl and H. Ohno, Rev. Mod. Phys. **86**, 187 (2014).

[14] A. Kaminski and S. Das Sarma, Phys. Rev. Lett. **88**, 247202 (2002).

[15] T. Jungwirth, J. Sinova, J. Mašek, J. Kučera, and A. H. MacDonald, Rev. Mod. Phys. **78**, 809 (2006).

[16] B. König, I. A. Merkulov, D. R. Yakovlev, W. Ossau, S. M. Ryabchenko, M. Kutrowski, T. Wojtowicz, G. Karczewski, and J. Kossut, Phys. Rev. B **61**, 16870 (2000).

[17] R. Akimoto, K. Ando, F. Sasaki, S. Kobayashi, and T. Tani, Phys. Rev. B **57**, 7208 (1998).

[18] C. Camilleri, F. Teppe, D. Scalbert, Y. G. Semenov, M. Nawrocki, M. Dyakonov, J. Cibert, S. Tatarenko, and T. Wojtowicz, Phys. Rev. B **64**, 085331 (2001).

[19] S. A. Crooker, D. D. Awschalom, J. J. Baumberg, F. Flack, and N. Samarth, Phys. Rev. B **56**, 7574 (1997).

[20] R. Akimoto, K. Ando, F. Sasaki, S. Kobayashi, and T. Tani, Phys. Rev. B **56**, 9726 (1997).

[21] Z. Ben Cheikh, S. Cronenberger, M. Vladimirova, D. Scalbert, F. Perez, and T. Wojtowicz, Phys. Rev. B **88**, 201306 (2013).

[22] C. Thurn and V. M. Axt, Phys. Rev. B **85**, 165203 (2012).

[23] C. Thurn, M. Cygorek, V. M. Axt, and T. Kuhn, Phys. Rev. B **87**, 205301 (2013).

[24] C. Thurn, M. Cygorek, V. M. Axt, and T. Kuhn, Phys. Rev. B **88**, 161302(R) (2013).

[25] J. Kossut, phys. stat. sol. (b) **72**, 359 (1975).

[26] E. Tsitsishvili and H. Kalt, Phys. Rev. B **73**, 195402 (2006).

[27] J. H. Jiang, Y. Zhou, T. Korn, C. Schüller, and M. W. Wu, Phys. Rev. B **79**, 155201 (2009).

[28] Y. G. Semenov, Phys. Rev. B **67**, 115319 (2003).

[29] G. Dresselhaus, Phys. Rev. **100**, 580 (1955).

[30] Y. A. Bychkov and E. I. Rashba, J. Phys. C: Solid State Phys. **17**, 6039 (1984).

[31] G. Bastard, *Wave Mechanics Applied to Semiconductor Heterostructures*, Monographies de physique (Les Editions de Physique, JOUVE, France, 1990) pp. 35–54.

[32] S. A. Crooker, E. Johnston-Halperin, D. D. Awschalom, R. Knobel, and N. Samarth, Phys. Rev. B **61**, R16307 (2000).

[33] K. Kheng, R. T. Cox, Y. Merle d'Aubigné, M. Mamor, N. Magnea, H. Mariette, K. Saminadayar, and S. Tatarenko, Surf. Sci. **305**, 225 (1994).

[34] A. Esser, E. Runge, R. Zimmermann, and W. Langbein, Phys. Rev. B **62**, 8232 (2000).

[35] G. L. Bir, A. Aronov, and G. E. Pikus, Zh. Eksp. Teor. Fiz. **69**, 1382 (1975), [English translation: Sov. Phys. JETP, **42**, 702 (1975)].

[36] A. Golnik and J. Spałek, J. Magn. Magn. Mater. **54**, 1207 (1986).

[37] M. W. Wu, J. H. Jiang, and M. Q. Weng, Phys. Rep. **493**, 61 (2010).

[38] M. I. Dyakonov, ed., *Spin Physics in Semiconductors*, Springer Series in Solid-State Sciences, Vol. 157 (Springer, 2008) pp. 115–134.

[39] R. Winkler, *Spin-Orbit Coupling Effects in Two-Dimensional Electron and Hole Systems*, Springer Tracts in Modern Physics, Vol. 191 (Springer, 2003).

[40] F. Meier and B. P. Zakharchenya, eds., *Optical Orientation*, Modern Problems in Condensed Matter Sciences, Vol. 8 (North-Holland Amsterdam, 1984).

[41] E. A. Chekhovich, M. M. Glazov, A. B. Krysa, M. Hopkinson, P. Senellart, A. Lemaître, M. S. Skolnick, and A. Tartakovskii, Nature Physics **9**, 74 (2013).

[42] P. Löwdin, J. Chem. Phys. **19**, 1396 (1951).

[43] J. R. Schrieffer and P. A. Wolff, Phys. Rev. **149**, 491 (1966).

[44] L. L. Foldy and S. A. Wouthuysen, Phys. Rev. **78**, 29 (1950).

[45] M. Wu and C. Ning, Eur. Phys. J. B **18**, 373 (2000).

[46] M. I. D'yakonov and V. I. Perel', Zh. Eksp. Teor. Fiz. **60**, 1954 (1971), [English translation: Sov. Phys. JETP 33, 1053 (1971)].

[47] Y. Yafet, Solid State Physics, **14**, 1 (1963).

[48] R. J. Elliott, Phys. Rev. **96**, 266 (1954).

[49] J. Zhou and M. W. Wu, Phys. Rev. B **77**, 075318 (2008).

[50] R. Winkler, Phys. Rev. B **70**, 125301 (2004).

[51] F. Rossi and T. Kuhn, Rev. Mod. Phys. **74**, 895 (2002).

[52] J. Gaj, R. Planel, and G. Fishman, Solid State Commun. **29**, 435 (1979).

[53] A. Podlesnyak, S. Streule, J. Mesot, M. Medarde, E. Pomjakushina, K. Conder, A. Tanaka, M. W. Haverkort, and D. I. Khomskii, Phys. Rev. Lett. **97**, 247208 (2006).

[54] J. Kossut and J. Gaj, eds., *Introduction to the Physics of Diluted Magnetic Semiconductors*, Springer Series in Materials Science No. 144 (Springer, Berlin, 2011).

[55] J. Kondo, Prog. Theor. Phys. **32**, 37 (1964).

[56] B. E. Larson, K. C. Hass, H. Ehrenreich, and A. E. Carlsson, Phys. Rev. B **37**, 4137 (1988).

[57] I. A. Merkulov, D. R. Yakovlev, A. Keller, W. Ossau, J. Geurts, A. Waag, G. Landwehr, G. Karczewski, T. Wojtowicz, and J. Kossut, Phys. Rev. Lett. **83**, 1431 (1999).

[58] A. Bhattacharjee, G. Fishman, and B. Coqblin, Physica B **117&118**, 449 (1983).

[59] A. C. Hewson, *The Kondo Problem to Heavy Fermions* (Cambridge University Press, 1993).

[60] S. Cronenberger, M. Vladimirova, S. V. Andreev, M. B. Lifshits, and D. Scalbert, Phys. Rev. Lett. **110**, 077403 (2013).

[61] F. J. Teran, M. Potemski, D. K. Maude, D. Plantier, A. K. Hassan, A. Sachrajda, Z. Wilamowski, J. Jaroszynski, T. Wojtowicz, and G. Karczewski, Phys. Rev. Lett. **91**, 077201 (2003).

[62] E. Tsitsishvili and H. Kalt, Phys. Rev. B **77**, 155305 (2008).

[63] O. Morandi, P.-A. Hervieux, and G. Manfredi, Phys. Rev. B **81**, 155309 (2010).

[64] G. Bastard and R. Ferreira, Surf. Sci. **267**, 335 (1992).

[65] K. E. Rönnburg, E. Mohler, H. G. Roskos, K. Ortner, C. R. Becker, and L. W. Molenkamp, Phys. Rev. Lett. **96**, 117203 (2006).

[66] H. Bednarski and J. Spałek, Journal of Physics: Condensed Matter **24**, 235801 (2012).

[67] Y. Tian, Y. Li, M. He, I. A. Putra, H. Peng, B. Yao, S. A. Cheong, and T. Wu, Appl. Phys. Lett. **98**, 162503 (2011).

[68] D. E. Angelescu and R. N. Bhatt, Phys. Rev. B **65**, 075211 (2002).

[69] A. C. Durst, R. N. Bhatt, and P. A. Wolff, Phys. Rev. B **65**, 235205 (2002).

[70] M. Herbich, A. Twardowski, D. Scalbert, and A. Petrou, Phys. Rev. B **58**, 7024 (1998).

[71] P. A. Wolff, R. N. Bhatt, and A. C. Durst, J. Appl. Phys. **79**, 5196 (1996).

[72] H. Bednarski and J. Spałek, New J. Phys. **16**, 093060 (2014).

[73] M. D. Kapetanakis and I. E. Perakis, Phys. Rev. Lett. **101**, 097201 (2008).

[74] O. Morandi and P.-A. Hervieux, Phys. Rev. B **81**, 195215 (2010).

[75] C. Thurn, *Density matrix theory of diluted magnetic semiconductors: spin dynamics & magneto-optical properties*, Ph.D. thesis, Universität Bayreuth (2013).

[76] R. Kubo, J. Phys. Soc. Jpn. **17**, 1100 (1962).

[77] T. L. Gilbert, IEEE Transactions on Magnetics **40**, 3443 (2004).

[78] J. Kossut, *Diluted Magnetic Semiconductors*, edited by J. Furdyna and J. Kossut, Semiconductors and Semimetals, Vol. 25 (Academic Press, San Diego, 1988) p. 185.

[79] A. Haury, A. Wasiela, A. Arnoult, J. Cibert, S. Tatarenko, T. Dietl, and Y. M. d'Aubigné, Phys. Rev. Lett. **79**, 511 (1997).

[80] M. Vladimirova, S. Cronenberger, P. Barate, D. Scalbert, F. J. Teran, and A. P. Dmitriev, Phys. Rev. B **78**, 081305 (2008).

[81] F. Perez, J. Cibert, M. Vladimirova, and D. Scalbert, Phys. Rev. B **83**, 075311 (2011).

[82] P. M. Shmakov, A. P. Dmitriev, and V. Y. Kachorovskii, Phys. Rev. B **83**, 233204 (2011).

[83] P. Barate, S. Cronenberger, M. Vladimirova, D. Scalbert, F. Perez, J. Gòmez, B. Jusserand, H. Boukari, D. Ferrand, H. Mariette, J. Cibert, and M. Nawrocki, Phys. Rev. B **82**, 075306 (2010).

[84] D. Frustaglia, J. König, and A. H. MacDonald, Phys. Rev. B **70**, 045205 (2004).

[85] J. K. Zhou, *Differential Transformation and its Applications for Electrical Circuits* (Huarjung University Press, 1986).

[86] W. J. de Haas, J. de Boer, and G. J. van dën Berg, Physica **1**, 1115 (1934).

[87] A. Sumiyama, Y. Oda, H. Nagano, Y. Ōnuki, K. Shibutani, and T. Komatsubara, J. Phys. Soc. Jpn. **55**, 1294 (1986).

[88] S. Das Sarma, E. H. Hwang, and A. Kaminski, Phys. Rev. B **67**, 155201 (2003).

[89] J. Spałek, Phys. Rev. B **30**, 5345 (1984).

[90] A. V. Kavokin and K. V. Kavokin, Semiconductor Science and Technology **8**, 191 (1993).

[91] J. Schilp, T. Kuhn, and G. Mahler, Phys. Rev. B **50**, 5435 (1994).

[92] C. Fürst, A. Leitenstorfer, A. Laubereau, and R. Zimmermann, Phys. Rev. Lett. **78**, 3733 (1997).

[93] Y. S. Ang, Z. Ma, and Z. Chao, Sci. Rep. **5**, 7872 (2015).

[94] L. Allen, M. W. Beijersbergen, R. J. C. Spreeuw, and J. P. Woerdman, Phys. Rev. A **45**, 8185 (1992).

[95] G. F. Quinteiro and P. I. Tamborenea, Phys. Rev. B **82**, 125207 (2010).

[96] B. E. A. Saleh and M. C. Teich, *Fundamentals of Photonics* (Wiley, 1991).

[97] G. F. Quinteiro and T. Kuhn, Phys. Rev. B **90**, 115401 (2014).

[98] A. Twardowski, M. Nawrocki, and J. Ginter, phys. stat. sol. (b) **96**, 497 (1979).

[99] S.-K. Chang, A. V. Nurmikko, J.-W. Wu, L. A. Kolodziejski, and R. L. Gunshor, Phys. Rev. B **37**, 1191 (1988).

[100] V. M. Axt and S. Mukamel, Rev. Mod. Phys. **70**, 145 (1998).

[101] J. M. Luttinger and W. Kohn, Phys. Rev. **97**, 869 (1955).

[102] I. A. Merkulov and K. V. Kavokin, Phys. Rev. B **52**, 1751 (1995).

[103] F. X. Bronold, I. Martin, A. Saxena, and D. L. Smith, Phys. Rev. B **66**, 233206 (2002).

[104] B. A. Bernevig, T. L. Hughes, and S.-C. Zhang, Science **314**, 1757 (2006).

[105] B. Scharf, A. Matos-Abiague, I. Žutić, and J. Fabian, Phys. Rev. B **91**, 235433 (2015).

Part IV.

Publications

List of publications as parts of this thesis:

[Pub1]   M. Cygorek and V. M. Axt,
Comparison between a quantum kinetic theory of spin transfer dynamics in Mn-doped bulk semiconductors and its Markov limit for nonzero Mn magnetization,
Phys. Rev B **90**, 035206 (2014).

[Pub2]   M. Cygorek and V. M. Axt,
Effective equations for the precession dynamics of electron spins and electron-impurity correlations in diluted magnetic semiconductors,
Semicond. Sci. Technol. **30**, 085011 (2015).

[Pub3]   F. Ungar, M. Cygorek, P. I. Tamborenea, and V. M. Axt,
Ultrafast spin dynamics in II-VI diluted magnetic semiconductors with spin-orbit interaction,
Phys. Rev. B **91**, 195201 (2015).

[Pub4]   F. Ungar, M. Cygorek, P. I. Tamborenea, and V. M. Axt,
Relaxation and coherent oscillations in the spin dynamics of II-VI diluted magnetic quantum wells,
J. Phys.: Conf. Ser. **647**, 012010 (2015).

[Pub5]   M. Cygorek, P. I. Tamborenea, and V. M. Axt,
Carrier-impurity spin transfer dynamics in paramagnetic II-VI diluted magnetic semiconductors in the presence of a wave-vector-dependent magnetic field,
Phys. Rev. B **93**, 205201 (2016).

[Pub6]   M. Cygorek and V. M. Axt,
Non-Markovian Effects in the Spin Transfer Dynamics in Diluted Magnetic Semiconductors due to Excitation in Proximity to the Band Edge,
J. Phys.: Conf. Ser. **647**, 012042 (2015).

[Pub7]   M. Cygorek, P. I. Tamborenea, and V. M. Axt,
Nonperturbative correlation effects in diluted magnetic semiconductors,
Phys. Rev. B **93**, 035206 (2016) & Erratum: Phys. Rev. B **94**, 079906 (2016).

[Pub8]   M. Cygorek, F. Ungar, P. I. Tamborenea, and V. M. Axt,
Dependence of quantum kinetic effects in the spin dynamics of diluted magnetic semiconductors on the excitation conditions,
submitted to Proceedings of SPIE, Optics + Photonics: Nanoscience + Engineering, Spintronics IX (2016).

[Pub9]   M. Cygorek, P. I. Tamborenea, and V. M. Axt,
Insensitivity of spin dynamics to the orbital angular momentum transferred from twisted light to extended semiconductors,
Phys. Rev. B **92**, 115301 (2015).

[Pub10]   M. Cygorek, F. Ungar, P. I. Tamborenea, and V. M. Axt,
Influence of non-magnetic impurity scattering on the spin dynamics in diluted magnetic semiconductors,
arXiv:1609.02582v1, *submitted to* Phys. Rev. B

Other publications of the author:

Ref. [23]   C. Thurn, M. Cygorek, V. M. Axt, and T. Kuhn,
Non-Markovian spin transfer dynamics in magnetic semiconductors despite short memory times,
Phys. Rev. B **87**, 205301 (2013).

Ref. [24]   C. Thurn, M. Cygorek, V. M. Axt, and T. Kuhn,
Coherent spin-transfer dynamics in diluted magnetic semiconductor quantum wells even after optical excitation with zero net angular momentum,
Phys. Rev. B **88**, 161302(R) (2013).

Contributions to the publications

The author of the present thesis declares that he carried out most of the work for the publications [Pub1], [Pub2], [Pub5], [Pub6], [Pub7], [Pub8], [Pub9] and [Pub10]. In particular, he developed the concept of the papers, derived the equations presented there, wrote the C++ code for the numerical simulations, and wrote most of the text of the publications. The coauthors assisted in the presentation of the content and the discussion of the results, checked the results for soundness and pointed out relevant publications in the literature.

The publication [Pub3] is based on the results of Florian Ungar's Bachelor thesis, who numerically implemented the equations of motion based on a C++ framework provided by the author. Large parts of the text of [Pub3] were formulated by Pablo I. Tamborenea. The main contributions of the author of the present thesis to [Pub3] were the development of the concept of the paper, supervising the Bachelor thesis, checking the results and the numerical implementation and contributing to the interpretation and presentation of the paper.

Pablo I. Tamborenea proposed studying the situation presented in [Pub4] and he performed the calculations using the program provided by Florian Ungar. There, the author of the thesis contributed large parts of the interpretation, especially Eq. (1) and the idea to fit the numerical results with Gaussian functions rather than exponentials.

Contributions to Conferences/Seminars:

The author presented parts of this work to the scientific community at the following conferences:

talks:	NOEKS 12, Bremen, Germany (2014)
	OPON 2016, Wrocław, Poland (2016)
posters:	OPON 2013, Bayreuth, Germany (2013)
	EP2DS-20/MSS-16, Wrocław, Poland (2013)
	EDISON 19, Salamanca, Spain (2015)
	SPIE Optics + Photonics 2016, San Diego, USA (2016)

Beside the conferences, the author presented the work also in a seminary talk at the Wrocław University of Technology, Wrocław, Poland (2013), invited by Paweł Machnikowski and in the groups of Jigang Wang (Ames, USA, 2016), Igor Žutić (Buffalo, USA, 2016) as well as Paweł Hawrylak (Ottawa, Canada, 2016). Furthermore, the author worked together with Ilias Perakis during a research stay of about 5 weeks in Birmingham, USA (2016), on the topic of Fano line shapes in differential reflectivity signals measured at Co-doped $BaFe_2As_2$.

Publication 1

Comparison between a quantum kinetic theory of spin transfer dynamics in Mn-doped bulk semiconductors and its Markov limit for nonzero Mn magnetization

M. Cygorek and V. M. Axt

Comparison between a quantum kinetic theory of spin transfer dynamics in Mn-doped bulk semiconductors and its Markov limit for nonzero Mn magnetization

M. Cygorek and V. M. Axt

Theoretische Physik III, Universität Bayreuth, 95440 Bayreuth, Germany

We investigate the transfer between carrier and Mn spins due to the *s-d*-exchange interaction in a Mn-doped bulk semiconductor within a microscopic quantum kinetic theory. We demonstrate that the spin transfer dynamics is qualitatively different for components of the carrier spin parallel and perpendicular to the Mn magnetization. From our quantum kinetic equations we have worked out the corresponding Markov limit, which is equivalent to rate equations based on Fermi's golden rule. The resulting equations resemble the widely used Landau-Lifshitz-Gilbert equations, but also describe genuine spin transfer due to quantum corrections. Although it is known that the Markovian rate description works well for bulk systems when the initial Mn magnetization is zero, we find large qualitative deviations from the full quantum kinetic theory for finite initial Mn magnetizations. These deviations mainly reflect corrections of higher than leading order in the interaction, which are not accounted for in golden-rule-type rates.

I. INTRODUCTION

Diluted magnetic semiconductors (DMS) have been studied intensively in the past decades, since they combine the versatility of semiconductors with the spin degree of freedom, which promises future applications in spintronics [1–5]. The magnetic properties of DMS arise from the *s/p-d* exchange interaction [4,6,7] between carriers and magnetic impurities, which typically consist of Mn ions acting as localized spin-$\frac{5}{2}$ systems. Especially for short timescales and high Mn doping concentrations the exchange interaction can dominate the spin dynamics [8,9]. The description of the resulting spin transfer dynamics in DMS is usually based on rate equations, where the rates are computed using Fermi's golden rule [9,10]. The standard derivation of the golden rule involves a Markov approximation [8,11] and is perturbative with respect to the exchange coupling constant. In Ref. [12] a projection operator method was applied to derive spin relaxation rates for DMS quantum wells. There, also a Markovian assumption as well as a perturbative argument were used. Another approach to the description of the macroscopic magnetization dynamics is the use of the phenomenological Landau-Lifshitz-Gilbert equations [13,14].

Recently, starting from a Kondo-like interaction Hamiltonian a density matrix approach based on correlation expansion was developed [15] in order to describe the spin dynamics in the ultrafast regime. Until now, this quantum kinetic theory (QKT) has only been applied to the case of an initially zero Mn spin. There, it has been found that in three-dimensional systems, the time evolution of the carrier spin is exponentially decreasing, where the decay rate coincides with its value according to Fermi's golden rule [16]. The latter was shown by performing the Markov limit (ML) of the QKT using only terms in second order of J_{sd}. In lower-dimensional systems, excitation conditions can be found where significant differences between the ML and the QKT become visible although the memory induced by the exchange interaction is orders of magnitude shorter than the time scale for the evolution of the carrier and Mn dynamics [16]. In particular,

quantum kinetic effects are most pronounced when suitably tuned oppositely circular polarized two-color laser pulses are used for the excitation [17].

In this article, we study the spin dynamics of conduction band electrons in a bulk ZnMnSe semiconductor for the case of a nonzero initial Mn spin where electron spins can precess around the Mn magnetization. It turns out that the spin transfer dynamics that is superimposed to the precession is qualitatively different for electron spins aligned parallel or perpendicular to the Mn magnetization. Starting from our quantum kinetic equations we derive the corresponding Markov limit for finite Mn magnetization. The resulting equations can be interpreted as modified Landau-Lifshitz-Gilbert equations. Assuming Mn concentrations much larger than the itinerant electron density analytical solutions of these Markovian equations are presented. The resulting analytical expressions also exhibit a different dynamics for perpendicular and parallel spin transfer, which, however, quantitatively and qualitatively disagrees with the prediction of the full QKT. Here, the failure of the Markovian approach can be traced back to contributions of higher than leading order in the exchange coupling constant.

The outline of this paper is as follows: In a first step, we briefly summarize the QKT [15] that was used as a basis for our numerical calculation and introduce the model used in this paper. Then, we derive the Markov limit of the QKT along the lines described in Ref. [16] for an initially zero Mn magnetization $\langle \mathbf{S} \rangle$, but allow for a finite value of $\langle \mathbf{S} \rangle$ and an arbitrary angle between the conduction band electron spin and the Mn spin. In a subsequent section we present numerical results of our QKT for the spin transfer dynamics of the parallel and perpendicular components and compare them with the ML. The analytical solution of the ML equations in combination with a rearrangement of the contributions to our QKT allows for a clear physical interpretation of the pertinent source terms. By selectively studying the impact of different source terms we are able to demonstrate the importance of contributions of higher than leading order in the coupling constant.

II. QUANTUM KINETIC EQUATIONS

In Ref. [15], a quantum kinetic density matrix approach for the spin dynamics in Mn-doped semiconductors was developed starting from the Hamiltonian:

$$H = H_0 + H_{sd} + H_{pd} + H_{em}, \tag{1}$$

where H_0 describes the single particle band energies, H_{sd} accounts for the exchange interaction between the s-type conduction band electrons and the spins of the d-type electrons of the Mn dopands, while H_{pd} stands for the interaction of the latter with p-type holes. Finally, H_{em} comprises the dipole coupling to an external laser field. The exchange interactions $H_{sd} + H_{pd}$ as well as the random spatial distribution of Mn atoms give rise to a hierarchy of higher-order correlation functions. In order to obtain a finite set of dynamical variables a specially adapted correlation expansion has been worked out in Ref. [15].

Since the aim of the present paper is to investigate the spin transfer between conduction band electrons and Mn dopands, the model can be reduced to:

$$H = H_0 + H_{sd}. \tag{2}$$

H_0 now accounts only for electrons in a single spin degenerate conduction band:

$$H_0 = \sum_{l\mathbf{k}} E_{\mathbf{k}} c_{l\mathbf{k}}^\dagger c_{l\mathbf{k}}, \tag{3}$$

where $c_{l\mathbf{k}}^\dagger$ ($c_{l\mathbf{k}}$) are the creation (annihilation) operators of conduction band electrons with k vector $\mathbf{k}$ and spin index $l = 1, 2$. For simplicity we shall assume parabolic bands $E_{\mathbf{k}} = \frac{\hbar^2 k^2}{2m^*}$, with an effective mass m^*. The exchange interaction is given by [18,19]:

$$H_{sd} = J_{sd} \sum_{Ii} \hat{\mathbf{S}}_I \cdot \hat{\mathbf{s}}_i^e \delta(\mathbf{r}_i - \mathbf{R}_I), \tag{4}$$

where J_{sd} is the exchange constant and $\hat{\mathbf{S}}_I$ ($\hat{\mathbf{s}}_i^e$) are operators for the spin of the Mn atom (conduction band electron) in units of $\hbar$ at the position $\mathbf{R}_I$ ($\mathbf{r}_i$). As in Ref. [15] we assume an on average spatially homogeneous distribution of Mn positions $\mathbf{R}_I$.

According to the analysis in Ref. [15] the relevant dynamical variables for this reduced model are:

$$C_{l_1\mathbf{k}_1}^{l_2} = \langle c_{l_1\mathbf{k}_1}^\dagger c_{l_2\mathbf{k}_1} \rangle, \tag{5a}$$

$$M_{n_1}^{n_2} = \langle \hat{P}_{n_1 n_2}^I \rangle, \tag{5b}$$

$$K_{l_1 n_1 \mathbf{k}_1}^{l_2 n_2 \mathbf{k}_2} = \delta \langle c_{l_1\mathbf{k}_1}^\dagger c_{l_2\mathbf{k}_2} \hat{P}_{n_1 n_2}^I e^{i(\mathbf{k}_2 - \mathbf{k}_1)\mathbf{R}_I} \rangle, \tag{5c}$$

$$\bar{C}_{l_1\mathbf{k}_1}^{l_2\mathbf{k}_2} = \delta \langle c_{l_1\mathbf{k}_1}^\dagger c_{l_2\mathbf{k}_2} e^{i(\mathbf{k}_2 - \mathbf{k}_1)\mathbf{R}_I} \rangle, \tag{5d}$$

where $\hat{P}_{n_1 n_2}^I := |I, n_1\rangle \langle I, n_2|$ describes the spin state of the Ith Mn ion ($n = -\frac{5}{2}, \ldots, \frac{5}{2}$). The expectation value represented by the brackets involves a quantum mechanical average as well as the disorder average over the randomly distributed Mn positions. $C_{l_1\mathbf{k}_1}^{l_2}$ and $M_{n_1}^{n_2}$ are the electron and Mn density matrices. $K_{l_1 n_1 \mathbf{k}_1}^{l_2 n_2 \mathbf{k}_2}$ and $\bar{C}_{l_1\mathbf{k}_1}^{l_2\mathbf{k}_2}$ are the correlated parts of the corresponding density matrices, i.e., in these quantities all parts that can be factorized into products of lower-order correlations functions are subtracted from the expectation values. The explicit but lengthy definitions of $K_{l_1 n_1 \mathbf{k}_1}^{l_2 n_2 \mathbf{k}_2}$ and $\bar{C}_{l_1\mathbf{k}_1}^{l_2\mathbf{k}_2}$ can be found in Ref. [15].

It turns out that the resulting equations of motion can be simplified by introducing the following new correlation functions:

$$Q_{l_1 n_1 \mathbf{k}_1}^{l_2 n_2 \mathbf{k}_2} := K_{l_1 n_1 \mathbf{k}_1}^{l_2 n_2 \mathbf{k}_2} + M_{n_1}^{n_2} \bar{C}_{l_1\mathbf{k}_1}^{l_2\mathbf{k}_2}. \tag{6}$$

Rewriting the equations of motion from Ref. [15] in terms of these functions we obtain:

$$-i\hbar \frac{\partial}{\partial t} M_{n_1}^{n_2} = J_{sd} \frac{1}{V} \sum_{\mathbf{k}} \sum_{nll'} \mathbf{s}_{ll'} \left[C_{l\mathbf{k}}^{l'} \left(\mathbf{S}_{nn_1} M_n^{n_2} - \mathbf{S}_{n_2 n} M_{n_1}^n \right) + \frac{1}{V} \sum_{\mathbf{k}'} \left(\mathbf{S}_{nn_1} Q_{ln\mathbf{k}}^{l'n_2\mathbf{k}'} - \mathbf{S}_{n_2 n} Q_{ln_1\mathbf{k}}^{l'n\mathbf{k}'} \right) \right], \tag{7a}$$

$$-i\hbar \frac{\partial}{\partial t} C_{l_1\mathbf{k}_1}^{l_2} = J_{sd} n_{\mathrm{Mn}} \sum_{nn'l} \mathbf{S}_{nn'} \left[M_n^{n'} \left(\mathbf{s}_{ll_1} C_{l\mathbf{k}_1}^{l_2} - \mathbf{s}_{l_2 l} C_{l_1\mathbf{k}_1}^l \right) + \frac{1}{V} \sum_{\mathbf{k}} \left(\mathbf{s}_{ll_1} Q_{ln\mathbf{k}}^{l_2 n'\mathbf{k}_1} - \mathbf{s}_{l_2 l} Q_{l_1 n\mathbf{k}_1}^{ln'\mathbf{k}} \right) \right], \tag{7b}$$

$$\left(-i\hbar \frac{\partial}{\partial t} + E_{\mathbf{k}_2} - E_{\mathbf{k}_1} \right) Q_{l_1 n_1 \mathbf{k}_1}^{l_2 n_2 \mathbf{k}_2} = b_{l_1 n_1 \mathbf{k}_1}^{l_2 n_2 \mathbf{k}_2\, I} + b_{l_1 n_1 \mathbf{k}_1}^{l_2 n_2 \mathbf{k}_2\, II} + b_{l_1 n_1 \mathbf{k}_1}^{l_2 n_2 \mathbf{k}_2\, III}, \tag{7c}$$

with source terms

$$b_{l_1 n_1 \mathbf{k}_1}^{l_2 n_2 \mathbf{k}_2\, I} = \underbrace{J_{sd} \sum_{nl} \left\{ \mathbf{S}_{nn_1} \mathbf{s}_{ll_1} C_{l\mathbf{k}_2}^{l_2} M_n^{n_2} - \mathbf{S}_{n_2 n} \mathbf{s}_{l_2 l} C_{l_1\mathbf{k}_1}^l M_{n_1}^n \right\}}_{=:b_{l_1 n_1 \mathbf{k}_1}^{l_2 n_2 \mathbf{k}_2\, I.1}} - \underbrace{J_{sd} \sum_{nll'} \mathbf{s}_{ll'} C_{l\mathbf{k}_2}^{l_2} C_{l_1\mathbf{k}_1}^{l'} \left(\mathbf{S}_{nn_1} M_n^{n_2} - \mathbf{S}_{n_2 n} M_{n_1}^n \right)}_{=:b_{l_1 n_1 \mathbf{k}_1}^{l_2 n_2 \mathbf{k}_2\, I.2}}, \tag{7d}$$

$$b_{l_1 n_1 \mathbf{k}_1}^{l_2 n_2 \mathbf{k}_2\, II} = \underbrace{J_{sd} \sum_{nn'l} \mathbf{S}_{nn'} M_n^{n'} n_{\mathrm{Mn}} \left(\mathbf{s}_{ll_1} Q_{ln_1\mathbf{k}_1}^{l_2 n_2 \mathbf{k}_2} - \mathbf{s}_{l_2 l} Q_{l_1 n_1 \mathbf{k}_1}^{ln_2\mathbf{k}_2} \right)}_{b_{l_1 n_1 \mathbf{k}_1}^{l_2 n_2 \mathbf{k}_2\, II.1}} + \underbrace{J_{sd} \sum_{nll'} \mathbf{s}_{ll'} \frac{1}{V} \sum_{\mathbf{k}} C_{l\mathbf{k}}^{l'} \left(\mathbf{S}_{nn_1} Q_{l_1 n\mathbf{k}_1}^{l_2 n_2 \mathbf{k}_2} - \mathbf{S}_{n_2 n} Q_{l_1 n_1 \mathbf{k}_1}^{l_2 n\mathbf{k}_2} \right)}_{b_{l_1 n_1 \mathbf{k}_1}^{l_2 n_2 \mathbf{k}_2\, II.2}}, \tag{7e}$$

$$
b_{l_1 n_1 \mathbf{k}_1}^{l_2 n_2 \mathbf{k}_2 \, III} = \underbrace{J_{sd} \sum_{nl} \left\{ \frac{1}{V} \sum_{\mathbf{k}} \left[\mathbf{S}_{nn_1} \mathbf{s}_{ll_1} Q_{ln\mathbf{k}}^{l_2 n_2 \mathbf{k}_2} - \mathbf{S}_{n_2 n} \mathbf{s}_{l_2 l} Q_{l_1 n_1 \mathbf{k}_1}^{ln\mathbf{k}} \right] \right\}}_{b_{l_1 n_1 \mathbf{k}_1}^{l_2 n_2 \mathbf{k}_2 \, III.1}}
$$

$$
\underbrace{- J_{sd} \sum_{nll'} \mathbf{s}_{ll'} \left\{ \frac{1}{V} \sum_{\mathbf{k}} C_{l_1 \mathbf{k}_1}^{l'} \left[\mathbf{S}_{nn_1} Q_{ln\mathbf{k}}^{l_2 n_2 \mathbf{k}_2} - \mathbf{S}_{n_2 n} Q_{ln_1\mathbf{k}_1}^{l_2 n \mathbf{k}_2} \right] + \frac{1}{V} \sum_{\mathbf{k}} C_{l\mathbf{k}_2}^{l_2} \left[\mathbf{S}_{nn_1} Q_{l_1 n_1 \mathbf{k}_1}^{l' n_2 \mathbf{k}} - \mathbf{S}_{n_2 n} Q_{l_1 n_1 \mathbf{k}_1}^{l' n \mathbf{k}} \right] \right\}}_{b_{l_1 n_1 \mathbf{k}_1}^{l_2 n_2 \mathbf{k}_2 \, III.2}} , \qquad (7f)
$$

where $\mathbf{S}_{n_1 n_2}$ and $\mathbf{s}_{l_1 l_2}^e$ are the Mn and electron spin matrices, V is the volume of the DMS, and $n_{\mathrm{Mn}} = \frac{N_{\mathrm{Mn}}}{V}$ is the density of the Mn ions. We have subdivided the sources on the right-hand side of Eq. (7c) for later reference. The physical meaning of these terms and their respective importance will be discussed later.

In order to study the dynamics of the spin transfer we consider initial conditions where the electrons are initially spin polarized and the Mn magnetization corresponds to a thermal distribution while the correlations $Q_{l_1 n_1 \mathbf{k}_1}^{l_2 n_2 \mathbf{k}_2}$ are assumed to be zero. This is a situation typical for a system immediately after an ultrafast optical excitation has induced a finite electron spin polarization.

III. MARKOV LIMIT

It turns out to be instructive to derive the Markov limit of our QKT, first of all, because this greatly simplifies the theory as the higher-order correlation functions are formally eliminated in favor of the variables of most interest, i.e., the electronic densities and spins. Furthermore, the Markov limit provides a relevant reference for our QKT. In particular for bulk systems it has been found previously [16] that the memory of the exchange interaction is short and therefore it is tempting to think that the Markovian equations should yield valid results in our case.

In order to be able to work out the Markov limit starting from Eqs. (7), we follow the procedure that in Ref. [16] led to rates in accordance with Fermi's golden rule and neglect in a first step the source terms of higher than leading order in the exchange coupling J_{sd}. Due to the initial condition $Q_{l_1 n_1 \mathbf{k}_1}^{l_2 n_2 \mathbf{k}_2} = 0$ the correlations $Q_{l_1 n_1 \mathbf{k}_1}^{l_2 n_2 \mathbf{k}_2}$ are of first order in J_{sd} and thus we see from Eqs. (7) that $b_{l_1 n_1 \mathbf{k}_1}^{l_2 n_2 \mathbf{k}_2 \, II}$ and $b_{l_1 n_1 \mathbf{k}_1}^{l_2 n_2 \mathbf{k}_2 \, III}$ are of second order in J_{sd} and yield third-order contributions to the electron spin dynamics. Thus, we keep in Eq. (7c) only the first-order term $b_{l_1 n_1 \mathbf{k}_1}^{l_2 n_2 \mathbf{k}_2 \, I}$. This allows us to formally integrate the correlations:

$$
Q_{l_1 n_1 \mathbf{k}_1}^{l_2 n_2 \mathbf{k}_2}(t) = \frac{i}{\hbar} \int_0^t dt' e^{i(\omega_{\mathbf{k}_2} - \omega_{\mathbf{k}_1})(t' - t)} b_{l_1 n_1 \mathbf{k}_1}^{l_2 n_2 \mathbf{k}_2 \, I}(t'), \qquad (8)
$$

with frequency $\omega_{\mathbf{k}} = \frac{E_{\mathbf{k}}}{\hbar} = \frac{\hbar k^2}{2m^*}$. Substituting Eq. (8) back into the equations for $C_{l_1 \mathbf{k}_1}^{l_2}$ and $M_{n_1}^{n_2}$ we have to perform a k summation, which, due to interference resulting from the k-dependent phases $e^{i(\omega_{\mathbf{k}_2} - \omega_{\mathbf{k}_1})(t' - t)}$, leads to a finite memory. The Markov limit is established by assuming that the sources

$b_{l_1 n_1 \mathbf{k}_1}^{l_2 n_2 \mathbf{k}_2 \, I}$ change on a much slower time scale than the memory and can therefore be drawn out of the integral. The memory has been found to decay on a fs time scale while the spin dynamics evolves on a ps time scale [16]. Therefore, the lower limit of the integral can be extended to $-\infty$ resulting in the following approximation for the correlations:

$$
Q_{l_1 n_1 \mathbf{k}_1}^{l_2 n_2 \mathbf{k}_2}(t) \approx \frac{i}{\hbar} b_{l_1 n_1 \mathbf{k}_1}^{l_2 n_2 \mathbf{k}_2 \, I}(t) \int_{-\infty}^0 dt'' e^{i(\omega_{\mathbf{k}_2} - \omega_{\mathbf{k}_1}) t''}
$$

$$
= \frac{i}{\hbar} b_{l_1 n_1 \mathbf{k}_1}^{l_2 n_2 \mathbf{k}_2 \, I}(t) \left(\pi \delta(\omega_{\mathbf{k}_2} - \omega_{\mathbf{k}_1}) - \mathcal{P} \frac{i}{\omega_{\mathbf{k}_2} - \omega_{\mathbf{k}_1}} \right), \qquad (9)
$$

where $\mathcal{P}$ denotes the Cauchy principal value.

Starting from Eq. (7b) for the electron density $C_{l_1 \mathbf{k}_1}^{l_2}$ we can set up an equation of motion for the average electron spin $\langle \mathbf{s}_{\mathbf{k}_1} \rangle = \sum_{l_1 l_2} \mathbf{s}_{l_1 l_2}^e C_{l_1 \mathbf{k}_1}^{l_2}$ in the state with k vector $\mathbf{k}_1$. Feeding back the correlations $Q_{l_1 n_1 \mathbf{k}_1}^{l_2 n_2 \mathbf{k}_2}$ from Eq. (9) into these equations we finally obtain:

$$
\frac{\partial}{\partial t} \langle \mathbf{s}_{\mathbf{k}_1} \rangle = \frac{J_{sd} n_{\mathrm{Mn}}}{\hbar} \left(\langle \mathbf{S} \rangle \times \langle \mathbf{s}_{\mathbf{k}_1} \rangle \right)
$$

$$
+ \frac{J_{sd}^2 n_{\mathrm{Mn}}}{\hbar^2 V} \sum_{\mathbf{k}} \left\{ \frac{1}{2} \mathcal{P} \frac{n_{\mathbf{k}} - 1}{\omega_{\mathbf{k}_1} - \omega_{\mathbf{k}}} \left(\langle \mathbf{S} \rangle \times \langle \mathbf{s}_{\mathbf{k}_1} \rangle \right) \right.
$$

$$
+ \pi \delta(\omega_{\mathbf{k}_1} - \omega_{\mathbf{k}}) \left[\langle \mathbf{S} \rangle \frac{4 \langle \mathbf{s}_{\mathbf{k}_1} \rangle^2 - n_{\mathbf{k}_1}^2 + 2 n_{\mathbf{k}_1}}{4} \right.
$$

$$
+ \left(\langle \mathbf{s}_{\mathbf{k}} \rangle \times \left(\langle \mathbf{s}_{\mathbf{k}_1} \rangle \times \langle \mathbf{S} \rangle \right) \right)
$$

$$
\left. \left. + \frac{\langle \mathbf{S} \times (\mathbf{S} \times \langle \mathbf{s}_{\mathbf{k}} \rangle) \rangle + \langle (\langle \mathbf{s}_{\mathbf{k}} \rangle \times \mathbf{S}) \times \mathbf{S} \rangle}{2} \right] \right\}. \qquad (10)
$$

Applying the same procedure to the electron occupations $n_{\mathbf{k}_1} = \sum_l C_{l\mathbf{k}_1}^l$ at a given k vector $\mathbf{k}_1$ we find that on this level of theory $n_{\mathbf{k}_1}$ is time independent. It should be noted, that in the full QKT this is not the case. Instead it was shown in Refs. [15–17] that redistributions in k space take place, which are responsible for a number of features of the magnetization dynamics that are not expected in the Markovian theory.

The different terms in equation (10) can easily be interpreted. The first term describes the precession of the electron spin in an effective magnetic field due to the Mn magnetization $\langle \mathbf{S} \rangle$, which is also the result of a mean-field calculation [15].

The second term represents a renormalization of the precession frequency that depends on the density of states and therefore on the dimensionality of the system as well as the k vector, which can possibly lead to dephasing of the electron spin.

The magnitude of the renormalization for a bulk semiconductor can be estimated in the continuum limit by approximating the Brillouin zone (BZ) as a sphere with radius k_{BZ} and assuming a parabolic band structure as follows:

$$\Delta\omega_M = \omega_M^0 \frac{J_{sd}}{\hbar(2\pi)^2} \frac{2m^*}{\hbar} \underbrace{\int_0^{k_{\mathrm{BZ}}} dk \frac{k^2}{k^2 - k_1^2}(1 - n_{\mathbf{k}})}_{\approx k_{\mathrm{BZ}}}, \quad (11)$$

where $\omega_M^0 = \frac{J_{sd} n_{\mathrm{Mn}}}{\hbar}|\langle \mathbf{S} \rangle|$ is the mean-field precession frequency. The order of magnitude of the integral on the right-hand side of Eq. (11) can be determined by noting that the optically excited carriers occupy only very few states near the center of the BZ and therefore for the most part of the BZ $n_{\mathbf{k}} \approx 0$ holds, which also implies $\frac{k_1}{k} \ll 1$ for the occupied states. Approximating $n_{\mathbf{k}} \approx 0$ and $\frac{k_1}{k} \approx 0$ the integral yields the value k_{BZ}. For the parameters used in our study (see below) the renormalization is estimated in this way to be of the order of $\approx 1\%$ of the mean-field precession frequency.[1] The third term in Eq. (10), which is proportional to the Mn spin, describes a transfer of spin from the Mn to the electron system. The prefactor $\frac{4\langle \mathbf{s}_{\mathbf{k}_1} \rangle^2 - n_{\mathbf{k}_1}^2 + 2n_{\mathbf{k}_1}}{4}$ is zero for $n_{\mathbf{k}_1} \in \{0,2\}$. For $n_{\mathbf{k}_1} = 0$ no transfer can occur because there are no electrons that can exchange their spins with the Mn atoms; for $n_{\mathbf{k}_1} = 2$ the transfer vanishes due to Pauli blocking.

The term proportional to $\langle \mathbf{s}_{\mathbf{k}} \rangle \times (\langle \mathbf{s}_{\mathbf{k}_1} \rangle \times \langle \mathbf{S} \rangle)$ has the form of the relaxation term of a Landau-Lifshitz-Gilbert (LLG) equation and describes the tendency of a spin in a given effective magnetic field to align along the direction of the field. Unlike in the LLG equation, here, the prefactor is determined by the parameters of the microscopic model and is not a phenomenological fitting parameter.

The last term in Eq. (10) resembles a relaxation term that would be expected in the LLG equation for the Mn magnetization $\langle \mathbf{S} \rangle$. Here, it arises in the equation for the electron spin reflecting the conservation of total spin which is a feature also of the full QKT [15]. However, there is a crucial difference between the last term in Eq. (10) and the LLG relaxation term for the Mn magnetization: while the cross products in the LLG equation involve classical vectors, we are dealing here with vector operators. Here, the expectation value has to be taken after constructing the cross product in a symmetrized form. The physical consequences of this difference become most obvious by rewriting the last term in Eq. (10) as follows:

$$\frac{\langle \mathbf{S} \times (\mathbf{S} \times \langle \mathbf{s}_{\mathbf{k}} \rangle) \rangle + \langle (\langle \mathbf{s}_{\mathbf{k}} \rangle \times \mathbf{S}) \times \mathbf{S} \rangle}{2}$$
$$= -(\langle S^2 \rangle - \langle S^{\|2} \rangle)\langle \mathbf{s}_{\mathbf{k}}^{\|} \rangle - \frac{1}{2}(\langle S^2 \rangle + \langle S^{\|2} \rangle)\langle \mathbf{s}_{\mathbf{k}}^{\perp} \rangle, \quad (12)$$

where $\langle \mathbf{s}_{\mathbf{k}}^{\|} \rangle$ and $\langle \mathbf{s}_{\mathbf{k}}^{\perp} \rangle$ describe the electron spin of the states with k vector $\mathbf{k}$ in the direction parallel and perpendicular to the Mn spin vector $\langle \mathbf{S} \rangle$ and $S^{\|} = \mathbf{S} \cdot \frac{\langle \mathbf{S} \rangle}{|\langle \mathbf{S} \rangle|}$.

It is seen from Eq. (12) that even when the electron spin is aligned parallel to the Mn spin, a spin transfer can occur, and it was already noted in Ref. [16] that the corresponding parallel spin transfer rate coincides with the result of Fermi's golden rule. In contrast, the corresponding term in the standard LLG equation would be zero. This transfer is enabled because the factor $\langle S^2 \rangle - \langle S^{\|2} \rangle$ is nonzero as quantum mechanically the maximal value of $\langle S^{\|2} \rangle$ is $\hbar^2 S^2$, while $\langle S^2 \rangle = \hbar^2 S(S + 1)$, which reflects the uncertainty between the respective spin components. For classical vectors, as considered in the standard LLG equation, this factor would always be zero. Furthermore, in general the contribution in Eq. (12) is different for the parallel and perpendicular components of the electron spin. It is noteworthy that if the Mn spin had been represented by a pseudospin $\frac{1}{2}$, this feature would be lost as then independent of the Mn spin configuration we find $\langle S^2 \rangle = \frac{3}{4}$ and $\langle S^{\|2} \rangle = \frac{1}{4}$ resulting in the same prefactors for $\langle \mathbf{s}_{\mathbf{k}_1}^{\|} \rangle$ and $\langle \mathbf{s}_{\mathbf{k}_1}^{\perp} \rangle$ in Eq. (12).

In order to use Eq. (10) in practical calculations we have to know the values of the average Mn spin $\langle \mathbf{S} \rangle$ and according to Eq. (12) the second moment $\langle S^{\|2} \rangle$, which appear on the right-hand side of Eq. (10). The average Mn spin can be calculated from the knowledge of the electron spin and the initial total spin by using the total spin conservation [15]. Setting up an equation of motion for the second moment is cumbersome and not necessary for the cases that we shall discuss in this paper where it is assumed that the number of Mn ions by far exceeds the number of photo induced electrons ($N_{\mathrm{Mn}} \gg N_e$). In this case, the change of the average Mn spin as well as its second moment can be neglected and thus the second moment essentially coincides with its initial thermal value. Furthermore, for nearly constant Mn magnetization, the equations of motion for electron states with different energies $\hbar\omega_{\mathbf{k}}$ are decoupled in the Markov limit due to the δ distribution in Eq. (10) and the fact that $n_{\mathbf{k}}$ remains constant which allows using the initial occupation for the evaluation of the frequency renormalization.

The decoupling of the equations of motion in the Markov limit enables us to find analytical solutions for Eq. (10). To this end we split the electron spin into its components parallel and perpendicular to the Mn spin according to:

$$\langle \mathbf{s}_{\mathbf{k}_1} \rangle = s_{\mathbf{k}_1}^{\|} \frac{\langle \mathbf{S} \rangle}{S} + s_{\mathbf{k}_1}^{\perp} \left(\sin(\omega_M t) \frac{\langle \mathbf{S} \rangle \times \langle \mathbf{s}_{\mathbf{k}_1}(0) \rangle}{|\langle \mathbf{S} \rangle \times \langle \mathbf{s}_{\mathbf{k}_1}(0) \rangle|} \right.$$
$$\left. + \cos(\omega_M t) \frac{(\langle \mathbf{S} \rangle \times \langle \mathbf{s}_{\mathbf{k}_1}(0) \rangle) \times \langle \mathbf{S} \rangle}{|(\langle \mathbf{S} \rangle \times \langle \mathbf{s}_{\mathbf{k}_1}(0) \rangle) \times \langle \mathbf{S} \rangle|} \right), \quad (13)$$

where ω_M accounts for the precession of the perpendicular component that results from Eq. (10). With this decomposition,

---

[1]For lower-dimensional systems this crude approximation leads to a divergence of the frequency renormalization at $k \to k_1$. This fact supports the findings of Refs. [16,17] that the Markov limit is not a good approximation in systems with dimensions lower than 3.
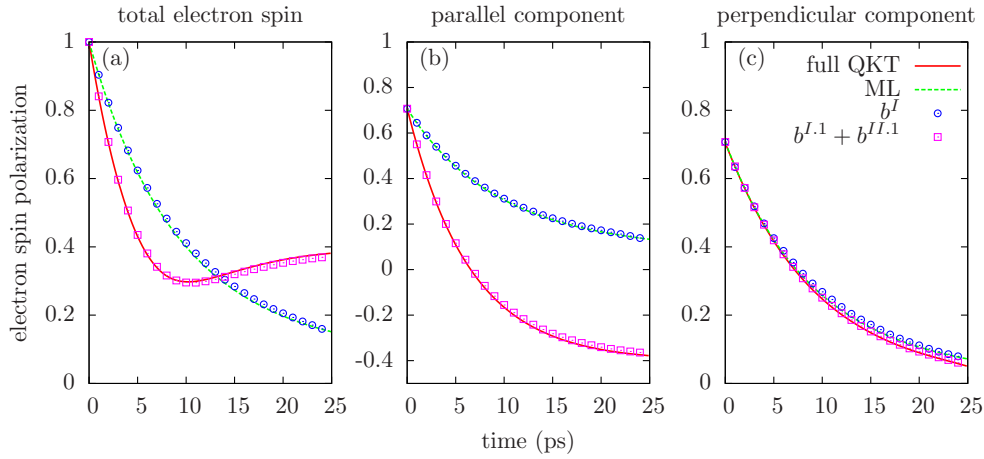
FIG. 1. (Color online) Time evolution of the total electron spin polarization (a) and its components parallel (b) and perpendicular (c) to the Mn spin assuming the electrons to be initially spin polarized along a direction at an angle of 45° relative to the Mn magnetization. The solid red line describes the spin dynamics according to the full quantum kinetic theory, the dashed green line shows its Markov limit (analytic solutions, cf. Appendix). Blue circles and purple squares correspond to approximate quantum kinetic calculations where only a subset of source terms for the correlations (as indicated in the key of the figure) has been accounted for.

Eq. (10) can be rewritten as:

$$\frac{\partial}{\partial t} s_{\mathbf{k}_1}^{\parallel} = \gamma_{\mathbf{k}_1} S \left(s_{\mathbf{k}_1}^{\parallel} \right)^2 + \gamma_{\mathbf{k}_1} S \frac{n_{\mathbf{k}_1}(2 - n_{\mathbf{k}_1})}{4}$$
$$- \gamma_{\mathbf{k}_1} \left(\langle S^2 \rangle - \langle S^{\parallel 2} \rangle \right) s_{\mathbf{k}_1}^{\parallel}, \tag{14a}$$

$$\frac{\partial}{\partial t} s_{\mathbf{k}_1}^{\perp} = \gamma_{\mathbf{k}_1} s_{\mathbf{k}_1}^{\parallel} s_{\mathbf{k}_1}^{\perp} S - \frac{1}{2} \gamma_{\mathbf{k}_1} \left(\langle S^2 \rangle + \langle S^{\parallel 2} \rangle \right) s_{\mathbf{k}_1}^{\perp}, \tag{14b}$$

with

$$\gamma_{\mathbf{k}_1} = \frac{J_{sd}^2 n_{\mathrm{Mn}}}{\hbar^2 V} \pi \sum_{\mathbf{k}} \delta(\omega_{\mathbf{k}_1} - \omega_{\mathbf{k}}), \tag{15a}$$

$$\omega_M = \frac{J_{sd} n_{\mathrm{Mn}}}{\hbar} S \left(1 + \frac{1}{2} \frac{J_{sd}}{\hbar V} \sum_{\mathbf{k}} \mathcal{P} \frac{n_{\mathbf{k}} - 1}{\omega_{\mathbf{k}_1} - \omega_{\mathbf{k}}} \right), \tag{15b}$$

and $S = |\langle \mathbf{S} \rangle|$. Equation (14a) is a Riccati differential equation with constant coefficients, which can be solved analytically. Its solutions can then be fed back into Eq. (14b) for the perpendicular electron spin. The explicit solutions are listed in Appendix.

It is noteworthy that by a rescaling of the time axis according to $\tau := \gamma_{\mathbf{k}_1} t$ all material parameters can be eliminated from Eqs. (14) for the moduli $s_{\mathbf{k}_1}^{\parallel}$ and $s_{\mathbf{k}_1}^{\perp}$. Therefore, with this choice of time units and given initial conditions we obtain the same universal solution for all material parameters. Reinserting the solutions for $s_{\mathbf{k}_1}^{\parallel}$ and $s_{\mathbf{k}_1}^{\perp}$ into Eq. (13) and choosing again $1/\gamma_{\mathbf{k}_1}$ as the unit of time, we conclude that for given initial conditions the time trace of the electron spin $\langle \mathbf{s}_{\mathbf{k}_1} \rangle$ is affected by the material parameters only via the ratio $\omega_M / \gamma_{\mathbf{k}_1}$.

IV. NUMERICAL RESULTS

The quantum kinetic equations of motion (7) have been solved numerically and compared with their Markov limit (10) for different initial conditions in a three-dimensional bulk DMS. The initial electron distribution over the single-particle energies $E_{\mathbf{k}}$ is taken to be Gaussian with its center at $E_{k=0}$ and a standard deviation of $\sigma = 3$ meV while the initial magnitude of the Mn spin is set to $\frac{1}{2}\hbar$ (i.e., 20% of its maximal value). The material parameters used were the same as in Ref. [16] for $\mathrm{Zn}_{0.93}\mathrm{Mn}_{0.07}\mathrm{Se}$ with $J_{sd} = 12$ meVnm^3 and $m_e = 0.21 m_0$.

First, we shall discuss results where at the beginning of the simulation the electron spins are assumed to be totally polarized in a direction with an angle of 45° with respect to the Mn magnetization vector. Displayed in Fig. 1 is the corresponding time evolution of the electron spin; (a) shows the total electron spin, while in (b) and (c) the components parallel and perpendicular to the Mn magnetization are plotted, respectively. The full quantum kinetic results are plotted as solid red lines whereas curves derived from the analytical solutions of the Markov limit equations are depicted as dashed green lines.

As seen from Fig. 1(a), the dynamics predicted by the full theory is qualitatively different from the Markovian result. On a short time scale (for our parameters $t < 5$ ps), the electron spin decays much faster for the full solution than in the Markov limit. Subsequently, the quantum kinetic curve exhibits a nonmonotonic time dependence and the electron spin eventually approaches a finite value. In contrast, in the Markov limit, we find a monotonic, almost exponential decay for all times. From the explicit analytical expression (cf. Appendix) it is seen that the long time limit of the electron spin in the Markov limit is zero.

The origin of the nonmonotonic behavior can be understood by splitting the total electron spin into its components parallel [Fig. 1(b)] and perpendicular [Fig. 1(c)] to the Mn spin. Both spin components decrease almost exponentially in the ML as well as in the full QKT. The time evolution of the perpendicular spin component essentially yields the same results for the full quantum kinetic calculation and the Markov limit. In the full QKT, however, the parallel spin component changes its sign and converges to a finite negative value, whereas both spin components in the ML and the perpendicular spin component of the QKT drop to zero. When the parallel spin component in
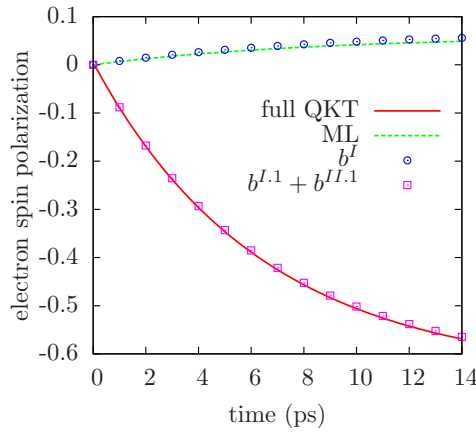
FIG. 2. (Color online) Dynamics of the electron spin polarization for initially unpolarized electron spins. Line styles and symbols have the same meaning as in Fig. 1.

the full QKT crosses the zero line, its modulus has a minimum, which leads to a minimum in the total spin.

The obvious discrepancy between the different levels of theory with regard to the dynamics of the parallel spin component does not arise due to the assumption of a short memory in the ML. This can be seen from calculations, where only the source terms $b_{l_1 n_1 \mathbf{k}_1}^{l_2 n_2 \mathbf{k}_2\, I}$, i.e., the terms used to derive the ML in the first place, have been taken into account but the finite memory expressed by the retardations in Eq. (8) are still kept [blue circles in Fig. 1]. The resulting curves almost coincide with the Markovian calculation. The main difference between the full QKT and the ML is due to the source term $b_{l_1 n_1 \mathbf{k}_1}^{l_2 n_2 \mathbf{k}_2\, II.1}$, which is demonstrated by simulations that incorporate only $b_{l_1 n_1 \mathbf{k}_1}^{l_2 n_2 \mathbf{k}_2\, I.1}$ and $b_{l_1 n_1 \mathbf{k}_1}^{l_2 n_2 \mathbf{k}_2\, II.1}$ [purple squares in Fig. 1]. The results of these calculations agree very well with the predictions of the full theory, suggesting that all other source terms are of minor importance, at least for the parameters used here. It should be noted, that especially the term $b_{l_1 n_1 \mathbf{k}_1}^{l_2 n_2 \mathbf{k}_2\, II.1}$, like $b_{l_1 n_1 \mathbf{k}_1}^{l_2 n_2 \mathbf{k}_2\, II.2}$ and $b_{l_1 n_1 \mathbf{k}_1}^{l_2 n_2 \mathbf{k}_2\, III}$, gives contributions to the reduced electron density matrices in the order of $\mathcal{O}(J_{sd}^3)$ while the leading-order contributions of the correlations are of $\mathcal{O}(J_{sd}^2)$. Thus, our results imply that a proper description of the coupled electron and Mn spin dynamics requires a treatment beyond perturbation theory.

The effect of these higher-order contributions on the dynamics is particularly dramatic in the case of initially unpolarized electron spins. Corresponding results are displayed in Fig. 2. Here, even the sign of the spin polarization is opposite for the QKT and ML calculations. Furthermore, also the predictions concerning the magnitude of the spin polarization deviate significantly.

V. INTERPRETATION OF THE SOURCE TERMS

By the numerical analysis in the last section, we were able to trace back the difference between the full quantum kinetic theory and its Markov limit to a few selected source terms for the correlations in Eqs. (7). In this section, we shall give a physical interpretation to the individual source terms which

will enable us to understand what determines their relative importance.

First of all, $b_{l_1 n_1 \mathbf{k}_1}^{l_2 n_2 \mathbf{k}_2\, I.1}$ is the most important source term, because it starts the correlation dynamics, i.e., without these sources the correlations would stay zero for all times. In the Markov limit, $b_{l_1 n_1 \mathbf{k}_1}^{l_2 n_2 \mathbf{k}_2\, I.1}$ yields a Landau-Lifshitz-Gilbert-like damping term described in Eq. (12) and a spin transfer term proportional to the Mn spin $\langle \mathbf{S} \rangle$. $b_{l_1 n_1 \mathbf{k}_1}^{l_2 n_2 \mathbf{k}_2\, I.2}$ provides corrections for Pauli blocking to the transfer term and yields another LLG-like damping term, where the electron spin appears twice in the double cross product [cf. Eq. (10)]. As seen above, the quantum kinetic $b_{l_1 n_1 \mathbf{k}_1}^{l_2 n_2 \mathbf{k}_2\, I}$ contributions act similarly to their Markov limit counterparts. The dominant role of these terms is further emphasized by the fact that they are the leading terms in a perturbative treatment with respect to the exchange coupling constant J_{sd}.

In order to understand the meaning of the $b_{l_1 n_1 \mathbf{k}_1}^{l_2 n_2 \mathbf{k}_2\, II}$ terms, it is instructive to reformulate the equations of motion of the QKT by introducing new correlation functions according to:

$$Q_{\beta \mathbf{k}_1}^{\alpha \mathbf{k}_2} := \sum_{\substack{l_1 l_2 \\ n_1 n_2}} S_{n_1 n_2}^{\beta} s_{l_1 l_2}^{\alpha} Q_{l_1 n_1 \mathbf{k}_1}^{l_2 n_2 \mathbf{k}_2}, \tag{16}$$

which are summed over the electron band and Mn state indices. Here, we use the conventions $\alpha = 0,1,2,3$ with $s_{l_1 l_2}^0 = \delta_{l_1 l_2}$ and $\beta = 1,2,3$. From Eq. (7c), we obtain the following equations of motion for the summed correlations:

$$\frac{\partial}{\partial t} Q_{\beta \mathbf{k}_1}^{0 \mathbf{k}_2} = -i\left(\omega_{\mathbf{k}_2} - \omega_{\mathbf{k}_1} \right) Q_{\beta \mathbf{k}_1}^{0 \mathbf{k}_2} + b_{\beta \mathbf{k}_1}^{0 \mathbf{k}_2\, \mathrm{Res}} \tag{17a}$$

$$\frac{\partial}{\partial t} Q_{\beta \mathbf{k}_1}^{\alpha \mathbf{k}_2} = -i\left(\omega_{\mathbf{k}_2} - \omega_{\mathbf{k}_1} \right) Q_{\beta \mathbf{k}_1}^{\alpha \mathbf{k}_2} + b_{\beta \mathbf{k}_1}^{\alpha \mathbf{k}_2\, \mathrm{Res}}$$
$$+ \sum_{\kappa \lambda} \epsilon_{\alpha \kappa \lambda} \omega_M^{\kappa} Q_{\beta \mathbf{k}_1}^{\lambda \mathbf{k}_2} + \sum_{\kappa \lambda} \epsilon_{\beta \kappa \lambda} \omega_E^{\kappa} Q_{\lambda \mathbf{k}_1}^{\alpha \mathbf{k}_2}, \tag{17b}$$

where

$$\omega_M^{\alpha} = \frac{J_{sd}}{\hbar} n_{\mathrm{Mn}} \langle S^{\alpha} \rangle, \tag{18a}$$

$$\omega_E^{\alpha} = \frac{J_{sd}}{\hbar} \frac{1}{V} \sum_{\mathbf{k}} \langle s_{\mathbf{k}}^{\alpha} \rangle, \tag{18b}$$

$$b_{\beta \mathbf{k}_1}^{\alpha \mathbf{k}_2\, \mathrm{Res}} = \sum_{\substack{l_1 l_2 \\ n_1 n_2}} S_{n_1 n_2}^{\beta} s_{l_1 l_2}^{\alpha} \left[b_{l_1 n_1 \mathbf{k}_1}^{l_2 n_2 \mathbf{k}_2\, I} + b_{l_1 n_1 \mathbf{k}_1}^{l_2 n_2 \mathbf{k}_2\, III} \right] \tag{18c}$$

and $\epsilon_{\alpha \beta \gamma}$ is the Levi-Civita symbol. We note in passing that the residual sources $b_{\beta \mathbf{k}_1}^{\alpha \mathbf{k}_2\, \mathrm{Res}}$ contain a term resulting from $b_{l_1 n_1 \mathbf{k}_1}^{l_2 n_2 \mathbf{k}_2\, III.1}$, which cannot be expressed by the summed correlations. Thus, Eqs. (17) are numerically advantageous only if $b_{l_1 n_1 \mathbf{k}_1}^{l_2 n_2 \mathbf{k}_2\, III.1}$ is disregarded. The point here is that the two terms in Eq. (17b) originating from $b_{l_1 n_1 \mathbf{k}_1}^{l_2 n_2 \mathbf{k}_2\, II.1}$ and $b_{l_1 n_1 \mathbf{k}_1}^{l_2 n_2 \mathbf{k}_2\, II.2}$ both involve the Levi-Civita symbol and can therefore be interpreted as describing precessions. This can be made more explicit, e.g., by introducing a vector with components α according to

$$\left(\mathbf{Q}_{\beta \mathbf{k}_1}^{\mathbf{k}_2} \right)_\alpha = Q_{\beta \mathbf{k}_1}^{\alpha \mathbf{k}_2}. \tag{19}$$

Then, the first of these terms, which stems from $b_{l_1 n_1 \mathbf{k}_1}^{l_2 n_2 \mathbf{k}_2 \, II.1}$, can be written as a cross product:

$$\boldsymbol{\omega}_M \times \mathbf{Q}_{\beta \mathbf{k}_1}^{\mathbf{k}_2} \qquad (20)$$

indicating a precession of the vector $\mathbf{Q}_{\beta \mathbf{k}_1}^{\mathbf{k}_2}$ around the direction $\boldsymbol{\omega}_M$ of the Mn magnetization with the same frequency as the mean-field precession of the electron spin. Likewise, the term originating from $b_{l_1 n_1 \mathbf{k}_1}^{l_2 n_2 \mathbf{k}_2 \, II.2}$ has a similar structure. It can also be written as a cross product

$$\boldsymbol{\omega}_E \times \mathbf{Q}_{\mathbf{k}_1}^{\alpha \mathbf{k}_2}, \qquad (21)$$

where now the index β is associated with the components of a vector $\mathbf{Q}_{\mathbf{k}_1}^{\alpha \mathbf{k}_2}$ formed from the correlations according to

$$\left(\mathbf{Q}_{\mathbf{k}_1}^{\alpha \mathbf{k}_2} \right)_\beta = Q_{\beta \mathbf{k}_1}^{\alpha \mathbf{k}_2}, \qquad (22)$$

i.e., now we are dealing with a precession around the direction $\boldsymbol{\omega}_E$ of the electron spin. Thus, not only the average spins of the electrons and Mn atoms exhibit a precession dynamics, but also their correlations, which is represented in the equations of motion by the $b_{l_1 n_1 \mathbf{k}_1}^{l_2 n_2 \mathbf{k}_2 \, II}$ terms.

Finally, the physical meaning of the $b_{l_1 n_1 \mathbf{k}_1}^{l_2 n_2 \mathbf{k}_2 \, III}$ source terms becomes clear by noting that their structure is analogous to the structure of the $b_{l_1 n_1 \mathbf{k}_1}^{l_2 n_2 \mathbf{k}_2 \, I}$ terms, where the products of electron and Mn density matrices are replaced by the corresponding unfactorized correlation functions. Thus, the $b_{l_1 n_1 \mathbf{k}_1}^{l_2 n_2 \mathbf{k}_2 \, III}$ sources provide the correlated parts of the $b_{l_1 n_1 \mathbf{k}_1}^{l_2 n_2 \mathbf{k}_2 \, I}$ sources, which represented a Landau-Lifshitz-Gilbert-like dynamics including Pauli blocking.

Now that all source terms have been physically interpreted, let us come back to the question of their relative importance in the case considered numerically in Sec. IV. As already noted, the sources $b_{l_1 n_1 \mathbf{k}_1}^{l_2 n_2 \mathbf{k}_2 \, I}$ always play a pivotal role, since no correlations would build up without these terms. The importance of the remaining terms depends on the physical situation. Looking at the definition Eqs. (7d)–(7f) of the sources, it is seen that the terms $b_{l_1 n_1 \mathbf{k}_1}^{l_2 n_2 \mathbf{k}_2 \, X.2}$, with $X \in \{I, II, III\}$, comprise similar factors as the corresponding contributions $b_{l_1 n_1 \mathbf{k}_1}^{l_2 n_2 \mathbf{k}_2 \, X.1}$, except that the former contain an additional factor proportional to the electron density matrix $C_{l_1 \mathbf{k}_1}^{l_2}$. From this observation we can conclude that the $b_{l_1 n_1 \mathbf{k}_1}^{l_2 n_2 \mathbf{k}_2 \, X.2}$ sources should be less important than the $b_{l_1 n_1 \mathbf{k}_1}^{l_2 n_2 \mathbf{k}_2 \, X.1}$ terms, if the electron density is moderate, as it is the case here. A criterion for being in the low density limit is particularly easy to formulate for the $b_{l_1 n_1 \mathbf{k}_1}^{l_2 n_2 \mathbf{k}_2 \, II}$ terms, since Eq. (7e) implies that $b_{l_1 n_1 \mathbf{k}_1}^{l_2 n_2 \mathbf{k}_2 \, II.2}$ is negligible compared with $b_{l_1 n_1 \mathbf{k}_1}^{l_2 n_2 \mathbf{k}_2 \, II.1}$ if $N_{\text{Mn}} \gg N_e$, which is fulfilled in our simulations. However, it is more challenging to give a condition for the negligibility of the $b_{l_1 n_1 \mathbf{k}_1}^{l_2 n_2 \mathbf{k}_2 \, I.2}$ term, as it strongly depends on the electron distribution in k space.

Finally, since the $b_{l_1 n_1 \mathbf{k}_1}^{l_2 n_2 \mathbf{k}_2 \, III}$ sources have the same structure as the $b_{l_1 n_1 \mathbf{k}_1}^{l_2 n_2 \mathbf{k}_2 \, I}$ term, except that the correlations $Q_{l_1 n_1 \mathbf{k}_1}^{l_2 n_2 \mathbf{k}_2}$ take the place of the product $C_{l_1 \mathbf{k}_1}^{l_2} M_{n_1}^{n_2}$, they will be of minor importance if the relation $\frac{Q_{l_1 n_1 \mathbf{k}_1}^{l_2 n_2 \mathbf{k}_2}}{C_{l_1 \mathbf{k}_1}^{l_2} M_{n_1}^{n_2}} \ll 1$ is satisfied. The latter relation is

expected to hold, when the conditions for the applicability of the correlation expansion are fulfilled. The numerical results shown in Fig. 1 indicate that the $b_{l_1 n_1 \mathbf{k}_1}^{l_2 n_2 \mathbf{k}_2 \, III}$ terms provide insignificant quantitative corrections, which confirms the consistency of the correlation expansion approach.

The fact that a source contains correlations is, however, not sufficient for concluding that it can be neglected compared with the $b_{l_1 n_1 \mathbf{k}_1}^{l_2 n_2 \mathbf{k}_2 \, I}$ terms, which do not involve correlations. In particular, the $b_{l_1 n_1 \mathbf{k}_1}^{l_2 n_2 \mathbf{k}_2 \, II.1}$ term was shown to qualitatively modify the spin dynamics (cf. Figs. 1 and 2). In view of our interpretation of the $b_{l_1 n_1 \mathbf{k}_1}^{l_2 n_2 \mathbf{k}_2 \, II.1}$ term, this implies physically that accounting for the precession of the correlations around the Mn magnetization is essential for a correct description of the spin dynamics. This also explains why previous studies in Refs. [16,17] reported a negligible contribution from the $b_{l_1 n_1 \mathbf{k}_1}^{l_2 n_2 \mathbf{k}_2 \, II.1}$ term, since there a situation was considered, where the average Mn spin was initially set to zero which suppresses the precession.

The features of the spin dynamics predicted in this article manifest themselves in the time evolution of the spin polarization which is a quantity accessible experimentally, e.g., by time- and polarization-resolved photoluminescence or Faraday-/Kerr-rotation measurements [20]. Favorable for the observation of such effects should be experiments measuring the time dependence of the spin polarization as well as the its equilibrium value where the angle between the Mn magnetization and the initial electron spin polarization induced by a circularly polarized laser beam is varied. For our purposes bulk materials are preferable compared with, e.g., quantum wells, since for heterostructures the anisotropy with respect to growth axis as well as structure inversion asymmetry can play a role [21], which would make it hard to separate the angular dependence predicted by our theory from anisotropy effects. Furthermore, II-VI DMS should be better suited for the proposed experiment than III-V DMS, since they have the advantage of isoelectrical doping. In III-V materials, the Bir-Aronov-Pikus interaction [22] between electron and hole spins can dominate the spin dynamics [9], while for II-VI DMS with sufficiently high Mn doping the s-d-exchange interaction is typically the most important spin relaxation mechanism [23].

VI. SUMMARY

In this article, we have analyzed the spin dynamics of conduction band electrons in Mn doped bulk DMS induced by the s-d-exchange interaction. In contrast to our previous studies [16,17], we now assume a nonzero Mn magnetization. This naturally leads to a distinction between the electron spin dynamics of the components parallel and perpendicular to the Mn spin which introduces an anisotropy in the spin relaxation. Starting from a microscopic quantum kinetic theory based on correlation expansion we have derived the Markov limit yielding equations similar to the widely used phenomenological Landau-Lifshitz-Gilbert equations. Our derivation yields microscopic expressions for the parameters in the Landau-Lifshitz-Gilbert equations and allows us to identify some quantum corrections. The resulting rate equations were solved analytically.

Numerical simulations within the quantum kinetic theory revealed that, while the dynamics of the perpendicular electron spin component can be well described by the Markovian theory, the parallel component exhibits qualitative deviations between the full quantum kinetic and the corresponding Markovian results. The differences between both levels of theory manifest themselves in a nonmonotonic temporal behavior of the total spin in the quantum kinetic theory as opposed to an almost exponential monotonic decay predicted by the Markovian theory. Moreover, for certain excitation conditions, even the sign of the spin polarization differs between these levels of theory.

A detailed analysis allowed us to assign a physical interpretation to all source terms for the correlations and to understand their relative importance found in our numerical studies. With the help of this analysis and our numerical results, the deviations between the full quantum kinetic theory and its Markov limit were traced back to the neglect of a precession dynamics of the correlations in the Markov theory. This precession is missing in the Markov limit not because of the assumption of a short memory but due to the perturbative treatment that is implicit in this approach.

ACKNOWLEDGMENT

APPENDIX: ANALYTICAL SOLUTIONS OF THE MARKOV EQUATIONS

Equation (14a) is a Riccati differential equation

$$\frac{\partial}{\partial t} s_{\mathbf{k}_1}^{\parallel} = f s_{\mathbf{k}_1}^{\parallel 2} - g s_{\mathbf{k}_1}^{\parallel} + h, \tag{A1}$$

with $f = \gamma_{\mathbf{k}_1} S$, $g = \gamma_{\mathbf{k}_1}(\langle S^2 \rangle - \langle S^{\parallel 2} \rangle)$ and $h = \gamma_{\mathbf{k}_1} S \frac{n_{\mathbf{k}_1}(2 - n_{\mathbf{k}_1})}{4}$. For $f = 0$, which is the case if $S = 0$, the solution of Eq. (A1) is simply:

$$s_{\mathbf{k}_1}^{\parallel}(t) = \left(s_{\mathbf{k}_1}^{\parallel}(0) - \frac{h}{g} \right) e^{-gt} + \frac{h}{g}. \tag{A2}$$

For $f \neq 0$, the Riccati equation can be rewritten in terms of a linear differential equation with eigenvalues:

$$\lambda_{1/2} = \underbrace{-\frac{g}{2}}_{=:\mu} \pm \underbrace{\sqrt{\frac{g^2}{4} - fh}}_{=:\nu}. \tag{A3}$$

The solution of Eq. (A1) is then given by:

$$s_{\mathbf{k}_1}^{\parallel}(t) = \frac{\mu}{f} - \frac{\nu}{f} \tanh\left(\frac{\varphi}{2} + \nu t \right) \tag{A4}$$

where φ is determined by the initial value of $s_{\mathbf{k}_1}^{\parallel}$.

Eq. (14b) for the perpendicular spin component assumes the form:

$$\frac{\partial}{\partial t} s_{\mathbf{k}_1}^{\perp} = \left(-\xi + f s_{\mathbf{k}_1}^{\parallel} \right) s_{\mathbf{k}_1}^{\perp}, \tag{A5}$$

where $\xi = \frac{1}{2} \gamma_{\mathbf{k}_1}(\langle S^2 \rangle + \langle S^{\parallel 2} \rangle)$. Eq. (A5) is solved by

$$s_{\mathbf{k}_1}^{\perp}(t) = s_{\mathbf{k}_1}^{\perp}(0) e^{-\xi t} \underbrace{e^{f \int_0^t s_{\mathbf{k}_1}^{\parallel}(t')dt'}}_{=:I}. \tag{A6}$$

For $f = 0$, $I = 1$ and the perpendicular spin component decreases exponentially. Inserting the solution for the parallel spin component from Eq. (A4) for nonzero f yields:

$$I = e^{\mu t} \frac{\cosh\left(\frac{\varphi}{2} \right)}{\cosh\left(\frac{\varphi}{2} + \nu t \right)}. \tag{A7}$$

[1] D. Awschalom and N. Samarth, J. Magn. Magn. Mater. **200**, 130 (1999).

[2] D. Awschalom and M. Flatté, Nature Phys. **3**, 153 (2007).

[3] S. A. Wolf, D. D. Awschalom, R. A. Buhrman, J. M. Daughton, S. von Molnr, M. L. Roukes, A. Y. Chtchelkanova, and D. M. Treger, Science **294**, 1488 (2001).

[4] I. Žutić, J. Fabian, and S. Das Sarma, Rev. Mod. Phys. **76**, 323 (2004).

[5] A. MacDonald, P. Schiffer, and N. Samarth, Nature Mater. **4**, 195 (2005).

[6] T. Dietl, H. Ohno, F. Matsukura, J. Cibert, and D. Ferrand, Science **287**, 1019 (2000).

[7] P. A. Wolff and J. Warnock, Jpn. J. Appl. Phys. **55**, 2300 (1984).

[8] O. Morandi, P.-A. Hervieux, and G. Manfredi, New J. Phys. **11**, 073010 (2009).

[9] J. H. Jiang, Y. Zhou, T. Korn, C. Schüller, and M. W. Wu, Phys. Rev. B **79**, 155201 (2009).

[10] B. König, I. A. Merkulov, D. R. Yakovlev, W. Ossau, S. M. Ryabchenko, M. Kutrowski, T. Wojtowicz, G. Karczewski, and J. Kossut, Phys. Rev. B **61**, 16870 (2000).

[11] L. Cywiński and L. J. Sham, Phys. Rev. B **76**, 045205 (2007).

[12] Y. G. Semenov, Phys. Rev. B **67**, 115319 (2003).

[13] M. D. Kapetanakis, J. Wang, and I. E. Perakis, J. Opt. Soc. Am. B **29**, A95 (2012).

[14] O. Morandi, Phys. Rev. B **83**, 224428 (2011).

[15] C. Thurn and V. M. Axt, Phys. Rev. B **85**, 165203 (2012).

[16] C. Thurn, M. Cygorek, V. M. Axt, and T. Kuhn, Phys. Rev. B **87**, 205301 (2013).

[17] C. Thurn, M. Cygorek, V. M. Axt, and T. Kuhn, Phys. Rev. B **88**, 161302 (2013).

[18] C. Zener, Phys. Rev. **81**, 440 (1951).

[19] J. Kossut, *Diluted Magnetic Semiconductors*, edited by J. Furdyna and J. Kossut, Semiconductors and Semimetals, Vol. 25 (Academic Press, San Diego, 1988), p. 185.

[20] J. Hübner and M. Oestreich, *Spin Physics in Semiconductors*, edited by M. I. Dyakonov, Springer Series in Solid-State Sciences, Vol. 157 (Springer, Berlin, 2008), pp. 115–134.

[21] Y. A. Bychkov and E. I. Rashba, J. Phys. C **17**, 6039 (1984).

[22] G. L. Bir, A. Aronov, and G. E. Pikus, JETP **42**, 705 (1975).

[23] M. Wu, J. Jiang, and M. Weng, Phys. Rep. **493**, 61 (2010).

Publication 2

Effective equations for the precession dynamics of electron spins and electron-impurity correlations in diluted magnetic semiconductors

M. Cygorek and V. M. Axt

Effective equations for the precession dynamics of electron spins and electron–impurity correlations in diluted magnetic semiconductors

M Cygorek and V M Axt

Theoretische Physik III, Universität Bayreuth, D-95440 Bayreuth, Germany

E-mail: Moritz.Cygorek@uni-bayreuth.de

CrossMark

Abstract

Starting from a quantum kinetic theory for the spin dynamics in diluted magnetic semiconductors, we derive simplified equations that effectively describe the spin transfer between carriers and magnetic impurities for an arbitrary initial impurity magnetization. Taking the Markov limit of these effective equations, we obtain good quantitative agreement with the full quantum kinetic theory for the spin dynamics in bulk systems at high magnetic doping. In contrast, the standard rate description where the carrier–dopant interaction is treated according to Fermi's golden rule, which involves the assumption of a short memory as well as a perturbative argument, has been shown previously to fail if the impurity magnetization is non-zero. The Markov limit of the effective equations is derived, assuming only a short memory, while higher order terms are still accounted for. These higher order terms represent the precession of the carrier–dopant correlations in the effective magnetic field due to the impurity spins. Numerical calculations show that the Markov limit of our effective equations reproduces the results of the full quantum kinetic theory very well. Furthermore, this limit allows for analytical solutions and for a physically transparent interpretation.

(Some figures may appear in colour only in the online journal)

1. Introduction

Diluted magnetic semiconductors (DMS), in particular Mn doped II–VI and III–V materials, have been studied for several decades [1–19]. However, the theoretical description of the ultrafast spin dynamics of the magnetic impurities and carriers is, so far, mostly limited to a single-particle mean-field picture, where transfer rates are calculated perturbatively by Fermi's golden rule. Interesting features of the spin dynamics in DMS that have been demonstrated in recent time-resolved Kerr measurements [20], like the non-monotonous magnetic field dependence of the transverse spin dephasing time in extremely diluted $Cd_{1-x}Mn_xTe$ quantum wells or the mismatch between the theoretically predicted and

experimentally measured dephasing times for zero magnetic field, still lack a satisfactory theoretical explanation. To provide a more elaborate theoretical framework for the discussion and quantitative calculation of the spin dynamics in DMS, a quantum kinetic theory based on a correlation expansion has been introduced [21] where the exchange interaction between free carriers and the d electrons of the Mn impurities was modelled by a Kondo Hamiltonian. The full quantum kinetic theory is, however, numerically challenging and the physical interpretation requires some effort. Hence, it is a difficult task to efficiently implement other mechanisms of spin exchange and dephasing into the theory in order to account for effects that are in many cases needed for a proper description of real experiments like, e.g., the D'yakonov–

Perel' [22], Elliot–Yafet [23, 24] and Bir–Aronov–Pikus [25] mechanisms. However, it was already shown that for three-dimensional systems in which the number of Mn impurities N_{Mn} exceeds the number of free carriers N_e, a simplification of the quantum kinetic theory can be established that reasonably reproduces results in the case of a vanishing initial Mn magnetization [26]. This was achieved by a perturbative treatment of the carrier–impurity interaction as well as the assumption of a short memory. This procedure yielded the same rate equations as Fermi's golden rule. In contrast, for a nonzero average Mn spin these rate equations were shown to describe only the electron spin component perpendicular to the Mn spin well, while a discrepancy in the dynamics of the parallel electron spin component could be attributed to neglected terms of higher than leading order in the coupling constant J_{sd} of the Kondo Hamiltonian (1) in the perturbative derivation of the rate equations in [27].

In the present article, we derive approximate equations of motion for the electron spins in the spirit of the equations in [27], but take the higher order corrections into account. These equations describe the effects of the precession of the electron spins around the effective magnetic field due to the Mn magnetization and effectively account for a precession-type dynamics of the electron–Mn correlations that has been identified previously in [27]. The resulting *precession of electron spins and correlations* (PESC) equations are then discussed and their Markov limit is established which can be solved analytically. Numerical calculations show that for $N_{Mn} \gg N_e$ these analytical solutions coincide with the results of the full quantum kinetic theory, at least in three-dimensional systems. The simplicity of the PESC equations makes it possible to easily interpret the basic physical processes involved in the quantum kinetic theory and allows the PESC equations to provide a suitable framework for further studies of non-Markovian effects as well as of the interplay between the s–d interaction and other mechanisms of spin relaxation and dephasing. In particular, it was shown in [29] on the basis of the PESC equations that in some materials the Dresselhaus [30] or Rashba [31] spin–orbit interactions can compete with the s–d exchange interaction.

It is noteworthy that the derived effective equations are expected to be applicable not only for the spin dynamics in DMS, but they can easily be extended to describe more generally any system, in which a continuum of states is coupled to localized magnetic impurities via a Kondo-like Hamiltonian

$$H_{sd} = J_{sd} \sum_{Ii} \hat{\mathbf{S}}^I \cdot \hat{\mathbf{s}}^i \delta(\mathbf{R}_I - \mathbf{r}_i), \tag{1}$$

where in the case of DMS $\hat{\mathbf{S}}^I$ and $\hat{\mathbf{s}}^i$ are the spin operators of the Ith Mn ion and the ith electron, respectively, and $\mathbf{R}_I$ as well as $\mathbf{r}_i$ are the corresponding positions. Similar magnetic interactions can also arise from nuclear spins due to the Fermi contact interaction or an effective interaction between conduction band electrons and localized states, such as in quantum dots, or quasi-particles, e.g. excitons, in a huge variety of systems ranging from semiconductor

heterostructures to novel materials such as graphene or dichalcogenides, since the main difference between these systems lies in the details of the single-particle band structures. Therefore, the equations of motion studied here are of prototypical character for the spin dynamics of extended systems.

The article is outlined as follows: first, we summarize the quantum kinetic theory and reproduce the basic equations of motion where we restrict ourselves to the terms that were shown in [27] to be numerically important in the case $N_{Mn} \gg N_e$. In a next step, we apply a rotating-wave-like approximation and derive the PESC equations of motion for the electron spins and occupations. Then, the Markov limit of the PESC equations is introduced, and the thereby described physical effects are discussed; in particular the spectral redistribution of electrons as well as Pauli blocking effects are shown to arise naturally on this level of theory. Subsequently, analytical solutions to the Markov limit of the PESC equations are presented and compared with numerical results of the full quantum kinetic theory.

2. Method: derivation of effective equations

We will give a short overview of the quantum kinetic theory for the spin dynamics in DMS developed in [21]. There, a systematic derivation of equations of motion for the spins of interacting carriers and Mn impurities in DMS has been presented accounting for conduction and valence band carriers, their coherences, the Mn impurity spins, the correlations between carriers and impurities as well as the effect of an external laser field, where a disorder average over the random distribution of the impurities in the semiconductor was performed. Apart from the corresponding band energies, the theory accounts for the exchange interaction between carriers and Mn impurities as well as for the dipole coupling to a classical laser field.

We want to focus our study on the spin dynamics in isoelectrically doped bulk DMS starting from a non-equilibrium state. Such kind of situation can be prepared, e.g., by optical excitation with circularly polarized light. Since in bulk systems, the typical timescale of the hole spin relaxation is of the order of 100 fs [28] due to the strong spin–orbit interaction, we can neglect the valence band and the interband coherences when concentrating on a ps timescale. The assumptions and parameters used in the present article can be realized best in II–VI DMS, whereas in III–V based DMS the situation can be more involved, e.g., the Mn doping usually leads to a p-doping in GaMnAs as a side effect. Furthermore, while the impurities in II–VI DMS are typically found in the spin-$\frac{5}{2}$ configuration of the Mn^{2+} state, substitutionally incorporated Mn^{3+} ions, e.g., in GaMnN can form spin-$\frac{4}{2}$ systems [19].

When only the conduction band electrons and the impurities together with their correlations are considered, the resulting equations of motion can be simplified as it was shown in [27]. As dynamical variables we can choose the

Pub 2

Semicond. Sci. Technol. **30** (2015) 085011   M Cygorek and V M Axt

spins $s_{\mathbf{k}}$ and occupations $n_{\mathbf{k}}$ of conduction band electrons with wave vector $\mathbf{k}$ and average impurity spin $\langle \mathbf{S} \rangle$ and second moments $\langle S^{\gamma_1} S^{\gamma_2} \rangle$ as well as the carrier–impurity correlations $Q_{\beta \mathbf{k}_1}^{\alpha \mathbf{k}_2}$ defined by:

$$n_{\mathbf{k}_1} = \sum_{\sigma_1 = \{\uparrow,\downarrow\}} \left\langle c_{\sigma_1 \mathbf{k}_1}^\dagger c_{\sigma_1 \mathbf{k}_1} \right\rangle, \tag{2a}$$

$$s_{\mathbf{k}_1}^\gamma = \sum_{\sigma_1,\sigma_2 = \{\uparrow,\downarrow\}} s_{\sigma_1 \sigma_2}^\gamma \left\langle c_{\sigma_1 \mathbf{k}_1}^\dagger c_{\sigma_2 \mathbf{k}_1} \right\rangle, \tag{2b}$$

$$\langle S^\gamma \rangle = \sum_{n_1,n_2 = -\frac{5}{2}}^{\frac{5}{2}} S_{n_1 n_2}^\gamma \hat{P}_{n_1 n_2}^I, \tag{2c}$$

$$\langle S^{\gamma_1} S^{\gamma_2} \rangle = \sum_{n_0,n_1,n_2 = -\frac{5}{2}}^{\frac{5}{2}} S_{n_0 n_1}^{\gamma_1} S_{n_1 n_2}^{\gamma_2} \left\langle \hat{P}_{n_0 n_2}^I \right\rangle, \tag{2d}$$

$$Q_{\beta \mathbf{k}_1}^{\alpha \mathbf{k}_2} = V \sum_{\sigma_1,\sigma_2 = \{\uparrow,\downarrow\}} \sum_{n_1,n_2 = -\frac{5}{2}}^{\frac{5}{2}} s_{\sigma_1 \sigma_2}^\alpha S_{n_1 n_2}^\beta$$
$$\times \left[\left\langle c_{\sigma_1 k_1}^\dagger c_{\sigma_2 \mathbf{k}_2} \hat{P}_{n_1 n_2}^I e^{i(\mathbf{k}_2 - \mathbf{k}_1)\mathbf{R}_I} \right\rangle - \left\langle c_{\sigma_1 \mathbf{k}_1}^\dagger c_{\sigma_2 \mathbf{k}_2} \right\rangle \left\langle \hat{P}_{n_1 n_2}^I \right\rangle \right], \tag{2e}$$

where $c_{\sigma_1 \mathbf{k}_1}^\dagger$ and $c_{\sigma_1 \mathbf{k}_1}$ are the electron creation and annihilation operators, $\hat{P}_{n_1 n_2}^I = |I, n_1\rangle \langle I, n_2|$ is the density operator for the spin-$\frac{5}{2}$ state of the d electrons of the Ith Mn ion, and the indices σ_i as well as n_i represent spin indices of the conduction band electrons and Mn spin states, respectively. The indices γ and β in equation (2) correspond to the three space components of the spin. In the definition of the correlations $Q_{\beta \mathbf{k}_1}^{\alpha \mathbf{k}_2}$ the index α runs from 0 to 3. $s_{\sigma_1 \sigma_2}^\alpha$ are the electron spin matrices and the identity matrix (for $\alpha = 0$), respectively, and $S_{n_1 n_2}^\beta$ are the spin-$\frac{5}{2}$ matrices for the Mn ions. The brackets symbolize the quantum mechanical average as well as the disorder average over the random distribution of the Mn positions $\mathbf{R}_I$ (see [21] and [27] for the details of the correlation expansion and the truncation scheme). The equations of motion for the dynamical variables are then given by [21, 27]:

$$\frac{\partial}{\partial t} n_{\mathbf{k}_1} = \frac{J_{\mathrm{sd}}}{\hbar} n_{\mathrm{Mn}} \frac{1}{V} \sum_{\mathbf{k}} \sum_{i=1}^{3} 2\Im\left(Q_{i\mathbf{k}_1}^{i\mathbf{k}}\right), \tag{3a}$$

$$\frac{\partial}{\partial t} s_{\mathbf{k}_1}^\alpha = \left(\boldsymbol{\omega}_M \times \mathbf{s}_{\mathbf{k}_1}\right)_\alpha$$
$$+ \frac{J_{\mathrm{sd}} n_{\mathrm{Mn}}}{V\hbar} \sum_{\mathbf{k}} \left[\frac{1}{2} \Im\left(Q_{\alpha \mathbf{k}_1}^{0\mathbf{k}}\right) + \sum_{i,j=1}^{3} \epsilon_{ij\alpha} \Re\left(Q_{i\mathbf{k}_1}^{j\mathbf{k}}\right) \right], \tag{3b}$$

$$\frac{\partial}{\partial t} Q_{\beta \mathbf{k}_1}^{\alpha \mathbf{k}_2} = -i(\omega_{\mathbf{k}_2} - \omega_{\mathbf{k}_1}) Q_{\beta \mathbf{k}_1}^{\alpha \mathbf{k}_2} + \sum_{\gamma,\delta=1}^{3} \epsilon_{\alpha\gamma\delta} \omega_M^\gamma Q_{\beta \mathbf{k}_1}^{\delta \mathbf{k}_2}$$
$$+ \frac{i}{\hbar} J_{\mathrm{sd}} \left(b_{\beta \mathbf{k}_1}^{\alpha \mathbf{k}_2 I} + b_{\beta \mathbf{k}_1}^{\alpha \mathbf{k}_2 \mathrm{Res}} \right), \tag{3c}$$

where V represents the volume of the sample, $n_{\mathrm{Mn}} = \frac{N_{\mathrm{Mn}}}{V}$ is the Mn density and the $\mathbf{k}$-sum has to be performed over all states in the first Brillouin zone. In equations (3b) and (3c), the mean field precession frequency and axis of the electrons

around the Mn magnetization $\boldsymbol{\omega}_M := \frac{J_{\mathrm{sd}}}{\hbar} n_{\mathrm{Mn}} \langle \mathbf{S} \rangle$ has been introduced. $\omega_{\mathbf{k}} = \frac{E_{\mathbf{k}}}{\hbar} = \frac{\hbar \mathbf{k}^2}{2m^*}$ describes the single-particle frequencies of the quasi-free conduction band electrons assuming a parabolic band structure with effective mass m^* without the electron–Mn exchange interaction. $b_{\beta \mathbf{k}_1}^{\alpha \mathbf{k}_2 \mathrm{Res}}$ comprise residual source terms that were identified in Ref. [27] to be insignificant if $N_{\mathrm{Mn}} \gg N_e$ and V is large. Therefore, we will henceforth neglect $b_{\beta \mathbf{k}_1}^{\alpha \mathbf{k}_2 \mathrm{Res}}$. The relevant source terms $b_{\beta \mathbf{k}_1}^{\alpha \mathbf{k}_2 I}$ for the correlations, which are given explicitly in appendix, describe the build-up of correlations between the impurities and the carriers [27]. The precession-type dynamics of the carrier–Mn correlations around the effective magnetic field due to the Mn magnetization are incorporated via the term proportional to $\boldsymbol{\omega}_M$ in equation (3c). The neglect of the latter has been found to be the reason for the failure of the golden rule-type rate equations of [27] in describing the parallel spin transfer between the carriers and the magnetic impurities.

It is, however, possible to account for this precession and to integrate equation (3c) formally. This is particularly easy if we use the assumption $N_{\mathrm{Mn}} \gg N_e$ that allows us to regard the Mn density matrix as nearly constant in time. If the z-axis is defined to point in the direction of the Mn magnetization, the correlations are given by:

$$Q_{\beta \mathbf{k}_1}^{0 \mathbf{k}_2} = \frac{i}{\hbar} J_{\mathrm{sd}} \int_0^t dt' \left\{ b_{\beta \mathbf{k}_1}^{0 \mathbf{k}_2 I}(t') e^{i(\omega_{\mathbf{k}_2} - \omega_{\mathbf{k}_1})(t'-t)} \right\}, \tag{4a}$$

$$Q_{\beta \mathbf{k}_1}^{x \mathbf{k}_2} = \frac{i}{2\hbar} J_{\mathrm{sd}} \int_0^t dt' \left\{ \left(b_{\beta \mathbf{k}_1}^{x \mathbf{k}_2 I}(t') + i b_{\beta \mathbf{k}_1}^{y \mathbf{k}_2 I}(t') \right) \right.$$
$$\times e^{i(\omega_{\mathbf{k}_2} - \omega_{\mathbf{k}_1} - \omega_M)(t'-t)}$$
$$\left. + \left(b_{\beta \mathbf{k}_1}^{x \mathbf{k}_2 I}(t') - i b_{\beta \mathbf{k}_1}^{y \mathbf{k}_2 I}(t') \right) e^{i(\omega_{\mathbf{k}_2} - \omega_{\mathbf{k}_1} + \omega_M)(t'-t)} \right\} \tag{4b}$$

$$Q_{\beta \mathbf{k}_1}^{y \mathbf{k}_2} = \frac{i}{2\hbar} J_{\mathrm{sd}} \int_0^t dt' \left\{ \left(b_{\beta \mathbf{k}_1}^{y \mathbf{k}_2 I}(t') - i b_{\beta \mathbf{k}_1}^{x \mathbf{k}_2 I}(t') \right) \right.$$
$$\times e^{i(\omega_{\mathbf{k}_2} - \omega_{\mathbf{k}_1} - \omega_M)(t'-t)}$$
$$\left. + \left(b_{\beta \mathbf{k}_1}^{y \mathbf{k}_2 I}(t') + i b_{\beta \mathbf{k}_1}^{x \mathbf{k}_2 I}(t') \right) e^{i(\omega_{\mathbf{k}_2} - \omega_{\mathbf{k}_1} + \omega_M)(t'-t)} \right\}, \tag{4c}$$

$$Q_{\beta \mathbf{k}_1}^{z \mathbf{k}_2} = \frac{i}{\hbar} J_{\mathrm{sd}} \int_0^t dt' \left\{ b_{\beta \mathbf{k}_1}^{z \mathbf{k}_2 I}(t') e^{i(\omega_{\mathbf{k}_2} - \omega_{\mathbf{k}_1})(t'-t)} \right\}. \tag{4d}$$

In order to simplify equations (4), we follow the line of [27] and identify fast and slowly changing terms. To this end, we express the electron spin in the state with wave vector $\mathbf{k}_1$

$$\mathbf{s}_{\mathbf{k}_1} := \begin{pmatrix} s_{\mathbf{k}_1}^\perp \cos\left(\omega_M t + \varphi_{\mathbf{k}_1}\right) \\ s_{\mathbf{k}_1}^\perp \sin\left(\omega_M t + \varphi_{\mathbf{k}_1}\right) \\ s_{\mathbf{k}_1}^\parallel \end{pmatrix}, \tag{5}$$

in terms of the spin component parallel to the Mn magnetization $s_{\mathbf{k}_1}^\parallel$, the perpendicular spin component $s_{\mathbf{k}_1}^\perp$ and the phase $\varphi_{\mathbf{k}_1}$. A rotating-wave-like approximation is established, by assuming that these variables $s_{\mathbf{k}_1}^\parallel$, $s_{\mathbf{k}_1}^\perp$ and $\varphi_{\mathbf{k}_1}$

as well as the electron occupation $n_{\mathbf{k}_1}$ of the states with k-vector $\mathbf{k}_1$ change only slowly in time, since they are constant in the mean field approximation. When they are drawn out of the integrals in equation (4) and the resulting expressions for the correlations are inserted in the equations of motion (3a) and (3b) for the electron occupations and spins, we get:

$$\frac{\partial}{\partial t} n_{\mathbf{k}_1}^{\uparrow/\downarrow} = \sum_{\mathbf{k}} \left\{ \Re\left(G_{\omega_{\mathbf{k}}}^{\omega_{\mathbf{k}_1}}\right) \frac{b^{\|}}{2} \left[n_{\mathbf{k}}^{\uparrow/\downarrow} - n_{\mathbf{k}_1}^{\uparrow/\downarrow} \right] \right.$$
$$\left. + \Re\left(G_{\omega_{\mathbf{k}}}^{\omega_{\mathbf{k}_1}\pm\omega_M}\right)\left[b^{\pm} n_{\mathbf{k}}^{\downarrow/\uparrow} - b^{\mp} n_{\mathbf{k}_1}^{\uparrow/\downarrow} \mp 2b^0 n_{\mathbf{k}_1}^{\uparrow/\downarrow} n_{\mathbf{k}}^{\downarrow/\uparrow} \right] \right\}$$
(6a)

$$\frac{\partial}{\partial t} \mathbf{s}_{\mathbf{k}_1}^{\perp} = -\sum_{\mathbf{k}} \left[\Re\left(G_{\omega_{\mathbf{k}}}^{\omega_{\mathbf{k}_1}-\omega_M}\right)\left(\frac{b^+}{2} - b^0 n_{\mathbf{k}}^{\uparrow}\right) \mathbf{s}_{\mathbf{k}_1}^{\perp} \right.$$
$$+ \Re\left(G_{\omega_{\mathbf{k}}}^{\omega_{\mathbf{k}_1}+\omega_M}\right)\left(\frac{b^-}{2} + b^0 n_{\mathbf{k}}^{\downarrow}\right) \mathbf{s}_{\mathbf{k}_1}^{\perp}$$
$$+ \Re\left(G_{\omega_{\mathbf{k}}}^{\omega_{\mathbf{k}_1}}\right)\frac{b^{\|}}{2}\left(\mathbf{s}_{\mathbf{k}}^{\perp} + \mathbf{s}_{\mathbf{k}_1}^{\perp}\right) \right]$$
$$+ \frac{\langle \mathbf{S}\rangle}{|\langle \mathbf{S}\rangle|} \times \left[\omega_M - \sum_{\mathbf{k}}\left\{ \Im\left(G_{\omega_{\mathbf{k}}}^{\omega_{\mathbf{k}_1}-\omega_M}\right)\left(\frac{b^+}{2} - b^0 n_{\mathbf{k}}^{\uparrow}\right) \right. \right.$$
$$\left. \left. - \Im\left(G_{\omega_{\mathbf{k}}}^{\omega_{\mathbf{k}_1}+\omega_M}\right)\left(\frac{b^-}{2} + b^0 n_{\mathbf{k}}^{\downarrow}\right)\right\}\right] \mathbf{s}_{\mathbf{k}_1}^{\perp},$$
(6b)

where in favor of a compact notation, the variables for the occupations and spins have been transformed into the occupations of the spin-up and spin-down band, i.e., the diagonal elements of the reduced electron density matrix, according to:

$$n_{\mathbf{k}_1}^{\uparrow/\downarrow} := \frac{n_{\mathbf{k}_1}}{2} \pm s_{\mathbf{k}_1}^{\|}.$$
(7)

The coefficients used in equation (6) are given by $b^{\pm} := \langle S^{\perp 2}\rangle \pm \frac{\langle S^{\|}\rangle}{2}$, $b^0 := \frac{\langle S^{\|}\rangle}{2}$ as well as $b^{\|} := \langle S^{\|2}\rangle$, where $S^{\|} := \hat{\mathbf{S}} \cdot \frac{\langle \hat{\mathbf{S}}\rangle}{|\langle \hat{\mathbf{S}}\rangle|}$ is the Mn spin operator component parallel to the average Mn spin and $\langle S^{\perp 2}\rangle = \frac{1}{2}\langle S^2 - S^{\|2}\rangle$. The remaining integral together with some prefactors are subsumed into the memory function

$$G_{\omega_{\mathbf{k}}}^{\omega_{\mathbf{k}_1}} := \frac{J_{\text{sd}}^2}{\hbar^2}\frac{n_{\text{Mn}}}{V}\int_{-t}^{0} dt'\, e^{i\left(\omega_{\mathbf{k}}-\omega_{\mathbf{k}_1}\right)t'}.$$
(8)

Equation (6) together with the memory in equation (8) describe the spin dynamics of the conduction band electron, where the precession of the electron spins and electron–impurity correlations are accounted for and will henceforth be referred to as the PESC (precession of electron spins and correlations) equations. Note that to account for finite memory effects, the memory $G_{\omega_{\mathbf{k}}}^{\omega_{\mathbf{k}_1}}$ has to be regarded as an integral operator and the spins and occupations in the rhs of equation (6) have to be evaluated at the time $t + t'$.

3. Results and discussion

3.1. Markov limit of effective equations

Equations (6) are written in terms of dynamical variables that depend on the k-vector including the angles. This is important for possible extensions of the theory with k-dependent effective magnetic fields resulting from, e.g., Dresselhaus [30] —and Rashba [31]—terms. Without such extensions, angle-averaged equations can be obtained after going over to the Markov limit from which the physical meaning of the individual terms in the PESC equation (6) will become most obvious. Technically, this is done by letting the lower integral bound $-t$ go to $-\infty$ in the memory function $G_{\omega_{\mathbf{k}}}^{\omega_{\mathbf{k}_1}}$. The memory is then given by:

$$G_{\omega_{\mathbf{k}}}^{\omega_{\mathbf{k}_1}} \approx \frac{J_{\text{sd}}^2}{\hbar^2}\frac{n_{\text{Mn}}}{V}\left\{ \pi\delta(\omega_{\mathbf{k}} - \omega_{\mathbf{k}_1}) - \mathcal{P}\frac{i}{\omega_{\mathbf{k}} - \omega_{\mathbf{k}_1}} \right\}.$$
(9)

The memory $G_{\omega_{\mathbf{k}}}^{\omega_{\mathbf{k}_1}}$ contains a Dirac delta distribution with respect to the frequencies $\omega_{\mathbf{k}}$. This allows us to derive from the PESC equation (6) closed equations for dynamical variables that depend only on the frequencies. To this end, we define the following averaged quantities:

$$n_{\omega_1}^{\uparrow/\downarrow} := \frac{\sum_{\mathbf{k}} n_{\mathbf{k}}^{\uparrow/\downarrow}\delta(\omega_{\mathbf{k}} - \omega_1)}{\sum_{\mathbf{k}}\delta(\omega_{\mathbf{k}} - \omega_1)},$$
(10a)

$$\mathbf{s}_{\omega_1}^{\perp} := \frac{\sum_{\mathbf{k}} \mathbf{s}_{\mathbf{k}}^{\perp}\delta(\omega_{\mathbf{k}} - \omega_1)}{\sum_{\mathbf{k}}\delta(\omega_{\mathbf{k}} - \omega_1)}.$$
(10b)

Due to the delta distribution in equation (9), it becomes clear that the first term in equation (6a) for the spin-up and spin-down occupations disappears. Therefore, performing the Markov limit of equation (6) and averaging over the angles, we obtain the following equations for the averaged variables $n_{\omega_1}^{\uparrow/\downarrow}$ and $s_{\omega_1}^{\perp} := |\mathbf{s}_{\omega_1}^{\perp}|$:

$$\frac{\partial}{\partial t} n_{\omega_1}^{\uparrow} = cD(\omega_2)\left\{ b^+ n_{\omega_2}^{\downarrow} - b^- n_{\omega_1}^{\uparrow} - 2b^0 n_{\omega_1}^{\uparrow} n_{\omega_2}^{\downarrow} \right\},$$
(11a)

$$\frac{\partial}{\partial t} n_{\omega_2}^{\downarrow} = cD(\omega_1)\left\{ b^- n_{\omega_1}^{\uparrow} - b^+ n_{\omega_2}^{\downarrow} + 2b^0 n_{\omega_1}^{\uparrow} n_{\omega_2}^{\downarrow} \right\},$$
(11b)

$$\frac{\partial}{\partial t} s_{\omega_1}^{\perp} = -c\left\{ \left(D(\omega_0) + D(\omega_2)\right)\frac{\langle S^{\perp 2}\rangle}{2} + D(\omega_1)\langle S^{\|2}\rangle + \right.$$
$$\left. - \frac{\langle S^{\|}\rangle}{2}\left(D(\omega_0)n_{\omega_0}^{\uparrow} - D(\omega_2)n_{\omega_2}^{\downarrow}\right) \right\} s_{\omega_1}^{\perp},$$
(11c)

where $\omega_0 := \omega_1 - \omega_M$ and $\omega_2 := \omega_1 + \omega_M$. Here, we have used that in the quasi-continuum limit $\sum_{\mathbf{k}} \to \int d\omega D(\omega)$

with $D(\omega)$ being the density of states (DOS), and thus:

$$\sum_{\mathbf{k}} \Re\left(G_{\omega_{\mathbf{k}}}^{\omega_{\mathbf{k}_1}}\right) = \frac{J_{sd}^2}{\hbar^2} \frac{n_{Mn}}{V} \pi \sum_{\mathbf{k}} \delta(\omega_{\mathbf{k}} - \omega_{\mathbf{k}_1})$$

$$= \underbrace{\frac{J_{sd}^2}{\hbar^2} \frac{n_{Mn}}{V} \pi}_{=:c} D(\omega_1). \qquad (12)$$

Therefore, it can be seen from equations (11*a*) and (11*b*) that in the Markov limit of the PESC equations, the only dynamical variables entering the equation of motion for the spin-up electrons $n_{\omega_1}^{\uparrow}$ with frequency ω_1 are $n_{\omega_2}^{\downarrow}$ and $n_{\omega_1}^{\uparrow}$ itself. Equally, the time evolution of $n_{\omega_2}^{\downarrow}$ only depends on $n_{\omega_1}^{\uparrow}$ and $n_{\omega_2}^{\downarrow}$, so that this pair of occupations is completely decoupled from the rest of the dynamical variables. Furthermore, the total number of electrons in the pair of occupations $n_{\omega_1}^{\uparrow}$ and $n_{\omega_2}^{\downarrow}$ is conserved, since from equations (11*a*) and (11*b*) it follows:

$$\frac{\partial}{\partial t} z_{\omega_1} = 0, \qquad (13a)$$

where

$$z_{\omega_1} := D(\omega_1) n_{\omega_1}^{\uparrow} + D(\omega_2) n_{\omega_2}^{\downarrow}. \qquad (13b)$$

Equation (13*a*) allows us to merge equations (11*a*) and (11*b*) into a one-dimensional differential equation:

$$\frac{\partial}{\partial t} x_{\omega_1} = 2cb^0 x_{\omega_1}^2 - c\left[D(\omega_1)b^+ + D(\omega_2)b^- + 2b^0 z_{\omega_1}\right] x_{\omega_1}$$

$$+ cD(\omega_1)b^+ z_{\omega_1} \qquad (14)$$

for the spectral electron density in the spin-up subband $x_{\omega_1} := D(\omega_1) n_{\omega_1}^{\uparrow}$.

The last term in equations (11*a*) and (11*b*), respectively, is a consequence of the source terms $b_{\beta\mathbf{k}_1}^{\alpha\mathbf{k}_2 I,2}$ in [27] which were associated with Pauli blocking in the golden rule-type rate equations that did not account for the precession of the correlations. This fact is also visible here, since for $n_{\omega_1}^{\uparrow} \approx 1$, equation (11*a*) yields

$$\frac{\partial}{\partial t} n_{\omega_1}^{\uparrow} = cD(\omega_2)\left(\left\langle S^{\perp 2}\right\rangle - \frac{\langle S^{\|}\rangle}{2}\right)\left(n_{\omega_2}^{\downarrow} - 1\right), \qquad (15a)$$

while without the last term of equation (11*a*), the limit would be

$$\frac{\partial}{\partial t} n_{\omega_1}^{\uparrow} = cD(\omega_2)\left(\left\langle S^{\perp 2}\right\rangle\left(n_{\omega_2}^{\downarrow} - 1\right) + \frac{\langle S^{\|}\rangle}{2}\left(n_{\omega_2}^{\downarrow} + 1\right)\right). \qquad (15b)$$

Since the minimal value of $\langle S^{\perp 2}\rangle$ is $\frac{35}{12}$ which is greater than the maximal value of $\frac{\langle S^{\|}\rangle}{2}$ of $\frac{5}{4}$, the rhs of equation (15*a*) is always non-positive, so an over-occupation of $n_{\omega_1}^{\uparrow}$ with values greater than 1 is averted. In contrast, in equation (15*b*) the occupation $n_{\omega_1}^{\uparrow}$ can exceed the physically reasonable limit of 1, e.g., in the case $n_{\omega_2}^{\downarrow} \approx 1$. Thus, again, the terms resulting

from $b_{\beta\mathbf{k}_1}^{\alpha\mathbf{k}_2 I,2}$ in [27] are shown to provide for Pauli blocking effects.

The equation of motion (11*c*) for the electron spin component perpendicular to the Mn magnetization suggest an almost exponential decay to zero, but the occupations of the spin-up electrons at $\omega_1 - \omega_M$ and spin-down electrons at $\omega_1 + \omega_M$ enter in the effective decay rate. The appearance of the occupations is also due to the $b_{\beta\mathbf{k}_1}^{\alpha\mathbf{k}_2 I,2}$ terms Here, they do not represent Pauli blocking, but are a remnant of the Landau–Lifshitz–Gilbert-like damping term structure in the Markov limit in [27], since:

$$\frac{\langle S^{\|}\rangle}{2}\left(D(\omega_0)n_{\omega_0}^{\uparrow} - D(\omega_2)n_{\omega_2}^{\downarrow}\right)s_{\mathbf{k}_1}^{\perp}$$

$$= \frac{\langle S^{\|}\rangle}{2}\left(\frac{z_{\omega_0} - z_{\omega_1}}{2} + s_{\omega_1}^{\|}\right)s_{\mathbf{k}_1}^{\perp} \qquad (16)$$

and

$$\left[\mathbf{s}_\omega \times \left(\mathbf{s}_{\omega_1} \times \langle\mathbf{S}\rangle\right)\right]_\perp = \langle S^{\|}\rangle s_\omega^{\|} s_{\omega_1}^{\perp}. \qquad (17)$$

In fact, comparing the derivation of the Markov limit with and without accounting for the precession of the correlations it can easily be seen that the PESC Markov equation (12) lead to the Markov equation (10) of [27], when ω_M is set to zero in the memory terms $G_\omega^{\omega_1 \pm \omega_M}$.

3.2. Analytical solutions

The Markov limit of the PESC equations allows us to find analytic solutions which we will derive in the following.

3.2.1. Without Pauli blocking. If the terms resulting from $b_{\beta\mathbf{k}_1}^{\alpha\mathbf{k}_2 I,2}$ are neglected, equations (11*a*) and (11*b*) yield:

$$\frac{\partial}{\partial t} x_{\omega_1} = -c\left(D(\omega_1)b^+ + D(\omega_2)b^-\right)x_{\omega_1} + cD(\omega_1)b^+ z_{\omega_1}. \qquad (18)$$

The solution of equation (18) decays exponentially:

$$x_{\omega_1}(t) = \left(x_{\omega_1}(0) - \xi_{\omega_1}\right)e^{-\eta_{\omega_1} t} + \xi_{\omega_1}, \qquad (19a)$$

with

$$\eta_{\omega_1} := c\left(D(\omega_1)b^+ + D(\omega_2)b^-\right), \qquad (19b)$$

$$\xi_{\omega_1} := \frac{D(\omega_1)b^+}{D(\omega_1)b^+ + D(\omega_2)b^-} z_{\omega_1}. \qquad (19c)$$

It should be noted that for $D(\omega_2) \to D(\omega_1)$, the rate η_{ω_1} reaches the same value as for the rate equations of [27] and Fermi's golden rule [1, 26] when only the parabolic band energy is accounted for the initial and final states. Here, η_{ω_1} describes rates that can be derived with Fermi's golden rule, when the mean field energy difference between electrons in the spin-up and spin-down subbands $\hbar\omega_M$ is substituted into the band structure and transitions between these now non-degenerate subbands are considered.

Furthermore, without the terms originating from $b_{\beta \mathbf{k}_1}^{\alpha \mathbf{k}_2 I.2}$, the perpendicular component of the electron spin changes according to

$$
\frac{\partial}{\partial t} s_{\omega_1}^{\perp}
$$

$$
= -c \underbrace{\left\{ \left(D(\omega_0) + D(\omega_2) \right) \frac{\langle S^{\perp 2} \rangle}{2} + D(\omega_1) \langle S^{\| 2} \rangle \right\}}_{\gamma_{\omega_1}^{\perp} :=} s_{\omega_1}^{\perp} \qquad (20)
$$

which is solved by

$$
s_{\omega_1}^{\perp}(t) = s_{\omega_1}^{\perp}(0) e^{-\gamma_{\omega_1}^{\perp} t}. \qquad (21)
$$

It should be noted that neglecting the $b_{\beta \mathbf{k}_1}^{\alpha \mathbf{k}_2 I.2}$ terms in the rate equations without accounting for the precession of the correlations yielded the same expression for the rate that can also be obtained by letting $D(\omega_0)$ and $D(\omega_2)$ go to $D(\omega_1)$ in equation (20). In [27] it was found that including the precession of the correlation in the calculation did not significantly change the spin dynamics of the perpendicular component. Now, this can be understood by Taylor-expanding the DOS. Since in three dimensions, the DOS is proportional to the square root of ω, we find:

$$
D(\omega_1 \pm \omega_M) = D(\omega_1) \sqrt{1 \pm \frac{\omega_M}{\omega_1}} \qquad (22a)
$$

and therefore

$$
D(\omega_0) + D(\omega_2) = 2 D(\omega_1) + \mathcal{O}\!\left(\left(\frac{\omega_M}{\omega_1} \right)^2 \right). \qquad (22b)
$$

Since the difference between the rates for the perpendicular component with and without accounting for the precession of the correlations is of second order of the ratio $\frac{\omega_M}{\omega_1}$, significant deviations can only be expected for small values of ω_1. There, however, the DOS is rather small.

3.2.2. With Pauli blocking. Equation (14) is a Riccati differential equation with constant coefficients. Also in the case of golden rule-type rate equations derived from the original quantum kinetic theory, where the precession of the correlations around the Mn magnetization is neglected, we found an equation for the parallel electron spin component of this form [27]. The solutions of equation (14) can be obtained along the line of the appendix in [27]:

$$
x_{\omega_1}(t) = \frac{\mu_{\omega_1}}{2 c b^0} - \frac{\nu_{\omega_1}}{2 c b^0} \tanh\!\left(\frac{\varphi_{\omega_1}}{2} + \nu_{\omega_1} t \right), \qquad (23a)
$$

with

$$
\mu_{\omega_1} = \frac{c}{2} \Big[D(\omega_1) b^+ + D(\omega_2) b^- + 2 b^0 z_{\omega_1} \Big],
$$
$$
\nu_{\omega_1} = \sqrt{\mu^2 - 2 c^2 D(\omega_1) b^+ b^0 z_{\omega_1}}, \qquad (23b)
$$

where z_{ω_1} and φ_{ω_1} are determined by the initial values of $n_{\omega_1}^{\uparrow}$ and $n_{\omega_2}^{\downarrow}$.

Finally, the time dependence of the perpendicular spin component can be calculated using the analytical expressions for $n_{\omega_0}^{\uparrow}$ and $n_{\omega_2}^{\downarrow}$ and reads:

$$
s_{\omega_1}^{\perp}(t) = s_{\omega_1}^{\perp}(0) e^{-\gamma_{\omega_1}^{\perp} t} e^{-b^0 c \int_0^t \mathrm{d}t' \left(D(\omega_0) n_{\omega_0}^{\uparrow}(t') - D(\omega_2) n_{\omega_2}^{\downarrow}(t') \right)}. \qquad (24)
$$

In order to explicitly give the corresponding analytical expressions we have to distinguish two cases:

For $\omega_1 < \omega_M$, $D(\omega_0)$ vanishes and we find from equation (24):

$$
s_{\omega_1}^{\perp}(t) = s_{\omega_1}^{\perp}(0) e^{-\gamma_{\omega_1}^{\perp} t} e^{\left(b^0 c z_{\omega_1} - \frac{1}{2} \mu_{\omega_1} \right) t} \sqrt{\frac{\cosh\left(\frac{\varphi_{\omega_1}}{2} + \nu_{\omega_1} t \right)}{\cosh\left(\frac{\varphi_{\omega_1}}{2} \right)}}, \qquad (25a)
$$

and for $\omega_1 > \omega_M$ we obtain:

$$
s_{\omega_1}^{\perp}(t) = s_{\omega_1}^{\perp}(0) e^{-\gamma_{\omega_1}^{\perp} t} e^{\left(b^0 c z_{\omega_1} - \frac{1}{2} \mu_{\omega_0} - \frac{1}{2} \mu_{\omega_1} \right) t}
$$
$$
\times \sqrt{\frac{\cosh\left(\frac{\varphi_{\omega_1}}{2} + \nu_{\omega_1} t \right)}{\cosh\left(\frac{\varphi_{\omega_1}}{2} \right)}} \sqrt{\frac{\cosh\left(\frac{\varphi_{\omega_0}}{2} + \nu_{\omega_0} t \right)}{\cosh\left(\frac{\varphi_{\omega_0}}{2} \right)}}. \qquad (25b)
$$

3.3. Numerical studies

The validity of the approximations used to derive the Markov limit PESC equation (11) is now checked by comparing the predicted spin dynamics with the results of the full quantum kinetic theory of [21] including also the residual terms that are denoted as $b_{\beta \mathbf{k}_1}^{\alpha \mathbf{k}_2 \mathrm{Res}}$ in equation (3c). We modeled a bulk DMS of $\mathrm{Zn}_{0.93}\mathrm{Mn}_{0.07}\mathrm{Se}$ with the following parameters: the Kondo coupling constant $J_{\mathrm{sd}} = 12$ meVnm^3, the effective mass $m_e = 0.21\, m_0$ and an initial average Mn spin of $\frac{1}{2}\hbar$ along the z-axis. These parameters are chosen as a compromise between, on the one hand, realistic parameters to model situations that could be explored experimentally, and on the other hand to provide a resonable test for the derived equation: a particularly large effective mass and a relatively high doping concentration lead to strong effects of the s–d interaction on the spin dynamics [26]. The coupling constant does not vary drastically between the different DMS materials. Furthermore, the difference between the different levels of theory, especially the role of the Pauli blocking terms, can be particularly highlighted by choosing initial non-equilibrium conditions, where the initial electron occupations are modeled by step functions (cf figure 1)[1].

In a first calculation, the spin-up subband occupation was initially a step function with a cut-off energy at $\mu = 3$ meV for electrons in the spin-up subband, while the spin-down subband was totally unoccupied for $t = 0$. The results are

---

[1] If the Pauli blocking terms are neglected, the equations are linear in $\mathbf{s_k}$ and $n_\mathbf{k}$. Therefore, the solutions of the equations for other initial occupations can be written as linear combinations of the solutions for the step functions.
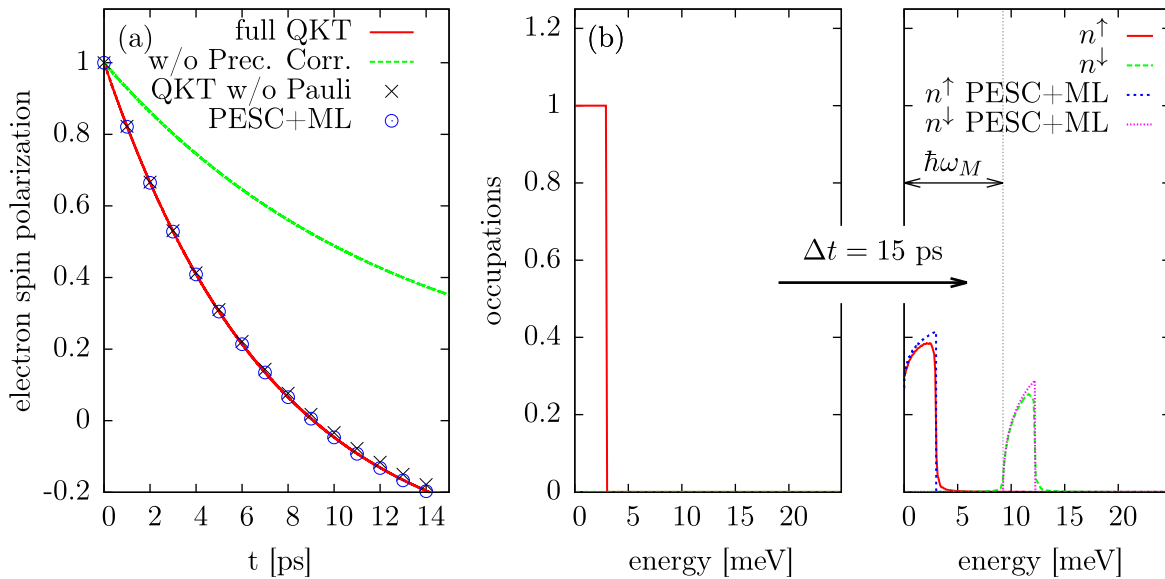
Figure 1. (a) Time evolution of the electron spin polarization of an initially step-like electron occupation in the spin-up subband. The red solid line is the result of a calculation using the full quantum kinetic theory (QKT) (see [21]). The green dashed line is derived from the rate equations without taking the precession of the correlations (w/o Prec. Corr.) into account (see [27]). The black crosses represent calculations of the quantum kinetic theory where the Pauli blocking terms $b^{\alpha \mathbf{k}_1 I.2}_{\beta \mathbf{k}_2}$ are neglected. The blue circles describe the spin dynamics according to the Markov limit of the PESC equation (11). (b) Electron distributions at times $t = 0$ ps and $t = 15$ ps calculated using the full quantum kinetic theory and the Markov limit PESC equations, respectively.

shown in figure 1(a) where we plot the modulus of the total spin polarization

$$\mathbf{s}_{\text{tot}} = \left(\sum_{\mathbf{k}} \mathbf{s}_{\mathbf{k}} \right) \left(\sum_{\mathbf{k}} \frac{1}{2} n_{\mathbf{k}} \right)^{-1}. \qquad (26)$$

There, the spin polarization is shown to decrease almost exponentially from the initially completely polarized configuration to a negative value according to the full quantum kinetic theory. While the calculation without accounting for the precession of the correlations deviates from the full quantum kinetic theory significantly, as it was already found in [27], the Markov limit of the PESC equations is able to reproduce the results of the full quantum kinetic theory almost perfectly. By comparison with the calculation neglecting the source terms $b^{\alpha \mathbf{k}_1 I.2}_{\beta \mathbf{k}_2}$ it can be seen that for the initial values used in this calculation, Pauli blocking effects are of minor importance.

Figure 1(b) depicts the energetic redistribution of the electrons: the initial step-like spin-up occupation evolves into a structure with two peaks; one in the spin-down and one in the spin-up band. The spin-up electrons with energy $\hbar\omega_1$ are redistributed to states with energy $\hbar\omega_1 + \hbar\omega_M$ which is predicted by the Markov limit of the PESC equation (6) due to terms proportional to $\delta(\omega_{\mathbf{k}} - (\omega_{\mathbf{k}_1} \pm \omega_M))$. In contrast, when the precession of the correlations are neglected, the spin-down peak builds up at the same energetic position as the spin-up peak as the shift by $\hbar\omega_M$, which accounts for the precession-like dynamics of the Mn-carrier correlations, is missing in the delta distribution. The skewness of the peaks in figure 1(b) arises from the square-root dependence of the DOS on the energy in a three-dimensional system. The fact that a small

tail is found below the spin-down peak representing occupations of states with energies lower than $\hbar\omega_M$ as well as a build-up of a high energy tail of the spin-up peak demonstrate slight non-Markovian deviations from the Dirac delta-like memory in the Markov limit of equation (9). These effects are, however, too small to influence the time dependence of the total spin polarization significantly.

Figure 2 displays the time evolution of the electron spin polarization for a situation where the initial conditions were chosen as in the calculations for figure 1, except that the average Mn spin is now turned 90° away from the electron spin. Unlike the case discussed before, the spin polarization vector $\mathbf{s}_{\text{tot}}$ now has components parallel and perpendicular to the Mn magnetization. Figure 2(a) shows a build-up of the spin polarization parallel to the Mn magnetization according to the full quantum kinetic theory which coincides with the calculations in the Markov limit of the PESC equations and the simulations without accounting for Pauli blocking. As in the previous calculations, the solution of the golden rule-type rate equation of [27] deviates significantly from the other calculations, since the energetic redistribution of the electrons is neglected. The time evolution of the perpendicular electron spin shown in figure 2(b), however, is almost the same in all of the above calculations which can be understood by considering equation (22).

In the following, we want to discuss the effects of Pauli blocking. To this end, we study a case, where both subbands are initially partly occupied and where the spin dynamics is especially clear: we use initial conditions that describe a situation, where the spin polarization is expected to be nearly constant if Pauli blocking is taken into account. Then, if we calculate the spin dynamics while neglecting the terms
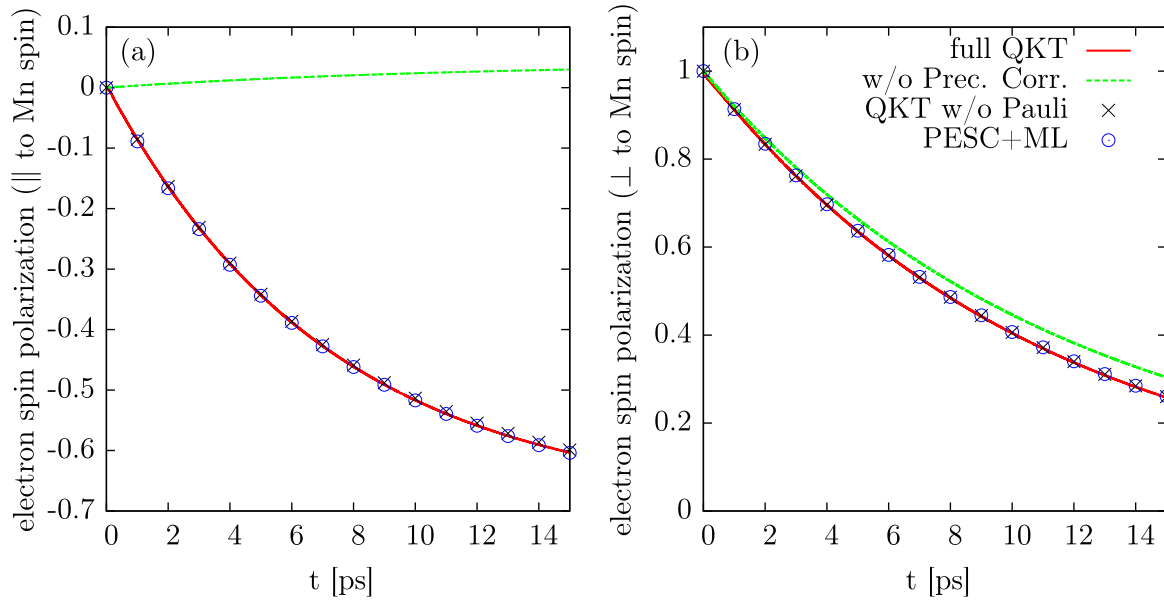
Figure 2. Time evolution of the spin polarization parallel (a) and perpendicular (b) to the Mn magnetization. The initial electron distribution is the same as in figure 1, except that the Mn magnetization was rotated 90° into a direction perpendicular to the initial electron spin (key as in figure 1(a).
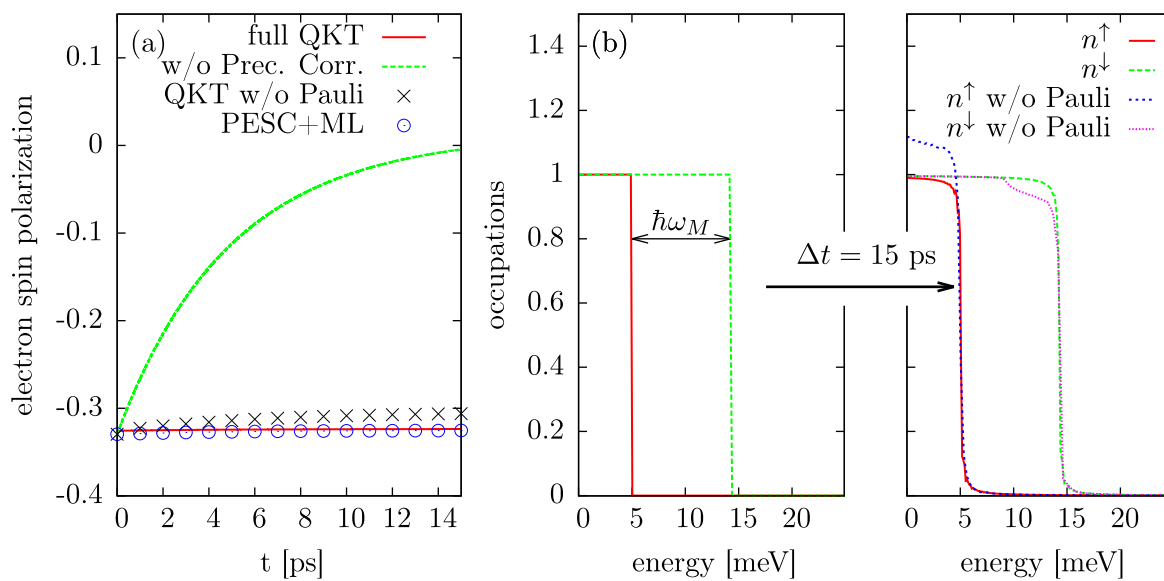
Figure 3. Time evolution of the spin polarization (a) and electron redistribution (b) of an initially step-like occupation of electrons where the difference of the cut-offs of the spin-up and spin-down subband occupations is $\hbar\omega_M$. In (b), the occupations are plotted for calculations based on the full quantum kinetic theory with and without the terms $b_{\beta\mathbf{k}_2}^{\alpha\mathbf{k}_1 1,2}$ accounting for Pauli blocking.

responsible for Pauli blocking effects, we can attribute the non-constant behavior to these effects. If the Hamiltonian (1) is treated on the mean field level, the equilibrium occupations at $T = 0$ of the spin-down and spin-up subbands follow spin-split Fermi distributions, i.e., step-functions, whose cut-off energies, measured from the respective band edge, differ by $\hbar\omega_M$. The results of the calculations with these initial conditions are given in figure 3. Since the full quantum kinetic theory also accounts for the correlation energies, very small changes in the electron spin polarization are found, which are due to the build-up of correlations over the course of time.

Figure 3(a) shows that the Markov limit of the PESC equations again yields nearly the same spin dynamics as the full quantum kinetic theory, while the rate equations without precession of the correlations fail to describe the spin polarization, since different states are coupled due to the neglect of ω_M in the Dirac delta function of the memory. The calculations involving the quantum kinetic theory without the Pauli blocking terms lead to surprisingly small deviations from the full quantum kinetic theory concerning the total spin polarization displayed in figure 3(a), despite the unphysical build-up of occupations $n_\omega^\uparrow > 1$ for some values of ω seen in

figure 3(b). The electron occupations after $t = 15$ ps depicted in figure 3(b) essentially follow the original step functions for the two spin orientations, but since the edges are smoothed due to the non-Markovian deviations from the delta distribution in the memory, they resemble Fermi distributions with an finite effective temperature.

4. Conclusion

We have derived effective equations of motion (cf equation (6)) for the conduction band electron spins and occupations starting from a microscopic quantum kinetic theory using a rotating-wave-like ansatz. These equations account for the precession of the electron spins around the effective magnetic field due to the Mn magnetization as well as for a precession-like dynamics of the electron–Mn correlation functions. Therefore, in this article they are referred to as PESC equations. The PESC equations can be more easily interpreted as the original quantum kinetic equations. They also provide an important speed-up of the numerics, in particular, when the Markov limit of the PESC equations is used. The spin dynamics for high Mn doping in three-dimensional systems derived from our effective equations in the Markov limit are demonstrated by numerical calculations to agree well with the corresponding results of the original quantum kinetic theory. This resolves the deficiency of the golden rule-type rate equations of [27] for the case of a finite initial impurity magnetization. Even though the PESC equations can in principle describe non-Markovian effects as well as Pauli blocking, the numerical studies suggest that these are of minor importance for the time evolution of the total electron spin polarization, at least for the situations studied in this paper.

The Markov limit of the PESC equation (11) can be readily interpreted: for a positive coupling constant J_{sd}, spin-up electrons can gain energy in the mean field due to the Mn magnetization by a spin-flip process to the spin-down subband. Due to the total energy conservation, this energy is transformed into kinetic energy. Therefore, a spin-up state couples effectively only to a spin-down state with a kinetic energy $\hbar\omega_M$ greater than the spin-up state energy and vice-versa. The resulting equation can be solved analytically yielding a time dependence of the electron spin polarization following a tanh-function. If the Pauli blocking terms are neglected, the equations are solved by a simple decaying exponential function with a rate that can also be obtained by applying Fermi's golden rule, if the mean field energy of an electron in the effective field of the Mn magnetization is included into the single particle energies.

Numerical studies of the energetic redistribution of the electrons in the full quantum kinetic theory support the findings of the delta-like coupling of states in energy space in general, but slight deviations from this Markovian prediction can be seen especially in the smoothing of sharp edges of the initial electron occupations. It is expected that the non-Markovian features will be more important in two-dimensional systems [26, 32]. The PESC equations in the Markov limit

derived in this paper can provide a suitable framework for further investigations of these effects. In addition, their numerical simplicity allows for the introduction of other mechanisms of spin relaxation to study reliably their competition with the s–d exchange interaction which would be a demanding task within the original quantum kinetic theory.

Acknowledgments

Appendix. Source terms for the carrier–impurity correlations

The source terms $b_{\beta\mathbf{k}_1}^{\alpha\mathbf{k}_2 I}$ for the carrier–impurity correlations $Q_{\beta\mathbf{k}_1}^{\alpha\mathbf{k}_2}$ in equation (3c) are

$$b_{\beta\mathbf{k}_1}^{\alpha\mathbf{k}_2 I} = \sum_{\gamma}\left(\langle S^{\gamma}S^{\beta}\rangle\langle s^{\gamma}s^{\alpha}\rangle_{\mathbf{k}_2\mathbf{k}_1} - \langle S^{\beta}S^{\gamma}\rangle\langle s^{\alpha}s^{\gamma}\rangle_{\mathbf{k}_1\mathbf{k}_2}\right), \quad \text{(A.1)}$$

where for $\alpha = \{1, 2, 3\}$

$$\langle s^{\gamma}s^{\alpha}\rangle_{\mathbf{k}_2\mathbf{k}_1} = \frac{1}{2}\delta_{\alpha\gamma}\left(\mathbf{s}_{\mathbf{k}_1}\cdot\mathbf{s}_{\mathbf{k}_2}\right) - \frac{1}{2}\left(s_{\mathbf{k}_1}^{\gamma}s_{\mathbf{k}_2}^{\alpha} + s_{\mathbf{k}_1}^{\alpha}s_{\mathbf{k}_2}^{\gamma}\right)$$
$$+ \frac{i}{2}\sum_{\kappa}\epsilon_{\gamma\alpha\kappa}\left[\left(1 - \frac{n_{\mathbf{k}_1}}{2}\right)s_{\mathbf{k}_2}^{\kappa} + \frac{n_{\mathbf{k}_2}}{2}s_{\mathbf{k}_1}^{\kappa}\right], \quad \text{(A.2)}$$

and $\alpha = 0$

$$\langle s^{\gamma}s^{0}\rangle_{\mathbf{k}_2\mathbf{k}_1} = \left(1 - \frac{n_{k_1}}{2}\right)s_{\mathbf{k}_2}^{\gamma} - \frac{n_{\mathbf{k}_2}}{2}s_{\mathbf{k}_1}^{\gamma} - \frac{i}{2}\sum_{\kappa\lambda}\epsilon_{\gamma\lambda\kappa}s_{\mathbf{k}_1}^{\lambda}s_{\mathbf{k}_2}^{\kappa}, \quad \text{(A.3)}$$

$$\langle s^{0}s^{\gamma}\rangle_{\mathbf{k}_1\mathbf{k}_2} = \left(1 - \frac{n_{k_2}}{2}\right)s_{\mathbf{k}_1}^{\gamma} - \frac{n_{\mathbf{k}_1}}{2}s_{\mathbf{k}_2}^{\gamma} - \frac{i}{2}\sum_{\kappa\lambda}\epsilon_{\gamma\lambda\kappa}s_{\mathbf{k}_1}^{\lambda}s_{\mathbf{k}_2}^{\kappa}. \quad \text{(A.4)}$$

References

[1] Kossut J 1975 *Phys. Status Solidi* b **72** 359–67
[2] Furdyna J K 1988 *J. Appl. Phys.* **64** 29–64
[3] Krenn H, Kaltenegger K, Dietl T, Spałek J and Bauer G 1989 *Phys. Rev.* B **39** 10918–34
[4] Crooker S A, Awschalom D D, Baumberg J J, Flack F and Samarth N 1997 *Phys. Rev.* B **56** 7574–88
[5] Kikkawa J M and Awschalom D D 1998 *Phys. Rev. Lett.* **80** 4313–6
[6] Akimov A V, Scherbakov A V, Yakovlev D R, Merkulov I A, Bayer M, Waag A and Molenkamp L W 2006 *Phys. Rev.* B **73** 165328
[7] Rönnburg K E, Mohler E, Roskos H G, Ortner K, Becker C R and Molenkamp L W 2006 *Phys. Rev. Lett.* **96** 117203
[8] Cywiński L and Sham L J 2007 *Phys. Rev.* B **76** 045205

[9] Jiang J H, Zhou Y, Korn T, Schüller C and Wu M W 2009 *Phys. Rev. B* **79** 155201

[10] Kapetanakis M D, Perakis I E, Wickey K J, Piermarocchi C and Wang J 2009 *Phys. Rev. Lett.* **103** 047404

[11] Wu M, Jiang J and Weng M 2010 *Phys. Rep.* **493** 61–236

[12] Kossut J and Gaj J (ed) 2011 *Introduction to the Physics of Diluted Magnetic Semiconductors (Springer Series in Materials Science* vol 144) (Berlin: Springer)

[13] Camilleri C, Teppe F, Scalbert D, Semenov Y, Nawrocki M, Dyakonov M, Cibert J, Tatarenko S and Wojtowicz T 2001 *Phys. Rev. B* **64** 085331

[14] Myers R C, Mikkelsen M H, Tang J M, Gossard A C, Flatté M E and Awschalom D D 2008 *Nat. Mater.* **7** 203–8

[15] Cronenberger S, Vladimirova M, Andreev S, Lifshits M and Scalbert D 2013 *Phys. Rev. Lett.* **110** 077403

[16] Chen W *et al* 2003 *Phys. Rev. B* **67** 125313

[17] Smyth J, Tulchinsky D, Awschalom D, Samarth N, Luo H and Furdyna J 1993 *Phys. Rev. Lett.* **71** 601–4

[18] Chen Y, Wiater M, Karczewski G, Wojtowicz T and Bacher G 2013 *Phys. Rev. B* **87** 155301

[19] Stefanowicz S *et al* 2013 *Phys. Rev. B* **88** 081201

[20] Ben Cheikh Z, Cronenberger S, Vladimirova M, Scalbert D, Perez F and Wojtowicz T 2013 *Phys. Rev. B* **88** 201306

[21] Thurn C and Axt V M 2012 *Phys. Rev. B* **85** 165203

[22] D'yakonov M I and Perel' V I 1971 *Zh. Eksp. Teor. Fiz* **60** 1954

D'yakonov M I and Perel' V I 1971 *Sov. Phys.—JETP* **33** 1053

[23] Yafet Y 1963 *Solid State Physics* vol 14 (New York: Academic)

[24] Elliott R J 1954 *Phys. Rev.* **96** 266–79

[25] Bir G L, Aronov A and Pikus G E 1975 *JETP* **42** 705

[26] Thurn C, Cygorek M, Axt V M and Kuhn T 2013 *Phys. Rev. B* **87** 205301

[27] Cygorek M and Axt V M 2014 *Phys. Rev. B* **90** 035206

[28] Hilton D J and Tang C L 2002 *Phys. Rev. Lett.* **89** 146601

[29] Ungar F, Cygorek M, Tamborenea P I and Axt V M 2015 *Phys. Rev. B* **91** 195201

[30] Dresselhaus G 1955 *Phys. Rev.* **100** 580–6

[31] Bychkov Y A and Rashba E I 1984 *J. Phys. C: Solid State Phys.* **17** 6039

[32] Thurn C, Cygorek M, Axt V M and Kuhn T 2013 *Phys. Rev. B* **88** 161302(R)

Publication 3

Ultrafast spin dynamics in II-VI diluted magnetic semiconductors with spin-orbit interaction

F. Ungar, M. Cygorek, P. I. Tamborenea, and V. M. Axt

Phys. Rev B **91**, 195201 (2015)

Ultrafast spin dynamics in II-VI diluted magnetic semiconductors with spin-orbit interaction

F. Ungar,[1] M. Cygorek,[1] P. I. Tamborenea,[2,1] and V. M. Axt[1]

[1]*Theoretische Physik III, Universität Bayreuth, 95440 Bayreuth, Germany*

[2]*Departamento de Física and IFIBA, FCEN, Universidad de Buenos Aires, Ciudad Universitaria, Pabellón I,*

C1428EHA Buenos Aires, Argentina

We study theoretically the ultrafast spin dynamics of II-VI diluted magnetic semiconductors in the presence of spin-orbit interaction. Our goal is to explore the interplay or competition between the exchange sd coupling and the spin-orbit interaction in both bulk and quantum-well systems. For bulk materials we concentrate on $Zn_{1-x}Mn_xSe$ and take into account the Dresselhaus interaction, while for quantum wells we examine $Hg_{1-x-y}Mn_xCd_yTe$ systems with a strong Rashba coupling. Our calculations were performed with a recently developed formalism which incorporates electronic correlations beyond mean-field theory originating from the exchange sd coupling. For both bulk and quasi-two-dimensional systems we find that, by varying the system parameters within realistic ranges, either of the two interactions can be chosen to play a dominant role or they can compete on an equal footing with each other. The most notable effect of the spin-orbit interaction in both types of system is the appearance of strong oscillations where the exchange sd coupling by itself causes only an exponential decay of the mean electronic spin components. The mean-field approximation is also studied and an analytical interpretation is given as to why it shows a strong suppression of the spin-orbit-induced dephasing of the spin component parallel to the Mn magnetic field.

I. INTRODUCTION

Diluted magnetic semiconductors (DMSs) are multifunctional materials that combine the outstanding electronic and optical properties of semiconductors with highly controllable magnetic properties [1,2]. With the prospect of spintronic applications of DMSs in mind, much effort has focused recently on the study of ultrafast spin dynamics and control [3–9]. At the same time, spin-orbit interaction (SOI) effects have been intensely studied in nonmagnetic bulk and nanostructured semiconductors [10–15]. The interplay between the exchange interaction characteristic of DMSs and the more generic SOI can lead to new possibilities for applications and basic research [16–21]. In particular, the spin-orbit torque effect in DMSs has attracted much interest in recent years [22–29].

In this article we explore this interplay theoretically by studying the ultrafast spin dynamics of a nonequilibrium electron distribution in the conduction band of II-VI Mn-doped semiconductors. Our work is based on a microscopic density-matrix theory that models on a quantum-kinetic level the spin precession and the spin transfer between electrons in the conduction band of such semiconductors and the manganese electrons, and which accounts for exchange-induced correlations beyond the mean-field level and considers the localized character of the Mn spins [30]. This recently developed formalism is quite general and can be computationally costly to apply in some circumstances. For this reason, in the present study we consider a particular situation which is nevertheless experimentally relevant and theoretically interesting: the limit of high Mn density compared to the electron density, which is normally realized in photoexcitation experiments. In this particular regime we can apply a simplified formalism which captures the essential physics that is relevant here and which greatly reduces the numerical effort [31].

The purpose of our study is to determine under which conditions, if any, the spin-orbit-interaction mechanisms present in semiconductors can become relevant or even dominant in the picosecond-time-scale spin dynamics in DMSs. As will be seen here, for both bulk and quasi-two-dimensional systems, depending on the choice of material parameters and excitation conditions, there can be a strong interplay or competition between the two types of interaction. This rather unexplored combined effect between exchange and SOI in DMS could lead in principle to new forms of spin control suitable for spintronic applications.

This article is organized as follows. In Sec. II A we present the model Hamiltonian of the DMSs with spin-orbit interaction and in Sec. II B we review the equations of motion that describe the spin dynamics in the formalism adopted here. In Secs. III and IV we present and discuss our results for bulk $Zn_{1-x}Mn_xSe$ and for $Hg_{1-x-y}Mn_xCd_yTe$ quantum wells, respectively. Finally, we provide some concluding remarks.

II. QUANTUM-KINETIC FORMALISM

A. DMS Hamiltonian

The theoretical model of DMSs for our work includes the exchange sd coupling between electrons in the conduction band and d electrons of the doping Mn atoms and the SOI of conduction-band electrons expressed in the envelope-function approximation. The Hamiltonian has the form

$$H = H_0 + H_{sd} + H_{SO}, \qquad (1)$$

where $H_0 = \sum_i \mathbf{p}_i^2/2m^*$, with conduction-band effective mass m^*, and the Kondo-like Hamiltonian [30]

$$H_{sd} = J_{sd} \sum_{iI} \mathbf{s}_i \cdot \mathbf{S}_I \, \delta(\mathbf{r}_i - \mathbf{R}_I) \qquad (2)$$

describes the coupling due to the exchange interaction between the conduction-band electrons and the Mn electrons. The spin

operator and position of the Ith Mn atom (ith conduction-band electron) are denoted as $\mathbf{S}_I$ and $\mathbf{R}_I$ ($\mathbf{s}_i$ and $\mathbf{r}_i$), respectively. The coupling constant J_{sd} is negative here, corresponding to a ferromagnetic coupling [32]. In the present work the negative Landé factor of Mn will always be combined with the negative sign of the coupling constant J_{sd}. In addition, all spin variables will be considered dimensionless and the coupling constant accordingly modified.

For bulk materials, the SOI Hamiltonian H_{SO} of zinc blende semiconductors is the Dresselhaus Hamiltonian [33]

$$H_D = \gamma_D \sum_i \left[\sigma_{i,x} k_{i,x} \left(k_{i,y}^2 - k_{i,z}^2 \right) + \text{cyclic perm.} \right], \quad (3)$$

where $\boldsymbol{\sigma}$ is the vector of Pauli matrices and $\mathbf{k}$ is the operator $\mathbf{p}/\hbar$. For quasi-two-dimensional systems, we consider asymmetric quantum wells which display the Rashba SOI [34]

$$H_R = \alpha_R \sum_i (k_{i,y} \sigma_{i,x} - k_{i,x} \sigma_{i,y}). \quad (4)$$

These effective spin-orbit couplings can be thought of as interactions of a spin with $\mathbf{k}$-dependent magnetic fields.

B. Equations of motion

In Refs. [30,31,35], the Heisenberg equations of motion of the density matrix for DMSs without SOI were posed and analyzed in terms of a correlation hierarchy which includes averaging of the Mn-atom positions, thus rendering the problem spatially homogeneous. In this work we follow that formalism and extend it in a simple fashion in order to study the effects of the SOI on the electronic spin degree of freedom.

When the number of Mn atoms (N_{Mn}) is much larger than the number of conduction-band electrons (N_e), i.e. in the limit $N_{\mathrm{Mn}} \gg N_e$, the quantum-kinetic equations established in Ref. [30] can be significantly simplified. This assumption can be easily fulfilled for intrinsic semiconductors in which the Mn^{2+} ions are incorporated isoelectronically, as in the case of II-VI semiconductors [36]. Unlike the situation in, for example, III-V-based DMSs, where the Mn doping results in a large number of holes, in isoelectronically doped systems the density of free carriers is controlled solely by the photoexcitation and thus can be kept much smaller than the Mn density simply by using low laser intensities. Here we consider electrons excited with typical narrowband laser pulses with near-band-gap energies and low intensities. Employing the approximation of low electron density as compared to the Mn doping density, we have developed a simplified formalism [31] based on the full model of Ref. [30], which allows

a numerically efficient handling of electronic correlations. Here we adopt the low-electron-density limit and follow the formalism of Ref. [31].
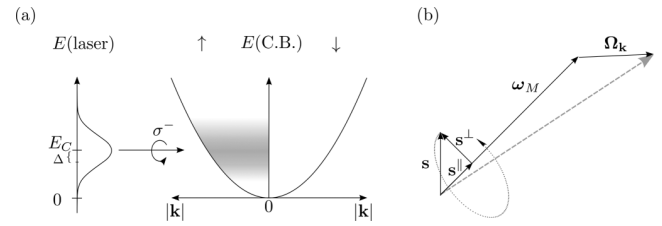

FIG. 1. (a) Schematic representation of the conduction band (CB) and the spectrum of the circularly polarized Gaussian laser pulse that excites electrons from the valence band to a Gaussian distribution of spin-up electrons in the conduction band (centered at an energy E_C above the band edge and with standard deviation Δ). (b) The electron spin and its components $\langle \mathbf{s}_{\mathbf{k}}^\perp \rangle$ and $\langle \mathbf{s}_{\mathbf{k}}^\parallel \rangle$, perpendicular and parallel to the Mn magnetic field (or equivalently angular frequency $\boldsymbol{\omega}_M$), respectively. Also represented is $\boldsymbol{\Omega}_{\mathbf{k}}$, the angular frequency associated with the $\mathbf{k}$-dependent spin-orbit effective magnetic field. The electron spin precesses about $\boldsymbol{\omega}_M + \boldsymbol{\Omega}_{\mathbf{k}}$.

In the regime $N_{\mathrm{Mn}} \gg N_e$ the Mn density matrix can be considered stationary and we take the z axis along the mean Mn magnetization $\langle \mathbf{S} \rangle$. The assumption of a stationary Mn density matrix has been numerically tested under conditions comparable with our present case in Refs. [31,35,37,38]. We introduce a precession frequency for the conduction-band electrons in the effective magnetic field of the Mn atoms:

$$\omega_{\mathrm{M}} = \frac{J_{\mathrm{sd}}}{\hbar} n_{\mathrm{Mn}} S, \quad (5)$$

where n_{Mn} is the Mn density and $S = |\langle \mathbf{S} \rangle|$, with $0 \leqslant S \leqslant \frac{5}{2}$.

We study the time evolution of the mean value of the spin operator associated with the state with wave vector $\mathbf{k}$,

$$\langle \mathbf{s}_{\mathbf{k}} \rangle = \sum_{\sigma\sigma'} \mathbf{s}_{\sigma\sigma'} \langle c_{\sigma\mathbf{k}}^\dagger c_{\sigma'\mathbf{k}} \rangle = (\langle \mathbf{s}_{\mathbf{k}}^\perp \rangle, \langle \mathbf{s}_{\mathbf{k}}^\parallel \rangle), \quad (6)$$

where $\langle \mathbf{s}_{\mathbf{k}}^\perp \rangle$ and $\langle \mathbf{s}_{\mathbf{k}}^\parallel \rangle$ are the mean spin components perpendicular and parallel to the mean Mn magnetization, respectively [see Fig. 1(b)]. We take as system variables $\langle \mathbf{s}_{\mathbf{k}}^\perp \rangle$ and the populations $n_{\mathbf{k}}^\sigma = \langle c_{\sigma\mathbf{k}}^\dagger c_{\sigma\mathbf{k}} \rangle$. The parallel mean spin can be obtained from the latter as

$$\langle s_{\mathbf{k}}^\parallel \rangle = \tfrac{1}{2}(n_{\mathbf{k}}^\uparrow - n_{\mathbf{k}}^\downarrow). \quad (7)$$

Leaving aside for the moment the SOI, the time evolution of these variables induced by H_0 and the sd interaction is given by [31]

$$\frac{\partial}{\partial t} n_{\mathbf{k}}^{\uparrow/\downarrow} \bigg|_{\mathrm{sd}} = \sum_{\mathbf{k}'} \left[\mathrm{Re}\big(G_{\omega_{\mathbf{k}'}}^{\omega_{\mathbf{k}}}\big) \frac{b^\parallel}{2} \big(n_{\mathbf{k}'}^{\uparrow/\downarrow} - n_{\mathbf{k}}^{\uparrow/\downarrow}\big) + \mathrm{Re}\big(G_{\omega_{\mathbf{k}'}}^{\omega_{\mathbf{k}}\pm\omega_{\mathrm{M}}}\big) \big(b^\pm n_{\mathbf{k}'}^{\downarrow/\uparrow} - b^\mp n_{\mathbf{k}}^{\uparrow/\downarrow} \mp 2b^0 n_{\mathbf{k}}^{\uparrow/\downarrow} n_{\mathbf{k}'}^{\downarrow/\uparrow}\big) \right], \quad (8)$$

$$\frac{\partial}{\partial t} \langle \mathbf{s}_{\mathbf{k}}^\perp \rangle \bigg|_{\mathrm{sd}} = -\sum_{\mathbf{k}'} \left\{ \left[\mathrm{Re}\big(G_{\omega_{\mathbf{k}'}}^{\omega_{\mathbf{k}}-\omega_{\mathrm{M}}}\big) \left(\frac{b^+}{2} - b^0 n_{\mathbf{k}'}^\uparrow \right) + \mathrm{Re}\big(G_{\omega_{\mathbf{k}'}}^{\omega_{\mathbf{k}}+\omega_{\mathrm{M}}}\big) \left(\frac{b^-}{2} + b^0 n_{\mathbf{k}'}^\downarrow \right) \right] \langle \mathbf{s}_{\mathbf{k}}^\perp \rangle + \mathrm{Re}\big(G_{\omega_{\mathbf{k}'}}^{\omega_{\mathbf{k}}}\big) \frac{b^\parallel}{2} (\langle \mathbf{s}_{\mathbf{k}}^\perp \rangle + \langle \mathbf{s}_{\mathbf{k}}^\perp \rangle) \right\}$$

$$+ \left\{ \omega_{\mathrm{M}} - \sum_{\mathbf{k}'} \left[\mathrm{Im}\big(G_{\omega_{\mathbf{k}'}}^{\omega_{\mathbf{k}}-\omega_{\mathrm{M}}}\big) \left(\frac{b^+}{2} - b^0 n_{\mathbf{k}'}^\uparrow \right) - \mathrm{Im}\big(G_{\omega_{\mathbf{k}'}}^{\omega_{\mathbf{k}}+\omega_{\mathrm{M}}}\big) \left(\frac{b^-}{2} + b^0 n_{\mathbf{k}'}^\downarrow \right) \right] \right\} \frac{\langle \mathbf{S} \rangle}{S} \times \langle \mathbf{s}_{\mathbf{k}}^\perp \rangle. \quad (9)$$

The constants in Eqs. (8) and (9) depend only on the setting of the Mn magnetization and are given by $b^\pm = \langle S^{\perp 2}\rangle \pm b^0$, $b^0 = \langle S^\parallel\rangle/2$, $b^\parallel = \langle S^{\parallel 2}\rangle$, where $S^\parallel = \mathbf{S}\cdot\langle\mathbf{S}\rangle/S$, and $\langle S^{\perp 2}\rangle = \langle S^2 - S^{\parallel 2}\rangle/2$. We also set $\omega_\mathbf{k} = E_\mathbf{k}/\hbar = \hbar\mathbf{k}^2/2m^*$.

The function $G^{\omega_\mathbf{k}}_{\omega_{\mathbf{k}'}}$ can be interpreted as a memory function and has the form

$$G^{\omega_\mathbf{k}}_{\omega_{\mathbf{k}'}}(t) = \frac{J^2_{\mathrm{sd}}\, n_{\mathrm{Mn}}}{V\hbar^2}\int_{-t}^{0}dt'\, e^{i(\omega_{\mathbf{k}'} - \omega_\mathbf{k})t'}$$

$$\approx \frac{J^2_{\mathrm{sd}}\, n_{\mathrm{Mn}}}{V\hbar^2}\pi\delta(\omega_{\mathbf{k}'} - \omega_\mathbf{k}), \qquad (10)$$

where in the last step we neglected the imaginary part and the finite memory, i.e., we applied a Markov limit which is a good approximation for not too large values of J^2_{sd} and excitations not too close to the band edge [38].

The spin-orbit Hamiltonians of Eqs. (3) and (4) introduce, to a first approximation, an additional **k**-dependent spin precession. If the contribution of a single electron with wave vector **k** to the spin-orbit Hamiltonian is written in the form

$$H_{\mathrm{SO}} = \frac{\hbar}{2}\hat{\Omega}_\mathbf{k}\cdot\boldsymbol{\sigma}, \qquad (11)$$

then the mentioned spin precession is described by the Heisenberg equation of motion of the mean value of the spin operator introduced in Eq. (6),

$$\left.\frac{\partial}{\partial t}\langle\mathbf{s}_\mathbf{k}\rangle\right|_{\mathrm{SO}} = \Omega_\mathbf{k}\times\langle\mathbf{s}_\mathbf{k}\rangle. \qquad (12)$$

Note that while $\hat{\Omega}_\mathbf{k}$ is an operator, we introduced $\Omega_\mathbf{k}$ as the corresponding regular vector where **k** is interpreted simply as a wave vector and not as an operator as in Eqs. (3) and (4) [see Fig. 1(b)]. In the present study we take into account the influence of the spin-orbit interaction at this level, in order to elucidate how this added **k**-dependent precession alters the quantum spin dynamics in bulk and quasi-two-dimensional DMSs.

III. BULK Zn$_{1-x}$Mn$_x$Se

In this section we present results for ultrafast spin dynamics in bulk semiconductors. For concreteness we focus on Zn$_{1-x}$Mn$_x$Se which is currently one of the best studied II-VI DMSs, and, as we will see, it can display an interesting interplay between exchange and SOI. We first examine numerically and analytically the dephasing caused by the Dresselhaus spin-orbit coupling and then we proceed to calculate and analyze the full dynamics under the influence of both exchange coupling and SOI.

A. Dresselhaus-induced dephasing

As mentioned in Sec. II A, the spin-orbit interaction in the envelope-function approximation plays the role of an effective **k**-dependent magnetic field around which the electron spin precesses. This spin precession in the case of an electron gas leads to global spin dephasing and decay, which is at the root of the D'yakonov-Perel spin-relaxation mechanism [39]. As initial condition for the conduction-band electrons
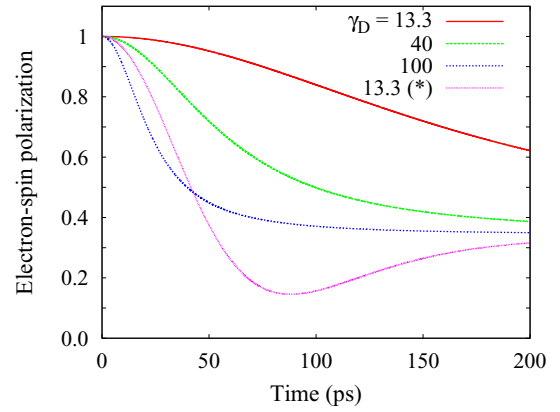

FIG. 2. (Color online) Dephasing after isotropic Gaussian excitation of the spin-up band (standard deviation $\Delta = 3$ meV) without exchange sd coupling in an effective Dresselhaus spin-orbit magnetic field with prefactor γ_D, specified in ps^{-1} nm^3. Three of the curves correspond to a Gaussian excitation centered at the band edge ($E_C = 0$), while the fourth, marked with (*), corresponds to a displacement of the excitation to $E_C = 10$ meV above the band edge.

we assume a Gaussian distribution caused by a pulsed optical excitation, similar to the one illustrated in Fig. 1(a). For the moment we consider a Gaussian distribution centered at $E_C = 0$ (the band edge) and later we will consider an excitation centered at $E_C = 10$ meV, always with standard deviation $\Delta = 3$ meV. We assume that the optical excitation populates only the spin-up conduction-band states thanks to its appropriate circular polarization. In Fig. 2 we plot the spin polarization, $\langle s_z\rangle(t) = 2N_e^{-1}\sum_\mathbf{k}\langle s_{\mathbf{k},z}\rangle(t)$ (normalized to 1), of the initially spin-up electron population (the z axis coincides with the main axis of the zinc blende lattice) in the conduction band versus time for different values of the Dresselhaus spin-orbit coupling constant γ_D.

The accepted standard value of $\gamma_D/\hbar = 13.3$ ps^{-1} nm^3 is included [10], and two artificially high values (40 and 100 ps^{-1} nm^3) are added to explore the tendencies of the decay behavior. We use for the conduction-band effective mass of ZnSe the value $m^* = 0.134m_0$ [40], where m_0 is the bare electron mass. The expected dephasing and decay mentioned above are clearly observed, with faster decay obtained for increasing SOI coupling constant. Note that the decay, however, is not exponential from the beginning, but rather quadratic at short times. Another interesting feature is that for an excitation 10 meV above the band edge the evolution displays a nonmonotonic behavior. Below we shall indicate the origin of this incipiently oscillatory behavior.

The long-time limit of the spin polarization seen in Fig. 2, which corresponds to the equilibrium distribution caused by the SOI effective field dephasing, is given by the value $1/3$:

$$\lim_{t\to\infty}\langle s_z\rangle(t) =: \langle s_{\mathrm{eq}}\rangle = \tfrac{1}{3}\langle s_z\rangle(t=0). \qquad (13)$$

This equilibrium value can be understood analytically as follows. The equation of motion for the spin under the SOI effective magnetic field, $\frac{\partial}{\partial t}\langle\mathbf{s}_\mathbf{k}\rangle|_{\mathrm{SO}} = \Omega_\mathbf{k}\times\langle\mathbf{s}_\mathbf{k}\rangle$, can be cast in

the matrix form $\frac{\partial}{\partial t}\langle \mathbf{s_k}\rangle|_{\mathrm{SO}} = \mathbb{M}_\mathbf{k}\langle \mathbf{s_k}\rangle$, where

$$
\mathbb{M}_\mathbf{k} = \begin{pmatrix} 0 & -\Omega_{\mathbf{k},z} & \Omega_{\mathbf{k},y} \\ \Omega_{\mathbf{k},z} & 0 & -\Omega_{\mathbf{k},x} \\ -\Omega_{\mathbf{k},y} & \Omega_{\mathbf{k},x} & 0 \end{pmatrix}, \qquad (14)
$$

and has the formal solution

$$
\langle \mathbf{s_k}\rangle(t) = \exp(\mathbb{M}_\mathbf{k} t)\,\langle \mathbf{s_k}\rangle(0). \qquad (15)
$$

The Taylor expansion of the matrix exponential can be simplified using that $\mathbb{M}_\mathbf{k}^3 = -\Omega_\mathbf{k}^2\,\mathbb{M}_\mathbf{k}$ and $\mathbb{M}_\mathbf{k}^4 = -\Omega_\mathbf{k}^2\,\mathbb{M}_\mathbf{k}^2$, with $\Omega_\mathbf{k} = |\boldsymbol{\Omega}_\mathbf{k}|$. One obtains

$$
\exp(\mathbb{M}_\mathbf{k} t) = 1 + \sin(\Omega_\mathbf{k} t)\frac{\mathbb{M}_\mathbf{k}}{\Omega_\mathbf{k}} + [1 - \cos(\Omega_\mathbf{k} t)]\left(\frac{\mathbb{M}_\mathbf{k}}{\Omega_\mathbf{k}}\right)^2. \qquad (16)
$$

The diagonal elements of this matrix are given by

$$
\exp(\mathbb{M}_\mathbf{k} t)|_{ii} = \frac{\Omega_{\mathbf{k},i}^2}{\Omega_\mathbf{k}^2} + \left(1 - \frac{\Omega_{\mathbf{k},i}^2}{\Omega_\mathbf{k}^2}\right)\cos(\Omega_\mathbf{k} t). \qquad (17)
$$

Assuming that initially only the ith spin component is nonzero, from Eqs. (15) and (17) we obtain $\langle s_{\mathbf{k}i}\rangle(t) = \exp(\mathbb{M}_\mathbf{k} t)|_{ii}\langle s_{\mathbf{k}i}\rangle(0)$. Thus, for large times t, this spin component, averaged over the isotropically occupied $\mathbf{k}$ states, tends to $\langle s_i\rangle = \overline{\Omega_i^2/\Omega^2} = 1/3$ since the effective field is isotropic (the overbar denotes the average over $\mathbf{k}$ states).

Note again that in Fig. 2 the curve corresponding to the excitation above the band edge displays a nonmonotonic behavior which is the precursor of an oscillation that can be seen under stronger SOI. These oscillations will be observed later in the quantum-well situation, and originate from the cosine term in Eq. (17), appropriately averaged over the occupied $\mathbf{k}$ states.

B. Interplay between exchange and Dresselhaus interactions

Having verified the dephasing caused by the $\mathbf{k}$-dependent Dresselhaus effective magnetic field, we now wish to study the interplay between the exchange sd (sd) and Dresselhaus (D) couplings. The material parameters of $\mathrm{Zn}_{1-x}\mathrm{Mn}_x\mathrm{Se}$ related to the Mn doping used in our simulations are as follows. The exchange coupling constant of $\mathrm{Zn}_{1-x}\mathrm{Mn}_x\mathrm{Se}$ is $N_0\alpha = 260$ meV [41], where N_0 is the number of unit cells per unit volume, and $\alpha = J_{\mathrm{sd}}$ in our notation. The lattice constant of ZnSe is 0.569 nm, the volume of the primitive unit cell is 0.0455 nm^3; thus $N_0 = 22$ nm^{-3}, and then $J_{\mathrm{sd}} \approx 12$ meV nm^3. We assume a relatively low percentage of Mn doping of 0.3% which gives a Mn density of 6.6×10^{-2} nm^{-3}. The density of photoexcited electrons is assumed to be 5×10^{-5} nm^{-3}, i.e., three orders of magnitude lower than the Mn density.

We first consider a Gaussian distribution for the conduction-band electrons centered at the band edge, and take an average Mn magnetization of $S = 0.5$. The Mn magnetization can be simply tuned by applying an external magnetic field in the desired direction and waiting for the Mn spin to reach its thermal equilibrium. Thus, we envision an experiment where the magnetic field is turned off before the pump laser pulse arrives. Note that the Mn spin-lattice relaxation time is of the order of $0.1\,\mu$s [42], which suffices to carry
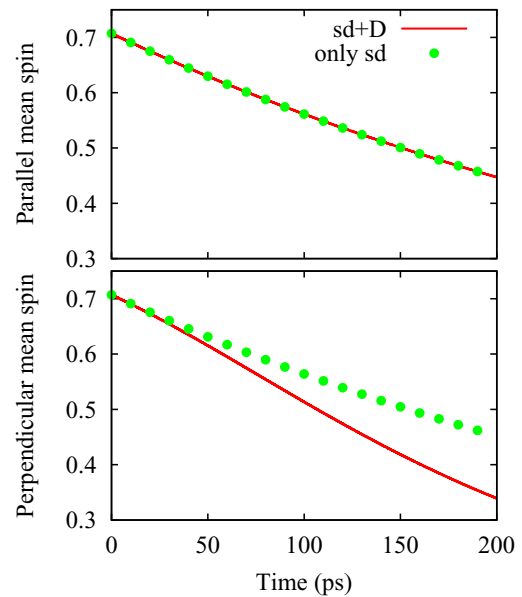

FIG. 3. (Color online) Influence of the Dresselhaus spin-orbit coupling (D) on the spin dynamics in bulk $\mathrm{Zn}_{1-x}\mathrm{Mn}_x\mathrm{Se}$ with exchange sd coupling (sd) for an initially Gaussian electron occupation centered at the band edge with standard deviation $\Delta = 3$ meV and initial spin polarization rotated $45°$ with respect to the z axis. The Mn concentration is $x_{\mathrm{Mn}} = 0.3\%$ and the net Mn magnetization $S = 0.5$. Red solid lines correspond to the full calculation (sd + D) and green dotted lines to the calculation leaving out the Dresselhaus coupling (only sd).

out the ensuing optical excitation experiment studied here under almost constant Mn magnetization. Figure 3 shows the time evolution of the parallel, $\langle s_z\rangle(t)$, and perpendicular, $|\langle \mathbf{s}^\perp\rangle(t)| = 2N_e^{-1}|\sum_\mathbf{k}\langle \mathbf{s}_\mathbf{k}^\perp\rangle(t)|$, mean spin components. From now on we use only the realistic value $\gamma_D/\hbar = 13.3$ ps^{-1} nm^3 for the Dresselhaus constant and for concreteness we take the initial spin polarization rotated $45°$ with respect to the z axis. The specific choice for this angle is not very relevant, but it is important to set it to a value different from zero in order to have spin precession about the Mn field. Since the Dresselhaus Hamiltonian is cubic in the wave vector, we expect it to have a relatively weak effect, as compared to the exchange coupling, on electrons populating low-energy states around the band edge, and Fig. 3 confirms this expectation. Indeed, we see that for the parallel spin component the presence of the Dresselhaus coupling does not modify the dynamics noticeably [the red solid line (sd + D) and the green dots (only sd) are superimposed]. For the perpendicular components there is a noticeable difference, but the two curves are still qualitatively similar. We have checked that if the Mn concentration and/or the Mn magnetization are increased the effect of the spin-orbit coupling becomes rapidly negligible also for the perpendicular spin component. Roughly speaking, the exchange sd coupling can be thought of as causing two main effects: a spin precession about the mean Mn magnetization and spin transfer between conduction-band and Mn electrons. On the other hand, as seen above, the Dresselhaus spin-orbit Hamiltonian, by providing a $\mathbf{k}$-dependent effective magnetic
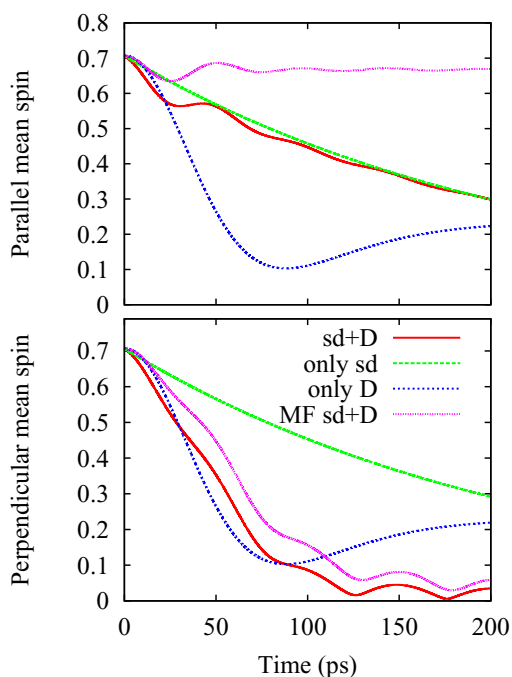
FIG. 4. (Color online) Influence of the Dresselhaus spin-orbit coupling (D) on the spin dynamics in bulk $Zn_{1-x}Mn_xSe$ with exchange sd coupling (sd) for an initially Gaussian electron occupation centered at $E_C = 10$ meV above the band edge with standard deviation $\Delta = 3$ meV and initial spin polarization rotated $45°$ with respect to the z axis. The Mn concentration is $x_{Mn} = 0.3\%$ and the net Mn magnetization $S = 0.1$. Red solid lines, full calculation with sd + D interactions; green long-dashed lines, only sd; blue short-dashed line: only D; pink dotted lines, mean-field approximation with sd + D.

field, induces a global dephasing in the electron population. The decay seen in both spin components in Fig. 3 is thus a result of both exchange-induced spin transfer and spin-orbit dephasing, but the former dominates the dynamics for the chosen set of parameters.

This raises the question of whether a parameter regime can be reached experimentally in which the dephasing caused by the spin-orbit effective field has a considerable influence on or even dominates the spin dynamics. As mentioned above, shifting the optical excitation away from the band edge to higher **k** values should enhance the effect of the SOI on the spin dynamics. Furthermore, the influence of the exchange sd coupling can be reduced by lowering both the Mn concentration and/or the average Mn magnetization. Thus, in Fig. 4 we show the time evolution of the parallel and perpendicular spin components as in Fig. 3, but centering the Gaussian occupation 10 meV above the band edge and reducing the Mn magnetization to $S = 0.1$. The Mn doping is kept at $x_{Mn} = 0.3\%$ as before, and for the conduction-band electrons we choose again an initial spin orientation rotated $45°$ away from the z axis. In the parallel spin component there is now a noticeable difference between the full calculation (sd + D) (red solid line) and the sd-only case (green long-dashed line). A qualitatively new feature is that the combination of sd and Dresselhaus couplings now produces not only a decay

but also oscillations, revealing a combined spin precession. In the perpendicular component the spin-orbit coupling has now an enormous effect, greatly accelerating the decay and causing superimposed oscillations. The oscillations seen in Fig. 4 have a frequency close to the precession frequency associated with the mean Mn magnetic field ($\omega_M = \omega_M \hat{z}$), $\omega_M = 0.124$ Thz (period $T_M = 50.7$ ps). We come back to this issue after discussing the mean-field approximation which we now introduce.

It is interesting to elucidate whether a similar spin dynamics would also be obtained in a simpler scenario combining the Dresselhaus SOI with a constant magnetic field of appropriate strength. (This type of problem has been studied recently from the point of view of impurity entanglement [43] and spin relaxation [44].) We can readily answer this question by intentionally leaving the correlation terms out of the equations of motion [keeping in the right-hand side of Eq. (9) only the first term of the second line] thus reverting to a mean-field approximation, which for a given Mn magnetization is equivalent to adding a constant magnetic field. The result is given by the pink dotted lines in Fig. 4. For the perpendicular component we see that the mean-field calculation resembles the full one, although there is a clearly distinguishable difference between them. On the other hand, both results are far away from the sd-only result, and we have to conclude that in this sense the mean-field approximation does capture an important part of the interplay between the exchange and spin-orbit couplings. For the parallel component the mean-field approximation radically modifies the dynamics. We see here that when the sd correlations are removed the spin-orbit dephasing is not capable by itself of inducing a decay in the presence of the spin precession about the Mn magnetization. In other words, the longitudinal component does not decay since its Dresselhaus dephasing is in a sense prevented by the "naked" (without exchange-induced correlations) precession about the Mn magnetization. To confirm this point we show in Fig. 4 the spin dynamics with only the Dresselhaus SOI (no sd coupling) with blue dotted lines. These curves show the strong decay induced by spin-orbit dephasing in the absence of both the spin precession and the spin transfer caused by the exchange coupling.

The origin and frequency of the oscillations mentioned above, which appear when both interactions are present, and in both the full and mean-field calculations, can be interpreted with the help of Eq. (17). For a given **k** state the precession frequency is now $\Omega \equiv \Omega_{\mathbf{k}} + \omega_M \mathbf{z}$. In the limit $\omega_M \gg \Omega_{\mathbf{k}}$ we can assume that $\Omega_z \approx \Omega \approx \omega_M$, and using Eqs. (15) and (17) we obtain $\langle s_z \rangle(t) = \langle s_z \rangle(0)$. This argument applies to every **k** state and thus can be extended to the whole electron population. Then, the precession about the spin-orbit effective magnetic field of the longitudinal component is suppressed by the dominant precession about the Mn magnetic field, a feature that can be seen clearly in the mean-field result of Fig. 4. If the spin-orbit angular frequency is not completely neglected we obtain oscillations in the parallel component with frequency $|\Omega_{\mathbf{k}} + \omega_M|$ and small amplitude proportional to $1 - (\Omega_{\mathbf{k},z} + \omega_M)^2/|\Omega_{\mathbf{k}} + \omega_M|^2$, as seen in Fig. 4. We have verified that increasing the Dresselhaus coupling increases the amplitude of the oscillations (not shown here). Oscillations of the same frequency are also present in the perpendicular spin component.

IV. $Hg_{1-x-y}Mn_xCd_yTe$ QUANTUM WELLS

We now turn to the study of the influence of the spin-orbit coupling in II-VI semiconductor quantum wells. In this case the SOI that we consider is the Rashba coupling (R), which is present when the quantum-well confinement lacks inversion symmetry. As explained in the Introduction, the role of the spin-orbit coupling is conceptually similar in bulk and in quantum wells, since in both cases it can be thought of as a **k**-dependent Zeeman Hamiltonian which induces global dephasing in an electron gas. However, quantum wells offer greater flexibility to control the SOI and also display high electron mobilities in high-quality modulation-doped samples. High mobilities amount to longer momentum-scattering times and therefore to more coherent quantum dynamics.

In line with the bulk studies discussed above, we first tested the spin dynamics in $Zn_{1-x}Mn_xSe$ quantum wells. For realistic parameters for this material, it turned out that the Rashba coupling was too weak to modify the dynamics driven by the exchange sd coupling. The root of this difficulty seems to be the large band gap (about 2.8 eV) of ZnSe, which results in a small Rashba coupling constant. Thus for the quantum-well calculations we looked for a family of materials with stronger and more controllable Rashba interaction. $Hg_{1-x}Mn_xTe$ is a good candidate since the energy gap E_g of this ternary compound depends strongly on the Mn concentration [45], going to zero at $x \leqslant 6.5\%$, while its spin-orbit valence-band splitting Δ is insensitive to it [46]. This interesting combination leads to flexible spin-orbit properties, which are generally controlled by the ratio Δ / E_g. By choosing a Mn concentration slightly above 6.5% we can select a very low energy gap, which leads in turn to a strong Rashba coupling [47]. However, this lower limit for the Mn concentration is still too high and leads again to a completely dominant exchange interaction even for as low a Mn magnetization as $S = 0.01$ (with sd-coupling-induced spin relaxation times below 5 ps). This drawback can be overcome by considering instead the compound $Hg_{1-x-y}Mn_xCd_yTe$ in which the nonmagnetic Cd atoms replace some of the Mn dopants. This change maintains the gap tunability via the doping fraction $x + y$ giving full flexibility regarding the concentration of magnetic ions [46]. The Rashba coupling constant can be calculated with the expression [16,47]

$$\alpha_R = \frac{\hbar^2}{2m^*} \frac{\Delta}{E_g} \frac{2E_g + \Delta}{(E_g + \Delta)(3E_g + 2\Delta)} \frac{V_{qw}}{d}. \quad (18)$$

We work with the effective mass of HgTe $m^* = 0.093\, m_0$ [40], and take the spin-orbit valence-band splitting as $\Delta = 1.08$ eV [48]. Assuming $E_g = 300$ meV, a quantum-well width $d = 200$ Å, and a potential energy drop of $V_{qw} = 50$ meV across the quantum well, we obtain $\alpha_R = 4.87$ meV nm ($\alpha_R/\hbar = 7.4\, ps^{-1}$ nm). Note that for ZnSe one obtains $\alpha_R = 0.015$ meV nm ($\alpha_R/\hbar = 0.023\, ps^{-1}$ nm), a very low value which leads to negligible spin-orbit effects, as mentioned before. For the exchange sd coupling constant of HgMnTe we take $N_0\alpha = 400$ meV [49], and the lattice constant of 0.645 nm leads to $J_{sd} = 26.8$ meV nm^3. We keep the previous Mn concentration of $x = 0.3\%$.

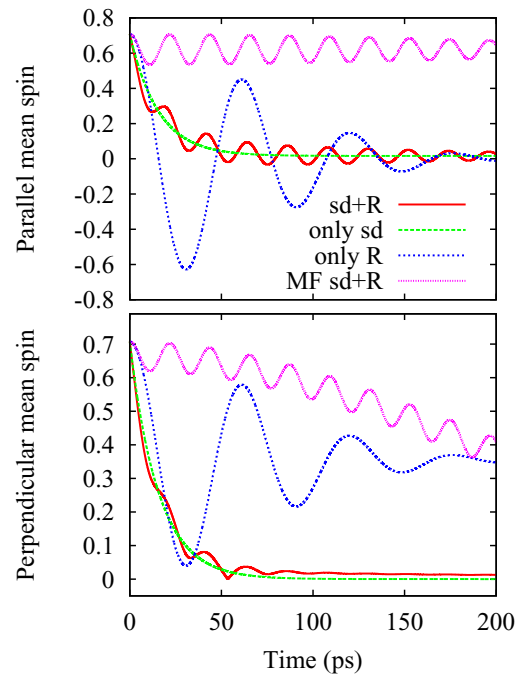In Fig. 5 we show the time evolution of the parallel and perpendicular spin components for quantum wells, where now

FIG. 5. (Color online) Influence of the Rashba spin-orbit coupling (R) on the spin dynamics in a $Hg_{1-x-y}Mn_xCd_yTe$ quantum well with exchange sd coupling (sd) for an initially Gaussian electron occupation centered 10 meV above the band edge with standard deviation of 3 meV and initial spin polarization rotated 45° with respect to the z axis. The Mn concentration is $x_{Mn} = 0.3\%$ and the net Mn magnetization $S = 0.1$. Red solid lines, full calculation with sd + R; green long-dashed lines, only sd; blue short-dashed lines, only R; pink dotted lines, mean-field approximation with sd + R.

the parallel component corresponds to the growth direction of the quantum well (z axis). The Gaussian occupation is centered 10 meV above the band edge and we consider a Mn magnetization of $S = 0.1$. The initial spin orientation is rotated 45° away from the z axis.

Figure 5 shows that while the sd-only curve (green long-dashed line) follows the usual exponential decay, the full dynamics with sd + R displays clear oscillations in both components. We have verified that the amplitude of these oscillations increases with increasing Rashba coefficient, which in turn is obtained by lowering the energy gap. The pink dotted lines in Fig. 5 show the mean-field approximation results with both sd and R interactions. Here the decay seen in the perpendicular component is due to the Rashba-induced dephasing since exchange correlations are absent. The parallel component maintains an approximately constant mean value in agreement with the analysis done in the previous section, and shows a slight decrease of the oscillation amplitude due to the dephasing induced by the Rashba SOI. We verified that this amplitude reduction is accelerated by increasing the Rashba coupling constant. The blue short-dashed lines show the evolution of the spin with only the Rashba interaction present (no sd). Here we see the full-fledged oscillations that had been anticipated in the discussion of Fig. 2. These oscillations are the collective result of the individual spin precessions about the effective **k**-dependent Rashba magnetic

field. There appears to be no analytical expression or simple interpretation for the frequency of these oscillations at present. This frequency depends on many factors such as the Rashba coefficient, the electron density, and the electronic distribution (which in our simulations is determined by the mean value and the standard deviation of the initial Gaussian population). We have checked numerically that there is a roughly linear dependence of this frequency on the Rashba coefficient for an excitation 10 meV above the band edge.

It is unexpected and noteworthy that, in the quantum-well case, the addition of the spin-orbit interaction to the DMS produces strong oscillations while at the same time leaves fairly unchanged the decay rate for our parameters, as can be seen in Fig. 5 ("only sd" versus "sd + R" curves). Finally, we point out that the main qualitative difference between the results shown in Fig. 4 for bulk and Fig. 5 for a quantum well is that, for the perpendicular spin component in the quantum well, the sd-only curve stays near the full result and the mean-field curve moves strongly away, while the opposite behavior occurs in bulk.

V. CONCLUSION

We studied theoretically the combined effects of the exchange sd coupling and the spin-orbit interaction in II-VI diluted magnetic semiconductors, both in bulk and in quantum wells. Although our results can be considered generally valid in zinc blende semiconductor systems, we focused on particular materials that show clearly the interplay between the two mechanisms: $Zn_{1-x}Mn_xSe$ for bulk and $Hg_{1-x-y}Mn_xCd_yTe$ for quantum wells. In our calculations we employed a recently developed formalism which incorporates electronic correlations originating from the exchange sd coupling. The main conclusion of our study is that for both bulk and quasi-two-dimensional systems there can be a strong interplay or competition between the two types of interaction, leading to experimentally detectable signatures (for example in time-resolved Faraday and Kerr rotation experiments) of the spin-orbit interaction in DMSs. In bulk we find that the

spin components parallel and perpendicular to the net Mn magnetization have rather different responses to the presence of the spin-orbit (Dresselhaus) interaction, the latter being much more affected by it. Indeed, coherent oscillations—with a frequency reflecting the precession around a combination of the Mn magnetization and the Dresselhaus field—develop as a consequence of the interplay between the two interactions, which are completely absent when the exchange interaction dominates. In addition, the decay rate is greatly enhanced for the perpendicular component by the presence of the Dresselhaus interaction in the studied regime. Regarding quantum wells, we find that the exchange interaction tends to be more dominant over the spin-orbit interaction (Rashba coupling in this case), which led us to consider a family of materials with large valence-band-splitting spin-orbit constant and tunable energy gap. For these DMS materials we obtained again a strong effect of the spin-orbit interaction, manifesting itself in the occurrence of oscillations which are not seen when the exchange interaction acts alone. Remarkably, even though the combination of exchange and spin-orbit interaction leads to clearly visible oscillations, the decay of the spin polarization is practically unaffected by the presence of the Rashba interaction. These signatures should be detectable experimentally in pump-and-probe experiments. Finally, for both bulk and quantum wells we find that in the mean-field approximation treatment of the exchange interaction there is a strong suppression of the spin-orbit-induced dephasing of the spin component parallel to the Mn magnetic field. The studied interplay between the spin-orbit interaction and the exchange coupling could improve spin control and thereby facilitate potential spintronic applications of DMSs.

[1] *Introduction to the Physics of Diluted Magnetic Semiconductors*, edited by Jacek Kossut and Jan A. Gaj (Springer, Heidelberg, 2010).

[2] J. Xia, W. Ge, and K. Chang, *Semiconductor Spintronics* (World Scientific, Singapore, 2012).

[3] A. Kirilyuk, A. V. Kimel, and T. Rasing, Rev. Mod. Phys. **82**, 2731 (2010).

[4] J. Qi, Y. Xu, A. Steigerwald, X. Liu, J. K. Furdyna, I. E. Perakis, and N. H. Tolk, Phys. Rev. B **79**, 085304 (2009).

[5] Y. Hashimoto, S. Kobayashi, and H. Munekata, Phys. Rev. Lett. **100**, 067202 (2008).

[6] L. Cywiński and L. J. Sham, Phys. Rev. B **76**, 045205 (2007).

[7] O. Morandi, P.-A. Hervieux, and G. Manfredi, Phys. Rev. B **81**, 155309 (2010).

[8] M. D. Kapetanakis, I. E. Perakis, K. J. Wickey, C. Piermarocchi, and J. Wang, Phys. Rev. Lett. **103**, 047404 (2009).

[9] C. Thurn, V. M. Axt, A. Winter, H. Pascher, H. Krenn, X. Liu, J. K. Furdyna, and T. Wojtowicz, Phys. Rev. B **80**, 195210 (2009).

[10] R. Winkler, *Spin-Orbit Coupling Effects in Two-Dimensional Electron and Hole Systems* (Springer-Verlag, Berlin, 2003).

[11] I. Žutić, J. Fabian, and S. Das Sarma, Rev. Mod. Phys. **76**, 323 (2004).

[12] J. Fabian, A. Matos–Abiague, C. Ertler, P. Stano, and I. Žutić, Acta Phys. Slov. **57**, 565 (2007).

[13] *Spin Physics in Semiconductors*, edited by M. I. Dyakonov (Springer-Verlag, Berlin, 2008).

[14] M. W. Wu, J. H. Jiang, and M. Q. Weng, Phys. Rep. **493**, 61 (2010).

[15] *Handbook of Spin Transport and Magnetism*, edited by E. Y. Tsymbal and I. Žutić (Chapman & Hall/CRC, Boca Raton, FL, 2011).

[16] K. Gnanasekar and K. Navaneethakrishnan, Physica E **35**, 103 (2006).

[17] W. Yang, Kai Chang, X. G. Wu, H. Z. Zheng, and F. M. Peeters, Appl. Phys. Lett. **89**, 132112 (2006).

[18] R. Vali and S. M. Mirzanian, Solid State Commun. **149**, 2032 (2009).

[19] J. H. Jiang, Y. Zhou, T. Korn, C. Schüller, and M. W. Wu, Phys. Rev. B **79**, 155201 (2009).

[20] S. M. Mirzanian, A. A. Shokri, and S. M. Elahi, J. Mater. Sci. **49**, 88 (2014).

[21] K. S. Denisov and N. S. Averkiev, JETP Lett. **99**, 400 (2014).

[22] A. Manchon and S. Zhang, Phys. Rev. B **79**, 094422 (2009).

[23] I. Garate and A. H. MacDonald, Phys. Rev. B **80**, 134403 (2009).

[24] K. M. D. Hals, A. Brataas, and Y. Tserkovnyak, Europhys. Lett. **90**, 47002 (2010).

[25] A. Chernyshov, M. Overby, X. Liu, J. K. Furdyna, Y. Lyanda-Geller, and L. P. Rokhinson, Nat. Phys. **5**, 656 (2009).

[26] M. Endo, F. Matsukura, and H. Ohno, Appl. Phys. Lett. **97**, 222501 (2010).

[27] D. Fang, H. Kurebayashi, J. Wunderlich, K. Výborný, L. P. Zârbo, R. P. Campion, A. Casiraghi, B. L. Gallagher, T. Jungwirth, and A. J. Ferguson, Nat. Nanotechnol. **6**, 413 (2011).

[28] H. Li, X. Wang, F. Doan, and A. Manchon, Appl. Phys. Lett. **102**, 192411 (2013).

[29] P. C. Lingos, J. Wang, and I. E. Perakis, arXiv:1411.6662 [cond-mat.str-el] [Phys. Rev. B (to be published)].

[30] C. Thurn and V. M. Axt, Phys. Rev. B **85**, 165203 (2012).

[31] M. Cygorek and V. M. Axt, arXiv:1412.5898 [cond-mat.mes-hall].

[32] J. D. Cibert and D. Scalbert, *Spin Physics in Semiconductors* (Springer-Verlag, Heidelberg, 2008), Chap. 13.

[33] G. Dresselhaus, Phys. Rev. **100**, 580 (1955).

[34] E. I. Rashba, Sov. Phys. Solid State **2**, 1109 (1960).

[35] M. Cygorek and V. M. Axt, Phys. Rev. B **90**, 035206 (2014).

[36] *Semiconductors and Semimetals*, edited by J. K. Furdyna and J. Kossut (Academic Press, San Diego, CA, 1988), Vol. 25.

[37] C. Thurn, M. Cygorek, V. M. Axt, and T. Kuhn, Phys. Rev. B **88**, 161302(R) (2013).

[38] C. Thurn, M. Cygorek, V. M. Axt, and T. Kuhn, Phys. Rev. B **87**, 205301 (2013).

[39] M. I. D'yakonov and V. I. Perel', Sov. Phys. JETP **33**, 1053 (1971).

[40] P. Y. Yu and M. Cardona, *Fundamentals of Semiconductors*, 4th ed. (Springer-Verlag, Heidelberg, 2010).

[41] A. Twardowski, M. von Ortenberg, M. Demianiuk, and R. Pauthenet, Solid State Commun. **51**, 849 (1984).

[42] B. König, I. A. Merkulov, D. R. Yakovlev, W. Ossau, S. M. Ryabchenko, M. Kutrowski, T. Wojtowicz, G. Karczewski, and J. Kossut, Phys. Rev. B **61**, 16870 (2000).

[43] A. Metavitsiadis, R. Dillenschneider, and S. Eggert, Phys. Rev. B **89**, 155406 (2014).

[44] Y. Zhou, T. Yu, and M. W. Wu, Phys. Rev. B **87**, 245304 (2013).

[45] J. Furdyna, J. Appl. Phys. **64**, R29 (1988).

[46] J. Kossut, in *Semiconductors and Semimetals* (Ref. [36]) (Academic Press, San Diego, 1988), Chap. 5.

[47] E. A. de Andrada e Silva, G. C. La Rocca, and F. Bassani, Phys. Rev. B **55**, 16293 (1997).

[48] Y.-H. Zhu and J.-B. Xia, Europhys. Lett. **82**, 37004 (2008); *Physics of II-VI and I-VII Compounds: Semimagnetic Semiconductors*, edited by O. Madelung, M. Schulz, and H. Weiss, Landolt-Börnstein, New Series, Group III, Vol. 17, Part b (Springer-Verlag, Berlin, 1982).

[49] Jian Liu, H. Buhmann, E. G. Novik, Yongsheng Gui, V. Hock, C. R. Becker, and L. W. Molenkamp, Phys. Status Solidi B **243**, 835 (2006).

Publication 4

Relaxation and coherent oscillations in the spin dynamics of II-VI diluted magnetic quantum wells

F. Ungar, M. Cygorek, P. I. Tamborenea and V. M. Axt

Relaxation and coherent oscillations in the spin dynamics of II-VI diluted magnetic quantum wells

F. Ungar[1], M. Cygorek[1], P. I. Tamborenea[1,2] and V. M. Axt[1]

[1] Theoretische Physik III, Universität Bayreuth, 95440 Bayreuth, Germany

[2] Departamento de Física and IFIBA, FCEN, Universidad de Buenos Aires, Ciudad Universitaria, Pab. I, C1428EHA Buenos Aires, Argentina

Abstract. We study theoretically the ultrafast spin dynamics of II-VI diluted magnetic quantum wells in the presence of spin-orbit interaction. We extend a recent study where it was shown that the spin-orbit interaction and the exchange sd coupling in bulk and quantum wells can compete resulting in qualitatively new dynamics when they act simultaneously. We concentrate on $Hg_{1-x-y}Mn_xCd_yTe$ quantum wells, which have a highly tunable Rashba spin-orbit coupling. Our calculations use a recently developed formalism which incorporates electronic correlations originating from the exchange sd-coupling. We find that the dependence of electronic spin oscillations on the excess energy changes qualitatively depending on whether or not the spin-orbit interaction dominates or is of comparable strength with the sd interaction.

Ultrafast spin dynamics in semiconductors is attracting nowadays a great deal of attention. In a recent article we explored the interplay between the exchange sd interaction (EXI) and the spin-orbit interaction (SOI) in II-VI diluted magnetic semiconductors (DMS) [1]. In that study we found that the EXI and the SOI can be tuned to overrun each other or to compete on an equal level in realistic bulk and quantum well systems. Importantly, we found that the inclusion of the SOI introduces oscillations in the spin dynamics which are completely absent when only the EXI is relevant. In the present article, we characterize systematically the decay and the periods of oscillations seen in the spin dynamics in quantum wells, as functions of the excess energy of the electron population in the conduction band (mean energy of a Gaussian occupation of spin-polarized photoexcited electrons). We employ a microscopic density-matrix theory that models on a quantum-kinetic level the spin dynamics, taking into account the exchange-induced correlations and the localized character of the Mn spins [2, 3]. For the sake of brevity we shall only sketch the model here and refer the reader to Refs. [1] and [3] for a complete description.

We consider conduction band electrons in Mn-doped II-VI DMS coming from low-intensity optical excitations. We work in the regime of electron densities n_e much lower than the Mn density n_{Mn}, in which the Mn spin variables are nearly stationary [3, 4, 5, 6]. The spin dynamics is described by $\langle \mathbf{s}_{\mathbf{k}}^{\perp} \rangle(t)$ and $\langle s_{\mathbf{k}}^{\parallel} \rangle(t)$, the mean electronic spin components, perpendicular and parallel to the Mn magnetization, respectively, corresponding to the conduction-band state $\mathbf{k}$.

In this study we concentrate on $Hg_{1-x-y}Mn_xCd_yTe$ quantum wells, since this alloy offers great flexibility in the control of the Rashba SOI. This control is achieved thanks to the strong dependence of the band gap on the doping fraction $x + y$ [7]. With this material, Rashba coefficients of the order of $\alpha_R \approx 10\,ps^{-1}nm$ can be obtained for realistic quantum well specifications [1]. Throughout the paper we shall assume the Mn magnetization to be perpendicular to the quantum well. Furthermore, we take a Gaussian electron occupation
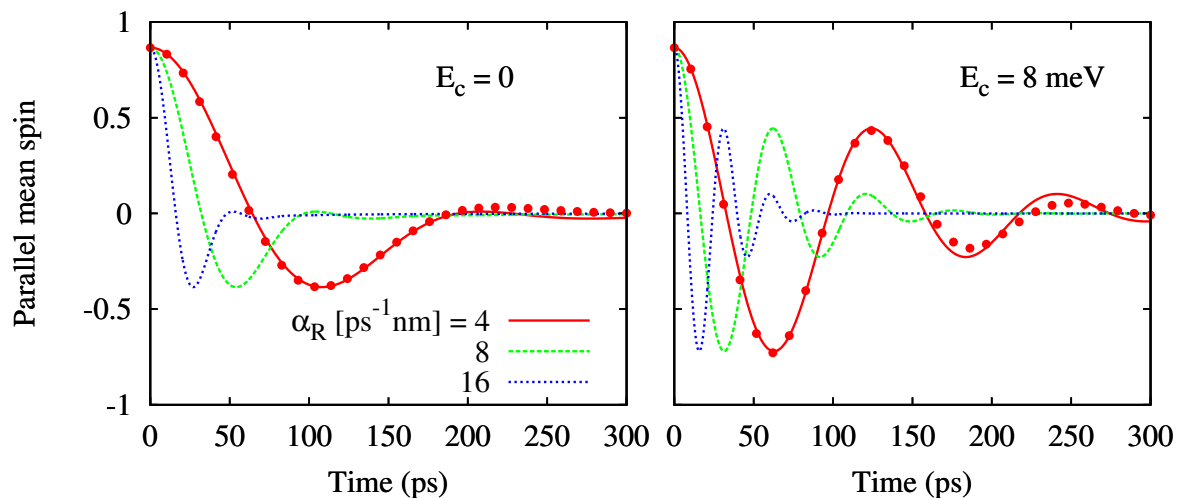
Figure 1. Electron spin dynamics in a $Hg_{1-x-y}Mn_xCd_yTe$ quantum well with Rashba interaction and no exchange sd coupling for a Gaussian electron distribution centered at E_c. Lines: simulations for different values of α_R expressed in units of $ps^{-1}nm$. Red dots: simple fits to the first oscillation of the curves with $\alpha_R = 4\,ps^{-1}nm$ (see text for details).

centered at an energy E_c above the conduction-band edge with a standard deviation of $E_s = 3$ meV and initial spin-polarization rotated $30°$ with respect to the Mn magnetization.

It is instructive to examine first the spin dynamics resulting only from the Rashba spin-orbit interaction (i.e., no exchange sd coupling is accounted for). In this case the Mn magnetization does not enter the dynamics. For later comparison we used, however, the above described initial condition where the direction of the initial electronic spin is related to direction of the Mn magnetization. Figure 1 shows the time evolution of the summed parallel spin component, $\langle s^{\parallel}\rangle(t) = \sum_{\mathbf{k}}\langle s_{\mathbf{k}}^{\parallel}\rangle(t)$, for three different values of the Rashba coupling constant α_R. The cases $E_c = 0$ (Gaussian occupation centered at the band edge) and $E_c = 8$ meV are shown. We see that the Rashba interaction produces well-defined oscillations and decay. Note that without the EXI, the time evolution of the total spin is given by coherent precessions of individual electron spins around the $\mathbf{k}$-dependent magnetic Rashba field, which are collectively responsible for the decay. Red dots in both panels of Fig. 1 are fits to the initial oscillations of the $\alpha_R = 4\,ps^{-1}nm$ evolutions, done with a function $f(t) \propto \exp\left[-(t/\tau)^2\right]\cos\left(2\pi t/T\right)$. For a Gaussian electron distribution with spins pointing in the growth direction, we find from Eq. (17) of Ref. [1]:

$$\langle s^{\parallel}(t)\rangle = C\int_0^\infty dk\,k\,\exp\left[-\frac{\left(\hbar^2 k^2 - 2m^*E_c\right)^2}{(2m^*E_s)^2}\right]\cos(2\alpha_R kt), \tag{1}$$

where m^* is the effective mass and C is a constant determined by the initial value of the total spin. The integral in Eq. (1) is close to the (half-sided) Fourier transform of a function with a single central peak indicating in time regime a damped oscillation with roughly the peak frequency. An initially exponential decay of $\langle s^{\parallel}(t)\rangle$ would require a Lorentzian decay in the energy domain. However, the function in Eq. (1) decays much faster for large k explaining why the initial behavior of $\langle s^{\parallel}(t)\rangle$ is much better approximated by a Gaussian than by an exponential. Indeed, Fig. 1 reveals that the Gaussian fit is almost perfect at early times but worsens somewhat later. Applying the Gaussian fit to a number of different cases we find that for given E_c both $\tau \propto \alpha_R^{-1}$ and $T \propto \alpha_R^{-1}$ hold to a very good approximation. A similar behavior is observed for $|\langle \mathbf{s}^{\perp}\rangle(t)| = |\sum_{\mathbf{k}}\langle \mathbf{s}_{\mathbf{k}}^{\perp}\rangle(t)|$, whose initial evolution can be well fitted with
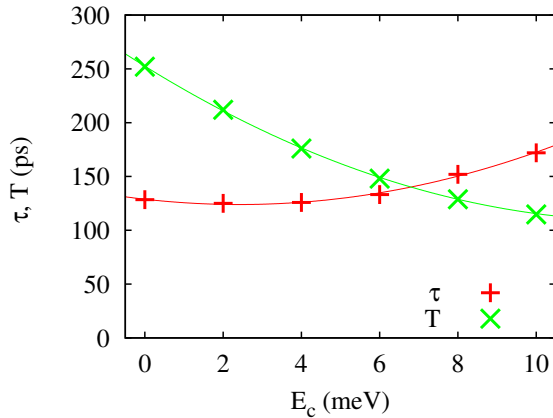
Figure 2. Gaussian electron spin relaxation time, τ, and period of the oscillations, T, in a $\mathrm{Hg_{1-x-y}Mn_xCd_yTe}$ quantum well with Rashba interaction $\alpha_R = 4\,\mathrm{ps^{-1}nm}$ and no exchange sd coupling as a function of the excess energy E_c. Symbols: full calculation; lines: parabolic fit.
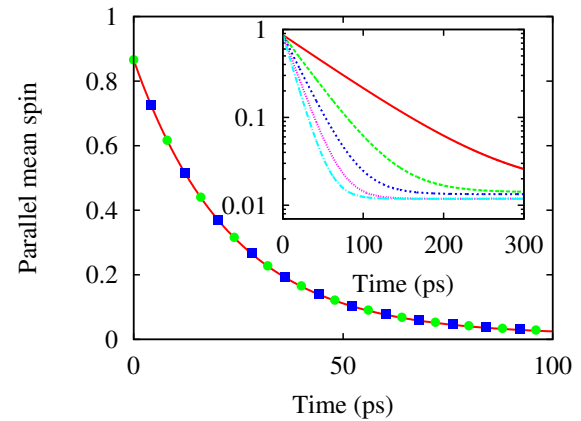
Figure 3. $\langle s^{\parallel}(t)\rangle$ with exchange sd and no Rashba interaction. $x_{\mathrm{Mn}} = 0.3\%$, $S = 0.1$, $E_c = 0$ (red line), $4\,\mathrm{meV}$ (green circles), $8\,\mathrm{meV}$ (blue squares). Inset: $E_c = 0$, $S = 0.1$, various x_{Mn}: 0.1% (red), 0.2% (green), 0.3% (blue), 0.4% (magenta), 0.5% (cyan).

$f(t) \propto \exp\left[-(t/\tau)^2\right]\cos\left(2\pi t/T\right) + 1$, with the same values of τ and T as for $\langle s^{\parallel}\rangle(t)$. We found that τ and T can be precisely fitted as functions of E_c with parabolas, as seen in Fig. 2. The decrease of T and the increase of τ with rising E_c reflect the fact that the effective Rashba field is k dependent becoming stronger for larger k.

Let us now look at the spin dynamics under the influence of the EXI only (no Rashba SOI). For the EXI coupling constant we take the value $J_{\mathrm{sd}} = 26.8\,\mathrm{meV\,nm^3}$ [1]. The effects of the EXI on the carrier spins can be controlled via the Mn concentration, x_{Mn}, and the initial net Mn magnetization, $S = |\langle \mathbf{S}\rangle|$ [1]. The dynamics of the electron spin component parallel to the Mn magnetization is shown in Fig. 3. As found previously, it is approximately described by an exponential decay to an in general non-zero equilibrium value with a decay time [cf. Eq.(19) of Ref. [3]] $\tau^{\parallel} = (J_{sd}^2 n_{Mn} m^*/\hbar^2 d)\langle S^2 - S^{\parallel 2}\rangle$, where d is the width of the quantum well and $\langle S^2 - S^{\parallel 2}\rangle$ is a second moment of the spin-$\frac{5}{2}$ Mn system. In particular, $\tau^{\parallel}$ is linear in x_{Mn} and independent of the excess energy E_c. Note that no oscillations appear in the time evolution of the parallel spin component when only the EXI is present. The perpendicular component decays to zero with a slightly different rate while it precesses around the Mn magnetization [3].

We now come to the combined effects of the Rashba SOI and EXI. Figure 4 shows the spin dynamics for $x_{\mathrm{Mn}} = 0.3\%$, $S = 0.1$, $\alpha_R \approx 4\,\mathrm{ps^{-1}nm}$, and three different values of E_c. Note the semilog scale chosen to better visualize the long time behavior. This set of parameters defines a "strong sd" and "weak Rashba" situation. Accordingly, the initial decay is exponential (not Gaussian like in Fig. 1), with an E_c-independent decay rate, like in Fig. 3. However, at later times fairly regular oscillations appear, with essentially constant, E_c-dependent amplitude, due to the presence of the Rashba interaction. We note that the frequency of the oscillations depends only slightly on E_c, becoming higher for higher E_c, which indicates a slight dependence on the Rashba mechanism. The frequency of the oscillations (period of about 35 ps) is close to the precession frequency about the net Mn magnetic field, which is independent of E_c. The oscillations do not decay because all electrons precess with nearly the same frequency governed mainly by the Mn magnetization and thus do not dephase. The fact that the amplitude of the oscillations does not
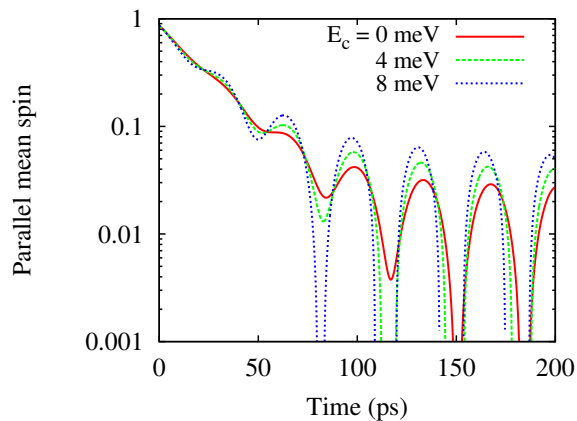
Figure 4. Evolution of the mean parallel electron spin under exchange sd and Rashba interactions. Parameters: $x_{\mathrm{Mn}} = 0.3\%$, $S = 0.1$, $\alpha_R \approx 4\,\mathrm{ps}^{-1}\mathrm{nm}$, and three values of E_c.
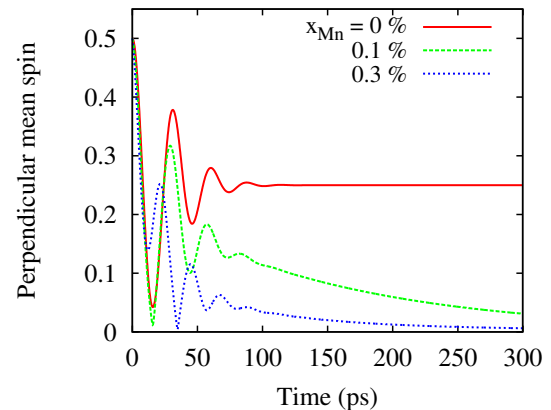
Figure 5. Evolution of the mean perpendicular electron spin component under exchange sd and Rashba interactions. Parameters: $\alpha_R = 16\,\mathrm{ps}^{-1}\mathrm{nm}$, $E_c = 8\,\mathrm{meV}$, $S = 0.1$, and three values of x_{Mn}.

decay with time and the near independence of the period on E_c distinguish qualitatively these oscillations from the ones observed with Rashba coupling alone. Also note that again there is a saturation value different from zero as seen above in the sd-only case. However, a new feature produced by the presence of the Rashba interactions is that the perpendicular spin component does not go to zero as in the sd-only evolution (not shown for brevity).

Finally, Fig. 5 shows the time evolution of the mean perpendicular spin component under EXI and SOI for fixed Rashba constant $\alpha_R = 16\,\mathrm{ps}^{-1}\mathrm{nm}$, $E_c = 8\,\mathrm{meV}$, and three different values of x_{Mn}. This figure shows the effect of an increasing EXI coupling in the presence of a strong Rashba coupling on the perpendicular spin component. We see that as the Mn concentration increases, starting from a Rashba-only situation in which the equilibrium value $\langle s_{\mathbf{k}}^{\perp} \rangle$ is half its initial value [1], a decay to zero sets in. At the same time, the frequency of the oscillations increases and their amplitude goes down.

In conclusion, we have studied theoretically the effects of the Rashba spin-orbit interaction in II-VI diluted-magnetic-semiconductor quantum wells. We characterized the dependence of the spin dynamics on the excess energy of a Gaussian population of electrons in the conduction band. Our findings provide qualitative signatures that could aid experimentalists in distinguishing the relative importance of spin-orbit and exchange interactions in DMS quantum wells.

References

[1] Ungar F, Cygorek M, Tamborenea P I and Axt V M 2015 *Phys. Rev* B **91** 195201
[2] Thurn C and Axt V M 2012 *Phys. Rev.* B **85** 165203
[3] Cygorek M and Axt V M 2015 *Semicond. Sci. Technol.* **30** 085011
[4] Cygorek M and Axt V M 2014 *Phys. Rev.* B **90** 035206
[5] Thurn C, Cygorek M, Axt V M and Kuhn T 2013 *Phys. Rev.* B **88** 161302(R)
[6] Thurn C, Cygorek M, Axt V M and Kuhn T 2013 *Phys. Rev.* B **87** 205301
[7] Kossut J 1988 *Diluted Magnetic Semiconductors (Semiconductors and Semimetals* vol 25) ed Furdyna J K and Kossut J (San Diego: Academic Press)

Publication 5

Carrier-impurity spin transfer dynamics in paramagnetic II-VI diluted magnetic semiconductors in the presence of a wave-vector-dependent magnetic field

M. Cygorek, P. I. Tamborenea, and V. M. Axt

Carrier-impurity spin transfer dynamics in paramagnetic II-VI diluted magnetic semiconductors in the presence of a wave-vector-dependent magnetic field

M. Cygorek,[1] P. I. Tamborenea,[1,2] and V. M. Axt[1]

[1]*Theoretische Physik III, Universität Bayreuth, 95440 Bayreuth, Germany*

[2]*Departamento de Física and IFIBA, FCEN, Universidad de Buenos Aires, Ciudad Universitaria, Pabellón I,*

1428 Ciudad de Buenos Aires, Argentina

Quantum kinetic equations of motion for carrier and impurity spins in paramagnetic II-VI diluted magnetic semiconductors in a **k**-dependent effective magnetic field are derived, where the carrier-impurity correlations are taken into account. In the Markov limit, rates for the electron-impurity spin transfer can be derived for electron spins parallel and perpendicular to the impurity spins corresponding to measurable decay rates in Kerr experiments in Faraday and Voigt geometry. Our rigorous microscopic quantum kinetic treatment automatically accounts for the fact that, in an individual spin flip-flop scattering process, a spin flip of an electron is necessarily accompanied by a flop of an impurity spin in the opposite direction and the corresponding change of the impurity Zeeman energy influences the final energy of the electron after the scattering event. This shift in the electron energies after a spin flip-flop scattering process, which usually has been overlooked in the literature, turns out to be especially important in the case of extremely diluted magnetic semiconductors in an external magnetic field. As a specific example for a **k**-dependent effective magnetic field the effects of a Rashba field on the dynamics of the carrier-impurity correlations in a $Hg_{1-x-y}Cd_yMn_xTe$ quantum well are described. It is found that, although accounting for the Rashba interaction in the dynamics of the correlations leads to a modified **k**-space dynamics, the time evolution of the total carrier spin is not significantly influenced. Furthermore, a connection between the present theory and the description of collective carrier-impurity precession modes is presented.

I. INTRODUCTION

Diluted magnetic semiconductors (DMSs) have attracted a great deal of interest [1–11] as their highly tunable magnetic properties are ideally suited for adding spintronic functionalities to otherwise well-established semiconductor technologies [12–14]. Particularly promising for future technological applications is the fact that some DMSs, such as $Ga_{1-x}Mn_xAs$, exhibit a ferromagnetic phase [2,15]. The convenient optical properties also allow, e.g., for the optical switching of the magnetization [16] in $Ga_{1-x}Mn_xAs$. While a comprehensive unified theoretical description of the magnetism in DMS is still missing, it is generally accepted that a carrier-mediated impurity-impurity spin interaction plays a key role [1,17]. Thus, it is crucial to understand the spin physics not only of the magnetic impurities, but also of the carriers as well as the details of the spin transfer between carriers and impurities.

Experimentally, the carrier spins in DMSs are often investigated optically using time-resolved magneto-optical Kerr effect (MOKE) measurements [3,10,18], a pump-probe technique that makes it possible to extract the carrier spin dynamics with a temporal resolution of ∼100 fs. The experimentally obtained carrier spin dephasing and relaxation rates, which also include the effects of the spin transfer between carriers and impurities, can then be used as an input for, e.g., the theoretical description of spin-wave excitations in ferromagnetic DMSs [8].

However, a quantitative theoretical explanation for the values of the carrier spin relaxation rates measured in MOKE experiments, even in the simplest possible case of conduction-band electrons in an intrinsic II-VI DMS, has yet to be found. For example, even such basic quantities as the magnetic field dependence of the spin transfer rate between the carrier and impurity systems in paramagnetic DMSs is still not satisfactorily explained [3]. This is, on the one hand, due to the large number of factors that simultaneously play a role in DMSs, like the spin-dependent *s-d* interaction between magnetic impurities and carriers, spin dephasing due to spin-orbit coupling mechanisms [19–21], carrier-carrier interaction [22], and disorder effects [23]. On the other hand, even the typically dominant *s-d* interaction is usually treated only on the level of the mean-field approximation [24–26], neglecting the effects of carrier-impurity correlations, which can be important [8,27,28]. The spin transfer between carriers and impurities is commonly described by rate equations where the rates are calculated using Fermi's "golden rule" [25,26,29–31].

One problem of this approach is that it is *a priori* not clear under which circumstances the perturbative scheme, which is implicit in the derivation of Fermi's golden rule, is applicable. For example, at the band edge, where the band energies, described by the Hamiltonian H_0 of an undoped semiconductor, are negligible, the *s-d* interaction cannot be thought of as a small perturbation to H_0. A second deficiency of the golden-rule treatment is that it gives, by construction, only the transition rate between energy eigenstates of the system. However, optical orientation also allows for an injection of carrier spins perpendicular to an external magnetic field (Voigt geometry) or the impurity magnetization, respectively [10], which corresponds to the excitation of superpositions of energy eigenstates. Thus, the relaxation rate of the transverse carrier spin component is not provided by Fermi's golden rule.

A more elaborate treatment of the *s-d* exchange interaction, which is also capable of deriving a rate for the spin transfer of the perpendicular electron-spin component, was given

by *Semenov* in a study based on a projection operator method [32]. Another notable approach to the spin dynamics in DMS has been provided by the group of Wu [22], which has developed the kinetic spin Bloch equations (KSBEs) that account not only for rates for the spin transfer due to the *s-d* exchange interaction, but also for a number of other effects, such as carrier-carrier and carrier-phonon interaction.

In the present paper, we describe the electron-spin dynamics in the conduction band, where we focus on paramagnetic intrinsic II-VI DMSs. We work with a quantum kinetic theory starting from the *s-d* exchange Hamiltonian H_{sd}, where a correlation expansion scheme was used to formulate equations of motion for the carrier and impurity density matrices as well as the carrier-impurity correlation functions [33]. This approach allows a nonperturbative description of far-from-equilibrium situations. The golden-rule rate equations can be deduced from the quantum kinetic theory as a Markovian limit [34,35]. In the same limit, also the rates for the carrier spin component perpendicular to the impurity magnetization can be derived [36]. Furthermore, the applicability of the Markovian limit and therewith the golden-rule rate equations can be checked by direct comparison of the full quantum kinetic theory with its Markovian limit [36]. It was found that for an agreement between the quantum kinetic and the Markovian predictions, it is essential to account for a precessionlike motion of the carrier-impurity correlations. Therefore, effective equations which capture the essential features of the full quantum kinetic equations that also include the correlation dynamics were called *precession of electron spins and correlations* (PESCs) equations [37].

For vanishing external magnetic field and impurity magnetization, all of the above theories contain the same rate equations that can also be found with Fermi's golden rule as a special case. In contrast, in the presence of an external magnetic field which leads to a finite impurity magnetization in the equilibrium of a paramagnetic DMS, the predictions of the different theories deviate from each other. In order to compare these theories, we extend the quantum kinetic theory of Ref. [33] to take into account the Zeeman interaction of carriers and impurities in a magnetic field.

We also allow for a **k** dependence of an effective magnetic field, which makes it possible to discuss the effects of Dresselhaus [20] or Rashba [19] spin-orbit coupling or a **k**-dependent *g* factor on the spin dynamics in DMSs. In contrast to previous treatments [21] where the PESC equations were extended by adding a **k**-dependent precession term to the time evolution of the carrier spins, in the present paper the **k**-dependent effective magnetic field is incorporated on a microscopic quantum kinetic level which also leads to a modification of the equations of motion for the carrier-impurity correlations. Another point of view is that, while the approach of Ref. [21] accounts for the **k**-dependent field *between* carrier-impurity spin-flip scattering events, in the present theory the effective magnetic field also acts *during* the spin-flip scattering. Formally this situation is similar to that of, e.g., the intracollisional field effect [38], where the effects of an external field that acts during a scattering event (phonon-emission in the case of Ref. [38]) can indeed change the optical and transport properties qualitatively.

Furthermore, here we account for the fact that the impurity spin is a *z*-dependent (growth direction of the quantum well) dynamical variable which can change over time. This connects the present theory to the description of collective carrier-impurity precession modes [11,39,40].

The paper is outlined as follows: First, we derive the Markov limit of quantum kinetic equations accounting for the *s-d* interaction, a possibly **k**-dependent effective magnetic field and the *z* dependence of the carrier envelope function. Then, we present results for the magnetic field dependence of the carrier-impurity spin transfer rates and compare it with the results predicted by several other theories. Next, we answer the question to what extent spin-orbit couplings that lead to a **k**-dependent effective magnetic field influence the spin transfer dynamics, in particular with respect to the dynamics of the carrier-impurity correlations. Finally, we show how the theory of the present paper can be related to the theory employed in the discussion of collective carrier-impurity precession modes [39].

II. THEORY

A. DMS Hamiltonian

The Hamiltonian for electrons and impurities in DMS can be modelled by

$$H = H_0 + H_Z^e + H_Z^{Mn} + H_{sd}, \qquad (1)$$

where H_0 describes the conduction band of a semiconductor crystal and can be written as

$$H_0 = \sum_{\mathbf{k}} \sum_{\sigma} \hbar\omega_{\mathbf{k}} c_{\mathbf{k}\sigma}^\dagger c_{\mathbf{k}\sigma} + \sum_{\mathbf{k}} \sum_{\sigma,\sigma'} \hbar\boldsymbol{\Omega}_{\mathbf{k}} \cdot \mathbf{s}_{\sigma\sigma'} c_{\mathbf{k}\sigma}^\dagger c_{\mathbf{k}\sigma'}. \quad (2)$$

$c_{\mathbf{k}\sigma}^\dagger$ and $c_{\mathbf{k}\sigma}$ are the creation and annihilation operators for electrons with wave vector **k** in the spin subband $\sigma \in \{\uparrow,\downarrow\}$. $\omega_{\mathbf{k}}$ describes the diagonal, i.e., the spin independent, part of H_0 while $\boldsymbol{\Omega}_{\mathbf{k}}$ is the **k**-dependent effective magnetic field, e.g., due to spin-orbit interactions. The electron-spin matrix vector $\mathbf{s}_{\sigma\sigma'} = \frac{1}{2}\boldsymbol{\sigma}_{\sigma\sigma'}$ is proportional to the vector of Pauli matrices $\boldsymbol{\sigma}_{\sigma\sigma'}$.[1]

H_Z^e and H_Z^{Mn} are the Zeeman energies for carriers and impurities, respectively:

$$H_Z^e = \sum_{\mathbf{k}\sigma\sigma'} g_e(\mathbf{k})\mu_B \mathbf{B} \cdot \mathbf{s}_{\sigma\sigma'} c_{\mathbf{k}\sigma}^\dagger c_{\mathbf{k}\sigma'}, \qquad (3)$$

$$H_Z^{Mn} = \sum_{Inn'} g_{Mn}\mu_B \mathbf{B} \cdot \mathbf{S}_{nn'} \hat{P}_{nn'}^I, \qquad (4)$$

where g_e and g_{Mn} are the electron and impurity *g* factors and **B** is the externally applied magnetic field. In general, g_e may depend on the electron wave vector which, e.g., gives rise to the imhomogeneous-*g*-factor spin dephasing mechanism [41,42] which is essential for the description of the magnetic field dependence of the spin decay time in nonmagnetic semiconductors [43]. $\mathbf{S}_{nn'}$ are the spin matrices

----

[1]Here, we use the convention that the factor $\hbar$ which appears in the spin matrices in the SI system is instead included in μ_B and J_{sd}, respectively.

for the impurities with, in the case of manganese, $S = \frac{5}{2}$, so that $n, n' \in \{-\frac{5}{2}, -\frac{3}{2}, \ldots, \frac{5}{2}\}$. The impurity spin is described by the operator $\hat{P}_{nn'}^I = |I, n\rangle \langle I, n'|$ where $|I, n\rangle$ is the nth spin state of the Ith impurity ion.

The most important part of the Hamiltonian for the spin dynamics in DMSs is the s-d exchange interaction which, in real space, has the form

$$H_{sd} = J_{sd} \sum_{\substack{I,n,n', \\ i,\sigma,\sigma'}} \left(\mathbf{S}_{nn'} \hat{P}_{nn'}^I\right) \cdot \mathbf{s}_{\sigma\sigma'} \psi_\sigma^\dagger(\mathbf{r}_i) \psi_{\sigma'}(\mathbf{r}_i) \delta(\mathbf{R}_I - \mathbf{r}_i), \quad (5)$$

where $\mathbf{R}_I$ and $\mathbf{r}_i$ are the position vectors of the Ith impurity and ith electron and $\psi_\sigma^\dagger(\mathbf{r}_i)$ as well as $\psi_\sigma(\mathbf{r}_i)$ are the corresponding real-space field operators for the electrons. Since most experiments on DMSs are performed on two-dimensional structures, we choose a single-particle basis comprised of product states of a z-dependent envelope, where z is defined to point along the growth direction, and an in-plane part described by plane waves. When restricting to the lowest confined state of the envelope function $\psi(z)$, we can formulate the effective s-d Hamiltonian for the in-plane part as

$$H_{sd} = \frac{J_{sd}}{V} d \sum_I |\psi(Z_I)|^2 \mathbf{S}_{nn'} \cdot \mathbf{s}_{\sigma\sigma'} c_{\mathbf{k}\sigma}^\dagger c_{\mathbf{k}'\sigma'} \hat{P}_{nn'}^I e^{i(\mathbf{k}'-\mathbf{k})\mathbf{R}_I^\parallel}, \quad (6)$$

where V is the volume of the sample, d is the quantum well width, Z_I is the z component of the Ith impurity position vector, and $\mathbf{R}_I^\parallel$ is the in-plane part of the position vector of the Ith impurity. Assuming infinitely high barriers, the envelope is given by

$$\psi(z) = \sqrt{\frac{2}{d}} \cos\left(\frac{\pi}{d} z\right), \quad (7)$$

for $z \in [-\frac{d}{2}; \frac{d}{2}]$ and zero otherwise. Thus, due to the factor $|\psi(Z_I)|^2$, magnetic impurities at the border of the quantum well couple much more weakly to the electrons than impurities at the center of the well.

B. Quantum kinetic equations of motion

In Ref. [33], a set of quantum kinetic equations of motion based on a correlation expansion scheme has been developed for the carrier and impurity density matrix as well as the carrier-impurity correlations in the case of zero external and effective-spin-orbit magnetic fields. In the present paper, we additionally consider an in general wave-vector-dependent effective magnetic field for the carriers and the Zeeman energy term for the magnetic impurities to the Hamiltonian. Since all of the terms that are added are effective single-particle contributions, they do not lead to a buildup of a new hierarchy of correlations, but only connect the density matrices and the correlations with themselves. Therefore, the truncation scheme and the factorization of higher correlations laid out in Ref. [33] can still be applied when the aforementioned

additional Hamiltonians are accounted for. If an on-average homogeneous distribution of magnetic impurities in the quantum-well plane is assumed, equations of motion can be formulated for the dynamical variables [36]

$$C_{\sigma_1 \mathbf{k}_1}^{\sigma_2} = \langle c_{\mathbf{k}_1 \sigma_1}^\dagger c_{\mathbf{k}_1 \sigma_2} \rangle, \quad (8a)$$

$$M_{n_1}^{n_2}(z) = \frac{d}{N_{Mn}} \sum_I \delta(z - Z_I) \langle \hat{P}_{n_1 n_2}^I \rangle, \quad (8b)$$

$$Q_{\sigma_1 n_1 \mathbf{k}_1}^{\sigma_2 n_2 \mathbf{k}_2}(z) = \frac{V}{N_{Mn}} d \sum_I \delta(z - Z_I)$$
$$\times \langle c_{\mathbf{k}_1 \sigma_1}^\dagger c_{\mathbf{k}_2 \sigma_2} \hat{P}_{n_1 n_2}^I e^{i(\mathbf{k}_2 - \mathbf{k}_1)\mathbf{R}_I^\parallel} \rangle, \quad (8c)$$

where $C_{\sigma_1 \mathbf{k}_1}^{\sigma_2}$ and $M_{n_1}^{n_2}(z)$ are the electron and impurity density matrices and $Q_{l_1 n_1 \mathbf{k}_1}^{l_2 n_2 \mathbf{k}_2}(z)$ (for $\mathbf{k}_1 \neq \mathbf{k}_2$) represent the carrier-impurity correlations, where the mean-field part has been subtracted. N_{Mn} is the number of impurity ions in the DMSs.

Instead of the density matrices, also the average carrier $\mathbf{s}_{\mathbf{k}_1}$ and impurity spins $\langle \mathbf{S}(z) \rangle$ as well as the electron occupations $n_{\mathbf{k}_1}$ can be used as dynamical variables [36] which helps to understand the dynamics of the physical variables and simplifies the equations of motion,

$$\langle \mathbf{S}(z) \rangle = \sum_{nn'} \mathbf{S}_{nn'} M_n^{n'}(z), \quad (9a)$$

$$n_{\mathbf{k}_1} = \sum_\sigma C_{\sigma \mathbf{k}_1}^\sigma, \quad (9b)$$

$$\mathbf{s}_{\mathbf{k}_1} = \sum_{\sigma_1 \sigma_2} \mathbf{s}_{\sigma_1 \sigma_2} C_{\sigma_1 \mathbf{k}_1}^{\sigma_2}, \quad (9c)$$

$$Q_{j\mathbf{k}_1}^{\alpha \mathbf{k}_2} := \sum_{\substack{\sigma_1 \sigma_2 \\ n_1 n_2}} S_{n_1 n_2}^j s_{\sigma_1 \sigma_2}^\alpha Q_{\sigma_1 n_1 \mathbf{k}_1}^{\sigma_2 n_2 \mathbf{k}_2}. \quad (9d)$$

From now on, we will use the convention that σ indices describe spin-up and spin-down subbands, n indices enumerate the impurity states, while all other Latin indices represent three-dimensional geometric directions, e.g., $j \in \{1,2,3\}$, and Greek indices range from 0 to 3, where the 0 describes occupations. In this notation, the zeroth spin matrix is defined to be the 2×2 identity matrix $s_{\sigma_1 \sigma_2}^0 = \delta_{\sigma_1 \sigma_2}$. Furthermore, we adopt the Einstein notation, so that when the same index appears twice, a summation is implied. Sub- and superscripts are used, e.g., to distinguish the carrier and impurity degrees of freedom of the correlations, and do not represent a covariant formulation. Sums over $\mathbf{k}$ vectors, on the other hand, will be stated explicitly and no sum is implied, if an index $\mathbf{k}_i$ appears twice in an expression.

In this notation, the equations of motion of Refs. [36,37], extended by terms due to the $\mathbf{k}$-dependent effective magnetic field and the impurity and carrier Zeeman energies, are

$$\frac{\partial}{\partial t} \langle S^l(z) \rangle = (\boldsymbol{\omega}_{Mn}(z) \times \langle \mathbf{S}(z) \rangle)_l - \frac{J_{sd} |\psi(z)|^2 d}{\hbar V^2} \sum_{\mathbf{k}\mathbf{k}'} \epsilon_{ijl} \text{Re}\left(Q_{i\mathbf{k}}^{j\mathbf{k}'}(z)\right), \quad (10a)$$

$$\frac{\partial}{\partial t} n_{\mathbf{k}_1} = \int_{-d/2}^{d/2} dz \frac{J_{sd} |\psi(z)|^2 N_{Mn}}{\hbar V^2} \sum_{\mathbf{k}} 2\text{Im}\left(Q_{i\mathbf{k}_1}^{i\mathbf{k}}(z)\right), \quad (10b)$$

$$\frac{\partial}{\partial t} s_{\mathbf{k}_1}^l = (\mathbf{\Omega}_{\mathbf{k}_1}' \times \mathbf{s}_{\mathbf{k}_1})_l + \int_{-d/2}^{d/2} dz \, \frac{J_{sd}|\psi(z)|^2 N_{Mn}}{\hbar V^2} \sum_{\mathbf{k}} \mathrm{Im}\left[\frac{1}{2} Q_{l\mathbf{k}_1}^{0\mathbf{k}}(z) + i\epsilon_{ijl} Q_{i\mathbf{k}_1}^{j\mathbf{k}}(z)\right], \tag{10c}$$

$$\frac{\partial}{\partial t} Q_{l\mathbf{k}_1}^{\alpha\mathbf{k}_2}(z) = -i(\omega_{\mathbf{k}_2} - \omega_{\mathbf{k}_1}) Q_{l\mathbf{k}_1}^{\alpha\mathbf{k}_2}(z) + (A_{\mathbf{k}_1} + A_{\mathbf{k}_2}^*)_{\alpha\gamma} Q_{l\mathbf{k}_1}^{\gamma\mathbf{k}_2}(z) + \epsilon_{ijl}\omega_{Mn}^i(z) Q_{j\mathbf{k}_1}^{\alpha\mathbf{k}_2}(z) + b_{l\mathbf{k}_1}^{\alpha\mathbf{k}_2}(z) + c_{l\mathbf{k}_1}^{\alpha\mathbf{k}_2}(z), \tag{10d}$$

$$b_{l\mathbf{k}_1}^{\alpha\mathbf{k}_2}(z) = \frac{i}{\hbar} J_{sd} d |\psi(z)|^2 \left[\langle S^i S^l(z)\rangle \langle s^i s^\alpha\rangle_{\mathbf{k}_2}^{\mathbf{k}_1} - \langle S^l S^i(z)\rangle \langle s^\alpha s^i\rangle_{\mathbf{k}_1}^{\mathbf{k}_2}\right], \tag{10e}$$

where the mean-field precession frequencies for impurities and carriers are defined as

$$\boldsymbol{\omega}_{Mn}(z) := \frac{g_{Mn}\mu_B}{\hbar}\mathbf{B} + \frac{J_{sd}|\psi(z)|^2 d}{\hbar V}\sum_{\mathbf{k}} \mathbf{s}_{\mathbf{k}}, \tag{11a}$$

$$\mathbf{\Omega}_{\mathbf{k}}' := \mathbf{\Omega}_{\mathbf{k}} + \boldsymbol{\omega}_e(\mathbf{k}), \tag{11b}$$

$$\boldsymbol{\omega}_e(\mathbf{k}) := \frac{g_e(\mathbf{k})\mu_B}{\hbar}\mathbf{B} + \int_{-d/2}^{d/2} dz \, \frac{J_{sd}|\psi(z)|^2 N_{Mn}}{\hbar V}\langle \mathbf{S}(z)\rangle. \tag{11c}$$

The $\mathbf{k}$-dependent precessionlike movement of the electron degree of freedom of the correlations is described by the 4×4 matrix

$$A_{\mathbf{k}_1} := \begin{pmatrix} 0 & \left(i\mathbf{\Omega}_{\mathbf{k}_1}'\right)^T \\ \left(\frac{i}{4}\mathbf{\Omega}_{\mathbf{k}_1}'\right) & \frac{1}{2}\left[\mathbf{\Omega}_{\mathbf{k}_1}'\right]_\times \end{pmatrix}, \tag{11d}$$

where $[\mathbf{\Omega}_{\mathbf{k}_1}']_\times$ is the 3×3 cross-product matrix with $[\mathbf{\Omega}_{\mathbf{k}_1}']_\times \mathbf{v} = \mathbf{\Omega}_{\mathbf{k}_1}' \times \mathbf{v}$.

The source terms $b_{l\mathbf{k}_1}^{\alpha\mathbf{k}_2}(z)$ involve electron variables $n_{\mathbf{k}}$ and $\mathbf{s}_{\mathbf{k}}$ in the form

$$\langle s^i s^j\rangle_{\mathbf{k}_1}^{\mathbf{k}_2} := \delta_{ij}\left[\frac{1}{4}\left(1 - \frac{n_{\mathbf{k}_2}}{2}\right)n_{\mathbf{k}_1} + \frac{1}{2}\mathbf{s}_{\mathbf{k}_1}\cdot\mathbf{s}_{\mathbf{k}_2}\right] - \frac{1}{2}s_{\mathbf{k}_1}^i s_{\mathbf{k}_2}^j$$
$$- \frac{1}{2}s_{\mathbf{k}_1}^j s_{\mathbf{k}_2}^i + \frac{i}{2}\epsilon_{ijl}\left[\left(1 - \frac{n_{\mathbf{k}_2}}{2}\right)s_{\mathbf{k}_1}^l + \frac{n_{\mathbf{k}_1}}{2}s_{\mathbf{k}_2}^l\right], \tag{12a}$$

and

$$\langle s^i s^0\rangle_{\mathbf{k}_2}^{\mathbf{k}_1} := \left(1 - \frac{n_{\mathbf{k}_1}}{2}\right)s_{\mathbf{k}_2}^i - \frac{n_{\mathbf{k}_2}}{2}s_{\mathbf{k}_1}^i - i\epsilon_{ijl}s_{\mathbf{k}_1}^j s_{\mathbf{k}_2}^l, \tag{12b}$$

$$\langle s^0 s^i\rangle_{\mathbf{k}_1}^{\mathbf{k}_2} := \left(1 - \frac{n_{\mathbf{k}_2}}{2}\right)s_{\mathbf{k}_2}^i - \frac{n_{\mathbf{k}_1}}{2}s_{\mathbf{k}_1}^i - i\epsilon_{ijl}s_{\mathbf{k}_1}^j s_{\mathbf{k}_2}^l. \tag{12c}$$

Also, $b_{l\mathbf{k}_1}^{\alpha\mathbf{k}_2}(z)$ contains second moments of the impurity variables:

$$\langle S^i S^j(z)\rangle = \langle S^{\perp^2}(z)\rangle\delta_{ij} + \langle S^{\|^2}(z) - S^{\perp^2}(z)\rangle$$
$$\times \frac{\langle S^i(z)\rangle\langle S^j(z)\rangle}{\langle \mathbf{S}(z)\rangle^2} + \frac{i}{2}\epsilon_{ijl}\langle S^l(z)\rangle, \tag{13}$$

where $S^\| := \frac{\mathbf{S}\cdot\langle\mathbf{S}\rangle}{\langle\mathbf{S}\rangle^2}$ is the spin operator projected onto the direction of the average impurity spin and $\langle S^{\perp^2}\rangle = \frac{1}{2}\langle S^2 - S^{\|^2}\rangle$ is the perpendicular second moment, with $\langle S^2\rangle = \frac{S(S+1)}{4} = \frac{35}{4}$ for a spin-$\frac{5}{2}$ system.

By going over from the density matrices in Eqs. (8) as dynamical variables to the variables defined in Eqs. (9), one ends up with a set of equations that is not closed. Thus, some approximations have to be employed to evaluate the right-hand side of Eqs. (10): First of all, it is necessary to evaluate the second moments of the impurity magnetization, for which the equations of motion can in principle be calculated, but they involve even higher moments. We reduce the complexity of the equations by calculating a quasithermal impurity density matrix in each time step, which is consistent with the average spin $\langle\mathbf{S}(z)\rangle$. Furthermore, the source terms $c_{l\mathbf{k}_1}^{\alpha\mathbf{k}_2}(z)^2$ contain degrees of freedom of the original correlation functions $Q_{\sigma_1 n_1 \mathbf{k}_1}^{\sigma_2 n_2 \mathbf{k}_2}$ that are not expressible in terms of $Q_{l\mathbf{k}_1}^{\alpha\mathbf{k}_2}$. However, the terms $c_{l\mathbf{k}_1}^{\alpha\mathbf{k}_2}(z)$ were shown to be irrelevant in numerical calculations in the situation described in Ref. [37]. Since these terms are proportional to some correlation functions $Q_{\sigma n \mathbf{k}}^{\sigma' n' \mathbf{k}'}$, they mainly renormalize the frequencies with which the correlations oscillate. As will be seen later, the values of these frequencies determine the difference in kinetic energies of the initial and final states of carriers scattered due to the s-d interaction. On the other hand it will be shown that neglecting the terms $c_{l\mathbf{k}_1}^{\alpha\mathbf{k}_2}(z)$ leads to equations that conserve the mean-field energies of the carriers, so that the role of these terms is mainly to ensure energy conservation including the carrier-impurity correlation energy. However, this correlation energy is typically of the order of a few μeV [28], so that it is typically a good approximation to neglect the source terms $c_{l\mathbf{k}_1}^{\alpha\mathbf{k}_2}(z)$, as we will henceforth do.

With these approximations, it seems straightforward to solve the coupled system of ordinary differential equations (10) numerically. However, this task is very challenging, since the correlations are indexed by two $\mathbf{k}$ vectors, where each one is an element of a two-dimensional continuum in the case of a quantum well. The problem therefore has the complexity $\mathcal{O}(N_k^4 N_z N_t)$, where N_k, N_z, and N_t are the numbers of discretization points of the k-space (linear dimension), the growth direction in real space, and the time, respectively. Our strategy to make the calculation tractable follows Ref. [37]: The computation time can be strongly reduced, if the correlations are eliminated and only their effects on the electron and impurity variables are kept. This can be achieved by formally integrating the equations of motion for the correlations at the cost of introducing a memory integral. This memory integral can in turn be eliminated by a

---

[2] The source terms $c_{l\mathbf{k}_1}^{\alpha\mathbf{k}_2}$ are given by $c_{l\mathbf{k}_1}^{\alpha\mathbf{k}_2} := \sum_{\sigma_1\sigma_2 n_1 n_2} S_{n_1 n_2}^l s_{\sigma_1\sigma_2}^\alpha b_{\sigma_1 n_1 \mathbf{k}_1}^{\sigma_2 n_2 \mathbf{k}_2\,III}$ with $b_{\sigma_1 n_1 \mathbf{k}_1}^{\sigma_2 n_2 \mathbf{k}_2\,III}$ being defined in Ref. [36].

short-memory or Markov approximation, which is established in the next section.

C. Derivation and applicability of the Markov limit

Before we discuss the Markov limit of the correlations including the precessionlike movement of the correlations, we briefly recapitulate the standard way [36,44] of deriving the Markov limit of quantum kinetic equations in the simplest possible situation with $\boldsymbol{\Omega}'_{\mathbf{k}} = 0$ and $\boldsymbol{\omega}_{Mn}(z) = 0$. There, the equation of motion (10d) for the correlations becomes

$$\frac{\partial}{\partial t} Q_{l\mathbf{k}_1}^{\alpha\mathbf{k}_2} = -i(\omega_{\mathbf{k}_2} - \omega_{\mathbf{k}_1}) Q_{l\mathbf{k}_1}^{\alpha\mathbf{k}_2} + b_{l\mathbf{k}_1}^{\alpha\mathbf{k}_2}. \tag{14}$$

If the source term $b_{l\mathbf{k}_1}^{\alpha\mathbf{k}_2}$ is regarded as a time-dependent inhomogeneity, one can first solve the homogeneous part of the equation and take the inhomogeneity into account by a variation of constants, which yields

$$Q_{l\mathbf{k}_1}^{\alpha\mathbf{k}_2}(t) = e^{-i(\omega_{\mathbf{k}_2}-\omega_{\mathbf{k}_1})t}\Bigg[Q_{l\mathbf{k}_1}^{\alpha\mathbf{k}_2}(t_0) \\ + \int_{t_0}^{t} dt'\, e^{i(\omega_{\mathbf{k}_2}-\omega_{\mathbf{k}_1})t'} b_{l\mathbf{k}_1}^{\alpha\mathbf{k}_2}(t') \Bigg]. \tag{15}$$

We assume that the carriers stem exclusively from optical excitation and therefore also the correlations are zero before the laser pulse is applied. Therefore, $Q_{l\mathbf{k}_1}^{\alpha\mathbf{k}_2}(t_0) = 0$ for $t_0 \to -\infty$. The correlations act back on the carrier and impurity variables only via sums over correlations with respect to at least one $\mathbf{k}$ index. Thus, we consider, e.g.,

$$\sum_{\mathbf{k}_2} Q_{l\mathbf{k}_1}^{\alpha\mathbf{k}_2}(t) = \int_0^{\omega_{BZ}} d\omega\, D(\omega) \int_{-\infty}^{t} dt'\, e^{i(\omega-\omega_{\mathbf{k}_1})(t'-t)} b_{l\mathbf{k}_1}^{\alpha\mathbf{k}(\omega)}(t'), \tag{16}$$

with the quasicontinuous limit

$$\sum_{\mathbf{k}} \cdots \to \int_{BZ} dk\, D(k) \cdots = \int_0^{\omega_{BZ}} d\omega\, D(\omega)\dots, \tag{17}$$

where $\hbar\omega$ are the spin-independent single-particle energies of H_0 and $\hbar\omega_{BZ}$ is a cutoff energy corresponding to the upper end of the conduction band. Although this expression is valid also for nonparabolic band structures, we simplify the discussion by first assuming an effective-mass approximation in two dimensions, so that $D^{2D} := D(\omega) = \frac{Am^*}{2\pi\hbar}$ is constant.

Now, the Markov or short-memory approximation can be applied to Eq. (16) as follows: Assuming that, because of the $\mathbf{k}$ sum, the effects of the correlations on the carrier and impurity dynamics dephase fast for not too small values of $t' - t$ in the integral kernel, the largest contribution of the integrals stems from source terms $b_{l\mathbf{k}_1}^{\alpha\mathbf{k}(\omega)}(t')$ with $t' \approx t$. Then, Eq. (16) can be approximated by

$$\sum_{\mathbf{k}_2} Q_{l\mathbf{k}_1}^{\alpha\mathbf{k}_2}(t) \approx D^{2D} \int_0^{\omega_{BZ}} d\omega\, b_{l\mathbf{k}_1}^{\alpha\mathbf{k}(\omega)}(t) \int_{-\infty}^{t} dt'\, e^{i(\omega-\omega_{\mathbf{k}_1})(t'-t)}. \tag{18}$$

Using the Sokhotski-Plemelj formula

$$\int_{-\infty}^{0} dt'\, e^{ixt'} = \pi\left(\delta(x) - \mathcal{P}\frac{i}{\pi x}\right) =: \pi\bar{\delta}(x), \tag{19}$$

where $\mathcal{P}$ denotes the Cauchy principal value, allows us to express the correlations solely in terms of carrier and impurity variables evaluated at $t' = t$. For the real part of $\bar{\delta}$, the $\mathbf{k}$ sum reduces to an integration over a single energy shell. The imaginary part has been shown to lead to a small renormalization of the precession frequencies [28] that can only reach values over 1% for a small range of realistic material parameters and excitation conditions, so that we consider only the real part of $\bar{\delta}$ in the further discussion of the Markov limit.

In the above treatment, it was postulated that the memory induced by the correlations is short. To see in which cases this is indeed a good approximation and how the time scale of the memory can be defined, we briefly summarize the findings of Ref. [45]: The source terms $b_{l\mathbf{k}_1}^{\alpha\mathbf{k}_2}$ that enter, e.g., in the dynamics for the carrier spin $\mathbf{s}_{\mathbf{k}_1}$, involve the variables $n_{\mathbf{k}_1}$, $\mathbf{s}_{\mathbf{k}_1}$, $n_{\mathbf{k}_2}$, and $\mathbf{s}_{\mathbf{k}_2}$. For the parts that only contain variables at $\mathbf{k}_1$, which we will refer to as $b_{l\mathbf{k}_1}^{\alpha}$, the real part of the integral on the right-hand side of Eq. (16) yields

$$\mathrm{Re}\int_{-\infty}^{t} dt' \int_0^{\omega_{BZ}} d\omega\, e^{i(\omega-\omega_{\mathbf{k}_1})(t'-t)} b_{l\mathbf{k}_1}^{\alpha}(t') \\ = \mathrm{Re}\int_{-\infty}^{0} dt''\, \frac{\sin[(\omega_{BZ}-\omega_{\mathbf{k}_1})t''] + \sin(\omega_{\mathbf{k}_1}t'')}{t''} b_{l\mathbf{k}_1}^{\alpha}(t+t''). \tag{20}$$

Since $\frac{\sin\Delta\omega t}{t} \to \pi\delta(t)$ for $\Delta\omega \to \infty$, this way of expressing the integral now shows that the memory has two time scales, one corresponding to $(\omega_{BZ} - \omega_{\mathbf{k}_1})^{-1}$, which is typically of the order of a few fs due to values of ω_{BZ} in the eV range, and the other one at $\omega_{\mathbf{k}_1}^{-1}$. This can explain why, for a δ-like initial electron occupation at $\mathbf{k}_1 = 0$, the spin transfer rate extracted from the quantum kinetic calculations in Ref. [45] is exactly $\frac{1}{2}$ of the Markovian expression for the rate. Thus, non-Markovian effects are found to be mainly due to the spectral proximity of the electrons to the band edge. Therefore, if the initial carrier distribution has a width of a few meV, the Markovian results coincide with the quantum kinetic calculations [45].

For the other parts of the source terms $b_{l\mathbf{k}_1}^{\alpha\mathbf{k}_2}$ which depend also on the electron variables at $\mathbf{k}_2$, a new time scale emerges which corresponds to the inverse of the frequency difference $\tau_{\mathbf{k}_1,\mathbf{k}_2}$ for which the electron variables $\mathbf{s}_{\mathbf{k}_2}$ ($n_{\mathbf{k}_2}$) start to differ notably from $\mathbf{s}_{\mathbf{k}_1}$ ($n_{\mathbf{k}_1}$).

In summary, it can therefore be said that the correlation time τ_{cor}, i.e., the time scale of the memory induced by the correlations, depends on the details of the spectral carrier distributions. Thus, in order to obtain meaningful results by using the Markov approximation, it is of key importance that the dynamics of the source terms takes place on a much slower time scale than the buildup of correlations τ_{cor}. If this is not the case, e.g., due to a fast precession of the electron spins with a frequency ω_e, it is necessary to split this precession off of the correlation induced spin transfer, yielding a modified integral kernel $e^{i(\omega_{\mathbf{k}_2}-\omega_{\mathbf{k}_1}\pm\omega_e)t'}$ and therefore a shift of $\pm\omega_e$ in the respective δ functions [37]. Therefore, the identification of fast and slowly changing parts of the source terms $b_{l\mathbf{k}_1}^{\alpha\mathbf{k}_2}$ is crucial for the derivation of the Markov limit of the quantum kinetic equations of motion (10).

D. Markov limit of the quantum kinetic equations

In the last section, the standard procedure of deriving a Markov limit was summarized starting from a simple set of equations where all the relevant spin precessions in DMSs were neglected. Now, for the more general theory of the present paper, we repeat the same steps while accounting for all terms in Eqs. (10). As above, first of all, the homogeneous part of the differential equation for the correlations has to be solved,

$$\frac{\partial}{\partial t} Q_{l\mathbf{k}_1}^{\alpha \mathbf{k}_2 \, \text{hom}} = -i(\omega_{\mathbf{k}_2} - \omega_{\mathbf{k}_1}) Q_{l\mathbf{k}_1}^{\alpha \mathbf{k}_2 \, \text{hom}} \\ + \left(A_{\mathbf{k}_1} + A_{\mathbf{k}_2}^* \right)_{\alpha\gamma} Q_{l\mathbf{k}_1}^{\gamma \mathbf{k}_2 \, \text{hom}} + \epsilon_{ijl} \omega_{Mn}^i Q_{j\mathbf{k}_1}^{\alpha \mathbf{k}_2 \, \text{hom}}. \tag{21}$$

Equation (21) can be represented in a more abstract form, if $Q_{l\mathbf{k}_1}^{\alpha \mathbf{k}_2 \, \text{hom}}$ is rewritten as a single vector $\mathbf{Q}^{\text{hom}}$ with respect to the set of indices l, α, $\mathbf{k}_1$, and $\mathbf{k}_2$. Then, Eq. (21) becomes

$$\frac{\partial}{\partial t} \mathbf{Q}^{\text{hom}} = M \mathbf{Q}^{\text{hom}}, \tag{22}$$

where the matrix M is defined by the terms on the right-hand side of Eq. (21). The formal solution of Eq. (22) is the time-ordered exponential:

$$\mathbf{Q}^{\text{hom}}(t_0 + \Delta t) = \mathcal{T} e^{\int_{t_0}^{t_0 + \Delta t} dt' M(t')} \mathbf{Q}^{\text{hom}}(t_0) \tag{23}$$

However, since in the Markov limit the solution of the homogeneous differential equation is only required on a time scale comparable to τ_{cor} in the fs range, we can assume that neither the precession frequencies nor the precession axes will change significantly on this time scale. This assumption makes it possible to approximate $M(t') \approx M(t_0)$ in Eq. (23) so that the time-ordering operator $\mathcal{T}$ can be dropped.

The expression for the solution for $\mathbf{Q}^{\text{hom}}$ can be further simplified, because the different contributions to the right-hand side of Eq. (21) act on different degrees of freedom of $Q_{l\mathbf{k}_1}^{\alpha \mathbf{k}_2 \, \text{hom}}$ and therefore commute. As also $A_{\mathbf{k}_1}$ and $A_{\mathbf{k}_2}^*$ commute, which can be checked directly using the explicit expression for those matrices in Eq. (11d), the homogeneous part of the equation of motion for the correlation is solved by

$$Q_{l\mathbf{k}_1}^{\alpha \mathbf{k}_2 \, \text{hom}}(t_0 + \Delta t) = e^{-i(\omega_{\mathbf{k}_2} - \omega_{\mathbf{k}_1})\Delta t} \left(e^{A_{\mathbf{k}_1} \Delta t} e^{A_{\mathbf{k}_2}^* \Delta t} \right)_{\alpha\gamma} \\ \times (e^{[\boldsymbol{\omega}_{Mn}]_\times \Delta t})_{ll'} Q_{l'\mathbf{k}_1}^{\alpha \mathbf{k}_2 \, \text{hom}}(t_0). \tag{24}$$

The exponential $e^{[\boldsymbol{\omega}_{Mn}]_\times t}$ of the cross product matrix $[\boldsymbol{\omega}_{Mn}]_\times$ is

$$e^{[\boldsymbol{\omega}_{Mn}]_\times t} = R_{\boldsymbol{\omega}_{Mn}}(\omega_{Mn} t), \tag{25}$$

where $R_{\mathbf{n}}(\alpha)$ is the 3×3 matrix describing a rotation around the axis $\mathbf{n}$ with an angle α. Similarly, it is possible to calculate an exponential of the matrices $A_{\mathbf{k}}$:

$$E_{\mathbf{k}_1}(t) := e^{A_{\mathbf{k}_1} t} \\ = \cos\left(\frac{\Omega'_{\mathbf{k}_1}}{2} t\right) \mathbf{1} + \sin\left(\frac{\Omega'_{\mathbf{k}_1}}{2} t\right) \begin{pmatrix} 0 & 2i \frac{\Omega'_{\mathbf{k}_1}}{\Omega'_{\mathbf{k}_1}}^T \\ \frac{i}{2} \frac{\Omega'_{\mathbf{k}_1}}{\Omega'_{\mathbf{k}_1}} & \left[\frac{\Omega'_{\mathbf{k}_1}}{\Omega'_{\mathbf{k}_1}}\right]_\times \end{pmatrix}, \tag{26}$$

with the inverse $[E_{\mathbf{k}_1}(t)]^{-1} = E_{\mathbf{k}_1}(-t)$.

Now, the solution to the inhomogeneous equation can be found by a variation of constants yielding

$$Q_{l\mathbf{k}_1}^{\alpha \mathbf{k}_2}(t_0 + \Delta t) \\ = e^{-i(\omega_{\mathbf{k}_2} - \omega_{\mathbf{k}_1})\Delta t} \left[E_{\mathbf{k}_1}(\Delta t) E_{\mathbf{k}_2}^*(\Delta t) \right]_{\alpha\gamma} \\ \times \left[R_{\boldsymbol{\omega}_{Mn}}(\omega_{Mn} \Delta t) \right]_{ll'} \left[Q_{l\mathbf{k}_1}^{\alpha \mathbf{k}_2}(t_0) + \int_{t_0}^{t_0 + \Delta t} dt' \, e^{i(\omega_{\mathbf{k}_2} - \omega_{\mathbf{k}_1})t'} \right. \\ \left. \times \left[E_{\mathbf{k}_1}(-t') E_{\mathbf{k}_2}^*(-t') \right]_{\gamma\kappa} \left[R_{\boldsymbol{\omega}_{Mn}}(-\omega_{Mn} t') \right]_{l'l''} b_{l''\mathbf{k}_1}^{\kappa \mathbf{k}_2}(t') \right] \tag{27}$$

Equation (27) can be further simplified by decomposing the matrices $R_{\boldsymbol{\omega}_{Mn}}(\omega_{Mn} t)$ and $E_{\mathbf{k}_1}$ as well as $E_{\mathbf{k}_2}^*$ in components oscillating with different frequencies:

$$R_{\mathbf{n}}(\omega t) = R_{\mathbf{n}}^0 + R_{\mathbf{n}}^+ e^{i\omega t} + R_{\mathbf{n}}^- e^{-i\omega t}, \tag{28a}$$

$$E_{\mathbf{k}_1}(t) = E_{\mathbf{k}_1}^0 + E_{\mathbf{k}_1}^+ e^{i(1/2)\Omega'_{\mathbf{k}_1} t} + E_{\mathbf{k}_1}^- e^{-i(1/2)\Omega'_{\mathbf{k}_1} t}, \tag{28b}$$

$$E_{\mathbf{k}_2}^*(t) = \left(E_{\mathbf{k}_2}^* \right)^0 + \left(E_{\mathbf{k}_2}^* \right)^+ e^{i(1/2)\Omega'_{\mathbf{k}_2} t} + \left(E_{\mathbf{k}_2}^* \right)^- e^{-i(1/2)\Omega'_{\mathbf{k}_2} t}, \tag{28c}$$

where the components of $E_{\mathbf{k}}$ can directly be read off from the definition in Eq. (26) and the decomposition of $R_{\mathbf{n}}(\alpha)$ is

$$\left(R_{\mathbf{n}}^0 \right)_{ij} = \frac{n_i n_j}{|\mathbf{n}|^2}, \tag{29a}$$

$$\left(R_{\mathbf{n}}^\pm \right)_{ij} = \frac{1}{2} \left(\delta_{ij} - \frac{n_i n_j}{|\mathbf{n}|^2} \pm i\epsilon_{ijk} \frac{n_k}{|\mathbf{n}|} \right). \tag{29b}$$

For the components defined in Eq. (28), an important relation is

$$R_{\mathbf{n}}^{\chi_1} R_{\mathbf{n}}^{\chi_2} = \delta_{\chi_1 \chi_2} R_{\mathbf{n}}^{\chi_1}, \tag{30a}$$

$$E_{\mathbf{k}_1}^{\chi_1} E_{\mathbf{k}_1}^{\chi_2} = \delta_{\chi_1 \chi_2} E_{\mathbf{k}_1}^{\chi_1}, \tag{30b}$$

$$(E_{\mathbf{k}_2}^*)^{\chi_1} (E_{\mathbf{k}_2}^*)^{\chi_2} = \delta_{\chi_1 \chi_2} (E_{\mathbf{k}_2}^*)^{\chi_1}, \tag{30c}$$

where from now on we assume $\chi_i \in \{-1, 0, 1\}$ for any χ index.

As stated earlier, it is necessary to identify fast oscillating and slowly changing contributions to the source terms $b_{l\mathbf{k}_1}^{\alpha \mathbf{k}_2}$. To this end, we consider the dynamics of $b_{l\mathbf{k}_1}^{\alpha \mathbf{k}_2}$ in the mean-field approximation, where

$$\langle S^i S^j (t_0 + \Delta t) \rangle \approx \left[R_{\boldsymbol{\omega}_{Mn}}(\omega_{Mn} \Delta t) \right]_{ii'} \\ \times \left[R_{\boldsymbol{\omega}_{Mn}}(\omega_{Mn} \Delta t) \right]_{jj'} \langle S^{i'} S^{j'}(t_0) \rangle, \tag{31a}$$

$$n_{\mathbf{k}}(t_0 + \Delta t) \approx n_{\mathbf{k}}(t_0), \tag{31b}$$

$$s_{\mathbf{k}}^i(t_0 + \Delta t) \approx \left[R_{\Omega'_{\mathbf{k}}}(\Omega'_{\mathbf{k}} \Delta t) \right]_{ii'} s_{\mathbf{k}}^{i'}(t_0). \tag{31c}$$

With these approximations, the source terms can be decomposed into

$$b_{l\mathbf{k}_1}^{\alpha \mathbf{k}_2}(t_0 + \Delta t) \approx \sum_m b_{l\mathbf{k}_1}^{\alpha \mathbf{k}_2 (\omega_m)}(t_0) e^{i\omega_m \Delta t}, \tag{32}$$

where m counts all the possible oscillation frequencies ω_m which consist of combinations of the frequencies $\omega_{Mn}(z)$ and $\Omega'_{\mathbf{k}}$.

Now, the Markov limit of Eqs. (10) can be established by using the Markov approximation in Eq. (18) with the Sokhotski-Plemelj formula in Eq. (19) on the expression for the time evolution of the correlations in Eq. (27), simplifying the products of exponential matrices with the relations (30) and decomposing the source terms according to Eq. (32):

$$Q_{l\mathbf{k}_1}^{\alpha\mathbf{k}_2} \approx \pi \sum_m \sum_{\chi_{Mn},\chi_{\mathbf{k}_1},\chi_{\mathbf{k}_2}} \bar{\delta}\left[\omega_{\mathbf{k}_2} - \left(\omega_{\mathbf{k}_1} + \chi_{Mn}\omega_{Mn} + \frac{1}{2}\chi_{\mathbf{k}_1}\Omega'_{\mathbf{k}_1} + \frac{1}{2}\chi_{\mathbf{k}_2}\Omega'_{\mathbf{k}_2} - \omega_m\right)\right]\left[E_{\mathbf{k}_1}^{\chi_{\mathbf{k}_1}}\left(E_{\mathbf{k}_2}^*\right)^{\chi_{\mathbf{k}_2}}\right]_{\alpha\gamma}\left(R_{\omega_{Mn}}^{\chi_{Mn}}\right)_{ll'}b_{l'\mathbf{k}_1}^{\gamma\mathbf{k}_2(\omega_m)}(t') \quad (33)$$

or more explicitly

$$Q_{l\mathbf{k}_1}^{\alpha\mathbf{k}_2}(z) \approx \pi\frac{i}{\hbar}J_{sd}|\psi(z)|^2 d \sum_{\chi_{\mathbf{k}_1},\chi'_{\mathbf{k}_1},\chi_{\mathbf{k}_2},\chi'_{\mathbf{k}_2},\chi_{Mn}} \bar{\delta}\left\{\omega_{\mathbf{k}_2} - \left[\omega_{\mathbf{k}_1} + \left(\frac{1}{2}\chi_{\mathbf{k}_1} - \chi'_{\mathbf{k}_1}\right)\Omega'_{\mathbf{k}_1} + \left(\frac{1}{2}\chi_{\mathbf{k}_2} - \chi'_{\mathbf{k}_2}\right)\Omega'_{\mathbf{k}_2} - \chi_{Mn}\omega_{Mn}(z)\right]\right\}$$

$$\times \left\{\left[E_{\mathbf{k}_1}^{\chi_{\mathbf{k}_1}}\left(E_{\mathbf{k}_2}^*\right)^{\chi_{\mathbf{k}_2}}\right]_{\alpha 0}\left(\frac{\langle S^l S^{j'}(z) + S^{j'}S^l(z)\rangle}{2}\left(R_{\omega_{Mn}(z)}^{\chi_{Mn}}\right)_{jj'}\left[\delta_{\chi'_{\mathbf{k}_1},0}\left(R_{\Omega'_{\mathbf{k}_2}}^{\chi'_{\mathbf{k}_2}}\right)_{jk'}s_{\mathbf{k}_2}^{k'} - \delta_{\chi'_{\mathbf{k}_2},0}\left(R_{\Omega'_{\mathbf{k}_1}}^{\chi'_{\mathbf{k}_1}}\right)_{jk'}s_{\mathbf{k}_1}^{k'}\right]\right.\right.$$

$$+ \frac{i}{2}\epsilon_{j'li''}\langle S^{i''}(z)\rangle\left(R_{\omega_{Mn}(z)}^{\chi_{Mn}}\right)_{jj'}\left[\delta_{\chi'_{\mathbf{k}_1},0}(1-n_{\mathbf{k}_1})\left(R_{\Omega'_{\mathbf{k}_2}}^{\chi'_{\mathbf{k}_2}}\right)_{jk'}s_{\mathbf{k}_2}^{k'} + \delta_{\chi'_{\mathbf{k}_2},0}(1-n_{\mathbf{k}_2})\left(R_{\Omega'_{\mathbf{k}_1}}^{\chi'_{\mathbf{k}_1}}\right)_{jk'}s_{\mathbf{k}_1}^{k'}\right.$$

$$\left.- 2i\epsilon_{jki}\left(R_{\Omega'_{\mathbf{k}_1}}^{\chi'_{\mathbf{k}_1}}\right)_{kk'}\left(R_{\Omega'_{\mathbf{k}_2}}^{\chi'_{\mathbf{k}_2}}\right)_{ii'}s_{\mathbf{k}_1}^{k'}s_{\mathbf{k}_2}^{i'}\right]\right) + \left[E_{\mathbf{k}_1}^{\chi_{\mathbf{k}_1}}\left(E_{\mathbf{k}_2}^*\right)^{\chi_{\mathbf{k}_2}}\right]_{\alpha k}\left(\left(R_{\omega_{Mn}(z)}^{\chi_{Mn}}\right)_{kj'}\delta_{\chi'_{\mathbf{k}_1},0}\delta_{\chi'_{\mathbf{k}_2},0}\right.$$

$$\times \left[\frac{\langle S^l S^{j'}(z) + S^{j'}S^l(z)\rangle}{2}\frac{n_{\mathbf{k}_2} - n_{\mathbf{k}_1}}{4} + \frac{i}{2}\epsilon_{j'li''}\langle S^{i''}(z)\rangle\left(\frac{n_{\mathbf{k}_2} + n_{\mathbf{k}_1} - n_{\mathbf{k}_1}n_{\mathbf{k}_2}}{4}\right)\right]$$

$$+ \frac{i}{2}\epsilon_{j'li''}\langle S^{i''}(z)\rangle(\delta_{jk}\delta_{k'k''} - \delta_{jk'}\delta_{kk''} - \delta_{jk''}\delta_{kk'})\left(R_{\omega_{Mn}(z)}^{\chi_{Mn}}\right)_{jj'}\left(R_{\Omega'_{\mathbf{k}_1}}^{\chi'_{\mathbf{k}_1}}\right)_{k'i}\left(R_{\Omega'_{\mathbf{k}_2}}^{\chi'_{\mathbf{k}_2}}\right)_{k''i'}s_{\mathbf{k}_1}^{i}s_{\mathbf{k}_2}^{i'}$$

$$+ \frac{i}{2}\epsilon_{jki}\frac{\langle S^l S^{j'}(z) + S^{j'}S^l(z)\rangle}{2}\left(R_{\omega_{Mn}(z)}^{\chi_{Mn}}\right)_{jj'}\left[\left(R_{\Omega'_{\mathbf{k}_2}}^{\chi'_{\mathbf{k}_2}}\right)_{il'}\delta_{\chi'_{\mathbf{k}_1},0}s_{\mathbf{k}_2}^{l'} + \left(R_{\Omega'_{\mathbf{k}_1}}^{\chi'_{\mathbf{k}_1}}\right)_{il'}\delta_{\chi'_{\mathbf{k}_2},0}s_{\mathbf{k}_1}^{l'}\right]$$

$$\left.- \frac{1}{4}\epsilon_{jki}\epsilon_{j'li''}\langle S^{i''}(z)\rangle\left(R_{\omega_{Mn}(z)}^{\chi_{Mn}}\right)_{jj'}\left[\left(R_{\Omega'_{\mathbf{k}_2}}^{\chi'_{\mathbf{k}_2}}\right)_{il'}\delta_{\chi'_{\mathbf{k}_1},0}(1-n_{\mathbf{k}_1})s_{\mathbf{k}_2}^{l'} - \left(R_{\Omega'_{\mathbf{k}_1}}^{\chi'_{\mathbf{k}_1}}\right)_{il'}\delta_{\chi'_{\mathbf{k}_2},0}(1-n_{\mathbf{k}_2})s_{\mathbf{k}_1}^{l'}\right]\right)\right\}, \quad (34)$$

Finally, inserting the expression for $Q_{l\mathbf{k}_1}^{\kappa\mathbf{k}_2}$ of Eq. (34) into the quantum kinetic equations of motion (10a)–(10c) for the carrier and impurity variables yields the desired set of ordinary differential equations for $n_{\mathbf{k}}$, $s_{\mathbf{k}}$, and $\langle\mathbf{S}\rangle$ where the correlations are eliminated, but their effects are still accounted for.

E. Numerical implementation of the Markovian equations of motion

The numerical advantage of the Markov limit over the original quantum kinetic equations is mainly that, because of the δ function in Eq. (34), only those electronic states with wave vectors $\mathbf{k}_2$ contribute to the time evolution of electron variables with wave vector $\mathbf{k}_1$ that are allowed by energy conservation. Here, the total energy consists of the kinetic energy as well as Zeeman-like spin-dependent energies due to the impurity magnetization, the external magnetic field, and the $\mathbf{k}$-dependent effective magnetic field due to the Rashba or Dresselhaus terms as well as the impurity Zeeman energy.

The complicated interplay of the different contributions to the total energy makes it hard to find the roots of the argument of the δ function in Eq. (34), which is necessary in order to identify the wave vectors $\mathbf{k}_2$ of the electronic states which are relevant for the calculation of the time evolution of electronic states with wave vector $\mathbf{k}_1$. In particular, the $\mathbf{k}$ dependence of the energies, the dimensionality of the $\mathbf{k}$ vector, and the fact that the number of roots is in general not known turn out to be major obstacles for the direct numerical solution of Eq. (34).

Here, we solve this problem by rediscretizing the electron variables. The roots of the argument of the δ function in Eq. (34) are given by

$$\bar{\omega}_{\mathbf{k}_2}(\xi_2) = \bar{\omega}_{\mathbf{k}_1}(-\xi_1) - \chi_{Mn}\omega_{Mn}(z) \quad (35a)$$

with

$$\bar{\omega}_{\mathbf{k}}(\xi) := \omega_{\mathbf{k}} - \xi\Omega'_{\mathbf{k}}, \quad (35b)$$

$$\xi \in \left\{-\frac{3}{2}, -\frac{1}{2}, \frac{1}{2}, \frac{3}{2}\right\}. \quad (35c)$$

After the space of $\bar{\omega}$ is discretized into small intervals, we create a list of discretization points in $\mathbf{k}$ space which contribute to the corresponding interval with respect to $\bar{\omega}$. Since the construction of this list has the complexity $\mathcal{O}(N_k^2)$, where N_k is the number of discretization points of a linear dimension in the two-dimensional $\mathbf{k}$ space, and the correlations $\sum_{\mathbf{k}_2} Q_{l\mathbf{k}_1}^{\alpha\mathbf{k}_2}$ which enter in the equation for a single electron variable with wave vector $\mathbf{k}_1$ become of the order of $\mathcal{O}(N_k^0)$ due to the δ function, the problem of solving the Markovian equations in the full $\mathbf{k}$ space is $\mathcal{O}(N_k^2)$. This provides a significant advantage over the full quantum kinetic theory which has the complexity $\mathcal{O}(N_k^4)$ for a quantum well.

F. Case $N_{Mn} \gg N_e$ without spin-orbit fields

The Markov limit (34) of the equations of motion (10) yields quite lengthy expressions. However, these can be simplified dramatically in a case which is very common for experimentally studied DMS samples: If the number of the magnetic impurities N_{Mn} exceeds largely the number of quasifree carriers N_e, such as in the case of optically excited intrinsic DMSs, the impurity spin $\langle S \rangle$ only changes marginally due to the influence from the quasifree carriers. One can therefore assume that the impurity spin will approximately be defined by its thermal equilibrium value in the external magnetic field. In particular in the paramagnetic regime, the impurity spin will be parallel ($\sigma_S^B = +1$) or antiparallel ($\sigma_S^B = -1$) to the magnetic field,

$$\langle S \rangle = \sigma_S^B |\langle S \rangle| \frac{\mathbf{B}}{|\mathbf{B}|}. \tag{36a}$$

Since usually the Zeeman contribution to the energy of the magnetic ions is much stronger than the mean-field s-d term due to the carrier spins [39], we assume that

$$\boldsymbol{\omega}_{Mn} = \sigma_{Mn}^B \omega_{Mn} \frac{\mathbf{B}}{|\mathbf{B}|} \tag{36b}$$

and that $\boldsymbol{\omega}_{Mn}$ is independent of z. If only electrons with small wave vectors are excited, no electric field is applied, and the sample has a rather high impurity concentration, the s-d interaction usually dominates over spin-orbit coupling effects, so that one can neglect the latter [21]. Here, we shall first concentrate on this case and defer the discussion of the

interplay between s-d interactions and spin-orbit coupling to Sec. III B. Since the external magnetic field as well as the effective s-d field due the impurity spins are parallel, we find also

$$\boldsymbol{\Omega}_{\mathbf{k}} = \boldsymbol{\omega}_e = \sigma_e^B \omega_e \frac{\mathbf{B}}{|\mathbf{B}|}. \tag{36c}$$

Because of the $\mathbf{k}$ independence of the effective magnetic field for the carriers, the matrix $E_{\mathbf{k}_1} E_{\mathbf{k}_2}^*$ can be simplified to

$$E_{\mathbf{k}_1} E_{\mathbf{k}_2}^* = \begin{pmatrix} 1 & 0 \\ 0 & R_{\boldsymbol{\omega}_e} \end{pmatrix}. \tag{37}$$

Additionally, comparing Eq. (13) with Eq. (29) yields

$$\langle S^{i'} S^{j'} \rangle = \langle S^{\|2} \rangle \big(R_{\langle S \rangle}^0 \big)_{i'j'} + \langle S^{\perp 2} \rangle (R_{\langle S \rangle}^+ + R_{\langle S \rangle}^-)_{i'j'}$$
$$+ |\langle S \rangle| \tfrac{1}{2} \big(R_{\langle S \rangle}^+ - R_{\langle S \rangle}^- \big)_{i'j'}. \tag{38}$$

Now, the products of matrices in Eq. (34) can be evaluated using

$$R_{\langle S \rangle}^{\sigma_S^B \chi} = R_{\omega_{Mn}}^{\sigma_{Mn}^B \chi} = R_{\omega_e}^{\sigma_e^B \chi} = R_{\mathbf{B}}^\chi, \tag{39}$$

and the relation (30a). After a lengthy but straightforward calculation, we arrive at the Markov limit of the equations of motion for the occupations of the spin-up and -down subbands with respect to the direction of the external magnetic field $n_{\mathbf{k}}^{\uparrow/\downarrow} := \frac{n_{\mathbf{k}}}{2} \pm \frac{\mathbf{B}}{|\mathbf{B}|} \cdot \mathbf{s}_{\mathbf{k}}$ and the perpendicular spin component $\mathbf{s}_{\mathbf{k}}^\perp := \mathbf{s}_{\mathbf{k}} - \frac{\mathbf{B}}{|\mathbf{B}|} \big(\frac{\mathbf{B}}{|\mathbf{B}|} \cdot \mathbf{s}_{\mathbf{k}} \big)$:

$$\frac{\partial}{\partial t} n_{\mathbf{k}_1}^{\uparrow/\downarrow} \big|_{\text{cor}} \approx \int_{-d/2}^{d/2} dz\, \pi \frac{J_{sd}^2 |\psi(z)|^4 N_{Mn} d}{\hbar^2 V^2} \sum_{\mathbf{k}_2} \Bigg\{ \delta(\omega_{\mathbf{k}_2} - \omega_{\mathbf{k}_1}) \frac{\langle S^{\|2} \rangle}{2} (n_{\mathbf{k}_2}^{\uparrow/\downarrow} - n_{\mathbf{k}_1}^{\uparrow/\downarrow}) + \delta\big(\omega_{\mathbf{k}_2} - \big[\omega_{\mathbf{k}_1} \pm \big(\sigma_e^B \omega_e - \sigma_e^B \omega_{Mn}\big)\big]\big)$$

$$\times \Bigg[\bigg(\langle S^{\perp 2} \rangle \pm \sigma_S^B \frac{|\langle S \rangle|}{2} \bigg)(1 - n_{\mathbf{k}_1}^{\uparrow/\downarrow}) n_{\mathbf{k}_2}^{\downarrow/\uparrow} - \bigg(\langle S^{\perp 2} \rangle \mp \sigma_S^B \frac{|\langle S \rangle|}{2} \bigg)\big(1 - n_{\mathbf{k}_2}^{\downarrow/\uparrow}\big) n_{\mathbf{k}_1}^{\uparrow/\downarrow} \Bigg] \Bigg\}, \tag{40a}$$

$$\frac{\partial}{\partial t} \mathbf{s}_{\mathbf{k}_1}^\perp \big|_{\text{cor}} \approx \int_{-d/2}^{d/2} dz\, \pi \frac{J_{sd}^2 |\psi(z)|^4 N_{Mn} d}{\hbar^2 V^2} \sum_{\mathbf{k}_2} \Bigg\{ -\delta(\omega_{\mathbf{k}_2} - \omega_{\mathbf{k}_1}) \frac{\langle S^{\|2} \rangle}{2} (\mathbf{s}_{\mathbf{k}_2}^\perp + \mathbf{s}_{\mathbf{k}_1}^\perp)$$

$$- \delta\big(\omega_{\mathbf{k}_2} - \big[\omega_{\mathbf{k}_1} + \big(\sigma_e^B \omega_e - \sigma_e^B \omega_{Mn}\big)\big]\big) \bigg[\frac{1}{2} \bigg(\langle S^{\perp 2} \rangle - \sigma_S^B \frac{|\langle S \rangle|}{2} \bigg) + n_{\mathbf{k}_2}^\uparrow \sigma_S^B \frac{|\langle S \rangle|}{2} \bigg] \mathbf{s}_{\mathbf{k}_1}^\perp$$

$$- \delta\big(\omega_{\mathbf{k}_2} - \big[\omega_{\mathbf{k}_1} - \big(\sigma_e^B \omega_e - \sigma_e^B \omega_{Mn}\big)\big]\big) \bigg[\frac{1}{2} \bigg(\langle S^{\perp 2} \rangle + \sigma_S^B \frac{|\langle S \rangle|}{2} \bigg) - n_{\mathbf{k}_2}^\downarrow \sigma_S^B \frac{|\langle S \rangle|}{2} \bigg] \mathbf{s}_{\mathbf{k}_1}^\perp$$

$$- \frac{1}{\pi} \frac{1}{\omega_{\mathbf{k}_2} - \big[\omega_{\mathbf{k}_1} + \big(\sigma_e^B \omega_e - \sigma_e^B \omega_{Mn}\big)\big]} \bigg[\frac{1}{2} \bigg(\langle S^{\perp 2} \rangle - \sigma_S^B \frac{|\langle S \rangle|}{2} \bigg) + n_{\mathbf{k}_2}^\uparrow \sigma_S^B \frac{|\langle S \rangle|}{2} \bigg] \frac{\mathbf{B}}{|\mathbf{B}|} \times \mathbf{s}_{\mathbf{k}_1}^\perp$$

$$+ \frac{1}{\pi} \frac{1}{\omega_{\mathbf{k}_2} - \big[\omega_{\mathbf{k}_1} - \big(\sigma_e^B \omega_e - \sigma_e^B \omega_{Mn}\big)\big]} \bigg[\frac{1}{2} \bigg(\langle S^{\perp 2} \rangle + \sigma_S^B \frac{|\langle S \rangle|}{2} \bigg) - n_{\mathbf{k}_2}^\downarrow \sigma_S^B \frac{|\langle S \rangle|}{2} \bigg] \frac{\mathbf{B}}{|\mathbf{B}|} \times \mathbf{s}_{\mathbf{k}_1}^\perp \Bigg\}, \tag{40b}$$

where $\frac{\partial}{\partial t} n_{\mathbf{k}_1}^{\uparrow/\downarrow} \big|_{\text{cor}}$ and $\frac{\partial}{\partial t} \mathbf{s}_{\mathbf{k}_1}^\perp \big|_{\text{cor}}$ describe the contributions to the time derivative of the respective quantities beyond the mean-field dynamics. In the case studied here, the total time evolution is given by

$$\frac{\partial}{\partial t} n_{\mathbf{k}_1}^{\uparrow/\downarrow} = \frac{\partial}{\partial t} n_{\mathbf{k}_1}^{\uparrow/\downarrow} \big|_{\text{cor}}, \tag{41a}$$

$$\frac{\partial}{\partial t} \mathbf{s}_{\mathbf{k}_1}^\perp = \boldsymbol{\omega}_e \times \mathbf{s}_{\mathbf{k}_1}^\perp + \frac{\partial}{\partial t} \mathbf{s}_{\mathbf{k}_1}^\perp \big|_{\text{cor}}, \tag{41b}$$

$$\frac{\partial}{\partial t} \langle S \rangle = \boldsymbol{\omega}_{Mn} \times \langle S \rangle + \frac{\partial}{\partial t} \langle S \rangle \big|_{\text{cor}}, \tag{41c}$$

where $\frac{\partial}{\partial t}\langle \mathbf{S}\rangle|_{\text{cor}}$ can be obtained by replacing $N_{Mn}\int_{-d/2}^{d/2}dz$ by $-d\sum_{\mathbf{k}_1}$ on the right-hand side of Eq. (40b). This follows directly from the fact that the s-d interaction conserves the total spin.

Note that Eqs. (40) generalize Eqs. (6) of Ref. [37] by incorporating a $\mathbf{k}$-dependent precession frequency for the electrons, an external magnetic field and the z dependence of the coupling due to the form of the envelope function of the quantum well.

Equation (40a) can be interpreted like equations resulting from Fermi's golden rule: A spin-up electron is scattered either to another spin-up state with the same value of the kinetic energy $\hbar\omega_{\mathbf{k}}$ [term proportional to $\delta(\omega_{\mathbf{k}_2}-\omega_{\mathbf{k}_1})$] or to a spin-down state with kinetic energy $\hbar\omega_{\mathbf{k}_2}=\hbar\omega_{\mathbf{k}_1}+\hbar(\sigma_e^B\omega_e-\sigma_e^B\omega_{Mn})$ and vice versa. To understand the latter term it is important to keep in mind that the total mean-field energy of a spin-up electron is $\hbar(\omega_{\mathbf{k}}+\frac{1}{2}\sigma_e^B\omega_e)$ while for a spin-down electron one finds $\hbar(\omega_{\mathbf{k}}-\frac{1}{2}\sigma_e^B\omega_e)$. Also, since the s-d interaction conserves the sum of the electron and impurity spins, a flip of an electron spin in one direction is always accompanied by a flip of an impurity spin in the opposite direction. Thus, in order to fulfill the conservation of the total mean-field energy, the energy $\hbar(\sigma_e^B\omega_e-\sigma_e^B\omega_{Mn})$ that is freed by an impurity mediated flip of an electron from the spin-up to the spin-down state has to be compensated by a difference of the kinetic energies of the electronic states $\omega_{\mathbf{k}_2}-\omega_{\mathbf{k}_1}$.

Although Eq. (40a) for the spin-up and spin-down occupations can also be derived by Fermi's golden rule, the energy shifts in the δ functions are often not correctly accounted for in the literature [22,32]. The consequences are discussed in Sec. III A. Here, the spin-flip terms of Eq. (40a) also correctly account for Pauli-blocking effects by the terms proportional to $(1-n_{\mathbf{k}}^{\uparrow/\downarrow})$ which are usually put in by hand in a golden-rule derivation. Furthermore, a golden-rule treatment only allows us to derive transition rates between energy eigenstates and does not provide equations governing the dynamics of the coherences between those eigenstates, i.e., the components of the electron and impurity spins perpendicular to the direction of the external magnetic field, which is given in our derivation by Eq. (40b). As in the equations for the spin-up and spin-down occupations, we find that the equations for the perpendicular spin components connect states whose difference in kinetic energies $\hbar(\omega_{\mathbf{k}_2}-\omega_{\mathbf{k}_1})$ is either zero or $\pm\hbar(\sigma_e^B\omega_e-\sigma_{Mn}^B\omega_{Mn})$. Note that in contrast to the equations for $n_{\mathbf{k}_1}^{\uparrow/\downarrow}$, here we find terms proportional to the imaginary part of $\bar{\delta}$. While the real part leads to a ratelike damping of the perpendicular electron spin, the imaginary part yields an additional contribution to the precession frequency. Such frequency renormalizations have been extensively discussed in Ref. [28].

From Eqs. (40) one can also find decay rates for spin-up $[(\tau_{\mathbf{k}_0}^{\uparrow})^{-1}]$ and spin-down $[(\tau_{\mathbf{k}_0}^{\downarrow})^{-1}]$ electron states as well as the spin components parallel $[(\tau_{\mathbf{k}_0}^{\parallel})^{-1}]$ perpendicular $[(\tau_{\mathbf{k}_0}^{\perp})^{-1}]$ to the external magnetic field, if it is assumed that only very few quasifree carriers are excited, so that one can regard only single electrons by setting $n_{\mathbf{k}_2}^{\uparrow/\downarrow}=\delta_{\mathbf{k}_1,\mathbf{k}_2}n_{\mathbf{k}_1}^{\uparrow/\downarrow}$ and $\mathbf{s}_{\mathbf{k}_2}^{\perp}=\delta_{\mathbf{k}_1,\mathbf{k}_2}\mathbf{s}_{\mathbf{k}_1}^{\perp}$:

$$\left(\tau_{\mathbf{k}_0}^{\uparrow}\right)^{-1}=\Gamma^-\Theta\big[\omega_{\mathbf{k}_0}+\big(\sigma_e^B\omega_e-\sigma_{Mn}^B\omega_{Mn}\big)\big], \quad (42a)$$

$$\left(\tau_{\mathbf{k}_0}^{\downarrow}\right)^{-1}=\Gamma^+\Theta\big[\omega_{\mathbf{k}_0}-\big(\sigma_e^B\omega_e-\sigma_{Mn}^B\omega_{Mn}\big)\big], \quad (42b)$$

$$\left(\tau_{\mathbf{k}_0}^{\parallel}\right)=\left(\tau_{\mathbf{k}_0}^{\uparrow}\right)^{-1}+\left(\tau_{\mathbf{k}_0}^{\downarrow}\right)^{-1}, \quad (42c)$$

$$\left(\tau_{\mathbf{k}_0}^{\perp}\right)^{-1}=\Gamma^0+\frac{1}{2}\big[\left(\tau_{\mathbf{k}_0}^{\uparrow}\right)^{-1}+\left(\tau_{\mathbf{k}_0}^{\downarrow}\right)^{-1}\big], \quad (42d)$$

with

$$\Gamma^0=I\pi D^{2D}\frac{J_{sd}^2 N_{Mn}}{\hbar^2 V^2}\langle S^{\parallel^2}\rangle, \quad (42e)$$

$$\Gamma^\pm=I\pi D^{2D}\frac{J_{sd}^2 N_{Mn}}{\hbar^2 V^2}\left(\langle S^{\perp^2}\rangle\pm\sigma_S^B\frac{|\langle\mathbf{S}\rangle|}{2}\right), \quad (42f)$$

$$I=d\int_{-d/2}^{d/2}dz\,|\psi(z)|^4, \quad (42g)$$

where $\Theta(x)$ is the Heaviside step function.

Thus, the main effect of the frequency shifts due to the precession of the correlations is the opening and closing of decay channels due to the corresponding step functions which originate from the step of the two-dimensional density of states at $\omega_{\mathbf{k}=0}$.

III. RESULTS

A. Magnetic field dependence of the spin transfer rates

Now, we compare the theory derived in the present paper with the different treatments of the s-d interaction presented by other groups. To this end, we focus on the case without spin-orbit interactions and $N_{Mn}\gg N_e$, so that the correlation induced changes in the carrier variables can be described by Eqs. (40). Often in the literature rates for the carrier-impurity spin transfer dynamics are obtained from Fermi's golden rule [25,29–31]. In two-dimensional systems one finds in the absence of magnetic fields:

$$\frac{\partial}{\partial t}s_{\omega_1}^i=-I\pi\frac{J_{sd}^2}{\hbar^2}\frac{N_{Mn}}{V^2}\frac{2}{3}[S(S+1)]$$

$$\times\int d\omega\,D^{2D}(\omega)\delta(\omega-\omega_1)s_\omega^i=-\tau_{\text{FGR}}s_{\omega_1}^i, \quad (43a)$$

$$\tau_{\text{FGR}}=I\pi\frac{J_{sd}^2}{\hbar^2}\frac{N_{Mn}}{V^2}\frac{2}{3}[S(S+1)]\frac{Am^*}{2\pi\hbar}, \quad (43b)$$

where we assume isotropy so that the carrier spin variables are independent of the angle of the wave vector and can equivalently be described by $s_{|\mathbf{k}|}^i$ or s_ω^i, with the kinetic energy $\hbar\omega=\frac{\hbar^2|\mathbf{k}|^2}{2m}$. τ_{FGR} is Fermi's golden-rule spin-transfer rate at $B=0$. In contrast, if an external magnetic field is applied, the conduction band is energetically split by $\sigma_e^B\omega_e$. This leads to the appearance of an additional energy offset in the δ function. In our treatment, we also find an energy offset corresponding to the impurity Zeeman splitting $\sigma_{Mn}^B\omega_{Mn}$ which is necessary for the simultaneous conservation of the total carrier and impurity energy as well as the total spin. Furthermore, Fermi's golden rule is only able to predict transitions between energy eigenstates, whereas it makes no statement about the transfer of the carrier spin components perpendicular to the quantization axis. The distinction between parallel and perpendicular components does not arise for $B=0$, since in this case all directions are equivalent. Additionally, the factor $S(S+1)$ has to be modified in the presence of a magnetic field that causes a nonzero paramagnetic impurity magnetization.

In particular, the energetic offset caused by the impurity Zeeman splitting is often overlooked in studies based on the golden-rule approach [22,29]. In Ref. [22], which is based on the kinetic spin Bloch equations (KSBEs), even the band splitting $\sigma_e^B \omega_e$ is disregarded, but the magnetic field dependence of the second moments of the impurity spin, which enters in the rates, was kept. There are also studies [25,26,30] that explicitly include the band splitting as well as the impurity Zeeman terms, but since there the rates are derived by Fermi's golden rule, no expression for the perpendicular spin transfer component was given.

In this context, one particularly notable theoretical derivation of magnetic field dependent carrier-impurity spin transfer rates was given by *Semenov* in Ref. [32], which is based on a projection operator method. There, the electron spins are treated as a subsystem which interacts with a bath of impurity ions. In Ref. [32], it was assumed that the electron density matrix can be factorized into one part accounting for the spin degree of freedom and the **k**-dependent part, which is described by a Fermi distribution. Tracing out the **k**-dependent part of the carrier density matrix as well as the impurity system, rates were obtained for the spin degree of freedom of the carriers. In contrast to the theory of the present paper, where only energetic shifts associated with the spin-flip-flop processes of the form $|\sigma_e^B \omega_e - \sigma_{Mn}^B \omega_{Mn}|$ appear, the projection operator method of Ref. [32] also finds terms proportional to $|\sigma_e^B \omega_e + \sigma_{Mn}^B \omega_{Mn}|$. As mentioned earlier, such energy shifts are in conflict with the conservation of the total carrier and impurity energy. We trace the appearance of the energy nonconserving terms in Ref. [32] back to the fact that, there, only the positive frequency component of the electron-spin precession was regarded, whereas the negative frequency component explicitly shows up in the theory of the present paper and leads to a cancellation of terms in the expression for the correlations which oscillate with $\pm(\sigma_e^B \omega_e + \sigma_{Mn}^B \omega_{Mn})$.

Having discussed the different expressions for the magnetic field dependence of the carrier-impurity spin transfer rates that can be found in the literature, we compare them at the example of the situation discussed in Ref. [32]. There, it was assumed that the spectral electron distribution is

$$n^\uparrow(\omega) = n^\downarrow(\omega) \propto e^{-\omega/T} \qquad (44)$$

for some carrier temperature T, irrespective of the spin-split subband. With this assumption, the decay rate of the total parallel (T_1^{-1}) and perpendicular (T_2^{-1}) carrier spin with respect to the magnetic field direction can be obtained from Eqs. (42) of the present theory:

$$T_1^{-1} \propto \int_0^\infty d\omega\, e^{-\omega/T} [\tau^\parallel(\omega)]^{-1} \propto T_\uparrow^{-1} + T_\downarrow^{-1}, \qquad (45a)$$

$$T_2^{-1} \propto \int_0^\infty d\omega\, e^{-\omega/T} [\tau^\perp(\omega)]^{-1} \propto \Gamma^0 + \frac{1}{2}(T_\uparrow^{-1} + T_\downarrow^{-1}), \qquad (45b)$$

$$T_\uparrow^{-1} \propto \int_0^\infty d\omega\, e^{-\omega/T} [\tau^\uparrow(\omega)]^{-1} \propto \Gamma^-$$
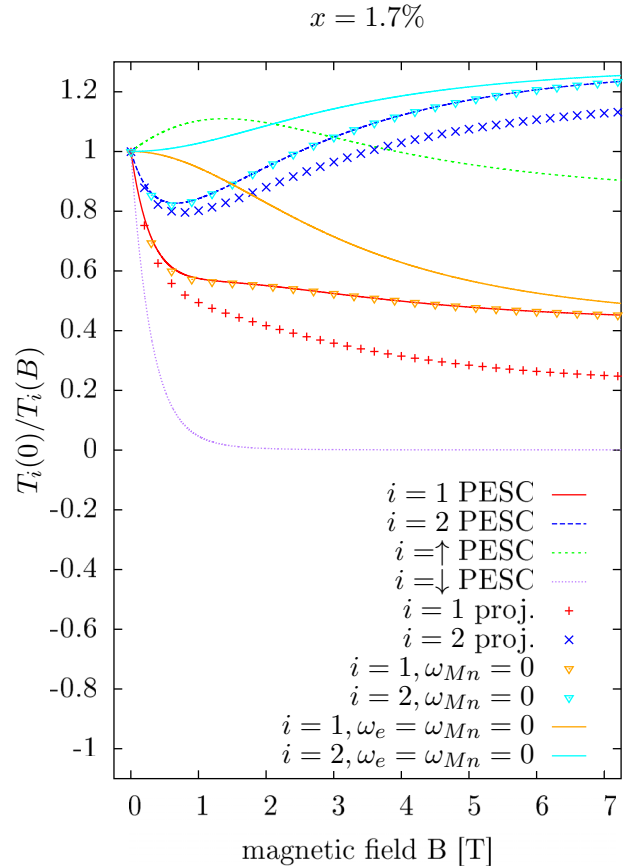$$\times \min(1, e^{(\sigma_e^B \omega_e - \sigma_{Mn}^B \omega_{Mn})/T}), \qquad (45c)$$

$$x = 1.7\%$$

FIG. 1. Magnetic field dependence of the parallel ($i = 1$) and perpendicular ($i = 2$) spin transfer rates normalized with respect to $B = 0$ in a 8-nm-wide Cd$_{0.983}$Mn$_{0.017}$Te quantum well at temperature $T = 4$ K. Red and blue lines (PESC) represent rates according to the theory of the present article [Eqs. (45)] and red and blue crosses show the rates calculated by the projection operator method (proj.) of Ref. [32]. Furthermore, cyan and orange triangles and lines show the results of Eqs. (45), when the energetic shifts due to the Zeeman impurity splittings in spin-flip-flop processes ($\omega_{Mn} = 0$) or additionally the spin splittings ($\omega_e = \omega_{Mn} = 0$) are neglected. $T_\uparrow$ and $T_\downarrow$ are the relaxation rates of spin-up and spin-down occupations, respectively.

$$T_\downarrow^{-1} \propto \int_0^\infty d\omega\, e^{-\omega/T} [\tau^\downarrow(\omega)]^{-1} \propto \Gamma^+$$
$$\times \min(1, e^{-(\sigma_e^B \omega_e - \sigma_{Mn}^B \omega_{Mn})/T}), \qquad (45d)$$

where also the values for the decay rate of the spin-up ($T_\uparrow^{-1}$) and spin-down occupations ($T_\downarrow^{-1}$) are given explicitly. For $B = 0$, the rates $T_1^{-1} = T_2^{-1} = 2T_\uparrow^{-1} = 2T_\downarrow^{-1}$ coincide with the rate calculated by Fermi's golden rule τ_{FGR}, which defines the normalization of the rates in Eq. (45).

Figure 1 shows the magnetic field dependence of the parallel and perpendicular spin transfer rates according to Eqs. (45) with the parameters of Ref. [32], where a $d = 8$-nm-wide Cd$_{0.983}$Mn$_{0.017}$Te quantum well was considered at $T = 4$ K. The value for the coupling constant is $J_{sd} = 15$ meV nm^3 and the electron and Mn g factors are $g_e = -1.77$ and $g_{Mn} = 2.0$ respectively. The present theory predicts that the parallel spin
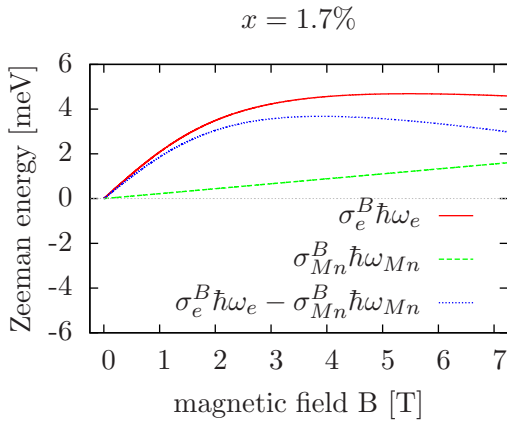
FIG. 2. Magnetic field dependence of the electron (red solid line) and impurity Zeeman energy (green dashed line) as well as their difference (blue dotted line) for a DMS quantum well (same parameters as for Fig. 1).

transfer rate T_1^{-1} first decays fast from $B = 0$ to $B \approx 1$ T, then levels off. The perpendicular spin transfer rate T_2^{-1} first decays with increasing magnetic field, reaches a minimum at $B \approx 1$ T, and finally increases again. This behavior of T_1^{-1} and T_2^{-1} can be explained by considering the rates $T_\uparrow^{-1}$ and $T_\downarrow^{-1}$ separately, together with the values of the energy shifts $\sigma_e^B \omega_e - \sigma_{Mn}^B \omega_{Mn}$ presented in Fig. 2. The mean-field impurity energy $\hbar \sigma_e^B \omega_{Mn}$ is mainly dominated by its Zeeman energy and therefore increases linearly with B. In contrast, the mean-field carrier energy $\hbar \sigma_e^B \omega_e$ is strongly modified by a contribution proportional to a $S = \frac{5}{2}$ Brillouin function due to the impurity magnetization, which starts linearly in B but begins to saturate at $B \approx 2$ T. For high magnetic fields ($B > 6$ T), $\hbar \sigma_e^B \omega_e$ decreases again, when the impurity magnetization is fully saturated and the negative electron g factor becomes important. Although $\sigma_e^B \omega_e - \sigma_{Mn}^B \omega_{Mn}$ eventually becomes negative for very high magnetic fields (not shown in Fig. 2), for typical experimentally accessible fields, it is mostly positive and increases linearly up to $B \approx 2$ T, just like $\sigma_e^B \omega_e$.

It follows from Eq. (45c) that $T_\downarrow^{-1}$ decreases approximately exponentially with B in the regime where $\sigma_e^B \omega_e - \sigma_{Mn}^B \omega_{Mn}$ increases linearly. Therefore, we find that the spin-splitting introduced by the external magnetic field closes the transfer channel $T_\downarrow^{-1}$. In the case studied here, the magnetic field dependence of the rate $T_\uparrow^{-1}$ comes exclusively from the prefactor, since due to the positive value of $\sigma_e^B \omega_e - \sigma_{Mn}^B \omega_{Mn}$ the corresponding transfer channel is maximally open. Noting that

$$\Gamma^0(B \to \infty) \to \frac{15}{14}\tau_{\text{FGR}}, \tag{46a}$$

$$\Gamma^+(B \to \infty) \to 0, \tag{46b}$$

$$\Gamma^-(B \to \infty) \to \frac{3}{7}\tau_{\text{FGR}}, \tag{46c}$$

we find that T_1^{-1} approaches $\frac{5}{8}\tau_{\text{FGR}}$ and $T_2^{-1} \to \frac{9}{7}\tau_{\text{FGR}} \approx 1.29\tau_{\text{FGR}}$ for large values of B.

The magnetic field dependence of rates predicted from the projection operator method of Ref. [32] is qualitatively similar
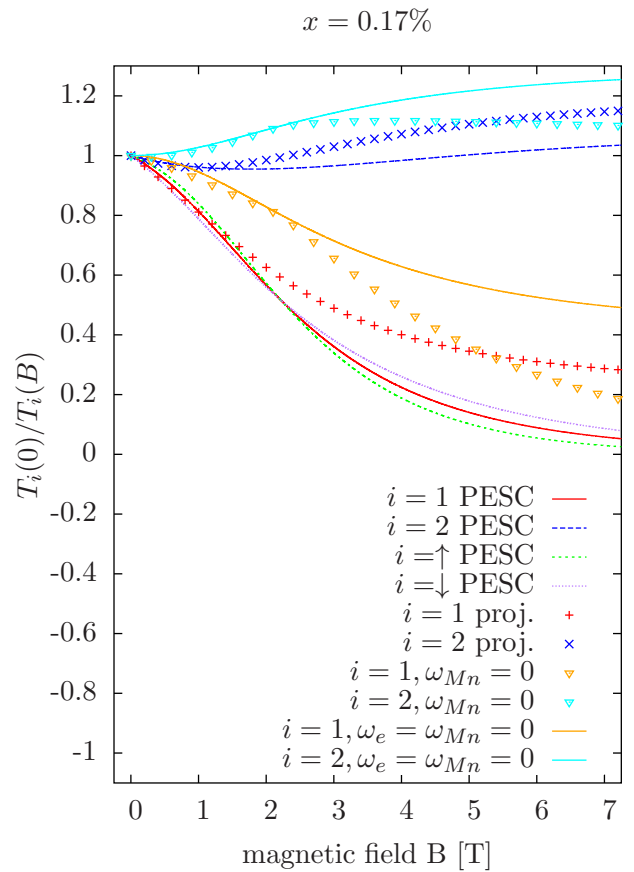

FIG. 3. Magnetic field dependence of spin transfer rates for a $Cd_{0.9983}Mn_{0.0017}Te$ quantum well (cf. Fig. 1).

to that of the present theory, as can be seen in Fig. 1. However, they suggest quantitatively smaller values for the rates, with deviations of the order of $\sim 0.2\tau_{\text{FGR}}$. In the case studied here, the offset due to the impurity Zeeman splitting $\sigma_{Mn}^B \omega_{Mn}$ plays a less significant role, so that the rates calculated neglecting these terms (triangles in Fig. 1) coincide with the calculation which conserves the total energy. However, neglecting the spin splittings $\sigma_{Mn}^B \omega_{Mn}$ is found to lead to the correct rates only for large values of the magnetic field while for smaller magnetic fields qualitative features, such as the minimum in T_2^{-1}, are not obtained.

In our analysis of the magnetic field dependence of the spin transfer rates it was important that $\sigma_e^B \omega_e - \sigma_{Mn}^B \omega_{Mn} > 0$. The situation can change significantly, if this is not the case. In order to study this regime of parameters, we repeat the same calculations shown in Figs. 1 and 2 but we assume a Mn concentration $x = 0.17\%$ which is smaller by a factor of 10 than in the previous calculations. The results are displayed in Figs. 3 and 4 respectively. We find in Fig. 4 that now also the electron spin splitting is dominated by the Zeeman term and the mean-field contribution from the impurity magnetization is rather small. In particular, one finds that $\sigma_e^B \omega_e - \sigma_{Mn}^B \omega_{Mn}$ is now negative for all values of $B > 0$. This fact has immediate consequences on the magnetic field dependence of the spin transfer rates. The main qualitative difference between the rates shown in Fig. 3 and in the previous case is that now
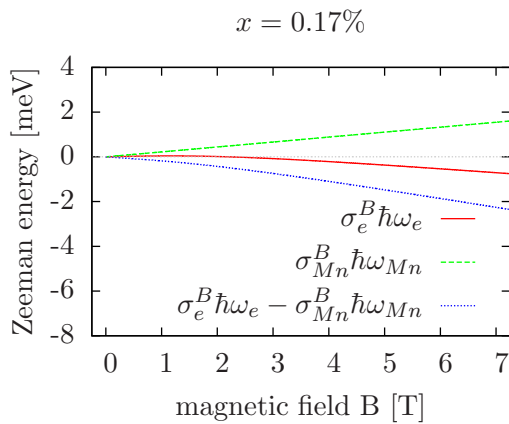
FIG. 4. Magnetic field dependence of the Zeeman energies for a $Cd_{0.9983}Mn_{0.0017}Te$ quantum well (cf. Fig. 2).

the parallel spin transfer rate T_1^{-1} decays to zero for large values of B. Here, the spin transfer channel corresponding to $T_\uparrow^{-1}$ is closed due to the energy splitting, whereas $T_\downarrow^{-1}$ decreases to zero, because the prefactor Γ^+ tends to zero for $B \to \infty$. The physical reason for this behavior is that due to the negativity of $\sigma_e^B \omega_e - \sigma_{Mn}^B \omega_{Mn}$ spin flips from the spin-up to the spin-down band face an energy penalty, while a flip from the spin-down to the spin-up band would require a corresponding decrease of an impurity spin in order to satisfy the spin conservation. However, for $B \to \infty$ the impurity spins are already fully aligned antiparallel to the magnetic field, so that this spin flip is also forbidden. The magnetic field dependence of the perpendicular spin transfer rate T_2^{-1} for $x = 0.17\%$ is quantitatively similar to the case of $x = 1.7\%$. However, here, the asymptotic value for strong magnetic fields is $T_2^{-1}(B \to \infty) \to \frac{15}{14}\tau_{FGR}$.

For the smaller impurity concentrations, the projection operator method of Ref. [32] overestimates the spin transfer rates. Figure 3 also shows that, in this case, neglecting the impurity Zeeman terms leads to significant deviations from the energy-conserving rates.

In order to establish a connection between the theories discussed above and the experimentally determined electron-spin relaxation rates, it has to be noted that in most magneto-optical experiments on II-VI DMS quantum wells so far (cf. Ref. [3] and references therein) the pump laser is tuned to the electron-heavy-hole exciton energy. To model these experiments also the Coulomb correlations between electrons and holes have to be taken into account, which is beyond the scope of the present paper. It was found in Ref. [3] that different groups consistently measured perpendicular electron-spin relaxation rates T_2^{-1} which are about five times larger than τ_{FGR} at $B = 0$. This discrepancy can be understood by the fact that the effective electron mass has to be replaced by the exciton mass in the expression for the rate τ_{FGR}^{-1} [46], which yields an increase of the rate by a factor of ~ 4.6 in the case of CdMnTe. Nevertheless, the finding of the present paper that the rate T_2^{-1} varies only weakly with the magnetic field and stays essentially within 30% of τ_{FGR}^{-1} is consistent with the tendency of most of the experimental results summarized in Ref. [3]. However, especially for samples with low impurity concentration at

low temperatures, there are also some experiments which measured a maximum (instead of a minimum predicted by the present theory) of the magnetic field dependence of the perpendicular spin transfer rate as well as changes in the rate which span about one order of magnitude of its value at $B = 0$, which was suggested [3] to stem from local fluctuations of the impurity magnetization. In order to distinguish these imhomogeneity effects from Coulomb correlation effects we suggest experiments where the pump pulse is tuned to energies well above the exciton resonance.

B. Interplay between *s-d* and Rashba interactions

The fact that in the derivation of Eq. (34) the **k** dependence of an effective magnetic field was taken into account makes it possible to discuss the interplay between the spin-orbit coupling and the *s-d* interaction on a rigorous microscopic basis, where the spin-orbit interaction also acts during *s-d* scattering events. In earlier works, the interplay between these effects was studied [21,47], where only the direct effects of the spin-orbit coupling on the electron spins was considered, yielding an additional **k**-dependent contribution to the mean-field precession frequency, whereas the dynamics of the correlations was not modified, i.e., the spin-orbit interaction was only accounted for between *s-d* scattering events. It was found that already on a mean-field level, the carrier spin dephasing due to the **k** dependence of the precession frequencies can be strongly suppressed by a motional-narrowing-type mechanism caused by the precession in the mean field of the impurity magnetization. Furthermore, it was argued that both mechanisms can be tuned in a wide range, especially in $Hg_{1-x-y}Cd_yMn_xTe$ quantum wells with applied electric fields. In this material, the strength of the *s-d* interaction is determined by the Mn concentration x, while the Cd concentration y can be used to change the gap between conduction and valence bands which controls the strength of the Rashba [19] field. When both types of interaction are similarly important, a complex oscillatory time evolution of the carrier spin was found, which is absent when either one of the interactions dominates.

Now, the question arises whether neglecting the effects of the Rashba field on the dynamics of the correlations is indeed a good approximation or if qualitative changes have to be expected if they are accounted for. We study this question in a case in which the strengths of the Rashba and the *s-d* interactions are comparable. We consider a $d = 20$ nm wide $Hg_{1-x-y}Cd_yMn_xTe$ quantum well with electric and magnetic fields applied along the growth direction z. The voltage drop between the barriers of the quantum well leads to a strong Rashba interaction of the form

$$H_R = 2\hbar\alpha_R \sum_{\mathbf{k}\sigma\sigma'} \left(k_y s_{\sigma\sigma'}^x - k_x s_{\sigma\sigma'}^y\right) c_{\mathbf{k}\sigma}^\dagger c_{\mathbf{k}\sigma'}, \qquad (47)$$

where we assume a value of $\alpha_R = 4.87$ meV nm [21].

Further parameters that enter the calculation are the effective mass $m^* = 0.093m_0$, the *s-d* coupling constant $J_{sd} = 15$ meV nm^3, the lattice constant $a = 0.645$ nm and the Mn concentration $x = 7\%$. The initial Mn state is modelled by a thermal equilibrium state following a Brillouin function with temperature $T = 4$ K in an external magnetic field pointing in

the $-z$ direction with $|\mathbf{B}| = 50$ mT. The g factors for impurities and conduction-band electrons are $g_{Mn} = 2.$ and $g_e = -1.5$, respectively. Furthermore, as we consider an intrinsic DMS where the quasifree carriers originate purely from optical excitation, $N_{Mn} \gg N_e$ is clearly fulfilled, so that we can neglect the back action of the carriers on the impurities. Thus, the Mn magnetization remains homogeneous, which allows us to integrate along the growth direction yielding a factor of $I = 1.5$. The initial electron spin was modelled by a Gaussian distribution in the spin-up band centered at the band edge with standard deviation $E_s = 1$ meV corresponding to a σ^- polarized laser with pulse duration (full width at half maximum) ~ 140 fs. For these parameters, the mean-field energy splitting caused by the impurity magnetization is ~ -0.75 meV (the spin-up-subband is energetically favored), while the strength of the Rashba interaction for an electron with kinetic energy $\frac{\hbar^2 k_0^2}{2m^*} = 1$ meV is $2\hbar\alpha_R k_0 \sim 0.89$ meV. Here, the Zeeman terms yield significantly smaller contributions of $g_e \mu_B |\mathbf{B}| \approx -0.004$ meV and $g_{Mn} \mu_B |\mathbf{B}| \approx 0.006$ meV to the respective spin splittings.

Figure 5 shows the results of numerical simulations for this set of parameters. As reported earlier [21], the Rashba interaction alone (blue dashed line) leads to a fast dephasing of the carrier spins. If additionally magnetic impurities with a finite magnetization are present, already a mean-field treatment (purple circles) can lead to a strong suppression of the
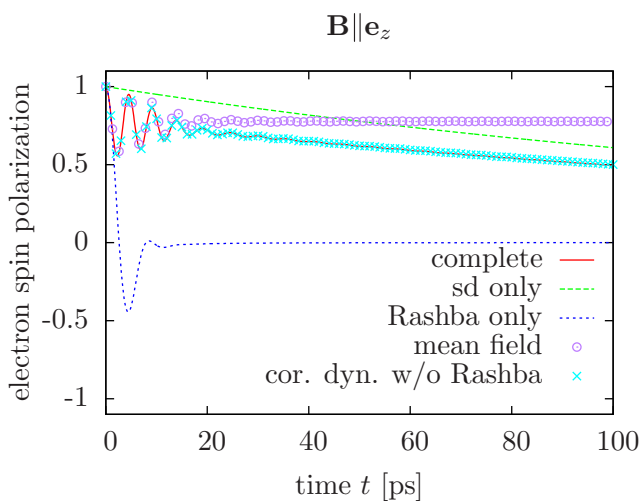

FIG. 5. Time evolution of the total electron-spin polarization after spin-polarized optical excitation in a magnetic field perpendicular to the quantum well plane (cf. text for parameters). The red solid line describes the results according to Eqs. (10b) and (10c) with the Markovian expression for the correlations from Eq. (34). The green dashed line corresponds to a calculation without Rashba coupling, where only the s-d interaction is considered. The blue dotted line presents the results of the case in which only the Rashba interaction is present. The mean-field calculation, which is obtained by dropping the correlations completely, is shown as the purple circles. The cyan crosses describe the results where the effects due to the Rashba interaction on the dynamics of the carrier-impurity correlations are neglected, so that in addition to the mean-field terms, the time derivative of the carrier variables obtains the correlation induced contribution of Eqs. (40).
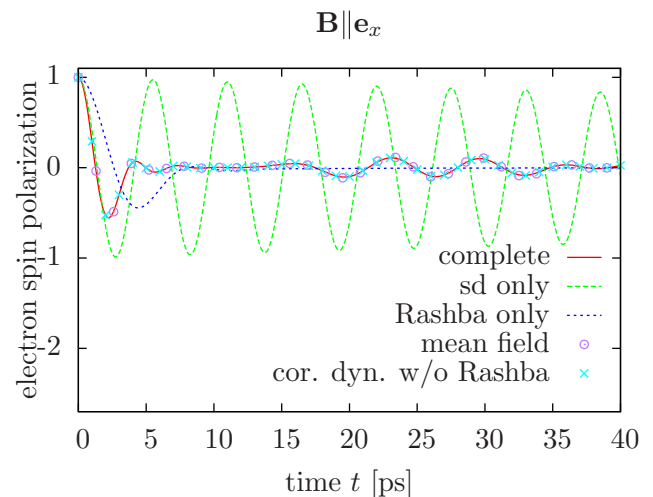

FIG. 6. Time evolution of the total electron-spin polarization after spin-polarized optical excitation in a magnetic field parallel to the quantum-well plane (cf. Fig. 5).

dephasing by motional narrowing caused by the precession of the carrier spin in the mean field of the impurity magnetization. Without the Rashba interaction, the s-d interaction causes a spin transfer from the carriers to the impurities which can be seen in Fig. 5 as an exponential decay to a nonvanishing equilibrium value. In the previous studies [21], the correlation induced spin transfer was combined with the mean-field precession, but the effects of the Rashba interaction on the dynamics of the correlations were neglected (here shown as cyan crosses). In Fig. 5, also the complete carrier spin dynamics is shown, where the Rashba interaction is explicitly accounted for in the calculation of the correlations (red solid line). By comparing both calculations, it can be seen that the total carrier spin is hardly influenced by the effects of the Rashba spin-orbit coupling on the correlation dynamics. The same result is also obtained for the situation where the magnetic field is applied parallel to the quantum well plane, as shown in Fig. 6.

Similar to the fact that the precession-type motion of the correlations discussed so far leads to changes in the kinetic energy of scattered carriers, also the Rashba inter-action enforces a precession of the correlations resulting in corresponding changes in the electron energies. In Fig. 7 the carrier occupations at $t = 0$ and $t = 50$ ps are shown for calculations with and without accounting for the Rashba effect on the correlation dynamics for the situation described in Fig. 5 with magnetic field parallel to the growth direction. Without the Rashba interaction, the kinetic-energy dependence of the occupations at $t = 50$ ps shows a distinctive step at $\hbar\omega_{\mathbf{k}} = |\hbar\sigma_e^B \omega_e - \hbar\sigma_{Mn}^B \omega_{Mn}|$ which corresponds to a redistribution of carriers with an excess energy in the spin degree of freedom to states with higher kinetic energies. When the Rashba coupling is turned on, the step shifts towards slightly higher kinetic energies. This can be explained by the fact that in the configuration with a magnetic field along the growth direction and a Rashba field in the quantum well plane the energy
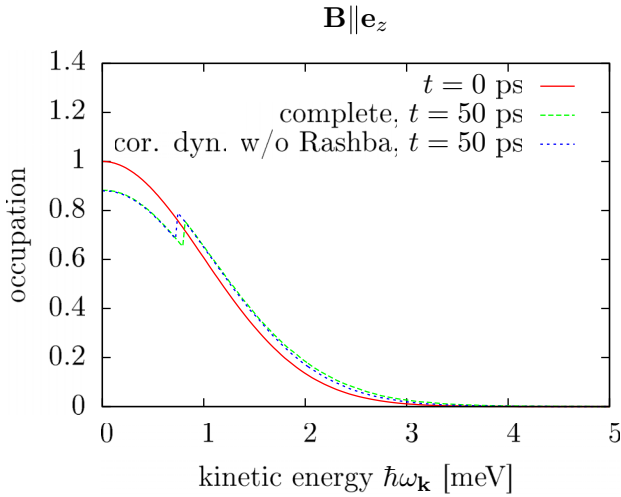
B∥e_z

FIG. 7. Kinetic-energy dependence of the occupation of carrier states at times $t = 0$ ps and $t = 50$ ps for the calculations shown in Fig. 5.

eigenvalues of an electron with wave vector $\mathbf{k}$ are

$$E_\pm = \hbar\omega_\mathbf{k} \pm \tfrac{1}{2}\hbar\sqrt{(2\alpha_R|\mathbf{k}|)^2 + (\sigma_e^B\omega_e)^2}. \tag{48}$$

Including the shifts due to the impurity Zeeman splittings, the step in the kinetic-energy dependence of the occupation is therefore shifted to $\hbar\sqrt{(2\alpha_R|\mathbf{k}|)^2 + (\sigma_e^B\omega_e - \sigma_{Mn}^B\omega_{Mn})^2}$. However, the shift of the energy splitting is too small to cause a significant impact on the time evolution of the total spin.

C. Connection to the theory of collective carrier-impurity precession modes in DMSs

In the derivation of the theory, the z dependence of the carrier envelope function was taken into account. We see from Eqs. (42) that one effect of this z dependence is that the spin transfer rate obtains the prefactor I. Assuming a constant linear impurity density $\frac{N_{Mn}}{d}$, a constant z envelope yields a value of $I = 1$ while the extreme case of a quantum well with infinite barriers yields $I = \frac{3}{2}$. This effect has also been found in previous studies of DMSs [3,15,32].

Like the spin transfer rates, also the electron-spin precession is influenced by the z dependence of the envelope of the electron wave function. In particular, it can be seen from Eq. (11c) that the contribution to the electron-spin precession frequency from the impurity spin is proportional to

$$\int_{-d/2}^{d/2} dz\, |\psi(z)|^2 \langle \mathbf{S}(z)\rangle.$$

Thus, the impurity spin as a function of z can be decomposed into this mode which couples to the electron-spin precession and $N_{Mn} - 1$ orthogonal modes, which do not influence the electron spins directly on a mean-field level. In the parameter regime where the precession frequencies of the electron and impurity spins almost coincide, the coupling between the above impurity mode and the electron spin is particularly large, leading to an avoided crossing indicating a collective motion of impurity and carrier spins. This fact has been discussed in a number of recent papers by different groups [6,11,39,40,48,49]. In these works, however, the carrier-impurity correlations have been disregarded.

In the following, we will derive equations describing the situation studied, e.g., in Ref. [39] taking the effects due to the correlations into account. There, an n-type CdMnTe quantum well in an external magnetic field parallel to the quantum well plane (x direction) was considered, leading to equilibrium values of the impurity and carrier spins antiparallel to the magnetic field. A circularly polarized pump beam induces electron-hole pairs with spin polarization along the z direction. During the decay of the hole spins on a time scale of ∼5 ps, the impurity magnetization precesses around the p-d exchange field of the holes, causing a small tilt of the impurity spins away from the equilibrium x axis into the y axis. The optically induced electron spins contribute to the z component of the total carrier spin. Thus, after the holes are decayed, one ends up with a situation where the impurity and carrier spins precess around each other.

The fact that the spin components perpendicular to the equilibrium values are small compared with the parallel components allows one to linearize Eqs. (40) and (41) with the expression for the rates from Eq. (42):

$$\frac{\partial}{\partial t}\mathbf{s}_{>/<}^\perp = \frac{g_e\mu_B}{\hbar}\mathbf{B}\times\mathbf{s}_{>/<}^\perp + \frac{J_{sd}N_{Mn}}{\hbar V}\mathbf{S}^{x,(1)}\times\mathbf{s}_{>/<}^\perp - \frac{J_{sd}N_{Mn}}{\hbar V}\mathbf{s}_{>/<}^x\times\mathbf{S}^{\perp,(1)} - \frac{1}{d}\int_{-d/2}^{d/2}dz\,\Gamma^{>/<}(z)\mathbf{s}_{>/<}^\perp, \tag{49a}$$

$$\frac{\partial}{\partial t}\mathbf{S}^{\perp,(j)} = \frac{g_{Mn}\mu_B}{\hbar}\mathbf{B}\times\mathbf{S}^{\perp,(j)} - \frac{J_{sd}}{V\hbar}\mathbf{S}^{x,(j+1)}\times(\mathbf{s}_>^\perp + \mathbf{s}_<^\perp) + \frac{J_{sd}}{V\hbar}(\mathbf{s}_>^x + \mathbf{s}_<^x)\times\mathbf{S}^{\perp,(j+1)}$$

$$+ d^{j-1}\int_{-d/2}^{d/2}dz\,|\psi(z)|^{2j}[\Gamma^>(z)\mathbf{s}_>^\perp + \Gamma^<(z)\mathbf{s}_<^\perp], \tag{49b}$$

$$\Gamma(\mathbf{k},z) := \pi\frac{Am^*}{2\pi\hbar}\frac{J_{sd}^2N_{Mn}}{\hbar^2V^2}d^2|\psi(z)|^4\left[\langle S^{\|2}\rangle + \left(\frac{\langle S^{\perp 2}\rangle}{2} - \sigma_S^B\frac{|\langle\mathbf{S}\rangle|}{4}\right)\Theta\{\omega_\mathbf{k} + [\sigma_e^B\omega_e - \sigma_e^B\omega_{Mn}(z)]\}\right.$$

$$\left. + \left(\frac{\langle S^{\perp 2}\rangle}{2} + \sigma_S^B\frac{|\langle\mathbf{S}\rangle|}{4}\right)\Theta\{\omega_\mathbf{k} - [\sigma_e^B\omega_e - \sigma_e^B\omega_{Mn}(z)]\}\right] \tag{49c}$$

with

$$s_{>/<}^{x/\perp} := \sum_{\mathbf{k}}^{>/<} s_{\mathbf{k}}^{x/\perp}, \tag{50a}$$

$$\Gamma^{>/<}(z) := \sum_{\mathbf{k}}^{>/<} \Gamma(\mathbf{k},z), \tag{50b}$$

$$\mathbf{S}^{x/\perp,(j)} := d^{j-1} \int_{-d/2}^{d/2} dz\, |\psi(z)|^{2j} \langle \mathbf{S}^{x/\perp}(z) \rangle, \tag{50c}$$

where the indices x and $\perp$ denote the spin components parallel and perpendicular to the equilibrium axis x and $\sum_{\mathbf{k}}^{>/<}$ describes the sum over all wave vectors $\mathbf{k}$ with $\omega_{\mathbf{k}} > \omega_0$ or $\omega_{\mathbf{k}} < \omega_0$, respectively, where $\omega_0 = |\sigma_e^B \omega_e - \sigma_{Mn}^B \omega_{Mn}|$. The distinction between states with higher or lower kinetic energy than ω_0 is a direct consequence of the steplike $\mathbf{k}$ dependence of the spin transfer rates.

Equations (49) of the present paper differ mainly from Eqs. (4) and (5) of Ref. [39] in that carriers with $\omega_{\mathbf{k}} < \omega_0$ are distinguished from carriers with $\omega_{\mathbf{k}} > \omega_0$ and in that the terms proportional to the rate $\Gamma^{>/<}(z)$ are omitted in the mean-field treatment of Ref. [39]. Instead, a phenomenological relaxation rate τ_e^{-1} was added manually in Ref. [39]. Another difference is the appearance of the corresponding spin transfer term in the equations for the impurities. This is due to the fact that the s-d interaction is spin conserving so that the electron spin that is removed from $s_{>/<}^{\perp}$ has to be transferred to the impurity system. Taking these corrections with respect to the description of Ref. [39] into account would lead to a more accurate modelling of the collective carrier-impurity precession modes. However, as discussed earlier, the variation of the perpendicular spin transfer rate in the presence of an external magnetic field is limited to $\lesssim 30\%$ of the golden rule value at $\mathbf{B} = 0$, so that the spin transfer rate remains in the same order of magnitude. Thus, the phenomenological treatment of the rate can be justified for the purpose of the discussion in Ref. [39].

IV. CONCLUSION

A quantum kinetic description of the carrier spin dynamics in paramagnetic intrinsic II-VI DMSs was presented which, in contrast to previous works [33,36,37], also accounts for a wave-vector-dependent effective magnetic field as well as Zeeman terms for carriers and impurities. The Markov limit of the quantum kinetic equations allow us to extract rates for spin transfer processes between carriers and magnetic impurities. From the rigorous treatment of a precession-type dynamics of the carrier-impurity correlations it is found that the redistribution of carriers in $\mathbf{k}$ space is not only influenced by the spin splitting of the electron subbands due to the Zeeman energy enhanced by the impurity magnetization, but also acquires an energetic shift corresponding to the Zeeman level splitting of the magnetic impurities. This shift accounts for the fact that a spin flip of an electron involves a spin flop of the magnetic impurity in the opposite direction and the total energy of the magnetic impurity and the electron spin has to be conserved. The energetic shifts in the description of the

spin-flip-flop processes are often not correctly accounted for in the literature.

The impact of these energy shifts was investigated using the example of the magnetic-field dependence of the carrier-impurity spin transfer rates parallel and perpendicular to the impurity magnetization. Two distinct parameter regimes were identified, one for rather high doping concentrations of the order of $x \sim 1\%$ and one for extremely diluted systems with $x \lesssim 0.1\%$. These regimes correspond to cases where the total change of the kinetic electron energy as given by $(\sigma_e^B \omega_e - \sigma_{Mn}^B \omega_{Mn})$ is mainly positive or negative. In both situations the perpendicular spin transfer rate T_2^{-1} varies within $\sim 30\%$ of the value for $B = 0$, which also coincides with the results for T_1^{-1} obtained by Fermi's golden rule. However, in the first case, the parallel spin transfer rate T_1^{-1} decays monotonically for an increasing magnetic field to $\frac{5}{8}$ of the golden-rule value at $B = 0$, while in the extremely diluted case, T_1^{-1} eventually vanishes. In calculations where the carrier spin splitting $\hbar\omega_e$ or the impurity Zeeman splitting $\hbar\omega_{Mn}$ is neglected, as is often done in the literature, the magnetic field dependence of the spin transfer rates deviates significantly from that predicted by the accurate description involving both energetic shifts. Accounting for the impurity Zeeman splitting for the spin-flip-flop processes turns out to be particularly important in the very dilute case.

Furthermore, the interplay between the s-d interaction between carrier and impurities and the Rashba interaction in a $Hg_{1-x-y}Cd_yMn_xTe$ quantum well was investigated. In the standard rate description approach one usually calculates for each interaction a corresponding scattering rate and ignores that other interactions might change the dynamics *during* the scattering process. This was the point of view adopted in previous studies of the combined dynamics of s-d and Rashba couplings [21,47]. However, such mutual dependencies of different interactions have been shown in the literature to be of importance, e.g., in the case of a static electric field acting during phonon-scattering process known as *intracollisional field effects* [38]. Technically, the dynamics during an ongoing interaction process is represented by correlation functions. In the present paper, we presented a quantum kinetic description where s-d and Rashba interactions have been fully accounted for in the combined dynamics of the single-particle density matrices and the carrier-impurity correlations, thus fully covering all mutual cross effects between these interactions. While it is *a priori* difficult to predict how important these cross effects actually are, we have demonstrated for the present case that the total carrier spin is hardly affected by this mechanism.

Finally, taking into account also the z dependence of the carrier envelope function makes it possible to show how the phenomenological treatment of the spin transfer rate in the description of collective carrier-impurity precession modes in Ref. [39] can be based on a solid microscopic foundation.

In summary, our microscopic treatment of the effects of a $\mathbf{k}$-dependent magnetic field and the impact of the shape of the carrier envelope function justifies the approximations made in earlier studies of the dynamics of the total electron spin [21,39]. Apart from this insight, the present theory further contributes to the progress in the field of spin physics in

DMS by not only deriving rates for carrier spins parallel but also perpendicular to the impurity magnetization in the presence of an external magnetic field. The latter are expected to be the dominant contribution to the carrier dephasing time in time-resolved magneto-optical Kerr measurements in Voigt configuration. In contrast to earlier approaches found in the literature [22,32], the rates derived in this paper are fully compatible with the energy conservation of an individual spin-flip-flop process. Our study reveals that the difference between the predictions of the discussed

theories is most prominent for extremely diluted magnetic semiconductors.

[1] T. Dietl and H. Ohno, Rev. Mod. Phys. **86**, 187 (2014).

[2] T. Dietl, H. Ohno, F. Matsukura, J. Cibert, and D. Ferrand, Science **287**, 1019 (2000).

[3] Z. Ben Cheikh, S. Cronenberger, M. Vladimirova, D. Scalbert, F. Perez, and T. Wojtowicz, Phys. Rev. B **88**, 201306 (2013).

[4] Y. S. Chen, M. Wiater, G. Karczewski, T. Wojtowicz, and G. Bacher, Phys. Rev. B **87**, 155301 (2013).

[5] S. Cronenberger, M. Vladimirova, S. V. Andreev, M. B. Lifshits, and D. Scalbert, Phys. Rev. Lett. **110**, 077403 (2013).

[6] F. Perez, J. Cibert, M. Vladimirova, and D. Scalbert, Phys. Rev. B **83**, 075311 (2011).

[7] M. D. Kapetanakis, I. E. Perakis, K. J. Wickey, C. Piermarocchi, and J. Wang, Phys. Rev. Lett. **103**, 047404 (2009).

[8] M. D. Kapetanakis and I. E. Perakis, Phys. Rev. Lett. **101**, 097201 (2008).

[9] H. Krenn, K. Kaltenegger, T. Dietl, J. Spałek, and G. Bauer, Phys. Rev. B **39**, 10918 (1989).

[10] S. A. Crooker, D. D. Awschalom, J. J. Baumberg, F. Flack, and N. Samarth, Phys. Rev. B **56**, 7574 (1997).

[11] P. Barate, S. Cronenberger, M. Vladimirova, D. Scalbert, F. Perez, J. Gòmez, B. Jusserand, H. Boukari, D. Ferrand, H. Mariette, J. Cibert, and M. Nawrocki, Phys. Rev. B **82**, 075306 (2010).

[12] I. Žutić, J. Fabian, and S. Das Sarma, Rev. Mod. Phys. **76**, 323 (2004).

[13] T. Dietl, Nat. Mater. **9**, 965 (2010).

[14] H. Ohno, Nat. Mater. **9**, 952 (2010).

[15] A. Haury, A. Wasiela, A. Arnoult, J. Cibert, S. Tatarenko, T. Dietl, and Y. Merle d'Aubigné, Phys. Rev. Lett. **79**, 511 (1997).

[16] M. D. Kapetanakis, J. Wang, and I. E. Perakis, J. Opt. Soc. Am. B **29**, A95 (2012).

[17] T. Jungwirth, J. Sinova, J. Mašek, J. Kučera, and A. H. MacDonald, Rev. Mod. Phys. **78**, 809 (2006).

[18] A. Patz, T. Li, X. Liu, J. K. Furdyna, I. E. Perakis, and J. Wang, Phys. Rev. B **91**, 155108 (2015).

[19] Y. A. Bychkov and E. I. Rashba, J. Phys. C **17**, 6039 (1984).

[20] G. Dresselhaus, Phys. Rev. **100**, 580 (1955).

[21] F. Ungar, M. Cygorek, P. I. Tamborenea, and V. M. Axt, Phys. Rev. B **91**, 195201 (2015).

[22] J. H. Jiang, Y. Zhou, T. Korn, C. Schüller, and M. W. Wu, Phys. Rev. B **79**, 155201 (2009).

[23] K. E. Rönnburg, E. Mohler, H. G. Roskos, K. Ortner, C. R. Becker, and L. W. Molenkamp, Phys. Rev. Lett. **96**, 117203 (2006).

[24] J. K. Furdyna, J. Appl. Phys. **64**, R29 (1988).

[25] B. König, I. A. Merkulov, D. R. Yakovlev, W. Ossau, S. M. Ryabchenko, M. Kutrowski, T. Wojtowicz, G. Karczewski, and J. Kossut, Phys. Rev. B **61**, 16870 (2000).

[26] O. Morandi, P.-A. Hervieux, and G. Manfredi, Phys. Rev. B **81**, 155309 (2010).

[27] O. Morandi and P.-A. Hervieux, Phys. Rev. B **81**, 195215 (2010).

[28] M. Cygorek, P. I. Tamborenea, and V. M. Axt, Phys. Rev. B **93**, 035206 (2016).

[29] E. Tsitsishvili and H. Kalt, Phys. Rev. B **73**, 195402 (2006).

[30] E. Tsitsishvili and H. Kalt, Phys. Rev. B **77**, 155305 (2008).

[31] J. Kossut, Phys. Status Solidi B **72**, 359 (1975).

[32] Y. G. Semenov, Phys. Rev. B **67**, 115319 (2003).

[33] C. Thurn and V. M. Axt, Phys. Rev. B **85**, 165203 (2012).

[34] C. Thurn, M. Cygorek, V. M. Axt, and T. Kuhn, Phys. Rev. B **87**, 205301 (2013).

[35] C. Thurn, M. Cygorek, V. M. Axt, and T. Kuhn, Phys. Rev. B **88**, 161302(R) (2013).

[36] M. Cygorek and V. M. Axt, Phys. Rev. B **90**, 035206 (2014).

[37] M. Cygorek and V. M. Axt, Semicond. Sci. Technol. **30**, 085011 (2015).

[38] J. Hader, T. Meier, S. W. Koch, F. Rossi, and N. Linder, Phys. Rev. B **55**, 13799 (1997).

[39] M. Vladimirova, S. Cronenberger, P. Barate, D. Scalbert, F. J. Teran, and A. P. Dmitriev, Phys. Rev. B **78**, 081305 (2008).

[40] F. J. Teran, M. Potemski, D. K. Maude, D. Plantier, A. K. Hassan, A. Sachrajda, Z. Wilamowski, J. Jaroszynski, T. Wojtowicz, and G. Karczewski, Phys. Rev. Lett. **91**, 077201 (2003).

[41] A. D. Margulis and Vl. A. Margulis, Fiz. Tverd. Tela (Leningrad) **25**, 1590 (1983) [Sov. Phys. Solid State **25**, 918 (1983)].

[42] N. R. Ogg, Phys. Soc. London **89**, 431 (1966).

[43] F. X. Bronold, I. Martin, A. Saxena, and D. L. Smith, Phys. Rev. B **66**, 233206 (2002).

[44] F. Rossi and T. Kuhn, Rev. Mod. Phys. **74**, 895 (2002).

[45] M. Cygorek and V. M. Axt, J. Phys.: Conf. Ser. **647**, 012042 (2015).

[46] G. Bastard and R. Ferreira, Surf. Sci. **267**, 335 (1992).

[47] F. Ungar, M. Cygorek, P. I. Tamborenea, and V. M. Axt, J. Phys.: Conf. Ser. **647**, 012010 (2015).

[48] P. M. Shmakov, A. P. Dmitriev, and V. Y. Kachorovskii, Phys. Rev. B **83**, 233204 (2011).

[49] D. Frustaglia, J. König, and A. H. MacDonald, Phys. Rev. B **70**, 045205 (2004).

Publication 6

Non-Markovian Effects in the Spin Transfer Dynamics in Diluted Magnetic Semiconductors due to Excitation in Proximity to the Band Edge

M. Cygorek and V. M. Axt

Non-Markovian Effects in the Spin Transfer Dynamics in Diluted Magnetic Semiconductors due to Excitation in Proximity to the Band Edge

M. Cygorek, V. M. Axt

Theoretische Physik III, Universität Bayreuth, 95440 Bayreuth, Germany

E-mail: `Moritz.Cygorek@uni-bayreuth.de`

Abstract. The non-Markovian effects in the spin dynamics in diluted magnetic semiconductors found in quantum kinetic calculations can be reproduced very well by a much simpler effective single electron theory, if a finite memory is accounted for. The resulting integro-differential equation can be solved by a differential transform method, yielding the Taylor series of the solution. From the comparison of both theories it can be concluded that the non-Markovian effects are due to the spectral proximity of the excited electrons to the band edge.

1. Introduction

Diluted magnetic semiconductors (DMS) are a class of workhorse materials in the field of semiconductor spintronics, since they combine the magnetic degree of freedom with the versatility and highly developed fabrication schemes of the semiconductor technology. Usually, Mn doped II-VI or III-V semiconductors are studied and a localized s-d interaction between the carrier and Mn spins modelled by a Kondo-like Hamiltonian has been found to describe the magnetic properties and the spin dynamics of DMS very well.

A numerical calculation based on a quantum kinetic theory (QKT) for the spin dynamics in DMS governed by the s-d interaction[1] showed that, among other phenomena, non-Markovian effects, such as overshoots or oscillations of the total spin polarization, can be found in one- and two-dimensional systems[2, 3]. The quantum kinetic theory can be presented in a more easy-to-use and intuitive way, by eliminating the correlations at the cost of a memory integral. Because it was found that, in doing so, it is crucial to account for a precession-like dynamics of the carrier-impurity correlations, the equations are referred to as *precession of electron spins and correlations* (PESC) equations[4]. In the present article, we show that the non-Markovian spin dynamics in DMS, found in the quantum kinetic theory, can be well described by an approximation of the PESC equations. The resulting integro-differential equation can be solved by a differential transform method (DTM)[5]. An analysis based on this simplified approach reveals that the non-Markovian effects are due to the proximity of the electronic excitations to the band edge.

2. Equation of motion

In Ref. [4] effective equations of motion for the correlation-induced spin dynamics in DMS were derived. For initially vanishing magnetization of the magnetic impurities, the time evolution of

the conduction band electron spin polarization in a DMS quantum well structure can be found from Eq. (7a) of Ref. [4]:

$$\frac{\partial}{\partial t}s_{\omega_1}(t) = -\frac{\eta}{\pi}\int_0^t dt'\int_0^{\omega_{BZ}} d\omega \cos[(\omega_1 - \omega)(t - t')]\left[s_{\omega_1}(t') + \frac{1}{4}(s_\omega(t') - s_{\omega_1}(t'))\right], \qquad (1)$$

where s_{ω_1} is the mean electron spin of electrons with energy $\hbar\omega_1$ (relative to the band minimum), η is the spin transfer rate in the Markov limit and $\hbar\omega_{BZ}$ is the energy at the end of the first Brillouin zone. If we assume a parabolic band structure, we find $\omega_1 = \frac{\hbar k_1^2}{2m^*}$ with effective mass m^* for an electron with wave vector $\mathbf{k}_1$ and $\eta = \frac{35}{12}\frac{J_{sd}^2 m^* n_{Mn}}{\hbar^3 d}$ with coupling constant J_{sd}, magnetic ion density n_{Mn} and quantum well width d.

It is noteworthy that in the time derivative for the total spin, where Eq. (1) is integrated over ω_1, the term $(s_\omega(t') - s_{\omega_1}(t'))$ cancels. Since this term can be expected to lead to an insignificant contribution to the total spin, we henceforth neglect this term which simplifies the analysis of the spin dynamics drastically. Despite this argument being valid only for the total spin, we shall show by numerical calculation that also the individual spin dynamics for an electron at the energy ω_1 is reasonably well described by this approximation (cf. Fig 1(c) and (d)). Thus, Eq. (1) can be reduced to

$$\frac{\partial}{\partial t}s_{\omega_1}(t) = -\frac{\eta}{\pi}\int_0^t dt'\left[\frac{\sin((\omega_{BZ} - \omega_1)(t' - t))}{t' - t} + \frac{\sin(\omega_1(t' - t))}{t' - t}\right]s_{\omega_1}(t') \qquad (2)$$

The phyiscal meaning of Eq. (2) becomes most obvious when the Markov limit is regarded, which assumes that s_{ω_1} changes on a much slower timescale than the oscillations of the integral kernel. Then, on the r. h. s. of Eq. (2), $s_{\omega_1}(t')$ can be evaluated at $t' = t$ and drawn out of the integral. Keeping in mind that $\lim_{\omega\to\infty}\sin(\omega t)/t = \pi\delta(t)$ and that the integral ranges only over one half of the $\sin(\omega t)/t$ peak, one finds: $\frac{\partial}{\partial t}s_{\omega_1} = -\eta s_{\omega_1}$, which shows a simple exponential decay of s_{ω_1} with the rate η. This corresponds to a golden rule-type transfer of the electron spin to the impurity system.

However, the condition for the applicability of the Markov limit was $\eta \ll \omega_1$ and $\eta \ll \omega_{BZ} - \omega_1$. For realistic parameters (e. g., the parameters used in Ref. [2, 3] yield $\hbar\eta \approx 0.45$ meV) and excitations far away from the end of the first Brillouin zone, only the latter condition is fulfilled, while for excitations close to the band edge, ω_1 can be of the same order of magnitude as η. Thus, we apply the Markov limit ($\omega_{BZ} \to \infty$) only on the first term of Eq. (2). The number of parameters can be reduced by substituting $\tau := \eta t$ and $\xi := \omega_1/\eta$. Then, the problem is transformed to:

$$\frac{\partial}{\partial\tau}\Phi_\xi(\tau) = -\frac{1}{2}\Phi_\xi(\tau) - \frac{1}{\pi}\int_0^\tau d\tau'\frac{\sin(\xi(\tau' - \tau))}{\tau' - \tau}\Phi_\xi(\tau'), \quad \Phi_\xi(0) := 1, \qquad (3)$$

where $s_{\omega_1}(t) = s_{\omega_1}(0)\Phi_{\omega_1/\eta}(\eta t)$. Thus, the shape of the time evolution depends only on the ratio between ω_1 and η.

3. Numerical Evaluation of the non-Markovian Spin Dynamics

We solve the integro-differtial equation (3) by a technique similar to Zhou's differential transform method (DTM)[5], which consists of Taylor-expanding all terms in Eq. (3) at $\tau = 0$. This yields
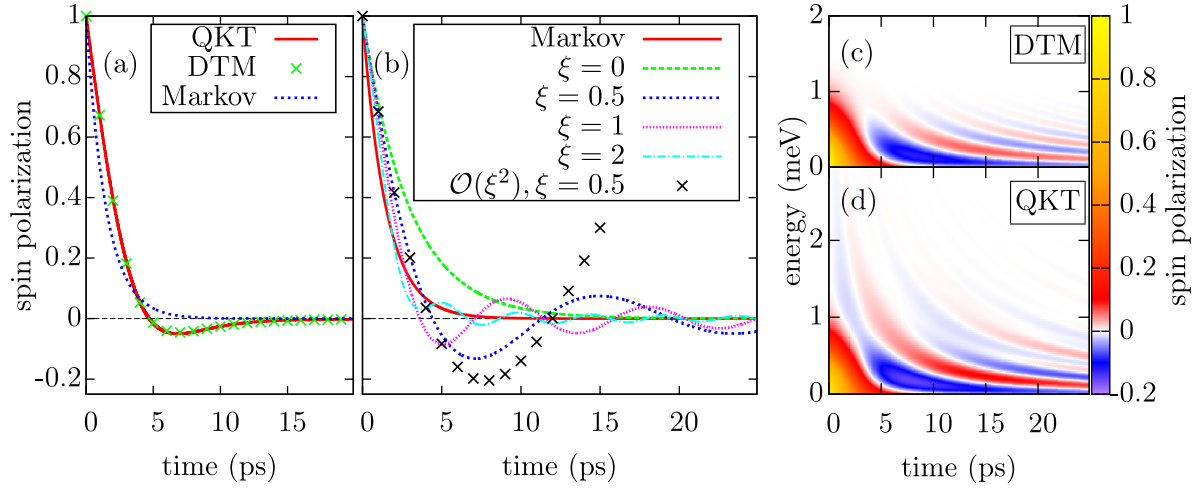
Figure 1. (a): Spin dynamics in a 4 nm wide $Zn_{0.93}Mn_{0.07}Se$ quantum well with $\eta \approx 0.67$ ps^{-1} with Gaussian excitaton at $\hbar\omega = 0$ and standard deviation $\Delta = 0.4$ meV (same as in Ref. [2]) according to the full quantum kinetic theory (QKT), the differential transform method (DTM, from Eq. (4)) and the Markov limit. (b): Time evloution of the spin of single electrons with fixed energies $\hbar\omega = \hbar\eta\xi$, compared with the Markov limit and the expression in Eq. (5) for the low-ξ approximation. The spectrally resolved time evolution of the spin polarization is shown in (c) for the DTM calculation, and in (d) for the QKT (cf. Ref. [2]).

a recursion relation between the derivatives of Φ_ξ:

$$\Phi_\xi^{(i)} = -\tfrac{1}{2}\Phi_\xi^{(i-1)} - \frac{1}{\pi}\sum_{0\le 2m\le i-2}\frac{(-1)^m}{2m+1}\xi^{(2m+1)}\Phi_\xi^{(i-2-2m)}, \qquad (4)$$

where $\Phi_\xi^{(i)}$ is the i-th derivative of Φ_ξ evaluated at $\tau = 0$. The numerical evaluation of Eq. (4) is very efficient and $\Phi_\xi(\tau)$ can be calculated to high orders by substituting the derivatives into the Taylor expansion. We refer to this algorithm as the DTM calculation.

It is noteworthy that from the recursion relation (4) closed expressions can be derived for $\Phi_\xi(\tau)$ to a certain order in the ratio ξ by combinatoric analysis of the paths from $\Phi_\xi^{(0)} = 1$ to $\Phi_\xi^{(n)}$ and comparing the Taylor series with that of known functions. E. g., to second order in ξ, we find:

$$\Phi_\xi(\tau) = e^{-\frac{\tau}{2}} + \frac{\xi}{\pi}[(2\tau + 4)e^{-\frac{\tau}{2}} - 4] + \left(\frac{\xi}{\pi}\right)^2\left[(2\tau^2 + 16\tau + 48)e^{-\frac{\tau}{2}} + 8\tau - 48\right] + \mathcal{O}(\xi^3) \quad (5)$$

which should be valid for excitations near the band edge where $\xi \ll 1$ can be fulfilled.

4. Results

To check the validity of the approximation of neglecting the last term of Eq. (1), we compare the DTM calculation with the results of a full quantum kinetic treatment. Fig. 1(a) shows that the non-Markovian dynamics of the total spin given in Fig. 1(b) of Ref.[2] can be reproduced almost perfectly with the DTM calculation. Also, the time evolution of an individual spin of an electron with energy $\hbar\omega_1$ is very similar in both calculations except for a high-energy tail appearing in the full quantum kinetic result, as can be seen from the spectrally resolved time evolution presented in Figs. 1(c) and (d) for DTM and QKT calculations, respectively. This finding confirms that Eq. (3) indeed captures the main non-Markovian features of the full quantum kinetic theory.

Fig. 1(b) shows the results of the DTM calculation for different values of ξ. For $\xi = 0$, the dynamics is given by an exponential decay with half the rate η, as can be seen also in the low-ξ approximation in Eq. (5). For larger values of ξ, the decay rate approaches η and oscillations start to appear whose amplitudes eventually decrease for even larger values of ξ, where the time evolution converges to the exponential decay of the Markov limit ($\omega_1 \to \infty$). Thus, the non-Markovian features are only present if the approximation $\xi \gg \eta$ breaks down, i. e., if the excited electrons are spectrally close to the band edge, where the characteristic energy scale is given by $\hbar\eta$.

This can easily be understood if another derivation of the Markov limit starting from Eq. (1) is considered. If the assumption of a vanishing memory is made and on the r. h. s. the functions $s_\omega(t')$ are evaluated at $t' = t$, we can first integrate over dt' and then over $d\omega$. Calculating the first interal gives

$$\frac{\partial}{\partial t}s_{\omega_1}(t) = -\frac{\eta}{\pi}\int\limits_0^{\omega_{BZ}} d\omega \frac{\sin[(\omega_1 - \omega)t]}{\omega_1 - \omega}\left[s_{\omega_1}(t) + \frac{1}{4}(s_\omega(t) - s_{\omega_1}(t))\right]. \quad (6)$$

Using again the fact that $\lim_{t\to\infty}\frac{\sin[\Delta\omega t]}{\Delta\omega} \to \pi\delta(\Delta\omega)$, one again ends up with the Markov limit. For finite time t, however, the integral kernel is not yet contracted to a δ-distribution and the finite integral limits cut off tails of the $\frac{\sin[\Delta\omega t]}{\Delta\omega}$ function. This cut-off is particularly significant, if the peak of the integral kernel, which is given by ω_1 is close to one of the integral limits.

Furthermore, it can be seen in Fig. 1(b) that the low-ξ approximation in Eq. (5) yields reasonable results for $\xi = 0.5$ for the initial exponential decay while it fails to reproduce the long-term oscillations.

5. Conclusion

The non-Markovian overshoots and oscillations in the time evolution of the carrier spins in DMS found in a quantum kinetic theory can be reproduced by integro-differential equation of a much simpler form that also simplifies the interpretation considerably. A differential transform method (DTM) is employed to solve the resulting equation and allows to find closed-form expressions for low excitation energies of electrons.

It is found that a non-exponential behaviour of the time evolution of the electron spin is only present for electrons excited close to the band edge, where the decay predicted by the rate and the oscillations with frequency corresponding to the electron energies take place on the same time scale. Technically, this is due to the fact that a sinc-function that converges to a δ-distribution in the Markov limit is cut off by the band edge. It is noteworthy that similar time evolutions have also been found in different setups, e. g., for the hole spin dynamics due to phonon scattering in a GaAs quantum well when the scattering rate is close to the phonon frequency[6].

Acknowledgments

[1] Thurn C and Axt V M 2012 Phys. Rev. B **85** 16520
[2] Thurn C, Cygorek M, Axt V M, and Kuhn T 2013 Phys. Rev. B **87**, 205301.
[3] Thurn C, Cygorek M, Axt V M, and Kuhn T 2013 Phys. Rev. B **88**, 161302
[4] Cygorek M and Axt V M 2014 Semicond. Sci. Technol. **30**, 085011.
[5] Zhou J K 1986 *Differential Transformation and its Applications for Electrical Circuits* (Wuuhahn: Huarjung University Press)
[6] Zhang P and Wu M W 2007 Phys. Rev. B **76**, 193312

Publication 7

Nonperturbative correlation effects in diluted magnetic semiconductors

M. Cygorek, P. I. Tamborenea and V. M. Axt

Phys. Rev B **93**, 035206 (2016)

&

Erratum: Nonperturbative correlation effects in diluted magnetic semiconductors

M. Cygorek, P. I. Tamborenea and V. M. Axt

Phys. Rev. B **94**, 079906 (2016).

Nonperturbative correlation effects in diluted magnetic semiconductors

M. Cygorek,[1] P. I. Tamborenea,[1,2] and V. M. Axt[1]

[1]*Theoretische Physik III, Universität Bayreuth, 95440 Bayreuth, Germany*

[2]*Departamento de Física and IFIBA, FCEN, Universidad de Buenos Aires, Ciudad Universitaria, Pabellón I,*

1428 Ciudad de Buenos Aires, Argentina

(Received 14 September 2015; revised manuscript received 5 November 2015; published 28 January 2016)

The effects of carrier-impurity correlations due to a Kondo-like spin-spin interaction in diluted magnetic semiconductors are investigated. These correlations are not only responsible for a transfer of spins between the carriers and the impurities, but also produce nonperturbative effects in the spin dynamics such as renormalization of the precession frequency of the carrier spins, which can reach values of several percent in CdMnTe quantum wells. In two-dimensional systems, the precession frequency renormalization for a single electron spin with defined wave vector shows logarithmic divergences similar to those also known from the Kondo problem in metals. For smooth electron distributions, however, the divergences disappear due to the integrability of the logarithm. A possible dephasing mechanism caused by the wave-vector dependence of the electron spin precession frequencies is found to be of minor importance compared to the spin transfer from the carrier to the impurity system. In the Markov limit of the theory, an expression for the stationary carrier-impurity correlation energy can be deduced indicating the formation of weakly correlated carrier-impurity states with binding energies in the μeV range.

I. INTRODUCTION

A perturbative treatment of the interaction between quasifree electrons in a metal with localized magnetic impurities predicts logarithmic divergences in several quantities such as resistivity and entropy at zero temperature [1,2]. This finding, the Kondo effect, is a famous example of a situation where perturbation theory leads to unphysical conclusions, whereas the measured values of the resistivity assume finite values. The Kondo problem, i.e., the question of how to properly describe the low-temperature limit of a system with a spin dependent carrier-impurity interaction theoretically, has opened up a wide field of physics. Although the Kondo problem, as it was originally formulated, has been solved [2], the Kondo physics experienced a revival since it has become possible to study experimentally similar problems in other systems, e.g., structures where quantum dots play the role of the magnetic impurities [3–12]. The common feature in these systems is that a microscopic exchange coupling gives rise to an effective Kondo Hamiltonian that assumes the form of a spin-spin contact interaction between the quasifree carriers and the localized magnetic impurities, or quantum dots, respectively.

Other systems which are usually modeled by a Kondo-like Hamiltonian are diluted magnetic semiconductors (DMS) where typically II-VI or III-V semiconductors are doped with magnetic impurities, usually Mn which effectively forms a spin-$\frac{5}{2}$ system. These materials have been studied extensively in the last decades [13–34] due to their optical and magnetic properties which make them promising candidates for future spintronics devices [35–37]. However, quantum mechanical correlations between the carriers and impurities in DMS, which are crucial for the Kondo effect, have so far not been investigated thoroughly, since a vast number of interesting effects, such as collective modes in the coherent spin precession of carriers and impurities [38], carrier mediated RKKY interaction [39] leading to a ferromagnetic order in

DMS [35], and bound or free magnetic polarons [40–47], can already be found using a semiclassical or mean-field approximation, where the carrier-impurity correlations are disregarded. It has been argued in the literature [48] that Kondo-type correlation effects are different in DMS than in magnetically doped metals because in the latter only a few magnetic impurities and a huge number of quasifree carriers are present in the metal, whereas in the former case, in particular in the case of (intrinsic) II-VI DMS, the number of impurities usually exceeds the number of carriers. On the other hand, a third-order many-body perturbation theory based on the pseudofermion formalism [49] reveals Kondo-like divergences in the propagator for the spin dynamics in DMS due to the hole-impurity exchange interaction. From this it was concluded that the carrier-impurity correlations should in fact be important for the dynamics in DMS.

The main goal of the present article is to calculate and discuss the magnitude of the additional effects arising in the description of DMS, when the carrier-impurity correlations are explicitly accounted for. It is assumed that only optically induced spin polarized carriers are present, which interact with magnetic impurities via the *s-d* exchange interaction. This assumption is particularly well met in II-VI DMS like CdMnTe, whereas the correlation effects might be modified in other DMS materials like GaMnAs due to Coulomb effects. We base our study on a microscopic quantum kinetic theory derived by a correlation expansion scheme [50] that is capable of a nonperturbative description of highly nonequilibrium situations. One aspect of the effects of the carrier-impurity correlations on the spin dynamics has already been found in previous works [51–55]: The correlations mediate the transfer of spins between the carriers and the impurities. Since in the Markovian limit the quantum kinetic theory contains the special case of rate equations which can also be derived by a Fermi's golden rule approach [51], this spin transfer can, in fact, be treated perturbatively [56]. Note that in some situations, e.g., for excitations close to the band edge in two-

and lower-dimensional DMS [57], the Markov limit is not a good approximation so that deviations from a golden-rule-like exponential decay are predicted.

In the present study we show that the carrier-impurity correlations are also responsible for another effect in the spin dynamics that is not predicted by a perturbative method: a renormalization of the precession frequency of carrier spins compared with its mean-field value. It is shown that the frequency renormalization contains logarithmic divergences in the Markov limit in two-dimensional systems similar to those known from diluted magnetic metallic alloys [58]. However, here we find that these divergences never lead to unphysical results in the spin dynamics. This is, first of all, due to the fact that the singularities are integrable and yield finite values for a nonsingular spectral electron distribution. Moreover, the divergence in the frequency renormalization is only found for $t \to \infty$ where the amplitude of the precessing electron spin has already decayed to zero. The Markov limit of the quantum kinetic theory also allows to find an expression for the carrier-impurity correlation energy which shows a similar behavior as the frequency renormalization, including Kondo-like logarithmic divergences in the two-dimensional case.

The article is structured as follows: First, the quantum kinetic theory is briefly reviewed as well as effective PESC (*precession of electron spins and correlations*) equations [54] based on the quantum kinetic theory. Then, the frequency renormalization described by the PESC equations is calculated and compared with the result of a Markovian approximation to the PESC equations in two and three dimensions. A possible electron spin dephasing mechanism due to the wave vector dependence of the frequency renormalization is discussed. Finally, we investigate the mean carrier-impurity correlation energy.

II. THEORY

A. System

The Hamiltonian for conduction band electrons in DMS is modeled by

$$H = H_0 + H_{\mathrm{sd}}, \tag{1a}$$

$$H_0 = \sum_{\mathbf{k}\sigma} \hbar\omega_{\mathbf{k}} c^\dagger_{\sigma\mathbf{k}} c_{\sigma\mathbf{k}}, \tag{1b}$$

$$H_{\mathrm{sd}} = \frac{J_{\mathrm{sd}}}{V} \sum_{Inn'\mathbf{k}\mathbf{k}'\sigma\sigma'} \mathbf{S}_{nn'} \cdot \mathbf{s}_{\sigma\sigma'} c^\dagger_{\sigma\mathbf{k}} c_{\sigma'\mathbf{k}'} e^{i(\mathbf{k}'-\mathbf{k})\mathbf{R}_I} \hat{P}^I_{nn'}, \tag{1c}$$

where H_0 describes the band structure and H_{sd} is the Kondo Hamiltonian which originates from the exchange interaction between the s-type conduction band electrons and the d electrons of the magnetic ions. Throughout this article we assume a parabolic band structure with $\omega_{\mathbf{k}} = \frac{\hbar k^2}{2m^*}$, where m^* is the effective mass. J_{sd} and V are the coupling constant and volume of the DMS and $c^\dagger_{\sigma\mathbf{k}}$ and $c_{\sigma\mathbf{k}}$ are the creation and annihilation operators for electrons with spin index σ and wave vector $\mathbf{k}$. $\mathbf{R}_I$ is the position of the Ith magnetic impurity and $\hat{P}^I_{nn'} = |I,n\rangle\langle I,n'|$ are the projection operators corresponding to the spin state of the Ith impurity, e.g., for

spin-$\frac{5}{2}$ Mn impurities, $n = \{-\frac{5}{2}, -\frac{3}{2}, \dots, \frac{5}{2}\}$. $\mathbf{S}_{nn'}$ and $\mathbf{s}_{\sigma\sigma'}$ are the spin matrices for spin-$\frac{5}{2}$ and $\frac{1}{2}$ systems, respectively.

B. Equations of motion

A microscopic quantum kinetic theory based on a correlation expansion scheme was constructed in Ref. [50], where equations of motion have been derived for the electron and impurity density matrices $C^{\sigma_2}_{\sigma_1\mathbf{k}}$ and $M^{n_2}_{n_1}$ as well as their correlations which are defined by

$$C^{\sigma_2}_{\sigma_1\mathbf{k}} = \langle c^\dagger_{\sigma_1\mathbf{k}} c_{\sigma_2\mathbf{k}}\rangle, \tag{2a}$$

$$M^{n_2}_{n_1} = \langle \hat{P}^I_{n_1 n_2}\rangle, \tag{2b}$$

$$Q^{\sigma_2 n_2 \mathbf{k}_2}_{\sigma_1 n_1 \mathbf{k}_1} = V\langle c^\dagger_{\sigma_1\mathbf{k}_1} c_{\sigma_2\mathbf{k}_2} e^{i(\mathbf{k}_2-\mathbf{k}_1)\mathbf{R}_I} \hat{P}^I_{n_1 n_2}\rangle (1 - \delta_{\mathbf{k}_1,\mathbf{k}_2}), \tag{2c}$$

where the brackets denote the quantum mechanical average as well as an average over spatially homogeneously distributed impurities [59]. From the assumption of a homogeneous distribution it also follows that off-diagonal elements of the carrier density matrix with respect to $\mathbf{k}$ average out, so that the electron density matrix in Eq. (2a) can be addressed by a single $\mathbf{k}$ index. The fact that the localized s-d interaction breaks the translational invariance of the system manifests itself in the theory, e.g., in a redistribution of carriers in $\mathbf{k}$ space [50]. The equations of motion for these dynamical variables are given in Ref. [53].

The full quantum kinetic equations are lengthy and their solution requires considerable numerical effort. However, it was found in Ref. [54] that they can be drastically simplified in the case where the number of impurity ions N_{Mn} is much larger than the number of the quasifree electrons N_e. This is usually fulfilled especially in II-VI DMS where the magnetic doping with Mn does not simultaneously lead to p or n doping and the carriers stem exclusively from optical excitation. To understand the effective equations derived in Ref. [54] it is instructive to first consider the mean-field dynamics for the spin $\mathbf{s}_{\mathbf{k}} = \sum_{\sigma_1\sigma_2} \mathbf{s}_{\sigma_1\sigma_2} C^{\sigma_2}_{\sigma_1\mathbf{k}}$ of electrons with wave vector $\mathbf{k}$ and the impurities $\langle\mathbf{S}\rangle = \sum_{n_1 n_2} \mathbf{S}_{n_1 n_2} M^{n_2}_{n_1}$. In the mean-field approximation, i.e., if the correlations are neglected, one finds

$$\frac{\partial}{\partial t}\mathbf{s}_{\mathbf{k}}\bigg|_{\mathrm{MF}} = \boldsymbol{\omega}_M \times \mathbf{s}_{\mathbf{k}}, \tag{3a}$$

$$\frac{\partial}{\partial t}\langle\mathbf{S}\rangle\bigg|_{\mathrm{MF}} = -\frac{1}{N_{\mathrm{Mn}}} \sum_{\mathbf{k}} \frac{\partial}{\partial t}\mathbf{s}_{\mathbf{k}}\bigg|_{\mathrm{MF}}, \tag{3b}$$

where $\boldsymbol{\omega}_M := \frac{J_{\mathrm{sd}}}{\hbar} n_{\mathrm{Mn}} \langle\mathbf{S}\rangle$. Equation (3b) follows from the total spin conservation of the Kondo Hamiltonian. In the case $N_{\mathrm{Mn}} \gg N_e$, the change of the impurity spin is marginal and can therefore be neglected. The precession of the electron spin around the mean field due to the impurity magnetization, on the other hand, is in general important. Equation (3a) is solved by

$$\mathbf{s}_{\mathbf{k}} = R_{\langle\mathbf{S}\rangle}(\omega_M t)\mathbf{s}'_{\mathbf{k}}, \tag{4}$$

where $R_{\mathbf{n}}(\alpha)$ is the matrix describing a rotation around the vector $\mathbf{n}$ with angle α and the precession frequency $\omega_M = \boldsymbol{\omega}_M \cdot \langle\mathbf{S}\rangle/|\langle\mathbf{S}\rangle|$ is defined so that it has the same sign as the coupling constant J_{sd}. In the mean-field approximation $\mathbf{s}'_{\mathbf{k}}$ is

constant. However, if we also account for the carrier-impurity correlations, $\mathbf{s}'_{\mathbf{k}}$ changes slowly in time and constitutes the electron spin in a rotating frame. If the correlations are formally integrated and inserted into the corresponding equations of motion for the electron variables, the effective equations for the electron spin component $\mathbf{s}'^{\perp}_{\mathbf{k}_1}$ perpendicular to the impurity magnetization can be given as [54]

$$
\begin{aligned}
\frac{\partial}{\partial t}\mathbf{s}'^{\perp}_{\mathbf{k}_1} = & -\sum_{\mathbf{k}}\Bigg[\mathrm{Re}\big(G^{\omega_{\mathbf{k}_1}-\omega_M}_{\omega_{\mathbf{k}}}\big)\Big(\frac{b^+}{2}-b^0 n^{\uparrow}_{\mathbf{k}}\Big)\mathbf{s}'^{\perp}_{\mathbf{k}_1} \\
& + \mathrm{Re}\big(G^{\omega_{\mathbf{k}_1}+\omega_M}_{\omega_{\mathbf{k}}}\big)\Big(\frac{b^-}{2}+b^0 n^{\downarrow}_{\mathbf{k}}\Big)\mathbf{s}'^{\perp}_{\mathbf{k}_1} \\
& + \mathrm{Re}\big(G^{\omega_{\mathbf{k}_1}}_{\omega_{\mathbf{k}}}\big)\frac{b^{\|}}{2}\big(\mathbf{s}'^{\perp}_{\mathbf{k}}+\mathbf{s}'^{\perp}_{\mathbf{k}_1}\big)\Bigg] \\
& -\frac{\langle \mathbf{S}\rangle}{|\langle \mathbf{S}\rangle|}\sum_{\mathbf{k}}\Bigg[\mathrm{Im}\big(G^{\omega_{\mathbf{k}_1}-\omega_M}_{\omega_{\mathbf{k}}}\big)\Big(\frac{b^+}{2}-b^0 n^{\uparrow}_{\mathbf{k}}\Big) \\
& -\mathrm{Im}\big(G^{\omega_{\mathbf{k}_1}+\omega_M}_{\omega_{\mathbf{k}}}\big)\Big(\frac{b^-}{2}+b^0 n^{\downarrow}_{\mathbf{k}}\Big)\Bigg]\mathbf{s}'^{\perp}_{\mathbf{k}_1}.
\end{aligned}
\tag{5}
$$

The coefficients in Eq. (5) are given by $b^{\pm} := \langle S^{\perp 2}\rangle \pm \frac{\langle S^{\|}\rangle}{2}$, $b^0 := \frac{\langle S^{\|}\rangle}{2}$, and $b^{\|} := \langle S^{\|2}\rangle$, where the component of the impurity spin operator in the direction of the mean impurity spin is $S^{\|} := \hat{\mathbf{S}}\cdot\frac{\langle\hat{\mathbf{S}}\rangle}{|\langle\hat{\mathbf{S}}\rangle|}$, and the relevant second moments of the impurity spin operator can be separated into parallel $\langle S^{\|2}\rangle$ and perpendicular parts $\langle S^{\perp 2}\rangle = \frac{1}{2}\langle S^2 - S^{\|2}\rangle$. The memory function

$$
G^{\omega_{\mathbf{k}_1}}_{\omega_{\mathbf{k}}} := \frac{J^2_{\mathrm{sd}}}{\hbar^2}\frac{n_{\mathrm{Mn}}}{V}\int_{-t}^0 dt'\, e^{i(\omega_{\mathbf{k}}-\omega_{\mathbf{k}_1}t')}
\tag{6}
$$

has to be interpreted as an integral operator and the time-dependent variables that appear after $G^{\omega_{\mathbf{k}_1}}_{\omega_{\mathbf{k}}}$ in Eq. (5) are evaluated at t'. Finally, $n^{\uparrow/\downarrow}_{\mathbf{k}}$ are the occupation numbers of the states with wave-vector $\mathbf{k}$, i.e., the diagonal elements of the density matrix with respect to the spin indices. Equation (5) together with the corresponding equations for $n^{\uparrow/\downarrow}_{\mathbf{k}}$ given in Ref. [54] are called precession of electron spins and correlations (PESC) equations, since besides the electron spins, also the correlations $Q^{\alpha\mathbf{k}_2}_{\beta\mathbf{k}_1} := \sum_{\sigma_1\sigma_2}\sum_{n_1 n_2}\mathbf{s}_{\sigma_1\sigma_2}\cdot\mathbf{S}_{n_1 n_2}Q^{\sigma_2 n_2\mathbf{k}_2}_{\sigma_1 n_1\mathbf{k}_1}$ exhibit a precessionlike movement around the mean field due to the impurity magnetization. Note that Eq. (5) is equivalent to the full quantum kinetic theory of Ref. [50] except that some source terms for the correlations are neglected that are numerically insignificant (cf. Ref. [54] for details).

Equation (5) is only complicated and numerically challenging due to the time integral induced by the memory function $G^{\omega_{\mathbf{k}_1}}_{\omega_{\mathbf{k}}}$. Now, working in the rotating frame allows us to assume that the electron variables change only slowly in time and can equally well be evaluated at t instead of t'. The memory integral consists then only of

$$
\int_{-t}^0 dt'\, e^{i(\omega_{\mathbf{k}}-\omega_{\mathbf{k}_1})t'} \approx \pi\delta(\omega_{\mathbf{k}}-\omega_{\mathbf{k}_1}) - i\mathcal{P}\frac{1}{\omega_{\mathbf{k}}-\omega_{\mathbf{k}_1}},
\tag{7}
$$

where $\mathcal{P}$ is the Cauchy principal value. The Markov approximation (7) was established by letting $t \to \infty$ in the lower

limit of the integral and using the Sokhotski-Plemelj theorem. The validity of the Markovian approximation can in general depend on the values of $\mathbf{k}$, $\mathbf{k}_1$, t as well as the time scale of the change of the electron variables and therefore has to be checked numerically.

If only the real part of the memory function is used in Markov approximation and the imaginary part is neglected, the PESC equations assume a golden-rule-type form, where the spin transfer dynamics follows approximately an exponential decay to the equilibrium value with rate

$$
(\tau_{\perp})^{-1} \approx \frac{J^2_{\mathrm{sd}} n_{\mathrm{Mn}}}{\hbar^2 V}\pi\Bigg[D(\omega_1-\omega_M)\frac{b^+}{2} + D(\omega_1+\omega_M)\frac{b^-}{2} + D(\omega_1)b^{\|}\Bigg]
\tag{8}
$$

for an electron with kinetic energy ω_1, if the terms of second order of the electron variables in Eq. (5) are neglected [54]. In the expression for the rate, $D(\omega)$ describes the spectral density of states and depends on the dimensionality of the system.

C. Frequency renormalization in the Markov limit

One issue that we would like to focus on in the present work is the change in the precession frequency described in Eq. (5) by the terms proportional to the imaginary part of the memory function. Such a renormalization of the precession frequency would be absent in any truncated perturbative approach [60]. It originates, like the spin transfer described by the real part of the memory function, from the carrier-impurity correlations.

It is noteworthy that the frequency renormalization is singular in the Markov limit described in Eq. (7), i.e., the imaginary part of the memory function $G^{\omega_{\mathbf{k}_1}}_{\omega_{\mathbf{k}}}$ diverges if $\omega_{\mathbf{k}} = \omega_{\mathbf{k}_1}$. However, this divergence does not lead to an unphysical behavior. First of all, the divergence is a feature of the Markovian limit. For finite times t, the left-hand side of Eq. (7) is a finite integral over an analytic function and is therefore itself analytic. For $\omega_{\mathbf{k}} = \omega_{\mathbf{k}_1}$, the value of the integral is t which only goes to infinity in the Markov limit. As only the electron spin component perpendicular to the impurity magnetization is affected by the frequency renormalization and this component decays approximately exponentially to zero, an infinite precession frequency is never observable.

Similar to the Markovian spin transfer rate in Eq. (8), an expression for the frequency renormalization $\Delta\omega$ can be given in the Markov limit of Eq. (5), if the imaginary part of Eq. (7) is used:

$$
\begin{aligned}
\Delta\omega(\omega_1) = & \frac{J^2_{\mathrm{sd}}}{\hbar^2}\frac{n_{\mathrm{Mn}}}{V}\int_0^{\omega_{\mathrm{BZ}}} d\omega\, D(\omega) \\
& \times\Bigg[\frac{b^+}{2}\frac{1}{\omega-(\omega_1-\omega_M)} - \frac{b^-}{2}\frac{1}{\omega-(\omega_1+\omega_M)}\Bigg],
\end{aligned}
\tag{9}
$$

where, for the sake of simplicity, the terms proportional to $n^{\uparrow/\downarrow}$ in Eq. (5) were neglected, since they only matter if a large number of carriers is present. In two-dimensional systems, the spectral density of states $D^{\mathrm{2D}}(\omega) = \frac{Am^*}{2\pi\hbar}\Theta(\omega)$ is constant, where A is the sample area and $\Theta(x)$ is the step function. In three dimensions, $D^{\mathrm{3D}}(\omega) = \frac{V}{4\pi^2}\big(\frac{2m^*}{\hbar}\big)^{3/2}\sqrt{\omega}\,\Theta(\omega)$ is propor-

tional to the square root of ω. The corresponding frequency renormalizations are

$$\Delta\omega^{2D}(\omega_1) = -\frac{J_{sd}^2}{\hbar^2}\frac{n_{Mn}}{d}\frac{m^*}{2\pi\hbar}\left\{\frac{b^+}{2}\ln\left|\frac{\omega_1-\omega_M}{\omega_{BZ}-(\omega_1-\omega_M)}\right|\right.$$

$$\left.-\frac{b^-}{2}\ln\left|\frac{\omega_1+\omega_M}{\omega_{BZ}-(\omega_1+\omega_M)}\right|\right\}, \quad (10a)$$

where $d = V/A$ is the quantum well width, and

$$\Delta\omega^{3D}(\omega_1) = \frac{J_{sd}^2}{\hbar^2}\frac{n_{Mn}}{4\pi}\left(\frac{2m^*}{\hbar}\right)^{3/2}\int_0^{\omega_{BZ}}d\omega$$

$$\times\left\{\frac{b^+}{2}\frac{\sqrt{\omega}}{\omega-(\omega_1-\omega_M)}-\frac{b^-}{2}\frac{\sqrt{\omega}}{\omega-(\omega_1+\omega_M)}\right\}, \quad (10b)$$

with

$$\int_0^{\omega_{BZ}}d\omega\frac{\sqrt{\omega}}{\omega-\omega_0}$$

$$=\begin{cases}2\sqrt{\omega_{BZ}}-\sqrt{\omega_0}\ln\left|\frac{\omega_0+\omega_{BZ}}{\omega_0-\omega_{BZ}}\right|, & \omega_0 > 0,\\ 2\sqrt{\omega_{BZ}}-2\sqrt{|\omega_0|}\tan^{-1}\left(\frac{\omega_{BZ}}{|\omega_0|}\right), & \omega_0 < 0.\end{cases} \quad (10c)$$

It should be noted that in two and three dimensions the frequency renormalization depends explicitly on the frequency ω_{BZ}, which corresponds to the energy at the end of the first Brillouin zone, and diverges in the limit $\omega_{BZ}\to\infty$. For typical pump-probe experiments with diluted magnetic semiconductors, carriers are optically excited relatively close to the band edge. For the excited electrons, one can safely assume $\omega_1\pm\omega_M\ll\omega_{BZ}$. In this case, we find a logarithmic dependence on ω_{BZ} in the two-dimensional frequency renormalization.

With the same assumption also the integral in Eq. (10c) for the three-dimensional renormalization can be simplified to

$$\int_0^{\omega_{BZ}}d\omega\frac{\sqrt{\omega}}{\omega-\omega_0}\approx 2\sqrt{\omega_{BZ}}-\pi\sqrt{|\omega_0|}\Theta(-\omega_0). \quad (11)$$

Thus, we find a square-root dependence of the frequency renormalization on the cut-off frequency ω_{BZ}, as well as a square-root dependence on $\omega_0 = \omega_1\pm\omega_M$ which only contributes if ω_0 is negative.

The divergence in the limit $\omega_{BZ}\to\infty$ is similar to the metallic Kondo effect where the divergence in the resistivity is also logarithmic in the bandwidth [2]. An effective spin-dependent Hamiltonian leading to a carrier spin precession which diverges logarithmically with the bandwidth has also been derived in Ref. [58] in the formulation a theory of spin resonance in diluted magnetic metallic alloys which is based on a Kadanoff-Baym-like gradient expansion combined with a Markovian approximation and the assumption of a thermal electron distribution. The fact that the metallic problem resembles rather the two-dimensional than the three-dimensional case in DMS originates from both systems being modeled by a constant density of states.

It is noteworthy that the divergence of the frequency renormalization at $\omega_0 = \omega_1\pm\omega_M$ vanishes in the three-dimensional

case due to the integral over the density of states. In two-dimensional systems, a diverging frequency renormalization remains, but only for electrons with a unique value of the kinetic energy. For realistic optical excitation, however, a smooth spectral electron distribution can be expected so that the change of the total precession frequency comprises an averaging over frequency renormalizations of nearby states. Since the logarithmic divergence is integrable, the total frequency renormalization remains finite.

III. NUMERICAL CALCULATIONS

In order to check the validity of the Markov approximation for the renormalization of the precession frequency of the electrons, we compare the Markov result with calculations, where the memory is taken into account explicitly. It seems straightforward to use Eq. (5) with the time-integral operator $G_{\omega_\mathbf{k}}^{\omega_{\mathbf{k}_1}}$ defined in Eq. (6) and solve the integrodifferential equations numerically. This is, however, a very challenging problem for the following reasons.

From the Markovian expression for the frequency renormalization, we find the explicit dependence on the value of the cut-off energy $\hbar\omega_{BZ}$. Therefore, also oscillations with frequencies close to ω_{BZ} have to be resolved, which are on the time scale of a few femtoseconds since $\hbar\omega_{BZ}$ is in the eV range. On the other hand, relevant changes of the total electron spin takes place in the 10–100 ps range. Furthermore, for each time step the calculation of each $s_{\mathbf{k}_1}'^{\perp}$ requires a sum over all possible $\mathbf{k}$ states so that the problem has the complexity $O(N_k^2)$, where N_k is the number of discretization points for the k space. Note that also in $\mathbf{k}$ space, the details of excitations close to the band edge in the meV range as well as the full Brillouin zone up to energies of a few eV have to be resolved. Such a problem also arises in the metallic Kondo effect where numerical procedures, such as the famous renormalization group [61], have been developed to deal with the large value of the bandwidth [2]. Note that solving the integrodifferential equation by finding an auxiliary variable, so that the problem can be transformed into an ordinary differential equation, is equivalent to using the original quantum kinetic theory [54].

Here we solve this problem by using approximations that allow a separation of electron spins with different wave vectors, so that we find a $O(N_k)$ problem for an individual electron with wave vector $\mathbf{k}_1$. First of all, it is noteworthy that $s_{\mathbf{k}_1}'^{\perp}$ in Eq. (5) couples to the occupations $n_\mathbf{k}^{\uparrow/\downarrow}$ of states with different wave vectors $\mathbf{k}$. These terms, however, are of second order in electron variables and have a marginal effect on the dynamics of the perpendicular spin component [54], especially if the electron density is small, as is usually the case for optically excited carriers. Neglecting these terms, we can formulate equations of motion for the complex perpendicular electron spin variable (in the rotating frame):

$$s_{\mathbf{k}_1}' := s_{\mathbf{k}_1}'^x + i s_{\mathbf{k}_1}'^y, \quad (12)$$

where it is assumed that the impurity magnetization points in the z direction. Then, the PESC-equations (5) assume the

form

$$\frac{\partial}{\partial t} s'_{\mathbf{k}_1}(t) = -\frac{J_{sd}^2}{\hbar^2} \frac{n_{Mn}}{V} \sum_{\mathbf{k}} \int_0^t dt'$$

$$\times \left\{ \frac{b^+}{2} e^{i[\omega_{\mathbf{k}} - (\omega_{\mathbf{k}_1} - \omega_M)](t'-t)} s'_{\mathbf{k}_1}(t') \right.$$

$$+ \frac{b^-}{2} e^{-i[\omega_{\mathbf{k}} - (\omega_{\mathbf{k}_1} + \omega_M)](t'-t)} s'_{\mathbf{k}_1}(t')$$

$$\left. + \frac{b^\parallel}{2} \cos\left[(\omega_{\mathbf{k}} - \omega_{\mathbf{k}_1})(t'-t)\right] \left[s'_{\mathbf{k}}(t') + s'_{\mathbf{k}_1}(t')\right] \right\}. \tag{13}$$

It can be seen immediately from Eq. (13) that in the equation for $s'_{\mathbf{k}_1}$, electron variables of states with other wave vectors only enter in the last term, i.e., the term proportional to $s'_{\mathbf{k}}(t') + s'_{\mathbf{k}_1}(t')$. Note that a time integration of $\cos[(\omega_{\mathbf{k}} - \omega_{\mathbf{k}_1})(t'-t)]$ yields $\frac{\sin[(\omega_{\mathbf{k}} - \omega_{\mathbf{k}_1})t]}{(\omega_{\mathbf{k}} - \omega_{\mathbf{k}_1})t}$ which has a pronounced peak at $\omega_{\mathbf{k}} = \omega_{\mathbf{k}_1}$. Thus, if the electron spin distribution is assumed to be a smooth function in $\mathbf{k}$ space, the main contribution of the last term in Eq. (13) will be approximately the same if we set

$$s'_{\mathbf{k}}(t') \approx s'_{\mathbf{k}_1}(t'). \tag{14}$$

This approximation was shown to reproduce the non-Markovian features of the spin transfer in Ref. [57]. Also, in contrast to the other terms, the last term of Eq. (13), where the approximation is used, does not influence the frequency renormalization, due to the absence of an imaginary part of the oscillating prefactor $\cos[(\omega_{\mathbf{k}} - \omega_{\mathbf{k}_1})(t'-t)]$. Now, with the help of approximation (14), we end up with completely decoupled equations for the spins $s'_{\mathbf{k}_1}$ of electrons with different wave vectors $\mathbf{k}_1$.

Finally, it is useful for the numerical solution of the integrodifferential equation (13) to transform it into an ordinary differential equation using auxiliary variables $G^j_{\mathbf{k}_1 \mathbf{k}}$:

$$\frac{\partial}{\partial t} s'_{\mathbf{k}_1} = -\frac{J_{sd}^2}{\hbar^2} \frac{n_{Mn}}{V} \sum_{j=1}^4 \sum_{\mathbf{k}} D(\mathbf{k}) G^j_{\mathbf{k}_1 \mathbf{k}}, \tag{15a}$$

$$\frac{\partial}{\partial t} G^j_{\mathbf{k}_1 \mathbf{k}} = \sigma_j i \left(\omega_{\mathbf{k}} - \omega_{\mathbf{k}_1} + \chi_j \omega_M\right) G^j_{\mathbf{k}_1 \mathbf{k}} + \frac{b_j}{2} s'_{\mathbf{k}_1}, \tag{15b}$$

with

$$\sigma_j = \{1, -1, 1, -1\}, \tag{15c}$$

$$\chi_j = \{1, -1, 0, 0\}, \tag{15d}$$

$$b_j = \{b^+, b^-, b^\parallel, b^\parallel\}, \tag{15e}$$

and initial conditions $G^j_{\mathbf{k}_1 \mathbf{k}} = 0$ for $t = 0$. This reflects the fact that before the preparation (e.g., optical excitation) there are no free carriers available and therefore the carrier-impurity correlations should initially be zero. Calculating the dynamics of a single electron spin using Eqs. (15) has the complexity $O(N_k)$ and can be done without the need for a numerical renormalization group procedure.

IV. RESULTS FOR THE FREQUENCY RENORMALIZATION

The parameters used for the numerical calculations describe a $Cd_{0.93}Mn_{0.07}Te$ sample with coupling constant $J_{sd} = -15$ meV nm^3, effective mass $m^* = 0.093 m_0$ [62], where m_0 is the free electron mass, and, in the case of a two-dimensional system, a quantum well width of $d = 5$ nm. The cut-off energy was taken to be $\hbar\omega_{BZ} = 3$ eV. The initial impurity magnetization was modeled to be thermally distributed and is therefore completely defined by the mean value $\langle S^\parallel \rangle \in [-\frac{5}{2}; \frac{5}{2}]$.

We assume that electrons have been spin selectively prepared by optical excitation with circularly polarized light so that the initial electron spin is perpendicular to the initial impurity magnetization (Voigt geometry). Equations (15) are used to calculate the finite-memory spin dynamics for electrons with a defined wave vector k_1 or, equivalently, kinetic energy $\hbar\omega_1 = \frac{\hbar^2 k_1^2}{2m^*}$. An exponentially decaying cosine

$$s'^x_{\omega_1}(t) \approx s'^x_{\omega_1}(0) e^{-t/\tau_\perp} \cos(\omega'_M t) \tag{16}$$

is fit to the non-Markovian spin dynamics in order to find a value for the effective decay rate $\tau_\perp^{-1}(\omega_1)$ and the precession frequency $\omega'_M(\omega_1)$. The relative renormalization of the precession frequency is given by $\frac{\Delta\omega}{\omega_M}$ with $\Delta\omega = \omega'_M - \omega_M$.

Figure 1 shows the relative frequency renormalization obtained from a fit to the non-Markovian calculation and the corresponding Markovian result for a δ-like initial spectral electron distribution as a function of the kinetic energy $\hbar\omega_1$. First of all, it can be seen that in three-dimensional as well as in two-dimensional systems the Markovian and non-Markovian results coincide. In the three-dimensional case, the square-root energy dependence of the renormalization for $\omega_1 < \omega_M$ can
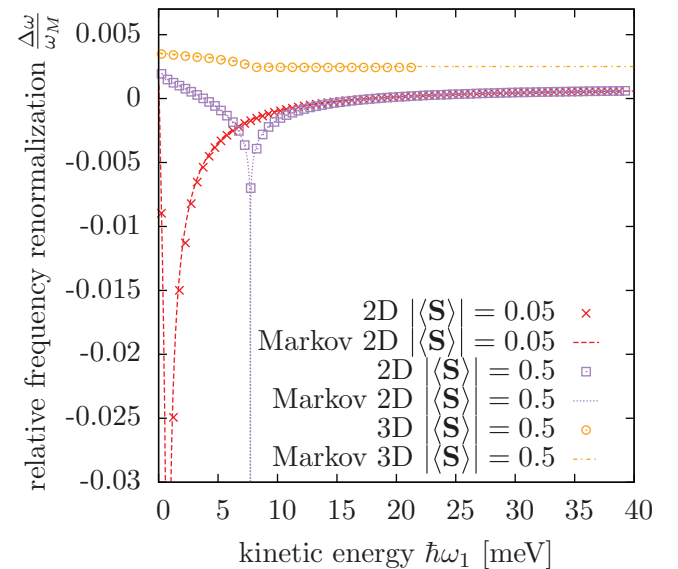

FIG. 1. Dependence of the relative frequency renormalization $\frac{\Delta\omega}{\omega_m}$ on the kinetic electron energy for two- and three-dimensional systems according to the calculation including a finite memory [Eqs. (15)] (points) and in the Markov limit [Eqs. (10)] (lines) for different values of the average impurity spin $|\langle \mathbf{S} \rangle|$ (in units of $\hbar$).
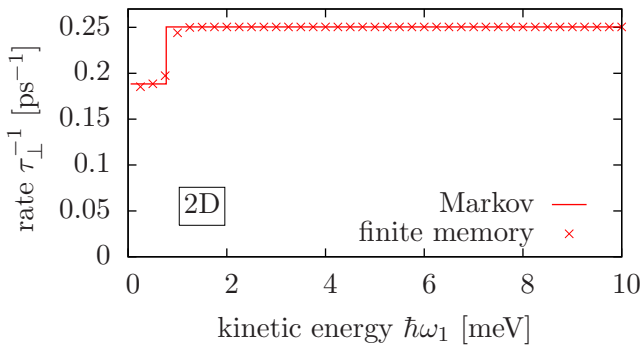
FIG. 2. Spin transfer rate $\tau_\perp^{-1}$ in Markov approximation (line) according to Eq. (8) and exponential fit to the calculation including a finite memory (crosses) using Eqs. (15) for $|\langle \mathbf{S} \rangle| = 0.05$ in a two-dimensional system.

be seen clearly, while in two dimensions, the logarithmic divergence at $\omega_1 = \omega_M$ is apparent. The positive relative frequency renormalization in three dimensions describes an increase in the modulus of the precession frequency. In two dimensions, the slightly positive background of the renormalization is overcompensated by a negative value in the region around the divergence.

In Fig. 2 the spin transfer rate according to the Markov approximation is compared with the value obtained by the exponential fit to the non-Markovian result for a calculation with $|\langle \mathbf{S} \rangle| = 0.05$ in two dimensions. The step in the rate $\tau_\perp^{-1}$ at $\omega_1 = \omega_M$, which is predicted in the Markov limit [cf. Eq. (8)], is found to be slightly rounded off in the non-Markovian calculation, but the deviations between both results are rather small.

In order to find an estimate for the strength of the change of the precession frequency for a more realistic electron distribution, Fig. 3 shows the relative precession frequency renormalization as a function of the average impurity spin where the initial spectral electron distribution [cf. inset of Fig. 3] was assumed to be Gaussian with center at $E_c = \hbar\omega_M$ and standard deviation $E_s = 1$ meV (0.1 meV) corresponding to a full width at half maximum (FWHM) of ≈ 2.35 meV (0.235 meV) or a Gaussian envelope of an exciting laser pulse with a duration (FWHM) of ≈ 140 fs (1.4 ps). The calculations for Fig. 3 were performed using the 2D Markovian expression for the rates in Eq. (8) and the renormalized precession frequencies in Eq. (10a). It can be seen that the magnitude of the frequency renormalization can reach values of several percent of the mean-field precession frequency and is negative for small values of $|\langle \mathbf{S} \rangle|$. For larger values of the impurity magnetization, the frequency renormalization approaches a small positive value. One could expect that the narrower electron distribution ($E_s = 0.1$ meV) is closer to the δ-like case than the wider distribution ($E_s = 1$ meV) and therefore the frequency renormalization should be more pronounced. However, it can be seen from Fig. 3 that this is only the case for very low values of $|\langle \mathbf{S} \rangle|$ (below 0.01 in the case studied here). For higher values of the impurity magnetization, the relative frequency renormalization approaches the positive background much faster in the calculations with the narrower electron distribution.
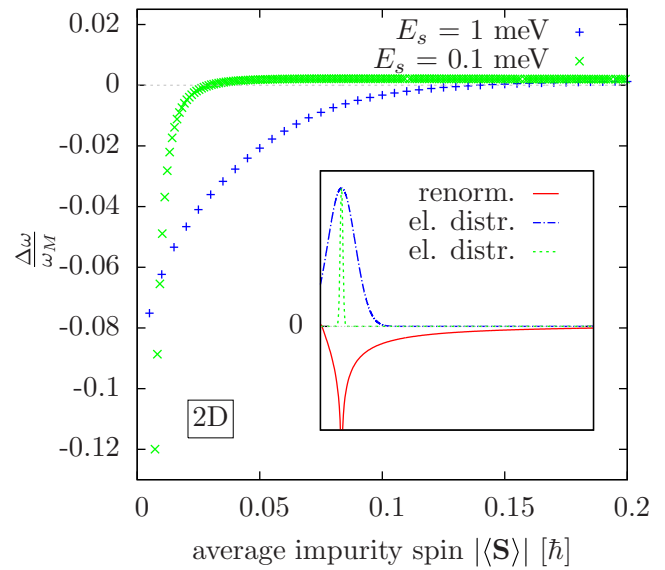

FIG. 3. Relative frequency renormalization $\frac{\Delta\omega}{\omega_M}$ in a two-dimensional system for a Gaussian spectral electron distribution centered at $E_c = \hbar\omega_M$ with standard deviations of $E_s = 1$ meV and $E_s = 0.1$ meV, respectively. The initial electron distribution as a function of the kinetic energy is visualized in the inset as the blue dash-dotted line ($E_s = 1$ meV) and green dotted line ($E_s = 0.1$ meV) together with the corresponding frequency renormalization for δ-like excitations (red line) for $|\langle \mathbf{S} \rangle| = 0.05$.

Note that in order to be able to measure or fit a precession frequency, at least one period of the oscillations should be visible before the spin polarization is decayed. Thus, the minimal value of the impurity magnetization, where one can reasonably deduce a precession frequency from the time evolution of the spin polarization, is given by $|\omega_M| \gtrsim \tau_\perp^{-1}$ which yields, for the parameters above, $|\langle \mathbf{S} \rangle| \gtrsim 0.01$. Therefore, we find that short laser pulses with pulse durations of the order of 100 fs provide the most promising configuration for experiments to measure the frequency renormalization. Under these conditions the precession frequency of the average spin could be directly measured, e.g., by time-resolved Kerr or Faraday rotation. According to our results, the precession frequency should be reduced by about a few percent compared with the mean-field value. We note in passing that Ref. [63] reported a measured enhancement of the spin transfer rates by roughly a factor of 5 compared with the value predicted theoretically for free carriers. This increase can be attributed to the excitation of excitons which implies that the total exciton mass replaces the effective electron mass m^* in the density of states [31,64]. While an explicit simulation involving excitonic effects is out of the scope of the present paper, a similar enhancement of the frequency renormalization should be expected recalling that also the latter is proportional to the density of states.

Since the frequency renormalization depends on the kinetic energy and therefore the wave vector of an electron, the question arises, whether this dependence leads to a dephasing of spins of electrons with different $\mathbf{k}$ vectors. To address this question, we show in Fig. 4 the value of the rate $\tau_\perp^{-1}$ obtained by an exponential fit to the time evolution of the total carrier spin polarization, where the same Gaussian initial
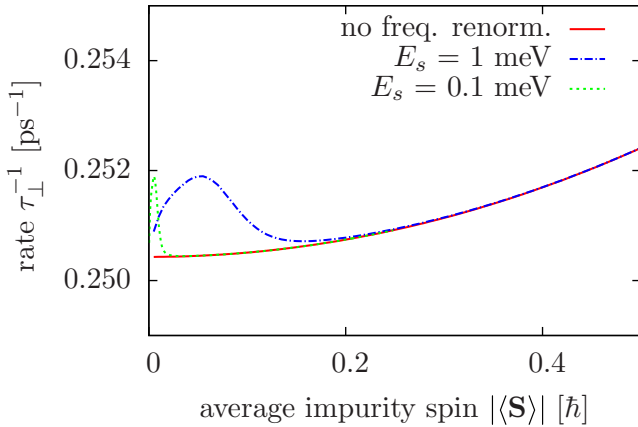
FIG. 4. Rate $\tau_\perp^{-1}$ obtained from an exponential fit for Gaussian initial spectral electron distributions (cf. Fig. 3) as a function of the average impurity spin with (blue dash-dotted line/green dotted line) and without (red solid line) accounting for a renormalization of the precession frequency.

electron distributions are used as in Fig. 3. It can be seen that calculations, where the correlation induced frequency renormalization is neglected, produce very similar decay rates as calculations that account for this renormalization for most of the possible values of the impurity magnetization. Only in a regime where the impurity spin is small we find a slightly larger value ($\lesssim 1\%$) of the rate at $|\langle \mathbf{S} \rangle| \approx 0.05$ for $E_s = 1$ meV and $|\langle \mathbf{S} \rangle| \approx 0.005$ for $E_s = 0.1$ meV. This increasing decay is the consequence of the dephasing of electron spins due to

the $\mathbf{k}$ dependence of the frequency renormalization. Since the expression for the rate in the Markov limit [cf. Eq. (8)] and the frequency renormalization [cf. Eq. (10a)] depend on the same parameters, this dephasing mechanism is always accompanied by a genuine spin transfer between impurities and carriers that is typically much faster than the dephasing itself.

V. CORRELATION ENERGY

Most studies on DMS which probe the energies of electrons in DMS use the mean-field approximation [24] and describe the effects of the impurity magnetization as a renormalization of the electron g factor which is known as the giant Zeeman effect [65]. If, however, the buildup of carrier-impurity correlations is taken into account, the mean s-d exchange interaction energy $\langle H_{\mathrm{sd}} \rangle$ will deviate from the mean-field value. The correlation energy can, in principle, have an impact on the thermodynamic properties of DMS which could help, e.g., in the description of the paramagnetic-ferromagnetic phase transition in GaMnAs.

Since the derivation of the PESC-equations in Ref. [54] required finding explicit expressions for the correlations, we can use this theory to get the correlation induced correction $\langle H_{\mathrm{sd}}^{\mathrm{cor}} \rangle$ to the mean-field exchange interaction energy analytically:

$$\langle H_{\mathrm{sd}} \rangle = \frac{J_{\mathrm{sd}}}{V} \sum_{\substack{Inn' \\ \sigma\sigma'\mathbf{kk'}}} \mathbf{S}_{nn'} \mathbf{s}_{\sigma\sigma'} \langle c_{\sigma\mathbf{k}}^\dagger c_{\sigma'\mathbf{k'}} e^{i(\mathbf{k'}-\mathbf{k})\mathbf{R}_I} \hat{P}_{nn'}^I \rangle$$

$$=: \sum_{\mathbf{k}} \hbar \boldsymbol{\omega}_M \cdot \mathbf{s}_{\mathbf{k}} + \langle H_{\mathrm{sd}}^{\mathrm{cor}} \rangle. \tag{17}$$

Using the time-integral form of the correlations from Ref. [54] we find

$$\langle H_{\mathrm{sd}}^{\mathrm{cor}} \rangle = \frac{J_{\mathrm{sd}}}{V} n_{\mathrm{Mn}} \sum_{\mathbf{kk'}} \sum_{\alpha=1}^{3} Q_{\alpha\mathbf{k}}^{\alpha\mathbf{k'}} = -\hbar \sum_{\mathbf{k}_1\mathbf{k}_2} \left(\mathrm{Im}\{G_{\omega_{\mathbf{k}_2}}^{\omega_{\mathbf{k}_1}+\omega_M}\} \left[\frac{b^+}{2} n_{\mathbf{k}_2}^\downarrow - \frac{b^-}{2} n_{\mathbf{k}_1}^\uparrow - \frac{b^0}{2} \left(n_{\mathbf{k}_1}^\uparrow n_{\mathbf{k}_2}^\downarrow + n_{\mathbf{k}_2}^\uparrow n_{\mathbf{k}_1}^\downarrow \right) \right] \right.$$

$$\left. + \mathrm{Im}\{G_{\omega_{\mathbf{k}_2}}^{\omega_{\mathbf{k}_1}-\omega_M}\} \left[\frac{b^-}{2} n_{\mathbf{k}_2}^\uparrow - \frac{b^+}{2} n_{\mathbf{k}_1}^\downarrow + \frac{b^0}{2} \left(n_{\mathbf{k}_1}^\uparrow n_{\mathbf{k}_2}^\downarrow + n_{\mathbf{k}_2}^\uparrow n_{\mathbf{k}_1}^\downarrow \right) \right] + \mathrm{Im}\{G_{\omega_{\mathbf{k}_2}}^{\omega_{\mathbf{k}_1}}\} \left\{ \frac{b^\parallel}{4} \left[\left(n_{\mathbf{k}_2}^\uparrow + n_{\mathbf{k}_2}^\downarrow \right) - \left(n_{\mathbf{k}_1}^\uparrow + n_{\mathbf{k}_1}^\downarrow \right) \right] \right\} \right). \tag{18}$$

To understand Eq. (18) it is important to recall that the correlations typically build up on the time scale of a few femtosecond [57], while the spin-up and spin-down occupations change on a picosecond time scale [51,54]. Thus, $\langle H_{\mathrm{sd}}^{\mathrm{cor}} \rangle$ is the stationary value of the correlation energy for given values of adiabatically changing occupations $n_{\mathbf{k}_1}^{\uparrow/\downarrow}$.

As in the discussion of the frequency renormalization, we neglect terms of second order in the electron variables and apply the Markov approximation to find for the two-dimensional case

$$\langle H_{\mathrm{sd}}^{\mathrm{cor}} \rangle \approx -\frac{J_{\mathrm{sd}}^2}{\hbar} \frac{n_{\mathrm{Mn}}}{V} \frac{Am^*}{2\pi\hbar} \sum_{\mathbf{k}_1} \left\{ \ln \left| \frac{\omega_{\mathrm{BZ}} - (\omega_{\mathbf{k}_1}+\omega_M)}{\omega_{\mathbf{k}_1}+\omega_M} \right| b^- n_{\mathbf{k}_1}^\uparrow + \ln \left| \frac{\omega_{\mathrm{BZ}} - (\omega_{\mathbf{k}_1}-\omega_M)}{\omega_{\mathbf{k}_1}-\omega_M} \right| b^+ n_{\mathbf{k}_1}^\downarrow + \ln \left| \frac{\omega_{\mathrm{BZ}}-\omega_{\mathbf{k}_1}}{\omega_{\mathbf{k}_1}} \right| \frac{b^\parallel}{2} \left(n_{\mathbf{k}_1}^\uparrow + n_{\mathbf{k}_1}^\downarrow \right) \right\}. \tag{19}$$

The mathematical structure of the correlation energy $\langle H_{\mathrm{sd}}^{\mathrm{cor}} \rangle$ in Eq. (19) is very similar to that of the frequency renormalization in Eq. (9). To see this relation, it is helpful to express the occupations $n_{\mathbf{k}_1}^{\uparrow/\downarrow}$ of the spin-up and spin-down subbands in terms of the occupation $n_{\mathbf{k}_1}$ of both bands and the spin component $s_{\mathbf{k}_1}^\parallel$ parallel to the impurity magnetization

(quantization axis) via

$$n_{\mathbf{k}_1}^{\uparrow/\downarrow} = \frac{n_{\mathbf{k}_1}}{2} \pm s_{\mathbf{k}_1}^\parallel. \tag{20}$$

As it is common for spin-dependent single particle energies like the Dresselhaus [66] or Rashba terms [67], one could

expect that the spin-dependent part of the correlation energy can be written as an effective magnetic field in which the electron spins precess. This additional precession movement could be made responsible for the frequency renormalization discussed above. However, although the corresponding effective field due to the correlation energy has the same form as the frequency renormalization, it is larger by a factor of 2. We attribute this to the fact that the correlation energy is not an average over a Hermitian single particle operator, but comprises multiparticle effects, where the naive identification of an effective magnetic field can lead to incorrect predictions.

A particularly interesting and transparent case is that where the impurity magentization $\langle \mathbf{S} \rangle$ vanishes. Then, the correlation energy takes the form

$$\langle H_{\text{sd}}^{\text{cor}} \rangle = -\frac{J_{\text{sd}}^2}{\hbar} \frac{n_{\text{Mn}}}{V} \langle S^2 \rangle \frac{Am^*}{2\pi\hbar} \sum_{\mathbf{k}_1} \ln \left| \frac{\omega_{\text{BZ}} - \omega_{\mathbf{k}_1}}{\omega_{\mathbf{k}_1}} \right| n_{\mathbf{k}_1}. \quad (21)$$

Thus, for $\langle \mathbf{S} \rangle = 0$, we find a logarithmic divergence of the correlation energy with respect to $\omega_{\text{BZ}} \to \infty$ and $\omega_{\mathbf{k}_1} \to 0$. In both limits, the correlation energy is negative and independent of the sign of the coupling constant J_{sd}. Note that this is different from the mean-field contribution to the interaction energy which is proportional to J_{sd} and therefore has a different sign for a ferromagnetic or antiferromagnetic s-d coupling. The negative correlation energy suggests that the formation of correlated carrier-impurity states is energetically favored, similar to the situation in metallic Kondo systems [2]. Again, we find that the divergence at $\omega_{\mathbf{k}_1} \to 0$ in Eq. (21) is integrable so that the total correlation energy always assumes finite values. To estimate the magnitude of the correlation energy in the case where $\langle \mathbf{S} \rangle = 0$ we consider a Gaussian spectral electron distribution centered at the band edge with standard deviation $E_s = 1$ meV. For the parameters of the $\text{Cd}_{0.93}\text{Mn}_{0.07}\text{Te}$ quantum well discussed above, we find from Eq. (21) a value of $\langle H_{\text{sd}}^{\text{cor}} \rangle \approx -1.8 \ \mu\text{eV}$ per electron. Thus, the correlations can be destroyed by thermal fluctuations when the temperature T exceeds 20 mK.

Note that, here, we describe the dynamic buildup of Kondo-type correlated carrier-impurity states that takes place on a short time scale after an initial preparation of a nonequilibrium spin distribution. On a longer time scale ($\sim$100 ps) the thermalization of excited carriers in DMS may lead to the formation of, e.g., bound (BMP), free (FMP), or exciton (EMP) magnetic polarons [30,40,46,47,68,69]. These states comprise carriers whose wave functions are limited to a finite volume in which the impurities are spin polarized. They become relevant, if their total free energy is lower than that of free carriers in a bath of homogeneously polarized ions. The treatment of such effects is beyond the scope of the present study. However, from the fact that the s-d interactions leads to correlation energies in the μeV range, while typical values of polaron binding energies are several tens of meV [30], we can conclude that a semiclassical treatment of H_{sd}, which is usually the case in the literature [30,40,46,47,68,69], is indeed justified for thermodynamic considerations that become relevant on time scales longer than those considered in this paper.

VI. CONCLUSION

A microscopic quantum kinetic theory is employed to describe the spin dynamics of carriers and magnetic impurities in diluted magnetic semiconductors (DMS) accounting also for the dynamics of the carrier-impurity correlations. The role of the correlations is examined to shed light into the controversy about their importance: While some authors assume that the Kondo physics due to carrier-impurity correlation is of minor importance [48], others [49] find divergences in a perturbative treatment of the spin dynamics in DMS, similarly to the appearance of divergences found in the metallic Kondo effect [1,58]. In the present study, we find that the correlations, besides mediating the spin transfer between carriers and impurities, are also responsible for a renormalization of the precession frequency.

We find by numerical simulations that simple Markovian expressions reproduce well the frequency renormalization obtained by using the quantum kinetic theory. The numerical calculations as well as the Markovian expressions predict that the frequency renormalization is small in three-dimensional DMS but diverges logarithmically in two-dimensional systems for electrons with a specific kinetic energy. However, we find that these divergences are integrable when a nonsingular electron distribution is considered, so that for realistic optical excitation scenarios the average frequency renormalization can reach values of up to a few percent. Since in these cases the relative frequency renormalization is negative, the precession frequency of the electron spin is reduced.

Although the $\mathbf{k}$ dependence of the frequency renormalization can in principle lead to a dephasing of carrier spins, the spin transfer from the carriers to the impurities is usually much faster, so that this dephasing mechanism yields only very small corrections to the total decay of the carrier spin.

In order to experimentally probe the correlation induced frequency renormalization, the spectral features of the laser pulse have to be precisely controlled. Furthermore, it was reported [70] that an antiferromagnetic impurity-impurity interaction influences the thermal equilibrium value of the Mn magnetization, which in turn changes the measured electron spin precession frequency. Therefore, it is common to introduce a fitting parameter T_0 and to describe the equilibrium Mn magnetization by a Brillouin function with effective temperature $T_{\text{eff}} = T_0 + T$, where T is the temperature of the sample. This complicates the identification of correlation induced changes in the precession frequency. To distinguish both effects it is useful that in addition to the dependence on the spectral position and shape of the exciting pulse, the relative frequency renormalization due to the correlations is independent of the impurity density, while the impurity-impurity interaction depends on the mean distance between the impurity ions and is not influenced by the excitation conditions. Because of this and from the different parameters entering the prefactor of the frequency renormalization, we find that the most promising samples for experimentally accessing the correlation induced frequency renormalization are very narrow quantum wells with large effective masses and a large coupling constant J_{sd} while the impurity concentration should be relatively low. Also, we find that the spectral properties of

ultrashort pulses with durations in the 100 fs range suit this purpose.

The explicit expressions for the correlations in the Markov limit also allow us to find a quasiequilibrium value for the correlation energy in terms of carrier and impurity variables. The form of the correlation energy is similar to the expression for the frequency renormalization and hints towards the appearance of Kondo-type correlated carrier-impurity states, independent of the sign of the coupling constant, which builds up dynamically on a femtosecond time scale after preparing an

initial nonequilibrium spin distribution which is initially not correlated.

[1] J. Kondo, Prog. Theor. Phys. **32**, 37 (1964).

[2] A. C. Hewson, *The Kondo Problem to Heavy Fermions* (Cambridge University Press, Cambridge, 1993).

[3] S. M. Cronenwett, T. H. Oosterkamp, and L. P. Kouwenhoven, Science **281**, 540 (1998).

[4] T. Inoshita, Science **281**, 526 (1998).

[5] A. Kaminski, Y. V. Nazarov, and L. I. Glazman, Phys. Rev. Lett. **83**, 384 (1999).

[6] W. G. van der Wiel, S. D. Franceschi, T. Fujisawa, J. M. Elzerman, S. Tarucha, and L. P. Kouwenhoven, Science **289**, 2105 (2000).

[7] J. Elzerman, S. De Franceschi, D. Goldhaber-Gordon, W. van der Wiel, and L. Kouwenhoven, J. Low Temp. Phys. **118**, 375 (2000).

[8] P. Nordlander, N. S. Wingreen, Y. Meir, and D. C. Langreth, Phys. Rev. B **61**, 2146 (2000).

[9] H. Jeong, A. M. Chang, and M. R. Melloch, Science **293**, 2221 (2001).

[10] D. Goldhaber-Gordon, H. Shtrikman, D. Mahalu, D. Abusch-Magder, U. Meirav, and M. A. Kastner, Nature (London) **391**, 156 (1998).

[11] A. Micolich, Nat. Phys. **9**, 530 (2013).

[12] B. Hemingway, S. Herbert, M. Melloch, and A. Kogan, Phys. Rev. B **90**, 125151 (2014).

[13] T. Dietl and H. Ohno, Rev. Mod. Phys. **86**, 187 (2014).

[14] M. W. Wu, J. H. Jiang, and M. Q. Weng, Phys. Rep. **493**, 61 (2010).

[15] Ł. Cywiński and L. J. Sham, Phys. Rev. B **76**, 045205 (2007).

[16] M. Nawrocki, R. Planel, G. Fishman, and R. Galazka, Phys. Rev. Lett. **46**, 735 (1981).

[17] S. A. Crooker, D. D. Awschalom, J. J. Baumberg, F. Flack, and N. Samarth, Phys. Rev. B **56**, 7574 (1997).

[18] J. H. Jiang, Y. Zhou, T. Korn, C. Schüller, and M. W. Wu, Phys. Rev. B **79**, 155201 (2009).

[19] T. Dietl, Nat. Mater. **9**, 965 (2010).

[20] D. Awschalom and M. Flatté, Nat. Phys. **3**, 153 (2007).

[21] K. Edmonds, G. van der Laan, and G. Panaccione, Semicond. Sci. Technol. **30**, 043001 (2015).

[22] M. D. Kapetanakis, J. Wang, and I. E. Perakis, J. Opt. Soc. Am. B **29**, A95 (2012).

[23] J. Kossut, Phys. Status Solidi B **72**, 359 (1975).

[24] J. K. Furdyna, J. Appl. Phys. **64**, R29 (1988).

[25] H. Krenn, K. Kaltenegger, T. Dietl, J. Spałek, and G. Bauer, Phys. Rev. B **39**, 10918 (1989).

[26] J. M. Kikkawa and D. D. Awschalom, Phys. Rev. Lett. **80**, 4313 (1998).

[27] A. V. Akimov, A. V. Scherbakov, D. R. Yakovlev, I. A. Merkulov, M. Bayer, A. Waag, and L. W. Molenkamp, Phys. Rev. B **73**, 165328 (2006).

[28] K. E. Rönnburg, E. Mohler, H. G. Roskos, K. Ortner, C. R. Becker, and L. W. Molenkamp, Phys. Rev. Lett. **96**, 117203 (2006).

[29] M. D. Kapetanakis, I. E. Perakis, K. J. Wickey, C. Piermarocchi, and J. Wang, Phys. Rev. Lett. **103**, 047404 (2009).

[30] J. Kossut and J. Gaj, Eds., *Introduction to the Physics of Diluted Magnetic Semiconductors*, Springer Series in Materials Science No. 144 (Springer, Berlin, 2011).

[31] C. Camilleri, F. Teppe, D. Scalbert, Y. G. Semenov, M. Nawrocki, M. Dyakonov, J. Cibert, S. Tatarenko, and T. Wojtowicz, Phys. Rev. B **64**, 085331 (2001).

[32] R. C. Myers, M. H. Mikkelsen, J.-M. Tang, A. C. Gossard, M. E. Flatté, and D. D. Awschalom, Nat. Mater. **7**, 203 (2008).

[33] S. Cronenberger, M. Vladimirova, S. V. Andreev, M. B. Lifshits, and D. Scalbert, Phys. Rev. Lett. **110**, 077403 (2013).

[34] J. Wang, C. Sun, Y. Hashimoto, J. Kono, G. A. Khodaparast, Ł. Cywiński, L. J. Sham, G. D. Sanders, C. J. Stanton, and H. Munekata, J. Phys. Condens. Matter **18**, R501 (2006).

[35] T. Dietl, H. Ohno, F. Matsukura, J. Cibert, and D. Ferrand, Science **287**, 1019 (2000).

[36] H. Ohno, Nat. Mater. **9**, 952 (2010).

[37] S. A. Wolf, D. D. Awschalom, R. A. Buhrman, J. M. Daughton, S. von Molnr, M. L. Roukes, A. Y. Chtchelkanova, and D. M. Treger, Science **294**, 1488 (2001).

[38] F. J. Teran, M. Potemski, D. K. Maude, D. Plantier, A. K. Hassan, A. Sachrajda, Z. Wilamowski, J. Jaroszynski, T. Wojtowicz, and G. Karczewski, Phys. Rev. Lett. **91**, 077201 (2003).

[39] G. Tang and W. Nolting, Phys. Rev. B **75**, 024426 (2007).

[40] H. Bednarski and J. Spałek, J. Phys. Condens. Matter **24**, 235801 (2012).

[41] Y. Tian, Y. Li, M. He, I. A. Putra, H. Peng, B. Yao, S. A. Cheong, and T. Wu, Appl. Phys. Lett. **98**, 162503 (2011).

[42] D. E. Angelescu and R. N. Bhatt, Phys. Rev. B **65**, 075211 (2002).

[43] A. C. Durst, R. N. Bhatt, and P. A. Wolff, Phys. Rev. B **65**, 235205 (2002).

[44] M. Herbich, A. Twardowski, D. Scalbert, and A. Petrou, Phys. Rev. B **58**, 7024 (1998).

[45] P. A. Wolff, R. N. Bhatt, and A. C. Durst, J. Appl. Phys. **79**, 5196 (1996).

[46] A. Golnik and J. Spałek, J. Magn. Magn. Mater. **54**, 1207 (1986).

[47] H. Bednarski and J. Spaek, New J. Phys. **16**, 093060 (2014).

[48] S. Das Sarma, E. H. Hwang, and A. Kaminski, Phys. Rev. B **67**, 155201 (2003).

[49] O. Morandi and P.-A. Hervieux, Phys. Rev. B **81**, 195215 (2010).

[50] C. Thurn and V. M. Axt, Phys. Rev. B **85**, 165203 (2012).

[51] C. Thurn, M. Cygorek, V. M. Axt, and T. Kuhn, Phys. Rev. B **87**, 205301 (2013).

[52] C. Thurn, M. Cygorek, V. M. Axt, and T. Kuhn, Phys. Rev. B **88**, 161302(R) (2013).

[53] M. Cygorek and V. M. Axt, Phys. Rev. B **90**, 035206 (2014).

[54] M. Cygorek and V. M. Axt, Semicond. Sci. Technol. **30**, 085011 (2015).

[55] F. Ungar, M. Cygorek, P. I. Tamborenea, and V. M. Axt, Phys. Rev. B **91**, 195201 (2015).

[56] In order to obtain physically meaningful results, care has to be taken that the mean-field exchange energy between carriers and impurities is taken into account in the corresponding δ function in the expression for Fermi's golden rule [54].

[57] M. Cygorek and V. M. Axt, J. Phys.: Conf. Ser. **647**, 012042 (2015).

[58] D. C. Langreth and J. W. Wilkins, Phys. Rev. B **6**, 3189 (1972).

[59] In Refs. [50,53] the correlations $Q^{\sigma_2 n_2 \mathbf{k}_2}_{\sigma_1 n_1 \mathbf{k}_1}$ were defined as the difference between the right-hand side of Eq. (2c) and factorized parts, which however vanish for $\mathbf{k}_2 \neq \mathbf{k}_1$ for the on average spatially homogeneous system considered here. Only the values of these correlations for $\mathbf{k}_2 \neq \mathbf{k}_1$ appear in the equations of motion .

[60] S. Doniach and E. H. Sondheimer, *Green's Functions for Solid State Physicists* (Imperial College Press, London, 1998).

[61] K. G. Wilson, Rev. Mod. Phys. **47**, 773 (1975).

[62] P. Y. Yu and M. Cardona, *Fundamentals of Semiconductors*, 4th ed. (Springer, Heidelberg, 2010).

[63] Z. Ben Cheikh, S. Cronenberger, M. Vladimirova, D. Scalbert, F. Perez, and T. Wojtowicz, Phys. Rev. B **88**, 201306 (2013).

[64] G. Bastard and R. Ferreira, Surf. Sci. **267**, 335 (1992).

[65] S. A. Crooker, E. Johnston-Halperin, D. D. Awschalom, R. Knobel, and N. Samarth, Phys. Rev. B **61**, R16307 (2000).

[66] G. Dresselhaus, Phys. Rev. **100**, 580 (1955).

[67] Y. A. Bychkov and E. I. Rashba, J. Phys. C **17**, 6039 (1984).

[68] J. Spałek, Phys. Rev. B **30**, 5345 (1984).

[69] A. V. Kavokin and K. V. Kavokin, Semicond. Sci. Technol. **8**, 191 (1993).

[70] J. Gaj, R. Planel, and G. Fishman, Solid State Commun. **29**, 435 (1979).

Erratum: Nonperturbative correlation effects in diluted magnetic semiconductors [Phys. Rev. B 93, 035206 (2016)]

M. Cygorek, P. I. Tamborenea, and V. M. Axt
(Received 16 July 2016; published 17 August 2016)

The starting point of this paper is the equation of motion (5) for the carrier spin component perpendicular to the impurity magnetization, which has been derived in Ref. [1]. In Eq. (5), a cross-product sign is not printed accurately. Furthermore, in the derivation of this equation in Ref. [1], it was assumed that the effective magnetic field $\boldsymbol{\omega}_M$ for the carrier spins caused by the impurity magnetization is parallel to the total impurity spin, i.e., the coupling constant J_{sd} is positive. In the present paper, however, this equation has been applied to the conduction band of CdTe where this condition is not fulfilled. To correct this error, the corresponding equation of motion needs to be derived for an arbitrary sign of J_{sd}. Toward that end, it is useful to define the quantization axis (z) as pointing in the direction of $\boldsymbol{\omega}_M$. Then, also the spin-up and spin-down occupations $n_{\mathbf{k}}^{\uparrow}$ and $n_{\mathbf{k}}^{\downarrow}$ as well as the parallel impurity spin operator $S^{\parallel} = \hat{\mathbf{S}} \cdot \frac{\boldsymbol{\omega}_M}{|\boldsymbol{\omega}_M|}$ in the definition of the factors b^i in Eq. (5) should be defined with respect to the direction of $\boldsymbol{\omega}_M$. In this coordinate system, Eq. (5) should be replaced by [2]

$$\frac{\partial}{\partial t}\mathbf{s'}_{\mathbf{k}_1}^{\perp} = -\sum_{\mathbf{k}}\left[\text{Re}\left(G_{\omega_{\mathbf{k}}}^{\omega_{\mathbf{k}_1}-\omega_M}\right)\left(\frac{b^+}{2} - b^0 n_{\mathbf{k}}^{\uparrow}\right)\mathbf{s'}_{\mathbf{k}_1}^{\perp} + \text{Re}\left(G_{\omega_{\mathbf{k}}}^{\omega_{\mathbf{k}_1}+\omega_M}\right)\left(\frac{b^-}{2} + b^0 n_{\mathbf{k}}^{\downarrow}\right)\mathbf{s'}_{\mathbf{k}_1}^{\perp} + \text{Re}\left(G_{\omega_{\mathbf{k}}}^{\omega_{\mathbf{k}_1}}\right)\frac{b^{\parallel}}{2}\left(\mathbf{s'}_{\mathbf{k}}^{\perp} + \mathbf{s'}_{\mathbf{k}_1}^{\perp}\right)\right]$$
$$-\sum_{\mathbf{k}}\left[\text{Im}\left(G_{\omega_{\mathbf{k}}}^{\omega_{\mathbf{k}_1}-\omega_M}\right)\left(\frac{b^+}{2} - b^0 n_{\mathbf{k}}^{\uparrow}\right) - \text{Im}\left(G_{\omega_{\mathbf{k}}}^{\omega_{\mathbf{k}_1}+\omega_M}\right)\left(\frac{b^-}{2} + b^0 n_{\mathbf{k}}^{\downarrow}\right)\right]\left(\frac{\boldsymbol{\omega}_M}{|\boldsymbol{\omega}_M|} \times \mathbf{s'}_{\mathbf{k}_1}^{\perp}\right). \tag{5'}$$

As a consequence, using the equation derived in Ref. [1] with a negative value of J_{sd} led to the wrong sign of the relative frequency renormalization $\frac{\Delta\omega}{\omega_M}$ in Figs. 1 and 3. Actually, the correlation-induced renormalization enhances the precession frequency instead of decreasing it, independently of the sign of J_{sd}. The magnitude of the renormalization, however, is not influenced.

Also, Eq. (6) has an error with parentheses. It should read

$$G_{\omega_{\mathbf{k}}}^{\omega_{\mathbf{k}_1}} := \frac{J_{sd}^2}{\hbar^2}\frac{n_{Mn}}{V}\int_{-t}^{0} dt' \, e^{i(\omega_{\mathbf{k}}-\omega_{\mathbf{k}_1})t'}. \tag{6'}$$

Furthermore, a factor $\frac{1}{2}$ is missing in Eq. (21). The corrected version of Eq. (21) is

$$\langle H_{sd}^{cor}\rangle = -\frac{J_{sd}^2}{\hbar}\frac{n_{Mn}}{V}\frac{\langle S^2\rangle}{2}\frac{Am^*}{2\pi\hbar}\sum_{\mathbf{k}_1}\ln\left|\frac{\omega_{BZ} - \omega_{\mathbf{k}_1}}{\omega_{\mathbf{k}_1}}\right|n_{\mathbf{k}_1}. \tag{21'}$$

Also, due to an error in the computer program, the evaluation of the correlation energy according to Eq. (21) led to a wrong value. For the situation described in this paper, the value of the average correlation energy per electron, $\langle H_{sd}^{cor}\rangle/(\sum_{\mathbf{k}} n_{\mathbf{k}})$, is not $-1.8\ \mu\text{eV}$, but rather -0.34 meV, which corresponds to a temperature of $T \approx 4$ K.

The above errors have little influence on the conclusion about the frequency renormalization. While the sign of the frequency renormalization has to be changed, the magnitude remains the same. However, the relatively large corrected value of the correlation energy indicates that the carrier-impurity correlations are strong in low-temperature experiments and should therefore not be neglected, as is usually done by invoking a semiclassical approximation [3–7].

[1] M. Cygorek and V. M. Axt, Semicond. Sci. Technol. **30**, 085011 (2015).
[2] M. Cygorek, P. I. Tamborenea, and V. M. Axt, Phys. Rev. B **93**, 205201 (2016).
[3] H. Bednarski and J. Spałek, J. Phys. Condens. Matter **24**, 235801 (2012).
[4] H. Bednarski and J. Spałek, New J. Phys. **16**, 093060 (2014).
[5] A. Golnik and J. Spałek, J. Magn. Magn. Mater. **54**, 1207 (1986).
[6] J. Spałek, Phys. Rev. B **30**, 5345 (1984).
[7] A. V. Kavokin and K. V. Kavokin, Semicond. Sci. Technol. **8**, 191 (1993).

Publication 8

Dependence of quantum kinetic effects in the spin dynamics of diluted magnetic semiconductors on the excitation conditions

M. Cygorek, F. Ungar, P. I. Tamborenea and V. M. Axt

Dependence of quantum kinetic effects in the spin dynamics of diluted magnetic semiconductors on the excitation conditions

M. Cygorek[a], F. Ungar[a], P. I. Tamborenea[b], and V. M. Axt[a]

[a]Theoretische Physik III, Universität Bayreuth, 95440 Bayreuth, Germany
[b]Departamento de Física and IFIBA, FCEN, Universidad de Buenos Aires, Ciudad Universitaria, Pabellón I, 1428 Ciudad de Buenos Aires, Argentina

ABSTRACT

Non-Markovian quantum kinetic features, that cannot be captured by rate equations, have been predicted theoretically in the spin dynamics in diluted magnetic semiconductors excited with a circularly polarized laser. In order to identify situations which are most promising for detecting the genuine quantum kinetic effects in future experiments, we study numerically the strength of these effects for a number of different excitation conditions. In particular, we show that laser pulse durations of the order of the spin-transfer rate or longer are well suited for studying the non-Markovian effects. Furthermore, in the presence of an external magnetic field, the quantum kinetic theory predicts a significantly different stationary value for the carrier spin polarization than Markovian rate equations, which can be attributed to the build-up of strong carrier-impurity correlations.

Keywords: Spintronics, diluted magnetic semiconductors, spin dynamics, optical excitation, quantum kinetics

1. INTRODUCTION

Diluted magnetic semiconductors (DMS) provide the possibility to investigate novel physical features caused by magnetic impurities in the well-studied field of semiconductor optics and transport.[1-8] In particular, DMS heterostructures have been in the focus of investigations in recent years.[9-12] Some of the static magnetic properties in DMS, such as the giant Zeeman effect and the corresponding spin-splitting of carrier levels, can be explained in the mean-field approximation, where the effects of the magnetic impurities on the carriers are regarded as a homogeneous effective magnetic field.[13] The spin dynamics in DMS is usually experimentally accessed by time-resolved magneto-optical Kerr or Faraday measurements.[7,14,15] These time-resolved experiments are typically described theoretically in terms of rate equations[15-18] where the rates are calculated from Fermi's golden rule.

In a series of papers,[19-26] we have developed a quantum kinetic description of the spin dynamics in DMS where the carrier-impurity correlations, which build up because of the s/p-d carrier-impurity exchange interaction, are explicitly taken into account. For zero magnetic field, the Markov limit of the quantum kinetic theory was shown to coincide with rate equations that can be obtained using Fermi's golden rule.[20,23,26] While in some cases the full quantum kinetic treatment yields a spin dynamics very similar to that predicted by a golden-rule-type description, pronounced deviations from the exponential time evolution of the spin have been identified in some situations, especially in two dimensions for optical excitations very close to the band edge.[20,21,27] Thus, these non-Markovian effects are sensitive to the details of the optical excitation. However, due to the numerical demands, most of the quantum kinetic studies so far focus on the conduction band and the optical excitation is modelled by the choice of an initial non-equilibrium carrier distribution. The optical excitation of a DMS with a time-dependent laser field within the dipole approximation was taken explicitly into account on a quantum kinetic level only in rare cases such as in Ref. 21.

For an experimental verification of the prediction of a non-Markovian carrier-impurity spin transfer, i. e. dynamics that cannot be described by a simple rate equation approach, it is important to find a regime of excitation conditions, where these effects are most pronounced. Especially important for experiments are the properties of the laser pulse: If the pulse duration τ_L is too short, i.e. the spectral width of the laser is large, the excitation can no longer be concentrated on states at $\mathbf{k} = 0$. If such broad distributions are taken as initial

carrier occupations, the quantum kinetic theory predicts the same behaviour as the rate equations.[20,27] On the other hand, if the pulse is too long, the spin transfer between carriers and impurities is already significant during the laser pulse and non-Markovian features might be smeared out. Also, in the presence of a magnetic field, the originally spin-degenerate conduction band is split and an energy conserving scattering from an initial state with wave vector $\mathbf{k} = 0$ scatters to a state with finite kinetic energy. Recalling that quantum kinetic effects are most pronounced near the band edge, the occupation of states with higher kinetic energy induced by a finite magnetic field suggests that deviations from the predictions of rate equations should be smaller for higher values of the magnetic field.

The goal of the present article is to provide a more comprehensive study of non-Markovian effects in the spin dynamics in DMS for a broader set of parameters and initial conditions. In particular, we study the effects of different pulse durations and external magnetic fields on the deviations of the quantum kinetic predictions from the results of rate equations.

Indeed, we find that the non-Markovian effects nearly vanish for pulses much shorter than the carrier-impurity spin transfer time, where rate equations turn out to provide a good approximation. For pulse durations of the order of the spin transfer time, the non-Markovian effects, such as overshoots, predicted by initial value calculations are confirmed for the more realistic description, where the light-matter interaction is treated explicitly. Surprisingly, the quantum kinetic features are still visible for much longer pulses and are not smoothed out, as it might be expected.

The presence of an external magnetic field reduces the overshoots that are characteristic for non-Markovian behavior. However, the stationary value of the spin polarization after the pulse is significantly different in both approaches, which can be attributed to the build-up of strong carrier-impurity correlations in the quantum kinetic theory.

The article is structured as follows: In section II, we briefly recapitulate the quantum kinetic theory of Ref. 19 and its extension in the presence of an external magnetic field.[26] In Section III we present quantum-kinetic numerical calculations for different pulse durations and with and without external magnetic fields.

2. THEORY

The quantum kinetic equations for the spin dynamics in DMS in the absence of an external magnetic field have been derived in Ref. 19, where the conduction and valence bands as well as the interband coherences have been taken into account. The Zeeman energies have been accounted for in Ref. 26, but there, only the conduction band has been considered and the optical excitation has been modelled by suitable non-equiblibirum initial carrier occupations. Here, we present the full set of quantum kinetic equations of motion including both, the optical excitation as well as the external magnetic field, on a quantum kinetic level.

2.1 Hamiltonian

A DMS quantum well in the presence of an external magnetic field is described by the total Hamiltonian

$$H = H_0 + H_{sd} + H_{pd} + H_{em} + H_Z^e + H_Z^h + H_Z^{Mn}, \tag{1a}$$

$$H_0 = \sum_{l\mathbf{k}} E_{l\mathbf{k}} c_{l\mathbf{k}}^\dagger c_{l\mathbf{k}} + \sum_{v\mathbf{k}} E_{v\mathbf{k}} d_{v\mathbf{k}}^\dagger d_{v\mathbf{k}}, \tag{1b}$$

$$H_{sd} = \frac{J_{\mathrm{sd}} d}{V} \sum_{\mathbf{k}\mathbf{k}'ll'} \sum_{Inn'} \mathbf{S}_{nn'} \cdot \mathbf{s}_{ll'}^e c_{l\mathbf{k}}^\dagger c_{l'\mathbf{k}'} e^{i(\mathbf{k}'-\mathbf{k})\mathbf{R}_I} \hat{P}_{nn'}^I, \tag{1c}$$

$$H_{pd} = \frac{J_{\mathrm{pd}} d}{V} \sum_{\mathbf{k}\mathbf{k}'vv'} \sum_{Inn'} \mathbf{S}_{nn'} \cdot \mathbf{s}_{vv'}^h d_{v\mathbf{k}}^\dagger d_{v'\mathbf{k}'} e^{i(\mathbf{k}'-\mathbf{k})\mathbf{R}_I} \hat{P}_{nn'}^I, \tag{1d}$$

$$H_{em} = -\sum_{lv\mathbf{k}} \left(\mathbf{E} \cdot \mathbf{M}_{vl\mathbf{k}}^* c_{l\mathbf{k}}^\dagger d_{v-\mathbf{k}}^\dagger + \mathbf{E} \cdot \mathbf{M}_{vl\mathbf{k}} d_{v-\mathbf{k}} c_{l\mathbf{k}} \right), \tag{1e}$$

$$H_Z^e = \sum_{ll'\mathbf{k}} g_e \mu_B \mathbf{B} \cdot \mathbf{s}_{ll'}^e c_{l\mathbf{k}}^\dagger c_{l'\mathbf{k}}, \tag{1f}$$

$$H_Z^h = \sum_{vv'\mathbf{k}} g_h \mu_B \mathbf{B} \cdot \mathbf{s}_{vv'}^h d_{v\mathbf{k}}^\dagger d_{v'\mathbf{k}}, \tag{1g}$$

$$H_Z^{Mn} = \sum_{nn'I} g_{Mn} \mu_B \mathbf{B} \cdot \mathbf{S}_{nn'} \hat{P}_{nn'}^I \tag{1h}$$

where H_0 denotes the crystal Hamiltonian and H_{em} incorporates the light-matter interaction describing the optical excitation of carriers in the semiconductor. The operators $c_{l\mathbf{k}}^{(\dagger)}$ and $d_{v\mathbf{k}}^{(\dagger)}$ annihilate (create) conduction band electrons in the l-th subband or valence band holes in the v-th subband with wave vector $\mathbf{k}$. $E_{l\mathbf{k}}$ and $E_{v\mathbf{k}}$ describe the electron and hole band structures, $\mathbf{E}$ is the electric field of the light and $\mathbf{M}_{vl\mathbf{k}}$ is the transition dipole moment between states in the v-th valence subband and the l-th conduction subband. The exchange interaction between electrons and the magnetic impurities is described by H_{sd}, where J_{sd} is the coupling constant, d is the quantum well width, V is the volume of the sample and $\mathbf{R}_I$ is the position of the I-th impurity ion. Similarly, H_{pd} represents the coupling between holes and the magnetic impurities, where J_{pd} is the corresponding coupling constant for the valence band. The operator $\hat{P}_{n_1 n_2}^I = |I, n_1\rangle\langle I, n_2|$ is the impurity density operator in the basis spanned by the n_i-th spin states of the I-th impurity, where $n_i \in \{-\frac{5}{2}, -\frac{3}{2}, \dots, \frac{5}{2}\}$ for spin-$\frac{5}{2}$ magnetic impurities like Mn. $\mathbf{s}_{l_1 l_2}^e$ and $\mathbf{s}_{v_1 v_2}^h$ are the electron (spin-$\frac{1}{2}$) and hole (spin-$\frac{3}{2}$) spin matrices and $\mathbf{S}_{n_1 n_2}$ denotes the impurity spin matrices. The Zeeman energies for electrons, holes and magnetic impurities in an external magnetic field are H_Z^e, H_Z^h and H_Z^{Mn}, respectively.

2.2 Equations of motion

Starting from the Hamiltonian in Eqs. (1a)–(1e), quantum kinetic equations of motion have been derived in Ref. 19 for the carrier and impurity density matrices and the carrier-impurity correlations[*]:

$$M_{n_1}^{n_2} = \langle \hat{P}_{n_1 n_2}^I \rangle, \tag{2a}$$

$$C_{l_1\mathbf{k}_1}^{l_2} = \langle c_{l_1\mathbf{k}_1}^\dagger c_{l_2\mathbf{k}_1} \rangle, \tag{2b}$$

$$D_{v_1\mathbf{k}_1}^{v_2} = \langle d_{v_1\mathbf{k}_1}^\dagger d_{v_2\mathbf{k}_1} \rangle, \tag{2c}$$

$$Y_{v_1\mathbf{k}_1}^{l_2} = \langle d_{v_1\mathbf{k}_1} c_{l_2 -\mathbf{k}_1} \rangle, \tag{2d}$$

$$QC_{l_1 n_1 \mathbf{k}_1}^{l_2 n_2 \mathbf{k}_2} = V \langle c_{l_1\mathbf{k}_1}^\dagger c_{l_2\mathbf{k}_2} \hat{P}_{n_1 n_2}^I e^{i(\mathbf{k}_2 - \mathbf{k}_1)\mathbf{R}_I} \rangle (1 - \delta_{\mathbf{k}_1, \mathbf{k}_2}), \tag{2e}$$

$$QD_{v_1 n_1 \mathbf{k}_1}^{v_2 n_2 \mathbf{k}_2} = V \langle d_{v_1\mathbf{k}_1}^\dagger d_{v_2\mathbf{k}_2} \hat{P}_{n_1 n_2}^I e^{i(\mathbf{k}_2 - \mathbf{k}_1)\mathbf{R}_I} \rangle (1 - \delta_{\mathbf{k}_1, \mathbf{k}_2}), \tag{2f}$$

$$QY_{v_1 n_1 \mathbf{k}_1}^{l_2 n_2 \mathbf{k}_2} = V \langle d_{v_1\mathbf{k}_1} c_{l_2\mathbf{k}_2} \hat{P}_{n_1 n_2}^I e^{i(\mathbf{k}_2 + \mathbf{k}_1)\mathbf{R}_I} \rangle (1 - \delta_{\mathbf{k}_1, -\mathbf{k}_2}), \tag{2g}$$

where the brackets denote a quantum mechanical average as well as an average over a random distribution of impurity positions $\mathbf{R}_I$.

Since the Zeeman energies (1f)–(1h) are single particle contributions and do not lead to a build-up of further many-particle correlations, it is straightforward to include them into the quantum kinetic theory. Taking these into account, the corresponding equations of motion for the variables defined in Eq. (2) in Ref. 19 are extended to:

$$
-i\hbar \frac{\partial}{\partial t} M_{n_1}^{n_2} = \sum_n \boldsymbol{\omega}_{Mn} \cdot \left(\mathbf{S}_{nn_1} M_n^{n_2} - \mathbf{S}_{n_2 n} M_{n_1}^n \right)
$$
$$
+ \frac{J_{\mathrm{sd}}}{V^2} \sum_{\mathbf{k}\mathbf{k}'} \sum_n \left[\sum_{ll'} \mathbf{s}_{ll'}^e \cdot \left(\mathbf{S}_{nn_1} QC_{ln\mathbf{k}}^{l' n_2 k'} - \mathbf{S}_{n_2 n} QC_{ln_1\mathbf{k}}^{l' n k'} \right) \right.
$$
$$
\left. + \sum_{vv'} \mathbf{s}_{vv'}^h \cdot \left(\mathbf{S}_{nn_1} QD_{ln\mathbf{k}}^{l' n_2 k'} - \mathbf{S}_{n_2 n} QD_{ln_1\mathbf{k}}^{l' n k'} \right) \right], \tag{3a}
$$

---

[*]Here, we use a slightly more condensed, but equivalent notation for the carrier-impurity correlations compared to Ref. 19.

$$-i\hbar\frac{\partial}{\partial t}C_{l_1\mathbf{k}_1}^{l_2} = -\left(E_{l_2\mathbf{k}_1} - E_{l_1\mathbf{k}_1}\right)C_{l_1\mathbf{k}_1}^{l_2} + \sum_v \mathbf{E}\cdot\left(\mathbf{M}_{vl_2\mathbf{k}_1}^*(Y_{v-\mathbf{k}_1}^{l_1})^* - \mathbf{M}_{vl_1\mathbf{k}_1}Y_{v-\mathbf{k}_1}^{l_2}\right)$$

$$+ \sum_l \boldsymbol{\omega}_e\cdot\left(\mathbf{s}_{ll_1}^e C_{l\mathbf{k}_1}^{l_2} - \mathbf{s}_{l_2l}^e C_{l_1\mathbf{k}_1}^l\right) + \frac{J_{\mathrm{sd}}N_{\mathrm{Mn}}}{V^2}\sum_{\mathbf{k}}\sum_{nn'l}\mathbf{S}_{nn'}\cdot\left(\mathbf{s}_{ll_1}^e Q_{Cln\mathbf{k}}^{l_2n'\mathbf{k}_1} - \mathbf{s}_{l_2l}^e Q_{Cl_1n\mathbf{k}_1}^{ln'\mathbf{k}}\right), \quad (3\mathrm{b})$$

$$-i\hbar\frac{\partial}{\partial t}D_{v_1\mathbf{k}_1}^{v_2} = -\left(E_{v_2\mathbf{k}_1} - E_{v_1\mathbf{k}_1}\right)D_{v_1\mathbf{k}_1}^{v_2} + \sum_l \mathbf{E}\cdot\left(\mathbf{M}_{v_2l-\mathbf{k}_1}^*(Y_{v_1\mathbf{k}_1}^l)^* - \mathbf{M}_{v_1l-\mathbf{k}_1}Y_{v_2\mathbf{k}_1}^l\right)$$

$$+ \sum_v \boldsymbol{\omega}_h\cdot\left(\mathbf{s}_{vv_1}^h D_{v\mathbf{k}_1}^{v_2} - \mathbf{s}_{v_2v}^h D_{v_1\mathbf{k}_1}^v\right) + \frac{J_{\mathrm{sd}}N_{\mathrm{Mn}}}{V^2}\sum_{\mathbf{k}}\sum_{nn'v}\mathbf{S}_{nn'}\cdot\left(\mathbf{s}_{vv_1}^h Q_{Dvn\mathbf{k}}^{v_2n'\mathbf{k}_1} - \mathbf{s}_{v_2v}^h Q_{Dv_1n\mathbf{k}_1}^{vn'\mathbf{k}}\right),$$
$$(3\mathrm{c})$$

$$-i\hbar\frac{\partial}{\partial t}Y_{v_1\mathbf{k}_1}^{l_2} = -\left(E_{v_1\mathbf{k}_1} + E_{l_2-\mathbf{k}_1}\right)Y_{v_1\mathbf{k}_1}^{l_2} + \mathbf{E}\cdot\mathbf{M}_{v_1l_2-\mathbf{k}_1}^* - \sum_l \mathbf{E}\cdot\mathbf{M}_{v_1l-\mathbf{k}_1}^* C_{l-\mathbf{k}_1}^{l_2} - \sum_v \mathbf{E}\cdot\mathbf{M}_{vl_2-\mathbf{k}_1}^* D_{v\mathbf{k}_1}^{v_1}$$

$$- \sum_l \boldsymbol{\omega}_e\cdot\mathbf{s}_{l_2l}^e Y_{v_1\mathbf{k}_1}^l - \sum_v \boldsymbol{\omega}_h\cdot\mathbf{s}_{v_1v}^h Y_{v\mathbf{k}_1}^{l_2}$$

$$- \frac{N_{\mathrm{Mn}}}{V^2}\sum_{nn'}\mathbf{S}_{nn'}\cdot\left(J_{\mathrm{sd}}\sum_l \mathbf{s}_{l_2l}^e Q_{Yv_1n\mathbf{k}_1}^{ln'\mathbf{k}} + J_{\mathrm{pd}}\sum_v \mathbf{s}_{v_1v}^h Q_{Yvn\mathbf{k}}^{l_2n'-\mathbf{k}_1}\right), \quad (3\mathrm{d})$$

$$-i\hbar\frac{\partial}{\partial t}Q_{Cl_1n_1\mathbf{k}_1}^{l_2n_2\mathbf{k}_2} = -\left(E_{l_2\mathbf{k}_2} - E_{l_1\mathbf{k}_1}\right)Q_{Cl_1n_1\mathbf{k}_1}^{l_2n_2\mathbf{k}_2} + b_{Cl_1n_1\mathbf{k}_1}^{\mathbf{E}\,l_2n_2\mathbf{k}_2} + b_{Cl_1n_1\mathbf{k}_1}^{I\,l_2n_2\mathbf{k}_2} + b_{C\,l_1n_1\mathbf{k}_1}^{II\,l_2n_2\mathbf{k}_2} + b_{C\,l_1n_1\mathbf{k}_1}^{III\,l_2n_2\mathbf{k}_2}, \quad (3\mathrm{e})$$

$$-i\hbar\frac{\partial}{\partial t}Q_{Dv_1n_1\mathbf{k}_1}^{v_2n_2\mathbf{k}_2} = -\left(E_{v_2\mathbf{k}_2} - E_{v_1\mathbf{k}_1}\right)Q_{Dv_1n_1\mathbf{k}_1}^{v_2n_2\mathbf{k}_2} + b_{Dv_1n_1\mathbf{k}_1}^{\mathbf{E}\,v_2n_2\mathbf{k}_2} + b_{Dv_1n_1\mathbf{k}_1}^{I\,v_2n_2\mathbf{k}_2} + b_{D\,v_1n_1\mathbf{k}_1}^{II\,v_2n_2\mathbf{k}_2} + b_{D\,v_1n_1\mathbf{k}_1}^{III\,v_2n_2\mathbf{k}_2}, \quad (3\mathrm{f})$$

$$-i\hbar\frac{\partial}{\partial t}Q_{Yv_1n_1\mathbf{k}_1}^{l_2n_2\mathbf{k}_2} = -\left(E_{l_2\mathbf{k}_2} + E_{v_1\mathbf{k}_1}\right)Q_{Yv_1n_1\mathbf{k}_1}^{l_2n_2\mathbf{k}_2} + b_{Yv_1n_1\mathbf{k}_1}^{\mathbf{E}\,l_2n_2\mathbf{k}_2} + b_{Yv_1n_1\mathbf{k}_1}^{I\,l_2n_2\mathbf{k}_2} + b_{Y\,v_1n_1\mathbf{k}_1}^{II\,l_2n_2\mathbf{k}_2} + b_{Y\,v_1n_1\mathbf{k}_1}^{III\,l_2n_2\mathbf{k}_2}, \quad (3\mathrm{g})$$

with mean-field electron, hole and impurity precession frequencies

$$\boldsymbol{\omega}_e := \frac{J_{\mathrm{sd}}N_{\mathrm{Mn}}}{V}\sum_{nn'}\mathbf{S}_{nn'}M_n^{n'} + g_e\mu_B\mathbf{B}, \quad (4\mathrm{a})$$

$$\boldsymbol{\omega}_h := \frac{J_{\mathrm{pd}}N_{\mathrm{Mn}}}{V}\sum_{nn'}\mathbf{S}_{nn'}M_n^{n'} + g_h\mu_B\mathbf{B}, \quad (4\mathrm{b})$$

$$\boldsymbol{\omega}_{Mn} := \frac{J_{\mathrm{sd}}}{V}\sum_{\mathbf{k}ll'}\mathbf{s}_{ll'}^e C_{l\mathbf{k}}^{l'} + \frac{J_{\mathrm{pd}}}{V}\sum_{\mathbf{k}vv'}\mathbf{s}_{vv'}^h D_{v\mathbf{k}}^{v'} + g_{Mn}\mu_B\mathbf{B}, \quad (4\mathrm{c})$$

where N_{Mn} is the total number of magnetic impurities in the DMS. The explicit expressions for the source terms of the correlations are given in appendix A. The source terms can be classified as follows:[22] the terms b^E represent interactions between the different correlations Q_C, Q_D and Q_Y via the light field. b^I are inhomogeneous source terms that only depend on the single particle density matrices C, D, Y and M. b^{II} are the homogeneous terms that describe a precession-type motion of the correlations about the effective magnetic field provided by the carrier and impurity magnetization as well as by the external magnetic field. These terms depend linearly on $\boldsymbol{\omega}_e$, $\boldsymbol{\omega}_h$ and $\boldsymbol{\omega}_{Mn}$ and correlations with the same $\mathbf{k}$-indices. The source terms b^{III} comprise the interaction between correlations with different $\mathbf{k}$-indices.

2.3 Assumptions and approximations

The full numerical solution of Eqs. (3) is very time consuming and it becomes necessary to introduce some simplifying and physically meaningful assumptions in order to reduce the huge numerical demands. In the present article, we focus on the situation of a narrow intrinsic paramagnetic DMS quantum well that is optically excited by a pulse of circularly polarized light for various parameters and excitation conditions. This allows for several simplifications:

(i) In an intrinsic DMS such as Mn-doped II-VI semiconductors like CdTe or ZnSe, the quasi-free carriers stem exclusively from optical excitation. Thus, the number of quasi-free carriers N_e is typically much smaller

than the number of magnetic impurities N_{Mn}. Therefore, the impurities act like an effective spin bath for the carriers and the change of the average impurity spin during the spin-transfer process is negligible,[22] so that the impurity density matrix M can be treated as constant in time.

(ii) In a typical narrow quantum well, the heavy- and light-hole bands are split, e.g., because of the different effective masses and the confinement potential or due to strain effects.[28] Here, we assume that the splitting is large enough to prohibit transitions between heavy- and light-hole states and that the heavy hole band lies above the light hole band. Confining our considerations to the basis set of conduction and heavy-hole bands, we find that the total Hamiltonian is diagonal with respect to the heavy-hole subband indices v. Thus, for a narrow well, the hole spin is pinned. Since the circular polarization of the light only couples to one of the heavy-hole subbands, only this band is important for further calculations. Therefore, non-trivial spin dynamics after the exciting laser pulse only takes place in the system of the conduction band electrons.

(iii) As we consider a situation where spin-orbit coupling is not important,[25] there is no preferred direction in $\mathbf{k}$-space. This allows us to regard all density matrices and correlations as depending on the corresponding wave vectors $\mathbf{k}$ only via its modulus $|\mathbf{k}|$. This reduces the dimensionality of the problem enormously.

(iv) The central frequency of the laser pulse, which is of the order of the band gap E_g, is much larger than any other energy scale in the system. It is therefore a good approximation to formulate the equations of motion (3) in a rotating-wave picture with respect to the laser frequency ω_L and neglect terms with frequency $\pm 2\omega_L$.

(v) It was found in earlier studies[22] that the source terms b^{III} are numerically insignificant. These terms describe how correlations are influenced by other correlations with different wave vectors. Since the correlations in general oscillate rapidly, the terms in b^{III} can be expected to interfere destructively which explains why these terms have been found in Ref.[22] to have little effects. We therefore neglect the source terms b^{III} in order to reduce the computation time.

(vi) We assume that there are no quasi-free carriers before the pump pulse arrives so that the density matrices C, D and Y as well as all correlations are zero for times $t \ll 0$, where $t = 0$ is defined by the center of the pump pulse. For a paramagnetic DMS, the value of the impurity density matrix M is determined by the thermal equilibrium with respect to the Zeeman energy H_Z^{Mn} for a given external magnetic field $\mathbf{B}$, the impurity g-factor $g_{Mn} \approx 2$ and the temperature $T = 2$ K.

2.4 Markov limit

Approximation (v), i.e. neglecting the source terms b^{III}, makes it possible to formally integrate the equations of motion for the correlations (3e)–(3g) and obtain expressions for the correlations, which have the form of memory integrals over the values of the single-particle density matrices at earlier times. In the Markov limit, where it is assumed that this memory is short, the quantum kinetic equations reduce to rate equations. For vanishing magnetic field and impurity magnetization, this procedure gives the same results as Fermi's golden rule.[26] Since the goal of the present paper is to work out the conditions under which the quantum kinetic results deviate from the Markovian rate equations, we also calculate the Markovian results in order to enable a direct comparison. Note that, here, the Markovian approximation is applied only to the s-d interaction, whereas the light-matter interaction is still taken into account fully coherently. The p-d interaction does not lead to a carrier-impurity spin transfer in the approximation of a narrow quantum well with strong heavy-hole–light-hole splitting (ii).

For the derivation of the Markovian rate equations, the reader is referred to Ref. 26. For a formulation of the rate equations, it is useful to define the spin-up and spin-down occupations $n_{\mathbf{k}_1}^{\uparrow/\downarrow}$ and the perpendicular carrier spin $\mathbf{s}_{\mathbf{k}_1}^{\perp}$ with respect to the quantization axis given by the external magnetic field direction $\mathbf{e}_{\parallel} = \frac{\mathbf{B}}{|\mathbf{B}|}$ by:

$$n_{\mathbf{k}_1}^{\uparrow/\downarrow} := \sum_{l_1 l_2} (\frac{1}{2}\delta_{l_1 l_2} \pm \mathbf{e}_{\parallel} \cdot \mathbf{s}_{l_1 l_2}) C_{l_1 \mathbf{k}_1}^{l_2},$$

$$\mathbf{s}_{\mathbf{k}_1}^{\perp} := \mathbf{s}_{\mathbf{k}_1} - \frac{1}{2}(n_{\mathbf{k}_1}^{\uparrow} - n_{\mathbf{k}_2}^{\downarrow})\mathbf{e}_{\parallel}, \tag{5a}$$

where $\mathbf{s}_{\mathbf{k}_1} := \sum_{l_1 l_2} \mathbf{s}_{l_1 l_2} C_{l_1 \mathbf{k}_1}^{l_2}$ is the average spin in the conduction band states with wave vector $\mathbf{k}_1$. In the Markov limit, the contribution of the correlations to the equations of motion for the carrier variables are:[26]

$$\frac{\partial}{\partial t} n_{\mathbf{k}_1}^{\uparrow/\downarrow}\Big|_{cor} \approx \frac{\pi J_{\mathrm{sd}}^2 N_{\mathrm{Mn}}}{\hbar^2 V^2} \sum_{\mathbf{k}_2} \delta\Big(\omega_{\mathbf{k}_2} - \big(\omega_{\mathbf{k}_1} \pm (\omega_e - \omega_{Mn})\big)\Big) \Big[\big(\langle S^{\perp\,2}\rangle \pm \frac{\langle S^{\|}\rangle}{2}\big)(1 - n_{\mathbf{k}_1}^{\uparrow/\downarrow}) n_{\mathbf{k}_2}^{\downarrow/\uparrow}$$

$$- \big(\langle S^{\perp\,2}\rangle \mp \frac{\langle S^{\|}\rangle}{2}\big)(1 - n_{\mathbf{k}_2}^{\downarrow/\uparrow}) n_{\mathbf{k}_1}^{\uparrow/\downarrow}\Big], \tag{6a}$$

$$\frac{\partial}{\partial t} \mathbf{s}_{\mathbf{k}_1}^{\perp}\Big|_{cor} \approx -\frac{\pi J_{\mathrm{sd}}^2 N_{\mathrm{Mn}}}{\hbar^2 V^2} \sum_{\mathbf{k}_2} \Big[\delta(\omega_{\mathbf{k}_2} - \omega_{\mathbf{k}_1})\langle S^{\|\,2}\rangle + \delta\Big(\omega_{\mathbf{k}_2} - \big(\omega_{\mathbf{k}_1} + (\omega_e - \omega_{Mn})\big)\Big) \frac{1}{2}\big(\langle S^{\perp\,2}\rangle - (1 - 2n_{\mathbf{k}_2}^{\uparrow})\frac{\langle S^{\|}\rangle}{2}\big)$$

$$+ \delta\Big(\omega_{\mathbf{k}_2} - \big(\omega_{\mathbf{k}_1} - (\omega_e - \omega_{Mn})\big)\Big) \frac{1}{2}\big(\langle S^{\perp\,2}\rangle + (1 - 2n_{\mathbf{k}_2}^{\downarrow})\frac{\langle S^{\|}\rangle}{2}\big)\Big] \mathbf{s}_{\mathbf{k}_1}^{\perp}, \tag{6b}$$

with operators $S^{\|} = \mathbf{e}_{\|} \cdot \mathbf{S}$ and $S^{\perp\,2} = \frac{1}{2}\big(S^2 - S^{\|\,2}\big)$ and band energies $\hbar\omega_{\mathbf{k}} := E_{l\mathbf{k}}$. In Eq. (6b) the quantitatively small correlation-induced renormalization of the spin precession frequency[24] has been neglected.

Equations (6) can be understood as follows:[26] The s-d interaction is responsible for spin-flip scattering processes, where a spin-up electron becomes a spin-down electron and vice-versa, while an impurity spin flips in the opposite direction. In this process, the energy $\hbar\omega_e$ of the spin degree of freedom of a spin-up electron is released and a quantum $\hbar\omega_{Mn}$ has to be spent in order to flip the corresponding impurity spin. The magnetic energy $\hbar\omega_e - \hbar\omega_{Mn}$ released in a spin-flip scattering process has to be accommodated by an increase of the kinetic energy of the scattered electron of the same magnitude. This explains the arguments of the δ-function in Eqs. (6). The terms $(1 - n_{\mathbf{k}}^{\uparrow/\downarrow})$ in Eq. (6a) account for Pauli blocking effects. The rate, i.e. the prefactor in Eq. (6), depends on the value of the impurity spins. A stationary value of the occupations $n_{\mathbf{k}_1}^{\uparrow/\downarrow}$ is reached when spin-flip scattering processes from spin-up to spin-down states balance spin-flips in the opposite direction. The perpendicular carrier spin component $\mathbf{s}_{\mathbf{k}_1}^{\perp}$ decays approximately exponentially towards zero.

Assuming a parabolic band structure we find for the Markovian rate equations

$$\frac{\partial}{\partial t} C_{l_1 \mathbf{k}_1}^{l_2} = \frac{i}{\hbar} \sum_v \mathbf{E} \cdot \big(\mathbf{M}_{v l_2 \mathbf{k}_1}^* (Y_{v-\mathbf{k}_1}^{l_1})^* - \mathbf{M}_{v l_1 \mathbf{k}_1} Y_{v-\mathbf{k}_1}^{l_2}\big) + \frac{\partial}{\partial t} C_{l_1 \mathbf{k}_1}^{l_2}\Big|_{cor}, \tag{7a}$$

$$\frac{\partial}{\partial t} D_{v_1 \mathbf{k}_1}^{v_2} = \frac{i}{\hbar} \sum_l \mathbf{E} \cdot \big(\mathbf{M}_{v_2 l-\mathbf{k}_1}^* (Y_{v_1 \mathbf{k}_1}^l)^* - \mathbf{M}_{v_1 l-\mathbf{k}_1} Y_{v_2 \mathbf{k}_1}^l\big), \tag{7b}$$

$$\frac{\partial}{\partial t} Y_{v_1 \mathbf{k}_1}^{l_2} = -\frac{i}{\hbar}\Big(E_g + \frac{\hbar^2 \mathbf{k}_1^2}{2 m_{hh}} + \frac{\hbar^2 \mathbf{k}_1^2}{2 m^*}\Big) Y_{v_1 \mathbf{k}_1}^{l_2} + \frac{i}{\hbar}\Big(\mathbf{E} \cdot \mathbf{M}_{v_1 l_2-\mathbf{k}_1}^* - \sum_l \mathbf{E} \cdot \mathbf{M}_{v_1 l-\mathbf{k}_1}^* C_{l-\mathbf{k}_1}^{l_2} - \sum_v \mathbf{E} \cdot \mathbf{M}_{v l_2-\mathbf{k}_1}^* D_{v \mathbf{k}_1}^{v_1}\Big), \tag{7c}$$

with effective electron and heavy-hole masses m^* and m_{hh}, band gap E_g and

$$\frac{\partial}{\partial t} C_{l_1 \mathbf{k}_1}^{l_2}\Big|_{cor} = \frac{1}{2}\delta_{l_1 l_2}\Big(\frac{\partial}{\partial t} n_{\mathbf{k}_1}^{\uparrow}\Big|_{cor} + \frac{\partial}{\partial t} n_{\mathbf{k}_1}^{\downarrow}\Big|_{cor}\Big) + (\mathbf{e}_{\|} \cdot \mathbf{s}_{l_1 l_2})\Big(\frac{\partial}{\partial t} n_{\mathbf{k}_1}^{\uparrow}\Big|_{cor} - \frac{\partial}{\partial t} n_{\mathbf{k}_1}^{\downarrow}\Big|_{cor}\Big) + 2 \mathbf{s}_{l_1 l_2} \cdot \frac{\partial}{\partial t} \mathbf{s}_{\mathbf{k}_1}^{\perp}\Big|_{cor} \tag{7d}$$

If no external magnetic field is applied, a single spin transfer rate T_1^{-1} can be identified:

$$\frac{\partial}{\partial t} C_{l_1 \mathbf{k}_1}^{l_2}\Big|_{cor} = -\frac{1}{T_1}\Big(C_{l_1 \mathbf{k}_1}^{l_2} - \delta_{l_1 l_2}\frac{1}{2}\sum_l C_{l \mathbf{k}_1}^l\Big), \tag{8a}$$

$$\frac{1}{T_1} = \frac{J_{\mathrm{sd}}^2 N_{Mn} m^*}{\hbar^3 V d} \frac{\langle S^2\rangle}{3}, \tag{8b}$$

where $\langle S^2\rangle = \frac{35}{4}$ for a spin-$\frac{5}{2}$ impurity system and d is the width of the quantum well.

Table 1. Material parameters for ZnSe [cf. Ref. 20] and CdTe [cf. Ref. 26]. a_0: (cubic) lattice constant, m_e: conduction band effective mass, m_{hh}: heavy-hole mass, J_{sd}: coupling constant for conduction band electrons, J_{pd}: coupling constant for holes in the valence band.

	a_0	m_e	m_{hh}	J_{sd}	J_{pd}
ZnSe	0.567 nm	0.21 m_0	1.44 m_0	-12 meVnm^3	60 meVnm^3
CdTe	0.648 nm	0.1 m_0	0.7 m_0	-15 meVnm^3	60 meVnm^3

3. RESULTS

We first consider a $Cd_{0.93}Mn_{0.07}Te$ quantum well excited with a Gaussian laser pulse with FWHM duration $\tau_L = 1.7$ ps and central frequency in resonance with the band gap. The material parameters used in our calculations are listed in Table 1. The pulse characteristics have been chosen here as in a previous study of a 4 nm wide $Zn_{0.93}Mn_{0.07}Se$ quantum well[21] which enables a conclusive comparison of the different materials. The time evolution of the carrier spins resulting from the quantum kinetic theory is shown in Fig. 1(a) together with mean-field and rate equation results. The corresponding curves for $Zn_{0.93}Mn_{0.07}Se$ from Ref. 21 are included for comparison in Fig. 2(d).

The carrier spin is normalized so that at long times $t \to \infty$ a value of 1 corresponds to the maximal spin polarization. For $B = 0$ and a paramagnetic impurity system, the s/p-d interaction has no effect whatsoever in the mean-field approximation. Thus, the mean-field result simply tracks the build-up of carrier occupations during the laser pulse. Similar to the ZnMnSe quantum well of Ref. 21, the differences between the results of the quantum kinetic theory and the Markovian rate equaitions are the following: First, the spin transfer in the quantum kinetic description is delayed with respect to the rate equations, so that the quantum kinetics follows the mean-field curve more closely in the first few hundred fs. After that, the carrier spin according to the quantum kinetic theory decreases faster than predicted by the rate equations and eventually leads to an overshoot, i.e. a non-monotonic time trace of the electronic spin polarization which in the case shown in Fig. 1(a) first falls below zero and then recovers.

Figure 1(b) shows the kinetic energy distribution of the electrons at $t = 0$. Note that in order to achieve comparable occupations for the quantum kinetic calculation and the rate equations (maximum of occupations at $E_{\mathbf{k}} = 0$ meV), it was necessary to slightly shift the laser energy with respect to the band edge about -0.25 meV (-0.68 meV for ZnSe) to compensate a renormalization of the carrier energies due to the s-d interaction. Still, the occupations obtained using the quantum kinetic theory form a broader peak than predicted by the rate equations. This is due to the scattering of carriers at the impurities which induces a redistribution in $\mathbf{k}$-space.[20]

In comparison with the ZnSe quantum well depicted in Fig. 2(d), the carrier spin in the CdTe quantum well in Fig. (1) decays slower and the overshoot of the quantum kinetic result is less pronounced, although the basic features are very similar in both figures. This agrees with the findings for initial value calculations[20, 27] that the non-Markovian effects are particularly strong when the rate is large. According to Eq. (8b) the spin relaxation times at $B = 0$ are $T_1 \approx 3.0$ ps for the CdTe DMS and $T_1 \approx 1.5$ ps for the ZnSe system. The difference between both sets of material parameters is mainly that the effective electron mass, which enters linearly in the expression for the rate, is about twice as large in ZnSe compared with CdTe.

Figure 2 shows the time evolution of the carrier spins in a $Zn_{0.93}Mn_{0.07}Se$ quantum well for different pulse durations τ_L. For the short pulses presented in Fig. 2(a) and Fig. 2(b), the quantum kinetic results show an almost exponential decay. The main difference between the quantum kinetic and the Markovian results is that an exponential fit to the quantum kinetic curves yields an increased rate by about 5% for $\tau_L = 0.17$ ps [Fig. 2(a)] and 7% for $\tau_L = 0.34$ ps [Fig. 2(b)]. The fact that the spin transfer is nearly exponential for short pulses, i.e. broad spectral distributions of the excited carriers, is compatible with the finding of previous initial value calculations,[27] where the non-Markovian features were shown to be particularly strong for excitation in close proximity to the band edge.

When the pulse duration reaches values close to the spin transfer time $T_1 \approx 1.5$ ps according to Fermi's golden rule, such as in Figs. 2(c) and (d) for $\tau_L = 0.85$ ps and $\tau_L = 1.7$ ps, the non-Markovian effects, i.e. a short delay of the spin transfer and an overshoot, become visible, as already discussed for the situation depicted in Fig. 1. Even for pulse durations much longer than the spin transfer time [cf. Figs. 2(e) and (f)], the non-Markovian
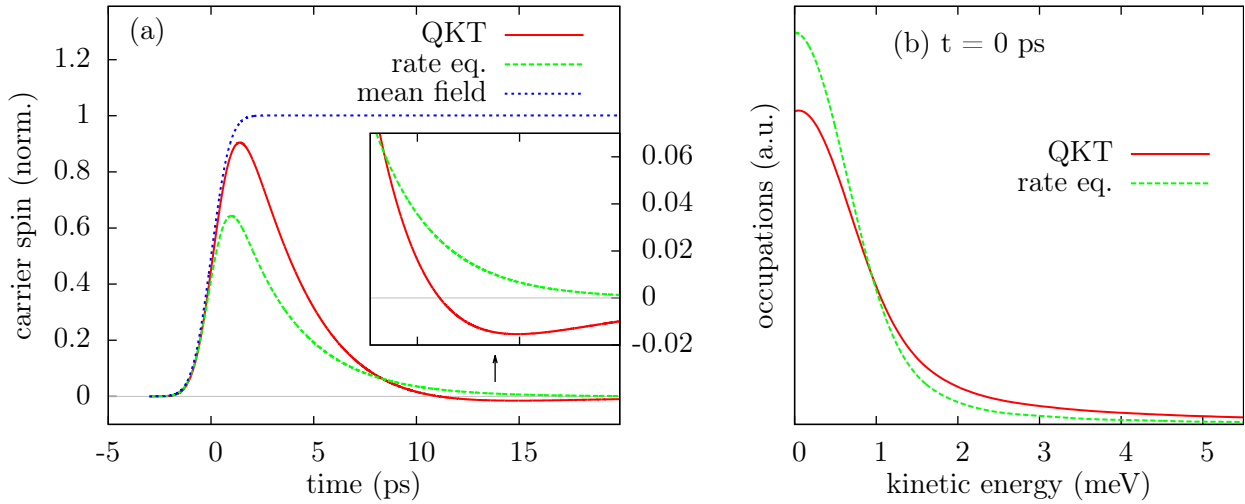
Figure 1. (a) Time evolution of the carrier spin in a 4 nm wide $Cd_{0.93}Mn_{0.07}Te$ quantum well after optical excitation with a circularly polarized Gaussian light beam with pulse duration (FWHM) $\tau_L = 1.7$ ps centered at $t = 0$. The inset shows a magnified picture of the region where the non-monotonic behavior of the spin dynamics occurs. Red solid lines describe the results of the quantum kinetic equations (3), green dashed lines represent the Markovian calculations based on Eqs. (7). The blue dotted line shows the mean-field result where the correlations are neglected. (b) Distribution of the electronic kinetic energy at $t = 0$.
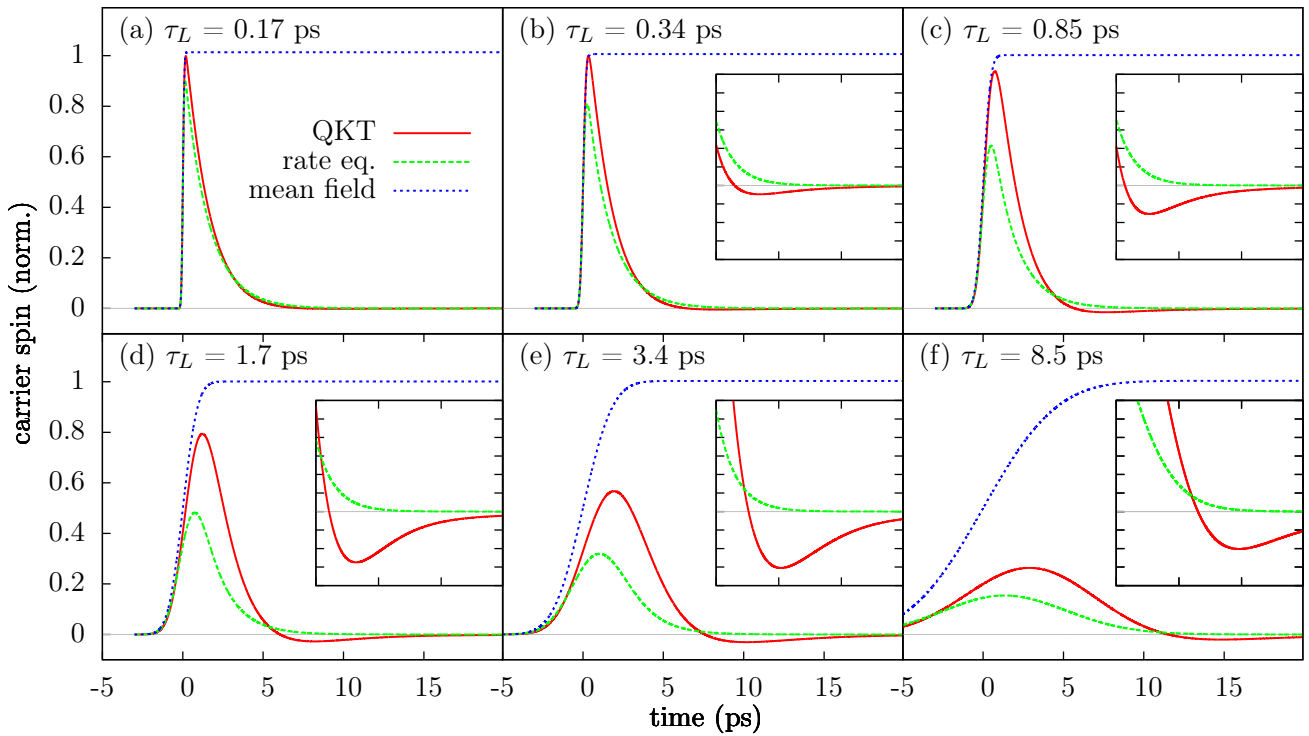

Figure 2. Time evolution of the carrier spin in a 4 nm wide $Zn_{0.93}Mn_{0.07}Se$ quantum well for different pulse durations τ_L. Key as in Fig. 1. The insets show magnifications of the regions from -0.04 to 0.06 of the normalized carrier spin in the time interval from 5 ps to 20 ps.
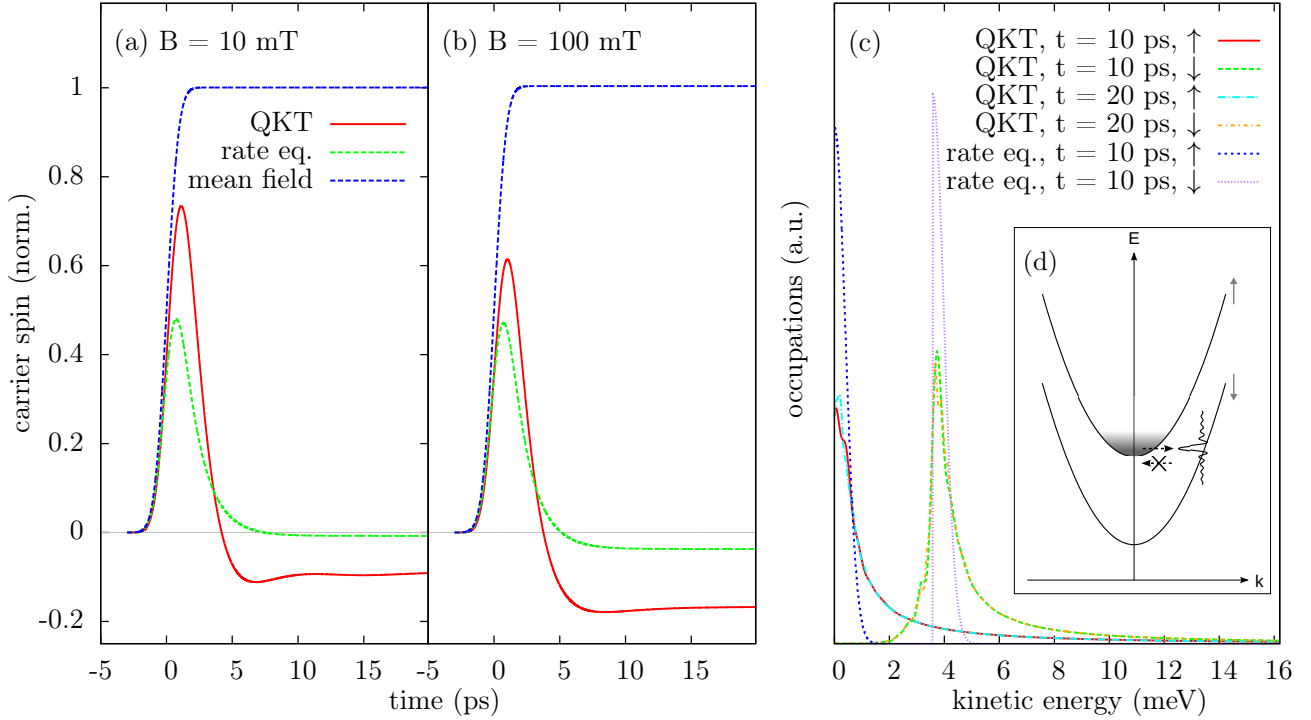
Figure 3. Time evolution of the carrier spin in a 4 nm wide $Zn_{0.93}Mn_{0.07}Se$ quantum well in the presence of external magnetic fields (a) $B = 10$ mT and (b) $B = 100$ mT, excited with pulse duration $\tau_L = 1.7$ ps. (c) spin-up and spin-down occupations at $t = 10$ ps and 20 ps, respectively, for the calculation with $B = 100$ mT. (d): Band diagram of spin-up and spin-down electrons in an external magnetic field.

effects are clearly observable. Thus, the overshoots are not destroyed due to a smoothing of the dynamics, which might be expected for long pulse durations.

The effects of an external magnetic field on the spin dynamics are shown in Fig. 3 for the $Zn_{0.93}Mn_{0.07}Se$ quantum well excited by a laser with pulse duration $\tau_L = 1.7$ ps. For small magnetic fields [$B = 10$ mT, Fig. 3(a)], the same deviations of the quantum kinetic results from the Markovian calculations are found as in the zero-magnetic-field case, in particular the non-monotonic time trace in the form of an overshoot as well as the short delay and subsequent increase of the carrier-impurity spin transfer. For higher magnetic fields [$B = 100$ mT, Fig. 3(b)], these effects are visibly reduced. However, the most striking genuine quantum kinetic effect, which is absent in the zero-magnetic-field case, is that the stationary value reached in the limit $t \to \infty$ is significantly different from the predictions of the rate equations. To understand this effect, the occupations of the spin-up and spin-down bands at $t = 10$ ps and $t = 20$ ps are presented in Fig. 3(c) and the spin-flip scattering process is visualized in Fig. 3(d). The rate equations predict that a spin-flip scattering process is strictly horizontal in the band structure, i.e. the spin-up occupations are transferred to the spin-down band at the same total energy, which due to the giant Zeeman splitting of the bands implies an increase of the kinetic energy of the scattered electron. Since the transition is δ-like in energy, the emerging occupation in the spin-down band in Fig. 3(c) is a replica of the optically induced occupation in the spin-up band. In the quantum kinetic calculations, one can observe a significant broadening of the scattered electron distribution. Note that the broadening of the spin-up occupations in Fig. 3(c) with respect to the prediction of the rate equations is due to the scattering during the light pulse, as already shown in Fig. 1(b) for $B = 0$. The stationary spin polarization is reached when there is a balance between scattering from the spin-up to the spin-down band and vice versa. The small non-zero stationary spin polarization in the case of the rate equations is a consequence of the different prefactors $\left(\langle S^{\perp^2} \rangle \pm \frac{1}{2} \langle S^{\parallel} \rangle \right)$ for the corresponding transition rates [cf. Eq. (6a)]. In contrast, the quantum kinetic theory predicts a broadening of the electron occupations in the spin-down band, so that a significant number of states below the energetic threshold corresponding to the band splitting are occupied [cf. Fig. 3(c)]. The probability of

these states to scatter back to the spin-up band is considerably reduced, as there are no spin-up states with the same total energy. Thus, the balance between the scattering from and to spin-up and spin-down bands becomes biased in the quantum kinetic theory, which leads to a different stationary value of the carrier spin. In this sense, the system acts effectively like a quantum ratchet[29] driven by the carrier-impurity correlations.

A broadening of carrier distributions is often found in quantum kinetic calculations at early times reflecting the energy-time uncertainty.[30,31] If the main reason for the broadening in the case studied here were the energy-time uncertainty, the distributions would be expected to narrow for later times. However, one can see clearly in Fig. 3(c) that the width of the distributions at $t = 20$ ps is practically identical to that at $t = 10$ ps. We propose that the reason for the broadening is not primarily the energy-time uncertainty, but rather the fact that the carriers and impurities become strongly correlated. Thus, the eigenstates of the system are many-particle states, which cannot be separated into products of independent single-particle states. Taking the partial trace of such a many-particle state to obtain the reduced single-particle density matrix means that the single-particle occupations do not correspond to states with well-defined single-particle energies. This picture is consistent with the fact that the distributions stay broad also for longer times. Thus, we attribute the broadening of the distributions observed in Fig. 3(c) rather to strong many-body correlation effects than to the energy-time uncertainty.

Note that the difference in the stationary values for the rate equations and the quantum kinetic theory can only be clearly distinguished if there is no significant thermalization, e.g. due to carrier-carrier or carrier-phonon interaction, during the lifetime of the optically excited carriers. If thermalization processes are active and enable a dissipation of energy, the system in the situation depicted in Fig. 3(d) will evolve into an equilibrium state, where only the spin-down band is occupied, which would lead to a negative spin polarization close to -1 also when exchange interaction is treated in the Markov limit. However, for low excitation intensities and temperatures and a band splitting well below the energy of LO phonons, thermalization is expected to play a minor role on the timescale considered here and the deviations of the degree of spin polarization from the prediction of rate equation a few T_1 after the laser pulse are indeed a signature of genuine quantum kinetic effects.

4. CONCLUSION

A quantum kinetic theory is employed to describe the spin dynamics in diluted magnetic semiconductors. Numerical calculations for different excitation conditions allow us to identify a regime where genuine quantum kinetic effects, which cannot be described by simple rate equations, are particularly pronounced.

We find that in order to experimentally access these non-Markovian quantum kinetic effects, it is advantageous to use laser pulses with durations on the order of or longer than the carrier-impurity spin transfer time, which can be obtained from Fermi's golden rule. For a 4 nm wide $Zn_{0.93}Mn_{0.07}Se$ we find pulse durations of more than $\sim$1 ps most suitable for this purpose. Earlier studies[20] already found that the non-Markovian effects are particularly strong for materials where the spin transfer rate is large. Numerical calculations confirm that due to the different sets of material parameters, Mn-doped ZnSe is slightly better suited than CdTe for experiments targeted at confirming non-Markovian effects in DMS.

Furthermore, in the presence of an external magnetic field, the quantum kinetic theory predicts a significantly different stationary value of the carrier spin polarization than Markovian rate equations, which is directly connected to a spectral broadening of the distribution of spin-flip scattered electrons. In contrast to the usual situation in quantum kinetic calculations,[30,31] this broadening stems not from the energy-time uncertainty, but it is rather a consequence of strong many-body correlations.

ACKNOWLEDGMENTS

APPENDIX A. SOURCE TERMS FOR CORRELATIONS

The source terms for the correlations $Q_C{}_{l_1 n_1 \mathbf{k}_1}^{l_2 n_2 \mathbf{k}_2}$ are:

$$b_C{}_{l_1 n_1 \mathbf{k}_1}^{\mathbf{E}\, l_2 n_2 \mathbf{k}_2} = \sum_v \mathbf{E} \cdot \left(\mathbf{M}_{v l_2 \mathbf{k}_2}^* (Q_Y{}_{v n_2 - \mathbf{k}_2}^{l_1 n_1 \mathbf{k}_1})^* - \mathbf{M}_{v l_1 \mathbf{k}_1} Q_Y{}_{v n_1 - \mathbf{k}_1}^{l_2 n_2 \mathbf{k}_2} \right), \tag{9a}$$

$$b_C{}_{l_1 n_1 \mathbf{k}_1}^{I\, l_2 n_2 \mathbf{k}_2} = J_{\mathrm{sd}} \sum_{n l l'} \left(\mathbf{S}_{n n_1} \cdot \mathbf{s}_{l l'}^e (\delta_{l_1 l'} - C_{l_1 \mathbf{k}_1}^{l'}) C_{l \mathbf{k}_2}^{l_2} M_n^{n_2} - \mathbf{S}_{n_2 n} \cdot \mathbf{s}_{l l'}^e (\delta_{l l_2} - C_{l \mathbf{k}_2}^{l_2}) C_{l_1 \mathbf{k}_1}^{l'} M_{n_1}^n \right)$$
$$+ J_{\mathrm{pd}} \sum_{n v v'} \mathbf{s}_{v v'}^h Y_{v' - \mathbf{k}_2}^{l_2} (Y_{v - \mathbf{k}_1}^{l_1})^* \cdot \left(\mathbf{S}_{n n_1} M_n^{n_2} - \mathbf{S}_{n_2 n} M_{n_1}^n \right), \tag{9b}$$

$$b_C{}_{l_1 n_1 \mathbf{k}_1}^{II\, l_2 n_2 \mathbf{k}_2} = \sum_l \boldsymbol{\omega}_e \cdot \left(\mathbf{s}_{l l_1}^e Q_C{}_{l n_1 \mathbf{k}_1}^{l_2 n_2 \mathbf{k}_2} - \mathbf{s}_{l_2 l}^e Q_C{}_{l_1 n_1 \mathbf{k}_1}^{l n_2 \mathbf{k}_2} \right) + \sum_n \boldsymbol{\omega}_{Mn} \cdot \left(\mathbf{S}_{n n_1} Q_C{}_{l_1 n \mathbf{k}_1}^{l_2 n_2 \mathbf{k}_2} - \mathbf{S}_{n_2 n} Q_C{}_{l_1 n_1 \mathbf{k}_1}^{l_2 n \mathbf{k}_2} \right), \tag{9c}$$

$$b_C{}_{l_1 n_1 \mathbf{k}_1}^{III\, l_2 n_2 \mathbf{k}_2} = \frac{J_{\mathrm{sd}}}{V} \sum_{\mathbf{k}} \sum_{n l} \Bigg[\left(\mathbf{S}_{n n_1} \cdot \mathbf{s}_{l l_1}^e Q_C{}_{l n \mathbf{k}}^{l_2 n_2 \mathbf{k}_2} - \mathbf{S}_{n_2 n} \cdot \mathbf{s}_{l_2 l}^e Q_C{}_{l_1 n_1 \mathbf{k}_1}^{l n \mathbf{k}} \right)$$
$$- \sum_{l'} \mathbf{s}_{l l'}^e C_{l_1 \mathbf{k}_1}^{l'} \cdot \left(\mathbf{S}_{n n_1} Q_C{}_{l n \mathbf{k}}^{l_2 n_2 \mathbf{k}_2} - \mathbf{S}_{n_2 n} Q_C{}_{l n_1 \mathbf{k}}^{l_2 n \mathbf{k}_2} \right) - \sum_{l'} C_{l \mathbf{k}_2}^{l_2} \mathbf{s}_{l l'}^e \cdot \left(\mathbf{S}_{n n_1} Q_C{}_{l_1 n \mathbf{k}_1}^{l' n_2 \mathbf{k}} - \mathbf{S}_{n_2 n} Q_C{}_{l_1 n_1 \mathbf{k}_1}^{l' n \mathbf{k}} \right) \Bigg]$$
$$+ \frac{J_{\mathrm{pd}}}{V} \sum_{\mathbf{k}} \sum_{n v v'} \mathbf{s}_{v v'}^h \cdot \Bigg[(Y_{v - \mathbf{k}_1}^{l_1})^* \left(\mathbf{S}_{n n_1} Q_Y{}_{v' n \mathbf{k}}^{l_2 n_2 \mathbf{k}_2} - \mathbf{S}_{n_2 n} Q_Y{}_{v' n_1 \mathbf{k}}^{l_2 n \mathbf{k}} \right)$$
$$+ Y_{v' - \mathbf{k}_2}^{l_2} \left(\mathbf{S}_{n n_1} (Q_Y{}_{v n_2 \mathbf{k}}^{l_1 n \mathbf{k}_1})^* - \mathbf{S}_{n_2 n} (Q_Y{}_{v n \mathbf{k}}^{l_1 n_1 \mathbf{k}_1})^* \right) \Bigg]. \tag{9d}$$

The source terms for the correlations $Q_D{}_{v_1 n_1 \mathbf{k}_1}^{v_2 n_2 \mathbf{k}_2}$ are:

$$b_D{}_{v_1 n_1 \mathbf{k}_1}^{\mathbf{E}\, v_2 n_2 \mathbf{k}_2} = \sum_l \mathbf{E} \cdot \left(\mathbf{M}_{v_2 l - \mathbf{k}_2}^* (Q_Y{}_{v_1 n_2 \mathbf{k}_1}^{l n_1 - \mathbf{k}_2})^* - \mathbf{M}_{v_1 l - \mathbf{k}_1} Q_Y{}_{v_2 n_1 \mathbf{k}_2}^{l n_2 - \mathbf{k}_1} \right), \tag{10a}$$

$$b_D{}_{v_1 n_1 \mathbf{k}_1}^{I\, v_2 n_2 \mathbf{k}_2} = J_{\mathrm{pd}} \sum_{n v v'} \left(\mathbf{S}_{n n_1} \cdot \mathbf{s}_{v v'}^h (\delta_{v_1 v'} - D_{v_1 \mathbf{k}_1}^{v'}) D_{v \mathbf{k}_2}^{v_2} M_n^{n_2} - \mathbf{S}_{n_2 n} \cdot \mathbf{s}_{v v'}^h (\delta_{v v_2} - D_{v \mathbf{k}_2}^{v_2}) D_{v_1 \mathbf{k}_1}^{v'} M_{n_1}^n \right)$$
$$+ J_{\mathrm{sd}} \sum_{n l l'} \mathbf{s}_{l l'}^e Y_{v_2 \mathbf{k}_2}^{l'} (Y_{v_1 \mathbf{k}_1}^l)^* \cdot \left(\mathbf{S}_{n n_1} M_n^{n_2} - \mathbf{S}_{n_2 n} M_{n_1}^n \right), \tag{10b}$$

$$b_D{}_{v_1 n_1 \mathbf{k}_1}^{II\, v_2 n_2 \mathbf{k}_2} = \sum_v \boldsymbol{\omega}_h \cdot \left(\mathbf{s}_{v v_1}^h Q_D{}_{v n_1 \mathbf{k}_1}^{v_2 n_2 \mathbf{k}_2} - \mathbf{s}_{v_2 v}^h Q_D{}_{v_1 n_1 \mathbf{k}_1}^{v n_2 \mathbf{k}_2} \right) + \sum_n \boldsymbol{\omega}_{Mn} \cdot \left(\mathbf{S}_{n n_1} Q_D{}_{v_1 n \mathbf{k}_1}^{v_2 n_2 \mathbf{k}_2} - \mathbf{S}_{n_2 n} Q_D{}_{v_1 n_1 \mathbf{k}_1}^{v_2 n \mathbf{k}_2} \right), \tag{10c}$$

$$b_D{}_{v_1 n_1 \mathbf{k}_1}^{III\, v_2 n_2 \mathbf{k}_2} = \frac{J_{\mathrm{pd}}}{V} \sum_{\mathbf{k}} \sum_{n v} \Bigg[\left(\mathbf{S}_{n n_1} \cdot \mathbf{s}_{v v_1}^h Q_D{}_{v n \mathbf{k}}^{v_2 n_2 \mathbf{k}_2} - \mathbf{S}_{n_2 n} \cdot \mathbf{s}_{v_2 v}^h Q_D{}_{v_1 n_1 \mathbf{k}_1}^{v n \mathbf{k}} \right)$$
$$- \sum_{v'} \mathbf{s}_{h h'}^e D_{v_1 \mathbf{k}_1}^{v'} \cdot \left(\mathbf{S}_{n n_1} Q_D{}_{v n \mathbf{k}}^{v_2 n_2 \mathbf{k}_2} - \mathbf{S}_{n_2 n} Q_D{}_{v n_1 \mathbf{k}}^{v_2 n \mathbf{k}_2} \right) - \sum_{v'} \mathbf{s}_{v v'}^h D_{v \mathbf{k}_2}^{v_2} \left(\mathbf{S}_{n n_1} Q_D{}_{v_1 n \mathbf{k}_1}^{v' n_2 \mathbf{k}} - \mathbf{S}_{n_2 n} Q_D{}_{v_1 n_1 \mathbf{k}_1}^{v' n \mathbf{k}} \right) \Bigg]$$
$$+ \frac{J_{\mathrm{sd}}}{V} \sum_{\mathbf{k}} \sum_{n l l'} \mathbf{s}_{l l'}^e \cdot \Bigg[(Y_{v_1 \mathbf{k}_1}^l)^* \left(\mathbf{S}_{n n_1} Q_Y{}_{v_2 n \mathbf{k}_2}^{l' n_2 \mathbf{k}} - \mathbf{S}_{n_2 n} Q_Y{}_{v_2 n_1 \mathbf{k}_2}^{l' n \mathbf{k}} \right)$$
$$+ Y_{v_2 \mathbf{k}_2}^{l'} \left(\mathbf{S}_{n n_1} (Q_Y{}_{v_1 n_2 \mathbf{k}_1}^{l n \mathbf{k}})^* - \mathbf{S}_{n_2 n} (Q_Y{}_{v_1 n \mathbf{k}_1}^{l n_1 \mathbf{k}})^* \right) \Bigg]. \tag{10d}$$

The source terms for the correlations $Q_Y{}_{v_1 n_1 \mathbf{k}_1}^{l_2 n_2 \mathbf{k}_2}$ are:

$$b_Y{}_{v_1 n_1 \mathbf{k}_1}^{\mathbf{E}\, l_2 n_2 \mathbf{k}_2} = - \sum_l \mathbf{E} \cdot \left(\mathbf{M}_{v_1 l - \mathbf{k}_1}^* Q_C{}_{l n_1 - \mathbf{k}_1}^{l_2 n_2 \mathbf{k}_2} - \mathbf{M}_{v l_2 \mathbf{k}_2}^* Q_D{}_{v n_1 - \mathbf{k}_2}^{v_1 n_2 \mathbf{k}_1} \right), \tag{11a}$$

$$b_Y{}_{v_1 n_1 \mathbf{k}_1}^{I\, l_2 n_2 \mathbf{k}_2} = - \sum_n \mathbf{S}_{n_2 n} \cdot \left[J_{\mathrm{sd}} \sum_l \mathbf{s}_{l_2 l}^e Y_{v_1 \mathbf{k}_1}^l M_{n_1}^n + J_{\mathrm{pd}} \sum_v \mathbf{s}_{v_1 v}^h Y_{v - \mathbf{k}_2}^{l_2} M_{n_1}^n \right]$$
$$- \sum_n \left(J_{\mathrm{sd}} \sum_{l l'} \mathbf{s}_{l l'}^e Y_{v_1 \mathbf{k}_1}^{l'} C_{l \mathbf{k}_2}^{l_2} + J_{\mathrm{pd}} \sum_{v v'} \mathbf{s}_{v v'}^h Y_{v' - \mathbf{k}_2}^{l_2} D_{v \mathbf{k}_1}^{v_1} \right) \cdot \left(\mathbf{S}_{n n_1} M_n^{n_2} - \mathbf{S}_{n_2 n} M_{n_1}^n \right), \tag{11b}$$

$$b_Y^{II}{}_{v_1 n_1 \mathbf{k}_1}^{l_2 n_2 \mathbf{k}_2} = -\sum_l \boldsymbol{\omega}_e \cdot \mathbf{s}_{l_2 l}^e Q_Y{}_{v_1 n_1 \mathbf{k}_1}^{l n_2 \mathbf{k}_2} - \sum_v \boldsymbol{\omega}_h \cdot \mathbf{s}_{v_1 v}^h Q_Y{}_{v n_1 \mathbf{k}_1}^{l_2 n_2 \mathbf{k}_2} + \sum_n \boldsymbol{\omega}_{Mn} \cdot \left(\mathbf{S}_{n n_1} Q_Y{}_{l_1 n \mathbf{k}_1}^{l_2 n_2 \mathbf{k}_2} - \mathbf{S}_{n_2 n} Q_Y{}_{l_1 n_1 \mathbf{k}_1}^{l_2 n \mathbf{k}_2} \right),$$

(11c)

$$\begin{aligned}
b_Y^{III}{}_{v_1 n_1 \mathbf{k}_1}^{l_2 n_2 \mathbf{k}_2} = & -\frac{1}{V} \sum_{\mathbf{k}} \sum_n \mathbf{S}_{n_2 n} \cdot \Big[J_{\mathrm{sd}} \sum_l \mathbf{s}_{l_2 l}^e Q_Y{}_{v_1 n_1 \mathbf{k}_1}^{l n \mathbf{k}} + J_{\mathrm{pd}} \sum_v \mathbf{s}_{v_1 v}^h Q_Y{}_{v n_1 \mathbf{k}}^{l_2 n \mathbf{k}_2} \Big] \\
& - \frac{J_{\mathrm{sd}}}{V} \sum_{\mathbf{k}} \sum_{n l l'} \mathbf{s}_{l l'}^e C_{l \mathbf{k}_2}^{l_2} \cdot \left(\mathbf{S}_{n n_1} Q_Y{}_{v_1 n \mathbf{k}_1}^{l' n_2 \mathbf{k}} - \mathbf{S}_{n_2 n} Q_Y{}_{v_1 n_1 \mathbf{k}_1}^{l' n \mathbf{k}} \right) \\
& - \frac{J_{\mathrm{pd}}}{V} \sum_{\mathbf{k}} \sum_{n v v'} \mathbf{s}_{v v'}^h D_{v \mathbf{k}_1}^{v_1} \cdot \left(\mathbf{S}_{n n_1} Q_Y{}_{v' n \mathbf{k}}^{l_2 n_2 \mathbf{k}_2} - \mathbf{S}_{n_2 n} Q_Y{}_{v' n_1 \mathbf{k}}^{l_2 n \mathbf{k}_2} \right) \\
& - \frac{J_{\mathrm{sd}}}{V} \sum_{n l l'} \mathbf{s}_{l l'}^e Y_{v_1 \mathbf{k}_1}^{l'} \cdot \left(\mathbf{S}_{n n_1} Q_C{}_{l n \mathbf{k}}^{l_2 n_2 \mathbf{k}_2} - \mathbf{S}_{n_2 n} Q_C{}_{l n_1 \mathbf{k}}^{l_2 n \mathbf{k}_2} \right) \\
& - \frac{J_{\mathrm{pd}}}{V} \sum_{n v v'} \mathbf{s}_{v v'}^h Y_{v' - \mathbf{k}_2}^{l_2} \cdot \left(\mathbf{S}_{n n_1} Q_D{}_{v n \mathbf{k}}^{v_1 n_2 \mathbf{k}_1} - \mathbf{S}_{n_2 n} Q_D{}_{v n_1 \mathbf{k}}^{v_1 n \mathbf{k}_1} \right)
\end{aligned}$$

(11d)

REFERENCES

[1] Žutić, I., Fabian, J., and Das Sarma, S., "Spintronics: Fundamentals and applications," *Rev. Mod. Phys.* **76**, 323–410 (2004).

[2] Žutić, I., Fabian, J., and Das Sarma, S., "Spin-polarized transport in inhomogeneous magnetic semiconductors: Theory of magnetic/nonmagnetic $p-n$ junctions," *Phys. Rev. Lett.* **88**, 066603 (2002).

[3] Ohno, H., Shen, A., Matsukura, F., Oiwa, A., Endo, A., Katsumoto, S., and Iye, Y., "(Ga,Mn)As: A new diluted magnetic semiconductor based on GaAs," *Applied Physics Letters* **69**(3), 363–365 (1996).

[4] Ohno, H., "A window on the future of spintronics," *Nat. Mater.* **9**, 952–954 (2010).

[5] Dietl, T. and Ohno, H., "Dilute ferromagnetic semiconductors: Physics and spintronic structures," *Rev. Mod. Phys.* **86**, 187–251 (2014).

[6] Dietl, T., Ohno, H., Matsukura, F., Cibert, J., and Ferrand, D., "Zener model description of ferromagnetism in zinc-blende magnetic semiconductors," *Science* **287**(5455), 1019–1022 (2000).

[7] Jiang, J. H., Zhou, Y., Korn, T., Schüller, C., and Wu, M. W., "Electron spin relaxation in paramagnetic Ga(Mn)As quantum wells," *Phys. Rev. B* **79**, 155201 (2009).

[8] Furdyna, J. K., "Diluted magnetic semiconductors," *J. Appl. Phys.* **64**(4), R29–R64 (1988).

[9] Zayachuk, D. M., Slobodskyy, T., Astakhov, G. V., Slobodskyy, A., Gould, C., Schmidt, G., Ossau, W., and Molenkamp, L. W., "Magnetic-field-induced exchange effects between Mn ions and free carriers in ZnSe quantum wells through the intermediate nonmagnetic barrier studied by photoluminescence," *Phys. Rev. B* **83**, 085308 (2011).

[10] Debus, J., Maksimov, A. A., Dunker, D., Yakovlev, D. R., Filatov, E. V., Tartakovskii, I. I., Ivanov, V. Y., Waag, A., and Bayer, M., "Heating of the Mn spin system by photoexcited holes in type-II (Zn,Mn)Se/(Be,Mn)Te quantum wells," *physica status solidi (b)* **251**(9), 1694–1699 (2014).

[11] Debus, J., Ivanov, V. Y., Ryabchenko, S. M., Yakovlev, D. R., Maksimov, A. A., Semenov, Y. G., Braukmann, D., Rautert, J., Löw, U., Godlewski, M., Waag, A., and Bayer, M., "Resonantly enhanced spin-lattice relaxation of Mn^{2+} ions in diluted magnetic (Zn,Mn)Se/(Zn,Be)Se quantum wells," *Phys. Rev. B* **93**, 195307 (2016).

[12] Schulz, R., Korn, T., Stich, D., Wurstbauer, U., Schuh, D., Wegscheider, W., and Schüller, C., "Ultrafast optical studies of diffusion barriers between ferromagnetic Ga(Mn)As layers and non-magnetic quantum wells," *Physica E: Low-dimensional Systems and Nanostructures* **40**(6), 2163 – 2165 (2008). 13th International Conference on Modulated Semiconductor Structures.

[13] Gaj, J., Planel, R., and Fishman, G., "Relation of magneto-optical properties of free excitons to spin alignment of Mn^{2+} ions in $Cd_{1-x}Mn_x Te$," *Solid State Commun.* **29**, 435 (1979).

[14] Crooker, S. A., Awschalom, D. D., Baumberg, J. J., Flack, F., and Samarth, N., "Optical spin resonance and transverse spin relaxation in magnetic semiconductor quantum wells," *Phys. Rev. B* **56**, 7574–7588 (1997).

[15] Ben Cheikh, Z., Cronenberger, S., Vladimirova, M., Scalbert, D., Perez, F., and Wojtowicz, T., "Electron spin dephasing in Mn-based II-VI diluted magnetic semiconductors," *Phys. Rev. B* **88**, 201306 (2013).

[16] Wu, M. W., Jiang, J. H., and Weng, M. Q., "Spin dynamics in semiconductors," *Phys. Rep.* **493**(24), 61 – 236 (2010).

[17] Krenn, H., Kaltenegger, K., Dietl, T., Spałek, J., and Bauer, G., "Photoinduced magnetization in dilute magnetic (semimagnetic) semiconductors," *Phys. Rev. B* **39**, 10918–10934 (1989).

[18] Camilleri, C., Teppe, F., Scalbert, D., Semenov, Y. G., Nawrocki, M., Dyakonov, M., Cibert, J., Tatarenko, S., and Wojtowicz, T., "Electron and hole spin relaxation in modulation-doped CdMnTe quantum wells," *Phys. Rev. B* **64**, 085331 (2001).

[19] Thurn, C. and Axt, V. M., "Quantum kinetic description of spin transfer in diluted magnetic semiconductors," *Phys. Rev. B* **85**, 165203 (2012).

[20] Thurn, C., Cygorek, M., Axt, V. M., and Kuhn, T., "Non-Markovian spin transfer dynamics in magnetic semiconductors despite short memory times," *Phys. Rev. B* **87**, 205301 (2013).

[21] Thurn, C., Cygorek, M., Axt, V. M., and Kuhn, T., "Coherent spin-transfer dynamics in diluted magnetic semiconductor quantum wells even after optical excitation with zero net angular momentum," *Phys. Rev. B* **88**, 161302(R) (2013).

[22] Cygorek, M. and Axt, V. M., "Comparison between a quantum kinetic theory of spin transfer dynamics in Mn-doped bulk semiconductors and its Markov limit for nonzero Mn magnetization," *Phys. Rev. B* **90**, 035206 (2014).

[23] Cygorek, M. and Axt, V. M., "Effective equations for the precession dynamics of electron spins and electron-impurity correlations in diluted magnetic semiconductors," *Semicond. Sci. Technol.* **30**(8), 085011 (2015).

[24] Cygorek, M., Tamborenea, P. I., and Axt, V. M., "Nonperturbative correlation effects in diluted magnetic semiconductors," *Phys. Rev. B* **93**, 035206 (2016).

[25] Ungar, F., Cygorek, M., Tamborenea, P. I., and Axt, V. M., "Ultrafast spin dynamics in II-VI diluted magnetic semiconductors with spin-orbit interaction," *Phys. Rev. B* **91**, 195201 (2015).

[26] Cygorek, M., Tamborenea, P. I., and Axt, V. M., "Carrier-impurity spin transfer dynamics in paramagnetic II-VI diluted magnetic semiconductors in the presence of a wave-vector-dependent magnetic field," *Phys. Rev. B* **93**, 205201 (2016).

[27] Cygorek, M. and Axt, V. M., "Non-Markovian Effects in the Spin Transfer Dynamics in Diluted Magnetic Semiconductors due to Excitation in Proximity to the Band Edge," *Journal of Physics: Conference Series* **647**(1), 012042 (2015).

[28] Bastard, G., [*Wave Mechanics Applied to Semiconductor Heterostructures*], Monographies de physique, Les Editions de Physique, JOUVE, France (1990).

[29] Ang, Y. S., Ma, Z., and Chao, Z., "Quantum ratchet in two-dimensional semiconductors with Rashba spin-orbit interaction," *Scientific Reports* **5**, 7872 (2015).

[30] Schilp, J., Kuhn, T., and Mahler, G., "Electron-phonon quantum kinetics in pulse-excited semiconductors: Memory and renormalization effects," *Phys. Rev. B* **50**, 5435–5447 (1994).

[31] Fürst, C., Leitenstorfer, A., Laubereau, A., and Zimmermann, R., "Quantum Kinetic Electron-Phonon Interaction in GaAs: Energy Nonconserving Scattering Events and Memory Effects," *Phys. Rev. Lett.* **78**, 3733–3736 (1997).

Publication 9

Insensitivity of spin dynamics to the orbital angular momentum transferred from twisted light to extended semiconductors

M. Cygorek, P. I. Tamborenea and V. M. Axt

Phys. Rev B **92**, 115301 (2015)

Insensitivity of spin dynamics to the orbital angular momentum transferred from twisted light to extended semiconductors

M. Cygorek,[1] P. I. Tamborenea,[1,2] and V. M. Axt[1]

[1]*Theoretische Physik III, Universität Bayreuth, 95440 Bayreuth, Germany*
[2]*Departamento de Física and IFIBA, FCEN, Universidad de Buenos Aires, Ciudad Universitaria, Pabellón I,*
1428 Ciudad de Buenos Aires, Argentina

We study the spin dynamics of carriers due to the Rashba interaction in semiconductor quantum disks and wells after excitation with light with orbital angular momentum. We find that although twisted light transfers orbital angular momentum to the excited carriers and the Rashba interaction conserves their total angular momentum, the resulting electronic spin dynamics is essentially the same for excitation with light with orbital angular momentum $l = +|l|$ and $l = -|l|$. The differences between cases with different values of $|l|$ are due to the excitation of states with slightly different energies and not to the different angular momenta per se and vanish for samples with large radii where a k-space quasicontinuum limit can be established. These findings apply not only to the Rashba interaction but also to all other envelope-function-approximation spin-orbit Hamiltonians like the Dresselhaus coupling.

I. INTRODUCTION

Light with orbital angular momentum (OAM), referred to as twisted light, is a relatively new field of research which has become increasingly popular [1–17] since Allen *et al.* showed how twisted light beams can be easily generated from conventional laser beams [18]. Recently, the theoretical foundation of the optical excitation of solids and nanostructures with twisted light has been established [19–27], and experimental studies with twisted light on semiconductors have been carried out [28,29].

One motivation for such studies is the prospect of using the large amounts of angular momentum that twisted light can carry in order to control the spin dynamics of electrons, thus adding a flexible tool to the active field of spin control [30–39]. In this context two different mechanisms need to be distinguished. First, angular momentum as well as energy selection rules can lead to selective optical excitation of carriers with a preferred spin direction. This mechanism enables fast spin-selective preparation of states during the photoexcitation process and has recently been studied for strongly confined systems such as quantum dots [27] and quantum rings [23]. Second, the spin-orbit interaction, like the Rashba [40] and Dresselhaus [41] couplings in semiconductor structures, is expected to couple the OAM of carriers transferred from the twisted light [19,22] to their spin degree of freedom. This would provide a slower carrier spin control, which would be dynamical and would remain active after the twisted light pulse.

In this paper, we study the spin dynamics of carriers in semiconductor quantum disks and wells excited with twisted light, taking into account the Rashba spin-orbit interaction. Our central finding is that, rather unexpectedly, the spin dynamics of the photoexcited electrons differs only slightly after excitation with light with and without OAM in the limit of large quantum disks, becoming insensitive to the OAM content of the twisted light beam for extended quantum wells. This result is consistent with the outcome of recent experiments which did not show traces of the OAM transferred from twisted light to bulk GaAs in spin-resolved photoemission measurements [29].

Analytically, we find that the Rashba interaction, while conserving the total angular momentum of the electrons,

has matrix elements which are independent of the OAM quantum number in the (k-space) quasicontinuum limit. As a consequence, the induced spin dynamics is almost identical, particularly for twisted light with components of the OAM in the growth direction $l = +|l|$ and $l = -|l|$. This finding can be generalized to all possible effective spin-orbit interactions stemming from a lattice-periodic potential in the envelope-function approximation, e.g., the Dresselhaus coupling. Our results suggest that for the search for materials supporting twisted-light-based spin control it is most promising to concentrate on small quantum structures and other discrete systems.

II. OPTICAL EXCITATION WITH TWISTED LIGHT

The discussion of the optical excitation of electrons with twisted light is especially clear when a basis of cylindrical states is chosen [22]. The wave functions of these basis states are expressed in cylindrical coordinates $\{r,\phi,z\}$ as

$$\psi_{bm\nu}(r,\phi,z) = \mathcal{N}_{m\nu} J_m(k_{m\nu}r)e^{im\phi}\Phi_b(z), \tag{1}$$

where J_m is the mth Bessel function, $\Phi_b(z)$ is the z envelope of the b subband (the band index includes the spin quantum number), and $\mathcal{N}_{m\nu} = [\sqrt{\pi}R J_{m+1}(k_{m\nu}R)]^{-1}$ is the normalization factor. For a circular quantum disk with radius R, width L, and growth direction z, the boundary conditions $\psi_{bm\nu}(R,\phi,z) = 0$ are satisfied if $k_{m\nu} = u_{m,\nu}/R$, where $u_{m,\nu}$ is the νth zero of the mth Bessel function. Note that $\psi_{bm\nu}$ is an eigenstate of the z component of the envelope OAM operator with eigenvalue $\hbar m$ and $k_{m\nu}$ determines the kinetic energy of state $\psi_{bm\nu}$ since in a parabolic band b with effective mass m_b^* the energy of the state is given by $\epsilon_{bm\nu} = \hbar^2 k_{m\nu}^2/(2m_b^*)$. Note also how the precise location of the energy eigenvalues is given by the zeros of the Bessel functions; this detailed information will be "smeared out" in the limit $R \to \infty$ as the allowed values of k become a quasicontinuum. For the sake of simplicity, we restrict our discussion to a case where only spin-degenerate conduction ($b = c = \{-1/2,1/2\}$) and heavy-hole ($b = v = \{-3/2,3/2\}$) bands are considered.

The matrix elements of the twisted-light–matter interaction Hamiltonian H_I (in the dipole approximation for only the
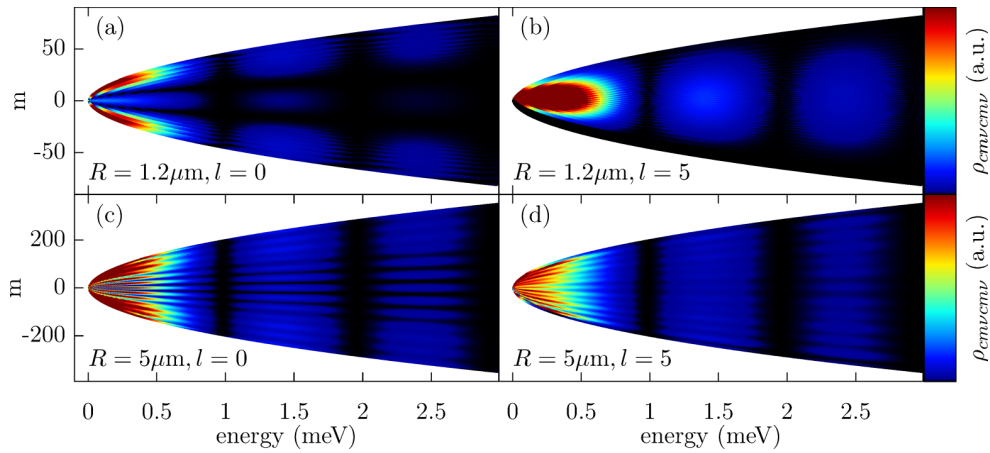
FIG. 1. (Color online) Diagonal elements of the density matrix ρ_{cmvcmv} after an excitation of a cylindrical quantum disk with radius R with a box-shaped pulse of length $t = 5$ ps and orbital angular momentum l of the light. (a) and (b) show the occupations of an $R = 1.2\ \mu$m quantum disk with $l = 0$ and $l = 5$, respectively. (c) and (d) display the occupations for a larger $R = 5\ \mu$m disk with $l = 0$ and $l = 5$. For a better comparison, the matrix elements are plotted against the energies ϵ_{cmv} instead of the indices ν, and the absolute values of the occupations are rescaled.

z component) in the cylindrical basis states were derived in Ref. [22]:

$$\langle cm'v'|H_I|vm\nu \rangle = \xi_{cvv'vm'}e^{-i\omega t}\delta_{m,m'-l}, \tag{2a}$$

$$\xi_{cvv'vm'} = -\frac{e}{m_e}A_0\,\boldsymbol{\epsilon}_\sigma \cdot \mathbf{p}_{cv}\langle\Phi_c|\delta_{k_z,q_z}|\Phi_v\rangle\mathcal{N}_{m'v'}\mathcal{N}_{mv}$$

$$\times \int_0^R dr\ r\,J_l(q_\parallel r)J_{m'}(k_{m'v'}r)J_{m'-l}(k_{mv}r), \tag{2b}$$

where e and m_e are the electron charge and (bare) mass, A_0 is the field strength, ω is the light frequency, $q_\parallel$ and q_z are the in-plane and growth-direction parts of the light

wave vector, respectively, k_z is the electron wave vector in the growth direction, l is the OAM of the light, $\boldsymbol{\epsilon}_\sigma$ is the light polarization vector, and $\mathbf{p}_{cv}$ is the dipole matrix element between heavy-hole and conduction-band states. Note that $\mathbf{p}_{cv}$ contains spin selection rules. Let us consider the case where due to excitation with circularly polarized light only spin-up electrons are excited.

In Ref. [22] equations of motion were presented for the density matrix under the influence of twisted light switched on with constant amplitude at $t = 0$. In the low-excitation limit, i.e., initially empty conduction and filled valence bands excited with a moderate light field so that the occupations can be well approximated by an expansion up to second order in the field strength, we find from Eqs. (16) and (17) of Ref. [22]

$$\rho_{cmvc'm'v'}(t) = \sum_{m_1\nu_1\nu} \delta_{\frac{3}{2},v}\xi_{cvv\nu_1m}\xi^*_{c'v\nu'\nu_1m'}\left[\frac{1-e^{-i(\epsilon_{cmv}-\epsilon_{c'm'v'})t/\hbar}}{\epsilon_{cmv}-\epsilon_{c'm'v'}}\left(\frac{1}{\epsilon_{c'm'v'}-\epsilon_{vm_1\nu_1}-\hbar\omega}-\frac{1}{\epsilon_{cmv}-\epsilon_{vm_1\nu_1}-\hbar\omega}\right)\right.$$

$$\left.+\frac{1}{(\epsilon_{cmv}-\epsilon_{vm_1\nu_1}-\hbar\omega)(\epsilon_{c'm'v'}-\epsilon_{vm_1\nu_1}-\hbar\omega)}\left(e^{i(\epsilon_{c'm'v'}-\epsilon_{vm_1\nu_1}-\hbar\omega)t/\hbar}+e^{-i(\epsilon_{cmv}-\epsilon_{vm_1\nu_1}-\hbar\omega)t/\hbar}-2\right)\right]\delta_{mm'}\delta_{c\frac{1}{2}}\delta_{c'\frac{1}{2}}. \tag{3}$$

Thus, the optical excitation yields only diagonal elements of $\rho_{cmvc'm'v'}$ with respect to m. Also, we find from Eqs. (2) that for every electron with OAM m there occurs an unoccupied state with OAM $m - l$ in the valence band, i.e., a hole with OAM $l - m$. From this we can conclude that the total envelope OAM $l^{\rm tot}$ induced in the valence and conduction bands together is $l^{\rm tot} = lN_e\hbar$, where N_e is the number of excited electrons or, equivalently, holes. The distribution of the total orbital momentum into conduction- and valence-band contributions depends on the details of the band structure, the pulse duration, and the laser frequency. For example, for the effective masses $m_c^* = 0.067m_e$ and $m_{hh}^* = 0.45m_e$ for conduction and heavy-hole bands, respectively, an excitation with a circularly polarized twisted-light pulse with OAM

$l = 5$, pulse duration $t = 5$ ps, and central frequency resonant to the band gap leads to a total OAM in the conduction band of $l_c^{\rm tot} = 2.866N_e\hbar$ for $R = 1.2\ \mu$m, $l_c^{\rm tot} = 3.145N_e\hbar$ for $R = 5\ \mu$m, and $l_c^{\rm tot} = 2.914N_e\hbar$ for $R = 10\ \mu$m.

Figure 1 shows the diagonal elements of the density matrix ρ_{cmvcmv} for the excitation conditions described above. The oscillatory structure of the occupations along the energy axis can be attributed to the finite pulse duration via the energy-time uncertainty relation. Along the m axis, there are also oscillations in the occupations. Since their frequency depends strongly on the radius R of the sample and they get smeared out for large values of R, we attribute these oscillations to finite-size effects. Note that in Fig. 1(b), where the occupation for light with $l = 5$ is plotted, the states with the

five lowest values of m for every energy shell are empty (seen more clearly at low energies) since there are no valence-band states which satisfy the condition $m' = m - l$ of the matrix element in Eq. (2a). Figures 1(c) and 1(d) show that for the larger $R = 5\,\mu$m quantum disk, the difference between the occupations after $l = 0$ and $l = 5$ excitations diminishes visibly.

III. SPIN DYNAMICS

Now, we focus on the spin dynamics after the optical excitation. We study the effects of spin-orbit coupling mechanisms, considering for concreteness the Rashba Hamiltonian H_R [40], which is usually the dominant mechanism in quasi-two-dimensional systems. In order to better work with the cylindrical states given in Eq. (1), we switch from the usual Cartesian-coordinate expression of H_R to its expression in polar coordinates:

$$H_R = \hbar\alpha_R(k_y\sigma_x - k_x\sigma_y) = \hbar\alpha_R(s^+\partial^- - s^-\partial^+), \quad (4a)$$

$$\partial^\pm := \frac{\partial}{\partial x} \pm i\frac{\partial}{\partial y} = e^{\pm i\phi}\left(\frac{\partial}{\partial r} \pm \frac{i}{r}\frac{\partial}{\partial\phi}\right), \quad (4b)$$

where α_R is the Rashba coefficient and σ_i and $s^\pm$ are the Pauli matrices and spin raising and lowering operators, respectively. With the relation

$$\int_0^R dr\; r J_m(pr)J_m(qr)$$
$$= R\frac{p J_m(qR)J_m'(pR) - q J_m(pR)J_m'(qR)}{q^2 - p^2}, \quad (5)$$

it is straightforward to calculate the matrix elements of H_R with respect to the cylindrical states:

$$\langle c'm'\nu'|\partial^\pm|cm\nu\rangle = \delta_{m',m\pm1}\frac{2}{R}\frac{k_{m\nu}k_{m'\nu'}}{k_{m\nu}^2 - k_{m'\nu'}^2}, \quad (6a)$$

$$\langle c'm'\nu'|H_R|cm\nu\rangle = \frac{\hbar\alpha_R k_{m\nu}k_{m'\nu'}}{R(k_{m\nu}^2 - k_{m'\nu'}^2)}(s_{c'c}^+\delta_{m',m-1} - s_{c'c}^-\delta_{m',m+1}). \quad (6b)$$

It can be seen from the form of the Rashba Hamiltonian in cylindrical coordinates that an electron with spin up (down) and envelope OAM m flips to a state with spin down (up) and OAM $m + 1$ ($m - 1$). In this sense, $\partial^\pm$ can be regarded as raising and lowering operators in m. If H_R is applied a second time, the electronic state is transferred back to the initial spin and OAM state, while a change in ν is possible. Note that the sum $J = m + s$ of the envelope OAM m and the spin s is conserved by the Rashba Hamiltonian.

Having derived the matrix elements of H_R in cylindrical coordinates, it is straightforward to calculate numerically the time evolution of the density matrix, where the initial conditions correspond to the final occupations generated by optical excitation with light with OAM l, illustrated in Fig. 1. The resulting dynamics for the total conduction-band spin is shown in Fig. 2. We show results for three different values of the disk radius, $R = \{1.2, 5, 10\}\,\mu$m. As in the case of optical excitation with light with zero OAM, the Rashba interaction leads to a dephasing of the initial electron spins. Since for small disks only a finite number of states contributes noticeably
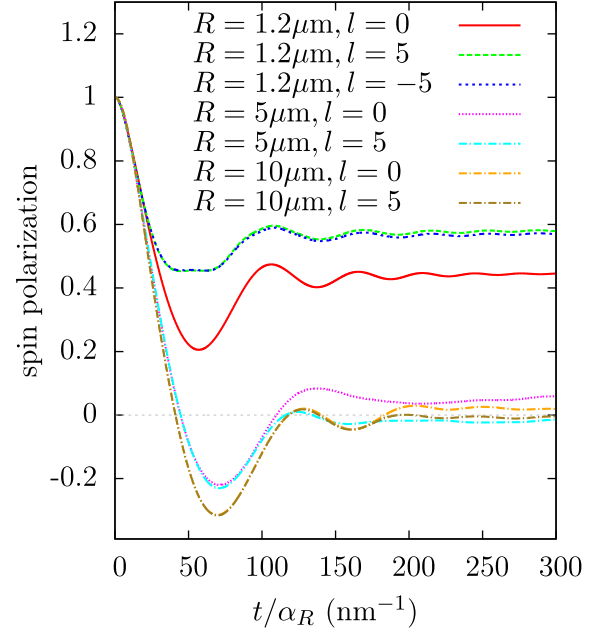

FIG. 2. (Color online) Spin dynamics after excitation with twisted light with orbital angular momentum $l = \{-5, 0, 5\}$ and quantum-disk radius $R = 1.2\,\mu$m and with $l = \{0, 5\}$ and $R = \{5\,\mu\text{m}, 10\,\mu\text{m}\}$.

to the dynamics, oscillations are found which do not cancel completely so that for long times the total spin reaches a nonzero value. Note that the curves for excitation with $l = 5$ and $l = -5$ almost coincide (shown for $R = 1.2\,\mu$m). This unexpected result shows clearly the insensitivity of the spin dynamics, in the presence of the Rashba spin-orbit interaction, to the content of OAM transferred from twisted light to the electron gas. For the same quantum disk, an excitation with $l = 0$ produces spin dynamics different from the $l = \pm 5$ excitation, but this difference decreases for larger radii. This tendency can be seen by comparing the excitations with $l = 5$ and $l = 0$ for the three different values of R used in Fig. 2.

To understand this finding, it is useful to analyze the case of an infinitely extended quantum well, obtained by letting $R \to \infty$. In this limit, the discrete $k_{m\nu}$ become continuous, and the eigenstates can be written as

$$\psi_{bkm}(r,\phi,z) := \sqrt{\frac{k}{2\pi}}J_m(kr)e^{im\phi}\Phi_b(z), \quad (7)$$

with the orthogonality relation $\langle bkm|b'k'm'\rangle = \delta_{bb'}\delta_{mm'}\delta(k - k')$. Using the fact that Bessel functions satisfy

$$\int_0^\infty dr\; r J_m(kr)J_m(k'r) = \frac{1}{k}\delta(k - k'), \quad (8)$$

the corresponding matrix elements become

$$\langle c'k'm'|\partial^\pm|ckm\rangle = \mp k\delta_{m',m\pm1}\delta(k - k'), \quad (9a)$$

$$\langle c'k'm'|H_R|ckm\rangle = \hbar\alpha_R k\,\delta(k - k')(s_{c'c}^+\delta_{m',m-1} + s_{c'c}^-\delta_{m',m+1}). \quad (9b)$$

Thus, in the quasicontinuum limit, the prefactor of the Rashba interaction depends only on the energy of the state via k but not on m. The spin dynamics is therefore a precession of the electron spin with a k-dependent frequency, which, for a given k, is the same for all different values of m. Since the effect of the excitation with twisted light was mainly that states with different m are excited, it is now easy to see why, for extended systems, the spin dynamics due to the Rashba Hamiltonian is almost the same for excitations with light with and without OAM.

It is noteworthy that this statement is also true for all effective Hamiltonians with a microscopic origin in the lattice-periodic crystal potential such as the Dresselhaus [41] spin-orbit coupling when treated in the envelope-function approximation: For a lattice-periodic potential, the solutions of the corresponding Schrödinger equation are given by the Bloch theorem as $\psi(\mathbf{r}) \propto e^{i\mathbf{kr}} u_{n\mathbf{k}}(\mathbf{r})$ with lattice-periodic Bloch function $u_{n\mathbf{k}}(\mathbf{r})$, band index n, and wave vector $\mathbf{k}$. The envelope-function approximation consists of integrating over the plane-wave part of the wave function, yielding an effective Hamiltonian [42] H_{eff} for $u_{n\mathbf{k}}$ which is diagonal in $\mathbf{k}$, and the matrix elements can be written as a power series in $\mathbf{k}$. The resulting effective Hamiltonian can be rewritten by decomposing k_x and k_y in terms of ∂^+ and ∂^-, as done in Eqs. (4). Thus, the dependence of the matrix elements of H_{eff} in cylindrical states on m is of the same character as that for the Rashba Hamiltonian and vanishes in the quasicontinuum limit. For systems with finite size, however, a weak dependence on m can be found due to the m dependence of the possible k values in the prefactor of the Rashba Hamiltonian in Eq. (6b). This means that, e.g., for small quantum disks, where the energy separation between the discrete cylindrical states becomes important, the OAM of the exciting light can influence the spin dynamics significantly.

IV. CONCLUSION

In conclusion, we have shown that although the OAM of twisted light can be transferred into the envelope OAM of electrons, the usual solid-state spin-orbit interactions, such as Rashba and Dresselhaus interactions, do not couple the envelope OAM of the carriers to their spin degree of freedom in such a way that a significant difference in the spin dynamics after excitation with light with and without OAM is found in large extended systems. This finding can explain why in recent experiments [29] no influence of the light's OAM on the spin polarization was found. However, for cylindrical quantum disks with small radii, the discreteness of the states plays an important role, so that the spin dynamics indeed depends on the OAM of the light. Nevertheless, also for small systems, the spin dynamics after excitation with OAM $l = |l|$ and $l = -|l|$ are very similar, in contrast to optical excitation with opposite circular polarization, where the spin dynamics acquires a different sign. Thus, twisted-light-based spin control is fundamentally different from traditional spin orientation, and combining these control schemes should therefore open new ways for spin manipulation. Our findings have direct implications for the search for systems where optical excitation with twisted light can be used to manipulate the spin dynamics: A continuum of states has to be avoided. Such systems can be confined structures like quantum dots [27] and rings [21,23], discrete states due to multiparticle effects, e.g., excitons, or localized states due to impurities and surface effects.

[1] E. Hemsing, M. Dunning, C. Hast, T. Raubenheimer, and D. Xiang, Phys. Rev. Lett. **113**, 134803 (2014).

[2] P. R. Ribič, D. Gauthier, and G. De Ninno, Phys. Rev. Lett. **112**, 203602 (2014).

[3] G. Gariepy, J. Leach, K. T. Kim, T. J. Hammond, E. Frumker, R. W. Boyd, and P. B. Corkum, Phys. Rev. Lett. **113**, 153901 (2014).

[4] M. Padgett, Proc. R. Soc. A **470**(2172), (2014).

[5] M.-E. Couprie, Nat. Phys. **9**, 531 (2013).

[6] S. Patchkovskii and M. Spanner, Nat. Phys. **8**, 707 (2012).

[7] J. Wang, J.-Y. Yang, I. M. Fazal, N. Ahmed, Y. Yan, H. Huang, Y. Ren, Y. Yue, S. Dolinar, M. Tur, and A. E. Willner, Nat. Photonics **6**, 488 (2012).

[8] N. V. Bloch, K. Shemer, A. Shapira, R. Shiloh, I. Juwiler, and A. Arie, Phys. Rev. Lett. **108**, 233902 (2012).

[9] P. Genevet, J. Lin, M. A. Kats, and F. Capasso, Nat. Commun. **3**, 1278 (2012).

[10] U. D. Jentschura and V. G. Serbo, Phys. Rev. Lett. **106**, 013001 (2011).

[11] M. Padgett and R. Bowman, Nat. Photonics **5**, 343 (2011).

[12] B. J. McMorran, A. Agrawal, I. M. Anderson, A. A. Herzing, H. J. Lezec, J. J. McClelland, and J. Unguris, Science **331**, 192 (2011).

[13] J. Verbeeck, H. Tian, and P. Schattschneider, Nature (London) **467**, 301 (2010).

[14] M. Uchida and A. Tonomura, Nature (London) **464**, 737 (2010).

[15] G. Molina-Terriza, J. P. Torres, and L. Torner, Nat. Phys. **3**, 305 (2007).

[16] A. T. O'Neil, I. MacVicar, L. Allen, and M. J. Padgett, Phys. Rev. Lett. **88**, 053601 (2002).

[17] H. He, M. E. J. Friese, N. R. Heckenberg, and H. Rubinsztein-Dunlop, Phys. Rev. Lett. **75**, 826 (1995).

[18] L. Allen, M. W. Beijersbergen, R. J. C. Spreeuw, and J. P. Woerdman, Phys. Rev. A **45**, 8185 (1992).

[19] G. F. Quinteiro and P. I. Tamborenea, Europhys. Lett. **85**, 47001 (2009).

[20] G. F. Quinteiro and P. I. Tamborenea, Phys. Rev. B **79**, 155450 (2009).

[21] G. F. Quinteiro and J. Berakdar, Opt. Express **17**, 20465 (2009).

[22] G. F. Quinteiro and P. I. Tamborenea, Phys. Rev. B **82**, 125207 (2010).

[23] G. F. Quinteiro, P. I. Tamborenea, and J. Berakdar, Opt. Express **19**, 26733 (2011).

[24] J. Wätzel, A. S. Moskalenko, and J. Berakdar, Opt. Express **20**, 27792 (2012).

[25] B. Sbierski, G. F. Quinteiro, and P. I. Tamborenea, J. Phys. Condens. Matter **25**, 385301 (2013).

[26] M. B. Farías, G. F. Quinteiro, and P. I. Tamborenea, Eur. Phys. J. B **86**, 432 (2013).

[27] G. F. Quinteiro and T. Kuhn, Phys. Rev. B **90**, 115401 (2014).

[28] Y. Ueno, Y. Toda, S. Adachi, R. Morita, and T. Tawara, Opt. Express **17**, 20567 (2009).

[29] N. B. Clayburn, J. L. McCarter, J. M. Dreiling, M. Poelker, D. M. Ryan, and T. J. Gay, Phys. Rev. B **87**, 035204 (2013).

[30] *Optical Orientation*, edited by F. Meier and B. P. Zakharchenya, Modern Problems in Condensed Matter Sciences Vol. 8 (North-Holland, Amsterdam, 1984).

[31] C. Flindt, A. S. Sørensen, and K. Flensberg, Phys. Rev. Lett. **97**, 240501 (2006).

[32] S. D. Ganichev, E. L. Ivchenko, S. N. Danilov, J. Eroms, W. Wegscheider, D. Weiss, and W. Prettl, Phys. Rev. Lett. **86**, 4358 (2001).

[33] P. Szumniak, S. Bednarek, B. Partoens, and F. M. Peeters, Phys. Rev. Lett. **109**, 107201 (2012).

[34] I. Žutić, J. Fabian, and S. Das Sarma, Rev. Mod. Phys. **76**, 323 (2004).

[35] K. Schmalbuch, S. Göbbels, P. Schäfers, C. Rodenbücher, P. Schlammes, T. Schäpers, M. Lepsa, G. Güntherodt, and B. Beschoten, Phys. Rev. Lett. **105**, 246603 (2010).

[36] F. G. G. Hernandez, G. M. Gusev, and A. K. Bakarov, Phys. Rev. B **90**, 041302 (2014).

[37] S. Kuhlen, K. Schmalbuch, M. Hagedorn, P. Schlammes, M. Patt, M. Lepsa, G. Güntherodt, and B. Beschoten, Phys. Rev. Lett. **109**, 146603 (2012).

[38] E. Poem, O. Kenneth, Y. Kodriano, Y. Benny, S. Khatsevich, J. E. Avron, and D. Gershoni, Phys. Rev. Lett. **107**, 087401 (2011).

[39] A. Greilich, S. E. Economou, S. Spatzek, D. R. Yakovlev, D. Reuter, A. D. Wieck, T. L. Reinecke, and M. Bayer, Nat. Phys. **5**, 262 (2009).

[40] Y. A. Bychkov and E. I. Rashba, J. Phys. C **17**, 6039 (1984).

[41] G. Dresselhaus, Phys. Rev. **100**, 580 (1955).

[42] G. Bastard, *Wave Mechanics Applied to Semiconductor Heterostructures*, Monographies de physique (Les Editions de Physique, Les Ulis, France, 1990), pp. 35–54.

Publication 10

Influence of non-magnetic impurity scattering on the spin dynamics in diluted magnetic semiconductors

M. Cygorek, F. Ungar, P. I. Tamborenea and V. M. Axt

Influence of non-magnetic impurity scattering on the spin dynamics in diluted magnetic semiconductors

M. Cygorek,[1] F. Ungar,[1] P. I. Tamborenea,[2] and V. M. Axt[1]

[1] *Theoretische Physik III, Universität Bayreuth, 95440 Bayreuth, Germany*
[2] *Departamento de Física and IFIBA, FCEN, Universidad de Buenos Aires,*
Ciudad Universitaria, Pabellón I, 1428 Ciudad de Buenos Aires, Argentina

The doping of semiconductors with magnetic impurities gives rise not only to a spin-spin interaction between quasi-free carriers and magnetic impurities, but also to a local spin-independent disorder potential for the carriers. Based on a quantum kinetic theory for the carrier and impurity density matrices as well as the magnetic and non-magnetic carrier-impurity correlations, the influence of the non-magnetic scattering potential on the spin dynamics in DMS after optical excitation with circularly polarized light is investigated using the example of Mn-doped CdTe. It is shown that non-Markovian effects, which are predicted in calculations where only the magnetic carrier-impurity interaction is accounted for, can be strongly suppressed in the presence of non-magnetic impurity scattering. This effect can be traced back to a significant redistribution of carriers in **k**-space which is enabled by the build-up of large carrier-impurity correlation energies. A comparison with the Markov limit of the quantum kinetic theory shows that, in the presence of an external magnetic field parallel to the initial carrier polarization, the asymptotic value of the spin polarization at long times is significantly different in the quantum kinetic and the Markovian calculations. This effect can also be attributed to the formation of strong correlations which invalidates the semiclassical Markovian picture and it is stronger when the non-magnetic carrier-impurity interaction is accounted for. In an external magnetic field perpendicular to the initial carrier spin, the correlations are also responsible for a renormalization of the carrier spin precession frequency. Considering only the magnetic carrier-impurity interaction, a significant renormalization is predicted for a very limited set of material parameters and excitation conditions. Accounting also for the non-magnetic interaction a relevant renormalization of the precession frequency is found to be more ubiquitous.

I. INTRODUCTION

Most of the devices based on the spintronics paradigm that are commercially available today use the fact that spin-up and spin-down carriers exhibit different transmission and reflection probabilities at interfaces involving ferromagnetic metals[1,2]. However, some applications, like spin transistors[3], require the control not only of spin-up and spin-down occupations, but also of the coherent precession of spins perpendicular to the quantization axis provided by the structure. For this purpose, spintronic devices based on semiconductors are preferable to metallic structures since the dephasing time in a metal is about three orders of magnitude shorter than in a semiconductor[4]. In the context of semiconductor spintronics[5–7], a particularly interesting class of materials for future applications are diluted magnetic semiconductors (DMS)[8–22], which are obtained when semiconductors are doped with transition metal elements, such as Mn, which act as localized magnetic moments. While some types of DMS, such as $Ga_{1-x}Mn_xAs$, exhibit a ferromagnetic phase[8,23], other types of DMS, like the usually paramagnetic CdMnTe, are especially valued for the enhancement of the effective carrier g-factor by the giant Zeeman effect that can be used, e.g., to facilitate an injection of a spin-polarized current into a light-emitting diode[24]. Besides causing the giant Zeeman effect, the s-d exchange interaction between the quasi-free carriers and

localized magnetic impurities also leads to other effects, such as inducing spin-flip scattering and thereby a direct transfer of spins from the carriers to the impurities and vice versa[25–28].

Typically, the s-d interaction is described by a Kondo-like[29] localized spin-spin interaction between carriers and impurities. However, in real DMS materials, the introduction of Mn impurities not only leads to a spin-dependent interaction Hamiltonian, but also to a spin-independent local potential for the carriers[30]. The reason for the appearance of this spin-independent potiential is that, in the case of $Cd_{1-x}Mn_xTe$, the semiconductor CdTe has a different band structure than MnTe and carriers located at unit cells with Mn impurities experience a larger local potiential energy than carriers at unit cells with Cd cations. The strength of this local potential can be estimated by the conduction and valence band offsets between CdTe and MnTe. Note, however, that usually, CdTe crystallizes in a zinc-blende structure, while MnTe is found in a wurzite structure. Thus, a better estimation for the strength of the spin-independent local potential is obtained by studying CdTe/$Cd_{1-x}Mn_x$Te heterostructures where both materials appear in the form of a zinc-blende lattice[31]. From such investigations, the strenght of the local spin-independent potential for carriers at Mn sites of about 1.6 eV can be estimated. In contrast, the spin-dependent local interaction in DMS is typically about 220 meV, i.e. one order of magnitude lower. This consideration suggests that the non-magnetic

impurity scattering caused by the local spin-independent interaction between carriers and impurities should not be disregarded in the study of the spin physics in DMS.

It is noteworthy that a theory which takes into account a local magnetic interaction as well as a non-magnetic local potential in a DMS, the V-J tight-binding model was employed to study the magnetic properties of GaMnAs[32] and it was found that taking into account the non-magnetic interaction is necessary in order to obtain results in good quantitative agreement with *ab initio* calculations for the Curie temperature and with experimental data for the optical conductivity.

For the spin dynamics, scattering at non-magnetic impurities has already important consequences in non-magnetic semiconductors[33] in the presence of spin-orbit fields, where scattering processes can enhance or reduce the spin relaxation and dephasing significantly, e.g., via the Elliott-Yafet[34] and D'yakonov-Perel'[35] mechanisms.

The goal of the present article is to investigate how the non-magnetic interaction between carriers and impurities affects the spin dynamics in paramagnetic II-VI DMS. To this end we employ a quantum kinetic theory for carrier and impurity density matrices including the carrier-impurity correlations starting from a system Hamiltonian that comprises a kinetic energy term, the magnetic and non-magnetic carrier-impurity interactions as well as the carrier and impurity Zeeman energies. Earlier quantum kinetic studies of the spin dynamics in DMS[25–27,36,37], which only considered the spin-dependent *s-d* interaction, predicted that in some cases, such as in narrow quantum wells optically excited very close to the band edge[38], the spin transfer between carriers and impurities cannot be well described by rate equations. Rather, the time evolution of the carrier spin is, in these cases, non-exponential and it can exhibit non-monotonic features such as overshoots. These effects are non-Markovian, as they can be traced back to the finite memory provided by the correlations, since the Markovian assumption of a δ-like memory leads to effective rate equations that predict an exponential spin dynamics[28].

Here, we find that these non-Markovian effects predicted in the theory of Refs. 25–27, 36, and 37 are suppressed in the case of the conduction band of a $Cd_{1-x}Mn_xTe$ quantum well when non-magnetic scattering of carriers at the impurities is taken into account. While, in this case, the non-monotonic behavior of the spin dynamics disappears, the quantum kinetic theory predicts quantitative changes in the effective spin transfer rate compared with the Fermi's golden rule value. The suppression of the non-Markovian features is mainly caused by a significant redistribution of carriers away from the band edge where the non-Markovian effects are particularly strong[38]. This carrier redistribution is facilitated by the build-up of strong carrier-impurity correlations providing a correlation energy of the order of a few meV per electron that leads to an increase of the average kinetic electron energy by about the same amount. Due to the different strengths of the interactions in the con-

duction band of $Cd_{1-x}Mn_xTe$, the non-magnetic carrier-impurity correlation energy is also much larger than the magnetic correlation energy studied before in Ref. 39.

In other cases, such as in the valence band of $Cd_{1-x}Mn_xTe$, the non-magnetic impurty scattering can be much weaker than the magnetic spin-flip scattering and the non-Markovian effects prevail.

In the presence of an external magnetic field parallel to the initial carrier spin polarization, it was shown[40] that a quantum kinetic treatment of the magnetic part of the carrier-impurity interaction in DMS leads to a significantly different asymptotic value of the carrier spin polarization at long times t. Because this is also a consequence of an energetic redistribution of carriers, including non-magnetic scattering increases this effect. If the initial carrier spin polarization is perpendicular to the external magnetic field, the carrier spins precess about the effective field comprised of the external field and the mean field due to the impurity magnetization. As shown in Ref. 39, the carrier-impurity correlations built up by the magnetic *s-d* interaction renormalize the carrier spin precession frequency. Here, we show that when both, the magnetic and the non-magnetic interactions are taken into account the renormalization of the carrier spin precession frequency can be different in sign and magnitude compared with calculations in which only the magnetic interaction is considered.

The article is structured as follows: First, quantum kinetic equations of motion for the carrier and impurity density matrices as well as for the magnetic and non-magnetic carrier-impurity correlations are formulated for a DMS with magnetic and non-magnetic carrier-impurity interactions. Then, we derive the Markov limit of the quantum kinetic theory which enables a comparison and allows us to distinguish the genuine quantum kinetic effects from the Markovian behavior. Furthermore, from the Markov limit we can derive analytic expressions for the carrier-impurity correlation energies as well as the correlation-induced renormalization of the carrier spin precession frequency. After having layed out the theory, we present numerical simulations of the quantum kinetic equations for the conduction band of a $Cd_{1-x}Mn_xTe$ quantum well including magnetic and non-magnetic scattering at the Mn impurities and discuss the energetic redistribution of carriers as well as the correlation energies. Then, we estimate the influence of non-magnetic impurity interaction on the spin dynamics in the valence band of $Cd_{1-x}Mn_xTe$. Finally, we discuss the effects of the non-magnetic impurity scattering on the spin dynamics in DMS in the presence of an external magnetic field parallel and perpendicular to an initial non-equilibrium carrier spin polarization.

II.   THEORY

A.   DMS Hamiltonian

Here, we consider an intrinsic DMS such as $Cd_{1-x}Mn_xTe$ in the presence of an external magnetic field. The total Hamiltonian of this DMS is given by

$$H = H_0 + H_{sd} + H_{imp} + H_Z^e + H_Z^{Mn}, \tag{1a}$$

$$H_0 = \sum_{\mathbf{k}\sigma} \hbar\omega_\mathbf{k} c_{\sigma\mathbf{k}}^\dagger c_{\sigma\mathbf{k}}, \tag{1b}$$

$$H_{sd} = \frac{J_{sd}}{V} \sum_{\mathbf{kk}'\sigma\sigma'} \sum_{Inn'} \mathbf{S}_{nn'} \cdot \mathbf{s}_{\sigma\sigma'} c_{\sigma\mathbf{k}}^\dagger c_{\sigma'\mathbf{k}'} e^{i(\mathbf{k}'-\mathbf{k})\mathbf{R}_I} \hat{P}_{nn'}^I, \tag{1c}$$

$$H_{imp} = \frac{J_0}{V} \sum_{\mathbf{kk}'\sigma} \sum_J c_{\sigma\mathbf{k}}^\dagger c_{\sigma\mathbf{k}'} e^{i(\mathbf{k}'-\mathbf{k})\mathbf{R}_J}, \tag{1d}$$

$$H_Z^e = \sum_{\mathbf{k}\sigma\sigma'} \hbar g_e \mu_B \mathbf{B} \cdot \mathbf{s}_{\sigma\sigma'} c_{\sigma\mathbf{k}}^\dagger c_{\sigma'\mathbf{k}}, \tag{1e}$$

$$H_Z^{Mn} = \sum_{Inn'} \hbar g_{Mn} \mu_B \mathbf{B} \cdot \mathbf{S}_{nn'} \hat{P}_{nn'}^I, \tag{1f}$$

where H_0 is the single-electron Hamiltonian due to the crystal potential, H_{sd} describes the magnetic s-d exchange interaction between the carriers and the impurities, H_{imp} describes the spin-independent scattering of carriers at impurities and H_Z^e and H_Z^{Mn} are the carrier and impurity Zeeman energies.

In Eqs. (1), $c_{\sigma\mathbf{k}}^\dagger$ and $c_{\sigma\mathbf{k}}$ denote the creation and annihilation operators for conduction band electrons with wave vector $\mathbf{k}$ in the spin subband $\sigma = \{\uparrow, \downarrow\}$. The magnetic Mn impurities are described by the operator $\hat{P}_{nn'}^I = |I, n\rangle\langle I, n'|$ where $|I, n\rangle$ is the n-th spin state ($n \in \{-\frac{5}{2}, -\frac{3}{2}, \ldots \frac{5}{2}\}$) of the I-th magnetic impurity located at $\mathbf{R}_I$. The band structure of the semiconductor is described by $\hbar\omega_\mathbf{k}$, which we assume to be parabolic $\omega_\mathbf{k} = \frac{\hbar\mathbf{k}^2}{2m^*}$ with effective mass m^*. V denotes the volume of the sample. J_{sd} is the s-d coupling constant for the spin-spin interaction between carriers and impurities and J_0 is the non-magnetic coupling constant. $\mathbf{S}_{n_1 n_2}$ and $\mathbf{s}_{\sigma_1\sigma_2}$ are the vectors with components consisting of spin-$\frac{5}{2}$ and spin-$\frac{1}{2}$ spin matrices for the impurities and the conduction band electrons, respectively, where the unit $\hbar$ has been substituted into the definition of J_{sd} so that $\mathbf{s}_{\sigma_1\sigma_2} = \frac{1}{2}\boldsymbol{\sigma}_{\sigma_1\sigma_2}$, where $\boldsymbol{\sigma}_{\sigma_1\sigma_2}$ are the Pauli matrices. Finally, g_e and g_{Mn} are the g-factors of the electrons and the impurities, respectively, and μ_B is the Bohr magneton.

In order to account for spin-independent scattering not only at Mn impurities but also additional non-magnetic scattering centers, such as in quaternary compound DMSs like HgCdMnTe[41], we allow the number of scattering centers N_{imp} in general to be larger than the number of magnetic impurities N_{Mn}. Here, we use the notation that the index I runs from 1 to N_{Mn} while the index J runs from 1 to N_{imp}.

B.   Quantum kinetic equations of motion

The goal of this artilce is to study the time evolution of the carrier spin polarization after optical excitation with circularly polarized light which can be extracted from the carrier density matrix. In this section, we derive the corresponding equations of motion starting from the total Hamiltonian in Eqs. (1).

Following Ref. 36, where for the conduction band only H_0 and H_{sd} in Eqs. (1) were considered, we seek to obtain a closed set of equations for the reduced carrier and impurity density matrices as well as for the carrier-impurity correlations:

$$M_{n_1}^{n_2} = \langle \hat{P}_{n_1 n_2}^I \rangle \tag{2a}$$

$$C_{\sigma_1 \mathbf{k}_1}^{\sigma_2} = \langle c_{\sigma_1 \mathbf{k}_1}^\dagger c_{\sigma_2 \mathbf{k}_1} \rangle, \tag{2b}$$

$$\bar{C}_{\sigma_1 \mathbf{k}_1}^{\sigma_2 \mathbf{k}_2} = V\langle c_{\sigma_1 \mathbf{k}_1}^\dagger c_{\sigma_2 \mathbf{k}_2} e^{i(\mathbf{k}_2-\mathbf{k}_1)\mathbf{R}_J} \rangle, \quad \text{for } \mathbf{k}_2 \neq \mathbf{k}_1, \tag{2c}$$

$$Q_{\sigma_1 n_1 \mathbf{k}_1}^{\sigma_2 n_2 \mathbf{k}_2} = V\langle c_{\sigma_1 \mathbf{k}_1}^\dagger c_{\sigma_2 \mathbf{k}_2} e^{i(\mathbf{k}_2-\mathbf{k}_1)\mathbf{R}_I} \hat{P}_{n_1 n_2}^I \rangle, \quad \text{for } \mathbf{k}_2 \neq \mathbf{k}_1. \tag{2d}$$

$M_{n_1}^{n_2}$ and $C_{\sigma_1 \mathbf{k}_1}^{\sigma_2}$ are the impurity and electron density matrices and $\bar{C}_{\sigma_1 \mathbf{k}_1}^{\sigma_2 \mathbf{k}_2}$ as well as $Q_{\sigma_1 n_1 \mathbf{k}_1}^{\sigma_2 n_2 \mathbf{k}_2}$ are the non-magnetic and magnetic carrier-impurity correlations, respectively. In Eqs. (2), the brackets denote not only the quantum mechanical average of the operators, but also an average over a random distribution of impurity positions, which we assume to be on average homogeneous so that $\langle e^{i(\mathbf{k}_2-\mathbf{k}_1)\mathbf{R}_J} \rangle = \delta_{\mathbf{k}_1 \mathbf{k}_2}$.

The equations of motion for the variables defined in Eqs. (2) can be derived using the Heisenberg equations of motion for the corresponding operators. Note, however, that this procedure leads to an infinite hierarchy of variables and equations of motion, since, e. g., the equation of motion for $\langle c_{\sigma_1 \mathbf{k}_1}^\dagger c_{\sigma_2 \mathbf{k}_2} e^{i(\mathbf{k}_2-\mathbf{k}_1)\mathbf{R}_I} \hat{P}_{n_1 n_2}^I \rangle$ contains also terms of the form $\langle c_{\sigma_1 \mathbf{k}_1}^\dagger c_{\sigma\mathbf{k}} e^{i(\mathbf{k}-\mathbf{k}_1)\mathbf{R}_I} e^{i(\mathbf{k}_2-\mathbf{k})\mathbf{R}_{I'}} \hat{P}_{n_1 n_2}^I \hat{P}_{nn'}^{I'} \rangle$ for $I' \neq I$ which cannot be expressed in terms of the variables in Eqs. (2). Thus, in order to obtain a closed set of equations, one has to employ a truncation scheme. Here, we follow the procedure of Ref. 36: we factorize the averages over products of operators and define the true correlations to be the remainder when all combinations of factorizations have been subtracted from the averages. For example, we define (for $\mathbf{k}_2 \neq \mathbf{k}_1$)

$$\delta\langle c_{\sigma_1 \mathbf{k}_1}^\dagger c_{\sigma_2 \mathbf{k}_2} e^{i(\mathbf{k}_2-\mathbf{k}_1)\mathbf{R}_I} \hat{P}_{n_1 n_2}^I \rangle :=$$
$$\langle c_{\sigma_1 \mathbf{k}_1}^\dagger c_{\sigma_2 \mathbf{k}_2} e^{i(\mathbf{k}_2-\mathbf{k}_1)\mathbf{R}_I} \hat{P}_{n_1 n_2}^I \rangle$$
$$- \Big(\langle c_{\sigma_1 \mathbf{k}_1}^\dagger c_{\sigma_2 \mathbf{k}_2} \rangle \langle e^{i(\mathbf{k}_2-\mathbf{k}_1)\mathbf{R}_I} \rangle \langle \hat{P}_{n_1 n_2}^I \rangle$$
$$+ \langle c_{\sigma_1 \mathbf{k}_1}^\dagger c_{\sigma_2 \mathbf{k}_2} e^{i(\mathbf{k}_2-\mathbf{k}_1)\mathbf{R}_I} \rangle \langle \hat{P}_{n_1 n_2}^I \rangle$$
$$+ \langle e^{i(\mathbf{k}_2-\mathbf{k}_1)\mathbf{R}_I} \rangle \langle c_{\sigma_1 \mathbf{k}_1}^\dagger c_{\sigma_2 \mathbf{k}_2} \hat{P}_{n_1 n_2}^I \rangle \Big) \tag{3}$$

where $\delta\langle \ldots \rangle$ denotes the true correlations. The basic assumption of the truncation scheme of Ref. 36 is that

all correlations higher than $\delta\langle c^{\dagger}_{\sigma_1\mathbf{k}_1} c_{\sigma_2\mathbf{k}_2} e^{i(\mathbf{k}_2-\mathbf{k}_1)\mathbf{R}_I}\rangle$ and $\delta\langle c^{\dagger}_{\sigma_1\mathbf{k}_1} c_{\sigma_2\mathbf{k}_2} e^{i(\mathbf{k}_2-\mathbf{k}_1)\mathbf{R}_I} \hat{P}^{I}_{n_1 n_2}\rangle$ are negligible. This assumption results in a closed set of equations of motion for the reduced density matrices and the true correlations. However, it turns out[26] that the equations of motion can be written down in a more condensed form when switching back to the full (non-factorized) higher order density matrices as variables, after the higher (true) correlations are neglected. For details of this procedure, the reader is referred to Refs. 26 and 36.

Applying this truncation scheme to the total Hamiltonian (1) including magnetic and non-magnetic carrier-impurity interactions as well as the Zeeman terms for carriers and impurities leads to the equations of motion for the variables defined in Eqs. (2):

$$-i\hbar\frac{\partial}{\partial t}M^{n_2}_{n_1} = \sum_n \hbar\boldsymbol{\omega}_{\mathrm{Mn}}\cdot(\mathbf{S}_{nn_1}M^{n_2}_n - \mathbf{S}_{n_2 n}M^n_{n_1}) + \frac{J_{\mathrm{sd}}}{V^2}\sum_n\sum_{\mathbf{k}\mathbf{k}'\sigma\sigma'}(\mathbf{S}_{nn_1}\cdot\mathbf{s}_{\sigma\sigma'}Q^{\sigma' n_2\mathbf{k}'}_{\sigma n\mathbf{k}} - \mathbf{S}_{n_2 n}\cdot\mathbf{s}_{\sigma\sigma'}Q^{\sigma' n\mathbf{k}'}_{\sigma n_1\mathbf{k}})], \quad (4\mathrm{a})$$

$$-i\hbar\frac{\partial}{\partial t}C^{\sigma_2}_{\sigma_1\mathbf{k}_1} = \sum_\sigma \hbar\boldsymbol{\omega}_e\cdot(\mathbf{s}_{\sigma\sigma_1}C^{\sigma_2}_{\sigma\mathbf{k}_1} - \mathbf{s}_{\sigma_2\sigma}C^{\sigma}_{\sigma_1\mathbf{k}_1}) + J_{\mathrm{sd}}\frac{N_{\mathrm{Mn}}}{V^2}\sum_{nn'}\sum_{\mathbf{k}\sigma}(\mathbf{S}_{nn'}\cdot\mathbf{s}_{\sigma\sigma_1}Q^{\sigma_2 n'\mathbf{k}_1}_{\sigma n\mathbf{k}} - \mathbf{S}_{nn'}\cdot\mathbf{s}_{\sigma_2\sigma}Q^{\sigma n'\mathbf{k}}_{\sigma_1 n\mathbf{k}_1}) +$$

$$+ J_0\frac{N_{\mathrm{imp}}}{V^2}\sum_{\mathbf{k}}(\bar{C}^{\sigma_2\mathbf{k}_1}_{\sigma_1\mathbf{k}} - \bar{C}^{\sigma_2\mathbf{k}}_{\sigma_1\mathbf{k}_1}), \quad (4\mathrm{b})$$

$$-i\hbar\frac{\partial}{\partial t}Q^{\sigma_2 n_2\mathbf{k}_2}_{\sigma_1 n_1\mathbf{k}_1} = \hbar(\omega_{\mathbf{k}_1}-\omega_{\mathbf{k}_2})Q^{\sigma_2 n_2\mathbf{k}_2}_{\sigma_1 n_1\mathbf{k}_1} + b^{\sigma_2 n_2\mathbf{k}_2\,I}_{\sigma_1 n_1\mathbf{k}_1} + b^{\sigma_2 n_2\mathbf{k}_2\,II}_{\sigma_1 n_1\mathbf{k}_1} + b^{\sigma_2 n_2\mathbf{k}_2\,III}_{\sigma_1 n_1\mathbf{k}_1} + b^{\sigma_2 n_2\mathbf{k}_2\,\mathrm{imp}}_{\sigma_1 n_1\mathbf{k}_1}, \quad (4\mathrm{c})$$

$$-i\hbar\frac{\partial}{\partial t}\bar{C}^{\sigma_2\mathbf{k}_2}_{\sigma_1\mathbf{k}_1} = \hbar(\omega_{\mathbf{k}_1}-\omega_{\mathbf{k}_2})\bar{C}^{\sigma_2\mathbf{k}_2}_{\sigma_1\mathbf{k}_1} + c^{\sigma_2\mathbf{k}_2\,I}_{\sigma_1\mathbf{k}_1} + c^{\sigma_2\mathbf{k}_2\,II}_{\sigma_1\mathbf{k}_1} + c^{\sigma_2\mathbf{k}_2\,III}_{\sigma_1\mathbf{k}_1} + c^{\sigma_2\mathbf{k}_2\,\mathrm{sd}}_{\sigma_1\mathbf{k}_1} \quad (4\mathrm{d})$$

with

$$b^{\sigma_2 n_2\mathbf{k}_2\,I}_{\sigma_1 n_1\mathbf{k}_1} = \sum_{n\sigma\sigma'} J_{\mathrm{sd}}[\mathbf{S}_{nn_1}\cdot\mathbf{s}_{\sigma\sigma'}(\delta_{\sigma_1\sigma'} - C^{\sigma'}_{\sigma_1\mathbf{k}_1})C^{\sigma_2}_{\sigma\mathbf{k}_2}M^{n_2}_n - \mathbf{S}_{n_2 n}\cdot\mathbf{s}_{\sigma\sigma'}(\delta_{\sigma\sigma_2} - C^{\sigma_2}_{\sigma\mathbf{k}_2})C^{\sigma'}_{\sigma_1\mathbf{k}_1}M^n_{n_1}], \quad (4\mathrm{e})$$

$$b^{\sigma_2 n_2\mathbf{k}_2\,II}_{\sigma_1 n_1\mathbf{k}_1} = \sum_\sigma \hbar\boldsymbol{\omega}_e\cdot(\mathbf{s}_{\sigma\sigma_1}Q^{\sigma_2 n_2\mathbf{k}_2}_{\sigma n_1\mathbf{k}_1} - \mathbf{s}_{\sigma_2\sigma}Q^{\sigma n_2\mathbf{k}_2}_{\sigma_1 n_1\mathbf{k}_1}) + \sum_n \hbar\boldsymbol{\omega}_{\mathrm{Mn}}\cdot(\mathbf{S}_{nn_1}Q^{\sigma_2 n_2\mathbf{k}_2}_{\sigma_1 n\mathbf{k}_1} - \mathbf{S}_{n_2 n}Q^{\sigma_2 n\mathbf{k}_2}_{\sigma_1 n_1\mathbf{k}_1}), \quad (4\mathrm{f})$$

$$b^{\sigma_2 n_2\mathbf{k}_2\,III}_{\sigma_1 n_1\mathbf{k}_1} = \frac{J_{\mathrm{sd}}}{V}\sum_n\sum_{\mathbf{k}\sigma}\Big\{(\mathbf{S}_{nn_1}\cdot\mathbf{s}_{\sigma\sigma_1}Q^{\sigma_2 n_2\mathbf{k}_2}_{\sigma n\mathbf{k}} - \mathbf{S}_{n_2 n}\cdot\mathbf{s}_{\sigma_2\sigma}Q^{\sigma n\mathbf{k}}_{\sigma_1 n_1\mathbf{k}_1})$$

$$- \sum_{\sigma'}\mathbf{s}_{\sigma\sigma'}\cdot\big[C^{\sigma'}_{\sigma_1\mathbf{k}_1}(\mathbf{S}_{nn_1}Q^{\sigma_2 n_2\mathbf{k}_2}_{\sigma n\mathbf{k}} - \mathbf{S}_{n_2 n}Q^{\sigma_2 n\mathbf{k}}_{\sigma n_1\mathbf{k}_1}) + C^{\sigma_2}_{\sigma\mathbf{k}_2}(\mathbf{S}_{nn_1}Q^{\sigma' n_2\mathbf{k}}_{\sigma_1 n\mathbf{k}_1} - \mathbf{S}_{n_2 n}Q^{\sigma' n\mathbf{k}}_{\sigma_1 n_1\mathbf{k}_1})\big]\Big\}, \quad (4\mathrm{g})$$

$$b^{\sigma_2 n_2\mathbf{k}_2\,\mathrm{imp}}_{\sigma_1 n_1\mathbf{k}_1} = J_0\big[(C^{\sigma_2}_{\sigma_1\mathbf{k}_2} - C^{\sigma_2}_{\sigma_1\mathbf{k}_1})M^{n_2}_{n_1} + \frac{1}{V}\sum_{\mathbf{k}}(Q^{\sigma_2 n_2\mathbf{k}_2}_{\sigma_1 n_1\mathbf{k}} - Q^{\sigma_2 n_2\mathbf{k}}_{\sigma_1 n_1\mathbf{k}_1})\big], \quad (4\mathrm{h})$$

and

$$c^{\sigma_2\mathbf{k}_2\,I}_{\sigma_1\mathbf{k}_1} = J_0(C^{\sigma_2}_{\sigma_1\mathbf{k}_2} - C^{\sigma_2}_{\sigma_1\mathbf{k}_1}), \quad (4\mathrm{i})$$

$$c^{\sigma_2\mathbf{k}_2\,II}_{\sigma_1\mathbf{k}_1} = \sum_\sigma \hbar\boldsymbol{\omega}_e\cdot(\mathbf{s}_{\sigma\sigma_1}\bar{C}^{\sigma_2\mathbf{k}_2}_{\sigma\mathbf{k}_1} - \mathbf{s}_{\sigma_2\sigma}\bar{C}^{\sigma\mathbf{k}_2}_{\sigma_1\mathbf{k}_1}), \quad (4\mathrm{j})$$

$$c^{\sigma_2\mathbf{k}_2\,III}_{\sigma_1\mathbf{k}_1} = \frac{J_0}{V}\sum_{\mathbf{k}}(\bar{C}^{\sigma_2\mathbf{k}_2}_{\sigma_1\mathbf{k}} - \bar{C}^{\sigma_2\mathbf{k}}_{\sigma_1\mathbf{k}_1}), \quad (4\mathrm{k})$$

$$c^{\sigma_2\mathbf{k}_2\,\mathrm{sd}}_{\sigma_1\mathbf{k}_1} = J_{\mathrm{sd}}\sum_{nn'}\sum_\sigma M_{nn'}\mathbf{S}_{nn'}\cdot(\mathbf{s}_{\sigma\sigma_1}C^{\sigma_2}_{\sigma\mathbf{k}_2} - \mathbf{s}_{\sigma_2\sigma}C^{\sigma}_{\sigma_1\mathbf{k}_1}) + \frac{J_{\mathrm{sd}}}{V}\frac{N_{\mathrm{Mn}}}{N_{\mathrm{imp}}}\sum_{nn'}\sum_{\mathbf{k}\sigma}\mathbf{S}_{nn'}\cdot(\mathbf{s}_{\sigma\sigma_1}Q^{\sigma_2 n'\mathbf{k}_2}_{\sigma n\mathbf{k}} - \mathbf{s}_{\sigma_2\sigma}Q^{\sigma n'\mathbf{k}}_{\sigma_1 n\mathbf{k}_1}), \quad (4\mathrm{l})$$

where $b^{\sigma_2 n_2\mathbf{k}_2\,X}_{\sigma_1 n_1\mathbf{k}_1}$ are the source terms for the magnetic carrier-impurity correlations, $c^{\sigma_2\mathbf{k}_2\,X}_{\sigma_1\mathbf{k}_1}$ are the sources for the non-magnetic correlations and

$$\boldsymbol{\omega}_{\mathrm{Mn}} = g_{\mathrm{Mn}}\mu_B\mathbf{B} + \frac{J_{\mathrm{sd}}}{\hbar}\frac{1}{V}\sum_{\mathbf{k}\sigma\sigma'}\mathbf{s}_{\sigma\sigma'}C^{\sigma'}_{\sigma\mathbf{k}}, \quad (5\mathrm{a})$$

$$\boldsymbol{\omega}_e = g_e\mu_B\mathbf{B} + \frac{J_{\mathrm{sd}}}{\hbar}\frac{N_{\mathrm{Mn}}}{V}\sum_{nn'}\mathbf{S}_{nn'}M_{nn'} \quad (5\mathrm{b})$$

are the mean-field precession frequencies of the impurity and carrier spins, respectively. The first terms on the right-hand side of Eqs. (4a) and (4b) represent the precession of the impurity and carrier spins in the mean field due to the carrier and impurity magnetization as well as the external magnetic field. The second terms in Eqs. (4a) and (4b) describe the effects of the magnetic carrier-impurity correlations on the impurity and carrier density matrices and the last term of Eq. (4b) describes the scattering of carriers at non-magnetic impurities.

In analogy to the situation without non-magnetic impurity scattering ($J_0 = 0$) studied in Ref. 26, we label the source terms of the correlations on the right-hand side of the Eqs. (4c) and (4d) as follows: The terms $b_{\sigma_1 n_1 \mathbf{k}_1}^{\sigma_2 n_2 \mathbf{k}_2\, I}$ are the inhomogeneous driving terms depending only on single-particle quantities. $b_{\sigma_1 n_1 \mathbf{k}_1}^{\sigma_2 n_2 \mathbf{k}_2\, II}$ are homogeneous terms which describe a precession-type motion of the correlations in the effective fields $\boldsymbol{\omega}_\mathrm{e}$ and $\boldsymbol{\omega}_\mathrm{Mn}$. The source terms $b_{\sigma_1 n_1 \mathbf{k}_1}^{\sigma_2 n_2 \mathbf{k}_2\, III}$ comprise the driving of the magnetic correlations by other magnetic correlations with different wave vectors and describe a change of the wave vectors of the correlations due to the s-d interaction. $b_{\sigma_1 n_1 \mathbf{k}_1}^{\sigma_2 n_2 \mathbf{k}_2\, \mathrm{imp}}$ denotes the contributions to the equation for the magnetic correlations due to the non-magnetic impurity scattering. The source terms $c_{\sigma_1 \mathbf{k}_1}^{\sigma_2 \mathbf{k}_2\, X}$ for the non-magnetic correlations are classified analogously.

A straightforward but lengthy calculation confirms that Eqs. (4) conserve the particle number as well as the total energy comprised of the single-particle contributions and the correlation energies.

C. Markov limit

Although Eqs. (4) can readily be used to calculate the spin dynamics given a set of appropriate initial conditions, it is instructive also to derive the Markov limit of the quantum kinetic equations[26–28]. On the one hand, this enables us to distinguish the Markovian behavior from genuine quantum kinetic effects. On the other hand, it allows us to derive analytic expressions for the correlation energies and the renormalization of the precession frequencies in the presence of an external magnetic field[39].

The derivation of the Markov limit comprises two steps[28]: First, the equations of motion for the correlations are formally integrated yielding explicit expressions for the correlations in the form of a memory integral. This yields integro-differential equations for the single-particle variables, where the values of the single-particle variables at earlier times enter. Second, the memory integral is eliminated by assuming a δ-like short memory.

However, the first step, which involves the formal integration of the carrier-impurity correlations, can, in general, be complicated. Nevertheless, if the source terms $b_{\sigma_1 n_1 \mathbf{k}_1}^{\sigma_2 n_2 \mathbf{k}_2\, III}$ and $c_{\sigma_1 \mathbf{k}_1}^{\sigma_2 \mathbf{k}_2\, III}$ as well as the correlation-

dependent part of $b_{\sigma_1 n_1 \mathbf{k}_1}^{\sigma_2 n_2 \mathbf{k}_2\, \mathrm{imp}}$ and $c_{\sigma_1 \mathbf{k}_1}^{\sigma_2 \mathbf{k}_2\, \mathrm{sd}}$ are neglected, the formal solution of Eqs. (4c-d) becomes much easier. In absence of non-magnetic impurity scattering, it has been shown that these source terms are indeed numerically insignificant[26]. Furthermore, a straightforward calculation shows that neglecting these terms also yields a consistent theory with respect to the conservation of the total energy. Whether neglecting the terms $b_{\sigma_1 n_1 \mathbf{k}_1}^{\sigma_2 n_2 \mathbf{k}_2\, III}$, $c_{\sigma_1 \mathbf{k}_1}^{\sigma_2 \mathbf{k}_2\, III}$ and the correlation-dependent parts of $b_{\sigma_1 n_1 \mathbf{k}_1}^{\sigma_2 n_2 \mathbf{k}_2\, \mathrm{imp}}$ and $c_{\sigma_1 \mathbf{k}_1}^{\sigma_2 \mathbf{k}_2\, \mathrm{sd}}$ is indeed a good approximation in the presence of non-magnetic impurity scattering can be tested by comparing the numerical results of the quantum kinetic equations with and without accounting for these source terms.

Neglecting the aforementioned source terms in Eqs. (4), we first formulate a set of quantum kinetic equations for the new dynamical variables

$$\langle S^i \rangle = \sum_{n_1 n_2} S_{n_1 n_2}^i M_{n_1 n_2}, \tag{6a}$$

$$n_\mathbf{k} = \sum_\sigma C_{\sigma \mathbf{k}}^\sigma, \tag{6b}$$

$$s_\mathbf{k}^i = \sum_{\sigma_1 \sigma_2} s_{\sigma_1 \sigma_2}^i C_{\sigma_1 \mathbf{k}}^{\sigma_2}, \tag{6c}$$

$$\bar{C}_{\ \mathbf{k}_1}^{\alpha \mathbf{k}_2} = \sum_{\sigma_1 \sigma_2} s_{\sigma_1 \sigma_2}^\alpha \bar{C}_{\sigma_1 \mathbf{k}_1}^{\sigma_2 \mathbf{k}_2} \tag{6d}$$

$$Q_{l \mathbf{k}_1}^{\alpha \mathbf{k}_2} = \sum_{\sigma_1 \sigma_2} \sum_{n_1 n_2} s_{\sigma_1 \sigma_2}^\alpha S_{n_1 n_2}^l Q_{\sigma_1 n_1 \mathbf{k}_1}^{\sigma_2 n_2 \mathbf{k}_2}, \tag{6e}$$

where $\langle \mathbf{S} \rangle$ is the average impurity spin and $n_\mathbf{k}$ and $\mathbf{s}_\mathbf{k}$ are the occupation density and spin density of the carrier states with wave vector $\mathbf{k}$, respectively. $\bar{C}_{\ \mathbf{k}_1}^{\alpha \mathbf{k}_2}$ as well as $Q_{l \mathbf{k}_1}^{\alpha \mathbf{k}_2}$ comprise the non-magnetic and magnetic carrier-impurity correlations. In Eqs. (6) we use a notation in which the Latin indices are in the range $\{1, 2, 3\}$, while the Greek indices also include the value 0, where $s_{\sigma_1 \sigma_2}^0 = \delta_{\sigma_1 \sigma_2}$ is the 2x2 identity matrix. The corresponding equations of motion for the variables defined in Eqs. (6) are explicitly given in appendix A.

Note that the source terms $b_{l \mathbf{k}_1}^{\alpha \mathbf{k}_2\, I}$ for the correlations $Q_{l \mathbf{k}_1}^{\alpha \mathbf{k}_2}$ depend on the second moments of the impurity spins $\langle S^i S^j \rangle = \sum_{n_1 n_2 n_3} S_{n_1 n_2}^i S_{n_2 n_3}^j M_{n_1 n_3}$ for which we do not present equations of motions, although such equations can, in principle, be derived from Eqs. (4). Here, we use the fact that for typical sample parameters the optically induced carrier density is usually much lower than the impurity concentration, so that the average impurity spin only changes marginally over time[26]. For the numerical calculations we assume that the impurity density matrix can be approximately described as being in thermal equilibrium at all times where the effective impurity spin temperature T_Mn can be obtained from the value of $\langle \mathbf{S} \rangle$. From this thermally occupied density matrix, the second moments $\langle S^i S^j \rangle$ consistent with $\langle \mathbf{S} \rangle$ can be calculated in each time step.

The equations of motion for the variables defined in Eqs. (6) are the starting point for the formal integration of the correlations. Note that Eqs. (A1d-g) for the correlations $Q_{l\mathbf{k}_1}^{\alpha\mathbf{k}_2}$ and $\bar{C}_{\mathbf{k}_1}^{\alpha\mathbf{k}_2}$ can be transformed into the general form

$$\frac{\partial}{\partial t}Q_{\mathbf{k}_1}^{\mathbf{k}_2} = -i(\omega_{\mathbf{k}_2} - \omega_{\mathbf{k}_1})Q_{\mathbf{k}_1}^{\mathbf{k}_2} + i\chi_1\omega_e Q_{\mathbf{k}_1}^{\mathbf{k}_2}$$
$$+ i\chi_2\omega_{\mathrm{Mn}}Q_{\mathbf{k}_1}^{\mathbf{k}_2} + b_{\mathbf{k}_1}^{\mathbf{k}_2 I}, \qquad (7)$$

where $\chi_1, \chi_2 \in \{-1, 0, 1\}$ and the terms proportional to $\omega_e = |\boldsymbol{\omega}_e|$ and $\omega_{\mathrm{Mn}} = |\boldsymbol{\omega}_{\mathrm{Mn}}|$ originate from the precession of the correlations described by the source terms $b_{\sigma_1 n_1 \mathbf{k}_1}^{\sigma_2 n_2 \mathbf{k}_2 II}$ and $c_{\sigma_1 \mathbf{k}_1}^{\sigma_2 \mathbf{k}_2 II}$. The term $b_{\mathbf{k}_1}^{\mathbf{k}_2 I}$ here denotes the contributions from the source terms $b_{\sigma_1 n_1 \mathbf{k}_1}^{\sigma_2 n_2 \mathbf{k}_2 I}$, $c_{\sigma_1 \mathbf{k}_1}^{\sigma_2 \mathbf{k}_2 I}$, $b_{\sigma_1 n_1 \mathbf{k}_1}^{\sigma_2 n_2 \mathbf{k}_2 \mathrm{imp}}$ and $c_{\sigma_1 \mathbf{k}_1}^{\sigma_2 \mathbf{k}_2 \mathrm{sd}}$ and only depends on the single-particle variables. The formal integration of Eq. (7) yields

$$Q_{\mathbf{k}_1}^{\mathbf{k}_2}(t) = \int_0^t dt' e^{i[\omega_{\mathbf{k}_2} - (\omega_{\mathbf{k}_1} + \chi_1\omega_e + \chi_2\omega_{\mathrm{Mn}})](t'-t)} b_{\mathbf{k}_1}^{\mathbf{k}_2 I}(t').$$
$$(8)$$

The Markov limit consists of assuming a short memory, i.e. the assumption that the correlations at time t depend only significantly on the single-particle variables at the same time t, so that one is inclined to evaluate $b_{\mathbf{k}_1}^{\mathbf{k}_2 I}(t')$ in Eq. (8) at $t' = t$ and to draw the source term out of the integral. However, first, one has to make sure that the source terms are indeed slowly changing variables.

For example, the carrier spin can precess rapidly about an external magnetic field. Therefore, we first analyze the mean-field precession of the single-particle quantities and split the source terms into parts oscillating with some frequencies ω of the form

$$b_{\mathbf{k}_1}^{\mathbf{k}_2 I}(t') \stackrel{\mathrm{MF}}{=} \sum_\omega \sum_{\chi \in \{-1,0,1\}} e^{i\chi\omega(t'-t)} b_{\mathbf{k}_1}^{\mathbf{k}_2 \omega,\chi}(t). \qquad (9)$$

Then, the different oscillating parts $b_{\mathbf{k}_1}^{\mathbf{k}_2 \omega,\chi}(t)$ can be drawn out of the memory integral and the remaining integral can be solved in the limit of large times t[28]:

$$\int_0^t dt' \, e^{i\Delta\omega(t'-t)} \xrightarrow{t\to\infty} \pi\delta(\Delta\omega) - \frac{i}{\Delta\omega}. \qquad (10)$$

This procedure yields particularly transparent results in the case where the external magnetic field and the impurity magnetization are collinear, as is usually the case when the number of impurities exceeds the number of quasi-free carriers ($N_{\mathrm{Mn}} \gg N_e$), and the impurity density matrix is initially occupied thermally. Choosing the direction of $\boldsymbol{\omega}_e$ as a reference and defining $s_{\mathbf{k}_1}^{\parallel} := \mathbf{s} \cdot \frac{\boldsymbol{\omega}_e}{\omega_e}$, $S^{\parallel} := \hat{\mathbf{S}} \cdot \frac{\boldsymbol{\omega}_e}{\omega_e}$ and $\omega_{\mathrm{Mn}}^{\parallel} := \boldsymbol{\omega}_{\mathrm{Mn}} \cdot \frac{\boldsymbol{\omega}_e}{\omega_e}$, the Markovian equations obtained for the spin-up and spin-down occupations and the perpendicular carrier spin component with respect to the direction of $\boldsymbol{\omega}_e$,

$$n_{\mathbf{k}_1}^{\uparrow/\downarrow} := \frac{n_{\mathbf{k}_1}}{2} \pm s_{\mathbf{k}_1}^{\parallel}, \qquad (11a)$$

$$\mathbf{s}_{\mathbf{k}_1}^{\perp} := \mathbf{s}_{\mathbf{k}_1} - \frac{\boldsymbol{\omega}_e}{\omega_e} s_{\mathbf{k}_1}^{\parallel}, \qquad (11b)$$

are given by:

$$\frac{\partial}{\partial t}n_{\mathbf{k}_1}^{\uparrow/\downarrow} = \frac{\pi}{\hbar^2 V^2}\sum_{\mathbf{k}_2}\left\{\delta(\omega_{\mathbf{k}_2} - \omega_{\mathbf{k}_1})\left[J_{\mathrm{sd}}^2 N_{\mathrm{Mn}}\frac{1}{2}\langle S^{\parallel^2}\rangle \pm J_{\mathrm{sd}}J_0(N_{\mathrm{Mn}} + N_{\mathrm{imp}})\langle S^{\parallel}\rangle + 2J_0^2 N_{\mathrm{imp}}\right](n_{\mathbf{k}_2}^{\uparrow/\downarrow} - n_{\mathbf{k}_1}^{\uparrow/\downarrow}) + \right.$$
$$\left. + \delta\left[\omega_{\mathbf{k}_2} - (\omega_{\mathbf{k}_1} \pm (\omega_e - \omega_{\mathrm{Mn}}^{\parallel}))\right]J_{\mathrm{sd}}^2 N_{\mathrm{Mn}}\left[\left(\langle S^{\perp^2}\rangle \pm \frac{1}{2}\langle S^{\parallel}\rangle\right)\left(1 - n_{\mathbf{k}_1}^{\uparrow/\downarrow}\right)n_{\mathbf{k}_2}^{\downarrow/\uparrow} - \left(\langle S^{\perp^2}\rangle \mp \frac{1}{2}\langle S^{\parallel}\rangle\right)\left(1 - n_{\mathbf{k}_2}^{\downarrow/\uparrow}\right)n_{\mathbf{k}_1}^{\uparrow/\downarrow}\right]\right\},$$
$$(12a)$$

$$
\begin{aligned}
\frac{\partial}{\partial t}\mathbf{s}_{\mathbf{k}_1}^{\perp} = &-\frac{\pi}{\hbar^2 V^2}\sum_{\mathbf{k}_2}\Bigg\{\delta(\omega_{\mathbf{k}_2}-\omega_{\mathbf{k}_1})\Big[J_{\mathrm{sd}}^2 N_{\mathrm{Mn}}\frac{1}{2}\langle S^{\parallel 2}\rangle(\mathbf{s}_{\mathbf{k}_2}^{\perp}+\mathbf{s}_{\mathbf{k}_1}^{\perp})-2J_0^2 N_{\mathrm{imp}}(\mathbf{s}_{\mathbf{k}_2}^{\perp}-\mathbf{s}_{\mathbf{k}_1}^{\perp})\Big]\\
&+\delta\big[\omega_{\mathbf{k}_2}-\big(\omega_{\mathbf{k}_1}+(\omega_{\mathrm{e}}-\omega_{\mathrm{Mn}}^{\parallel})\big)\big]\frac{1}{2}\Big(\langle S^{\perp 2}\rangle-\frac{1}{2}\langle S^{\parallel}\rangle(1-2n_{\mathbf{k}_2}^{\downarrow})\Big)\mathbf{s}_{\mathbf{k}_1}^{\perp}\\
&+\delta\big[\omega_{\mathbf{k}_2}-\big(\omega_{\mathbf{k}_1}-(\omega_{\mathrm{e}}-\omega_{\mathrm{Mn}}^{\parallel})\big)\big]\frac{1}{2}\Big(\langle S^{\perp 2}\rangle+\frac{1}{2}\langle S^{\parallel}\rangle(1-2n_{\mathbf{k}_2}^{\uparrow})\Big)\mathbf{s}_{\mathbf{k}_1}^{\perp}\Bigg\}\\
&+\boldsymbol{\omega}_{\mathrm{e}}\times\mathbf{s}_{\mathbf{k}_1}^{\perp}+\frac{1}{\hbar^2 V^2}\sum_{\mathbf{k}_2}\Bigg\{-\frac{J_{\mathrm{sd}}J_0}{\omega_{\mathbf{k}_2}-\omega_{\mathbf{k}_1}}\langle\mathbf{S}\rangle\times\big[(N_{\mathrm{imp}}-N_{\mathrm{Mn}})\mathbf{s}_{\mathbf{k}_2}^{\perp}+(N_{\mathrm{Mn}}+N_{\mathrm{imp}})\mathbf{s}_{\mathbf{k}_1}^{\perp}\big]\\
&-\frac{J_{\mathrm{sd}}^2 N_{\mathrm{Mn}}}{\omega_{\mathbf{k}_2}-\big(\omega_{\mathbf{k}_1}+(\omega_{\mathrm{e}}-\omega_{\mathrm{Mn}}^{\parallel})\big)}\frac{1}{2}\Big(\langle S^{\perp 2}\rangle-\frac{1}{2}\langle S^{\parallel}\rangle(1-2n_{\mathbf{k}_2}^{\downarrow})\Big)\Big(\frac{\boldsymbol{\omega}_{\mathrm{e}}}{\omega_{\mathrm{e}}}\times\mathbf{s}_{\mathbf{k}_1}^{\perp}\Big)\\
&+\frac{J_{\mathrm{sd}}^2 N_{\mathrm{Mn}}}{\omega_{\mathbf{k}_2}-\big(\omega_{\mathbf{k}_1}-(\omega_{\mathrm{e}}-\omega_{\mathrm{Mn}}^{\parallel})\big)}\frac{1}{2}\Big(\langle S^{\perp 2}\rangle+\frac{1}{2}\langle S^{\parallel}\rangle(1-2n_{\mathbf{k}_2}^{\uparrow})\Big)\Big(\frac{\boldsymbol{\omega}_{\mathrm{e}}}{\omega_{\mathrm{e}}}\times\mathbf{s}_{\mathbf{k}_1}^{\perp}\Big)\Bigg\}.
\end{aligned}
\tag{12b}
$$

The first line of the right-hand side of Eq. (12a), which is proportional to $n_{\mathbf{k}_2}^{\uparrow/\downarrow}-n_{\mathbf{k}_1}^{\uparrow/\downarrow}$, describes a redistribution of occupations of spin-up and spin-down states within a shell of defined kinetic energy via the term proportional to $\delta(\omega_{\mathbf{k}_2}-\omega_{\mathbf{k}_1})$. For a parabolic band structure, this implies a redistribution between states with the same modulus k of the wave vector $\mathbf{k}$, while the total carrier spin remains unchanged. If accompanied by a wave-vector dependent magnetic field like a Rashba or the Dresselhaus field, this term leads to a D'yakonov-Perel'-type suppression of the spin dephasing. Here, however, we do not consider any wave vector dependent field and the system under investigation is isotropic in $\mathbf{k}$-space, so that the first line in Eq. (12a) has no influence on the dynamics of the total spin. The second line in Eq. (12a) describes a spin-flip scattering from the spin-up band to the spin-down band and vice versa. Since these bands are energetically split by $\hbar\omega_{\mathrm{e}}$ and a flip of carrier spin involves a corresponding flip of an impurity spin in the opposite direction, which requires a magnetic (Zeeman) energy of $\hbar\omega_{\mathrm{Mn}}^{\parallel}$, the total magnetic energy released in a spin-flip process is $\pm\hbar(\omega_{\mathrm{e}}-\omega_{\mathrm{Mn}}^{\parallel})$. Thus, $\delta\big[\omega_{\mathbf{k}_2}-\big(\omega_{\mathbf{k}_1}\pm(\omega_{\mathrm{e}}-\omega_{\mathrm{Mn}}^{\parallel})\big)\big]$ ensures a conservation of the total single-particle energies in the Markov limit. It is noteworthy that, if the mean-field dynamics of the source terms as in Eq. (9) is not correctly taken into account, other energetic shifts are obtained in the δ-function, which yields equations in the Markov limit that are not consistent with the conservation of the single-particle energies[28]. Note also that the right-hand side of Eq. (12a) correctly deals with Pauli blocking effects. Because the non-magnetic impurity scattering enters in the equations of motion (12a) for the spin-up and spin-down occupation only via the first line which plays no role in an isotropic system, it has no influence on the spin dynamics in the Markov limit.

The first three lines in Eq. (12b) for the perpendicular carrier spin component, which are proportional to δ-functions, indicate an exponential decay of the per-

pendicular carrier spin component towards zero. The last three lines describe a precession of the perpendicular carrier spin component. The mean-field precession frequency ω_{e} is renormalized by the carrier-impurity correlations. This renormalization originates from the imaginary part of the memory integral in Eq. (10). Besides the terms proportional to $\frac{1}{\omega_{\mathbf{k}_2}-\big(\omega_{\mathbf{k}_1}\pm(\omega_{\mathrm{e}}-\omega_{\mathrm{Mn}}^{\parallel})\big)}$, which are also present when only the magnetic s-d interaction is taken into account[39], the non-magnetic impurity scattering introduces another contribution which is a cross-term, i.e. it is absent when either the magnetic or the non-magnetic impurity scattering is absent, which can be seen from the fact that it is proportional to the product of J_{sd} and J_0. In the quasi-continuous limit, the sum over $\mathbf{k}_2$ can be replaced by an integral over the spectral density of states. In quasi-two-dimensional systems like quantum wells, the spectral denstiy of states $D(\omega)=\frac{Am^*}{2\pi\hbar}$ is constant. Thus, the frequency renormalization can be integrated and yields logarithmic divergences

$$
\begin{aligned}
\sum_{\mathbf{k}_2}\frac{1}{\omega_{\mathbf{k}_2}-\omega_0} &= \int_0^{\omega_{BZ}} d\omega\, D(\omega)\frac{1}{\omega-\omega_0}\\
&= \frac{Am^*}{2\pi\hbar}\ln\left|\frac{\omega_{BZ}-\omega_0}{\omega_0}\right|.
\end{aligned}
\tag{13}
$$

at the poles $\omega_0=\omega_{\mathbf{k}_1}$ and $\omega_0=\omega_{\mathbf{k}_1}\pm(\omega_{\mathrm{e}}-\omega_{\mathrm{Mn}}^{\parallel})$. These logarithmic divergences are similar to the ones obtained in the discussion of the Kondo-effect in metals with magnetic impurities[29]. Despite the formal divergence, the summation over a non-singular carrier distribution always leads to a finite value of the precession frequency of the total carrier spin, since the logarithm is integrable[28]. From Eq. (13), one can see that the cut-off energy $\hbar\omega_{BZ}$, which corresponds to the width of the conduction band and is typically of the order of 1 eV, enters as a new model parameter in the theory and cannot be eliminated by assuming that $\omega_{BZ}\to\infty$, since then the frequency renormalization also diverges. As a consequence, the Markovian expression for the frequency renormalization

can only give an order-of-magnitude estimation and a more detailed treatment of the band structure is necessary if a quantitatively more accurate description is required.

For the special case of zero external magnetic field, vanishing impurity magnetization and low carrier densities, Eqs. (12) are equivalent to the simple rate equations

$$\frac{\partial}{\partial t}\mathbf{s}_{\mathbf{k}_1} = -\frac{1}{\tau}\mathbf{s}_{\mathbf{k}_1}, \tag{14}$$

where the values of the rates coincide with the Fermi's golden rule value. In two dimensions, one obtains[25]

$$\frac{1}{\tau^{2D}} = \frac{35}{12}\frac{J_{\mathrm{sd}}^2 m^*}{\hbar^3}\frac{N_{\mathrm{Mn}}}{V}\frac{1}{d}. \tag{15}$$

D. Correlation energy

In Eqs. (8) to (10), Markovian expressions for the carrier-impurity correlations are derived as functionals of the carrier and impurity variables. Using these expressions, it is straightforward to also obtain analytic expressions for the carrier-impurity correlation energies as functionals of the carrier spins and occupations[28]. Splitting the averages over the magnetic and non-magnetic carrier-impurity interactions into mean-field and correlated contributions

$$\langle H_{\mathrm{sd}}\rangle = \langle H_{\mathrm{sd}}^{\mathrm{MF}}\rangle + \langle H_{\mathrm{sd}}^{\mathrm{cor}}\rangle, \tag{16a}$$

$$\langle H_{\mathrm{imp}}\rangle = \langle H_{\mathrm{imp}}^{\mathrm{MF}}\rangle + \langle H_{\mathrm{imp}}^{\mathrm{cor}}\rangle, \tag{16b}$$

$$\langle H_{\mathrm{sd}}^{\mathrm{MF}}\rangle = \frac{J_{\mathrm{sd}}N_{\mathrm{Mn}}}{V}\sum_{\mathbf{k}}\langle\mathbf{S}\rangle\cdot\mathbf{s}_{\mathbf{k}} \tag{16c}$$

$$\langle H_{\mathrm{sd}}^{\mathrm{cor}}\rangle = \frac{J_{\mathrm{sd}}N_{\mathrm{Mn}}}{V^2}\sum_{\mathbf{k},\mathbf{k}'}\sum_i Q_{i\mathbf{k}}^{i\mathbf{k}'} \tag{16d}$$

$$\langle H_{\mathrm{imp}}^{\mathrm{MF}}\rangle = \frac{J_0 N_{\mathrm{imp}}}{V}\sum_{\mathbf{k}}n_{\mathbf{k}}, \tag{16e}$$

$$\langle H_{\mathrm{imp}}^{\mathrm{cor}}\rangle = \frac{J_0 N_{\mathrm{imp}}}{V^2}\sum_{\mathbf{k},\mathbf{k}'}\bar{C}_{\mathbf{k}}^{0\mathbf{k}'}, \tag{16f}$$

one obtains in the Markov limit

$$\langle H_{\mathrm{sd}}^{\mathrm{cor}}\rangle = -\frac{J_{\mathrm{sd}}N_{\mathrm{Mn}}}{V^2}\sum_{\mathbf{k}_1\mathbf{k}_2}\Bigg\{\frac{\frac{1}{2}J_{\mathrm{sd}}\langle S^{\|^2}\rangle n_{\mathbf{k}_1} + 2J_0\langle S^{\|}\rangle s_{\mathbf{k}_1}^{\|}}{\omega_{\mathbf{k}_2} - \omega_{\mathbf{k}_1}}$$

$$+ \frac{J_{\mathrm{sd}}\big(\langle S^{\perp}\rangle - \frac{1}{2}\langle S^{\|}\rangle\big)(1 - n_{\mathbf{k}_2}^{\downarrow})n_{\mathbf{k}_1}^{\uparrow}}{\omega_{\mathbf{k}_2} - (\omega_{\mathbf{k}_1} + (\omega_e - \omega_{\mathrm{Mn}}^{\|}))}$$

$$+ \frac{J_{\mathrm{sd}}\big(\langle S^{\perp}\rangle + \frac{1}{2}\langle S^{\|}\rangle\big)(1 - n_{\mathbf{k}_2}^{\uparrow})n_{\mathbf{k}_1}^{\downarrow}}{\omega_{\mathbf{k}_2} - (\omega_{\mathbf{k}_1} - (\omega_e - \omega_{\mathrm{Mn}}^{\|}))}\Bigg\}, \tag{17a}$$

$$\langle H_{\mathrm{imp}}^{\mathrm{cor}}\rangle = -2\frac{J_0 N_{\mathrm{imp}}}{V^2}\sum_{\mathbf{k}_1\mathbf{k}_2}\frac{J_0 n_{\mathbf{k}_1} + J_{\mathrm{sd}}\langle S^{\|}\rangle s_{\mathbf{k}_1}^{\|}}{\omega_{\mathbf{k}_2} - \omega_{\mathbf{k}_1}}. \tag{17b}$$

Eqs. (17) have the same poles as Eq. (12b) for the frequency renormalization and, thus, also contain formally logarithmic divergences in two-dimensional systems.

III. RESULTS

After having derived the quantum kinetic equations for the description of the spin dynamics in DMS including magnetic and non-magnetic scattering and having obtained rate-type Markovian equations, we now present results of numerical simulations. Here, we focus on the case of a 4-nm-wide $Cd_{0.93}Mn_{0.07}Te$ quantum well. For this material, the magnetic coupling constant is $J_{\mathrm{sd}} = -15$ meVnm^3 ($N_0 J_{\mathrm{sd}} = -220$ meV)[42], while the non-magnetic coupling constant is approximately $J_0 = 110$ meVnm^3 ($N_0 J_0 = 1.6$ eV)[31], where N_0 is the number of unit cells per unit volume. Furthermore, we use a conduction band effective mass of $m^* = 0.1\,m_0$ and assume that the impurity magnetization is described by a thermal distribution at a temperature of $T = 2$ K and the g-factors of the conduction band carriers and Mn impurities are $g_e = -1.77$ and $g_{\mathrm{Mn}} = 2$, respectively[40]. If not stated otherwise, we choose a value of 40 meV for the cut-off energy $\hbar\omega_{BZ}$ in the numerical calculations and we consider only Mn ions as sources of non-magnetic impurity scattering, i. e. $N_{\mathrm{imp}} = N_{\mathrm{Mn}}$. As initial value for the carrier distribution, we use a Gaussian distribution centered at the band edge of the spin-up band with standard deviation of $E_s = 0.4$ meV, which corresponds to an excitation with a circularly polarized light pulse with full width at half maximum (FWHM) pulse duration of about 350 fs.

We first discuss the spin dynamics in the conduction band of a $Cd_{0.93}Mn_{0.07}Te$ quantum well for zero magnetic field with a focus on the impact of non-magnetic impurity scattering on the spin dynamics and investigate the redistribution of carriers in $\mathbf{k}$-space as well as the build-up of correlation energy. Then, we study the spin dynamics in the valence band in a simplified model. Finally, we investigate the spin dynamics in the presence of an external magnetic field parallel and perpendicular to the carrier spin polarization and discuss, in the latter case, how the non-magnetic impurity scattering affects the carrier spin precession frequencies.

A. Zero magnetic field

Figure 1(a) shows the time evolution of an initially polarized carrier spin in a $Cd_{0.93}Mn_{0.07}Te$ quantum well for vanishing magnetic field. The Markovian equations (12) predict a simple exponential decay of the carrier spin, which is transferred to the impurities. Note that due to $N_{\mathrm{Mn}} \gg N_e$, the asymptotic value of the carrier spin for long times t is close to zero, since the impurities act as a spin bath. If only the magnetic spin-flip scattering is accounted for ($J_0 = 0$), the time evolution according to the quantum kinetic theory is non-monotonic and shows an overshoot below the asymptotic value. These non-Markovian effects are strongly suppressed in the calculations including non-magnetic impurity scattering ($J_0 = 110$ meVnm^3) and the time evo-
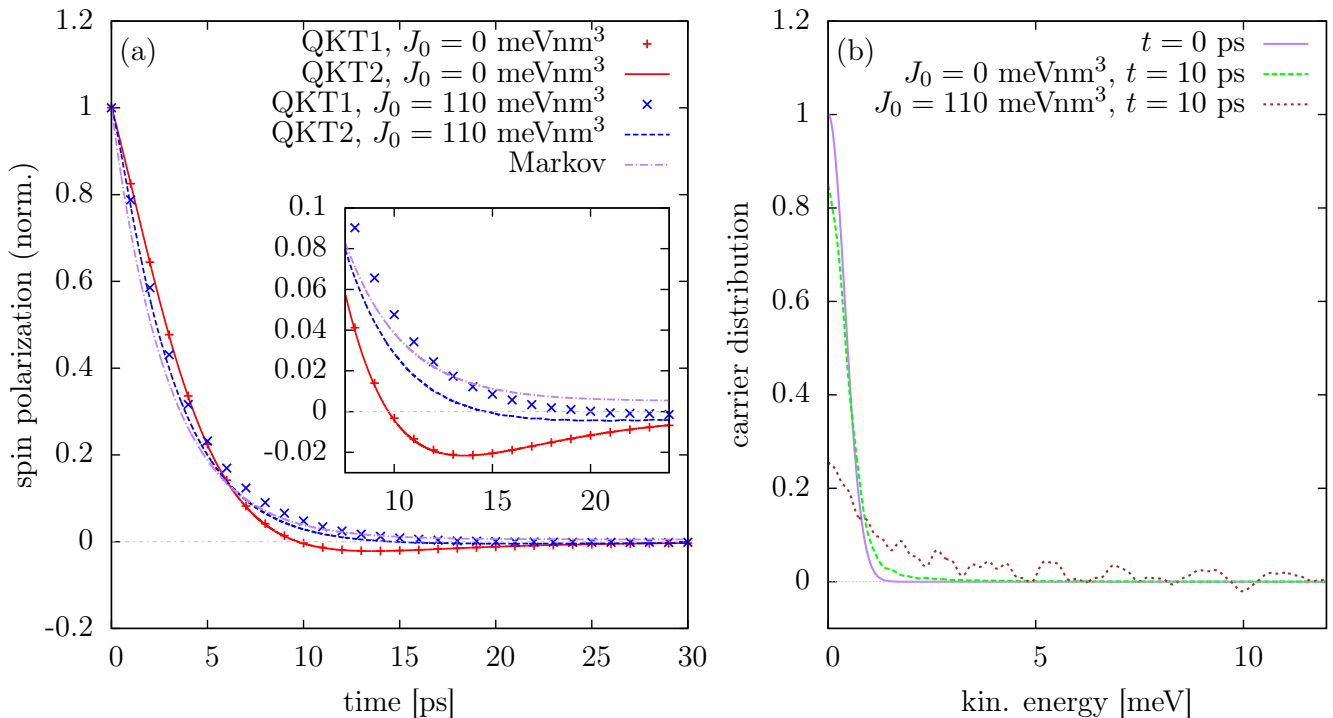
FIG. 1. (a): Time evolution of the carrier spin for zero magnetic field with $(J = 110 \text{ meVnm}^3)$ and without $(J = 0)$ non-magnetic impurity scattering. QKT1 (points) denotes the results according to the full quantum kinetic equations (4) while QKT2 (lines) describes the results of the reduced set of equations (A1). The purple dash-dotted line shows the results of the Markovian equations (12), which is independent of non-magnetic impurity scattering. The inset shows a magnification of the region where the quantum kinetic theory for $J_0 = 0$ predicts a non-monotonic behavior. (b) Occupation of carrier states at $t = 0$ and $t = 10$ ps for the calculations with and without non-magnetic impurity scattering.

lution of the total spin follows the Markovian dynamics more closely. An exponential fit to the dynamics of the full quantum kinetic theory yields an effective spin transfer rate about 15% smaller than the Markovian rate in Eq. (15).

Interestingly, while the full quantum kinetic equations (4) yield identical results as the reduced set of equations (A1) in the case without non-magnetic impurity scattering, deviations between both approaches can be clearly seen when the non-magnetic impurity scattering is taken into account.

In order to understand the suppression of the non-monotonic features in the spin dynamics with non-magnetic impurity scattering, it is useful to recapitulate the findings of Ref. 38, where the origin of the non-Markovian behavior of the spin dynamics in absence of non-magnetic impurity scattering was discussed: It was found that the depth of the memory induced by the correlations is of the order of the inverse energetic distance of the carrier state under consideration to the band edge times $\hbar$. Memory effects become insignificant if the kinetic energy of the carrier $\hbar\omega_{\mathbf{k}_1}$ is much higher than the energy scale of the carrier-impurity spin transfer rate $\frac{\hbar}{\tau}$. For the parameters used in the simulations, one obtains from Eq. (15) a value of $\tau^{2D} = 2.97$ ps and therefore $\frac{\hbar}{\tau} \approx 0.22$ meV. Figure 1(b) shows the redistribu-

tion of carriers in the calculations with and without non-magnetic impurity scattering. One can clearly see that, while without non-magnetic impurity scattering the carrier distribution at $t = 10$ ps is only slightly broadened, including the non-magnetic impurity scatterings leads to a drastic redistribution of carriers to states many meV away from the initial distribution. For these states, the memory is very short compared with the spin relaxation time and therefore the Markovian approximation is justified.

The redistribution of carriers to states several meV away from the band edge raises questions about the conservation of energy, since for zero magnetic field the mean-field energy of the system is comprised of only the kinetic energy of the carriers. In the quantum kinetic calculations, however, we also consider the carrier-impurity correlations which introduce correlation energies that are not captured in a simple single-particle picture. The different contributions to the total energy over the course of time for the simulations presented in Fig. 1 are shown in Fig. 2. There, it is shown that the average kinetic energy per electron increases from the initial value of the order of the width of the initial carrier distribution to a much larger value of about 4 meV on a timescale of about 0.5 ps. This energy is mostly provided by a decrease of non-magnetic correlation energy from zero to a negative value.
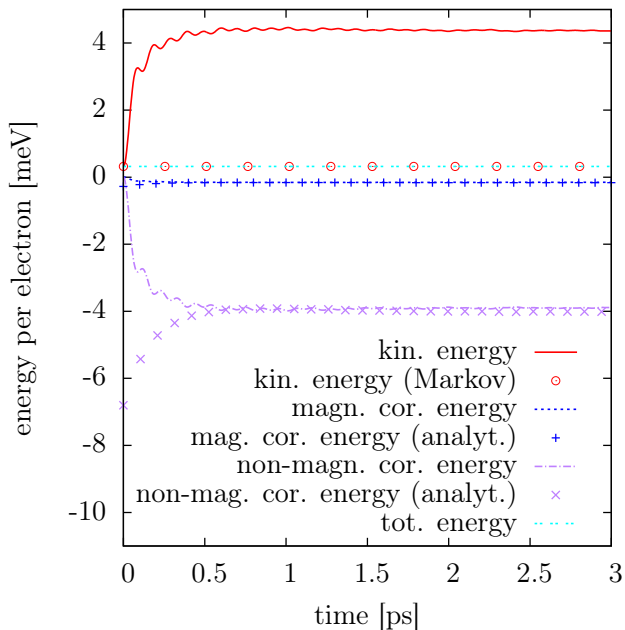
FIG. 2. Kinetic energy (red line), magnetic correlation energy (blue line), non-magnetic correlation energy (purple line) and total energy (cyan line) per electron for the quantum kinetic calculation shown in Fig. 1 with $J_0 = 110$ meVnm^3. The red circles show the kinetic energy obtained from the Markovian calculation in Fig. 1. The pluses and crosses depict the results according to the analytic Markovian expressions for the correlation energies in Eqs. (17) evaluated using the carrier distribution of the quantum kinetic calculation at selected time steps.

The magnetic correlation energy is comparatively small since the magnetic coupling constant J_{sd} is about one order of magnitude smaller than the non-magnetic coupling constant J_0. The pluses and crosses in Fig. 2 show the results of the analytic expressions (17) for the correlation energies evaluated using the carrier distributions of the full quantum kinetic theory in the respective time steps. The analytic results are found to coincide with the values extracted from the quantum kinetic theory after the first 0.5 ps. Even though the analytic expressions for the correlation energies are obtained within the Markovian description, it should be noted that in the Markovian equations of motion (12) for the spins and occupations only single-particle energies are considered for evaluating the energy balance. As in our case the single particle energies comprise only the kinetic energies of the carriers, the latter are constant in the Markovian description in sharp contrast to the quantum kinetic treatment.

Note also that the total energy comprised of single-particle and correlation energies remains constant in the quantum kinetic simulations, which provides a further test for the numerics.
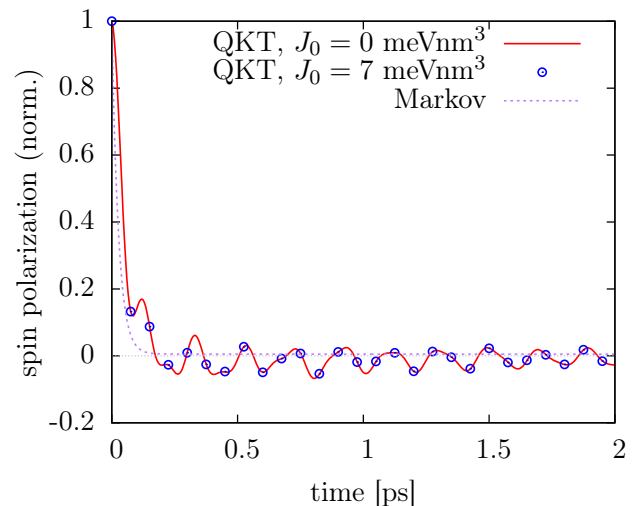

FIG. 3. Spin dynamics in a degenerate valence band of a Cd$_{0.93}$Mn$_{0.07}$Te quantum well with and without accounting for non-magnetic impurity scattering.

B. Valence band

The fact that in the conduction band of a Cd$_{1-x}$Mn$_x$Te quantum well the non-magnetic scattering at the impurities suppresses the characteristic non-monotonic features of genuine quantum kinetic behavior raises the question whether this statement is true in general and non-Markovian effects always only change the spin dynamics quantitatively. In this section, we provide an example of a situation where the non-Markovian features are not suppressed due to impurity scattering.

We consider now the valence band of a Cd$_{1-x}$Mn$_x$Te quantum well. The details of the valence band structure in a quantum well are influenced by, e.g., spin-orbit coupling, strain or the shape of the confinement potential. A realistic description of the band structure is beyond the scope of this article. Instead, we perform a model study, where we assume that heavy-hole and light-hole bands are degenerate. In this case, we can use the quantum kinetic theory derived for the conduction band and take the material parameters for the heavy holes. The magnetic coupling constant in the valence band is $J_{pd} = 60$ meVnm^3[42] and the heavy-hole mass is $m_h = 0.7m_0$[43]. The difference of the band gaps between CdTe and zincblende MnTe of about 1.6 eV is split into the conduction and valence band offsets by a ratio of 14:1[44]. Thus, one obtains a value for the non-magnetic coupling constant in the valence band of about $J_0 = 7$ meVnm^3. The results of the quantum kinetic simulations for these parameters are shown in Fig. 3.

In comparison with the conduction band, the 4 times larger magnetic coupling constant in the valence band leads to much stronger non-Markovian effects. In particular, one finds not a single overshoot, but pronounced oscillations of the spin polarization about its asymptotic
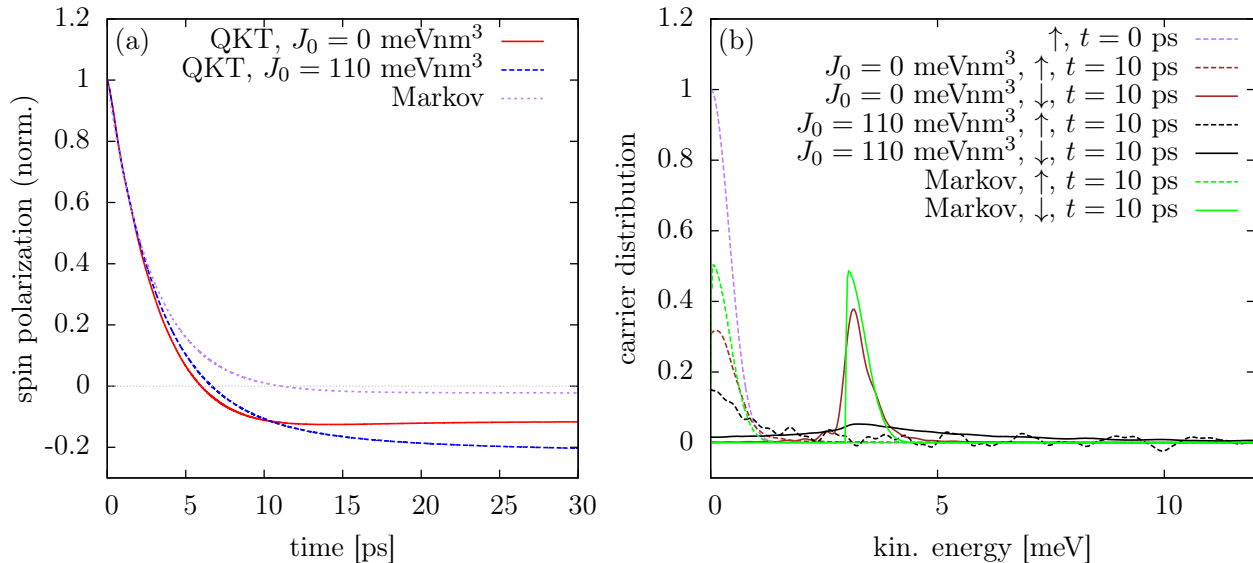
FIG. 4. (a): Time evolution of the carrier spin polarization parallel to an external magnetic field ($B = 100$ mT). (b): Spin-up ($\uparrow$) and spin-down occupations ($\downarrow$) at $t = 0$ and $t = 10$ ps.

value. In Fig. 3, the calculations with and without accounting for non-magnetic impurity scattering yield practically identical results. Thus, due to the fact that in the valence band the non-magnetic coupling constant is much smaller than the magnetic coupling constant, no suppression of non-Markovian effects in the spin dynamics is observed.

C. Finite magnetic field: Faraday configuration

Next, we investigate the effects of non-magnetic impurity scattering on the spin dynamics in DMS in the presence of an external magnetic field. In this section, we study the case in which the external field and the initial carrier spins are parallel, which is known as the Faraday configuration. This case has also been considered in Ref. 40, but without accounting for non-magnetic impurity scattering.

In Fig. 4(a) the time evolution of the carrier spin polarization parallel to an external magnetic field $B = 100$ mT is shown. Note that the non-monotonic behavior that can be seen in the case without an external magnetic field is suppressed for finite external fields even if the non-magnetic scattering is disregarded. The most striking feature in the time evolution of the carrier spin polarization is that the Markovian result and the quantum kinetic simulations predict very different asymptotic values of the spin polarization at long times t.

As discussed in Ref. 40, the different stationary values are related to a broadening of the distribution of scattered carriers in the spin-down band, which is shown in Fig. 4(b). Note that the broadening of the carrier distribution is not primarily an effect of energy-time un-

certainty, which is commonly found in quantum kinetic studies[45,46], since the width of the distribution does not shrink significantly over the course of time[40]. Rather, it is a consequence of the build-up of correlation energy which enables deviations from the conservation of the single-particle energies in spin-flip scattering processes.

In the Markov limit, the stationary value is obtained when a balance between scattering from the spin-up to the spin-down band and vice versa is reached. In the quantum kinetic calculations, the distribution of the scattered carriers is broadened, so that also spin-down states below the threshold $\hbar\omega_e - \hbar\omega_{Mn}^{\parallel}$ are occupied, whose back-scattering is suppressed since there are no states in the spin-up band with the matching single-particle energies. If additionally the non-magnetic impurity scattering is taken into account, the scattered impurity distribution is even broader and more spin-down states with kinetic energies below $\hbar\omega_e - \hbar\omega_{Mn}^{\parallel}$ are occupied, so that the back-scattering is more strongly suppressed and the deviation of the asymptotic value of the spin polarization from the Markovian value is even larger.

D. Finite magnetic field: Voigt configuration

The situation in which an external magnetic field and the optically induced carrier spin polarization are perpendicular to each other is usually referred to as the Voigt configuration and is the subject of this section. In this situation, the carrier spin precesses about the effective magnetic field $\boldsymbol{\omega}_e$ due to the external field and the impurity magnetization. As shown in Ref. 39, where the non-magnetic impurity scattering was disregarded, the carrier-impurity correlations are responsible for a renor-
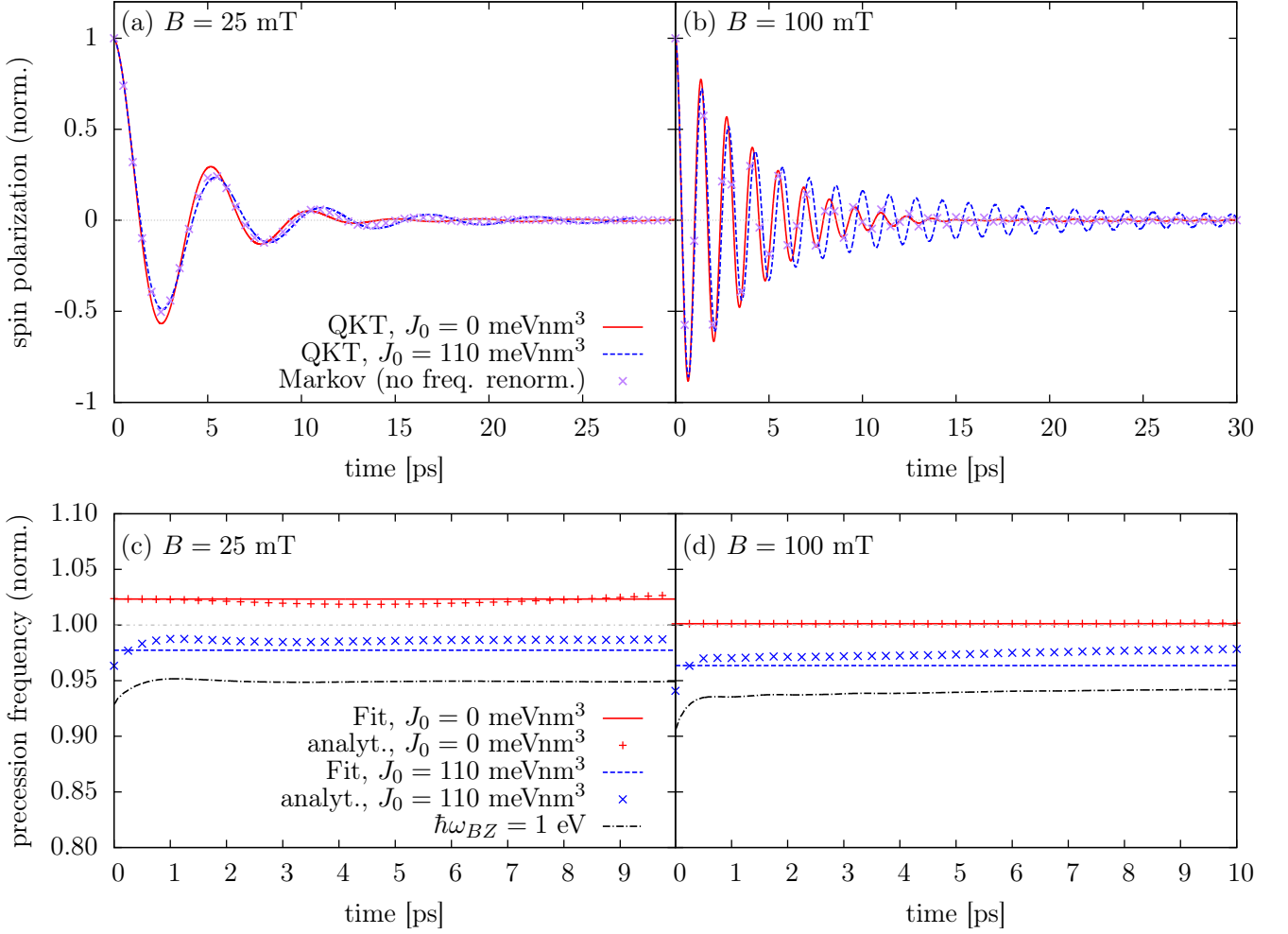
FIG. 5. (a) and (b): Time evolution of the carrier spin polarization for $B = 25$ mT (a) and $B = 100$ mT (b) using the quantum kinetic equations (4) and the Markovian equations Eq. (12b), where the terms responsible for the frequency renormalization in the Markovian equations have been dropped. The precession frequency normalized with respect to its mean-field value ω_e is shown in (c) and (d) using a fit of an exponentially decaying cosine to the quantum kinetic results and the analytic expressions obtained from Eq. (12b) and the occupations from the quantum kinetic calculations. The black dash-dotted lines in (c) and (d) show the analytic results for a cut-off energy of $\hbar\omega_{BZ} = 1$ eV.

malization of the precession frequency. There, it was also shown that the strength of this renormalization depends on the details of the carrier distribution and the strength of the effective field $\boldsymbol{\omega}_e$.

In Fig. 5(a), we present simulations of the spin dynamics in a DMS in Voigt geometry for an external magnetic field of $B = 25$ mT, which corresponds to a situation with $|\langle \mathbf{S} \rangle| \approx 0.05$, where the magnetic-correlation-induced frequency renormalization according to Ref. 39 is particularly strong. Simulations with ($J_0 = 110$ meVnm^3) and without ($J_0 = 0$) accounting for the non-magnetic impurity scattering are compared to Markovian calculations based on Eqs. (12). Note that for the Markovian calculation shown in Fig. 5 the frequency renormalization was not taken into account. The results of all simulations shown in Fig. 5(a) are very similar and follow closely the form of an exponentially damped cosine. Note that

at long times, the phases of the oscillations of the calculations accounting for non-magnetic impurity scattering matches the Markovian calculation without frequency renormalization, while accounting only for magnetic spin-flip scattering leads to oscillations with a slightly higher frequency.

The frequency renormalization for the simulations shown in Fig. 5(a) is presented in Fig. 5(c), where an exponentially decaying cosine is fit to the quantum kinetic results and, for comparison, the total precession frequency including the correlation-induced renormalization in the Markovian description in Eq. (12b) evaluated using the spin-up and spin-down occupations of the quantum kinetic simulations is depicted. Due to the time evolution of the occupations, also the renormalization predicted by Eq. (12b) becomes a function of time, which, however, is for all times close to the constant extracted

by fitting the quantum kinetic result. The calculations without non-magnetic impurity scattering predict an increase of the carrier spin precession frequency of about $2 - 3\%$ with respect to the mean-field value ω_e, which is consistent with the findings of Ref. 39. On the other hand, the contribution from the non-magnetic carrier-impurity correlations leads to a decrease of the precession frequency which partially cancels the contribution from the magnetic correlations.

In Figs. 5(b) and 5(d), the time evolution of the carrier spin polarization and the frequency renormalization are shown for an external magnetic field of $B = 100$ mT. In this case, the envelope of the spin polarization decays only exponentially for the calculations without non-magnetic impurity scattering. For $J_0 = 110$ meVnm^3, the spin polarization follows the exponential decay of the simulation with $J_0 = 0$ only up to about 5 ps. After that, it decays much slower, which is a new non-Markovian effect that is absent if the non-magnetic impurity scattering is disregarded. As can be seen in Fig. 5(d), the frequency renormalization due to the magnetic interaction alone is almost zero. Nevertheless, when the non-magnetic carrier-impurity correlations are taken into account, the precession frequency shows a decrease of about $2 - 3\%$. Thus, in contrast to the correlation-induced renormalization in absence of non-magnetic scattering where the renormalization is only observable for a very narrow set of initial conditions[39], including the non-magnetic carrier-impurity interaction results in a significant renormalization for a much broader set of excitation conditions.

It is noteworthy that the frequency renormalization in the quantum kinetic calculations is well reproduced by the Markovian expression in Eq. (12b). The numerical demands of the full quantum kinetic equations require a restriction of the conduction band width $\hbar\omega_{BZ}$ used in the calculations to a few tens of meV. However, in realistic band structures, the band widths are of the order of eV. In order to give an order-of-magnitude estimation of the frequency renormalization for such band widths, we present in Figs. 5(c) and 5(d) also the results of the Markovian expression for the frequency renormalizations using the value of $\hbar\omega_{BZ} = 1$ eV together with the occupations obtained in the quantum kinetic calculations for $\hbar\omega_{BZ} = 40$ meV. This estimation yields a renormalization of the precession frequencies due to the combined effects of magnetic and non-magnetic scattering of about $5 - 7\%$. A quantitatively more accurate description requires a more detailed treatment of the band structure, which is beyond the scope of this article.

Note also that the frequency renormalization due to the non-magnetic carrier-impurity correlations is dominated by a cross-term proportional to $J_{sd}J_0$ [cf. fourth line in Eq. (12b)]. Thus, the sign of the frequency renormalization depends on the relative signs of the coupling constants J_{sd} and J_0. In principle, this allows a determination of the sign of the magnetic coupling constant J_{sd} which cannot be obtained directly, e.g., by measuring the giant Zeeman splitting of excitons[42].

IV. CONCLUSION

We have investigated the influence of non-magnetic impurity scattering at Mn impurities on the spin dynamics in $Cd_{1-x}Mn_xTe$ diluted magnetic semiconductors. To this end, we have developed a quantum kinetic theory taking the magnetic and non-magnetic carrier-impurity correlations into account. The Markov limit of the quantum kinetic equation is derived in order to distinguish the Markovian dynamics from genuine quantum kinetic effects.

In contrast to earlier studies[25,27,37,40] in which only the magnetic contribution to the carrier-impurity interaction has been considered, some non-Markovian effects, such as a non-monotonic spin transfer between carriers and impurities, are strongly suppressed in the case of the conduction band of a $Cd_{1-x}Mn_xTe$ quantum well, while other features stemming from non-Markovian dynamics are enhanced, such as the large finite stationary value of the spin polarization in a magnetic field reached at long times. The reason for the suppression in the former case is that the non-magnetic impurity scattering leads to a strong redistribution of carriers in **k**-space away from the states at **k** = 0. Since memory effects are particularly strong for carriers in proximity to the band edge[27], this redistribution leads to spin dynamics that are well described by Markovian rate equations. The redistribution of the carriers implies an increase of their kinetic energies which is provided by a build-up of (negative) carrier-impurity correlation energy and which cannot be described by a mean-field or semiclassical approximation. We also provide analytic expressions for the correlation energies in the form of functionals of the spin-up and spin-down carrier occupations. Numerical calculations confirm that these expressions indeed describe the correlation energies obtained from the full quantum kinetic theory very well.

Even though doping with magnetic impurities unavoidably also provides a contribution to non-magnetic impurity scattering, there can still be situations where the latter is too weak to influence the spin dynamics and to suppress otherwise visible non-Markovian effects. This is substantiated by a model study of a $Cd_{1-x}Mn_xTe$ quantum well with degenerate valence bands, where the spin polarization exhibits a non-monotonic time dependence in the form of oscillations, while the Markovian treatment predicts a simple exponential decay. Further investigations using a more realistic valence band structure are needed in order to make more precise predictions about possible non-Markovian features in the hole spin dynamics in DMS.

In the presence of an external magnetic field parallel to the initial carrier spin (Faraday geometry), earlier studies[40] that did not consider non-magnetic impurity scattering predicted that the asymptotic value of the car-

rier spins in the conduction band of a DMS quantum well at long times t are significantly different in quantum kinetic and Markovian calculations. This was attributed to a broadening of the distribution of the scattered electrons due to the build-up of strong carrier-impurity correlations, which, because of the correlation energy, leads to a non-conservation of single-particle energies. The broadening results in an occupation of states by electrons whose back-scattering to the original band is strongly suppressed due to the lack of states with matching single-particle energies. This induces a bias between spin-flip scattering from the spin-up to the spin-down subband and vice versa. In the presence of a strong non-magnetic carrer-impurity interaction, the correlation energy becomes much larger and with it also the broadening of the scattered carrier distribution and the deviations of the asymptotic value of the carrier spin polarization from its value obtained in Markovian calculations.

In the Voigt geometry, where the initial carrier spin polarization is perpendicular to the external field, the carrier spin precesses about the effective magnetic field comprised of the external field and the mean field due to the impurity magnetization. There, the carrier-impurity correlations lead to a renormalization of the spin precession frequencies. An analytic expression for this renormalization is presented and it is found to be of a similar form as the expression for the correlation energies. The non-magnetic carrier-impurity interaction influences the frequency renormalization via a cross-term which vanishes if either the magnetic or the non-magnetic carrier-impurity interaction is neglected. In the case of the conduction band of $Cd_{1-x}Mn_xTe$, the magnetic and non-magnetic

contributions to the frequency renormalization have opposite signs. A measurement of the frequency renormalization can therefore indicate the sign of the exchange interaction. For magnetic fields at which the renormalization due to the magnetic correlations is particularly strong, the magnetic and non-magnetic contributions almost cancel each other. However, in most situations, the purely magnetic contribution is relatively weak[39], so that the cross-term dominates the total frequency renormalization. The order of magnitude of the frequency renormalization for the cases considered here is about a few percent of the mean-field precession frequency.

To summarize, the influence of the non-magnetic impurity scattering on the spin dynamics in DMS is two-fold: First, it leads to a significant redistribution of carriers in $\mathbf{k}$-space, which facilitates the suppression of some non-Markovian effects in certain situations. Second, it causes a formation of strong many-body correlations between carriers and impurities, which result in large correlation energies and a significant renormalization of the carrier spin precession frequency.

Appendix A: Reduced set of equations of motions

The equations of motions for the variables defined in Eq. (6) are:

$$\frac{\partial}{\partial t}\langle S^l\rangle = \sum_{im}\epsilon_{lim}\omega^i_{\text{Mn}}\langle S^m\rangle + \frac{J_{\text{sd}}}{V}\sum_{\mathbf{kk'}}\sum_{im}\epsilon_{lim}\text{Re}\{Q^{i\mathbf{k'}}_{m\mathbf{k}}\}, \tag{A1a}$$

$$\frac{\partial}{\partial t}n_{\mathbf{k}_1} = \frac{J_{\text{sd}}N_{\text{Mn}}}{\hbar V^2}\sum_{\mathbf{k}}\sum_i 2\text{Im}\{Q^{i\mathbf{k}}_{i\mathbf{k}_1}\} + \frac{J_0 N_{\text{imp}}}{\hbar V^2}\sum_{\mathbf{k}}2\text{Im}\{\bar{C}^{0\mathbf{k}}_{\mathbf{k}_1}\}, \tag{A1b}$$

$$\frac{\partial}{\partial t}s^l_{k_1} = \sum_{ij}\epsilon_{lij}\omega^i_{\text{e}}s^j_{\mathbf{k}_1} + \frac{J_{\text{sd}}N_{\text{Mn}}}{\hbar V^2}\sum_{\mathbf{k}}\left[\frac{1}{2}\text{Im}\{Q^{0\mathbf{k}}_{l\mathbf{k}_1}\} + \sum_{ij}\epsilon_{lij}\text{Re}\{Q^{j\mathbf{k}}_{i\mathbf{k}_1}\}\right] + \frac{J_0 N_{\text{imp}}}{\hbar V^2}\sum_{\mathbf{k}}2\text{Im}\{\bar{C}^{l\mathbf{k}}_{\mathbf{k}_1}\}, \tag{A1c}$$

$$\frac{\partial}{\partial t}Q^{0\mathbf{k}_2}_{l\mathbf{k}_1} = -i(\omega_{\mathbf{k}_2} - \omega_{\mathbf{k}_1})Q^{0\mathbf{k}_2}_{l\mathbf{k}_1} + \sum_{ii'}\epsilon_{lii'}\omega^i_{\text{Mn}}Q^{0\mathbf{k}_2}_{i'\mathbf{k}_1} + \frac{i}{\hbar}b^{0\mathbf{k}_2}_{l\mathbf{k}_1}{}^I + \frac{i}{\hbar}b^{0\mathbf{k}_2}_{l\mathbf{k}_1}{}^{\text{imp}}, \tag{A1d}$$

$$\frac{\partial}{\partial t}Q^{j\mathbf{k}_2}_{l\mathbf{k}_1} = -i(\omega_{\mathbf{k}_2} - \omega_{\mathbf{k}_1})Q^{j\mathbf{k}_2}_{l\mathbf{k}_1} + \sum_{ii'}\epsilon_{jii'}\omega^i_{\text{e}}Q^{i'\mathbf{k}_2}_{l\mathbf{k}_1} + \sum_{ii'}\epsilon_{lii'}\omega^i_{\text{Mn}}Q^{j\mathbf{k}_2}_{i'\mathbf{k}_1} + \frac{i}{\hbar}b^{j\mathbf{k}_2}_{l\mathbf{k}_1}{}^I + \frac{i}{\hbar}b^{j\mathbf{k}_2}_{l\mathbf{k}_1}{}^{\text{imp}}, \tag{A1e}$$

$$\frac{\partial}{\partial t}\bar{C}^{0\mathbf{k}_2}_{\mathbf{k}_1} = -i(\omega_{\mathbf{k}_2} - \omega_{\mathbf{k}_1})\bar{C}^{0\mathbf{k}_2}_{\mathbf{k}_1} + \frac{i}{\hbar}c^{0\mathbf{k}_2}_{\mathbf{k}_1}{}^I + \frac{i}{\hbar}c^{0\mathbf{k}_2}_{\mathbf{k}_1}{}^{\text{sd}}, \tag{A1f}$$

$$\frac{\partial}{\partial t}\bar{C}^{j\mathbf{k}_2}_{\mathbf{k}_1} = -i(\omega_{\mathbf{k}_2} - \omega_{\mathbf{k}_1})\bar{C}^{j\mathbf{k}_2}_{\mathbf{k}_1} + \sum_{ii'}\epsilon_{jii'}\omega^i_{\text{e}}\bar{C}^{i'\mathbf{k}_2}_{\mathbf{k}_1} + \frac{i}{\hbar}c^{j\mathbf{k}_2}_{\mathbf{k}_1}{}^I + \frac{i}{\hbar}c^{j\mathbf{k}_2}_{\mathbf{k}_1}{}^{\text{sd}}, \tag{A1g}$$

with

$$b_{l\mathbf{k}_1}^{0\mathbf{k}_2\,I} = J_{\mathrm{sd}}\sum_i \left[\mathrm{Re}\{\langle S^i S^l\rangle\}(s_{\mathbf{k}_2}^i - s_{\mathbf{k}_1}^i) + i\sum_m \epsilon_{ilm}\frac{\langle S^m\rangle}{2}\Big((1-n_{\mathbf{k}_1})s_{\mathbf{k}_2}^i + (1-n_{\mathbf{k}_2})s_{\mathbf{k}_1}^i\Big) + \langle S^i\rangle(s_{\mathbf{k}_1}^l s_{\mathbf{k}_2}^i - s_{\mathbf{k}_1}^i s_{\mathbf{k}_2}^l)\right], \tag{A1h}$$

$$b_{l\mathbf{k}_1}^{j\mathbf{k}_2\,I} = J_{\mathrm{sd}}\sum_i \left[\mathrm{Re}\{\langle S^i S^l\rangle\}\Big[\delta_{ij}\big(\frac{n_{\mathbf{k}_2}}{4} - \frac{n_{\mathbf{k}_1}}{4}\big) + \frac{i}{2}\epsilon_{ijk}(s_{\mathbf{k}_1}^k + s_{\mathbf{k}_2}^k)\Big] + \frac{i}{2}\sum_m \epsilon_{ilm}\langle S^m\rangle\Big[\delta_{ij}\frac{n_{\mathbf{k}_1} + n_{\mathbf{k}_2} - n_{\mathbf{k}_1}n_{\mathbf{k}_2}}{4}\right.$$
$$\left. + \delta_{ij}\mathbf{s}_{\mathbf{k}_1}\cdot\mathbf{s}_{\mathbf{k}_2} - (s_{\mathbf{k}_1}^i s_{\mathbf{k}_2}^j + s_{\mathbf{k}_2}^i s_{\mathbf{k}_1}^j) + \frac{i}{2}\epsilon_{ijk}\big((1-n_{\mathbf{k}_1})s_{\mathbf{k}_2}^k - (1-n_{\mathbf{k}_2})s_{\mathbf{k}_1}^k\big)\Big]\right], \tag{A1i}$$

$$b_{l\mathbf{k}_1}^{0\mathbf{k}_2\,\mathrm{imp}} = J_0\langle S^l\rangle(n_{\mathbf{k}_2} - n_{\mathbf{k}_1}), \tag{A1j}$$

$$b_{l\mathbf{k}_1}^{j\mathbf{k}_2\,\mathrm{imp}} = J_0\langle S^l\rangle(s_{\mathbf{k}_2}^j - s_{\mathbf{k}_1}^j), \tag{A1k}$$

$$c_{\mathbf{k}_1}^{0\mathbf{k}_2\,I} = J_0(n_{\mathbf{k}_2} - n_{\mathbf{k}_1}), \tag{A1l}$$

$$c_{\mathbf{k}_1}^{j\mathbf{k}_2\,I} = J_0(s_{\mathbf{k}_2}^j - s_{\mathbf{k}_1}^j), \tag{A1m}$$

$$c_{\mathbf{k}_1}^{0\mathbf{k}_2\,\mathrm{sd}} = J_{\mathrm{sd}}\langle S^i\rangle(s_{\mathbf{k}_2}^i - s_{\mathbf{k}_1}^i), \tag{A1n}$$

$$c_{\mathbf{k}_1}^{j\mathbf{k}_2\,\mathrm{sd}} = J_{\mathrm{sd}}\left[\frac{1}{4}\langle S^j\rangle(n_{\mathbf{k}_2} - n_{\mathbf{k}_1}) + \frac{i}{2}\epsilon_{ijk}\langle S^i\rangle(s_{\mathbf{k}_2}^k + s_{\mathbf{k}_1}^k)\right]. \tag{A1o}$$

[1] M. N. Baibich, J. M. Broto, A. Fert, F. N. Van Dau, F. Petroff, P. Etienne, G. Creuzet, A. Friederich, and J. Chazelas, Phys. Rev. Lett. **61**, 2472 (1988).

[2] S. A. Wolf, D. D. Awschalom, R. A. Buhrman, J. M. Daughton, S. von Molnár, M. L. Roukes, A. Y. Chtchelkanova, and D. M. Treger, Science **294**, 1488 (2001).

[3] S. Datta and B. Das, Appl. Phys. Lett. **56**, 665 (1990).

[4] D. Awschalom and M. Flatté, Nat. Phys. **3**, 153 (2007).

[5] I. Žutić, J. Fabian, and S. Das Sarma, Rev. Mod. Phys. **76**, 323 (2004).

[6] T. Dietl, Nat. Mater. **9**, 965 (2010).

[7] H. Ohno, Nat. Mater. **9**, 952 (2010).

[8] T. Dietl and H. Ohno, Rev. Mod. Phys. **86**, 187 (2014).

[9] T. Dietl, H. Ohno, F. Matsukura, J. Cibert, and D. Ferrand, Science **287**, 1019 (2000).

[10] Z. Ben Cheikh, S. Cronenberger, M. Vladimirova, D. Scalbert, F. Perez, and T. Wojtowicz, Phys. Rev. B **88**, 201306 (2013).

[11] Y. S. Chen, M. Wiater, G. Karczewski, T. Wojtowicz, and G. Bacher, Phys. Rev. B **87**, 155301 (2013).

[12] S. Cronenberger, M. Vladimirova, S. V. Andreev, M. B. Lifshits, and D. Scalbert, Phys. Rev. Lett. **110**, 077403 (2013).

[13] J. Debus, V. Y. Ivanov, S. M. Ryabchenko, D. R. Yakovlev, A. A. Maksimov, Y. G. Semenov, D. Braukmann, J. Rautert, U. Löw, M. Godlewski, A. Waag, and M. Bayer, Phys. Rev. B **93**, 195307 (2016).

[14] J. Debus, A. A. Maksimov, D. Dunker, D. R. Yakovlev, E. V. Filatov, I. I. Tartakovskii, V. Y. Ivanov, A. Waag, and M. Bayer, phys. stat. sol. (b) **251**, 1694 (2014).

[15] A. A. Maksimov, D. R. Yakovlev, J. Debus, I. I. Tartakovskii, A. Waag, G. Karczewski, T. Wojtowicz, J. Kossut, and M. Bayer, Phys. Rev. B **82**, 035211 (2010).

[16] F. Perez, J. Cibert, M. Vladimirova, and D. Scalbert, Phys. Rev. B **83**, 075311 (2011).

[17] M. D. Kapetanakis, I. E. Perakis, K. J. Wickey, C. Piermarocchi, and J. Wang, Phys. Rev. Lett. **103**, 047404 (2009).

[18] M. D. Kapetanakis and I. E. Perakis, Phys. Rev. Lett. **101**, 097201 (2008).

[19] H. Krenn, K. Kaltenegger, T. Dietl, J. Spałek, and G. Bauer, Phys. Rev. B **39**, 10918 (1989).

[20] S. A. Crooker, D. D. Awschalom, J. J. Baumberg, F. Flack, and N. Samarth, Phys. Rev. B **56**, 7574 (1997).

[21] P. Barate, S. Cronenberger, M. Vladimirova, D. Scalbert, F. Perez, J. Gòmez, B. Jusserand, H. Boukari, D. Ferrand, H. Mariette, J. Cibert, and M. Nawrocki, Phys. Rev. B **82**, 075306 (2010).

[22] J. H. Jiang, Y. Zhou, T. Korn, C. Schüller, and M. W. Wu, Phys. Rev. B **79**, 155201 (2009).

[23] H. Ohno, A. Shen, F. Matsukura, A. Oiwa, A. Endo, S. Katsumoto, and Y. Iye, Appl. Phys. Lett. **69**, 363 (1996).

[24] R. Fiederling, M. Keim, G. Reuscher, W. Ossau, G. Schmidt, A. Waag, and L. W. Molenkamp, Nature **402**, 787 (1999).

[25] C. Thurn, M. Cygorek, V. M. Axt, and T. Kuhn, Phys. Rev. B **87**, 205301 (2013).

[26] M. Cygorek and V. M. Axt, Phys. Rev. B **90**, 035206 (2014).

[27] M. Cygorek and V. M. Axt, Semicond. Sci. Technol. **30**, 085011 (2015).

[28] M. Cygorek, P. I. Tamborenea, and V. M. Axt, Phys. Rev. B **93**, 205201 (2016).

[29] J. Kondo, Prog. Theor. Phys. **32**, 37 (1964).

[30] J. Kossut, phys. stat. sol. (b) **72**, 359 (1975).

[31] A. Twardowski, M. Nawrocki, and J. Ginter, phys. stat. sol. (b) **96**, 497 (1979).

[32] R. Bouzerar and G. Bouzerar, EPL (Europhysics Letters) **92**, 47006 (2010).

[33] M. W. Wu, J. H. Jiang, and M. Q. Weng, Phys. Rep. **493**, 61 (2010).

[34] R. J. Elliott, Phys. Rev. **96**, 266 (1954).

[35] M. I. D'yakonov and V. I. Perel', Zh. Eksp. Teor. Fiz. **60**, 1954 (1971), [Sov. Phys. JETP 33, 1053 (1971)].

[36] C. Thurn and V. M. Axt, Phys. Rev. B **85**, 165203 (2012).

[37] C. Thurn, M. Cygorek, V. M. Axt, and T. Kuhn, Phys. Rev. B **88**, 161302(R) (2013).

[38] M. Cygorek and V. M. Axt, Journal of Physics: Conference Series **647**, 012042 (2015).

[39] M. Cygorek, P. I. Tamborenea, and V. M. Axt, Phys. Rev. B **93**, 035206 (2016); **94**, 079906 (2016).

[40] M. Cygorek, F. Ungar, P. I. Tamborenea, and V. M. Axt, *submitted to* Proceedings of SPIE, Optics + Photonics: Nanoscience + Engineering, Spintronics IX (2016).

[41] F. Ungar, M. Cygorek, P. I. Tamborenea, and V. M. Axt, Phys. Rev. B **91**, 195201 (2015).

[42] J. Kossut and J. Gaj, eds., *Introduction to the Physics of Diluted Magnetic Semiconductors*, Springer Series in Materials Science No. 144 (Springer, Berlin, 2011).

[43] F. Long, W. E. Hagston, P. Harrison, and T. Stirner, Journal of Applied Physics **82**, 3414 (1997).

[44] S.-K. Chang, A. V. Nurmikko, J.-W. Wu, L. A. Kolodziejski, and R. L. Gunshor, Phys. Rev. B **37**, 1191 (1988).

[45] J. Schilp, T. Kuhn, and G. Mahler, Phys. Rev. B **50**, 5435 (1994).

[46] C. Fürst, A. Leitenstorfer, A. Laubereau, and R. Zimmermann, Phys. Rev. Lett. **78**, 3733 (1997).

Erklärung

Hiermit versichere ich an Eides statt, dass ich die vorliegende Arbeit selbständig verfasst und keine anderen als die angegebenen Quellen und Hilfsmittel verwendet habe.

Weiterhin erkläre ich hiermit, dass ich bisher keinen anderweitigen Promotionsversuch unternommen habe und Hilfe von gewerblichen Promotionsberatern bzw. -vermittlern weder bisher in Anspruch genommen habe noch künftig in Anspruch nehmen werde.

Bayreuth, den . . . .

. . . .
Moritz Cygorek